



HAL
open science

Valorisation of urea into hydrogen by electro-oxidation: from mechanisms and kinetics studies to pilot-scale reactor design and optimisation

Guillaume Hopsort

► To cite this version:

Guillaume Hopsort. Valorisation of urea into hydrogen by electro-oxidation: from mechanisms and kinetics studies to pilot-scale reactor design and optimisation. Chemical engineering. Université Paul Sabatier - Toulouse III, 2023. English. NNT : 2023TOU30183 . tel-04726813v2

HAL Id: tel-04726813

<https://hal.science/tel-04726813v2>

Submitted on 22 Oct 2024

HAL is a multi-disciplinary open access archive for the deposit and dissemination of scientific research documents, whether they are published or not. The documents may come from teaching and research institutions in France or abroad, or from public or private research centers.

L'archive ouverte pluridisciplinaire **HAL**, est destinée au dépôt et à la diffusion de documents scientifiques de niveau recherche, publiés ou non, émanant des établissements d'enseignement et de recherche français ou étrangers, des laboratoires publics ou privés.



THÈSE

En vue de l'obtention du

DOCTORAT DE L'UNIVERSITÉ DE TOULOUSE

Délivré par : l'Université Toulouse 3 - Paul Sabatier

Présentée et soutenue le 06 octobre 2023 par :

Guillaume HOPSORT

Valorisation de l'urée en hydrogène par électro-oxydation :
des études cinétique et mécanistique
vers la conception et l'optimisation d'un réacteur à l'échelle pilote

JURY

Pr. Manuel A. RODRIGO, UNIVERSIDAD DE CASTILLA LA MANCHA	Rapporteur
Dr. Anna HANKIN, IMPERIAL COLLEGE LONDON	Rapporteuse
Dr. Alain BERGEL, DIRECTEUR DE RECHERCHE CNRS (LGC)	Président
Pr. Christine CACHET-VIVIER, UNIVERSITÉ PARIS-EST CRÉTEIL (ICMPE)	Examinatrice
Pr. Fabrice GROS, SIGMA CLERMONT (INSTITUT PASCAL)	Examineur
Pr. Théodore TZEDAKIS, UNIVERSITÉ TOULOUSE 3 (LGC)	Directeur de thèse
Dr. Karine LOUBIÈRE, DIRECTRICE DE RECHERCHE CNRS (LGC)	Co-directrice de thèse
Pr. Karine GROENEN SERRANO, UNIVERSITÉ TOULOUSE 3 (LGC)	Co-encadrante de thèse

École doctorale et spécialité :

MEGEP : Génie des procédés et de l'Environnement

Unité de Recherche :

UMR 5503 Laboratoire de Génie Chimique (LGC)



PhD THESIS

In order to obtain the
DOCTORATE FROM THE UNIVERSITY OF TOULOUSE

Delivered by: Université Toulouse 3 - Paul Sabatier

Presented and defended on 06th October 2023 by:

Guillaume HOPSORT

**Urea valorisation into hydrogen by electro-oxidation:
from mechanism and kinetic studies
to pilot-scale reactor design and optimisation**

COMITEE

Pr. Manuel A. RODRIGO, UNIVERSIDAD DE CASTILLA LA MANCHA	Referee
Dr. Anna HANKIN, IMPERIAL COLLEGE LONDON	Referee
Dr. Alain BERGEL, CNRS SENIOR RESEARCH SCIENTIST (LGC)	President
Pr. Christine CACHET-VIVIER, UNIVERSITÉ PARIS-EST CRÉTEIL (ICMPE)	Examiner
Pr. Fabrice GROS, SIGMA CLERMONT (INSTITUT PASCAL)	Examiner
Pr. Théodore TZEDAKIS, UNIVERSITÉ DE TOULOUSE (LGC)	Supervisor
Dr. Karine LOUBIÈRE, CNRS SENIOR RESEARCH SCIENTIST (LGC)	Co-supervisor
Pr. Karine GROENEN SERRANO, UNIVERSITÉ DE TOULOUSE (LGC)	Co-monitor

Doctoral school and speciality:

MEGEP: Process and Environmental Engineering

Research laboratory:

UMR 5503 Laboratoire de Génie Chimique (LGC)

This thesis has been prepared at

UMR 5503 Laboratoire de Génie Chimique

Campus de Rangueil
Bâtiment 2R1
118, Route de Narbonne
31062 Toulouse Cedex 4
France

☎ (33)(0)5 34 55 67 99
Web Site <https://lgc.cnrs.fr>



*There is a tide in the affairs of men.
Which, taken at the flood, leads on to
fortune;
Omitted, all the voyage of their life
Is bound in shallows and in miseries.
On such a full sea are we now afloat,
And we must take the current when it
serves,
Or lose our ventures.*

Brutus, Act IV, scene iii. *Julius
Caesar* (1599)

WILLIAM SHAKESPEARE

*Il y a une marée dans les affaires des
hommes,
Prise dans son flux elle porte au succès.
Mais si l'on manque sa chance,
Le grand voyage de la vie s'échoue mi-
sérablement sur le sable.
Or aujourd'hui, nous sommes à marée
haute,
Prenons le flot tant qu'il est favorable,
Ou tout ce que l'on a risqué sera perdu.*

Brutus, Acte IV, scène iii. *Jules César*
(1599)

WILLIAM SHAKESPEARE

**VALORISATION OF UREA INTO HYDROGEN BY ELECTRO-OXIDATION:
FROM MECHANISM AND KINETIC STUDIES TO PILOT-SCALE REACTOR DESIGN AND
OPTIMISATION**

Abstract

To face energy and environmental challenges, the electro-oxidation of urea offers a promising alternative for wastewater treatment. This operation, implemented at room temperature, allows, in addition to the depolluting action, the generation of hydrogen at the cathode. Using inexpensive electrodes, this method has potential for industrial application, and all the more by photo-assisting the process.

This thesis aims at developing a complete model including the design, implementation and optimisation of an electrochemical process allowing the recovery of urine effluents into hydrogen; optionally being assisted by sunlight. Most of the current studies on this subject focus on the functionalisation of electrode materials, without deeply investigating the electrochemical engineering aspects. It is precisely this gap that the work carried out in this thesis seeks to fill. The understanding of the reaction phenomena taking place during the UEO implies the availability of complementary analytical tools. Thus, a wide range of analytical methods (TOC, IC-CD/MS, GC, SEM, granulometry, BET, XRD) has been developed, adapted and rigorously optimised, enabling to establish complete mass balances on almost all the by-product formed.

Then, an electrochemical kinetic study has been carried out by plotting voltammetric curves under different conditions, in order: (i) to study the impact of the operating parameters ($[j]$, $\theta_{/^\circ\text{C}}$, $\omega_{/\text{RPM}}$) on the rate of each chemico-physical phenomenon (electro-catalytic layer generation, reagent transport, reaction kinetics) and (ii) to access key quantities describing the overall process (activation energy, diffusion and anodic charge transfer coefficients, heterogeneous electron transfer rate constant). The validation of the process on a lab-scale scale has been done by means of complete mass balances performed on electrolyses at a scale of 1 to 2 g of urea and for degradation rates of 50 to 90%, never reached to date, and this at different operating conditions ($[\text{OH}^-]$, $\theta_{/^\circ\text{C}}$, mono/bi-compartmented reactor). One of the noticeable results is that the content of the compounds OCN^- , CO_3^{2-} , NO_2^- ions and NH_3 represents $\sim 80\%$ of the degraded urea.

To better understanding of UEO mechanism, additional kinetic studies have been conducted by implementing an original strategy combining two different methods: either solid particles of NiOOH or electro-generated NiOOH on nickel. The analysis of the two kinetic rate laws obtained, coupled with the study of the nature of the oxidation products identified, has enabled to provide new insights on this complex system and to propose a detailed reactional mechanism of the overall process (adsorption, chemical reaction, desorption).

Then, a model combining the established kinetic law with diffusive transport phenomena has been proposed. Concentration profiles have been solved in the liquid volume, in the diffusion layer and in the porous solid layer of NiOOH at the electrode. Consistent agreement ($>95\%$) has been obtained when comparing the lab-scale electrolysis results with the model predictions, and this for different operating conditions.

Coupling the proposed multi-pathway mechanism with this predictive model paves the way for the design and operation of a pilot-scale reactor, the study of which forms the final part of the thesis. The effect of operating parameters ($[j]^\circ$, flow rate/rate, E) on urea conversion, transport phenomena, electrode stability and energy consumption, has been studied on urea solutions, and also on with real effluents. The findings have allowed the validation of the process at pilot-scale (~ 40 g urea).

At last, this thesis has initiated a multi-disciplinary research dynamic aiming at addressing both depollution and energy challenges by valorizing a waste into an energy vector.

Keywords: Urea, Electrochemical Engineering, Kinetic, Mechanism, Effluent valorization, Hydrogen

**VALORISATION DE L'URÉE EN HYDROGÈNE PAR ÉLECTRO-OXYDATION :
DES ÉTUDES CINÉTIQUE ET MÉCANISTIQUE VERS LA CONCEPTION ET L'OPTIMISATION
D'UN RÉACTEUR À L'ÉCHELLE PILOTE**

Résumé

Répondant aux défis énergétiques et écologiques, l'électro-oxydation de l'urée offre une alternative prometteuse au traitement biologique des eaux usées. Simple à mettre en œuvre et opérant à température ambiante, elle permet, outre l'action dépolluante, de générer du H_2 à la cathode. Utilisant des électrodes peu coûteuses, cette méthode présente un potentiel industriel accentué par la perspective de photo-assister le procédé.

Les travaux réalisés dans le cadre de cette thèse visent à développer un procédé électrochimique (conception, mise en œuvre et optimisation) permettant de valoriser l'urine en hydrogène et capable d'être assisté par la lumière solaire. La majorité des recherches actuelles se concentrent sur les matériaux d'électrode, négligeant la dimension Génie des Procédés, que cette thèse aborde.

La compréhension des phénomènes réactionnels liés à l'oxydation anodique de l'urée, implique de disposer d'outils analytiques et de caractérisation. À cet effet, un ensemble analytique (COT, IC-CD/MS, CPG, MEB, granulométrie, BET, DRX) a été développé, adapté et mis en œuvre, ce qui a permis d'établir des bilans de matière de la quasi-totalité des réactifs/produits impliqués.

L'étude de la cinétique électrochimique du système a été réalisée via les courbes $I=f(E)$ avec un double objectif : (i) étudier l'impact des paramètres opératoires ($[j]$, $\theta_{/^\circ C}$, $\omega_{/RPM}$) sur la vitesse de chaque phénomène physico-chimique (génération d'une couche électro-catalytique, transport des réactifs, cinétique de la réaction) et (ii) accéder à des grandeurs clés décrivant le processus global (énergie d'activation, coefficient de diffusion et de transfert électronique, constante de transfert électronique hétérogène). La validation du procédé à l'échelle laboratoire a été effectuée par des bilans de matière complets, sur des électrolyses à l'échelle de 1 à 2 g d'urée et à des taux de dégradation de 50 à 90%, jamais atteints à ce jour, et cela dans une large gamme de conditions opératoires ($[OH^-]$, $\theta_{/^\circ C}$, réacteur mono/bi-compartmenté). Le résultat marquant de cette étude est que les ions OCN^- , CO_3^{2-} , NO_2^- et NH_3 représentent $\sim 80\%$ de l'urée dégradée, le N_2 ne dépassant pas $\sim 15\%$.

Des études cinétiques de la dégradation de l'urée ont été par la suite conduites via une méthodologie originale combinant deux approches : l'analyse des lois de vitesse cinétique obtenues (i) sur particules solides de NiOOH et (ii) sur NiOOH électrogénéré. Couplée à l'identification des produits d'oxydation, ces résultats ont permis de mieux comprendre le système et de proposer un mécanisme réactionnel détaillé du processus global (adsorption, réaction chimique, désorption).

Un modèle combinant la loi cinétique établie avec les phénomènes de transport diffusifs et convectifs a été proposé. Les profils de concentration ont été déterminés : dans le liquide, la couche de diffusion et la couche solide poreuse de NiOOH à l'électrode. Les prédictions du modèle s'accordent à plus de 95% aux résultats d'électrolyses à l'échelle laboratoire, et ce pour différentes conditions de fonctionnement.

Du couplage de ce modèle prédictif avec le mécanisme à chemins réactionnels multiples proposé, un réacteur à l'échelle pilote a pu être conçu et élaboré, dont l'étude a fait l'objet de la dernière partie de la thèse. L'effet des paramètres opératoires ($[j]^\circ$, débit/régime d'écoulement,) sur les performances du procédé (conversion en urée, transport de matière, stabilité des électrodes et consommation énergétique) a été étudié avec l'urée commerciale puis avec de l'urine humaine, et a permis la validation du procédé à l'échelle pilote (~ 40 g d'urée).

L'ensemble de ces travaux ont contribué à une dynamique de recherche pluridisciplinaire, visant à valoriser un déchet en vecteur énergétique, qui est essentielle pour répondre aux enjeux contemporains de dépollution et d'énergie.

Mots clés : Urée, Génie Électrochimique, Cinétique, Mécanisme, Valorisation d'effluent, Hydrogène

Remerciements (acknowledgments)

J'aime à imaginer le parcours en thèse comme l'histoire d'un trio, un conte polygame, un scénario de passion et d'émotions, mêlant le thésard, ses encadrants ainsi que son sujet jusqu'au jour J, le *mariage* tant désiré. Évidemment, si j'écris ces quelques lignes, c'est que le mariage est maintenant consommé et il me faut donc remercier les principaux protagonistes qui ont permis le succès de cette union.

En premier lieu, je tiens à remercier (*ceux qui ont permis le financement de ce mariage*) l'Agence Nationale de la Recherche pour avoir subventionné le projet HYUREA dans lequel s'inscrit ces travaux de thèse.

Je remercie tous les membres du jury (*les témoins de ce mariage*), Mme. Anna Hankin, M. Manuel A. Rodrigo-Rodrigo, M. Alain Bergel, Mme. Christine Cachet-Vivier et M. Fabrice Gros pour l'attention que ces pairs ont pu porter à mon travail.

C'est maintenant le temps d'échanger les *vœux de mariage*, et je dois bien entendu remercier mes encadrants, qui m'ont permis de m'épanouir en toute autonomie en me faisant progresser dans un environnement presque familial. Je remercie chaleureusement Karine Groenen Serrano, pour avoir été le Ying et le Yang de cette famille, la quiétude quand les vagues remuaient l'embarcation. Je te remercie pour tes conseils toujours avisés. Karine Loubière, la « môman » qui m'a tant appris : sur moi-même, sur les autres, sur la Science, sur la politique, sur la recherche académique en France. Tu as toujours été là, avec mes mails en plein week-end, mes sms tard le soir quand j'étais inquiet ou lorsque j'avais une bonne nouvelle à fêter. La ligne téléphonique « Doctorant en détresse » peut maintenant se reposer et je sais que tu resteras toujours à l'écoute. J'en viens maintenant au « pôpa », l'ancien, le patriarche. Théo Tzedakis, a su dès les premiers jours de mon arrivée au laboratoire me tirer vers le haut. Le haut, toujours le haut. Fraichement sortit de l'école d'ingénieur avec un aplomb certain mais sans bagage en Génie Électrochimique, Théo m'a toujours montré la voie. Il m'a toujours accompagné sans compter ses heures. Il rassemble selon moi, tout ce que j'aspire dans ma carrière scientifique (en dépit de son bon caractère bien sûr). Je ne te remercierai jamais assez de m'avoir mis le pied à l'étrier, de m'avoir laissé ta porte ouverte par vents et marées, et de m'avoir fait autant rire que fatiguer ! Je suis particulièrement fier du parcours que nous avons effectué tous les quatre et j'espère que nos chemins se retrouveront dans le futur.

Je tiens également à remercier l'ensemble du personnel du Laboratoire de Génie Chimique. En premier lieu, je tiens à exprimer ma gratitude à Laure Latapie (ma demoiselle d'honneur), une boule d'énergie sans fin, qui a toujours su être là pour fêter les succès mais aussi et surtout quand le moral n'était pas au beau fixe. Venant d'un cursus tourné vers le Génie des Procédés, tu m'as donné goût aux techniques analytiques et tu sais tout le plaisir que j'ai à travailler avec toi, nos chemins pourront sans doute se croiser, qui sait ? Je remercie bien évidemment les services supports de Ranguel et Labège qui ont tous œuvrés à la réussite de ces résultats notamment Frédéric Barazzutti, Patrick Colombies, Sandrine Desclaux, Brigitte Dustou, Jean-Pierre Escafit, Lahcen Farhi, Stéphane Foulon, Sébastien Gaspard, Naïma Khoujane et Pierre Roblin. Je remercie tout particulièrement

Diana Pereira Dos Carmo et Elyes Piguet pour leurs aides précieuses au cours de leurs stages respectifs ; qui se sont à chaque fois, de par la qualité de leurs travaux, soldés par des publications scientifiques. Félicitations à eux. Je leurs suis gré pour leur bonne humeur constante qui vient revigorer la morosité qui peut s'installer durant la thèse.

Un grand merci aussi aux doctorants du LGC du site de Ranguelil : Abby, Brian, Marie, Marteen, Robin (merci pour avoir allumé l'étincelle \LaTeX), Mike, Alexandra ainsi qu'aux anciens qui ont bien passé le flambeau notamment Nabiil et Charaff.

Évidemment, l'être humain est complexe et il s'avère que les atomes s'accrochent plus avec certains collègues spécifiquement pour les transformer en quelque chose de particulier : des amis (préparez-vous aux compliments, c'est bien la seule fois que je me livre à un tel exercice). Je pense notamment à mes copines de bureau qui au quotidien ont subi les blagues, les colères, les soupirs, les surprises et surtout les bonnes musiques. Je commencerais par la plus jeune (ou pas, qui sait ?) Sanatou, la bonne humeur constante, un rayon de soleil avec qui nous avons eu la chance de partager le même directeur de thèse (et les mêmes plaintes ahah). Ta force de conviction est un modèle à suivre. Je te souhaite tout le meilleur et t'envoie tout le courage qu'il te faut pour rejoindre le club select des Docteurs. Chloé, un support sans faille lors des moments difficiles et des moments de commérages sans fin. Et enfin, Dihia. Mes journées au labo n'auraient pas eu le même goût sans toi (et je ne dis pas ça à cause des pâtisseries algériennes). Les longues soirées passées tous les deux à rédiger et travailler ne sont désormais qu'un mauvais souvenir sur lesquels nous nous moquerons d'ici quelques années. Enfin, je pense aux dernières arrivées dans cette aventure. Christelle et Marion sont entrées dans ma vie au début de la rédaction. Une vraie bouffée d'air frais. Marion, la maman du groupe, et Christelle, le clown. Je ne vous remercierais jamais assez pour tous ces moments qu'on a passé ensemble, d'une terrasse au bord de mer ou autour d'une bonne bière avec notre David national, que je remercie de m'avoir fait confiance pour les enseignements. Ma santé mentale vous doit une fière chandelle, et croyez-moi, tous ces moments passés ensemble resteront gravés.

Arrive la partie la plus difficile, les remerciements aux proches, ceux pour qui il m'est le plus dur d'exprimer mes sentiments. Je commencerais à remercier mes copines de la prépa (vous remarquez le nombre de filles qui m'entourent ?? ça ne s'arrête pas), Agathe, Anh-Lan, Bérénice et Marine. J'ai grandi avec et grâce à vous, et l'histoire n'est pas finie. Il y a aussi mes copines de l'école d'ingé. Lise, avec qui j'ai parcouru le monde jusqu'en Nouvelle-Zélande, et qui restera sûrement comme ma jumelle (je n'en reviens pas de ce que j'écris). Il y a aussi Alice. Dingue de voir à quel point, il est dur de parler de cette relation. Je te remercie pour toutes ces fois où tu as dû m'écouter, me rassurer, et surtout m'encourager. J'ai hâte de voir ce que l'avenir nous réserve.

Merci à tous les membres de ma famille pour leur soutien et encouragements. Des oncles et tantes en passant aux grands-parents (dont Adrien 91 ans tout de même !), je vous remercie tous pour la joie que vous m'avez apportée. Je pense particulièrement à ma petite sœur, Manon, avec qui j'ai rarement les bons mots pour lui exprimer toute la fierté de ce que tu as accompli. Bien sûr, je n'ai pas les mots suffisants pour exprimer la reconnaissance envers mes parents, qui m'ont toujours soutenu depuis que je suis parti de la maison. Papa, je ne te remercierai jamais assez pour toute la rigueur et surtout le soutien que tu nous as apporté depuis le début. Maman, tu sais à quel point il m'est difficile d'être loin de toi et combien tes bras me manquent. J'espère vous rendre fier aujourd'hui.

Enfin, Laurent. Je pourrais écrire un tome 2 du manuscrit pour toi. Présent depuis le début, tu me permets d'être meilleur chaque jour. Je souhaite à quiconque de pouvoir trouver la personne qui fasse ressentir ce que je ressens pour cet homme. Merci à toi.

Contents

Abstract	ix
Remerciements (acknowledgments)	xiii
Contents	xv
Nomenclature	xxi
Chemicophysical quantities	xxi
Latin letters	xxi
Greek letters	xxii
Abbreviations	xxiii
General introduction	1
I State of the art	7
I-1 Human urine storage and urea degradation	9
I-1.1 Historical considerations	9
I-1.2 Urine selective collection as an alternative to traditional sanitation systems	10
I-1.3 Urine composition, hydrolysis and stabilization	13
I-1.4 Conventional urea degradation processes	15
I-1.4.a Chemical degradation	15
I-1.4.b Chemical enzymatic degradation (urease action)	17
I-1.4.c Comparison of urea degradation methods	17
I-2 ElectroChemical treatment of urine simultaneously to the H ₂ production	19
I-2.1 ElectroChemical oxidation in physiological buffer medium	21
I-2.2 ElectroChemical oxidation in neutral/saline medium	23
I-2.3 Oxidation in alkaline medium	26
I-2.3.a Mechanisms	26
I-2.3.b Kinetics of the UEO	29
I-2.3.c By-product identification and formation routes	29
I-2.3.d Ongoing works and remaining challenges	33
I-2.3.e Concluding remarks	36
I-3 Highlights of the state of the art, context and strategy of the present study	37
II Material and methods	41
II-1 Experimental set-up	42
II-1.1 Laboratory scale	42
II-1.2 Pilot scale	45
II-1.3 Summary of the various EC set-up characteristics	50
II-2 Analytical methods for urea quantification	52
II-2.1 State of the art	52
II-2.1.a Electrochemical biosensor	52
II-2.1.b Chemiluminometric techniques	53
II-2.1.c Colorimetric & spectrophotometric methods	53

II-2.1.d	Chromatographic processes	54
II-2.1.e	Comparison and concluding comments	54
II-2.2	Total organic carbon (TOC) as a global tool to evaluate the carbonaceous load of the media	54
II-2.2.a	Analysis of Total Carbon (TC)	55
II-2.2.b	Analysis of Inorganic Carbon (IC)	56
II-2.2.c	Analysis of Non-Purgeable Organic Carbon (NPOC)	56
II-2.2.d	Assimilation of the NPOC measurement for urea determination	57
II-3	IC-CD/MS coupling	58
II-3.1	Principle	58
II-3.2	Instrumentation and analytical protocols	59
II-3.2.a	Chromatography	59
II-3.2.b	Mass spectroscopy	60
II-3.3	Application to urea solutions	60
II-4	Gas chromatography	64
II-4.1	Principle	64
II-4.2	Instrumentation and analytical protocols	64
II-4.3	Application to urea solutions	66
II-5	General operating procedure of the electrolysis at lab-scale	67
III	Study at lab-scale of the urea oxidation by electro-mediation of nickel(III)/nickel(II) system in alkaline media	71
III-1	Introduction	72
III-2	Effect of the operating parameters on UEO at lab-scale	72
III-2.1	Effect of urea concentration on overall rate of the indirect electro-oxidation	73
III-2.2	Effect of the scan rate as a tool for revealing the limitation of the HCR on the ER	75
III-2.3	Effect of the alkalinity on overall rate of the indirect electro-oxidation	79
III-2.4	Effect of temperature on chemico-physical properties affecting the global process (ER/HCR) as well as the mass transfer phenomena	83
III-2.5	Influence of nickel electrode angular velocity on mass transport processes	88
III-3	Mass balances at lab-scale and effect of process parameters	89
III-3.1	Identification of the electro-generated adducts and mass balance on carbon and nitrogen elements	89
III-3.2	Influence of the presence (or not) of the ionic separator (undivided cell vs divided cell)	91
III-3.3	Influence of the alkalinity	93
III-3.4	Influence of the temperature	95
III-4	Conclusion of Chapter 3	98
IV	From kinetics and mechanisms to reactor modeling of the reactions involving urea and nickel(III)	99
IV-1	Introduction	100
IV-2	Methodology of the kinetic study	101
IV-2.1	Kinetic study on nickel synthesized powders	101
IV-2.1.a	Synthesis protocol	101
IV-2.1.b	Powder characterization techniques	101
IV-2.2	Kinetics investigations of the reaction between urea and chemically synthesized nickel(III) sites in alkaline medium	105
IV-2.2.a	Experimental set-up and reaction monitoring	105

	IV-2.2.b Post-processing of the temporal pH-curves	107
	IV-2.3 Kinetic investigations of the reaction between urea and the electrochemically generated nickel(III) sites in alkaline medium	108
	IV-2.3.a Expression of reaction rate	108
IV-3	Results on the kinetic of the urea catalytic indirect oxidation	108
	IV-3.1 Case 1: with chemically synthesized nickel(III) sites	108
	IV-3.1.a Determination of the initial kinetic rate law	108
	IV-3.1.b Validation of the initial kinetic rate law by the integral method	111
	IV-3.2 Case 2: with the electrochemically synthesized nickel(III) sites on bare nickel electrode	113
IV-4	Establishment of a complete mechanism for the whole urea electro-oxidation	116
IV-5	Macro- and micro-modeling of the UEO	119
	IV-5.1 Establishment of the predictive model	119
	IV-5.1.a Model assumptions	120
	IV-5.1.b Governing equations: urea mass balances	121
	IV-5.1.c Boundary and initial conditions	122
	IV-5.1.d Comparison between predictions and experimental data	123
	IV-5.1.d.i Thicknesses of the diffusion film and the electrocatalytic layer	123
	IV-5.1.d.ii Urea electrolysis on nickel electrode : case results and comparison	123
IV-6	Conclusion of Chapter 4	127
V	Toward the process scaling-up: real effluent treatment and pilot-scale experiments	129
V-1	EC treatment of real matrix at lab-scale	130
	V-1.1 Complete mass-balances and proof of concept	130
	V-1.1.a Experimental information	131
	V-1.1.b Results and discussion	133
	V-1.1.b.i Electrolysis of urea synthetic solutions	133
	V-1.1.b.ii Electrolysis of human urine	136
	Effect of alkalization	136
	Chronoamperometry results	139
	V-1.1.b.iii Electrolysis of creatinine	142
	V-1.1.b.iv Energy cost assessments	144
	V-1.2 Linear voltammetry experiments as a tool to better understand the matrix effect during the electro-oxidation of human urine	145
	V-1.2.a Electrochemical behavior of urine stabilized by alkalization	146
	V-1.2.b Voltammetric response of different matrices spiked by each one of the most concentrated compounds in urine	149
	V-1.2.b.i KOH matrix	151
	V-1.2.b.ii Urea/KOH matrix	154
	V-1.2.b.iii Urine/KOH matrix	154
	V-1.2.c Matrix effect illustrated by means of kinetic study	155
V-2	From the lab-scale scale to the pilot-scale	157
	V-2.1 Complete mass balances during the course of the urea electrolysis at pilot-scale	157
	V-2.2 Effect of some key operating parameters on the urea synthetic solution electrolyses at pilot-scale	159
	V-2.2.a Influence of the surface of the nickel grid anode	160
	V-2.2.b Influence of the flow rate	160
	V-2.2.c Influence of the applied potential	161

V-2.3	Human urine electrolysis at pilot-scale	164
V-2.4	Evaluation of energy consumption at pilot-scale	166
V-3	Conclusion of Chapter 5	168
General Conclusion and Perspectives		171
Concluding remarks		171
Perspectives		175
A	Fresh urine composition	177
B	PEC reactor HyUrea concept	191
C	Pilot-scale plans of the EC cell	193
D	Validation of IC-CD/MS method	205
D-1	Introduction	206
D-2	Material and methods	207
D-2.1	Chemicals	207
D-2.2	Preparation of standards and urine samples	207
D-2.2.a	Preparation of standards	207
D-2.2.b	Preparation of urine samples	207
D-2.3	Validation of the method	207
D-2.3.a	Selectivity	208
D-2.3.b	Sensitivity	210
D-2.3.c	Linearity	210
D-2.3.d	Accuracy	211
D-2.3.e	Precision	212
D-2.3.f	Matrix effect	212
D-3	Results	213
D-3.1	Implementation of the IC-CD/MS method	213
D-3.2	Validation of the IC-CD/MS method	213
D-3.2.a	Linearity, LODs and LOQs	213
D-3.2.b	Precision	218
D-3.2.c	Accuracy	219
D-3.2.d	Matrix effect	222
D-3.3	Analysis of human urine samples	225
D-4	Discussions	228
D-5	Conclusions	230
D-6	Ethical approval	230
E	Repeatability of the initial rate	231
F	Model resolution	233
G	ICP-OES experimental details	235
H	Raw data of complete mass balance	237
I	I=f(E) for urine compounds	239
J	Langmuir model for histidine adsorption on nickel(III) sites	245
	Bibliography	247

Scientific production	265
Publications in peer-reviewed journals	265
Conference contributions	265
Other communications during the thesis	266

Nomenclature

Chemicophysical quantities

Latin letters

\mathcal{A}	Pre-exponential factor	\sim
BOD ₅	five-day Biochemical Oxygen Demand	[M.L ⁻³]
COD	Chemical Oxygen Demand	[M.L ⁻³]
D _i	Diffusion coefficient	[L ² .T ⁻¹]
E	Potential	[M.L ² .T ⁻³ .I ⁻¹]
E _a	Activation energy	[M.L ² .T ⁻² .N ⁻¹]
E _{peak}	Peak potential	[M.L ² .T ⁻³ .I ⁻¹]
E _{consumed}	Consumed energy of the electrolyser	[M.L ² .T ⁻²]
E _{eq. H₂ produced}	Energy contained in H ₂ gas at 25 °C and P _{atm}	[M.L ² .T ⁻²]
E _{I=0}	Open circuit potential	[M.L ² .T ⁻³ .I ⁻¹]
\mathcal{F}	Faraday's constant	96,485 A s mol ⁻¹
i	Current density	[I.L ⁻²]
I	Current	[I]
I _{peak}	Peak current	[I]
IC	Inorganic Carbon	[M.L ⁻³]
k	Kinetic constant	\sim
K	Reaction equilibrium constant	[-]
k ^o	Heterogeneous electron transfer rate constant	[T ⁻¹]
k _B	Boltzmann's constant	1.38 × 10 ⁻²³ J K ⁻¹
ME	Matrix Effect	[-]
m/z	Mass-to-charge ratio	[M]
n _e	Amount of electrons exchanged	[-]
NPOC	Non-Purgeable Organic Carbon	[M.L ⁻³]
POC	Purgeable Organic Carbon	[M.L ⁻³]

Q	Charge	[T.I]
Q_m	Mass flow rate	[M.T ⁻¹]
Q_v	Volumetric flow rate	[L ³ .T ⁻¹]
r_x	Chemical rate law	[N.T ⁻¹]
R	Gas constant	8.314 J K ⁻¹ mol ⁻¹
RE	Relative Error	[-]
RSD	Relative Standard Deviation	[-]
SD	Standard Deviation	[-]
S	Surface	[L ²]
SS	Suspended Solid	[M.L ⁻³]
T	Temperature	[Θ]
T_r	Retention time	[T]
TC	Total Carbon	[M.L ⁻³]
TN	Total Nitrogen	[M.L ⁻³]
TOC	Total Organic Carbon	[M.L ⁻³]
TP	Total Phosphorus	[M.L ⁻³]
$V_{H_2, \text{ produced}}$	Volume of H2 produced	[L ³]
$V_{i, \text{ after } j \text{ min}}$	Total volume of the compound i after j minutes of electrolysis symbol	[L ³]
X	Conversion rate	[-]
z_i	Ion charge of ion i	[-]

Greek letters

α, β, γ	Partial order of HCR	[-]
Γ_i	Surface concentration	[sites i.L ⁻²]
δ	Diffusion layer	[L]
ΔE	Differential between energies consumed and equivalent produced by H ₂ for an electrolyser	[M.L ² .T ⁻²]
$\Delta U_{\text{electrolyzer}}$	Cell potential	[M.L ² .T ⁻³ .I ⁻¹]
η	Dynamic viscosity	[M.L ⁻¹ .T ⁻¹]
λ_i	Molar conductivity of the ion i	[T ³ .I ² .N ⁻¹ .M ⁻¹]
λ_{H_2}	H ₂ gravimetric energy density	[L ² .T ⁻²]
ν	Kinematic viscosity	[L ² .T ⁻¹]
ν_{scan}	Potential scan rate	[M.L ² .T ² .I ⁻¹]
ρ_{H_2}	H ₂ volumetric density	[M.L ⁻³]
σ	Conductivity	[M ⁻¹ .L ⁻³ .T ³ .I ²]
τ	Tortuosity	[-]
τ_{reactor}	Residence time in the reactor	[T]
∇	Del operator	[-]

Abbreviations

AOR	Anode Oxidation Reaction
a.u.	Arbitrary Unit
BDD	Boron-Doped Diamond
BET	Brunauer, Emmett and Teller
C	Carbon
CD	Conductivity Detector
CE	Counter Electrode
CNTs	Carbon NanoTubes
CO ₂ RR	CO ₂ Reduction Reaction
CV	Cyclic Voltammetry
DFT	Density Functional Theory
EC	ElectroChemical
ER	Electro-generation Reaction
ESI	Electronic Spray Ionisation
FA	Formic Acid
FC	Fuel Cell
FE	Faradic Efficiency
FTO	Fluorine-doped Tin Oxide
GC	Gas Chromatography
HCR	Heterogeneous Chemical Reaction
HER	Hydrogen Evolution Reaction
HPLC	High Performance Liquid Chromatography
IC	Ion Chromatography
IC-CD/MS	Ion Chromatography - Conductivity Detector / Mass Spectroscopy
ICP-OES	Inductively Coupled Plasma - Optical Emission Spectroscopy
K	Potassium
KRPB	Krebs-Ringer Phosphate Buffer
LC	Liquid Chromatography
LGC	Chemical Engineering Laboratory (fr: Laboratoire de Génie Chimique)
LODs	Limits Of Detection
LOQs	Limits Of Quantification
LSV	Linear Sweep Voltammetry
MS	Mass Spectroscopy
MSA	Methane Sulfonic Acid
S	Sulfur

N	Nitrogen
N ₂ RR	N ₂ Reduction Reaction
NADP ⁺	Nicotinamide Adenine Dinucleotide Phosphate
NADPH	Nicotinamide Adenine Dinucleotide Phosphate reduced form
NDIR	Non-Dispersive Infrared
NF	Nickel Foam
NO _x	Nitrogen Oxides
OA	Oxalic Acid
OER	Oxygen Evolution Reaction
PCET	Proton-Coupled Electron Transfer
PEC	PhotoElectroChemical
POC	Proof Of Concept
RCS	Reactive Chlorine Species
RDE	Rotating Disk Electrode
RDS	Rate-Determining Step
RHE	Reversible Hydrogen Electrode
RPM	Revolutions per minute
SCE	Saturated Calomel Electrode
SEM	Scanning Electron Microscope
SHE	Standard Hydrogen Electrode
SS	Suspended Solids
STP	Standard Temperature and Pressure (i.e., 0 °C & 1 × 10 ⁵ Pa)
TAN	Total Ammonia Nitrogen
TCD	Thermal Conductivity Detector
TON	Turn Over Number
TP	Total Phosphorus
UBF	Urine-Based Fertilizers
UEO	Urea Electro-Oxidation
UOR	Urea Oxidation Reaction
UV	Ultra Violet
WE	Working Electrode
WWTPs	WasteWater Treatment Plants
XRD	X-Ray powder Diffraction

General introduction

The world population has been grown for many years, from 2.6 billion people in 1950 to 7 billion in 2011 and should end up, according to United Nations forecasts, at 11 billion people in 2100 [1]. This population growth, consequence of medical progresses and improved living standards, underlines the importance of a better management of the Earth's natural resources. The associated (*over*)consumption of energy inevitably leads to recycling issues that should be addressed to ensure a peaceful and sustainable future for next generations.

In practice, the **EU directives** impose to blend, convey and process urban domestic sewage in WasteWater Treatment Plants (WWTPs) prior to being discharged into natural environment (*i.e.*, rivers) since the 2000s. The diminution of disease transmission risks and the minimization of the environmental impact have been obtained by using such centralized approach for sewage treatment [2].

The biological decomposition treatment remains the method the most commonly used to degrade organic matter in WWTPs [3]. Also including the collection and disposal steps, the overall wastewater treatment process generally consists of a succession of unitary operations that are represented in Figure 1.

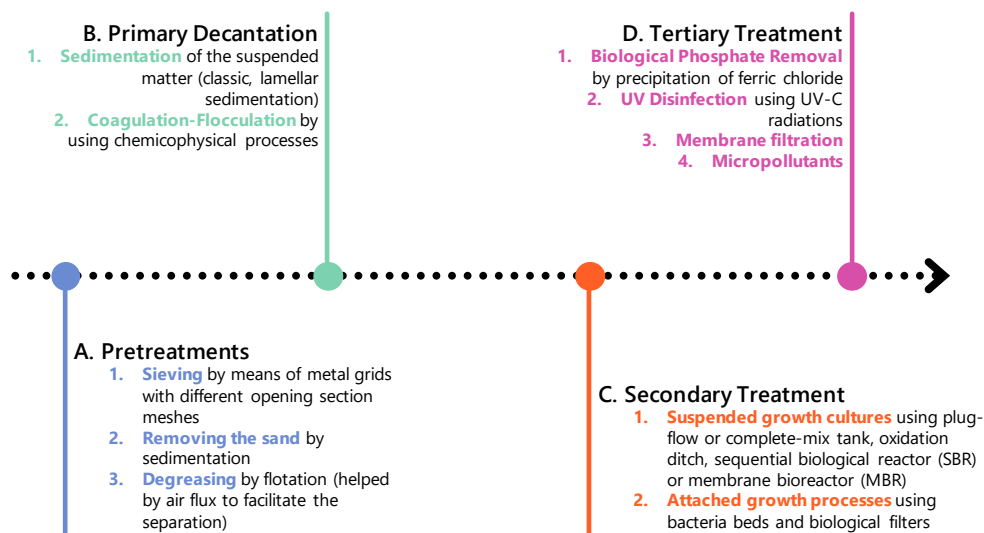


Fig. 1 – Schematic representation of the “classical” wastewater treatment in French WWTPs.

The process starts with a pre-treatment step allowing the separation of the coarse solids present in the wastewater (the bulky materials are separated by sieving while sand and greasy particles are separated by desanding). Then occurs the primary settling stage: the remaining suspended matters are separated by using, firstly, gravity to precipitates the particles, and secondly, chemico-physical settling (*i.e.*, coagulation, flocculation and then decantation) to remove the smallest particles. At the end of this second step, nearly 80% of

the suspended solids are retained. The secondary treatment stage is the most important one where, with the help of a microorganism consortium (bacteria, protozoa, metazoa and viruses), organic matter is biologically decomposed into mineral matter that can be later assimilated by plants.

Three main types of pollution have to be treated in WWTPs: carbon, nitrogen and phosphorus. The first is treated by heterotrophic bacteria that use organic carbon as a source of energy (aerobic conditions). The carbon organic matter is then transformed into carbon dioxide, water and new bacteria (called excess sludge). Nitrogen pollution (mainly urea, amino acids, uric acid, purine) is also very closely monitored because a reduced nitrogen discharge into water results in a very high oxygen consumption (about 4 mg of oxygen for 1 mg of nitrogen). To avoid any oxygen depletion in the natural aquatic environment, these nitrogen molecules are removed by successive oxidation-reductions:

- ammonification transforms organic matter by hydrolysis into ammonium. This step occurs naturally (*i.e.*, without any intervention) and thus starts before the treatment. As a consequence, when the effluent enters in the treatment plant, most of the nitrogenous molecules are already in the ammonia form;
- Nitrification is a two-step process using aerobic bacteria [4]:
 - nitritation, which converts ammonium ions to nitrites using nitrous bacteria (*Nitrosomonas*, *Nitrosococcus* and *Nitrospira*);
 - nitrating, which converts nitrites into nitrates with the help of nitrating bacteria (*Nitrobacter*, *Pseudomonas*)
- denitrification allows the reduction of organic matter in the form of nitrates. The process takes place in anoxia conditions.

One should note that *(i)* **during this last stage, nitrous oxide is produced which contributes to a significant part of greenhouse gas emissions** [5], and *(ii)* all these steps require to be finely optimize because the behavior of microorganisms remains very sensitive to any type of external stimuli (temperature, pressure, pH).

However, despite its rather good efficiency, this wastewater treatment process faces with many concerns that have been raised as early as the 1970s [6] and grown over the years [7, 8]:

- the presence of various (micro)pollutants makes treatment more costly, challenging, and even inefficient;
- the treatment mainly focuses on the improvement of the discharge quality, the wastewater transport requires the construction and maintenance of pipe networks, while the pipe leaking can lead to widespread water pollution. The adaptation of these systems to the constant population growth also remains a tricky issue.

In this context, the specific separation for recovery and further treatment of urine could be a relevant way:

- to reduce the release of environmental persistent pharmaceutical pollutants into the environment;

- by implementing some treatment processes that are economically more accessible due to the reduced volumes of effluent;
- to allow the valorisation and the recycling of Nitrogen (N), Phosphorus (P) and Potassium (K) nutrients thanks to their high contents in urban sewage.

Indeed, nearly 75% of the nitrogen present in wastewater come from human urine, resulting from the filtration of blood at the kidneys [9]. Multiple methods for urea degradation have emerged to face with the related large amount of nitrogen pollution produced every day. One can cite hydrolysis [10], enzymatic decomposition [11], biological treatment, chemical oxidation [12], adsorption [13, 14], catalytic decomposition [15]. However, these processes could require either expensive equipment and/or high energy consumption, and they are not all mature for industrial scale-up. As relatively simple to implement at room temperature, electro-oxidation appears as a promising alternative for pollution removal in wastewater, thus boosting the attention of the ElectroChemical (EC) community over the last two decades [16–19]. In general, the anodic half-electronic reaction enables pollutant degradation (industrial, human, or animal waste) while the cathodic half-electronic reaction enables producing hydrogen, that can be used later as fuel.

A key practical requirement for the Urea Electro-Oxidation (UEO) is the availability of highly efficient and cost-effective electrocatalysts. By performing UEO in alkaline medium, it was shown that the use of precious metals for the electrode is not mandatory [20, 21], which drastically reduces the process cost and opens prospects for transferring to an industrial scale. In particular, nickel-based alloys have the advantage of being cheap, widely available and able to efficiently degrade urea while producing hydrogen at a lower cell voltage than the one required for water splitting [22].

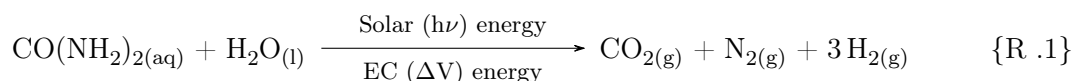
The H₂ production simultaneously to urea degradation represents a strong added-value of the UEO process.

In keeping with this context, the present thesis aims at contributing to the scientific advances in the UEO field by providing EC Engineering framework.

It has been funded by the ANR proposal “HyUrea” (ANR-19-CE04-0009) which overall objective is to propose a new concept of wastewater treatment, combining selective collection of urine and decentralized treatment (degradation into valuable products) through a PhotoElectroChemical (PEC) process.

By this way, the HyUrea project intends to propose a technology to mineralise effluents, considered as wastes, and to generate simultaneously products of interest (H₂), thus enabling to reduce the energy consumption and the greenhouse gas emissions of WWTPs.

To this end, and since the nitrogenous contribution of wastewater is composed in average of 75% by urea, the following {R .1} is the target reaction to carry out:



To achieve this objective, the project gathers an interdisciplinary consortium sharing their expertise in Electrochemistry, (electro)Chemical Engineering, (photo)Chemistry, Material Science and Water treatment. The different partners are:

- **ICMPE UMR 7182 Paris Est** (R. Benyahia, C. Cachet-Vivier, S. Bastide, M. Latroche, D. Muller),
- **LISE UMR 8235 Paris Sorbonne** (S. Akkari, V. Sanchez-Sanchez),
- **LRS UMR 7197 Paris Sorbonne** (V. Vivier),
- **LGC UMR 5503** (G. Hopsort, T. Tzedakis, K. Loubière, K. Groenen Serrano, L. Latapie),
- **SIAAP** (M. Lopez-Viveros, S. Azimi) as the Greater Paris sanitation authority.

The project is organized in four scientific tasks, as shown in the Figure 2.

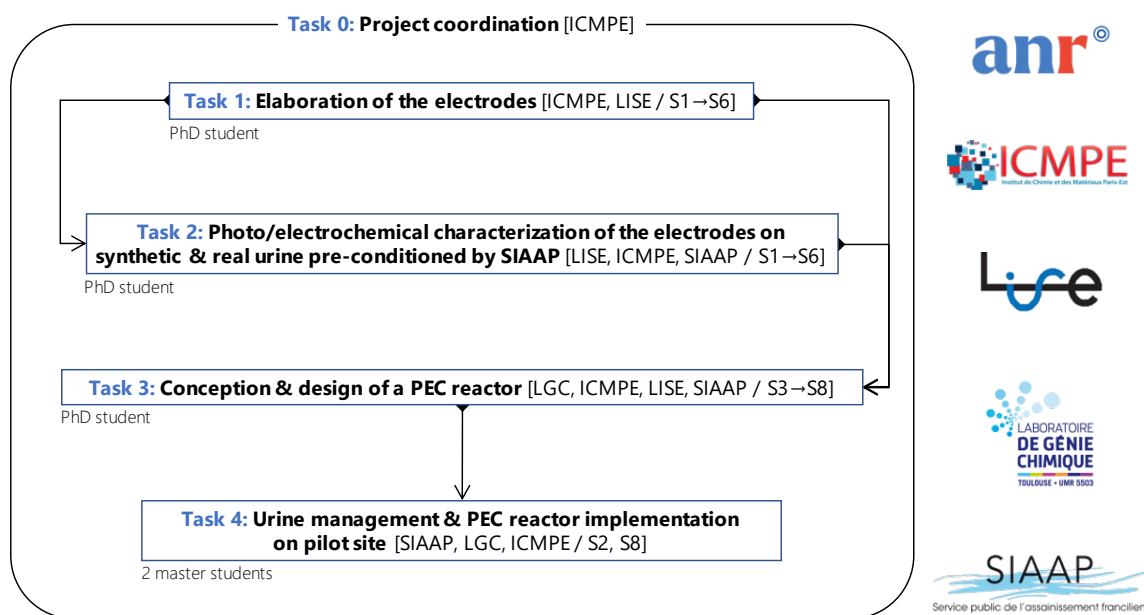


Fig. 2 – Description of the ANR HyUrea project.

As initially planned in the project, the PEC reactor should integrate photo-anodes irradiated by sun simulator. A first-generation of photo-anodes was elaborated and characterised at lab-scale by the ICMPE team. They were made of nano-structured semiconducting α - Fe_2O_3 layers deposited on transparent and conductive fluorine doped tin oxide (FTO), and decorated with Ni-based catalysts [23, 24]. Even if their performances were promising, they were not sufficient to scale them for their integration in the pilot-scale reactor designed in Toulouse. Because the second generation is currently under investigation, the implementation of these photo-anodes in the pilot-scale is still under progress and will not be presented in this manuscript.

As a consequence, the present thesis, that mainly focuses on Task 3, aims at designing, building and optimizing a EC reactor at pilot-scale that could be possibly photo-assisted and able to treat $5 \text{ L day}^{-1} \text{ m}_{\text{anode}}^{-2}$ of urea stored in external tanks at an average concentration of 0.33 mol L^{-1} using 100 cm^2 of electrode area.

This study has been carried in the Chemical Engineering Laboratory (*fr*: Laboratoire de Génie Chimique) (LGC), more specifically shared between two of its departments:

The *Electrochemical Processes (PE)* department through the team *Electre: Electrochemical Engineering for synthesis, pollution abatement and energy* which focuses on the design and the experimental or theoretical optimization of tools, methods and EC processes, in monophasic or multi-phase media, at scales ranging from μ -system to pilot.

The *Sciences and Technologies for Process Intensification (STPI)* department with its expertise in Photochemical reactor Engineering.

The manuscript is composed of five chapters. **Chapter I** is devoted to the state-of-the-art. The human urine storage, degradation as well as its EC treatment simultaneously with the H₂ production will be discussed.

Chapter II presents the experimental set-ups conceived and used (lab-scale cells and pilot-scale reactor) as well as the set of analytical methods that have been developed to establish complete mass balances in gas and liquid phases.

Chapter III explores the UEO in alkaline media at a lab-scale, investigating various parameters and cell configurations, while proposing guidelines for electrolyser design and operation for urea treatment.

Chapter IV investigates the kinetic behavior of urea oxidation on two types of NiOOH sites, determined kinetic rate laws, and established a multi-pathway mechanism using identified UEO by-products. It also proposed and validated a predictive model incorporating kinetic laws and transport phenomena, showing high agreement with lab results. The model, along with the multi-pathway mechanism, will be used for designing and operating a larger-scale UEO reactor.

Chapter V introduces a Proof Of Concept (POC) for a pilot-scale reactor enabling UEO, based on comprehensive mass balances and an energy study. The POC's application to real effluent treatment will also be discussed, facilitating a critical comparison with existing water treatment processes.

Finally, a conclusion will summarise present the main advances of this thesis work and present some key perspectives.

State of the art

Outline of the current chapter

I-1 Human urine storage and urea degradation	9
I-1.1 Historical considerations	9
I-1.2 Urine selective collection as an alternative to traditional sanitation systems	10
I-1.3 Urine composition, hydrolysis and stabilization	13
I-1.4 Conventional urea degradation processes	15
I-2 ElectroChemical treatment of urine simultaneously to the H₂ production	19
I-2.1 ElectroChemical oxidation in physiological buffer medium	21
I-2.2 ElectroChemical oxidation in neutral/saline medium	23
I-2.3 Oxidation in alkaline medium	26
I-3 Highlights of the state of the art, context and strategy of the present study	37

I believe that water will one day be employed as fuel, that hydrogen and oxygen which constitute it, used singly or together, will furnish an inexhaustible source of heat and light, of an intensity of which coal is not capable.

*Jules Verne, The Mysterious Island
(1874)*

Electrochemical Engineering seeks to solve contemporary societal problems, mainly in terms of environment and energy, which often go hand in hand. Since the discovery of the Volta cell, this discipline has developed considerably, both in terms of fundamental basics and applications in various sectors such as energy (production and storage), electro-synthesis, preparation of metals or reactive non-metals and analysis. The industrial applications of electrochemistry are diverse and the subject of ongoing research, particularly in the context of sustainable development and efficient management of matter and energy.

One of the major applications of this discipline is the development of electrolyzers. Electrolysis uses electrical energy (*i.e.*, a potential difference between two electrodes) to generate chemical reactions, such as the water electrolysis allowing the dissociation of water into H₂. Electrolysis has become an industrial-scale process in the late 1800s, consequence of the high demand for hydrogen in the newly emerging fertilizer industry, especially for catalytic ammonia synthesis purposes [25]. According to Hale in 1919 [26], the Royal College of France developed one of the first commercial systems in 1885, which generated approximately 300 liters (STP conditions) of H₂ per day. This system operated with an alkaline electrolyte comprising 30wt.% KOH. Several types of electrolyzer have emerged over the years, as knowledge has increased, mainly (*i*) alkaline electrolysis technology; (*ii*) acid electrolysis technology and (*iii*) high temperature electrolysis technology.

To address waste-scarcity situation, the optimal management of water resources and the wastewater treatment for reuse after depollution are seen as possible solutions [27]. Traditional processes such as physical, chemical and biological treatments are becoming more and more ineffective in producing safe water from the large amounts of wastewater generated by the agricultural, domestic and industrial sectors. Over the last years, one can observe that EC technologies have gained renewed importance worldwide, especially to face the challenges of (*i*) the high composition complexity of industrial wastewater [28] and of (*ii*) the ever-increasing standards of drinking water supply and increasingly strict environmental regulations on wastewater discharge. Indeed, they can be used to treat wastewater containing organic oils, organic pollutants, heavy metals and nitrates [29], by implementing different EC techniques, such as EC metal recovery, electrocoagulation and electro-oxidation [30].

In order to combine decontaminating power with the production of value-added products (H₂, etc.), hybrid solutions have been proposed to reduce the energy consumption of the processes, thus enabling development on a large scale. One can cite:

- (*i*) the implementation of other anode reactions to replace Oxygen Evolution Reaction (OER) and oxidative products (such as the urea oxidation);

- (ii) the design of functionalized electrodes with the aim of reducing the energy cost of electrolyzers;
- (iii) the bio-assistance through bioelectrochemical cells;
- (iv) the development of hybrid technologies assisted by photons (PhotoElectroChemical, Photocatalytic, PhotoVoltaic-ElectroChemical water splitting, etc.).

The present work is part of this scientific dynamic, by proposing an alternative method based on 3 main axes:

- Section I-1 describes the intrinsic properties of urine, including the main urea degradation methods;
- Section I-2 reports the main results of the EC treatment of urine in various media;
- Section I-3 ends this chapter by summarizing the major advances in this field and the lack in the literature. From this, the methodology and the expecting of the present thesis will be positioned.

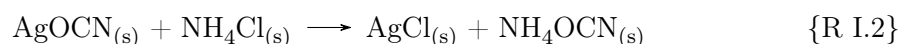
I-1 Human urine storage and urea degradation

This section is structured into 4 main areas and will present:

- (i) brief historical considerations and intrinsic features of urine;
- (ii) the ins and outs of the selective collection system of undiluted urine;
- (iii) the composition of urine;
- (iv) the methods currently used at lab-scale, knowing that the biological process implemented in WWTPs has been presented in the introduction of the manuscript).

I-1.1 Historical considerations

The abundance of urea (Figure I.1), in nature comes mainly from mammalian metabolism but also from the intensive industrial use of urea. For the urotelic species, urea, also called carbamide, is the final product of nitrogen compound degradation (mainly proteins) according to the ornithine cycle discovered by the German doctor Hans Adolf Krebs in 1932 [31] (in 1953, he was awarded the Nobel Prize in Physiology or Medicine for his identification of the citric acid cycle). Unearthed in 1773 by the French chemist Hilaire-Marin Rouelle (as “le cadet” *i.e.*, “the younger”), urea was first synthesized 50 years later in 1828, by chance when the German chemist Friedrich Wöhler expected to synthesize ammonium cyanate (NH_4OCN) by reacting silver cyanate (AgOCN) with ammonium chloride (NH_4Cl) according to the {R I.2}.



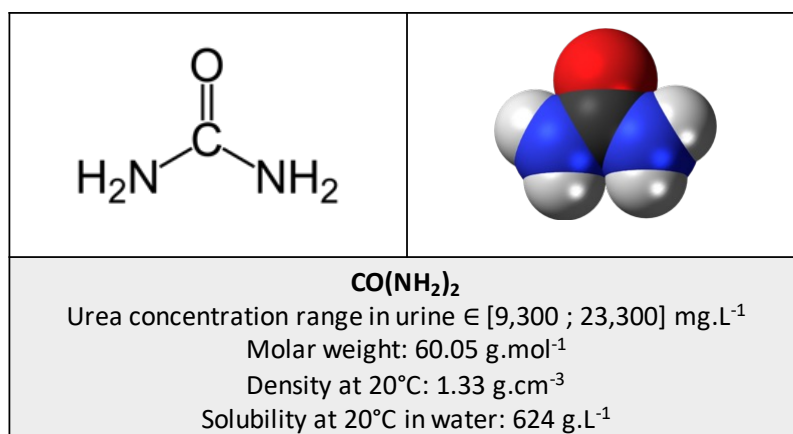


Fig. I.1 – Semi-developed formula, molecular modelling and some properties of urea.

He then observed that upon solvent evaporation, the cyanate was isomerized, leading to the formation of urea [32]. This “fortunate” synthesis became a key turning point in the history of chemistry because considered as the originator of organic chemistry.

Though being a major molecule at the origin of contemporary chemistry, urea remains necessary for all living beings as involved in many biological metabolisms (protein decomposition). Humans biologically produce urea, in the blood (at concentrations close to 5 mmol L⁻¹) but mainly in the urine at a level of 2.5% or an average concentration close to 330 mmol L⁻¹ (these concentrations vary depending on many physiological factors). One can estimate that human urine production is about 10 billion liters per day [33], which represents a huge nitrogen source.

Nowadays, urea is mainly used as fertilizer due to its high N-content (~ 46%) but also in food as feed additive for ruminants, in the synthesis of thermosetting plastics [34, 35] and as in motor vehicle exhaust pipes as a reducing agent of Nitrogen Oxides (NO_x). As industrial scale, urea is mostly produced either by CO₂ stripping (*i.e.*, the Stamicarbon process) or by ammonia stripping (*i.e.*, the Snam Progetti, Mitsui-Toatsu-Tokyo or Montedison/Technimont processes) [36]. However, significant waste amount are generated during the condensation stages involved in these processes, and then found in the environment, not only in the plant effluents but also in agriculture. To face this issue, various degradation processes have been developed, as described later.

I-1.2 Urine selective collection as an alternative to traditional sanitation systems

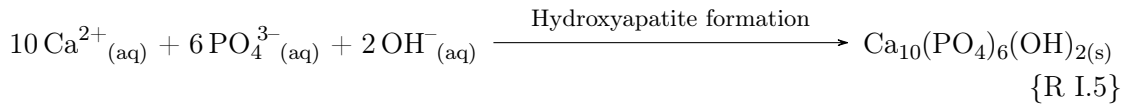
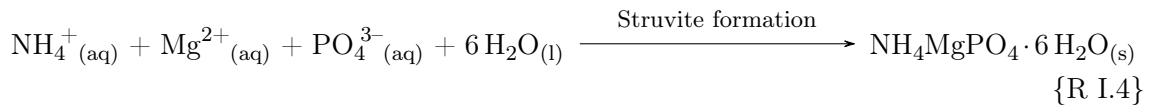
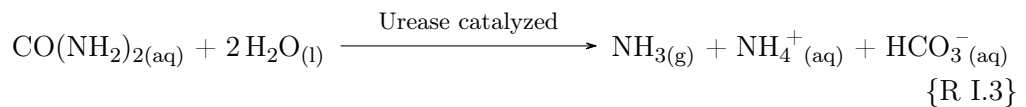
Urine should be collected separately from other forms contained in wastewater to prevent the dilution and/or contamination by pathogens [37]. This separation can be achieved by means of various toilet and urinal types, including waterless male urinals and urine-diverting toilets [38], even if some dilution may occur in toilets equipped with a flush [39]. Once separated, urine is treated to produce different fertilizers usable in agriculture, which are referred as Urine-Based Fertilizers (UBF) to identify their origin [40]. Over the past two decades, dozens of treatments have been developed, each of which has its own special objectives (nitrogen stabilization, volume reduction, nutrient oxidation, pharmaceutical residue and/or pathogen treatment), as outlined by Maurer et al. [39]. The separated urine is collected and then treated for various purposes. As described in Table I.1, urine diversion

has its benefits and cons, ranging from reduced water usage to potential health and hygiene issues [41].

Pros	Challenges
<p><i>Resource recovery:</i></p> <p>Urine contains valuable nutrients and minerals that can be recovered and used as fertilizer for crops;</p>	<p><i>Complexity:</i></p> <p>Implementation of urine diversion systems remains complex as requiring specialized knowledge and expertise;</p>
<p><i>Water savings:</i></p> <p>Urine separation allows reducing water amount for flushing toilets, but also, overall water usage;</p>	<p><i>Maintenance:</i></p> <p>Regular maintenance is required to ensure proper operation and sanitation (uncorking), assured by analytical monitoring;</p>
<p><i>Lower chemical usage:</i></p> <p>Conventional wastewater treatment requires chemicals (such as Cl) which amount can be reduced, and even eliminated when coupling urine diversion and alternative treatment ways;</p>	<p><i>Social acceptability:</i></p> <p>Urine diversion systems may be perceived by the general opinion as unhygienic, unsafe and/or unpleasant, thus limiting their wide adoption and acceptance; [42]</p>
	<p><i>Infrastructure:</i></p> <p>Significant infrastructure investments are required for implementing this technology [43].</p>
	<p><i>Matrix complexity:</i></p> <p>High variability and the presence of micro-pollutants must be taken into account. [43].</p>

Table I.1 – Pros and cons of urine diversion.

The process of urea hydrolysis in real situation (*i.e.*, pH, temperature, sewage pipe conditions) can cause a decline in the amount of organic nitrogen and a rise in Total Ammonia Nitrogen (TAN). The overall {R I.3} results in a pH increase from around 6-7 to around 9 [44]. This process also releases ammonia and bicarbonate and causes an increase in pH, leading to the precipitation of salts and a decrease in calcium, magnesium, and phosphate contents [45, 46]. The bacteria responsible for urea hydrolysis is called urease-positive bacteria: present in the urine collection systems, it can initiate this process within a few days [47].



This “natural” urea hydrolysis remains problematic for efficient urine valorisation, as a part of the ammonia is degassing during the collection and storage steps, and thus causes, nitrogen losses, unpleasant odors and environmental pollution [48]. Additionally, the spontaneous precipitation of calcium and magnesium salts (described in {R I.4-R I.5}) can clog collection system pipes (as shown in Figure I.2), thus inducing blockages, leaks and requiring frequent cleaning and maintenance [49, 50].



Fig. I.2 – Illustration of salt precipitations and subsequent deposits occurring inside collection systems (the pictures show a valve used in the “NoMix toilet” equipment from Roediger Vacuum GmbH) (extracted from [51]).

To prevent urea hydrolysis and subsequent precipitation, the microbial activity and urea-degrading enzyme should be inhibited. For that, some chemicals are added, such as acids, caustics, hydrogen peroxide or urease inhibitors [52, 53].

Based on the work of Eme et al. [54], Figure I.3 shows the typical composition of typical sewage (out of a family home). One can observe that organic matter coming from faecal matter and toilet paper represent an important contribution as well nutrients from urine. The nitrogen present in wastewater comes from urine (*i.e.*, 80%) and especially from urea, which is then converted by bacterial ureases into ammonia nitrogen. This nitrogen is concentrated in a limited amount of urine about 1.3L per person per day, while the total wastewater volume is about 41 L per person per day (*i.e.*, less than 5% of the total wastewater volume). This feature supports the implementation of selective collection systems on a larger scale, so as to treat concentrated nitrogen effluents instead of diluted ones.

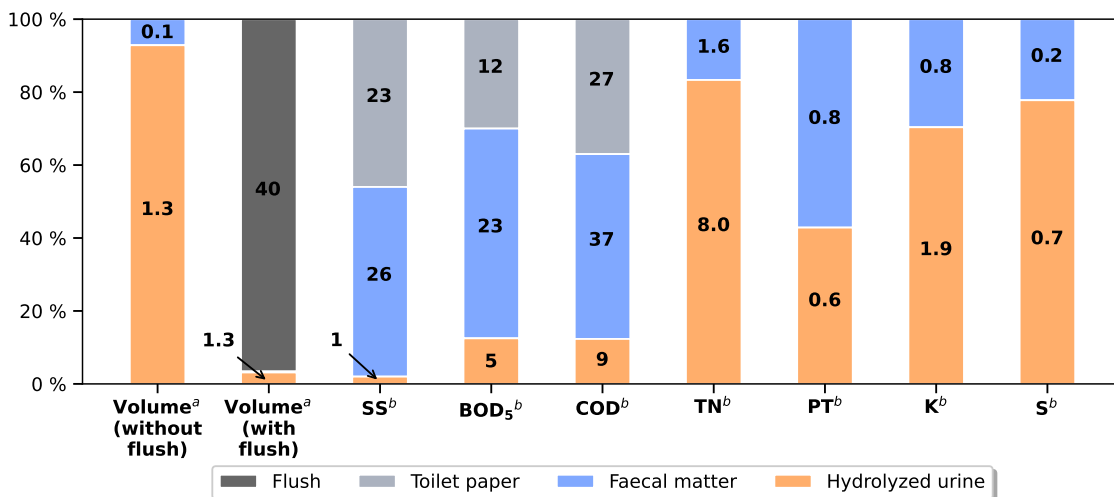


Fig. I.3 – Typical sewage composition in which the contribution with indexes ^a and ^b are expressed in L pers⁻¹ day⁻¹ and in g pers⁻¹ day⁻¹ respectively (extracted from [54]).

At last, one can mention that the use of source separation technologies and their optimization is increasingly studied in the state of the art as well as the coupling of selective collection with abatement processes [55], as illustrated in Figure I.4.

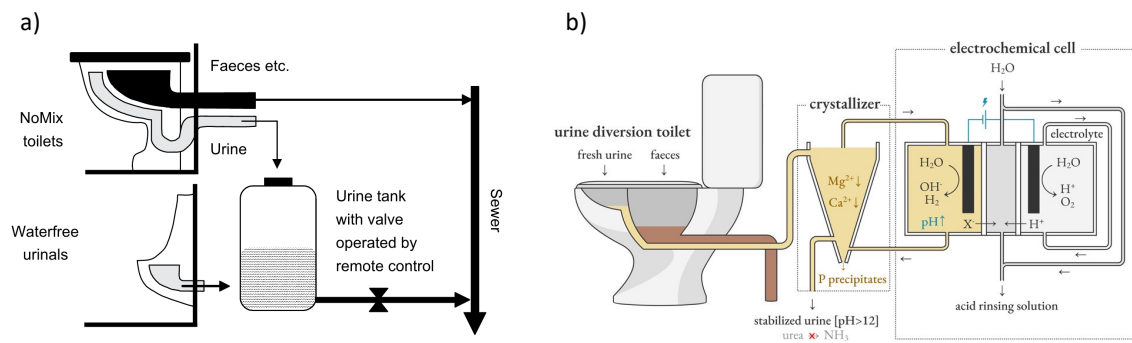


Fig. I.4 – a) Principle of urine source separation technology (“NoMix toilet” equipment from by Roediger Vacuum GmbH) with controlled release of urine to the sewer system (extracted from [38]). b) Schematic overview of a urine source separation set-up enabling nutrient recycling, facilitating wastewater management and conserving water (extracted from [56]).

I-1.3 Urine composition, hydrolysis and stabilization

Produced by the kidneys and stored in the bladder between urinations, urine has a composition, illustrated in Figure I.5, that depends on various factors, such as diet, lifestyle, and individual characteristics (*i.e.*, gender, age, weight, eating habits, etc.). When freshly excreted from the bladder, urine contains more than 98wt% of water. The dry substances present in urine are split into organic compounds ($\sim 60wt\%$) and inorganic compounds ($\sim 40wt\%$). Among organic compounds, urea represents more than 60wt% (with an average concentration of 0.33 mol L^{-1}), followed by ammonium salts ($\sim 20wt\%$), the rest including creatinine and other compounds (histidine, creatine, etc.). Inorganic salts are primarily sodium chlorides, then potassium chlorides, sulfates, carbonates, and phosphates. The composition of the urine is detailed in Appendix A based on the measurements made by D.F. Putnam from 1971 [57]. Proteins are present in trace amounts compared to their concentrations in blood plasma. In 2013, a study conducted by Bouatra et al. [58] identified more than 3,100 components in human urine. Among the comprehensive list of components, over 90 compounds were found to be consistently present in urine samples, irrespective of gender or collection time. Taking into account that each individual generates approximately between 1.5 and 2 L of urine daily and the global population stands at 7.7 billion people, the daily worldwide production of urine can be estimated between 11.6 and 15.4 billion liters. This translates to an annual global urine production ranging from 4.22 to 5.62 trillion liters. The criteria chosen for evaluating urine quality depend on the targeted use, namely medical analysis (through urinary ionograms), dietary purposes, agriculture applications or urine treatment for discharge or reuse.

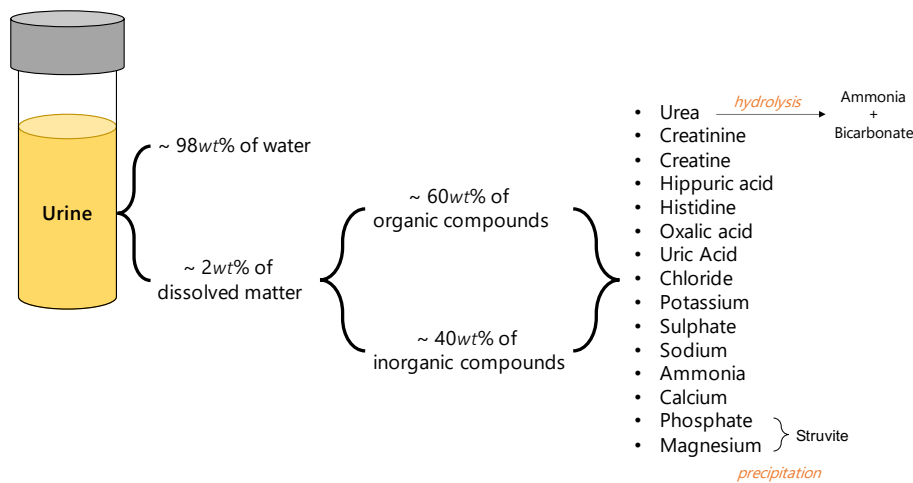


Fig. I.5 – Illustration of the human urine composition (adapted from [59]).

As discussed previously, the urea hydrolysis modifies the chemical composition of urine, depending whether urine has just been excreted or stored. To illustrate the importance of these variations, Table I.2 reports the urinary output of a person over 24 h. To stabilize urine, various methods have been used with their own advantages and disadvantages. One can cite : acidification [60, 61], alkalization [62, 63], electrochemistry [64, 65] or use of inhibitors or oxidants [66]. An inhibition of the urease contained in urine has been notably observed when the pH exceeds a value close to 10 and/or for temperatures higher than 80 °C [67, 68]. However, one should keep in mind that, the choice of the most appropriate stabilization method remains dependent on the urine collection method, on the targeted application and on the desired recovery form, because of the interdependent relationship between urine separation, stabilization, concentration and recycling [69].

Factor	Fresh urine	Hydrolyzed urine
pH	6.2 (2)	9.1 (1)
Suspended solids (SS) ^a	25 (1)	1 (2)
BOD ₅ ^a	6 (1)	5 (6)
COD ^a	16 (3)	9 (2)
TN ^a	11 (2)	8 (8)
including N _{NH₄}	4 (2)	8 (5)
including N _{urea}	7 (2)	- (-)
Total Phosphorus (TP) ^a	1.1 (2)	0.6 (8)
including P _{PO₄}	1.1 (2)	0.7 (2)
Potassium ^a	2.7 (2)	1.9 (8)
Sulfur ^a	1.3 (1)	1.9 (8)
including S _{SO₄}	1.2 (1)	0.6 (1)

^a given in g pers⁻¹ day⁻¹

Table I.2 – Illustration of the average daily loads of urine. Mean values are presented while the number of measures used for calculating these average values are presented in brackets. Data are extracted from [54].

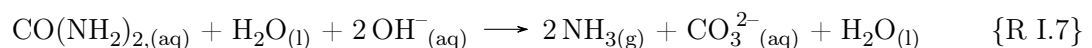
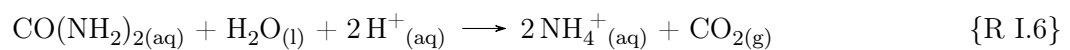
Udert et al. [47] have applied the Michaelis-Menten model, classically used for enzymatic reactions on a substrate, to describe the temporal decomposition of urea. They have found a hydrolysis kinetic constant equal to 960 g urea-N per day in the toilet separator pipes, and to 180 g urea-N per day in the storage tank filled with hydrolysed urine (0.1 m³). These differences have been explained by the fact that the bacteria in the pipes were in contact with fresh urine and thus developed the ability to secrete urease, while the elevated pH (~ 9) caused by the hydrolysed urine stored stop the bacterial development and hydrolysis. Another study by Liu et al. [70] have shown that, by mixing fresh and hydrolysed urine (20% hydrolysed and 80% fresh), the hydrolysis time could be reduced by more than 50% compared to fresh urine alone. They have also proven that temperatures above 20 °C favoured hydrolysis. These findings thus demonstrate that the urea hydrolysis kinetics is strongly influenced by the storage and collection conditions.

I-1.4 Conventional urea degradation processes

To face with this huge amount of urea produced each day, biological treatment in WWTPs is widely used. However to face to atmospheric pollution and/or high energy consumption, multiple degradation methods have emerged, such as hydrolysis, enzymatic decomposition, biological treatment, chemical oxidation, adsorption, catalytic decomposition and finally electro-oxidation. It should be noted that the capacity of existing set-ups based on these techniques are largely smaller than the biological treatment plants. Finally, these methods will be presented in the following section, while the urea EC treatment will be the object of a separate section (refer to section I-2).

I-1.4.a Chemical degradation

The products formed by urea chemical degradation (*i.e.*, hydrolysis) depend mainly on the pH. Thus, the reaction {R I.6} occurs with a strong acid solution, while in the presence of an alkaline base, the reaction {R I.7} preferentially takes place.



Therefore, hydrolysis will significantly modify the characteristics of urea-containing solutions: the pH of fresh urine solution (typically equal to 6.2) will after hydrolysis increase up to 9 [71] and its carbonate concentration from 0 to about 4 g_C L⁻¹. For fertilizer applications, once urea spread on the soil (UBF), the farmers must hydrolyze urea into ammonium during storage periode and then into nitrate so that the plants can absorb it, since NO₃⁻ is the main source of nitrogen for plant growth. Urea naturally hydrolyzes in the soil, as illustrated in Figure I.6, the reaction products alkalize the soil, and then change the chemical balance of dissolved ammonium by producing ammonia gas released in the atmosphere.

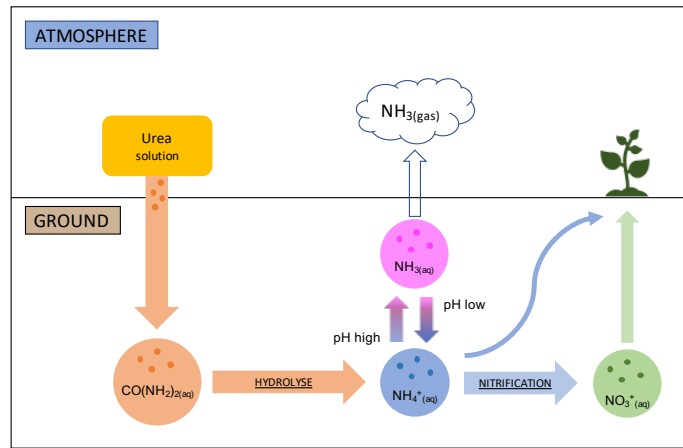
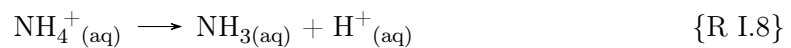


Fig. I.6 – Ammonia volatilisation and nitrogen loss when using urea as fertilizer (adapted from [72]).

In 2005, Behera et al. have estimated that 80.6% of ammonia emissions come from agriculture [73]. The use of urine as a fertilizer therefore presents an atmospheric pollution that needs to be taken into account. At the same time, this leads to soil and water acidification and eutrophication [74] due to the release of the protons according to the following mechanism {R I.8 - R I.9}:



To limit this atmospheric and terrestrial pollution, the use of other types of fertilizers is therefore to be preferred, such as ammonitrates (NH_4NO_3).

At last, it is interesting to report that urea hydrolysis is also used industrially. An aqueous urea solution is heated by a high-pressure steam stream, before separating the decomposition products [75] (urea stream heated for 30 min at 200 - 220 °C at a pressure of 2 - 3 MPa [76]). 94% of the nitrogen content is approximately reduced in the output stream. High temperatures remain the major drawback of this process (energy consumption) [10].

I-1.4.b Chemical enzymatic degradation (urease action)

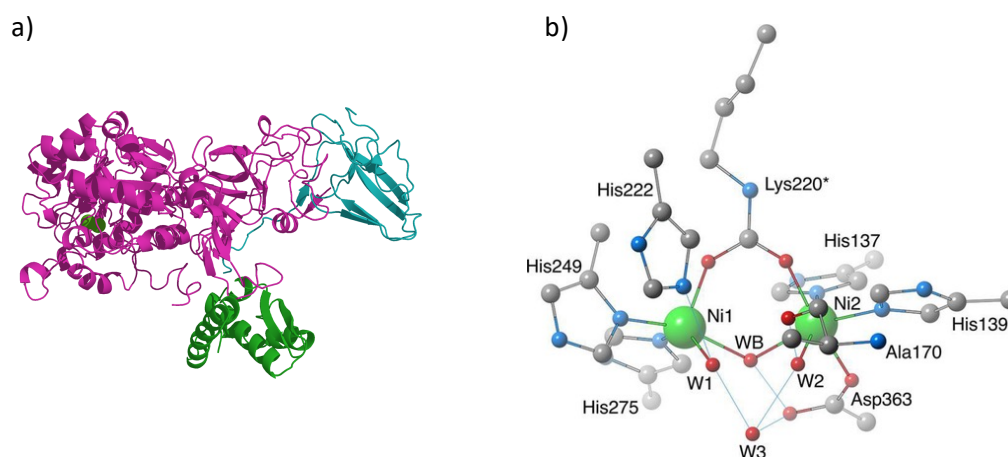
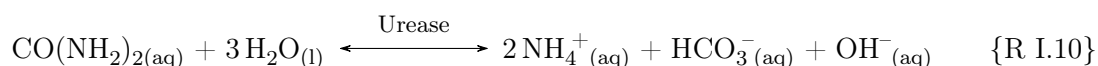


Fig. I.7 – a) Illustration of the ribbon diagram model of urease from *Klebsiella aerogenes* ($\alpha\beta\gamma$) subunits and two Ni^{+II} ions (green). [77] b) Representation of the crystal structure of *Sporosarcina pasteurii* urease active site which is a representative urease from soil bacterium. The Ni, C, N, and O atoms are shown in green, gray, blue and red, respectively. Hydrogen bonds are depicted by thin blue lines [78].

Hydrolysis can also be catalyzed by enzymes. Discovered in 1874, and characterized from the 1890s onwards, urease, illustrated in Figure I.7 is an enzyme produced by ureolytic bacteria. The urea decomposition is then accelerated thanks to the two nickel sites at the oxidation state +II. The related rate is estimated “ 10^{14} ” times faster [11] than that without urease. During the enzymatic reaction {R I.10}, urea is hydrolysed into ammonia and carbamic acid. As a result, this latter is then spontaneously decomposed into ammonia and carbonic acid. The carbonic acid ions and two molecules of ammonia are in equilibrium, that is affected by the pH of the solution.



The mechanisms related to the action of the nickel-containing active sites of urease onto the urea molecule are still under discussion in the literature. Whatever the explanations proposed over the years [79–81], a common feature can be highlighted: two active nickel sites linked by a hydroxide bridge (Figure I.7b, green atoms) are required and act as proton donor sites for hydrolyzing urea. The disagreement point inside the scientific community concerns the question of the urea sites affected by the urease: several groups [82, 83] have proposed an urease attack where one nickel atom is bonded to a carbon atom (from urea), while the other is combined with an oxygen atom. It will therefore be interesting to investigate whether urea degradation on nickel electrodes is similar to enzymatic degradation with its two nickel sites in urease.

I-1.4.c Comparison of urea degradation methods

Table I.3 summarises the conventional methods for urea degradation that have been previously presented. Three other methods are also reported in this table even if they are still rarely employed:

- chemical oxidation involves strong oxidizing compounds that must be chosen so as to convert urea into non-toxic products while being inexpensive and non-toxic, and reducing to non-ecotoxic forms. Currently, some studies have been carried out with ozone [12] or sodium chlorate [84] but there are still many obstacles to develop the process at large scale.
- adsorption consists of bringing a liquid or gaseous stream of urea into contact with a bed of sorbents, such as activated carbons [13], Faujasite type zeolites [14] and ion exchange resins [85] (R-SO₃-H⁺ type).
- catalytic decomposition (on Pt/SiO₂, Al₂O₃, TiO₂ catalysts) [15] remains an attractive method but is still too expensive to be used industrially

	General principle	Operating parameters	Decomposition products
<i>Hydrolysis</i>	High temperature and pressure	Residence time, Temperature (120 - 236 °C) Pressure (1.7 - 3.7 MPa)	NH ₃ , CO ₂
<i>Enzymatic decomposition</i>	Use of ureases	Enzyme immobilization pH (6.5-7.5)	NH ₃ , CO ₂
<i>Biologic degradation</i>	Use of a bacterial population	Nature of bacteria urea flow pH (7.0 - 9.0)	N ₂ , NO ₂ , NO _x , CO ₂
<i>Chemical oxidation</i>	Use of strong oxidants	Nature of oxidants pH	N ₂ , NO ₃ ⁻ , CO ₂
<i>Adsorption</i>	Use of sorbents	Sorbent properties Flow rate	/
<i>Catalytic degradation</i>	Use of catalysts	Nature of the catalyst Temperature (20 - 90 °C)	N ₂ , NO ₃ ⁻ , CO ₂ , NH ₃ , NO _x

Table I.3 – Comparison between the different non-EC methods of urea removal from aqueous solutions (adapted from [75]).

Various non-EC methods of urea removal are well-developed, with hydrolysis of urea being the most effective (around 94%). However, this process requires high temperature and pressure, limiting its industrial-scale application. Enzymatic decomposition of urea is also effective, but enzyme stability is a concern. Biological methods involve bacteria strains in biofilters but are not selective, and using oxidizing agents requires an affordable, non-toxic oxidant. Adsorbents are an evolving method, but optimization is still under investigation. Catalytic decomposition is expensive due to catalyst costs and requires optimization for maximum efficiency. The most promising industrial-scale method is hydrolysis of urea combined with enzymes. However, choosing the appropriate method depends on various factors, such as wastewater concentration, required purity, and process cost [75].

Following on from these techniques, the section I-2 focuses on EC methods for urea removal. This topic is of interest because EC treatment of urea-containing wastewater has potential applications in dialysis, WWTPs and Fuel Cells (FCs). The following section will

delve into this technique and provide a more complete understanding of the challenges and concerns associated with it.

I-2 ElectroChemical treatment of urine simultaneously to the H₂ production

UEO has emerged as a promising technology in the last decade, thanks to the compact system design, efficient treatment, and convenient operation [86, 87]. Under “strong” oxidation conditions, urea can be converted into mineralized products (N₂, CO₂) [88]. A notable feature of urine is its high solution conductivity, greater than 20 mS cm⁻¹, which minimizes energy losses in EC systems, resulting in improved EC performance. Various EC systems have been developed with different characteristics and purposes, but they still remain in its early development stages, thus requiring further exploration, in particular for large-scale applications.

The research dynamics and the future road-map on urea oxidation has been presented throughout Figure I.8, thus showing how, since the 1970s, the UEO development has gone through multiple stages in the mechanistic understanding. Noble catalysts (Pt, Ru, Ir, etc.) have been first used for de-ureation in life support systems, and the related investigations have been then centered on surface chemistry for urea adsorption models and direct oxidation behaviors. Later, urea oxidation have been considered by monitoring over time the products of electrolysis.

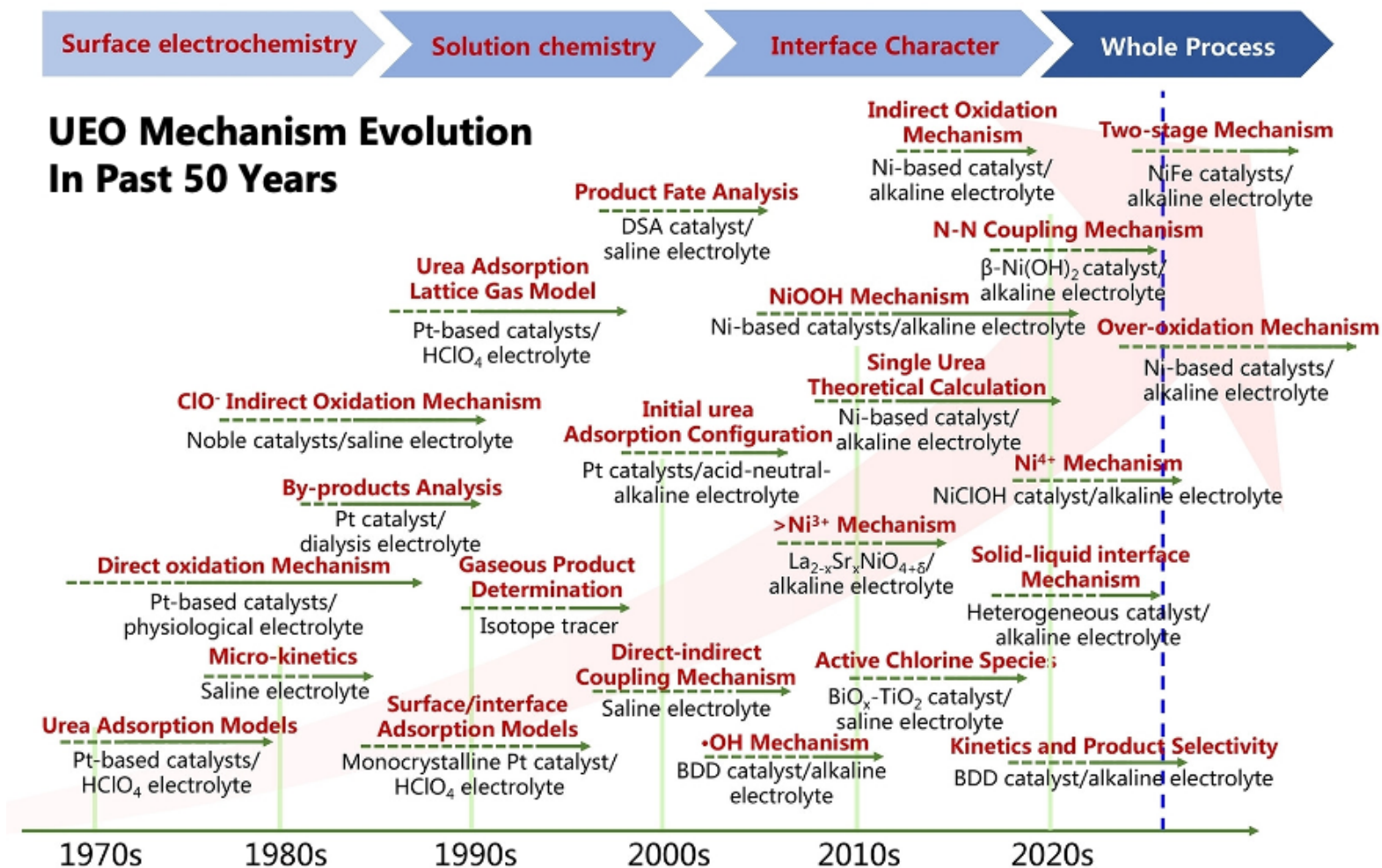


Fig. I.8 – Advancements in the mechanism of UEO over the last 50 years (extracted from [89]).

This chapter provides a summary of the current progresses in UEO made in various fields, such as human dialysis detoxification, chlorine-mediated nitrogen removal, and synergistic alkaline hydrogen production. The UEO mechanisms and the related key reaction intermediates will be discussed, from both experimental and computational results. By this way, a road-map of UEO over the past 50 years will be depicted, allowing to identify the challenges that still need to be addressed. At last, some development directions and promising prospects for future investigations will be proposed.

I-2.1 ElectroChemical oxidation in physiological buffer medium

For healthy adults, urea concentration in blood ranges between 1 and 10 mmol L⁻¹, with significant deviations due to health issues (*i.e.*, renal failure). The need to remove urea from blood dialysate fluid or to regenerate used adsorbent cartridges is at the origin of the works on anodic oxidation of urea.

Inspired from EC systems used for eliminating organic wastes in space and in manure lagoons [90], Sausse et al. [91] and Yao et al. [92] are reported as pionnering studies. The group of Sausse has explored the EC generation of ClO⁻ to directly degrade urea, while Yao et al. has examined the EC anodic oxidation of urea over a Pt disk electrode, in phosphate buffer (pH 7.4) solutions, with or without glucose. They have observed an oxidation peak at around 0.12 V *vs.* Ag/AgCl, and suggested that this peak could be attributed to urea degradation, which is chemically adsorbed on the electrode surface [93] leading to CO₂. These findings have thus demonstrated that urea could be directly oxidized on the Pt anode into CO₂, N₂, and H₂O as final products.

In Krebs-Ringer Phosphate Buffer (KRPB) solution, Keller et al. have investigated the effects of urea and glucose concentrations, pH and half-cell potential, on the shape of the anodic I=f(E) curves [93]. In a typical test, 108 mg of urea is removed from 300 mL of simulated dialysate within 100 h under a current density of 0.5 mA cm⁻². The solution's pH increases from 5 to 9 and then decreases to 6, possibly due to the water electrolysis. Only NH₄⁺ ions at concentrations close to 1 × 10⁻⁶ mol L⁻¹ has been detected as products. The response limit for urea is claimed to be 1 mg L⁻¹ over this Pt electrode.

Illustrated in Figure I.9, Patzer et al. have also proposed a mechanism for urea oxidation on Pt electrode, involving the following steps [94]:

- (i) potential-dependent urea adsorption on the electrode surface,
- (ii) formation of surface Pt-O or Pt-N bonds via one-electron transfer in the EC process,
- (iii) hydroxyl ion attack on the strained Carbon (C)-N bond, forming NH₃ and a carbonyl/carboxyl ion, similar to catalytic hydrolysis by urease,
- (iv) withdrawal of an electron from the carbonyl/carboxyl ion, breaking the other C-N bond through electrophilic attack by chemisorbed hydrogen atoms,
- (v) further EC oxidation of the formed ammonia into various nitrogenous products, with surface *CO/CO₂ species desorbing under strong potential, and regeneration of the electrode surface.

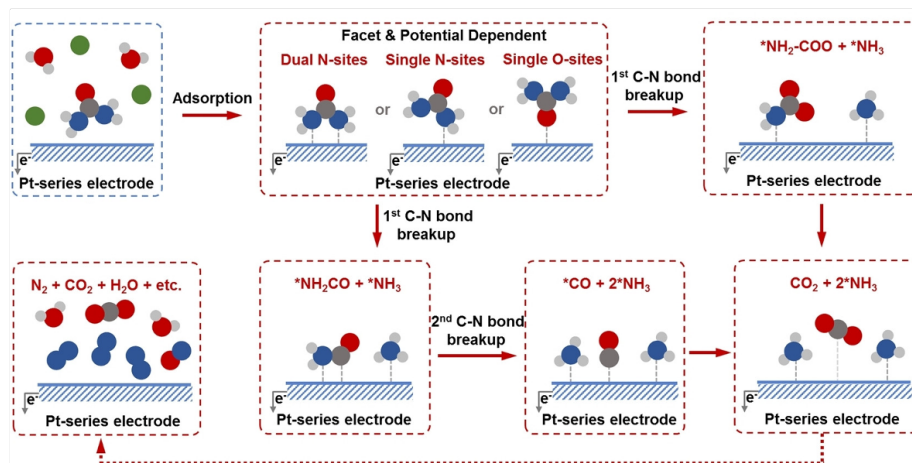


Fig. I.9 – Mechanism proposed by Patzer et al. [94] for urea electro-oxidation on a Pt-series electrode under physiological buffer conditions (adapted from [89]).

The urea oxidation constant has been determined to be $6.218 \times 10^{-7} \text{ g}_{\text{urea}} (\text{s mA})^{-1}$.

To achieve a urea removal rate of 2.08 mg s^{-1} within this chlorate-free (ClO^-) electrolyte system, Patzer et al. have estimated that a minimum current density of 0.25 A is required at an overpotential of 0.68 V vs. SHE [94]. Based on this knowledge, an electrolysis system with controlled potential and current has been developed. The total cell voltage has kept below 2 V to facilitate both urea elimination and electrode regeneration by avoiding chlorine generation. Removal rates of 0.75 , 0.9 , and $1.0 \text{ g (m}^2 \text{ h)}^{-1}$ have been obtained from human peritoneal dialysate [95], hemodialysate solution of a uremic diabetic dog, and urea KRPB solutions [96], respectively. Furthermore, a constant cell voltage was applied [97, 98]. The removal rate increases with the current and anode potential. However, when the potential of the working electrode exceeds 1.2 V , Cl^- is oxidized to hypochlorite. However, its impact on the direct oxidation rate is minimal in acidic solutions [99]. In addition to ammonia, trace amounts of other by-products, such as N_2O and NO_2 have been detected using Mass Spectroscopy (MS) [100]. The toxic effects of these by-products have discouraged the use of platinum electrolysis in dialysate regeneration for stringent clinical applications.

It is important to examine the adsorption and reactivity of urea at the molecular level. In a sulfate solution, the urea adsorption rate exceeds the oxidation rate at low potential ranges ($<1.2 \text{ V}$) [89]. However, at around 1.5 V , an significant acceleration of the oxidation is observed, in which the adsorbed $-\text{OH}$ play a key role, thus indicating the dominating influence of pH [101]. Using a radio-tracker method, urea has been found to exhibit anion-like adsorption behavior on the charged Pt electrode surface, akin to various anions (*e.g.*, HSO_4^- , H_2PO_4^- , Cl^-) and saturated aliphatic acids (*e.g.*, acetic, succinic, or Oxalic Acid (OA)).

The electrode surface properties and the supporting electrolyte nature seems to have a strong influence on urea adsorption [101]. For example, when replacing SO_4^{2-} electrolyte by KRPB phosphate buffer, urea chemisorption is inhibited due to a competition with phosphate anions. Urea can also adsorb on Pt, reducing the oxygen variation rate [102–104].

The crystallographic surface orientation of Pt has a strong impact on urea's voltammetry behavior, as shown by Gamboa-Aldeco et al. [103]. Langmuir and Virial isotherms have also been found to be applicable for describing urea adsorption behavior on copper, which are less hydrophobic than silver [105, 106]. Notably, the electrode hydrophilicity plays a crucial role in solid-liquid interface reactions, thus affecting urea adsorption and oxidation

during EC processes. This parameter should therefore be maximized to increase the amount of urea that can be oxidized at the electrode.

To overcome the use of costly Pt electrode, Yao et al. used using Ti and platinized Ti (Ti/Pt) [107]. The Pt loading per unit mass could decrease by 1,900 times. More recently, Fino et al. have examined the performance of urea (1 mol L⁻¹) oxidation over Pt, Ti-Ru oxide (DSA-Cl₂), Boron-Doped Diamond (BDD), and antimony-doped tin oxide (SnO₂-Sb₂O₅) electrodes in a perchlorate electrolyte with Na⁺ as the counter ion [108]. By Cyclic voltammetry (CV), they have showed that the presence of urea causes the decrease of the oxygen variation current on the Pt and Ti-Ru oxide surfaces, meaning that urea adsorption blocks the active sites for OER.

In contrast, a significant increase of the current density has been observed in proportion to the urea concentration on SnO₂-Sb₂O₅ and BDD surfaces, thus suggesting the potential role of OH^o via an indirect oxidation process. Different reaction pathways, product distributions, and kinetic behaviors have been observed across these electrodes. For instance, urea is degraded into N₂, NO₃⁻, and NH₄⁺ on BDD surfaces, with inorganic by-product fractions as high as 39% at a current density of 20 mA cm⁻². Both urea activation and by-product formation have been partially inhibited on SnO₂-Sb₂O₅ surfaces.

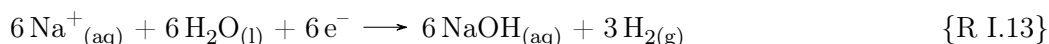
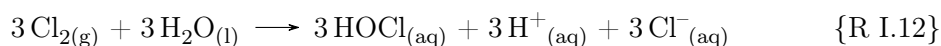
From this, one can conclude that the UEO in physiological buffers is significantly impacted by the choice of anode materials. To avoid corrosion issues in neutral or mildly acidic electrolytes, precious metals or inert electrodes are often preferred. In bodily fluids or KRPB buffer solutions, the surface-bound hydroxyl groups or trace amounts of hydroxyl radicals are suggested as the oxidative species involved in urea conversion. As a result, the development of effective electrocatalysts require to enhance the presence of hydroxyl groups or hydroxyl radicals on the surface, for instance through oxophilic components, potential range and/or facet orientations. Furthermore, the complex UEO mechanisms are directly influenced by various factors, including applied potential, pH, electrolyte composition, concentration and reaction temperature. For example, in acidic pH conditions, the primary degradation products are likely to be N₂ and CO₂, but small quantities of nitrogen oxides and ammonia species may still be present and the CO intermediate generated can sometimes poison Pt-based electrodes [89], significantly reducing their long-term stability. It should be noted that no mass balance has been carried out. Despite these extensive research efforts, it has to be said that this intricate system requires further investigations, particularly to understand the relationship between catalysts and UEO performances.

I-2.2 ElectroChemical oxidation in neutral/saline medium

Working with real dialysate or human urine necessitates to account for the presence of chloride ions (Cl⁻), because they act as precursors for active oxidative species and thus contribute to urea oxidation. As a result, the anodic reaction leads to the production of active chlorine (in acidic media) {R I.11} and hypochlorite (in neutral media) {R I.12}, collectively known as Reactive Chlorine Species (RCS). The Cl₂ or hypochlorite reductions may occur at the cathode, requiring to separate the anolyte and the catholyte so as to prevent energy waste. Depending on system operation, various products or intermediates have been observed, such as CO₂, N₂, H₂, CNO⁻, NO₃⁻, NO₂⁻, N₂O₂⁻, N₂O, NO₂, N₂H₄, chloramines,

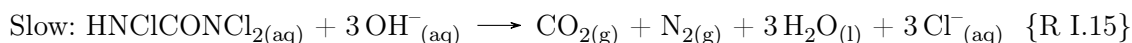
chlorinated urea, and urea cation radical $-\text{NH}_2\text{CONH}_2^{*+}$ [75]. It is therefore necessary to better understand how the formation of these products is influenced by operating parameters (electrode materials, potential, temperature, etc.). One can consider that this RCS-based system is in fact an enhanced and sophisticated version of the system from Bizot and Sausse [91], in which external NaOCl or HOCl is replaced by *in situ* electro-generated counterparts.

Fels et al. further studied the degradation of urea (500 mg L^{-1}) into dialysate matrices using a platinized Pt-black as both anode and cathode {R I.13} [109]. Urea degradation rates have been related to urea and hypochlorite concentrations, leading to a benchmark performance of $0.8 \text{ mg (h mm}_{\text{electrode}}^2)^{-1}$.



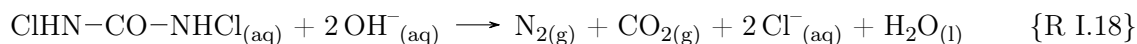
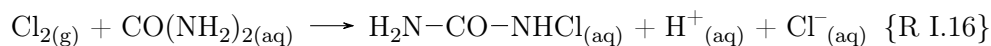
However, a cell potential of 6 V has been reached, and the current efficiency sharply declines, from over 90% to below 50%, for increasing potentials from 6 to 10 V. At the same time, the removal of unwanted by-products is found to be improved with increasing potential. During the urea degradation process, the pH dropped from 6.6 to 5.6 due to HOCl formation or CO_2 dissolution [109]. The impact of organic metabolism compounds, such as glucose or acetate, has been examined in a subsequent study. Without acetate, the solution significantly lost buffering capacity, resulting in a pH drop of 3-4 units. Additionally, by introducing oxygen, excess of ClO_x^- , including ClO^- , ClO_2^- , and ClO_3^- , have been detected and the ClO^- percentage decreases with increasing operational potential [110]. A treatment capacity of $40\text{-}80 \text{ mL min}^{-1}$ of urea solution could be successfully obtained by implementing a prototype device combined with a granulated charcoal adsorption cartridge [111].

A kinetic model involving RCS generation and urea oxidation has been proposed [112], guiding the development of an affordable, compact, and disposable oxidation cell. A test was carried out to put in contact NaOCl and urea. This last has revealed that the chlorination reaction {R I.14} occurs quickly, while the hydrolysis of chlorinated urea into CO_2 and N_2 {R I.15} is identified as the rate-limiting step [113].



Next, the focus has been shifted towards (*i*) the development of cost-effective electrodes and (*ii*) the understanding of the urea oxidation mechanism. Other platinum group metals, including Pd, Ru, and Ir, have been particularly investigated. Various techniques have been employed to create surface-enriched geometries of platinum metal on bulk electrodes, with the aim of enhancing the overall availability of the active precious metals. Additionally, some Pt-group free electrodes have been reported, such as carbon or Ti-based electrodes. For example, using the widely employed industrial electrode $\text{RuO}_2/\text{SnO}_2/\text{TiO}_2$ in 0.1 mol L^{-1} NaCl solution, urea chlorination has been found to occur in following multiple stages near the anode boundary layer, first by transforming urea into monochlorourea {R I.16} and subsequently into dichlorourea {R I.17}. At pH 7 or higher, the dichlorourea compound is decomposed into N_2 , CO_2 , and H_2 {R I.18}. Unlike the case with Pt electrodes, the initial step

of urea chlorination into monochlorourea is identified as the rate-determining step (RDS) under neutral to alkaline conditions [114].



Udert et al. have explored the performances of IrO₂ and Ti/IrO₂ electrodes for degrading urea and ammonia within artificial urine (freshly prepared) and synthetic stored urine matrices, respectively [71]. During the urea oxidation over IrO₂, NO₃⁻ (rather than NH₄⁺) has been identified as the primary by-product, suggesting that the indirect oxidation by bulk active chlorine would be the dominant pathway. Toxic by-products, such as chloramines, N₂H₄, and NO₂⁻, have been also detected in the IrO₂ electro-oxidation system [115].

Bimetallic Ti/Pt electrodes, with single or double-sided 3-10 μm Pt coatings on Ti foil, could be produced using EC and metallurgical techniques (explosion welding and combined with further rolling). Grinval'd et al. [116] have used an electrolyser with a capacity of 500 mL min⁻¹, and have examined the effect of current load, electrode working surface, mass transport factors, and presence of gas on the electrolysis performances and heat balance. Simka et al. [117, 118] have tested the effect of plate electrodes (containing Pt group metal including Ti/Pt, Ti/(Pt-Ir)_{70:30}, Ti/RuO₂, Ti/(RuO₂-TiO₂)_{40:60}, Ti/(RuO₂-TiO₂-IrO₂)_{20:60:20}, and Ti/(Ta₂O₅-IrO₂)_{70:30}) in terms of urea decomposition rate, current efficiency and electrode stability. From these two works, the electrode behavior could be classified into two categories:

- the presence or adsorption of urea obstructs the active site for chloride oxidation, resulting in a reduced chlorine release and current density for Ti/Pt, Ti/(Pt-Ir)_{70:30}, Ti/RuO₂, and Ti/(RuO₂-TiO₂-IrO₂)_{20:60:20};
- the current density increases with urea concentration, suggesting urea oxidation on Ti/(RuO₂-TiO₂)_{40:60} and Ti/(Ta₂O₅-IrO₂)_{70:30} surfaces.

A more economically interesting alternative is the use of BiO_x/TiO₂ sheets created using the chemical liquid deposition method. The surface titanol groups (*i.e.*, TiOH) offer active sites for hydroxyl radical formation, while BiO_x's redox transition (Bi^{+IV} → Bi^{+V}) acts as electron sinks [86].

Generally, one can describe the anodic oxidation of urea in a chloride-containing solution by three kinetically significant steps, occurring in the solution from the electrode surface, to the bulk:

- heterogeneous catalytic RCS generation on the inert electrode surface, with a contribution of water electro-activation into reactive oxygen species;
- initial RCS reactions with urea to produce monochlorourea or dichlorourea intermediates;
- subsequent oxidation reactions involving the initial reaction intermediates through free radical chain reactions to yield nitrogenous and/or Cl⁻ containing final products.

As a variety of electrode materials are widely employed, the active phases and sites exhibit high heterogeneity, resulting in significant variations in kinetics, reaction intermediates, and overall pathways, and thus in different product distributions and current efficiencies.

To briefly summarise, most of metallic catalysts are prone to corrosion in saline electrolytes and from protons released during urea oxidation (according to {R I.17-R I.18}). This considerably restricts the selection of available electrocatalysts to some options like novel metals, BDD and TiO₂-loaded electrodes. The results have demonstrated a strong correlation between current efficiency and applied anodic current density as well as urea concentration [75]. Nonetheless, the comprehensive evaluation of UEO cannot solely depend on current density, as several by-products also come into play. Among the studied electrodes for indirect oxidation of urea in a chlorate medium, plate Pt electrodes display unsatisfactory efficiency (with only 25% even at high current densities), whereas the Faradaic current efficiency of BDD and Ti/RuO₂ plate electrodes can reach nearly 100% [75]. Decreasing the formation of by-products such as chloramines and perchlorate [119], requires to drastically control certain operational parameters. For instance, the high urea content in fresh human urine can effectively suppress the over-generation of oxychlorides (approximately 1000 times lower than in hydrolyzed urine matrices [120]), thus indicating its suitability for point-source remediation prior to urine storage and hydrolysis. Furthermore, EC reactor configurations and operating parameters should affect the generation of these by-products [121, 122], but research works on this topic remain limited. Consequently, more intense research efforts should be paid on the development of effective electrocatalysts, on the optimization of reactor designs, and on the design of controllable system operations.

I-2.3 Oxidation in alkaline medium

I-2.3.a Mechanisms

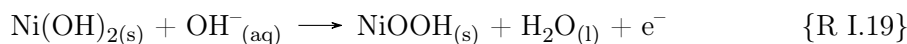
In recent years, the growing demand for renewable, sustainable, and eco-friendly energy, leads to recognize urea as an important N-based fuel molecule. Compared in Table I.4 to other molecules, such as ammonia or hydrazine (N₂H₄), urea offers competitive advantages: high solubility in aqueous media, low volatility, non-toxicity, excellent energy density, substantial hydrogen content, and a relatively low potential (theoretically -0.084 V *vs.* SHE, for {R .1}). Thus, the generation of renewable H₂ by urea electrolysis appears both as an alternative to water splitting and an attractive method for source-based water pollution removal.

N-based fuel molecules	Solubility (g _{compound} g _{water} ⁻¹ at 25 °C)	Vapor pressure (mm Hg at 25 °C)	Energy density (MJ kg ⁻¹)	Hydrogen content (wt%)
CO(NH ₂) ₂	55	23	12.7	6.7
NH ₃	32	7395	25.2	17.7
N ₂ H ₄	282	14	19.3	12.5 (7.9 in case of hydrous hydrazine)

Table I.4 – Summary table of nitrogen-based fuel molecules properties.

In alkaline conditions (pH>14), the Hydrogen Evolution Reaction (HER) is more likely to occur. Nickel, a non-precious metal, is considered as an electrocatalyst for alkaline

electrolyser anodes, because its corrosion resistance [123]. Indeed, native nickel oxidizes, and Ni(OH)₂ covers entirely the metal. Ni(OH)₂ can be electrochemically oxidized to generate NiOOH, according to {R I.19} [124], also a solid remaining on the metallic surface, which appears as a “strong” oxidizer.



Interestingly, the UEO on a nickel electrode takes place at 0.55 V (*vs.* Hg/HgO), nearly 0.1 V lower than that on Pt-Ir, Pt, or Rh electrodes. High-valent Ni^{+III} is suspected to be responsible for urea indirect oxidation [20]. *In situ* spectroscopy, cyclic voltammetry, potential oscillations and theoretical calculations have been used to try to elucidate the mechanism of urea oxidation on nickel-based catalysts [125–128].

Significant structural reconstructions of Ni-catalysts occur during the UEO in alkaline media, suggesting an electrochemical-chemical oxidation (E-C) mechanism based on the NiOOH/Ni(OH)₂ redox pair. This mechanism involves both direct chemical oxidation of urea over NiOOH and indirect oxidation through NiOOH, with EC catalyst regeneration. As illustrated in Figure I.10, the UEO proceeds via two routes once the urea molecules are adsorbed on Ni^{+III} active sites [129]:

- Route 1 involves the amine deprotonation by adsorbed OH[−] until the complete formation of [M[•]CO(N₂)]_{ads}. Further OH[−] attack induces N-N coupling, resulting in N₂ release and the generation of carbonate species on the surface.
- Route 2 is similar to Route 1 for the initial deprotonation step until the [M[•]CO(NH₂·NH)]_{ads} is formed. Then, an intramolecular rearrangement occurs between the H-N-H amine and N-H groups, followed by a series of deprotonations by adsorbed OH[−] to form [M[•]CO(N₂)]_{ads}. As in Route 1, further OH[−] attack produces N₂ and leaves carbonate species on the surface.

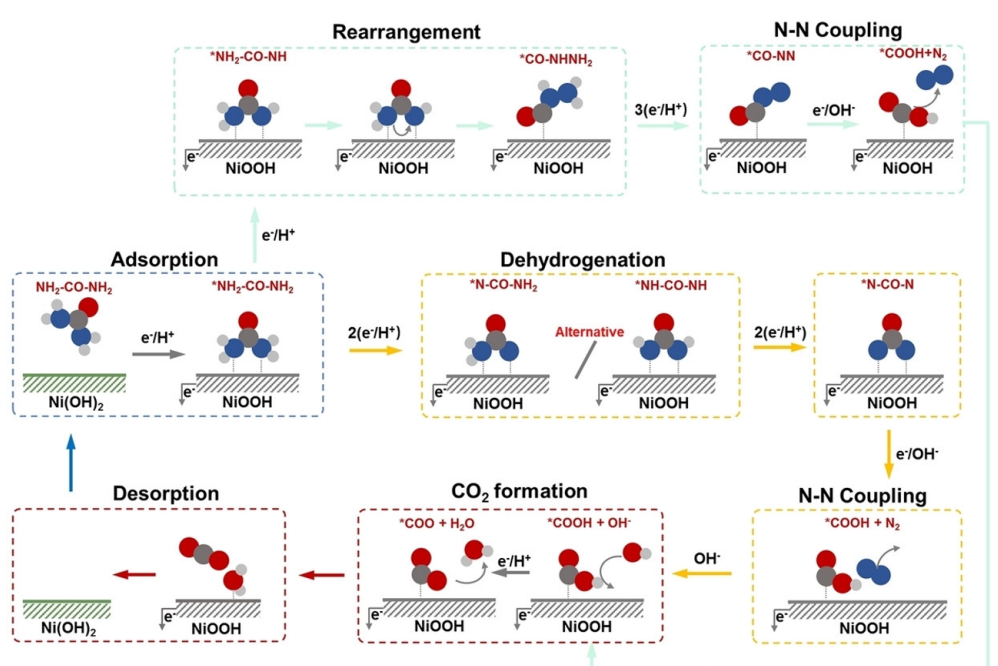


Fig. I.10 – Schematic representation of UEO in alkaline conditions (extracted from [89]).

In both routes, CO_2 desorption from the electrode surface is widely considered as the RDS for regenerating the electrode surface to its original state. Over time, the design of Ni-based electrocatalysts for Urea Oxidation Reaction (UOR) has been guided by the proposed mechanisms [88, 130, 131] and with the objective to enhance their activities, namely to increase both the number of active sites and the intrinsic activity of each site. By nanostructuring, a catalyst can provide much more exposed active sites. While the enhancement of the intrinsic UOR activity of each site can be achieved by facilitating the $-\text{COO}_{\text{ads}}$ desorption step. The acceleration of the generation of active species, configuring electrocatalysts with high oxidation states, constructing synergistic active sites, and/or forming heterojunction catalysts can be key parameters to optimize the reactional efficiency [130, 132]. For that, catalysts are mainly modified through element doping, material compositing, and/or catalyst loading.

Another important factor is the hydrophilicity of the catalytic material as this parameter acts on different phenomena:

- the adsorption rate constants are related to the electrode hydrophilicity [133];
- increased anode hydrophilicity leads to enhance the activity of the slow OER; [134, 135], as some key oxygen intermediates can be shared with the UOR system, suggesting a similar positive effect on the UOR system;
- higher hydrophilicities can strengthen the affinity between electrolyte and electrode, and enhance gas bubble dissipation during the UOR process, thus maintaining efficient EC interface charge transfer at high current activity [136];
- enhancing the hydrophilicity of a catalyst can increase the Proton-Coupled Electron Transfer (PCET) process, without suffering from transfer decay due to the coverage of gaseous products [137];
- the hydrophobicity of anodic oxides can be reduced due to electrowetting and OH^- accumulation at electrode surfaces [138], leading to more attached OH^- and enhanced UOR performance.

It is important to note that multiple regulation strategies are often used simultaneously to improve UOR performance, meaning that changing one factor may be accompanied by others.

Owing to the Ni- CO_2 or Ni-CO bounds, Ni-based catalysts may exhibit rapid deactivation and low stability, which constitutes a significant obstacle for practical use. However, by employing multi-metal catalysts, surface blockage can be reduced and current density enhanced. By electrodeposing a secondary metal, such as Pt, Pt-Ir, Rh, and Ru onto nickel foil, the selectivity towards OH^- , CO^- , and NH-species adsorption can be effectively adjusted. Among these, Ru-Ni have demonstrated the best performance, with a current density promotion of about 200 times [139].

Traditionally, the sustainability of UOR relies solely on the generation of harmless N_2 [20, 128]. Unfortunately, the literature does not mention the identification and the quantification of N-products in gaseous and liquid phases; generally, no mass balances are established.

In situ differential electrochemical mass spectrometry have allowed to monitor and compare, the mass-to-charge ratio of the generated N_2 product during UEO by incorporating

CO(¹⁴NH₂)₂ and CO(¹⁵NH₂)₂ at a 1:1 molar ratio into the KOH electrolyte. Interestingly, nearly equal proportions of ¹⁴N¹⁴N (~ 49%) and ¹⁵N¹⁵N (~ 49%), and only a trace amount of ¹⁴N¹⁵N (~ 2%) have been observed, thus indicating, that the intramolecular N-N bond coupling mechanism is the primary pathway for N₂ formation during the UOR process (as shown in Figure I.12-a) [140].

I-2.3.b Kinetics of the UEO

Concerning the UEO kinetics, only two studies have been reported in the literature:

- (i) Singh and Schechter [141] have analyzed the rate constant of the UOR in alkaline environments on Ni(OH)₂/Ni and β-Ni(OH)₂ surfaces. The reaction has been found to be slower on Ni(OH)₂/Ni compared to β-Ni(OH)₂. An indirect mechanism for the UOR has been then suggested.

The influence of KOH and urea concentrations on the UOR rate has been studied on these surfaces, enabling the researchers to determine some key reaction parameters. When the UOR occurs on β-Ni(OH)₂ at 1.43 V *vs.* Reversible Hydrogen Electrode (RHE), the reaction orders for KOH and urea have been identified as 1.22 and 0.26, respectively.

- (ii) Vedharathinam and Botte [142] have obtained reaction orders for KOH and urea equal to 2 and 0.3, respectively, at 0.440-0.455 V *vs.* Hg/HgO on a Ni electrode in an alkaline electrolyte by performing Linear Sweep Voltammetry (LSV) experiments under various OH⁻ or urea concentration in urea/KOH solutions.

The discrepancy in terms of reaction orders between these two studies could be ascribed to the different synthetic methods employed to create the Ni electrodes.

I-2.3.c By-product identification and formation routes

In 2021, Li et al. [143] have monitored the nitrogen content during UOR with considering nickel-based catalysts (*i.e.*, activated porous nickel foam) and by coupling chromatographic methods. Notably, these authors have observed the dominant nitrite formation (Faradic Efficiency (FE) of 80%) instead of N₂ (FE < 20%) as highlighted in Figure I.11. This product, often considered as a potential contaminant, is also prevalent on other typical nickel-based electrodes (NiMoO₄-Nickel Foam (NF), NiO-NF, Ni-C, Ac-NF) [115, 121]. The over-oxidation of urea on nickel-based electrodes, has been significantly underestimated for a long time. Furthermore, the authors have shown how the N-products distribution is dependent on the EC reaction parameters, such as electrolysis potentials, electrolysis time and electrolyte concentration.

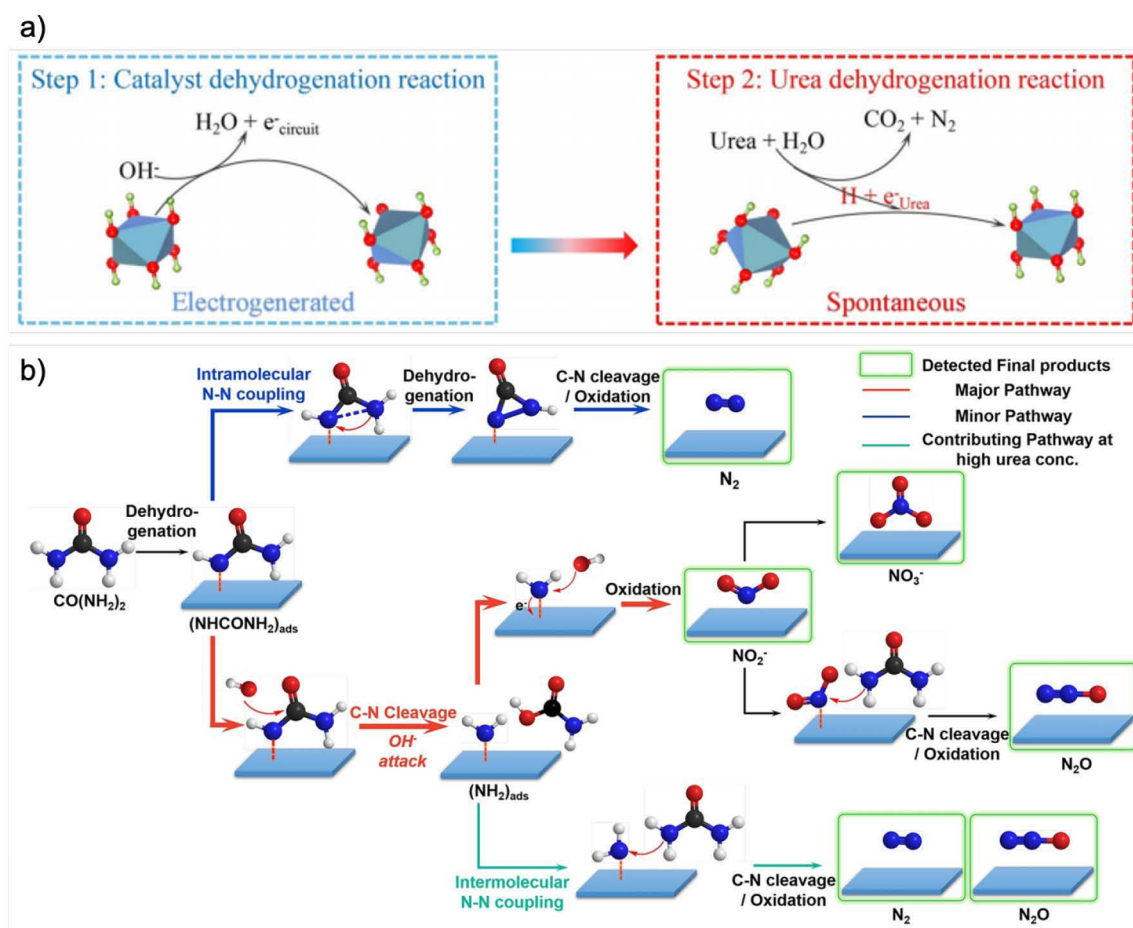


Fig. I.12 – a) UEO mechanism on the β -Ni(OH)₂ electrode proposed by Chen et al. [140] and b) schematic illustration of the UOR pathways proposed by Li et al. [143].

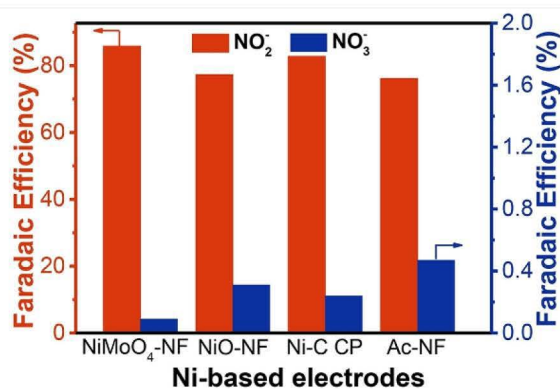


Fig. I.11 – The NO₂⁻ and NO₃⁻ FE during UOR using different Ni-based electrodes during electrolyses in divided EC cell (adapted from [143]).

Interestingly, using N-isotope labeling and urea analogues, Li et al. [143] have confirmed the intramolecular N-N coupling for urea conversion into N₂, as shown by Chen et al. [140]. Additionally, a trace of N₂O has been first detected through a selectively catalytic reduction-like pathway. Based on these findings, they have proposed a new pathway network and refined the mechanisms of UOR on Ni-based electrodes, as illustrated in Figure I.12-b. As a first step, urea adsorbs onto the active NiOOH surface, and then undergoes dehydrogenation at one -NH₂ site. Subsequently, two primary pathways emerge: intramolecular N-N coupling leading to N₂ formation, and C-N bond cleavage producing surface-bound -NH₂ species,

which further oxidizes into primary NO₂⁻ products. Theoretical calculations have supported these mechanisms and revealed that the OH⁻ assisted C-N direct cleavage pathway has a favorable overall barrier (0.953 eV), and that this barrier is sufficient to dominate but not to completely suppress the N-N coupling pathway (1.184 eV). This induces significant over-oxidation during UOR. As a result, Li et al. [140] have suggested a surface modification strategy of the anode to enhance N₂ production. This study is the pioneer to identify the over-oxidation issue in alkaline UOR, to significantly improve the understanding of the related mechanisms and to point out the need to analyse product and to verify mass balances.

Recently, Tatarchuk et al. (2022) have carried out both I=f(E) curves and the monitoring of by-products during electrolysis. LSVs have been recorded at Ni(OH)₂/NF in a KOH concentration of 1 mol L⁻¹, with and without urea (Figure I.13-a) in order to determine appropriate potentials for potentiostatic electrolysis and product analysis. Two waves have been observed in the absence of urea:

- (i) a peak at 1.4-1.6 V *vs.* RHE, attributed to the Ni^{+II}→Ni^{+III} transition (Ni(OH)₂ to NiOOH);
- (ii) and a second signal at >1.6 V *vs.* RHE, related to OER.

When introducing urea at 0.33 mol L⁻¹, the current of the Ni^{+II} oxidation is increasing, in agreement with the previous works [87, 88, 130, 144, 145]. Short-duration electrolyses at different anodic potentials (1.4-2.3 V) have been carried out to assess the effect of this applied potential on the product distribution (Figure I.13-b). The ionized products of the UOR have been analyzed by Ion chromatography (IC), while gas products by Gas Chromatography (GC). The main UOR products identified by Tatarchuk et al. include nitrites, N₂, and nitrates (Figure I.13-b):

- Nitrites prevail whatever the studied potentials, with an FE of up to 85% at 1.7 V, while N₂ selectivity remains generally modest (14-30%).
- The maximum FE of N₂ (30% at 1.4 V) appears for the lowest operating potential and slightly decreases with the increasing potential (to ~14% at 2.3 V).
- The formation of nitrates and oxygen is observed at potentials higher than 1.7 V. The related FE noticeably grow with increasing potentials, peaking at 2.3 V (17% for nitrate and 15% for O₂).

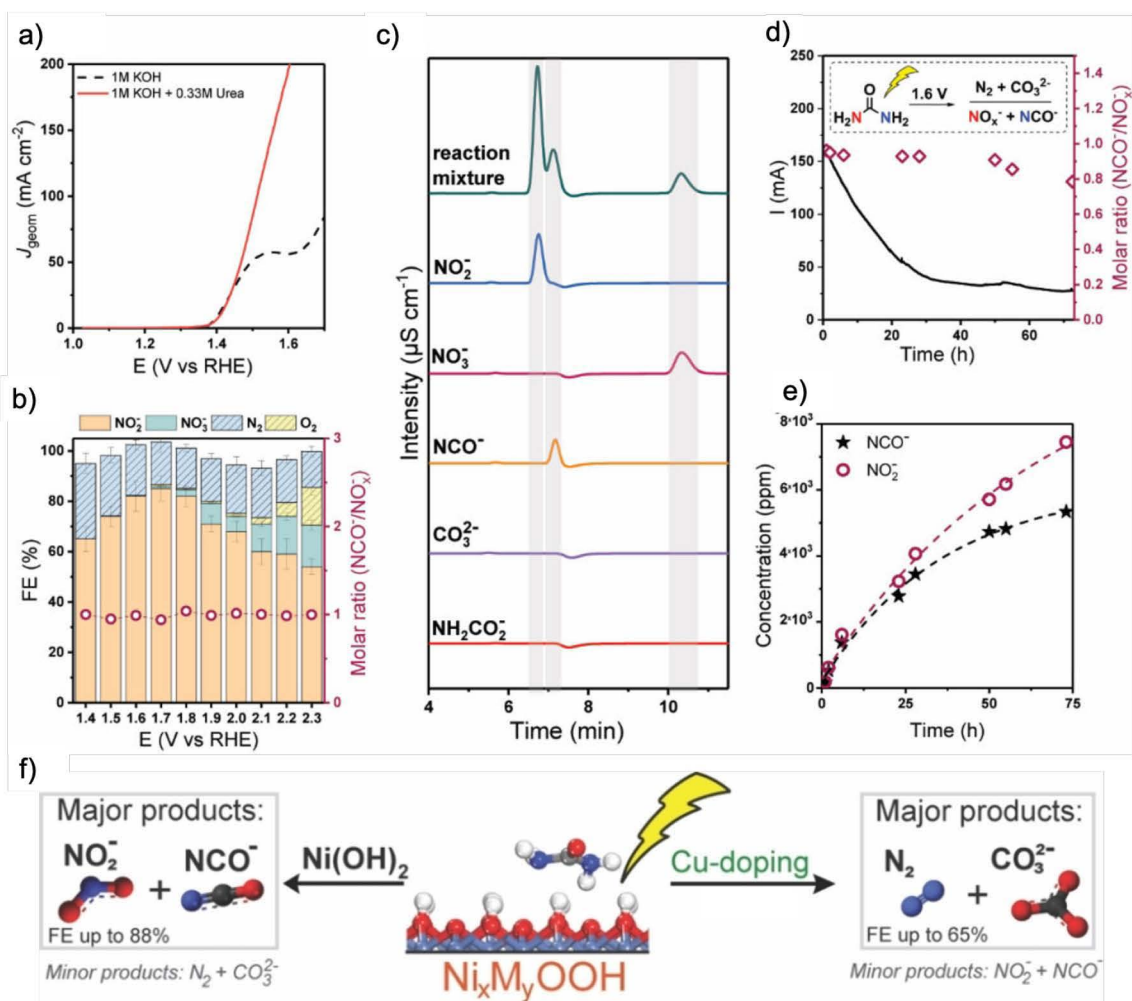


Fig. I.13 – Summary of the main results obtained by Tatarchuk et al. [146]. a) LSV curves have been obtained at a 5 mV s^{-1} scan rate using the $\text{Ni}(\text{OH})_2/\text{NF}$ anode in a 1 mol L^{-1} KOH solution, both with 0.33 mol L^{-1} urea (solid line) and without urea (dashed line); b) The FE of primary products from a 1-hour urea electrolysis and the $[\text{OCN}^- : \text{NO}_x^-]$ ($x=2, 3$) molar ratio have been analyzed as a function of applied potential; c) IC traces have been compared between the UOR reaction mixture and various standard anion solutions; d) a chrono-amperometry curve has been plotted for the electrolysis of 0.33 mol L^{-1} urea in 1 mol L^{-1} KOH at 1.6 V , along with the $[\text{OCN}^- : \text{NO}_x^-]$ ($x=2, 3$) molar ratio; e) the cyanate and nitrite concentrations in the electrolyte solution have been monitored over time during the electrolysis of 0.33 mol L^{-1} urea in 1 mol L^{-1} KOH at 1.6 V and f) a mechanistic analysis suggests that the binding site availability for both N atoms in urea is crucial for reaction selectivity (adapted from [146]).

Tatarchuk et al. [146] have found that the overall FE of the formed products deviates from 100% under the tested potentials (meaning that minor sub-reactions could occur). To identify the minor products during the urea electrolysis, in-line GC-MS analyses have been conducted at 1.5 V , 1.7 V , and 1.9 V vs. RHE . In addition to N_2 and O_2 , traces of N_2O and CO have been systematically detected, with FE of up to 1% and 0.3%, respectively. Furthermore, an additional peak has been observed by IC, suggesting that UOR produces another anionic product in significant amounts (Figure I.13-c). To determine this unidentified anion, the related IC retention time has been compared to carbon-containing anions that may possibly arise from urea, specifically carbamate and cyanate (OCN^-). At last, the retention time of the unknown anion has been found to be that of cyanate.

Note that the oxidation state of all the atoms contained in cyanate ions is identical to those in urea, thus implying that cyanate appears via acid/base equilibrium. Nevertheless

the polarization of the electrode is necessary to form cyanate. Note that IC analysis of an urea solution in KOH at 1 mol L⁻¹ have been carried out over three days: any cyanates have been detected. To identify the UOR pathway responsible for cyanate formation, the molar ratio of cyanate and other UOR products has been compared. Interestingly, whatever the potentials, the cyanate concentration generated during electrolysis at all potentials are nearly equal to the total concentration of NO_x⁻ products. This near-stoichiometric ratio thus suggests a mechanistic association between cyanate formation and the NO_x⁻ pathway, while cyanate does not form through the N₂ pathway.

Additionally, electrolysis of urea (0.33 mol L⁻¹) in KOH solution (1 mol L⁻¹) at 1.6 V *vs.* RHE has been performed to study how the concentrations of nitrite and cyanate evolve during electrolysis (Figure I.13-d,e). The current decreases almost linearly for the first 20 h of electrolysis, corresponding to a transfer of roughly 2 mol of electrons per mol of urea. After 20 h, the current exhibits an exponential decay before reaching a plateau (30 mA) when 3.2 mol of electrons per mol of urea have been transferred (around 62 h). The variation of the reaction medium with electrolysis time has been monitored using IC (Figure I.13-e). In the initial hours of electrolysis, the molar ratio of cyanate to nitrite is close to 1 : 1, in agreement with the results of the short-term electrolysis previously mentioned. However, the OCN : NO₂⁻ ratio declines with urea depletion, reaching 0.8 : 1 at the end of the electrolysis, indicating that cyanate can undergo EC oxidation as well. The final FE of nitrite has been found equal to 88%, with nitrite and cyanate concentrations at 0.16 mol L⁻¹ and 0.13 mol L⁻¹, respectively.

These findings show that N₂ and the urea overoxidation (when N-oxidation state is higher than 0) products are formed following two distinct reaction pathways, the latter involving the generation of cyanate as a by-product in a stoichiometric proportion to NO_x⁻. Conversely, Li et al. have identified carbamate (NH₂CO₂⁻) as UOR by-product [143]. In order to understand the involvement of these compounds in the UOR process, a comparison of the EC behavior of urea, carbamate, and cyanate with the same N-concentration at the Ni(OH)₂/NF anode has been conducted. Urea has been found to have the highest activity, followed by carbamate and cyanate with current density ratios of roughly 3.7 : 2.2 : 1, respectively. Potentiostatic electrolyses of either urea or cyanate solutions, performed at 1.6 V, have revealed very similar results for UOR and cyanate oxidation, with an FE of nitrite at 80%. This finding, together with the slow kinetics of cyanate oxidation, tends to support the hypothesis of a gradual cyanate depletion during extended UOR. The EC oxidation of carbamate leads to the formation of nitrite with an FE of 98%, with neither cyanate nor N₂ being produced, suggesting that carbamate cannot serve as an intermediate for either the N₂ pathway or the urea overoxidation pathway [146].

I-2.3.d Ongoing works and remaining challenges

Two main lines of research remain active in the community:

- (i) the search for a better understanding of reaction mechanisms to avoid the formation of unwanted by-products;
- (ii) the optimization of the EC process in order to reduce the energy consumption of the UEO process.

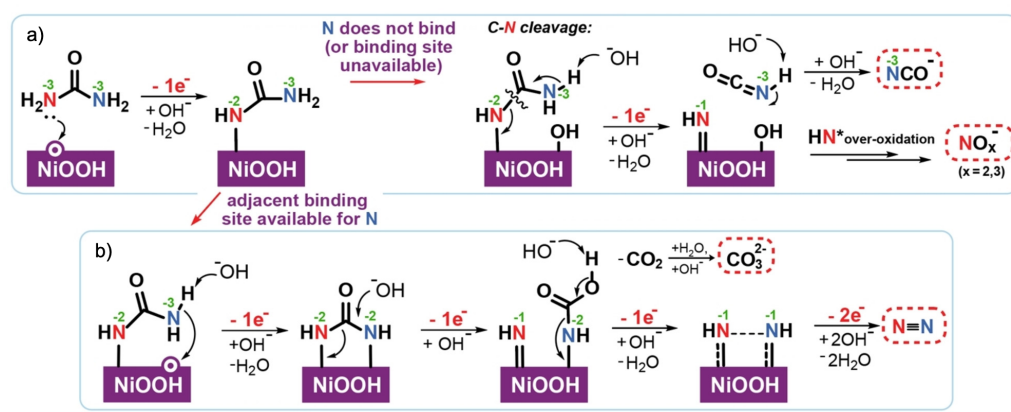


Fig. I.14 – Schematic illustration of the proposed pathways for UOR to a) N₂ & CO₃²⁻ and to b) NO_x⁻ & OCN⁻ on the NiOOH surface (the green numbers above N atoms correspond to the nitrogen oxidation state) (extracted from [146]).

By gathering the outcomes of the Tatarchuk et al. [146], the possible reaction mechanisms have been summarised in Figure I.14; they describe the NO_x⁻, OCN⁻, N₂ and CO₂ pathways (with CO₂ converting into CO₃²⁻ in basic media). The formation of NO_x⁻ & OCN⁻ requires only one N atom. The breaking of the bond between this second nitrogen atom and the carbon atom in the urea molecule gives rise to OCN⁻ formation and its release into the solution bulk; the *NH species undergo additional oxidations (Figure I.14-a). One should point out that these oxidation steps are analogous to the later stages of ammonia oxidation to nitrite and nitrate, which have been thoroughly detailed in recent studies [147, 148]. N₂ could also form through the latter pathway, although overoxidation pathways are more energetically favorable [146–148].

In summary, because its low oxidation potential (−0.46 V *vs.* Standard Hydrogen Electrode (SHE)), urea could be assumed as an interesting fuel for energy-efficient hydrogen production systems. It has been very recently shown that multiple electron and proton transfers occur and various by-products are formed (Figure I.8). Currently, research works in alkaline electrolytes focus on the enhancement of UEO (activity and stability), expecting to improve selectivity and to get a better understanding of the mechanism. More attention should be paid to the establishment of mass balance of the intermediates and the by-products and to the study of the products variation in UOR systems.

Additionally, one should note that few studies have investigated EC parameters under alkaline electrolytes (such as interference ions and organics) while they are commonly present in human urine or other urea-rich wastewater. The impact of reaction intermediates types, concentrations, and ratios on UEO activity, stability, and selectivity must be examined more closely for large-scale process development [89].

The UOR-integrated system has been the most extensively studied for hydrogen production [87, 88, 130].

In 2009, the work of Botte et al. have pioneered to develop UEO for pure hydrogen generation using affordable nickel catalysts [20]. They have estimated the voltages for urea and water electrolysis to be 1.4 V and 2.0 V, respectively, under 20 mA. Thus, urea electrolysis required 30% less energy (37.5 Wh g⁻¹) and produced 36% cheaper hydrogen

($2.63 \$ \text{kg}_{\text{H}_2}^{-1}$) compared to water electrolysis. This pioneered research has boosted the interest for energy-efficient hydrogen production through urea electro-oxidation with Ni electrodes in alkaline electrolysis, and subsequently, the integrated UOR||HER system has gained considerable attention.

In parallel, EC studies that transform greenhouse gases (such as CO₂) into valuable products have experienced growing advancements in recent years [149–152]. To reduce high energy electrolyser consumption, the cathodic CO₂ Reduction Reaction (CO₂RR) can be combined with a more efficient alternative Anode Oxidation Reaction (AOR), like UOR (Figure I.15). By this way, the overall cell potential and Gibbs free energy of the overall reaction combining CO₂RR with UOR can be theoretically decreased by approximately 0.9 ~ 1.2 V and 175 ~ 226 kJ mol⁻¹, respectively, when compared to the slow OER counterpart in the electrolyser [145]. Experimental data have further demonstrated that replacing OER by UOR in CO₂ electrolysers can reduce the overall potential in aqueous CO₂RR by 210 mV and up to 1 V in aprotic media, over a wide operating range and with high yields of electro-decarboxylation products. The UOR||CO₂RR coupling system thus allows in significant energy savings while simultaneously addressing the carbon/nitrogen footprint in a broader sense. Bertin et al. [153] have examined, during CO₂ electrolysis (for reducing the atmospheric pollution), the impact of the pH window on urea oxidation and found a strong dependence of UOR activity on pH, with a sharp decrease from pH 14 to 12, although it still occurs before OER potentials. The integrated UOR||CO₂RR system has showed a promising gain of 120 mV without significantly affecting the Faradic efficiency of CO₂ reduction into formate, thus confirming that the presence of urea in the electrolyte has not hindered the electrolyser's operation.

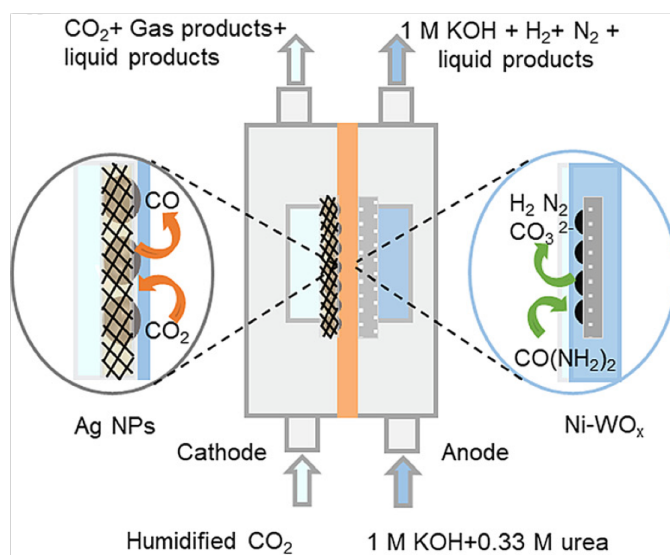


Fig. I.15 – The schematic image of the UOR||CO₂RR electrolyser (extracted from [154]).

The EC production of ammonia has recently emerged as sustainable alternative to the Haber-Bosch process that remains widely used for large-scale production, while consuming about 2% of global energy and contributing to over 1% of global CO₂ emissions. Indeed, NH₃ can be produced by the EC N₂ Reduction Reaction (N₂RR) at ambient temperature and pressure [155, 156]. UOR can be combined with EC N₂RR to create a more energy-efficient ammonia generation system.

Other applications can be encountered in environmental fields with different EC reduction in general. For example, the EC treatment of 4-nitrophenol (4-NP) has been studied [157, 158], as this molecule is a common toxin released from agricultural and industrial waste and posing significant threat to ecosystems and human health. The EC reduction of 4-NP leads to produce 4-aminophenol (4-AP) which is an important intermediate in drug synthesis, and thus offers a promising strategy for pollution control and resource recovery. Another example concerns the Cr-containing wastewater that are prevalent in various sectors, such as leatherworking and Cr plating. As Cr^{+VI} is 100-1,000 times more toxic than Cr^{+III} , numerous reduction technologies have been developed, and the EC reduction has been identified as the most promising one [159, 160]. This cathodic reaction could be also coupled with UOR into a single system. Even the huge potential, a very limited research effort has been so far dedicated to such (*non*)-environmental applications involving UOR system. This will require to carefully investigate the influence of several factors, including electrolyte, ions, and electrodes under mixed operating conditions. Fortunately, the existing integrated electrolysis systems can lay the groundwork for future UOR-counterpart energy-efficient electrolysis technologies in aqueous conditions.

I-2.3.e Concluding remarks

In the above sub-sections, the state of the art of reactional mechanisms involved in the UEO in alkaline medium have been discussed.

Among these, the classic E-C mechanism of NiOOH in alkaline UOR offers solid basis for thriving research in the following decade. Numerous advanced *in situ* characterizations have been employed for deciphering elementary mechanisms occurring at the EC interface between catalysts and electrolytes. At the same time, the role of active radicals generated on “inert” electrodes has been elucidated but the kinetic relationships between intermediates and by-products have yet to be established. By combining product analysis and reactive catalyst site design, the complex interactions between the urea molecules and multi-phase reaction surface have driven exploration.

To achieve a better understanding of the UOR system and more efficient designs of the EC reactor, several foreseeable challenges should be addressed:

- (i) UOR typically involves multiple proton/electron transfers and numerous surface interactions, leading to complex behaviors and mechanisms at local scale. To reveal them, **the key transient intermediate species at the interface need to be detected, which has not been yet done.**
- (ii) **The adsorption configurations of urea molecule on electrode have a direct impact on their EC oxidation mechanism.** Some fundamental studies have been conducted on Pt-based electrodes under acidic or dialysis electrolytes, but investigations on the adsorption forms present with alkaline and saline media have received less attention. They will greatly help to explain the differences observed between the various UOR system mechanisms.
- (iii) Concerning the **nitrites formed with nickel-based catalysts**, N-over-oxidation in alkaline UOR systems require deep investigations to prevent the formation of

environmental pollutants (NO_x). A special care has to be paid on the products generated by urea conversion during the UOR process, which has been generally overlooked in the literature. This consideration is also crucial for accurately interpreting UOR mechanisms.

- (iv) In real wastewater, particularly urine, many molecules are present with concentration levels close to the one of urea. **When using such wastewater as feed electrolyte, these interferent molecules could affect both electrocatalytic activity and product selectivity; this is still rarely studied, despite its importance for practical applications.**
- (v) OER in aqueous EC systems could be replaced by systems exhibiting lower oxidation potential. Current research works have demonstrated the feasibility of this integrated approach but they need deeper investigations.

I-3 Highlights of the state of the art, context and strategy of the present study

From the previous state-of-art, the following conclusions can be drawn:

- Urine is a complex effluent with a wide range of recovery options. The EC treatment of this fluid offers the advantage to both remove nitrogenous pollution from wastewater and to convert it into an energy carrier, thus facing environmental and energy challenges.
- In contrast to neutral medium, the UEO in alkaline medium is the most viable solution for treating this effluent (durability of the electrodes, formation of less toxic by-products, reduced energy consumption). The use of an alkaline medium has allowed the development of anode materials made of non-noble metals, of which nickel has the greatest catalytic activity.
- Despite the large amount of works carried out on UEO, they have rarely applied a Chemical Engineering approach. Many efforts have been made to functionalize and improve the performance and the stability of electrodes, while few works have been presented so far with long time experiments, high urea conversion rates, or complete mass balances.
- To the author's knowledge, no proof of concept of EC urea treatment at large-scale has been presented in a peer-reviewed journal.
- No energy and environmental balance of such a process has been found in the literature.
- The coupling of EC and photochemical processes has never been put into perspective on a pilot reactor scale.

Although much information gathered from the literature review, there exists many differences in the lab-scale-scale works reported and they generally involve short timescales, low conversion rates and small amounts of electrical charge. As a consequence, the ability of this process to reduce energy demand for H_2 production and for effluent recovery, remains

difficult to demonstrate. In this context, the ultimate objective of this thesis, which is part of the ANR HyUrea project, is to propose a EC process that allows efficient and low-cost production of H₂ coupled to wastewater treatment. Therefore, the main challenges of this project are:

- To understand the chemicophysical phenomena that take place during UEO on a 'basic' massive nickel electrode;
- To perform complete mass balances in both liquid and gas phases in order to identify the by-products, to establish reactional pathways and thus to rigorously quantify the efficiency of mineralisation of the UEO;
- To model the UEO kinetic law with the aim of designing larger scale EC reactor, possibly photo-assisted;
- To design, build and optimize a PEC reactor prototype allowing urea oxidation with simultaneous cathodic generation of H₂.

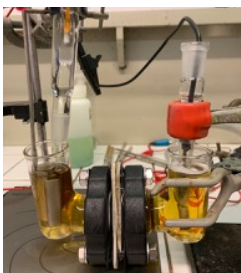
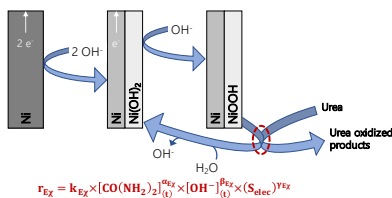
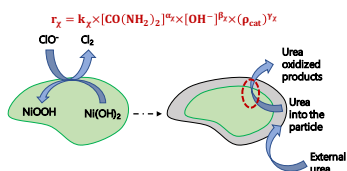
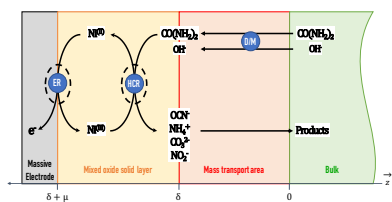
Figure I.16 intends to present the strategy of this thesis, which is organized as follows:

Chapter II Several devices and EC methodologies have been used, built and applied in this thesis. This chapter describes the principles and characteristics of these set-ups, as well as the large analytical panel that have been developed for establishing complete and accurate mass balances, for all reagents and by-products.

Chapter III This chapter is devoted to the study of the UEO in alkaline media at lab-scale-scale. It expects to deeply investigate the effects of operating conditions on the urea conversion and the formed by-products. The key parameters (activation energy, diffusion coefficient, anodic charge transfer coefficient, and heterogeneous electron transfer rate constant) will be determined. From these studies, some guidelines will be proposed, for further designing, building and optimization of an electrolyser for the urea mineralisation.

Chapter IV The **Chapter** focuses on the kinetic of urea oxidation; studies will be carried out by coupling in an original way two different NiOOH sites (chemically synthesized NiOOH solid particles and continuously electro-generated NiOOH layer on massive nickel electrode). The kinetic laws will be determined for both sites, and a multi-pathway mechanism will be established, on the basis of the by-products identified in the liquid phase. Additionally, a predictive model that combines the established UEO kinetic law with diffusive and convective transport phenomena will be proposed, and validated (>95%) by comparing with experimental results at the lab-scale for various operating conditions.

Chapter V This last chapter reports the building of a pilot-scale reactor as well as some experimental results obtained in this reactor. Results will constitute a proof of concept for scaling up the UEO process. Complete mass balances will be implemented and an energy study of the process done. Finally, the treatment of real effluents (instead of urea synthetic solutions) will also be investigated for the first time, allowing to identify the possible limitations induced by the direct use of the urine (*i.e.*, any eventual effect caused by the real matrix).



Step 1

New insights into the UEO on nickel anode at lab scale

- Impact of the operating parameters (concentration, temperature, angular velocity) & access of key parameters describing the overall process
- Urea electrolyzes achieving liquid mass balances for high urea conversion rates (~80%)

Step 2

Comparative study of the urea oxidation process

- Determination of kinetic rate laws
- Proposition of UEO mechanisms
- Modeling at macro- & micro-scale of the chemico-physical phenomena

Step 3

Real effluents treatment

- Parametric studies
- Matrice effects
- Validation of the process

Step 4

Design & building of a pilot-scale EC reactor, possibly photoassisted

Operate the EC pilot-scale reactor

- Mass and energy balances in liquid and gas phase
- Study of the operating parameters (E, flow rate, ...)
 - Proof-of-concept with real urine

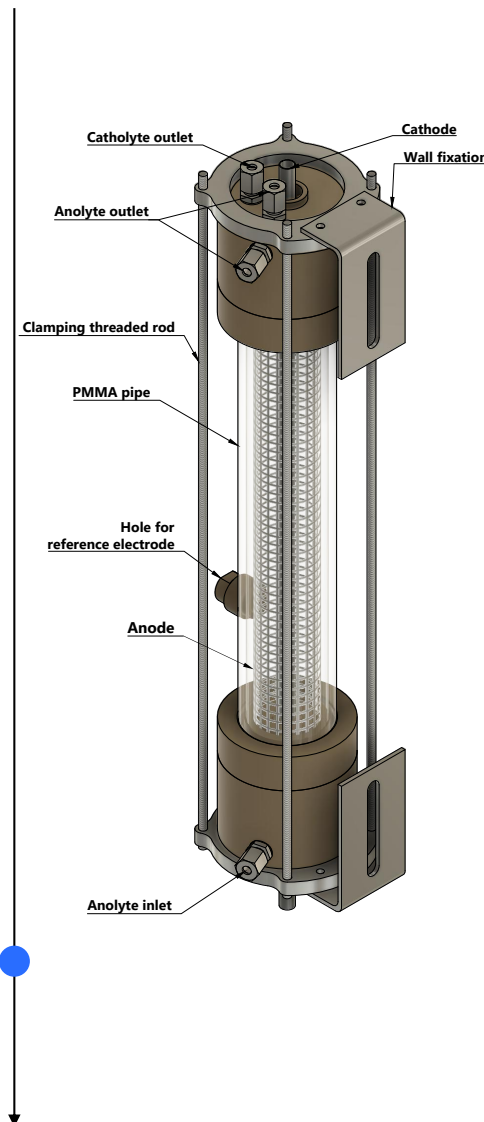


Fig. I.16 – Summary of the different stages of the thesis.

Material and methods

Outline of the current chapter

II-1 Experimental set-up	42
II-1.1 Laboratory scale	42
II-1.2 Pilot scale	45
II-1.3 Summary of the various EC set-up characteristics	50
II-2 Analytical methods for urea quantification	52
II-2.1 State of the art	52
II-2.2 Total organic carbon (TOC) as a global tool to evaluate the carbonaceous load of the media	54
II-3 IC-CD/MS coupling	58
II-3.1 Principle	58
II-3.2 Instrumentation and analytical protocols	59
II-3.3 Application to urea solutions	60
II-4 Gas chromatography	64
II-4.1 Principle	64
II-4.2 Instrumentation and analytical protocols	64
II-4.3 Application to urea solutions	66
II-5 General operating procedure of the electrolysis at lab-scale	67

This chapter introduces the set-ups and methods used in the next chapters. For the sake of clarity, the choice has been made to present here only the methods applied in all the studies while each specific method will be detailed in the relevant chapter. As a consequence, this chapter will focus on the methods used to carry out all electrolyses with urea solutions (and not with real urine solutions, see **Chapter V**) and to establish complete mass balances in both liquid and gas phases. The first part will present the EC devices on lab-scale and pilot-scales, the second part the analytical pool and the last part the operating procedure for carrying out rigorous and complete mass balance.

II-1 Experimental set-up

Three types of EC reactors were used: two lab-scale reactors (~ 100 mL, section II-1.1) and a pilot-scale reactor, that was especially designed and built for the present thesis (section II-1.2). The lab-scale reactors offered the benefit to allow electrolysis to be carried out over short times by reducing the molar amount of urea to be treated and thus optimizing the ratio of electrode surface area and electrolyte volume in **Chapter III** and **IV**.

II-1.1 Laboratory scale

A mono-compartment (undivided) reactor and a bi-compartment (divided) reactor were implemented in **Chapters III** and **IV** as illustrated in Figure II.1.

All the EC experiments were performed using a PGSTAT 128 N potentiostat (Metrohm Autolab[®]) controlled by NOVA software. A reference electrode Hg/HgO (Origasens, Orignalys[®]) located inside a Luggin capillary containing support electrolyte (1 mol L^{-1} of KOH) is used, and all the potentials were given with respect to Hg/HgO ($E_{\text{Hg}/\text{HgO}}^{\circ} = 107 \text{ mV vs. SCE for NaOH } 1 \text{ mol L}^{-1}$ [161]).

Cell a) consisted of a conventional three-electrodes thermoregulated tank (Metrohm type cell) that was used in this work for voltammetry studies ($I=f(E)$ curves). All the voltammograms were repeated 3 times. The temperature of the solution was regulated by circulating a thermostatic solution in the double-jacketed EC cell. The electrolyte volume was 50 mL. The Working Electrode (WE) was a Ni Rotating Disk Electrode (RDE) (3.14 mm^2) sealed in a Teflon rod, while the Counter Electrode (CE) consisted of a Pt plate (4 cm^2 , one face).

Cell b) was a H-shaped cell used for carrying out electrolysis at the lab-scale (around 1.4 g of urea). To that end, three massive nickel plate (4 , 6 and 28 cm^2 , corresponding to the geometric area of a single face) were used as anode in this study. Both anode and cathode (Pt) were introduced into the cell. The use of a magnetic stirring bar at 500 revolutions per min (RPM) provides the same agitation for all electrolysis into the anolyte compartment. If required, a membrane separator module could be placed between anolyte and catholyte compartments. Such design was used for comparing undivided or divided cell configurations in terms of urea degradation. The anionic nature of the membrane (IONAC MA-375, Lanxess[®]) ensured the migration of hydroxide ions produced at the cathode and consumed at the anode, while separating the other species. Note that, for rightly comparing both configurations, a special care was required to operate with constant volume in both divided and undivided cells, while using the same electroactive surface. Electrolytes were

alkaline solutions of KOH at concentrations in range of 0.5 to 5 mol L⁻¹. The solutions containing urea were prepared at a concentration close to those into the human urine. (*i.e.*, 0.33 mol L⁻¹ as presented in section [I-1.3](#)).

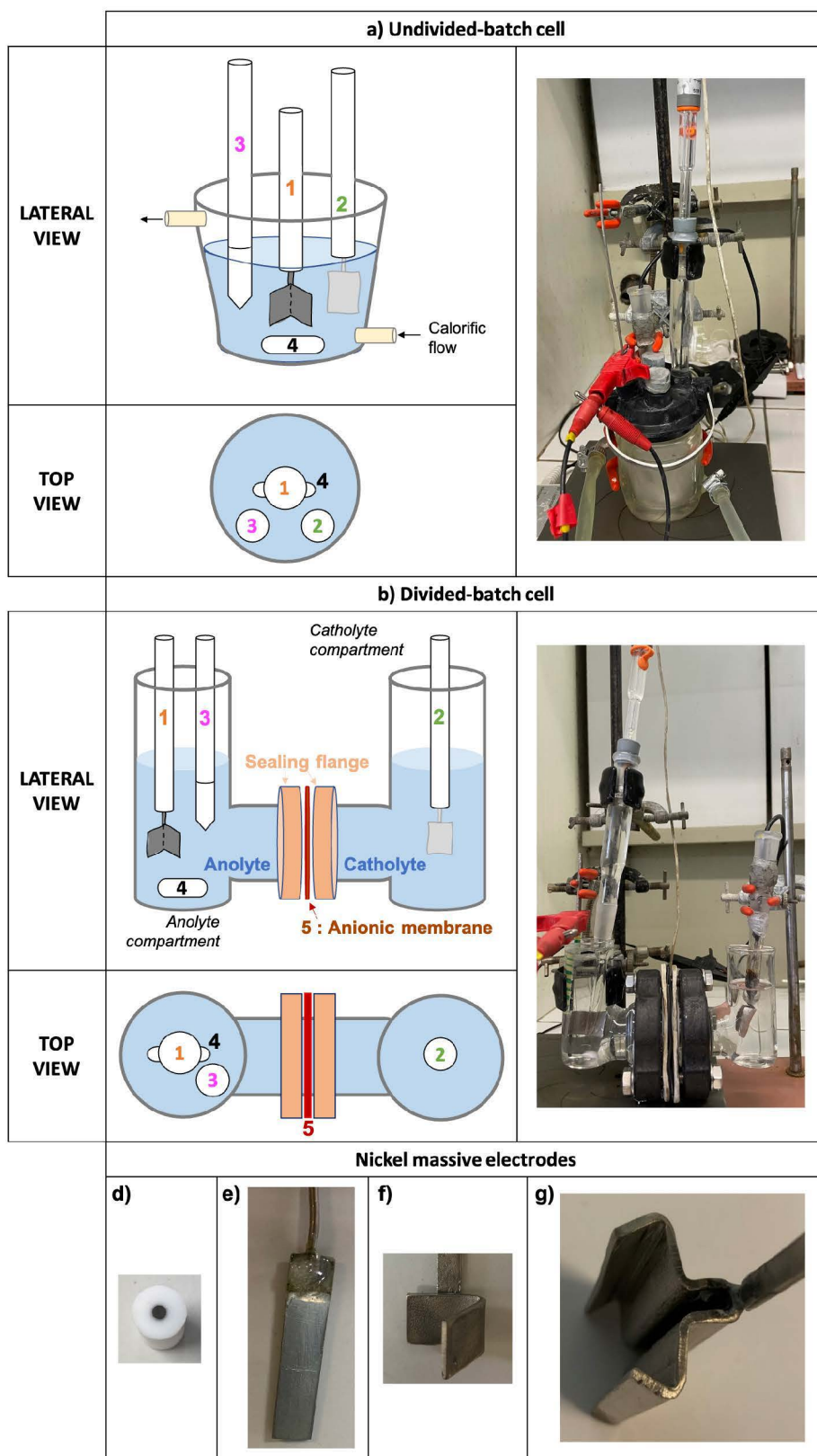


Fig. II.1 – Experimental set-up used for a) $I=f(E)$ curves and undivided electrolysis and b) un/divided cell for electrolysis. WE and CE are identified as 1 and 2. Reference electrode (Hg/HgO) is labeled 3. In the case of electrolysis, a magnetically stirring bar (mark 4) was used to mix the electrolyte solution. In case of divided cell, the membrane separator (mark 5) holds in place by flanges that maintain the seal. Nickel electrodes used in the present work with different surface areas: d) 3.14 mm^2 , e) 4 cm^2 , f) 6 cm^2 and g) 28 cm^2 .

These cells shown in Figure II.1 were used in **Chapters III** and **IV**, but unfortunately did not allow to collect the electro-generated gas. As a consequence, another H-type EC cell

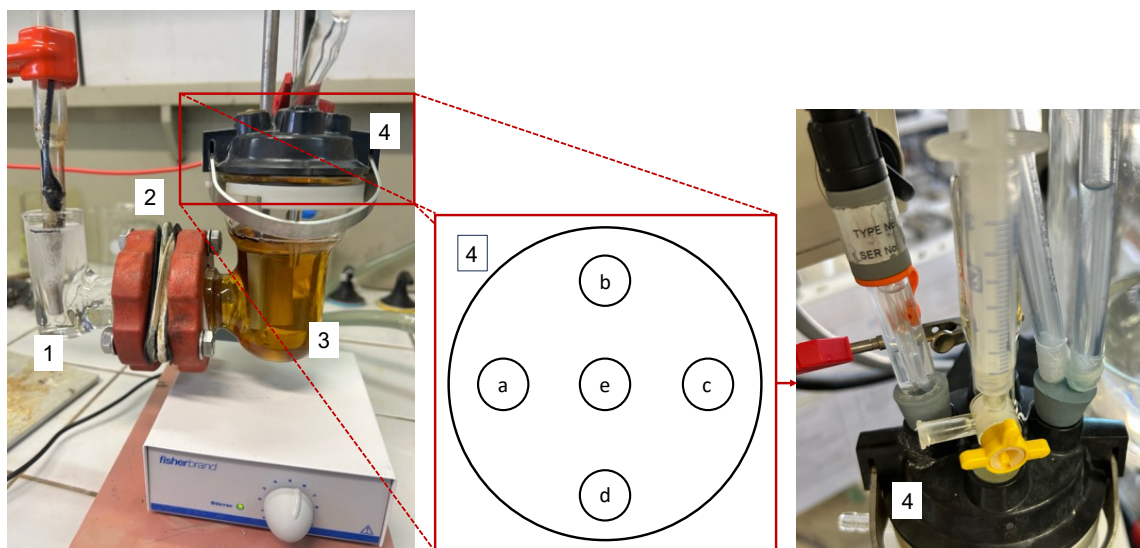


Fig. II.2 – Illustration of the H-type EC cell used in this work. Labels: 1) cathodic compartment, 2) anionic separator, 3) anodic compartment, 4) sealed-cap keeping the produced gases tight to the external ambient atmosphere. On this cap, various holes allow a) the positioning of the anode, b) the positioning of the reference electrode, c) argon bubbling, d) sampling syringe for the liquid phase and e) sampling of the gas phase to the GC.

(see Figure II.2) was developed in **Chapter V** enabling to maintain a controlled gaseous atmosphere in the EC cell. In fact, the upper part of cell a) was welded to cell b) by a glassmaker. As a result, the electrode surfaces, volumes and other features (use of membrane) of the cell b) are preserved, while still providing an atmosphere-tight seal. Note that, in **Chapters III** and **IV**, the mass balances presented are obtained for the liquid phase, while in **Chapter V**, they include the gas phase.

II-1.2 Pilot scale

In order to establish a proof-of-concept at larger scale on the UEO process, an EC reactor at pilot-scale and its environment were specially designed and built for this thesis. Note that the design of this pilot took into account the option of a photo-assistance on the UEO process. This led to choose a tubular geometry that could be externally illuminated while maximizing the surface of the photoanodes as imagined in Appendix B.

This geometry, illustrated in Figures II.3, II.4 and II.5, could allow irradiating several photo-anodes placed at different locations on the cylinder (or even photovoltaic panels associated to the external cylinder). Unfortunately, due to lack of time, it was not possible to implement photo-assistance, within the scope of this manuscript.

As a reminder, a set of requirements was laid down as part of the HyUrea project. Among which a number of points had to be met in the aim to design, manufacture and optimize a PEC reactor prototype. Typically the set-up must:

- (i) enables urea oxidation with simultaneous cathodic generation of H_2 by photo-assistance;
- (ii) uses of 100 cm^2 geometrical area electrodes;
- (iii) performs continuous electrolyses;
- (iv) treats $5 \text{ L day}^{-1} \text{ m}_{\text{anode}}^{-2}$ of solution (urea or urine) stored in an external tank with an average concentration of 0.33 mol L^{-1} of urea);

- (v) uses compartments made by transparent material walls (light transmittance $> 80\%$ for $\lambda > 300$ nm);
- (vi) present a connection at the top of each compartment to a gas collector, for further analyses;
- (vii) enables sampling of aliquots for the determination of mass balance on reagents and products.

As shown in Figure II.4, the main features of this pilot-scale reactor were:

- (i) a transparent PMMA tube; it is used to fix a tubular geometry for the reactor;
- (ii) a PEEK part located at the bottom (as well as at the top) of the reactor allowing fluid distribution (collection) in the reactor and maintaining the system's tightness;
- (iii) a central tubular cathode (94 cm^2) made of 316L stainless steel, enabling thermoregulation of the reactor;
- (iv) a nickel anode in the form of a wound grid provided by Neyco (1 mm square mesh), illustrated in Figure II.3 with a geometric surface that could be made varying depending on the number of turns of the wound grid. The surface area could then take the values of (i) 367, (ii) 734 and (iii) $1,101\text{ cm}^2$ (equivalent to the geometric surface area, calculated according to the number of wound cylinders);

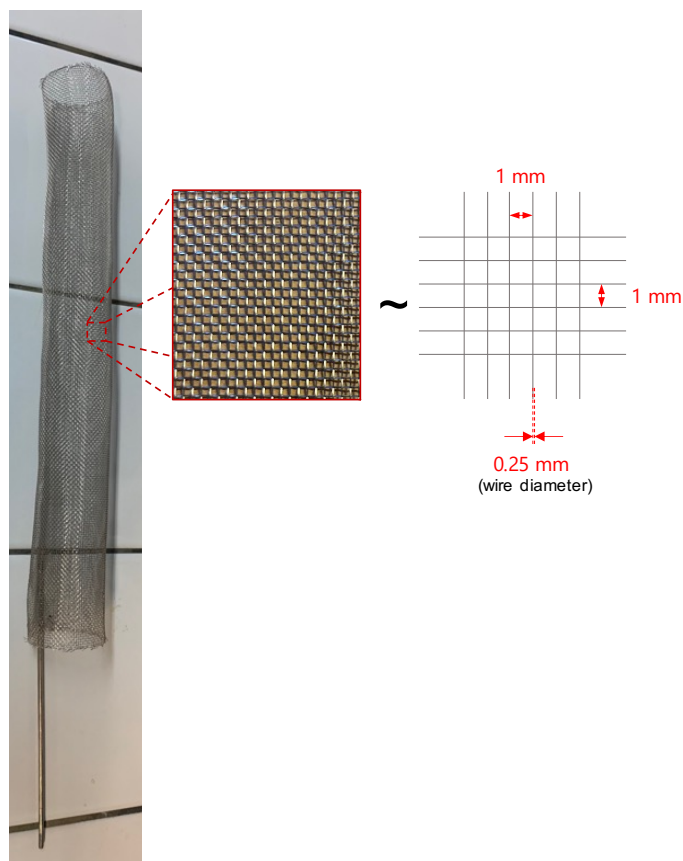


Fig. II.3 – Nickel grid used as anode in the pilot-scale reactor.

- (v) the possibility of working in mono- or bi-compartment when using a membrane separator. Grooves on the top and bottom of the PEEK rods, between the anode and the cathode allow a membrane cylindrical support to be located. A Teflon[®] support could be imagined, to keep the compartments sealed using a membrane separator;
- (vi) the volume of the solution to be treated could then range from 0.9 L in the case of single-compartment electrolysis (equivalent to a ratio S/V of 39 m^{-1} in case of one turn of grid or 117 m^{-1} for three turns) to 0.7 L (0.12 L for the cathode compartment) in the case of a divided-compartment electrolysis (equivalent to 53 m^{-1} in case of one turn of grid or 159 m^{-1} for three turns).

More information on the dimensions of the reactor parts, machined by the SEF company, can be found in the sketches of Appendix C.

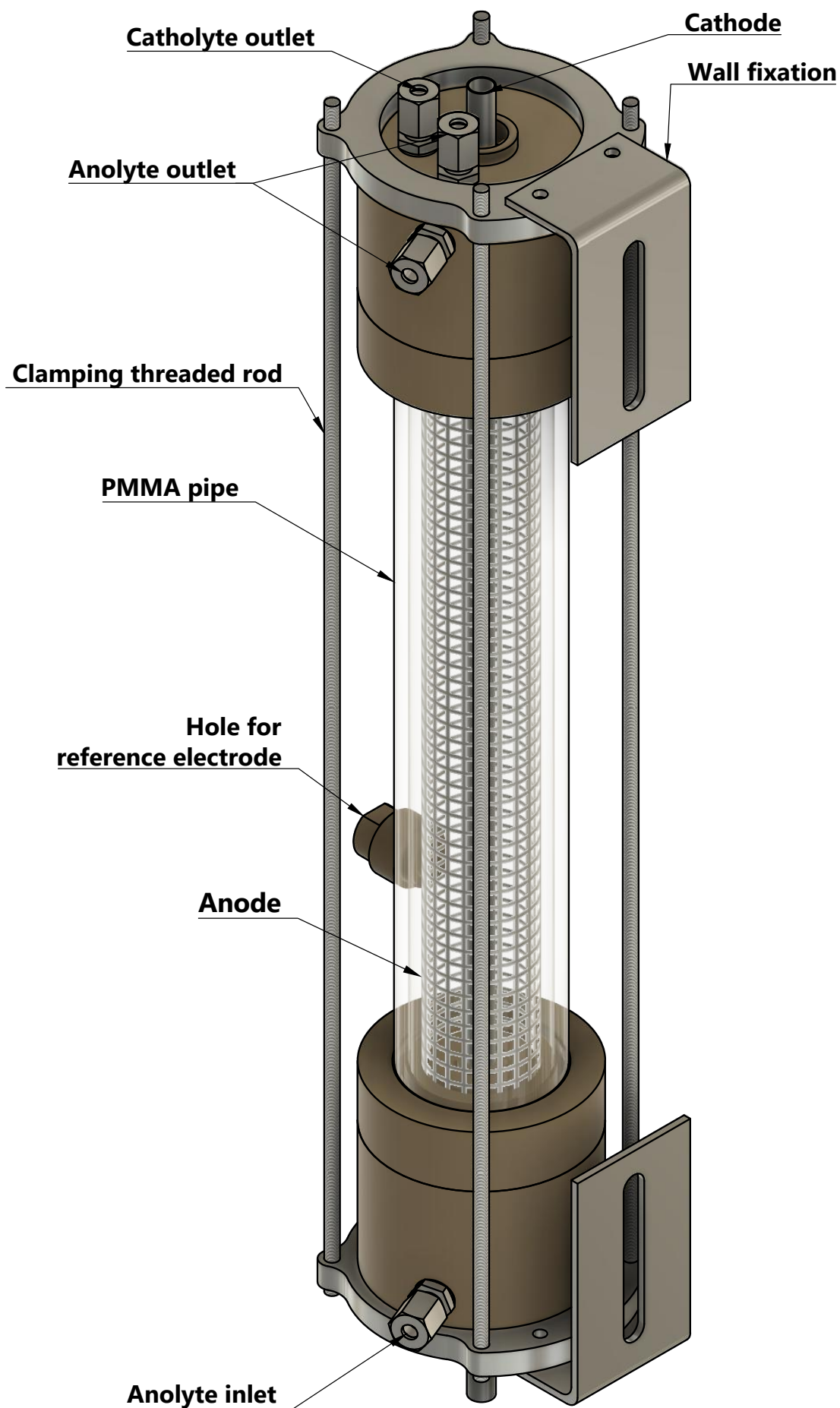


Fig. II.4 – Computer-aided design of pilot-scale EC reactor.

The reactor operated in multi-pass mode. Two thermoregulated storage tanks contain the electrolytes. A set of equipment was then installed, by the lab-scale's technical teams, so as to operate in such closed loop and under controlled conditions:

- (i) OrigaFlex 20A potentiostat (Orignalys, France);
- (ii) thermoregulated liquid storage tanks (capacity of ~ 2 L), which also enabled the degassing of the liquid phase. In order to reduce electrolysis time (in undivided compartment case), results were obtained with 1 L of solution. This means that, when operating, a very little liquid volume was remaining in the storage tank; all the electrolyte being thus in the reactor;
- (iii) magnetic pumps (M Pumps, T-MAG-P32) to feed the reactor at flow rates ranging from 0 to 60 kg h^{-1} ;
- (iv) Coriolis flow-meters (Micro Motion ELITE CMF010M Coriolis Meter) to measure the mass flow rate supplying the reactor
- (v) temperature (Pt-100) and pressure (KELLER OEM PR-21SR) sensors located at the reactor inlet (both in anolyte and catholyte paths);
- (vi) for the gas phase, the mass flow rate produced was quantified by a thermal mass flow meter (Brooks Instruments SR SLA5860S+0151). A Varian-450 GC was connected in-line to the system. The electrolysis process was flushed ($\sim 1.5 \text{ L h}^{-1}$) with argon gas to maintain a controlled atmosphere;
- (vii) a digital recorder (Honeywell Multitrend SX) to collect data generated by pilot instrumentation (liquid and gas flow meters, temperature and pressure sensors);
- (viii) an electric switchboard providing a safe power supply for the entire process.

Once summarised the EC set-ups used in this work, the next sections focus on the set of analytical methods used to perform mass balances in the liquid phase (determination of urea and liquid reaction by-products) and in the gas phase (N_2 , H_2 and O_2).

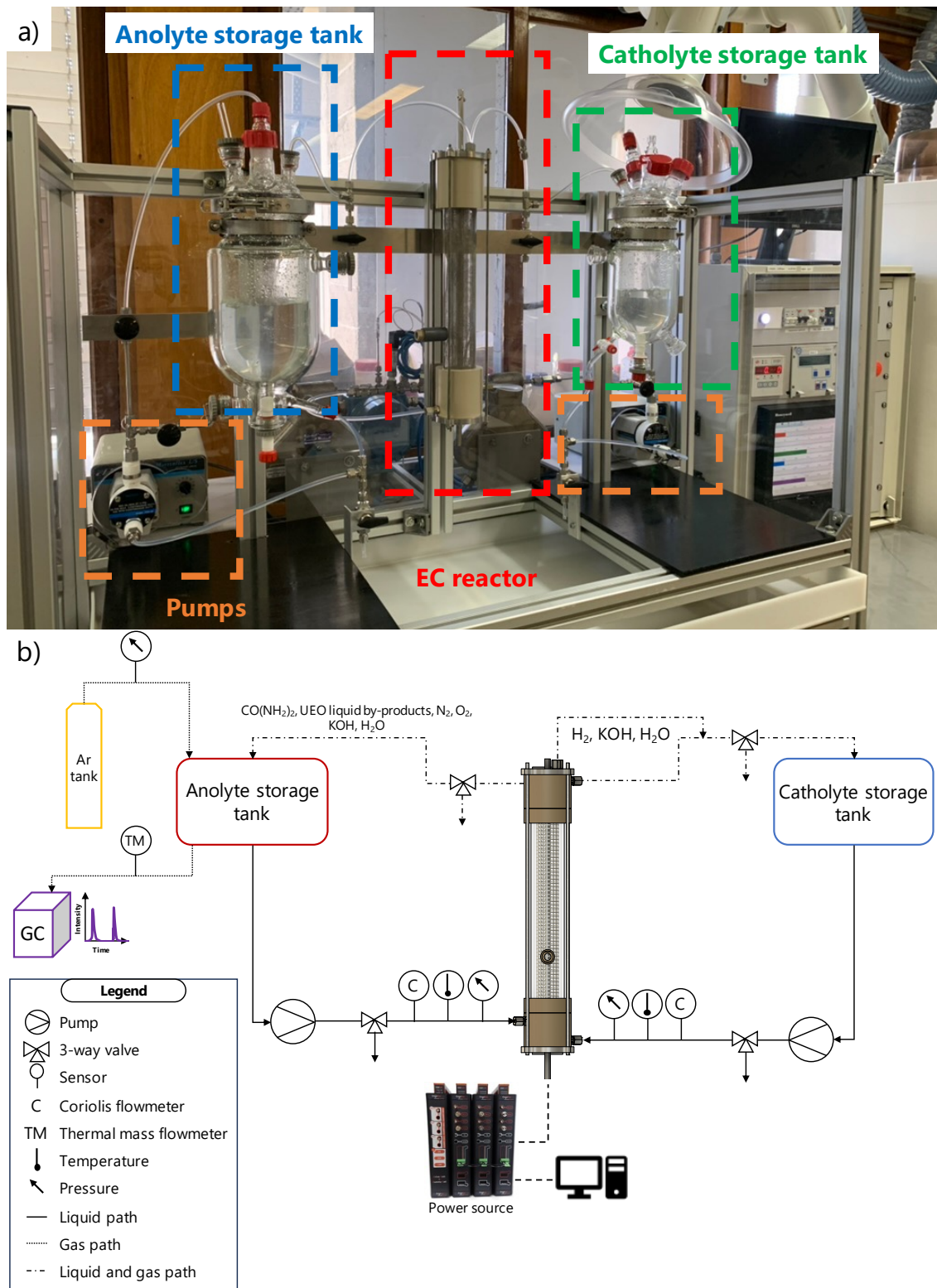


Fig. II.5 – a) Picture of the EC set-up at pilot-scale operating in closed loop and b) scheme set-up.

II-1.3 Summary of the various EC set-up characteristics

<i>EC reactor type</i>	Metrohm type cell				H-type cell			Pilot scale (for 1 L of solution to be treated) ^c								
<i>Single-compartment</i>	X				X			X								
<i>Bi-compartment</i>								X			X					
<i>Anode material</i>					Ni plate			Ni mesh								
<i>Cathode material</i>					Pt			316L stainless steel								
S_{anode} (m ²)	3.2×10^{-6}	4.0×10^{-4}	6.0×10^{-4}	2.8×10^{-3}	4.0×10^{-4}	6.0×10^{-4}	2.8×10^{-3}	4.0×10^{-4}	6.0×10^{-4}	2.8×10^{-3}	3.7×10^{-2}	7.3×10^{-2}	1.1×10^{-1}	3.7×10^{-2}	7.3×10^{-2}	1.1×10^{-1}
S_{cathode} (m ²)					4×10^{-4}			9.4×10^{-3}								
<i>Urea solution volume to treat</i> (m ³)	5.0×10^{-5}				1.2×10^{-4}			6.0×10^{-5}			9.4×10^{-4}			6.9×10^{-4}		
<i>S/V ratio</i> (m ⁻¹)	0.1	8.0	12.0	56.0	3.3	5.0	23.3	6.7	10.0	46.7	39.0	78.1	117.1	53.2	106.4	159.6
Q_m (kg h ⁻¹)											30 - 60					
Q_v (L h ⁻¹) ^a											29 - 58					
<i>Residence time τ_{reactor}</i> (s)					N.A.						58 - 117			43 - 85 (anodic compartment)		
<i>Number of passes through reactor in one hour</i>											31 - 62			42 - 84 (anodic compartment)		
<i>Reynolds number range</i> ^b											155 - 311			112 - 224 (anodic compartment)		

^a Density of KOH 1 mol L⁻¹ solution equal to 1040 kg m⁻³.

^b The Reynolds number for flow in an annular section (with inner and outer radius, R_1 and R_2 respectively) is calculated as follows: $Re = \frac{2 \times (R_2 - R_1) \times V_d}{\nu}$ with V_d as the velocity through the annular section as $V_d = \frac{Q_v}{\pi \times (R_2^2 - R_1^2)}$ and ν as the dynamic viscosity equal to 1.14 mPa.s.

^c In this thesis, only experiments with single-compartment were done at pilot-scale.

Table II.1 – Presentation of the different characteristics of the EC reactors used.

II-2 Analytical methods for urea quantification

In order to monitor the degradation of urea in the different EC set-up, it was necessary to establish and develop a complete analytical method. In this section, the analytical methods that are commonly encountered to measure urea concentration in different fields (wastewater treatment, health, food, etc.) will be first presented. The second part of this section will describe the total organic carbon measurement used in this thesis, while the method based on the coupling of Ion Chromatography - Conductivity Detector / Mass Spectroscopy (IC-CD/MS) will be explained in Section II-3.

II-2.1 State of the art

II-2.1.a Electrochemical biosensor

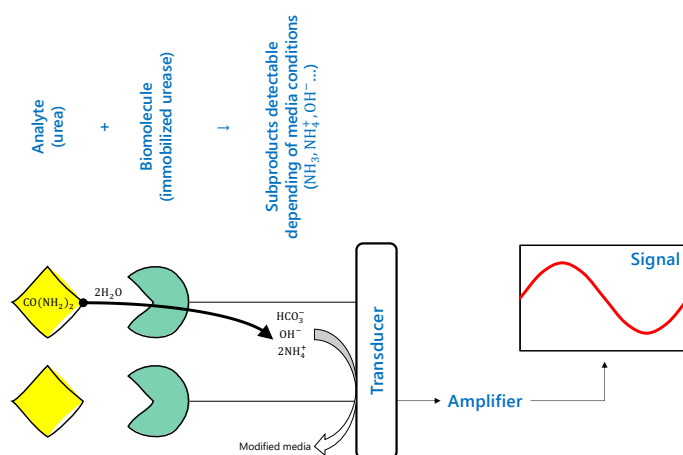


Fig. II.6 – Schematic representation of a typical biosensor used for urea concentration measurement.

As early as the 1970s, Guilbault et al. [162] have pioneered to design a biosensor for urea by implementing an enzyme electrode as a transducer, as illustrated in Figure II.6. It consists of a thin film of urease enzyme in an acrylamide gel on a Beckman cationic electrode surface that is responsive to ammonium ions. The enzymes on the surface catalyzed the urea decomposition into ammonium and the electrode detects the changes of the zero current potential (even pH) induced by the changes of the ammonium concentrations. Recent developments concern biosensors able to detect urea levels in different biological media [163–165]. Most of these urea biosensors involve urease as enzyme: by catalyzing the hydrolysis reaction, urease produces ammonium and carbonate ions and thus impacts the pH, which is logarithmically correlated to the urea concentration [166]. The main challenges of biosensors come down to (i) the enzyme immobilization techniques (entrapment, cross-linking, covalent binding, encapsulation, adsorption), (ii) the stability (enzyme), (iii) the characteristic response time (ranging from few seconds to several minutes) and finally (iv) the transducers (amperometric [167], potentiometric [168], piezoelectric [169], optical [170], calorimetric [171], conductometric [172], fluorometric [173]). This technology is well developed for determining urea level in human sweat [174], by using electropolymerization of 3,4-ethylenedioxythiophene (EDOT) monomer on the hierarchical network of Carbon NanoTubes (CNTs), with a Limits Of Detection (LODs) equals to 0.1 mmol L⁻¹. Recently,

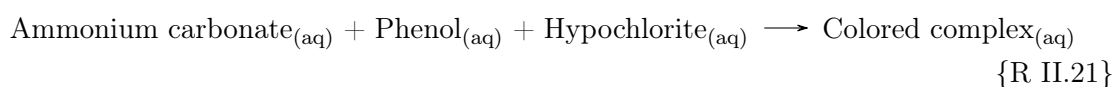
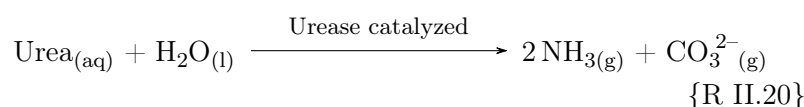
in May 2023, Janyasupab et al. have explored a method based on a non-enzymatic urea detection in dialysate that used an indirect urea oxidation process involving nickel, nitrogen-doped carbon, surface roughness, and double layer current. A unique reaction, evidenced by specific oxidation peaks in voltammetry techniques, allowed for precise urea concentration measures in dialysate. Various tests in simulated and patient dialysates have demonstrated excellent accuracy, with a sensitivity of $-5.136 \times 10^{-5} \text{ A (mmol L}^{-1}\text{)}^{-1}$ and a LODs equals to $60.2 \mu\text{mol L}^{-1}$. This method yielded a recovery percentage between 99.18% and 102.68% compared to the clinical standard, and thus opens up prospects for future monitoring and wearable artificial kidney technology [175]. Unfortunately, this type of sensor is not yet at the commercialization stage.

II-2.1.b Chemiluminometric techniques

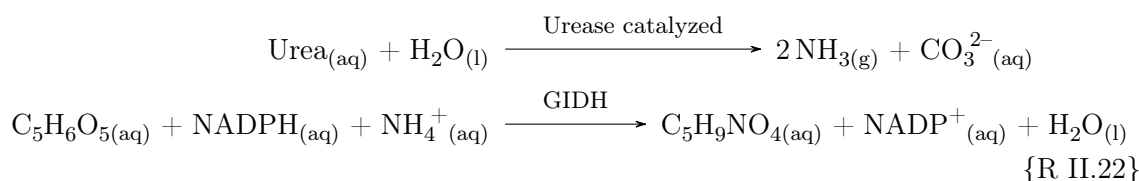
Most of these methods are based on the chemiluminescence reaction of urea with oxidants and chemiluminescence reagent. This enzyme-free technique has received a growing interest, in particular by coupling the use of strong oxidants (hypobromite BrO^- at 510 nm [176, 177], luminol $\text{C}_8\text{H}_7\text{N}_3\text{O}_2$ at 360 nm / permanganate MnO_4^- at 525 nm [178]) with chemiluminescence emitted detection. This technique is only at the research stage to the author's knowledge.

II-2.1.c Colorimetric & spectrophotometric methods

Urea concentration can be measured by colorimetric methods [179, 180]. The principle consists in determining the urea concentration in presence of a colored reagent (for example salicylate, α -isonitrosopropiophenone, diacetyl monoxime [181–184]), with or without enzymatic assistance. With enzyme, the color reaction is preceded by a reaction catalyzed by an enzyme. As the enzyme is specific to a particular substrate, more accurate results can be obtained. An example with urease is reported in the following equations {R II.20-R II.21}.



The most widely used technique works in the UltraViolet (UV) domain in which the difference in absorbance at 340 nm is measured between Nicotinamide Adenine Dinucleotide Phosphate (NADP^+) and Nicotinamide adenine dinucleotide phosphate reduced form (NADPH) according to {R II.22}.



where the amount of NADP^+ formed is stoichiometrically related to the amount of urea and ammonia in the sample.

Other colorimetric techniques involving various reagent types have been studied including nesslerization (treatment of a mixture with a solution of mercuric iodide in potassium iodide and KOH) [185], phenol-hypochlorite [186] or Berthelot's method [187] and diacetyl monoxime method [181]. The use of these reagents requires the addition of reagents, and therefore increases sample preparation.

They are commonly used for the assessment of blood urea levels, in particular in combination with a serum creatinine test [166]. The urea detection limit of commercial tests (*e.g.*, Sigma-Aldrich[®], Thermo-Fisher Scientific[™]) ranges around 0.1 mg L^{-1} .

II-2.1.d Chromatographic processes

High Performance Liquid Chromatography (HPLC) is the most commonly used chromatography methods for urea measurements. Urea is then separated from other components contained in the sample by means of a column filled with a stationary phase, typically silica-based. After separation, urea is detected and quantified using a spectrophotometer at 190 nm [188] ($\sim 0.2 \text{ mg L}^{-1}$) or a refractive index detector [189]. Some applications of Liquid Chromatography (LC) coupled with MS have exhibited higher quantification level of urea [190, 191] ($\sim 2 \times 10^{-4} \text{ mg L}^{-1}$).

II-2.1.e Comparison and concluding comments

The conventional methods, such as chromatography and colorimetric analysis, suffer from relatively long time-consuming sample preparation, high equipment cost and/or long analysis time [192]. In addition, they are generally not suitable in highly alkaline media, such as the ones involved in the UEO process (see **Chapter I** in section I-2). There is thus an obvious need to develop more efficient and rapid methods for urea measurements.

At the beginning of this thesis, we have focused on the development of successful analytical methods for the determination of urea under conditions of high alkalinity. After several tests, the enzymatic assay (in the case of this work, Urea/Ammonia Assay Kit (Rapid) from Megazyme), involving the urease enzymatic reaction, did not show conclusive results, certainly due to the enzyme's instability under the extreme conditions of pH (around 14). Two methods were therefore specifically optimized: (*i*) the measurement of TOC and (*ii*) MS coupled with ion chromatography. The next two sections is focusing on these studies.

II-2.2 Total organic carbon (TOC) as a global tool to evaluate the carbonaceous load of the media

In water, two forms of carbon can be found: organic carbon (TOC) and inorganic carbon (IC). TOC combines with hydrogen or oxygen to create organic molecules while, IC is related to inorganic compounds like dissolved CO_2 and carbonate ions. TC and IC have been measured and TOC is calculated following the Eq. II.1.

$$\text{TOC} = \text{TC} - \text{IC} \quad (\text{II.1})$$

This organic carbon contribution can also be classified according to the volatile nature of these compounds. As shown in Eq. II.2, a distinction is then made between NPOC

(Non-Purgeable Organic Carbon) and POC (Purgeable Organic Carbon).

$$\text{TOC} = \text{POC} + \text{NPOC} \quad (\text{II.2})$$

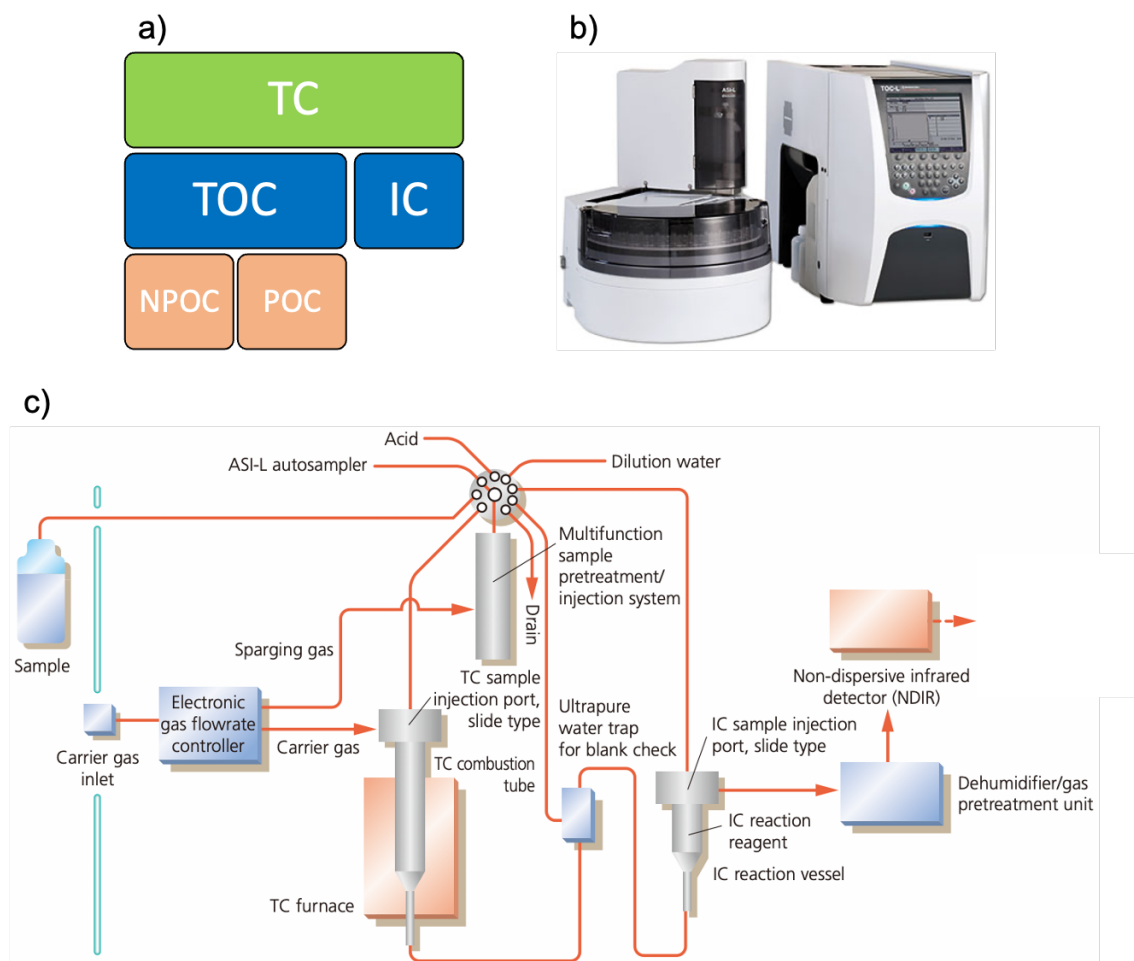


Fig. II.7 – a) Characterization of the different forms of carbon molecules (only applicable in aqueous medium), b) TOC-L analyzer from Shimadzu[®] and c) flow diagram of the analyzer (adapted from the user manual).

II-2.2.a Analysis of Total Carbon (TC)

In the TOC-L system (used in this thesis, illustrated Figure II.7-b and detailed in Figure II.7-c), a pressure regulator and mass flow controller manage the carrier gas flow. The carrier gas (synthetic air, $\text{CO}_2 < 1 \text{ ppmv}$) flows at a rate of 150 mL min^{-1} towards the combustion tube, which is filled with an oxidation catalyst (alumina beads with 0.5% of Pt) and heated to 680°C . The TC within a sample burns in the combustion tube, forming CO_2 . The carrier gas, now containing CO_2 and other combustion by-products, proceeds from the combustion tube to an electronic dehumidifier, where it is cooled and dehydrated. Subsequently, the gas passes through a halogen scrubber before reaching the Non-Dispersive Infrared (NDIR) gas analyzer's cell, where CO_2 is detected. The NDIR's analog detection signal thus generates a peak (Figure II.8-a), which area is measured by a data processor.

The peak area is directly proportional to the TC concentration of the sample. After analyzing a TC standard solution, the calibration curve equation (*i.e.*, the relationship between TC concentration and peak area) could be established (Figure II.8b), and then the

sample's TC concentration determined.

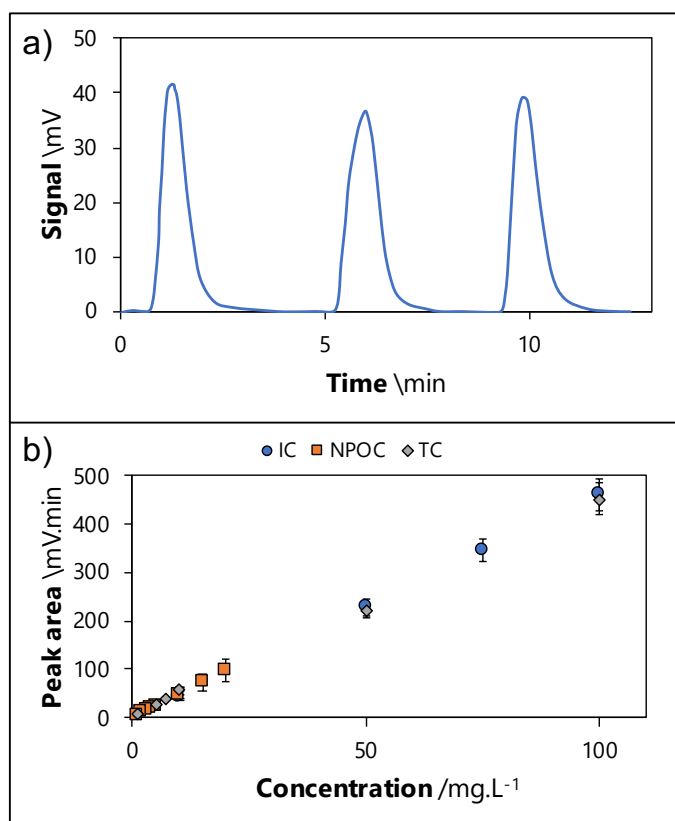
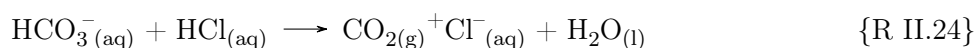
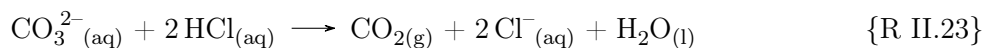


Fig. II.8 – a) Typical results obtained for triplicate injections of TC analysis of urea solution at 0.33 mol L^{-1} in 1 mol L^{-1} KOH and b) TC, IC and NPOC calibration curves obtained for various concentrations of carbon.

II-2.2.b Analysis of Inorganic Carbon (IC)

The IC includes the carbon within carbonate, hydrogen carbonate, carbonic acid and dissolved carbon dioxide.

To release all the carbonates as carbon dioxide form, the sample was acidified using a small quantity of hydrochloric acid (38 wt.%), resulting in a pH below 3. This process triggered the reactions {R II.23-R II.24}, where CO_3^{2-} transformed into CO_2 .



The CO_2 and dissolved carbon dioxide in the sample were then volatilized by bubbling (sparging) air or a gas (that did not contain carbon dioxide) through the sample. Once in the form of carbon dioxide, the quantity of material is measured by infrared by a NDIR.

II-2.2.c Analysis of Non-Purgeable Organic Carbon (NPOC)

The measurement of TOC, considered as an indicator of the mineralisation degree of the solution, could be decomposed as shown in Figure II.7-a, into:

- (i) POC (referring to the organic carbon that was sparged or removed from a sample, such as volatile acids or solvents)

(ii) and NPOC (referring to the organic carbon remaining in an acidified sample after purging the sample with carbon-free gas).

After acidifying the sample by adding acid until pH 2 to 3, synthetic air (without CO₂) was bubbled through it to remove the IC component. The remaining TC in the sample after acidification and sparging was then measured, leading to determine the TOC, using Eq. II.2. In the end, when NPOC was measured, POC and IC were volatilized, and the TC measurement was directly equal to NPOC.

II-2.2.d Assimilation of the NPOC measurement for urea determination

If the sample contains Purgeable Organic Carbon (POC) substances in significant amount, these components may be lost during the sparging step. In that case, TOC should not be measured using the NPOC method. This property was used, in an unexpected way, to titrate urea in our electrolysis samples *only in the case of urea solutions*. **Indeed, assimilating the urea concentration to the TOC concentration is not suitable for real effluents, thus requiring to develop a specific analysis**, as shown in the next section II-3. The carbon compounds identified during our electrolysis (as discussed in **Chapter III**) were only urea and cyanate as organic carbon, and carbonate as IC. As a consequence, the experimental protocol was modified as follows: when measuring NPOC, an excess of hydrochloric acid (38wt.%) as poured in to acidify the sample so that inorganic matter and weak acids (cyanate in our case) were removed as CO₂ gas or volatile acid (cyanic acid in the present case). It was then necessary to verify that the NPOC measurement allowed direct access to the urea concentration, namely was not deviated by the presence of cyanate in the sample. To do this, various alkaline standards with urea and cyanate concentrations were prepared and then analyzed to determine the corresponding NPOC values. The results, shown in Table II.2, confirmed the direct relationship between NPOC measurements and urea concentrations.

Sample	[CO(NH ₂) ₂] (mol L ⁻¹)	[CO(NH ₂) ₂] (eq g _C L ⁻¹)	[OCN ⁻] (mol L ⁻¹)	[OCN ⁻] (eq g _C L ⁻¹)	[NPOC _{result}] (g _C L ⁻¹)
#1	0.3	3.6	0	0	3.6 ± 0.2
#2	0.2	2.4	0.1	1.2	2.4 ± 0.2
#3	0.1	1.2	0.2	2.4	1.2 ± 0.2
#4	0	0	0.3	3.6	0.12

Table II.2 – Evidence of the direct relationship between NPOC measurements and urea concentrations.

Finally, measuring NPOC enabled efficient quantification of urea in alkaline media without the need for extensive sample preparation (as required with enzymatic assays). However, in the case of real matrices where many other carbonaceous organic molecules can be found, this technique becomes inadequate. The coupling of Ion Chromatography (IC) (that was already present in the lab-scale at the beginning of the thesis), with the mass spectroscopy (MS) (that arrived during the course of the thesis), enables to solve this problem. In fact, with a single injection, it will become possible to monitor both urea and

reaction by-products concentrations under alkaline conditions, and in both synthetic and real matrices. The following section will present the implementation of this original analysis, as never reported in the literature before.

II-3 Coupling of Ion chromatography/Conductivity Detector to Mass Spectroscopy (IC-CD/MS) for efficient monitoring of UEO process

II-3.1 Principle

Ion chromatography and mass spectroscopy are two powerful analytical techniques, frequently used separately in analytical chemistry.

IC is a form of liquid chromatography, used to separate ions and polar molecules, which principle is based on ion exchange. Indeed, ions of interest are separated according to their affinity with respect to the resin composing the chromatographic column. Ions present in the sample will thus exchange with ions of the same charge present on the column material. The degree of retention will depend on the affinity of the ions for the resin column. At the column's outlet, a detector (a Conductivity Detector (CD) in this work) is used to qualify this separation as illustrated in Figure II.9-b.

By MS the m/z of ionized molecules can be measured. It is a powerful tool for the qualitative and quantitative analysis of organic and inorganic compounds. The sample is first ionized (by a Electronic Spray Ionisation (ESI) in this work), then the ions are separated according to their m/z ratio in the mass analyzer. Finally, the ions are detected and the mass spectrum generated.

The advantages of this coupling IC-CD/MS include:

- Separation and precise identification: IC separates ions, while MS provides precise identification and quantification of these ions. This enables complete sample analysis;
- Sensitivity: MS is highly sensitive, enabling the detection of very small quantities of ions in the sample (in the picogram to femtogram range) [193];
- Analysis of polar and ionic compounds: IC-MS coupling is particularly useful for the analysis of polar and ionic compounds, which are difficult to analyze by other techniques [194];
- Wide range of applications: This method is used in many fields, including water analysis, environmental analysis, pharmaceuticals and biochemistry [195].

However, there are also disadvantages to consider:

- Cost: The equipment required is expensive (between 200,000 and 250,000 € *vs.* 85,000 for IC in 2022);
- Expertise: Interpretation of IC-MS data requires specific training and expertise;
- Maintenance: IC-MS instruments require regular servicing to ensure optimal operation.

II-3.2 Instrumentation and analytical protocols

A scheme of the system configuration for IC-CD/MS analysis is provided in Figure II.9.

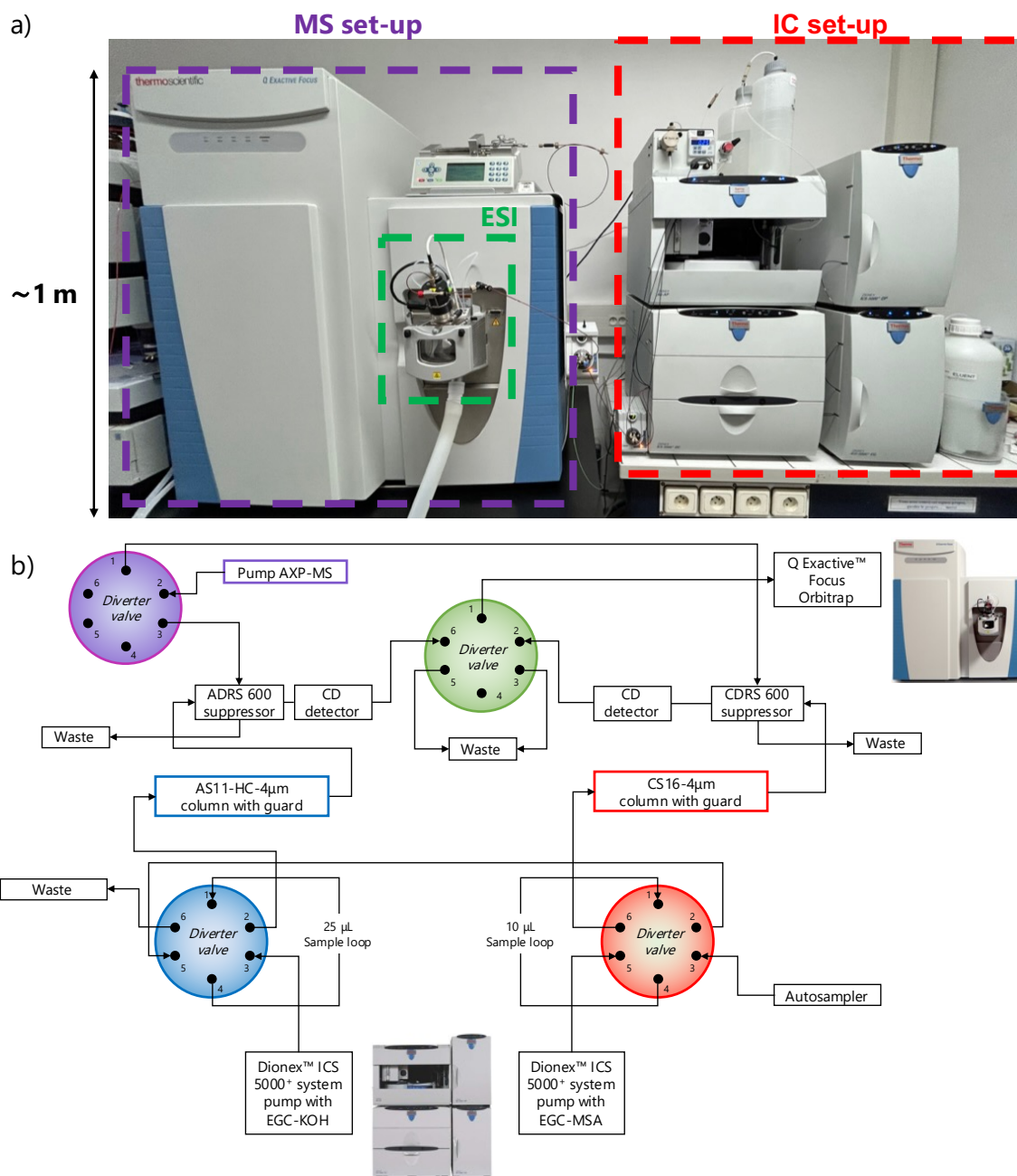


Fig. II.9 – a) Picture of the IC-CD/MS set-up and b) configuration set-up for IC-CD/MS analysis of urine.

In the following section, the analytical protocols that I developed in collaboration with *Laure Latapie* (CNRS engineer) will be detailed.

II-3.2.a Chromatography

Analyses were performed using an IC-CD system (Thermo Scientific Dionex™ ICS-5000+) equipped with a DP analytical pump, an AS-AP auto-sampler, and a DC-5 module with double oven containing (i) Dionex™ CDRS 600 and Dionex™ ADRS 600 suppressors for cation and anion detections respectively as well as (ii) two conductivity detectors (CD). A Dionex™ AXP Auxiliary Pump (water, 0.25 mL min^{-1}) was used to ensure a neutral pH

at the mass spectrometry inlet by connecting it to the relevant suppressor. The injection loop volumes were 25 μL and 10 μL , respectively for cation and anion pathways (full loop). Thermo Scientific™ Chromeleon™ Chromatography Data System software 7.2.10 was used for IC control and data processing. An IonPac CS16-4 μm analytical column (2 mm \times 250 mm and its guard CG16 2 mm \times 50 mm) from Thermo Scientific™ was used for cation separation. The cationic eluent (Methane Sulfonic Acid (MSA)) was generated at a flow rate of 0.16 mL min^{-1} by using a Thermo Scientific™ Dionex™ EGC 500 MSA Eluent Generator Cartridge. The column temperature was 40 °C. An IonPac AS11-HC-4 μm analytical column (2 mm \times 250 mm and its guard AG11 2 mm \times 50 mm)) from Thermo Scientific was used for anion separation. The anionic eluent (KOH) was generated at a flow rate of 0.25 mL min^{-1} by using a Thermo Scientific™ Dionex™ EGC III 500 KOH Potassium Hydroxide Eluent Generator Cartridge. The column temperature was 25 °C. Both eluent concentration profiles are provided in Figure II.10. The overall run time was 35 min.

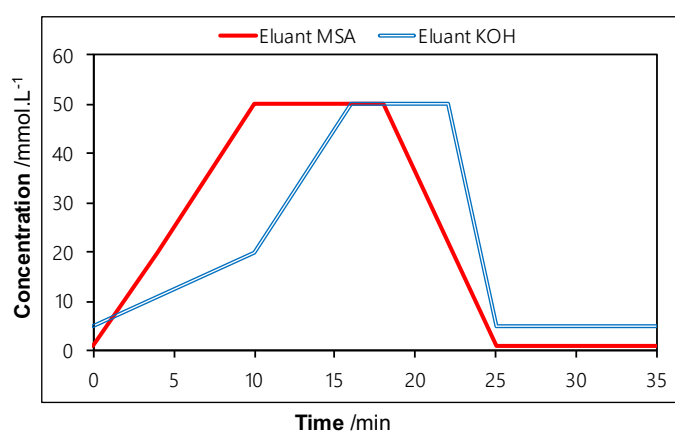


Fig. II.10 – Concentration gradient of anionic (KOH) and cationic (MSA) eluents for an optimal ionic separation.

II-3.2.b Mass spectroscopy

The IC system was coupled to a high-resolution (*i.e.*, high mass accuracy measurements with four-decimal precision) mass spectroscopy analyzer Orbitrap (Thermo Scientific Q Exactive™ Focus). Thermo Scientific™ Q Exactive™ Plus software 2.11 was employed for MS control and data processing proceeded by Thermo Scientific™ Chromeleon™ Chromatography Data System software 7.2.10 and Thermo Scientific™ Xcalibur™ software. MS was performed using the full-scan method in the negative mode (0-35 min, m/z 50-500) and positive mode (0-35 min, m/z 50-500) using a heated ESI source. Concerning the negative mode, the optimal parameters were set as follows: sheath gas flow rate (nitrogen) set to 40 Arbitrary Unit (*a.u.*); auxiliary gas flow rate (nitrogen) set to 20 *a.u.*; spray voltage, 3.5 kV; capillary temperature, 300 °C; S-lens RF level, 60; auxiliary gas heater temperature, 450 °C. Concerning the positive mode, the optimal parameters were set as follows: sheath gas flow rate (nitrogen) set to 30 *a.u.*; auxiliary gas flow rate (nitrogen) set to 10 *a.u.*; spray voltage, 4.5 kV; capillary temperature, 300 °C; S-lens RF level, 60; auxiliary gas heater temperature, 320 °C.

II-3.3 Application to urea solutions

This section will present the “raw” results obtained from various injections into the IC-CD/MS system. The related samples were obtained during potentiostatic electrolysis of

urea solutions in KOH 1 mol L⁻¹.

An identical approach, together with a characterization study (accuracy, repeatability, matrix effect, etc.) was also carried out in the case of the real urine matrix. This work leads to a research paper in the journal *Analytical and Bioanalytical Chemistry*, as presented in Appendix D [196].

To avoid saturating the signal, sample dilution was necessary. In the case of this thesis, the electrolyses were performed in conditions as close as possible to the real matrix, the electrolysis medium was thus concentrated. All samples were therefore diluted 1000-fold before injection into the IC-CD/MS.

As a first step, it was necessary to identify all the peaks observed, which was done by combining standard injection and bibliographic researches. The various ions identified were then classified according to the following categories:

Spectator ions: sodium, potassium, magnesium and calcium;

Anions: chloride, nitrite, cyanate, carbonate, sulfate and phosphate;

Cations: ammonium.

Typical chromatograms obtained by injecting mixed-standard solutions are shown in Figure II.11, as well as the related calibration curves. Peak area versus concentration is related by Kohlrausch's law, shown in Eq. II.3, demonstrating the linear nature of the calibration curves. In the case shown in Figure II.11, the wide concentration range induces a quadratic profile of the curves. This behavior is common in IC.

$$\sigma = \sum_i |z_i| \times \lambda_i \times C_i \quad (\text{II.3})$$

where σ is the ionic conductivity (Ωm), z_i is the charge of the ion i (dimensionless), λ_i is the molar conductivity of the ion i ($\text{S m}^{-2} \text{mol}^{-1}$), and C_i is the concentration of the ion i (mol m^{-3}).

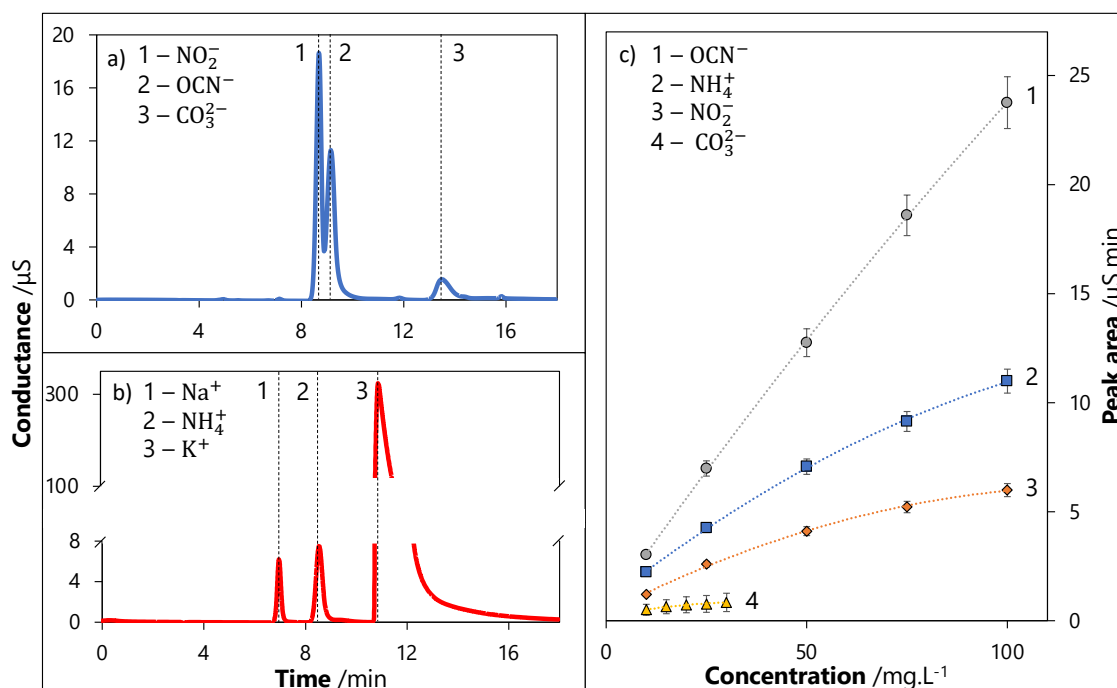


Fig. II.11 – Typical a) anionic and b) cationic chromatographs obtained during urea electrolysis experiment, and c) calibration curves for the major by-products formed during urea electrolysis.

Once analyzed by the CD detector, the sample was then directly conducted to the MS system. Typical chromatogram obtained and calibration curve are shown in Figure II.12 for urea.

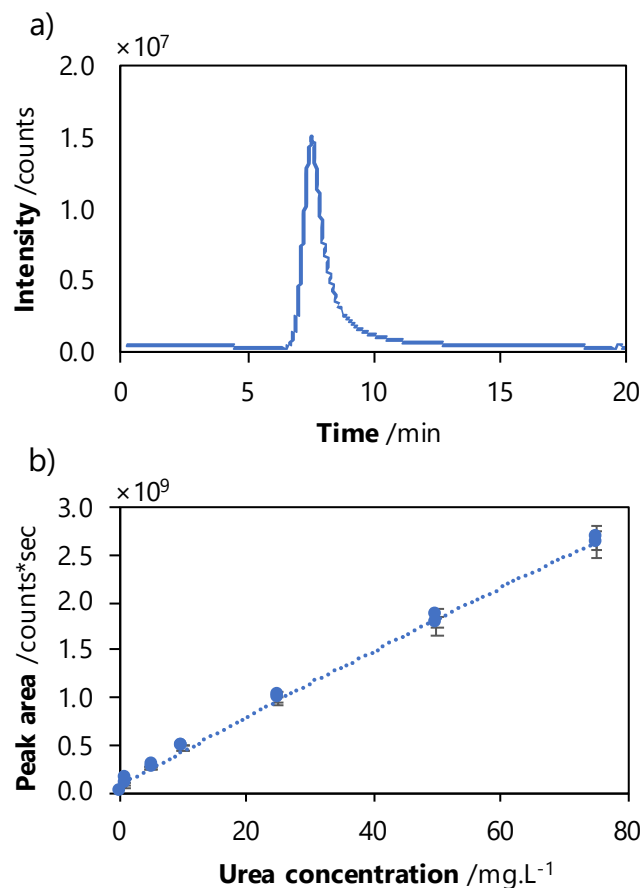


Fig. II.12 – Typical a) MS-chromatogram and b) calibration curve, obtained for urea.

During an electrolysis experiment, samples were taken after different times. Typical chromatograms are plotted in Figure II.13. They show an increase in the signal for nitrite, cyanate, carbonate and ammonium with a concomitant decrease of the urea's signal as far as this molecule was converted.

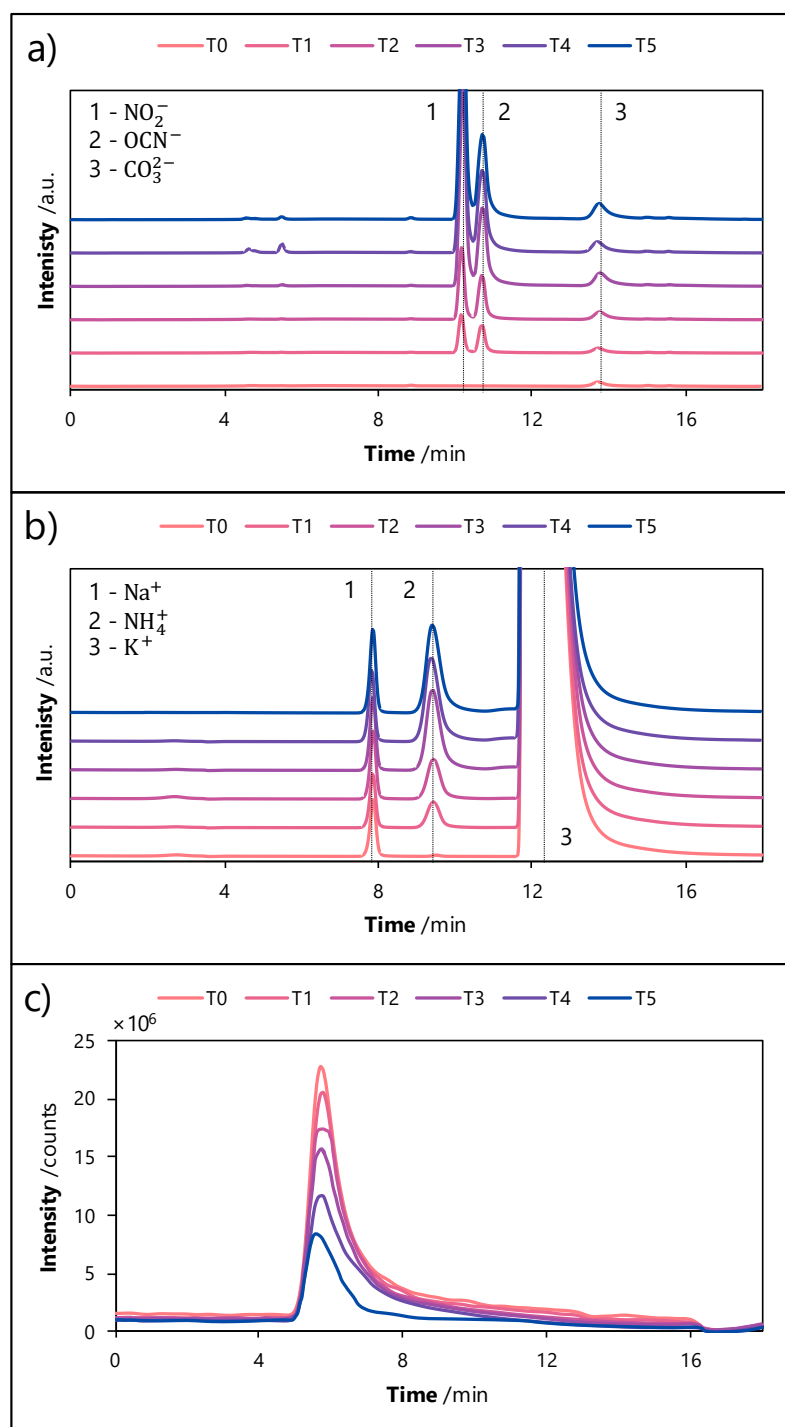


Fig. II.13 – Typical variation of the IC-CD/MS signal as a function of the electrolysis's time concerning a) anionic by-products, b) cationic by-products and c) urea.

As a consequence, the IC-CD/MS technique that we developed enables, with a single injection and in 35 min, to measure concentration of liquid-phase compounds present in an electrolysis sample. In order to obtain a complete mass balance, it was also necessary to develop a GC method for monitoring the gaseous compounds formed during the UEO process. This is the objective of the next section. The coupling of IC-CD/MS and GC was

only obtained at the end of the thesis, and the results in **Chapter V** were the only ones to present mass balances for both phases.

II-4 Gas chromatography

II-4.1 Principle

GC is a widely used technique for separating and analyzing the components in a gas mixture. The principle is based on the differential partitioning of components between a stationary and a mobile phase. The main elements of this technique are summarised below:

Mobile phase: An inert gas, usually helium, nitrogen or argon, is used as mobile phase.

The components of the mixture to be analyzed are transported by this gas through a column.

Stationary phase: The column, usually made of stainless steel or glass, is filled with a high-surface-area material coated with the stationary phase, often a liquid at high vaporization temperature. The interactions between this stationary phase and the components of the mixture will determine the rate at which each component elutes through the column.

Separation: It depends on the differential affinity of the molecules for the stationary and mobile phases. The compounds that are strongly interacting with the stationary phase will spend more time in the column and are therefore eluted (*i.e.*, removed from the column) later than those with weak interactions. The order of elution of the compounds (*i.e.*, the order in which they leave the column) is generally a function of the compound volatility. More volatile compounds (*i.e.*, those with a low boiling temperature) have small interactions with the stationary phase and thus are eluted first, while poor volatile compounds (*i.e.*, those with a higher boiling temperature) are eluted later.

Detector: After passing through the column, each component arrives at the detector, often a Thermal Conductivity Detector (TCD). The TCD measures the difference in thermal conductivity between the inert gas and the gas containing the components to be detected. As each compound has a different thermal conductivity, the detector can identify and quantify the components in the mixture.

It is important to note that this technique requires the components to be analyzed to be volatile, or to be rendered volatile without decomposition. It is therefore particularly well suited to the analysis of gases and volatile compounds (hydrocarbons, alcohols, ethers).

II-4.2 Instrumentation and analytical protocols

A Varian 450-GC GC, illustrated in Figure II.14-a was used to quantify the composition of the gas phase during the UEO process (Haysep N 80/100 Mesh, Haysep Q 80/100, Molsieve 13X, oven temperature 50 °C, TCD, carrier gas Ar, injector temperature 140 °C and TCD temperature 200 °C).

The internal diagram of the GC is shown on Figure II.14-b. Using a pneumatic valve, the system enabled semi-continuous analysis of the gas phase in the EC reactor:

Fill mode: at this stage, an injection loop (250 μL) was continuously swept by the sample gas and the carrier gas passed through the GC system without passing through this loop;

Injecting mode: once the V-1 valve was turned, the carrier gas flowed in the opposite direction in the injection loop, carrying a fixed volume of sample gas with it to the column, and the analysis has begun. The valve could then be returned to its initial position, and the injection loop was again continuously swept by sample gas.

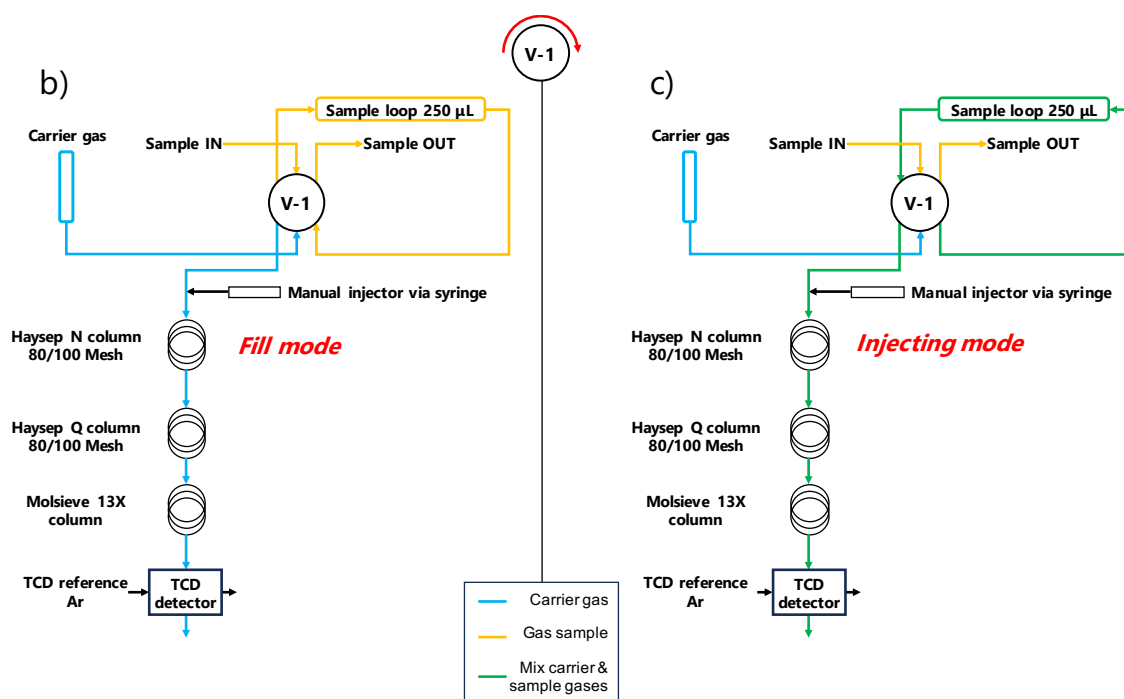
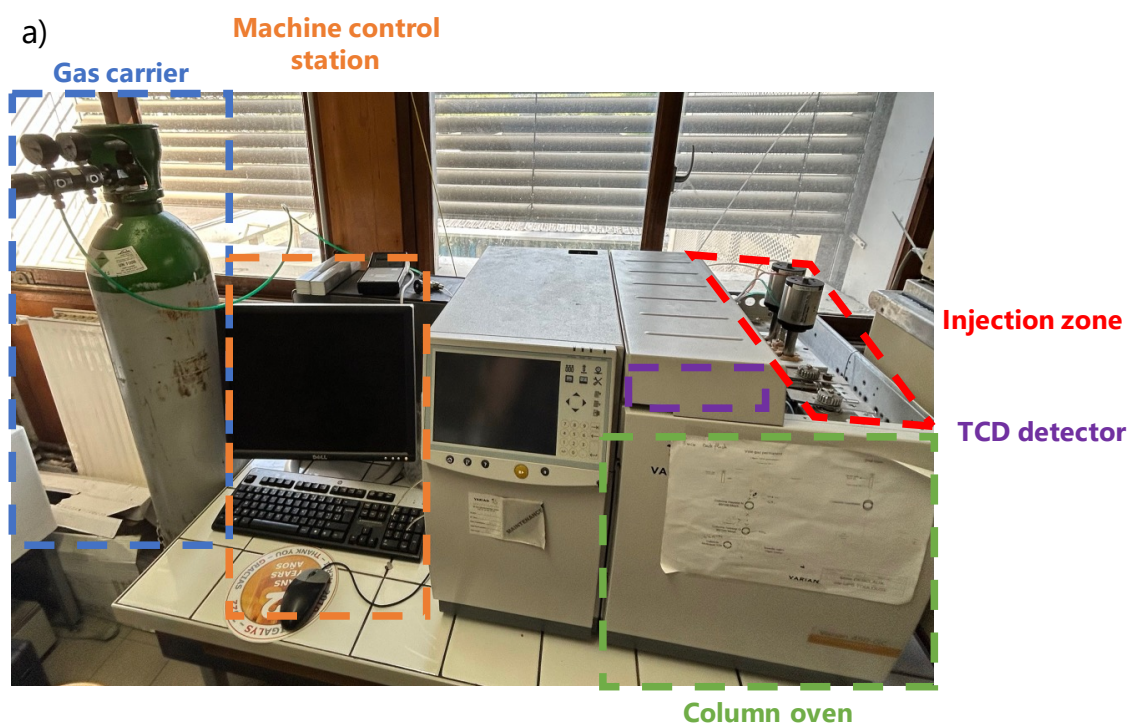


Fig. II.14 – a) Illustration of the GC system used to analyze the gas mixture obtained during electrolysis. Schemes of the analytical set-up during b) fill mode and c) injecting mode.

II-4.3 Application to urea solutions

An initial test is carried out to analyze and qualify the gas phase produced in the reactor. Three main peaks are identified: N_2 , O_2 and H_2 . Typical chromatograms and calibration curves are presented in II.15. The calibration curves were obtained by mixing ambient air with pure H_2 at different volumes in a syringe (with a Teflon[®] plunger) and presented in Eqs. II.4-II.6.

$$\text{Peak area}_{N_2} = 879.0 \times V_{N_2} \text{ with } T_r = 2.4 \text{ min} \ \& \ R^2 = 0.998 \quad (\text{II.4})$$

$$\text{Peak area}_{O_2} = 1,241.1 \times V_{O_2} \text{ with } T_r = 1.8 \text{ min} \ \& \ R^2 = 0.997 \quad (\text{II.5})$$

$$\text{Peak area}_{H_2} = 9,849.2 \times V_{H_2} \text{ with } T_r = 1.2 \text{ min} \ \& \ R^2 = 0.991 \quad (\text{II.6})$$

where Peak area_i is the peak area obtained by GC analysis ($\mu\text{V min}$), T_r is the retention time (min) in the GC and V_i is the injected volume at atmospheric pressure of the compound i (μL).

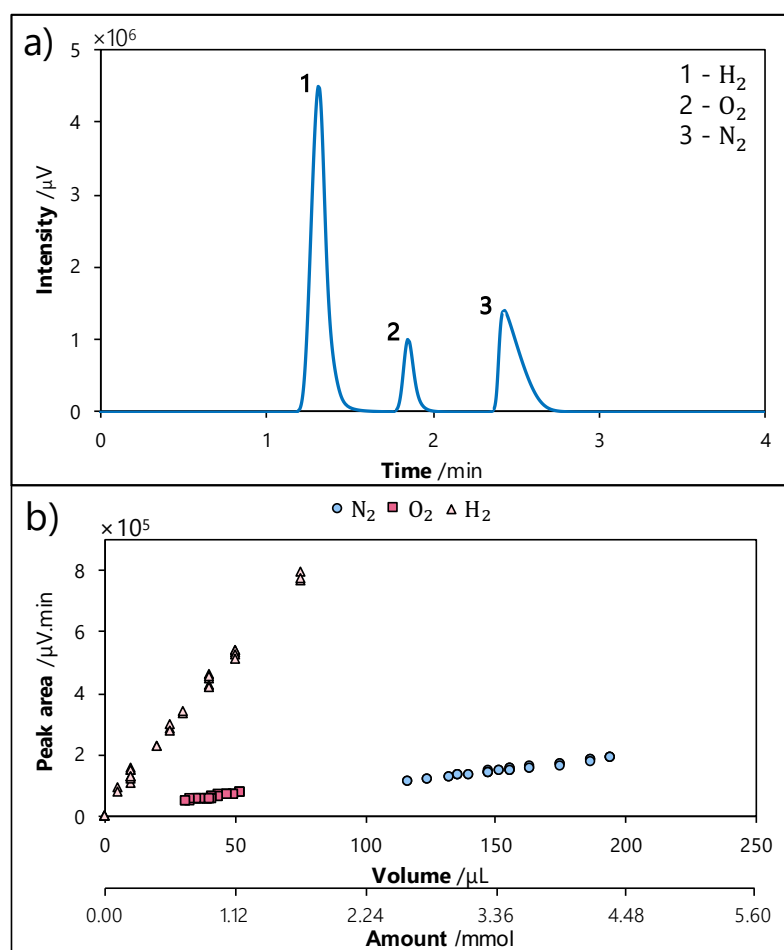


Fig. II.15 – a) Typical GC chromatogram obtained when analyzing mixed gases containing N_2 , H_2 and O_2 , as typically observed during some potentiostatic electrolysis (0.55 V vs. Hg/HgO) of urea solution in alkaline medium, and b) calibration curves for N_2 , O_2 and H_2 .

When running an electrolysis experiment, discrete values for the gas phase composition ($v_{i,t}$ in $\mu\text{L min}^{-1}$) were typically measured, as shown in Figure II.16, with an uncertainty of 5% when the same sample is introduced several times. In order to carry out a mass balance, the cumulative quantity of the compounds produced ($V_{i, \text{ after } j \text{ min}}$ in μL) should

be determined, using Eq. II.7.

$$V_{i, \text{ after } j \text{ min}} = \int_0^t v_{i, t} \times dt \quad (\text{II.7})$$

Before starting an electrolysis experiment, it was carefully checked that the EC cells were sufficiently purged using argon bubbling to ensure that no N_2 nor O_2 remained from leaks (and dead areas). For lab-scale cells, consistent bubbling was applied for 1 hour. In the case of the pilot, a minimum of 2 h of bubbling was required to avoid any variation in the peak area of N_2 and O_2 .

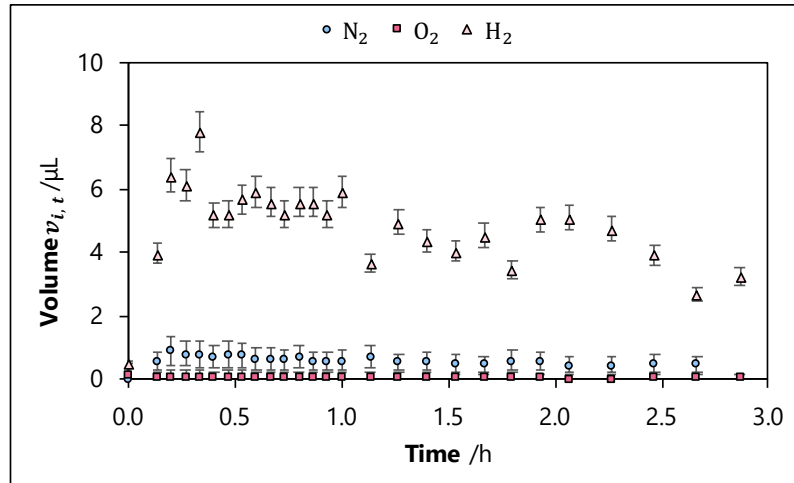


Fig. II.16 – Typical discrete value of gas volumes formed during a urea electrolysis experiment.

The predominant form of ammonia in alkaline media is NH_3 . A 24h-potentiostatic electrolysis was carried out to check whether ammonia was lost during the electrolysis or not. For that, the overhead gas was connected to a bubbler filled with hydrochloric acid so as to trap the possible gaseous NH_3 formation. Sampling of the acid solution before and after electrolysis was then analyzed by IC. It was observed that no increase in ammonium existed, thus confirming that all the ammonia formed remained dissolved in the solution. In addition, observed in the work of Tatarchuk et al. [146], no traces of N_2O or CO were observed in our case.

II-5 General operating procedure of the electrolysis at lab-scale

To summarise this chapter, Figure II.17 presents a flow chart showing all the steps required to perform mass balance in gas and liquid phases during potentiostatic electrolyses.

After preparing the set-up and allowing the necessary purge time to remove residual N_2 and O_2 from the ambient air, electrolysis can be started. To get a theoretical idea of the urea conversion X , presented in Eq. II.8, during electrolysis, we determine the total amount of urea to be oxidized according to Eq. II.9.

$$X(t) = \frac{[CO(NH_2)_2]^{ini} - [CO(NH_2)_2]_{(t)}}{[CO(NH_2)_2]^{ini}} \quad (\text{II.8})$$

$$n_{\text{CO}(\text{NH}_2)_2} = V_{\text{cell}} \times [\text{CO}(\text{NH}_2)_2]^{\text{ini}} \quad (\text{II.9})$$

This amount of matter can be oxidized with a number of electron, as a function of the final product (*i.e.*, 6 for N_2 and NH_3). In our case, the theoretical charge, $Q_{\text{theoretical}}$ is estimated each time by the oxidation conversion of urea when it produces N_2 (*i.e.*, 6 electrons, and if the FE is equal to 100% for the UEO), as shown in the Eq. II.10.

$$Q_{\text{theoretical}} = 6 \times \mathcal{F} \times n_{\text{CO}(\text{NH}_2)_2} \quad (\text{II.10})$$

Thus, the ratio of theoretical and actual charges supplied to the system can be used to estimate the urea-X, as depicted in Eq. II.11.

$$X = \frac{Q_{\text{supplied},(t)}}{Q_{\text{theoretical}}} \quad (\text{II.11})$$

where Q_{supplied} was directly calculated by the software of the potentiostat as the integral of the current over time (C).

In order to monitor this conversion rate analytically, various aliquots of the liquid phase were collected over time (approximately 0.5 mL in the case of the lab-scale cell, and 1-2 mL in the case of the pilot-scale cell).

In order to carry out complete N-mass balances, it was also necessary to calculate the number of equivalent moles released by each N-molecule, as illustrated in Eq. II.12.

$$\begin{aligned} n_{\text{CO}(\text{NH}_2)_2, \text{ eq. N}} &= 2 \times n_{\text{CO}(\text{NH}_2)_2} \\ n_{\text{N}_2, \text{ eq. N}} &= 2 \times n_{\text{N}_2} \\ n_{\text{NH}_3, \text{ eq. N}} &= n_{\text{NH}_3} \\ n_{\text{OCN}^-, \text{ eq. N}} &= n_{\text{OCN}^-} \\ n_{\text{NO}_2^-, \text{ eq. N}} &= n_{\text{NO}_2^-} \end{aligned} \quad (\text{II.12})$$

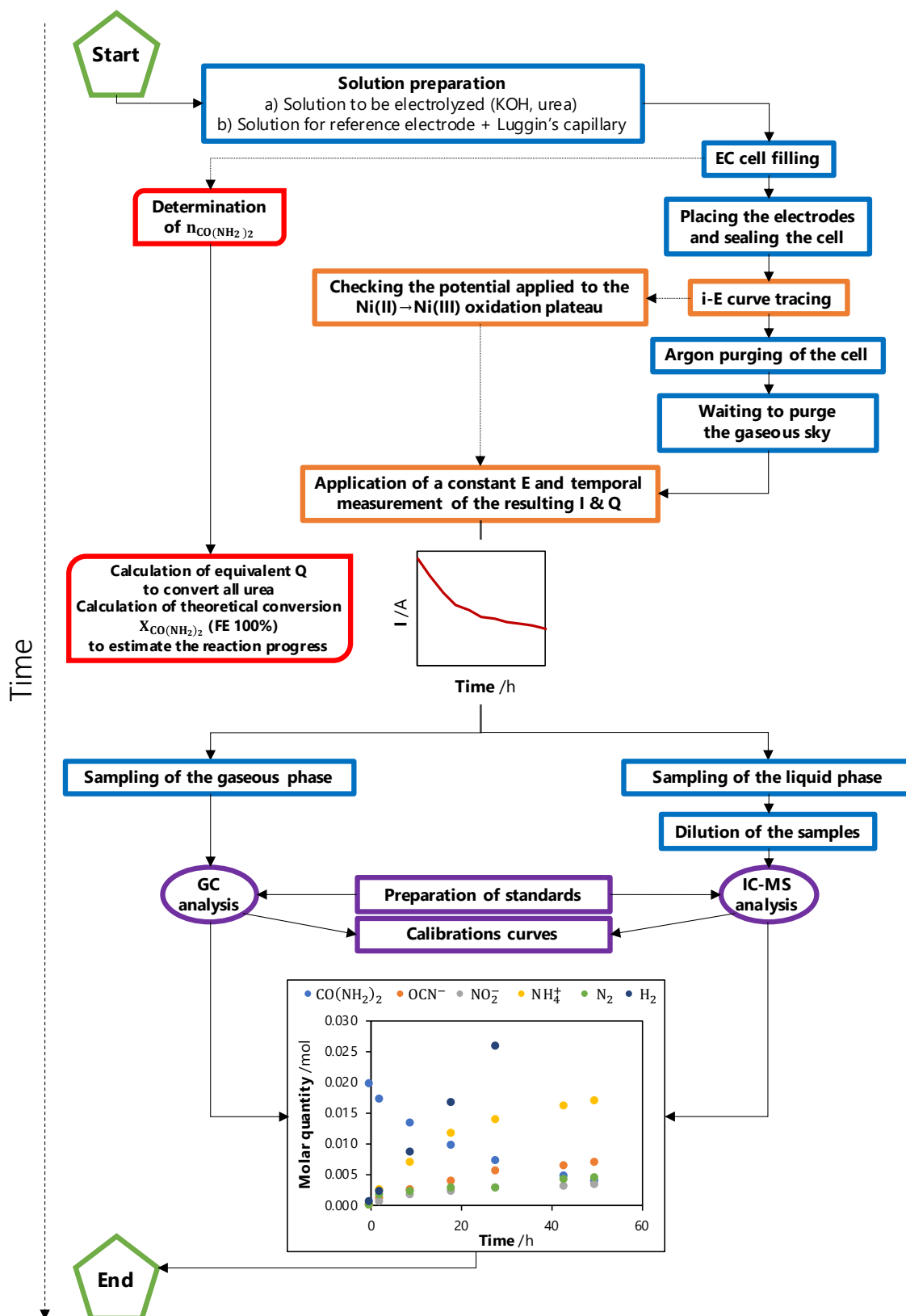


Fig. II.17 – Schematic flow chart summarizing the experimental procedure for carrying out potentiostatic electrolysis with urea solutions and for sample's processing to perform mass balances (green: start/end; blue: experimental set-up; red: calculation; orange: data processing; violet: analytical techniques).

Study at lab-scale of the urea oxidation by electro-mediation of nickel(III)/nickel(II) system in alkaline media

Outline of the current chapter

III-1	Introduction	72
III-2	Effect of the operating parameters on UEO at lab-scale	72
III-2.1	Effect of urea concentration on overall rate of the indirect electro-oxidation	73
III-2.2	Effect of the scan rate as a tool for revealing the limitation of the HCR on the ER	75
III-2.3	Effect of the alkalinity on overall rate of the indirect electro-oxidation	79
III-2.4	Effect of temperature on chemico-physical properties affecting the global process (ER/HCR) as well as the mass transfert phenomena	83
III-2.5	Influence of nickel electrode angular velocity on mass transport processes	88
III-3	Mass balances at lab-scale and effect of process parameters	89
III-3.1	Identification of the electro-generated adducts and mass balance on carbon and nitrogen elements	89
III-3.2	Influence of the presence (or not) of the ionic separator (undivided cell vs divided cell)	91
III-3.3	Influence of the alkalinity	93
III-3.4	Influence of the temperature	95
III-4	Conclusion of Chapter 3	98

This chapter presents the results obtained from the article “G. Hopsort*, D. Pereira Do Carmo, L. Latapie, K. Loubière, K. Groenen Serrano, T. Tzedakis* (2023). Progress toward a better understanding of the urea oxidation by electromediation of nickel(III)/nickel(II) system in alkaline media. *Electrochimica Acta*, 442. [10.1016/j.electa.2023.141898](https://doi.org/10.1016/j.electa.2023.141898)”.

Consequently, to maintain consistency, the introduction have been rewritten and the material and methods section removed as already described in **Chapter II**.

III-1 Introduction

This Chapter aims at investigating the treatment of urea by electro-oxidation on nickel(III)/nickel(II) system in alkaline medium. The main objective is to get a better understanding of the EC mechanisms and kinetics of the oxidation of the urea by the electromediation of the system NiOOH/Ni(OH)₂. For that, this work is going:

- (i) to introduce the turn over number and determine the activation energies (chemical reaction and mass transport). In addition, the EC characteristics of the NiOOH/Ni(OH)₂ system (heterogeneous electron transfer rate constant and anodic charge transfer coefficient) were evaluated, which is not done in the existing literature;
- (ii) to carry out lab-scale electrolysis exhibiting high (>80%) urea conversion on massive nickel electrode, and consequently;
- (iii) to open new analytical roads to detect the whole electro-generated products in liquid phase and to perform the corresponding mass balances.

By this way, it is expected to validate the process at the lab-scale (70 cm³ of urea) which constitutes a preliminary step before designing a urea EC process operating at larger scale.

For this purpose, three experimental set-ups (described in **Chapter II**) are implemented for the EC kinetic study and lab-scale electrolysis using both undivided and divided EC cell. The set of analytical techniques (IC and TOC), presented in section II-2.2, is used to identify the products electro-generated, determine their concentration and the urea conversion.

Firstly, a characterization of the studied EC system is presented through voltammetry experiments; the influence of the potential scan rate, the concentration of reactants and rotational speed is particularly studied. Secondly, lab-scale electrolysis, for which complete mass balances are systematically established, are performed. In these experiments, a special attention is paid for varying the concentrations of urea and KOH in a large range, as well as the temperature and of the presence of a membrane separator.

III-2 Effect of the operating parameters on electrokinetics for the characterization of the coupling ER to HCR

In this section, the involved EC system is characterized through voltammogram experiments. The influence of the scan rate, the concentration of reactants, temperature and agitation speed on the overall rate of the UEO is studied, expecting to elucidate the mechanism of the process.

III-2.1 Effect of urea concentration on overall rate of the indirect electro-oxidation

The effect of the urea concentration on the rate of the overall process is examined by plotting voltammograms on nickel RDE, in 1 mol L^{-1} KOH solutions at a scan rate of 1.36 mV s^{-1} . Figure III.1 shows the obtained voltammograms for urea concentrations ranging from 0 to 0.33 mol L^{-1} .

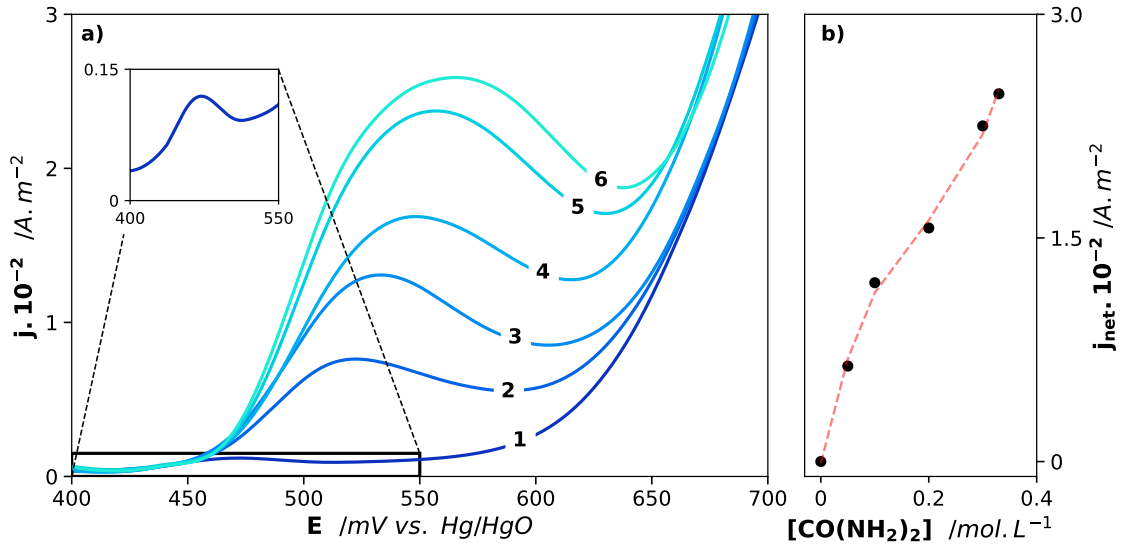
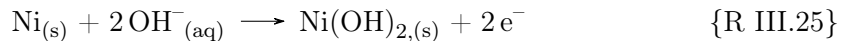


Fig. III.1 – Effect of the urea concentration a) on the shape of voltammograms obtained on nickel RDE without agitation. $[\text{KOH}] = 1 \text{ mol L}^{-1}$; $\nu = 1.36 \text{ mV s}^{-1}$; $T = 298 \text{ K}$, $S_{\text{anode}} = 3.14 \text{ mm}^2$. The urea concentration used was 0 mol L^{-1} (1), 0.05 mol L^{-1} (2), 0.1 mol L^{-1} (3), 0.2 mol L^{-1} (4), 0.3 mol L^{-1} (5) and 0.33 mol L^{-1} (6). b) shows the variation of the current magnitude of the oxidation peak as a function of the urea concentration.

Curve **1** (without urea), obtained on a nickel RDE freshly polished, exhibits a signal showing a peak at around 470 mV . According to Seghioeur et al. [197], this peak corresponds to the oxidation of nickel(II) to nickel(III) following the reaction {R I.19}. The oxidation of nickel(0) into nickel(II), as {R III.25} occurs theoretically at potentials close to -800 mV [197].



Note that this signal peak at around 470 mV is attributed [198] to the reaction {R I.19}. For higher potentials ($> 600 \text{ mV}$), the solvent oxidation to oxygen occurs. If the nickel oxidation signal is observed at such high potentials (400 mV), this means that, immediately after polishing, the nickel surface is spontaneously oxidized by the oxygen of the air, and that the nickel is covered by some oxides. Consequently, the observation can be translated by the {R III.26}.



Curves **2** to **6**, obtained when urea was added at various concentrations into the electrolyte, exhibit peaks shifting to the anodic potentials as the urea concentration increases, while the solvent oxidation potential does not seem to be affected. Note that the KOH

concentration (1 mol L^{-1}) is three times more concentrated than the highest concentration of urea used (0.33 mol L^{-1}). The variation of this peak current (from which the blank have been subtracted at each potential) *vs.* the urea concentration, plotted in the Figure III.1, does not show a linear behavior, meaning that the observed signal may not be attributed to a single direct oxidation of urea as already demonstrated [142] for urea concentration higher than 0.33 mol L^{-1} . Consequently, a catalytic process occurs at the electrode: urea is oxidized chemically by the nickel peroxide at the electrode surface and gives products while regenerating $\text{Ni}(\text{OH})_2$. In order to get a better understanding of the overall process, the oxidation of urea by the electromediation of the system $\text{NiOOH}/\text{Ni}(\text{OH})_2$ in alkaline medium consisted of an indirect or two-step mechanism, could be schematically [199] represented, according to Figure III.2.

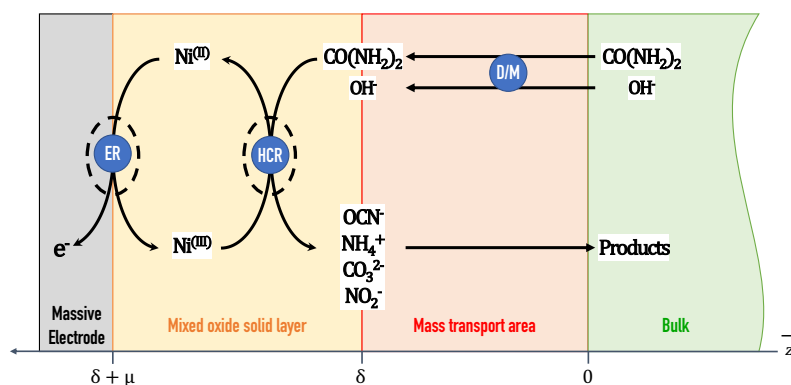
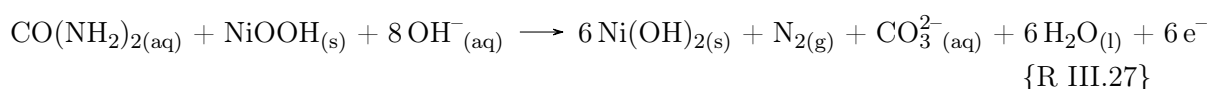


Fig. III.2 – Schematic representation of the indirect oxidation of the urea, by the electromediation of the system $\text{NiOOH}/\text{Ni}(\text{OH})_2$ operating on the surface of a massive nickel anode, and in presence of alkaline medium. ER, HCR, and D/M indicate respectively the locations where the NiOOH Electro-generation Reaction (ER), the Heterogeneous Chemical Reaction (HCR) and the mass transport (limited by the diffusion) occur.

Various phenomena occur during the UEO on a massive nickel anode and their locations depend to the distance from the massive electrode (*i.e.*, z -axis dependent):

- at $z = \delta + \mu$: the massive Ni surface is oxidized to successively form $\text{Ni}(\text{OH})_2$ and NiOOH by the ER;
- in $\delta + \mu < z < \delta$ area: corresponds to the thickness of the catalytic system $\text{NiOOH}/\text{Ni}(\text{OH})_2$ (solid layer), in which the HCR is assumed to occur;
- in $\delta < z < 0$ area: corresponds to the layer in which external mass transfer limitations exist for urea (and eventually KOH); [200]
- at $0 \geq z$: corresponds to the bulk (none reaction occurs).

After the “first spontaneous” oxidation of metallic Ni and the electro-generation of NiOOH , three phenomena are expected to occur: an ER involving insoluble oxides ($\{\text{R I.19}\}$), HCR occurring into the solid layer of NiOOH ($\{\text{R III.27}\}$), and as function of the operating conditions, a mass transfer process (diffusion and migration according to Eq. (III.1)).



$$\begin{cases} \frac{\partial[\text{CO}(\text{NH}_2)_2]}{\partial t} + \nabla \cdot \mathbf{j}_{\text{D,CO}(\text{NH}_2)_2} = 0 \\ \frac{\partial[\text{OH}^-]}{\partial t} + \nabla \cdot (\mathbf{j}_{\text{D,OH}^-} + \mathbf{j}_{\text{M,OH}^-}) = 0 \end{cases} \quad (\text{III.1})$$

Where j_i is the molar flux (diffusion or migration) of the species i ($\text{mol m}^{-2} \text{s}^{-1}$). Each elementary process being dependent of the other, it is therefore important to understand how a given operating parameter could impact each of them. In alkaline medium, note that the {R III.27} represents the global equation, namely the one corresponding to a complete mineralisation of urea involving $6 e^-$ and produce carbonates.

III-2.2 Effect of the scan rate as a tool for revealing the limitation of the HCR on the ER

To confirm previous assumptions and validate the overall process schema reported Figure III.2, the effect of the scan rate, is examined in the cases of the blank (NiOOH/KOH, Figure III.3-a) and an alkaline solution of urea (NiOOH/KOH/Urea, Figure III.3-b).

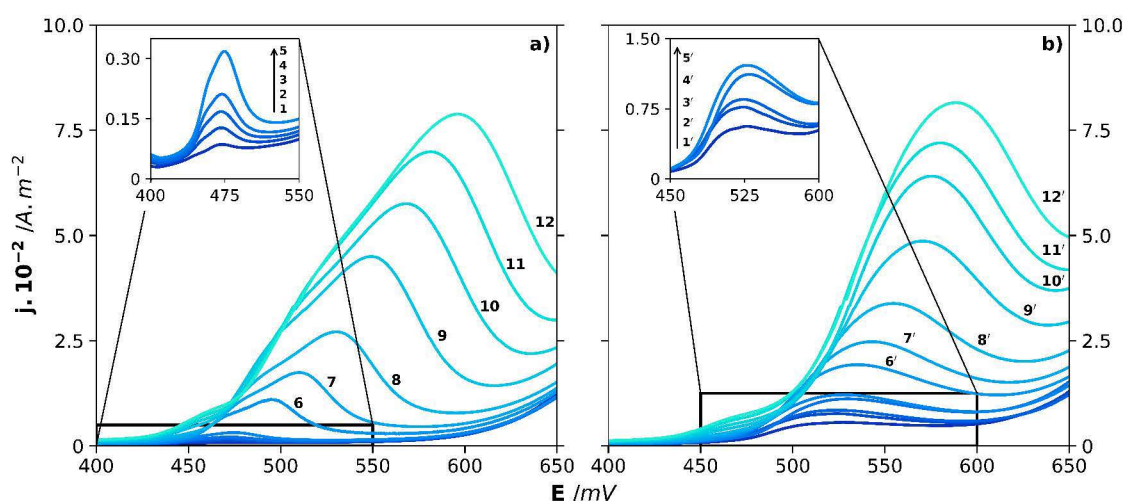


Fig. III.3 – Effect of potential scan rate on the voltammograms obtained without agitation on nickel RDE immersed into a) in 1 mol L^{-1} KOH solution and b) in 1 mol L^{-1} KOH containing 0.05 mol L^{-1} of urea. The scan rate used was 0.58 mV s^{-1} (1-1'), 1.36 mV s^{-1} (2-2'), 2.16 mV s^{-1} (3-3'), 2.91 mV s^{-1} (4-4'), 5 mV s^{-1} (5-5'), 25 mV s^{-1} (6-6'), 50 mV s^{-1} (7-7'), 100 mV s^{-1} (8-8'), 200 mV s^{-1} (9-9'), 300 mV s^{-1} (10-10'), 400 mV s^{-1} (11-11') and 500 mV s^{-1} (12-12'). The insets show a zoom in the oxidation peaks at low potential scan rate.

Regarding the voltammogram obtained in a KOH solution without urea (Figure III.3-a), a complex signal is observed containing two shoulders and one peak respectively, at about 460 mV , 475 to 525 mV and, 480 to 600 mV depending on the potential scan rate. The initial surface of the Ni, even polished, appears to be partially oxidized and the oxidation of the various intermediates ({R III.26}) could be responsible of the observed shoulders. Whatever the oxidation state of the surface, the final product is nickel(III). Moreover, the main peak is attributed to the oxidation of the nickel(II) to nickel(III). Conversely, resolute peaks are observed on the curves obtained with urea (Figure III.3-b). It seems that, as reacting with nickel peroxide and thus regenerating the reagent $\text{Ni}(\text{OH})_2$, urea allows to obtain only one predominant redox system.

As showed by the {R I.19}, $\text{Ni}(\text{OH})_2$ oxidation requires a hydroxide ion. As a result, the quasi-cancellation of the current density for potentials ranging from 600 to 650 mV

depending on the scan rate, could also be caused by the complete coverage of the anode surface by NiOOH, as already mentioned in various works [201, 202]. Note that in both cases (Figure III.3-a and b) at the end of the signal, the current decreases, meaning that mass transfer limitation exists. As the electrode reaction requires hydroxide ions, one could assume that the OH⁻ diffusion causes the current decrease. Besides, both the current and the potential of the peaks (Figure III.3-a and b) increase as the potential scan rate increases.

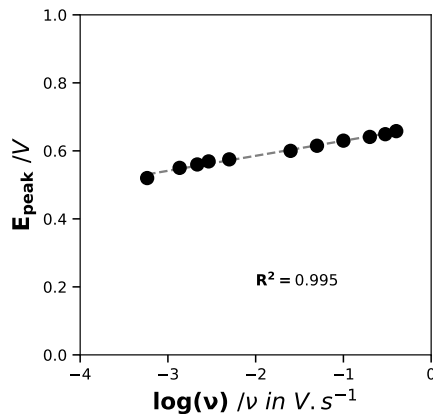


Fig. III.4 – Evolution of the anodic peak potential against the logarithm of the potential scan rate.

Regarding the variation of peak potentials as function of the logarithmic variation of the potential scan rate, illustrated in the Figure III.4, in the case of the NiOOH/urea system, extracted from Figure III.3-b, a linear variation (Eq. III.2, $R^2 = 0.995$) was observed between the potential of the anodic peak and the logarithm of the potential scan rate.

$$E_{\text{peak}} = 0.04 \times \log(\nu_{\text{scan}}) + 0.60 \quad (\text{III.2})$$

The variation of the potential against the potential scan rate is relatively low and the obtained slope (0.04) is ten times lower than the theoretical value (0.5), meaning that the corresponding NiOOH/Ni(OH)₂ system is slightly irreversible. The variation of the current magnitude of the peak as a function of the potential scan rate, shown in Figure III.5 is linear for scan rates higher than 100 mV s⁻¹ with a mean slope of 4×10^{-3} . This behavior could characterize an EC reaction of (i) adsorbed species on the anode surface or (ii) a thin layer of an electroactive species. Here, the system NiOOH/Ni(OH)₂ is considered to be two adsorbed species at the nickel surface. Consequently, this demonstrates that at high scan rates the EC reaction (Ni(OH)₂ → NiOOH) is the limiting step of the overall process of the urea indirect electro-oxidation.

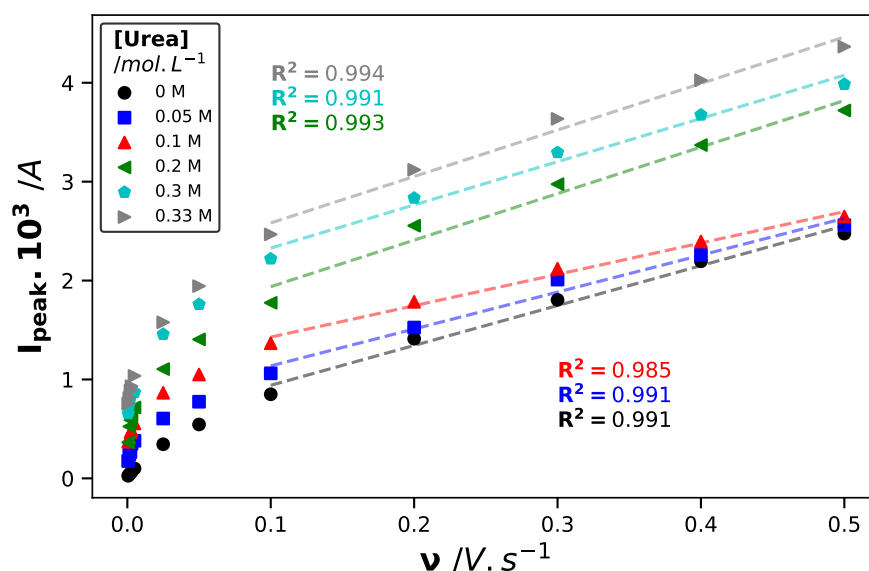


Fig. III.5 – Evolution of the current magnitude of anodic peak against the potential scan rate.

The effect of the potential scan rate is also studied for various KOH concentrations as well as urea, in order to get a better highlight of the overall process, *i.e.*, the HCR coupled to the ER. The influence of the potential scan rate on the peak current is plotted in Figure III.6, for the various concentrations of reagents (voltammograms are not illustrated here). For a ‘simple’ EC reaction, the normalized peak current by the square root of the potential scan rate, $\frac{I_{peak}}{\sqrt{\nu}}$, is expected to be constant against the square root of the potential scan rate, $\sqrt{\nu}$ [203, 204]. In the present case, the results do not present a linear variation in the whole examined range of ν . For potential scan rates in the range of 100 to 500 mV s^{-1} , the experimental variation of $\frac{I_{peak}}{\sqrt{\nu}}$ against $\sqrt{\nu}$, can be considered as linear in agreement with the theory. This means that for high ν , the dominant process is the EC oxidation of the nickel(II) to nickel(III). Decreasing ν seems to complexify the overall process, as, at scan rates lower than 25 mV s^{-1} , the values of $\frac{I_{peak}}{\sqrt{\nu}}$ decreases with $\sqrt{\nu}$ and this phenomenon is more pronounced at higher concentrations of both KOH (Figure III.6-a) and urea (Figure III.6-b).

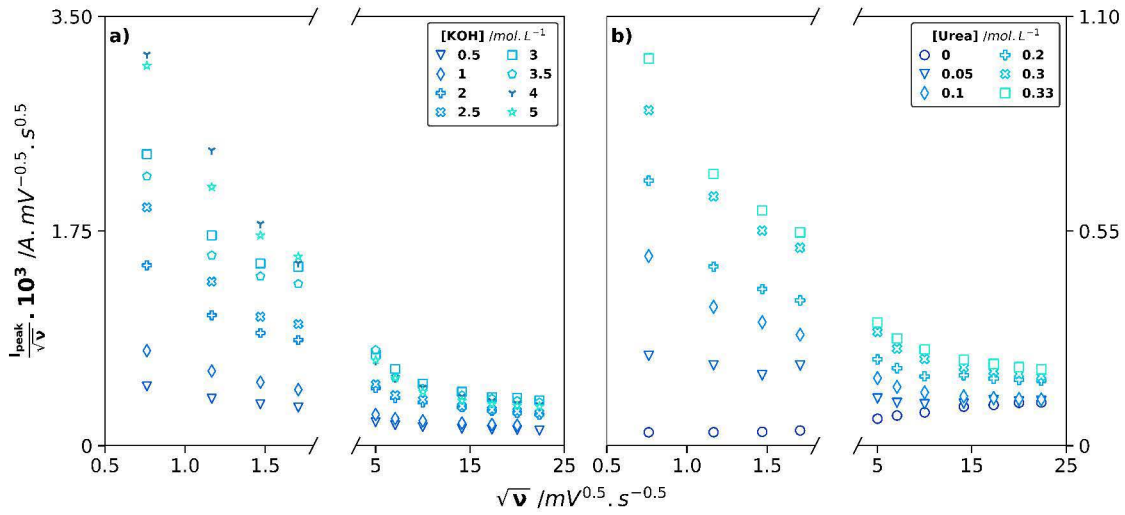
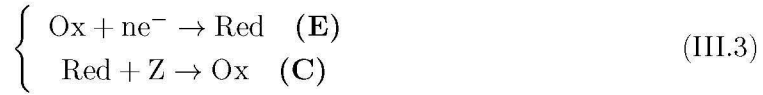
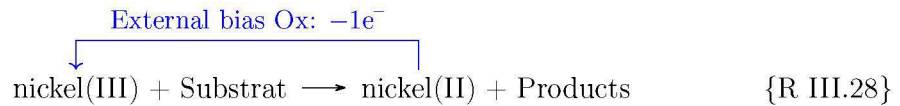


Fig. III.6 – Variations of the ratio between the current magnitude of anodic peak and \sqrt{v} at different concentrations of a) KOH in a solution of 0.33 mol L^{-1} urea and b) urea in a solution of 1 mol L^{-1} KOH. Results extracted from the current potential curves (not shown here) were plotted for various concentrations of a) KOH from 0.5 to 3 mol L^{-1} or b) urea from 0 to 0.33 mol L^{-1} .

This behavior is characteristic of an heterogeneous electron transfer followed by a chemical reaction which regenerate the reagent, thus increasing the current. Based on the work of Nicholson et Shain [205], the decrease of $\frac{I_{peak}}{\sqrt{v}}$ vs. \sqrt{v} is used as a diagnostic criterion to identify the mechanism of the reaction as an E-C catalyzed mechanism, the catalytic chemical reaction interposed between successive charge transfer following Eq. III.3.



Ohsaka et al. [206] has observed similar behavior in the study of the mechanism for the reaction of the initial stages of the electro-polymerization of 1-pyrenamine. Concerning the case of urea (Figure III.6-b), the system appears ‘simpler’. Decreasing the potential scan rate enables the HCR to occur and consequently to regenerate the $\text{Ni}(\text{OH})_2$ for starting a new catalytic cycle, following the scheme highlighted in {R III.28}. Note that in the absence of urea (*i.e.*, Figure III.6-b circles label), the slight increase of $\frac{I_{peak}}{\sqrt{v}}$ with \sqrt{v} could be attributed to a capacitive behavior of the $\text{NiOOH}/\text{Ni}(\text{OH})_2$ system.



An important parameter to characterize the nickel(III)/nickel(II) system in the presence of urea is the Turn Over Number (TON) presented in Eq. III.4.

$$\text{TON} = \frac{Q_{total}}{Q_{blank}} \quad \text{(III.4)}$$

It is defined as the ratio of the amount of charge Q_{total} corresponding to the whole anodic signal at $450 - 650 \text{ mV}$ (Figure III.3-b) attributed to the oxidation of the nickel(II) to nickel(III) in presence of urea and the amount of charge Q_{blank} corresponding to the whole signal of the oxidation of the nickel without urea (Figure III.3-a). This definition implies to

verify one of the two following conditions: (i) only one layer of the nickel oxidizes at the surface of the metal; (ii) if more than one layer reacts, the total volume of the reactive area ($\delta + \mu < z < \delta$, Figure III.2) is entirely permeable to the dissolved reagents, without any internal mass transfer limitation. The TON is thus plotted against the potential scan rate in Figure III.7.

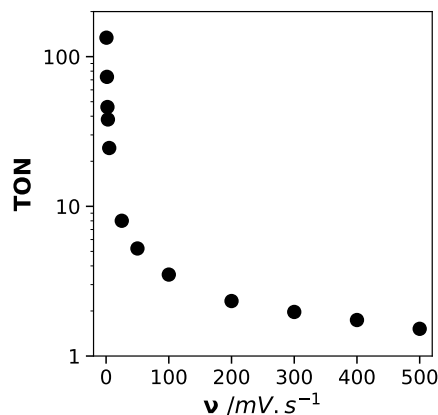


Fig. III.7 – Effect of the scan rate against values of TON.

Figure III.7 highlights two zones: for scan rate lower than 100 mV s^{-1} , high values (> 100) of TON are observed, while the ratio appears to tend towards 1 for scan rate higher than 500 mV s^{-1} . In this latter case, the electro-generated nickel(III) do not have enough time to react with urea and, as the whole metallic surface is covered with nickel(III), the current decreases and the TON tends to the unity. As the potential scan rate decreases, there is enough time for the HCR to occur (whatever the applied potentials). Nickel(III) is reduced by urea and the electro-generated nickel(II) can be oxidized again, thus enhancing the current. Note that because: (i) the continuous change of the applied potential during the monitoring of the $I=f(E)$ curve, and (ii) the definition of the TON as a “global” parameter based on the whole amount of charge of the $I=f(E)$ curve, it is difficult to estimate a value of the chemical rate, r_{χ} , of the HCR of which the reaction scheme appears also complex (see mass balances at the next section III-3).

III-2.3 Effect of the alkalinity on overall rate of the indirect electro-oxidation

Hydroxide ions are involved in both $\text{Ni}(\text{OH})_2$ oxidation ($\{\text{R I.19}\}$) and urea indirect oxidation by NiOOH ($\{\text{R III.27}\}$). The last reaction exhibits a stoichiometry based on 1 mole of urea for 8 moles of hydroxide ions, meaning that the alkalinity will affect the rate of the process. In order to examine the effect of KOH on the urea oxidation current, several $I=f(E)$ curves are plotted, using nickel RDE with KOH concentrations ranged from 0.05 to 5 mol L^{-1} , and two potential scan rates (1.36 and 500 mV s^{-1}). The urea concentration chosen is 0.33 mol L^{-1} and the obtained results presented in Figure III.8.

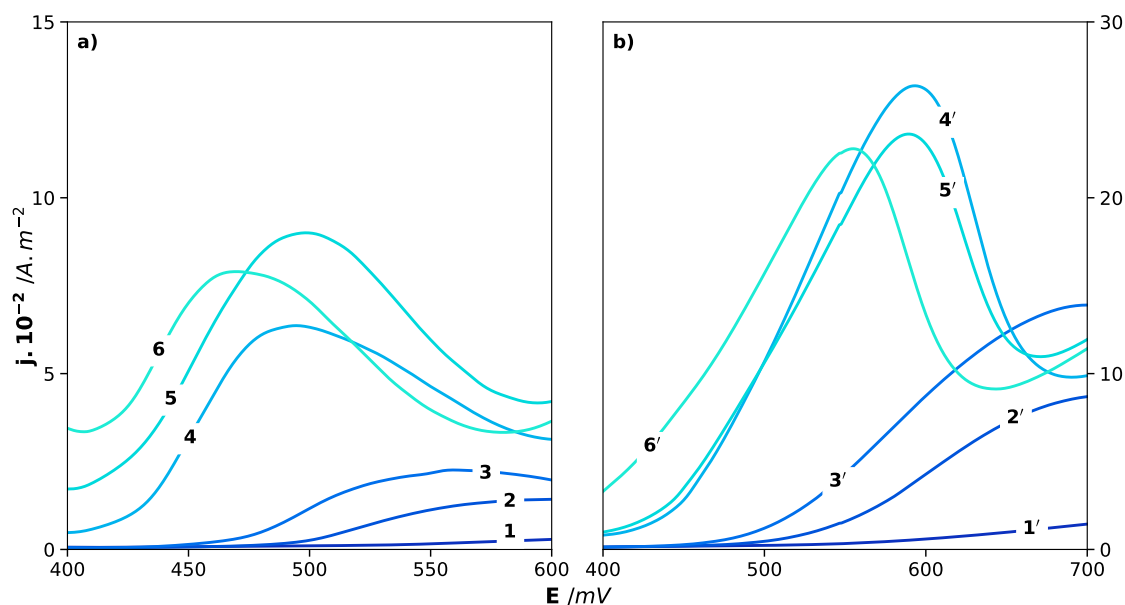


Fig. III.8 – Effect of KOH concentration by linear voltammogram of nickel RDE in a solution containing 0.33 mol L^{-1} urea at a) 1.36 and b) 500 mV s^{-1} without agitation at 298 K . The potassium hydroxide concentration used was 0.05 mol L^{-1} (1-1'), 0.5 mol L^{-1} (2-2'), 1 mol L^{-1} (3-3'), 3 mol L^{-1} (4-4'), 4 mol L^{-1} (5-5') and 5 mol L^{-1} (6-6').

The results show a strong effect of the KOH concentration on the shape of the curves. All the curves present, in the range from 400 to $600 \sim 700 \text{ mV}$ a signal mainly “peak shaped”, attributed to the $\text{Ni}(\text{OH})_2$ oxidation to NiOOH form. Both the magnitude of the current and the potential of the peak appear to be dependent of the KOH concentration. Indeed, for both potential scan rates, increasing the KOH concentration from 0.05 to 5 mol L^{-1} causes a peak potential shifting to the lower potentials, meaning that the system $\text{NiOOH}/\text{Ni}(\text{OH})_2$ becomes faster. The effect of KOH on the magnitude of the peak current of the $\text{Ni}(\text{OH})_2$ oxidation seems more complex, two distinct area can be evidenced: the peak current increases with the KOH concentrations until reaching 4 to 5 mol L^{-1} , and then decreases. As both reactions, in {R I.19 and R III.27}, require KOH, such increase of their reaction rates with the KOH concentration is understandable, however, a ‘quantitative’ kinetic study would be required to deeply investigate this issue and will constitute an upcoming study. For higher KOH concentration, the current of the curves decreases. This can be explained based on the E-pH diagram of nickel (see Figure III.9) which points out that the $\text{NiOOH}/\text{Ni}(\text{OH})_2$ couple is unstable at very high pH values. A part of this oxide can then dissolve and spread into the bulk, inducing a decrease of the rate of the anodic process.

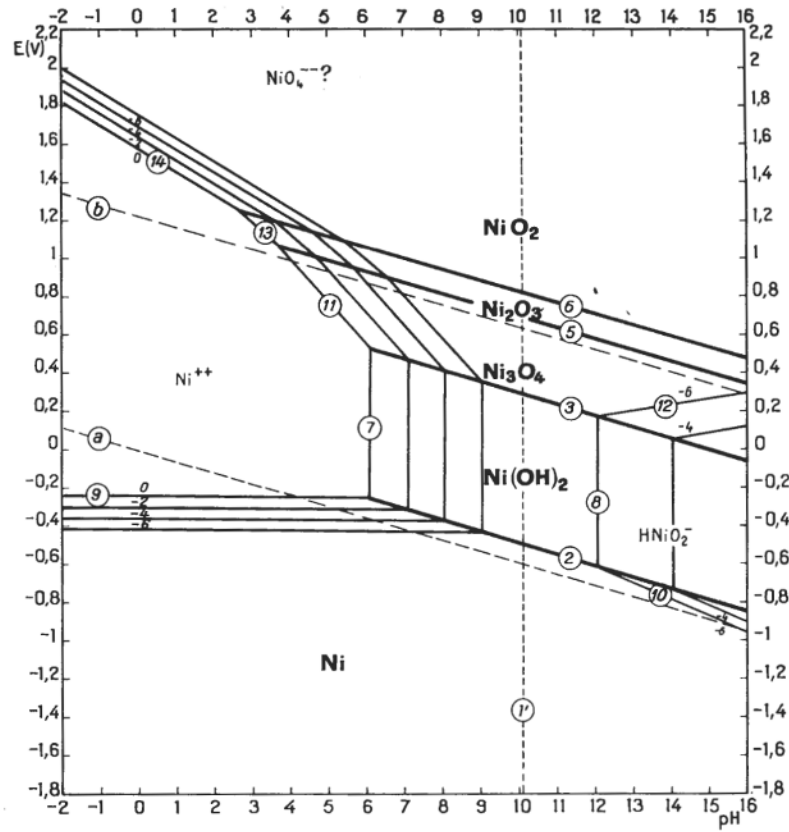


Fig. III.9 – Potential-pH equilibrium diagram for the system nickel-water at 298 K (adapted from [207]).

The comparison of the voltammograms obtained at two different scan rates, shows that at 500 mV s^{-1} the signal appears as ‘a more symmetrical peak’ than the one obtained at 1.36 mV s^{-1} (especially for the curves 4-4’, 5-5’ and 6-6’). Indeed, at 500 mV s^{-1} and for higher potentials than $550 \sim 600 \text{ mV}$, the decrease of the current is due to the fact that the electrode surface (the reaction area) is completely covered/filled by NiOOH, which has not time to react with urea (the EC reaction is fast, and there is no limitation by the KOH concentration). Consequently, there is no (electro-generated) Ni(OH)₂ to oxidize and the current falls down, inducing the occurrence of a dissymmetric peak in the curve. At 1.36 mV s^{-1} , there is enough time to enable the NiOOH to react with urea and be reduced to Ni(OH)₂, so the current slowly decreases after $450 \sim 500 \text{ mV}$.

Assuming that the curves obtained at 500 mV s^{-1} are mainly attributed to the ER (*i.e.*, without the effect of the HCR) and that the anodic activation limitation range of the curve obeys to the Butler-Volmer equation, the current can be expressed as Eq. III.5.

$$I = \left\{ n \times \mathcal{F} \times S_{\text{reaction area for } 0 \leq z \leq \delta + \mu} \times k_{\text{app}}^0 \times \Gamma_{\text{III}} \right\} \times \exp \left(\frac{\alpha n \mathcal{F}}{RT} \times (E - E_{I=0}) \right) \quad (\text{III.5})$$

where n is the exchanged electron number (dimensionless, here 1), \mathcal{F} the Faraday’s constant ($96\,500 \text{ C mol}^{-1}$), $S_{\text{reaction area for } 0 \leq z \leq \delta + \mu}$ the electro-active surface (m^2), k_{app}^0 the apparent intrinsic heterogeneous electron transfer rate constant (s^{-1}), which depends on $[\text{OH}^-]$ as $k_{\text{app}}^0 = \frac{k^0 \times [\text{OH}^-]^\delta}{\mu}$, where k^0 is the heterogeneous electron transfer rate constant (m s^{-1}), μ the thickness of the catalytic system NiOOH/Ni(OH)₂ (m), δ the partial order of {R III.27} for hydroxide (dimensionless), α the anodic charge transfer coefficient (dimensionless), E the

electrode potential (V), $E_{I=0}$ the open circuit potential (V) and Γ_{III} the nickel(III) surface concentration ($\text{mol m}_{\text{electrode}}^{-2}$).

The global nickel surface concentration, Γ_0 , can be expressed as Eq. III.6 where Γ_{II} is the nickel(II) surface concentration.

$$\Gamma_0 = \Gamma_{\text{II}} + \Gamma_{\text{III}} \quad (\text{III.6})$$

In these conditions (no chemical reaction at potential close to $E_{I=0}$ and 500 mV s^{-1}), Γ_{III} is considered as constant and equals to Γ_0 .

From Eq. III.5, it comes Eq. III.7.

$$\ln(I) = \left\{ \ln \left(n \times \mathcal{F} \times S_{\text{reaction area}} \right) + \ln(k_{\text{app}}^0) - \frac{\alpha n \mathcal{F}}{RT} \times E_{I=0} \right\} + \frac{\alpha n \mathcal{F}}{RT} \times E \quad (\text{III.7})$$

According to Eq. III.7, the natural logarithm plot of the current (in the activation zone) *vs.* applied potential, extracted from Figure III.8-b, is plotted Figure III.10 for $[\text{OH}^-]$ ranging from 0.05 to 5 mol L^{-1} .

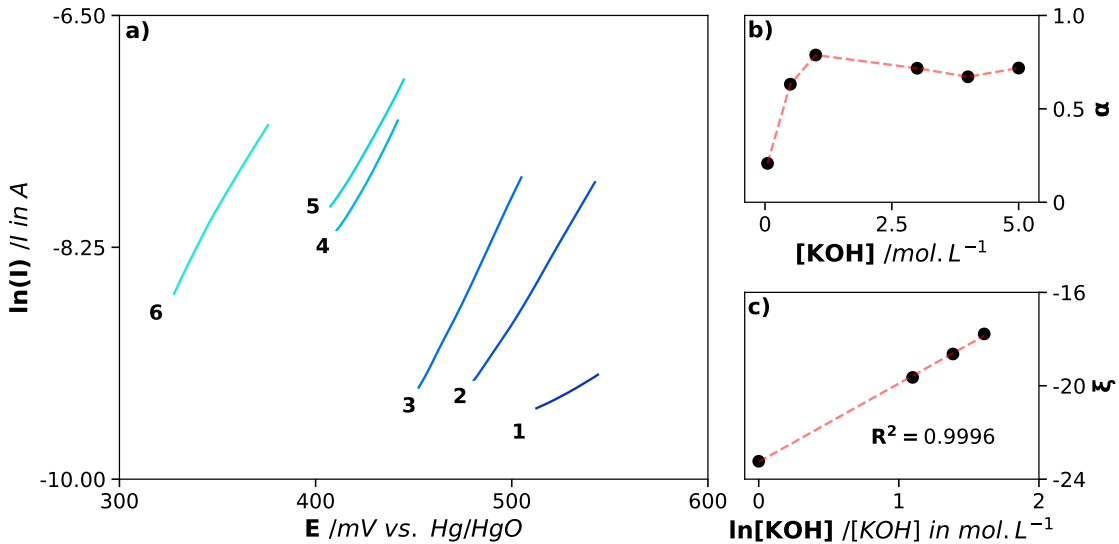
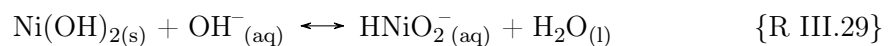


Fig. III.10 – a) Butler-Volmer analysis of voltammogram 1' to 6' extracted from Figure III.8-b. Figure b) shows the dependency of the anodic charge transfer coefficient α against the hydroxide concentration. Figure c) highlights the intercept of Butler-Volmer analysis against the natural logarithm of KOH concentration.

The anodic charge transfer coefficient α is deduced from the slope of the curves, as illustrated Figure III.10-a. Its variation against the KOH concentration is presented in Figure III.10-b and shows that α increases with the KOH concentration until becoming constant and equal to 0.7 at $[\text{OH}^-] \approx 1 \text{ mol L}^{-1}$. A similar value of 0.78 was obtained by Vedharathinam et al. [142]. One can note that this value is higher than 0.5 meaning a multi-step system. Other reactions can occur, such as {R III.29}, shown in the E-pH diagram of nickel.



The heterogeneous electron transfer rate constant k^0 and the hydroxide partial order δ in the {R III.27} are deduced from the y-intercept of the Eq. III.7, noted ξ . According

to Eq. III.8, ξ is directly proportional to the value of the natural logarithm of the KOH concentration.

$$\xi = \left\{ \ln \left(\frac{n \times \mathcal{F} \times S_{\text{reaction area for } 0 \leq z \leq \delta + \mu}}{\mu} \right) - \frac{\alpha n \mathcal{F}}{RT} \times E_{I=0} \right\} + \delta \times \ln([\text{OH}^-]) \quad (\text{III.8})$$

The variation of ξ against $\ln([\text{OH}^-])$ is represented in Figure III.10. The slope of this line, assimilated to the partial order of OH^- in the oxidation of nickel, is estimated to 3.3. A value of ‘three’ would mean that three hydroxide ions are involved at the associated reaction. Taking into account the strong KOH concentrations, one can suppose that the nickel oxidized may be partially dissolved and leave the electrode surface; in this case, the bare nickel oxidizes and three e^-/OH^- would be required. This fact means that to avoid the nickel dissolution, it is preferable to carry out the urea oxidation at concentrations of KOH lower than 1 mol L^{-1} , even if the EC conditions are not the more optimum.

Through the y-intercept of Eq. III.8, noted ξ' expressed in Eq. III.9, the value of k^0 , is obtained, as shown in Eq. III.10.

$$\xi' = \ln \left(\frac{n \times \mathcal{F} \times S_{\text{reaction area for } 0 \leq z \leq \delta + \mu}}{\mu} \right) - \frac{\alpha n \mathcal{F}}{RT} \times E_{I=0} \approx -14 \quad (\text{III.9})$$

$$k^0 = \left\{ \frac{\mu}{n \mathcal{F} S_{\text{reaction area for } 0 \leq z \leq \delta + \mu}} \right\} \times \exp \left(\xi' + \frac{\alpha n \mathcal{F}}{RT} \times E_{\text{eq}} \right) \quad (\text{III.10})$$

In order to estimate an order of magnitude of the reaction layer thickness, μ , the integration of $I=f(E)$ curves using a nickel RDE immersed in a 1 mol L^{-1} KOH solution (Figure III.3-a), is performed and allows to obtain the molar quantity transformed during the potential scan. Knowing the geometrical properties of the crystallographic phases from the work of Tkalych et al. [208], a thickness μ of 50 nm is obtained. $\text{NiOOH}/\text{Ni}(\text{OH})_2$ oxides are electronic conductors [209, 210]. In the reaction layer of thickness μ , no electronic limitation exists. The zero current potential is estimated from the Gibb’s free energy [211] and its value is taken as 490 mV *vs.* SHE. The value of k^0 is then estimated, at 298 K and with $1 e^-$ exchanged, to $8.1 \times 10^{-2} \text{ cm s}^{-1}$ a low value translating an irreversible system. As expected, this value is much lower than 0.3 cm s^{-1} which is associated the limit of reversibility for a simple one-electron process based on the work of Dickinson et Wain [212].

III-2.4 Effect of temperature on chemicophysical properties affecting the global process (ER/HCR) as well as the mass transfert phenomena

The effect of temperature in the range of 298 to 313 K on the voltammograms is presented in Figure III.11-a. These curves are obtained at low potential scan rates (0.66 mV s^{-1}) under stirring.

Note that, conversely to the previous cases (Figures III.1, III.3 and III.8) performed without stirring, here, the stirring enables to supply the interface with a constant flux of the dissolved reagents *i.e.*, the urea and the hydroxide ions. Besides, the low applied potential scan rate enables to the overall catalytic cycle ($\{\text{R III.28}\}$) to occur, thus the observed current is the overall catalytic current.

The increase in temperature leads to an increase in the overall current but does not seem to affect the position (potential) of the curves. This variation is in agreement with the simultaneous decrease of the solution viscosity implying an increase of the diffusion flux of (electro)reactive species to the electrode. Moreover, in general, the temperature causes the increase of the chemical rate according to the Arrhenius' law.

In Curve **1** obtained at 298 K, a quasi-plateau (with a very slight decrease of the current) is observed between 520 and 570 mV, exhibiting a diffusion limited current. This means that mass transport of dissolved reagents limits the overall process. The limitation is due to the urea present in the HCR. Indeed, the ER could not be limiting because the amount of OH^- required to oxidize $\text{Ni}(\text{OH})_2$ and regenerate NiOOH is low due to the low Γ_{II} surface concentration.

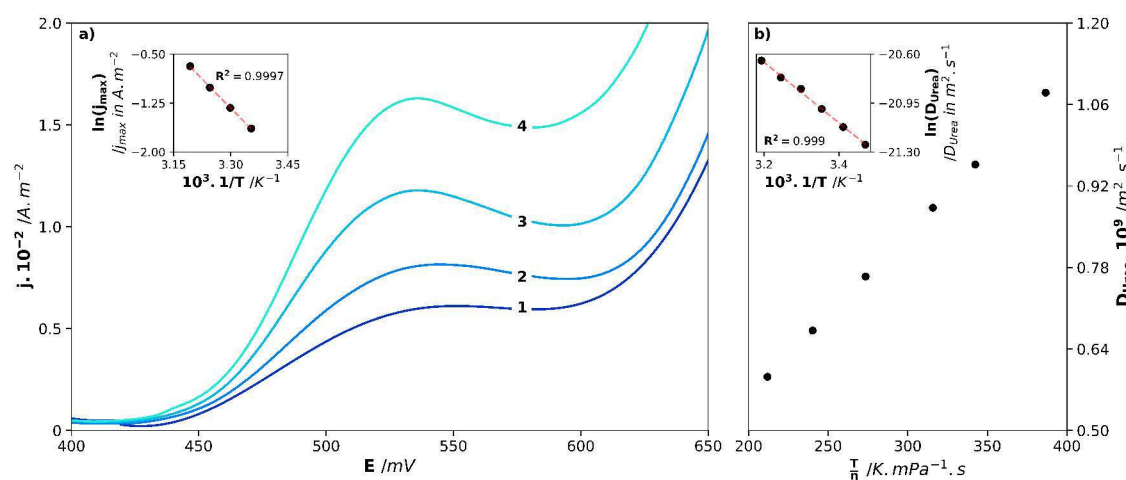


Fig. III.11 – a) Effect of temperature on the voltammograms obtained at 0.66 mV s^{-1} , on nickel RDE in a 1 mol L^{-1} KOH solution containing 0.33 mol L^{-1} urea. The temperature used was 298 K (1), 303 K (2), 308 K (3) and 313 K (4). $\omega = 200$ Revolutions per minute (RPM). Inset: $\ln(j_{\text{max}}) = f(1/T)$ plotted to determine the activation energy of the global process. b) Temperature dependence of the urea diffusion coefficient in 1 mol L^{-1} KOH solution between 288 and 313 K obtained by viscosity measurements. Inset: $\ln(D_{\text{urea,w}}) = f(1/T)$ plotted to determine the activation energy of the diffusion coefficient.

Increasing the temperature causes a deformation of the curves; typically, the current slightly decreases in the plateau area (520 and 570 mV), before reaching the oxidation potential of the solvent (600 mV), where it increases again. Note that the observed decrease of the current remains smaller than 10% (for the highest temperature). The decrease in current can be explained by a partial passivation of the nickel anode. This phenomenon does not appear to be strong or irreversible, as the solvent oxidation occurs in the same potential range as without urea. At least, two possibilities can be proposed to explain this partial passivation:

- Due to the OH^- depletion, at the limiting current, the interface may be partially neutralized and therefore carbonate, a by-product of the HCR (see next sections) may generate a gaseous layer of carbon dioxide. In addition, a higher temperature facilitates the degassing of CO_2 . The presence of such a gaseous layer may easily reduce the diffusion flux of urea [125, 213] and consequently distort the observed plateau.
- The increase in temperature leads to an increase of the current and at high currents,

the oxidation of urea may generate intermediates (even of small size) that would be adsorbed at the electrode and reduce the number of active nickel atoms (NiOOH), thus implying a decrease in the rate of the process.

A macroscopic mass balance of the nickel(III) can be expressed as Eq. III.11.

$$\left\{ \begin{array}{l} \text{Accumulation flux of nickel(III) + Chemical reaction flux - electro-generation flux} = 0 \\ \frac{\partial \Gamma_{\text{III}}}{\partial t} + \sum_{\forall \text{ reactions } i} \nu_i r_i - \frac{I}{n\mathcal{F}} \times \frac{1}{S_{\text{reaction area}} \text{ for } 0 \leq z \leq \delta + \mu} = 0 \end{array} \right. \quad (\text{III.11})$$

where Γ_{III} is the nickel(III) surface concentration ($\text{mol m}^{-2}_{\text{electrode}}$), ν_i the stoichiometric constant of nickel(III) (dimensionless) of the chemical reaction i , r_i the rate (nickel(III) $\text{s}^{-1} \text{m}^{-2}_{\text{electrode}}$) of the chemical reaction i , n the number of electron transferred (dimensionless, here 1), \mathcal{F} the Faraday's constant and $S_{\text{reaction area}} \text{ for } 0 \leq z \leq \delta + \mu$ the surface area of reaction (m^2).

Let's consider the following approximations:

- because the magnitude of the decreasing current after the plateau (due to the passivation) is smaller than 10%, the maximum current can be considered to be the limiting current.
- because a small value of scan rate is applied and a plateau is observed (*i.e.*, constant current at least for the first two temperatures), at each potential (in the range of 520 to 570 mV), the steady state is assumed to be reached for the nickel ($\frac{\partial \Gamma_{\text{III}}}{\partial t} = 0$).

Under these conditions, the rate of consumption of nickel(III) by the surface chemical reaction is equal to the electro-generation flux, which leads to Eq. III.12.

$$\sum_{\forall \text{ reactions } i} \nu_i r_i = \frac{I}{n\mathcal{F} S_{\text{reaction area}} \text{ for } 0 \leq z \leq \delta + \mu} \quad (\text{III.12})$$

Because the limitation of the current by the mass transfer of urea, this current can be expressed by Fick' first law as Eq. III.13.

$$I_{\text{max}} = n\mathcal{F} D S_{\text{reaction area}} \text{ for } 0 \leq z \leq \delta + \mu \times \nabla [\text{CO}(\text{NH}_2)_2]_{\text{reaction area}} \text{ for } 0 \leq z \leq \delta + \mu \quad (\text{III.13})$$

It is not obvious how to determine the $\nabla [\text{CO}(\text{NH}_2)_2]_{\text{reaction area}} \text{ for } 0 \leq z \leq \delta + \mu$. For that, one can suppose that (*i*) since the plateau is reached (520 to 570 mV), this gradient is constant with temperature, and (*ii*) there is no limitation by internal diffusion (Knudsen). Besides, the dependence of the diffusion coefficient on temperature may be expressed according to the Stokes-Einstein equation as Eq. III.14 and illustrated in Figure III.11-b.

$$D = \frac{k_B T}{6\pi r \eta} \quad (\text{III.14})$$

where k_B is the Boltzmann constant ($1.38 \times 10^{-23} \text{ J K}^{-1}$), T the absolute temperature (K), r the radius of the moving particle (r_{urea} calculated as $2.62 \times 10^{-10} \text{ m}$ [214]) and η the viscosity (Pa s^{-1}).

The dynamic viscosities of solutions were measured at different temperatures (applied by Peltier effect) using a rheometer Physica MCR301 Anton Paar, equipped with double-gap Couette system (standard measuring system DG26.7/T200/AL). To carry out these

measurements, about 5 mL of each solution was used and the shear rates varied between 20 and 100 s^{-1} . The viscosity of the solutions of urea in alkaline medium has been measured, as presented in the Figure III.12-a. These values are used to calculate the diffusion coefficients. This figure shows the influence of the KOH concentration on the dynamic viscosity of the solutions prepared in this work. The viscosity of a water solution was added as a reference. A classical viscosity decay profile was observed with increasing temperature. As an example, the viscosity of a 1 mol L^{-1} KOH solution decreased by 40% when varying the temperature from 288 to 313 K. Increasing the KOH concentration led to an increase in viscosity. For example, at 293 K, the increase in hydroxide concentration from 1 to 5 mol L^{-1} led to a 40% increased in viscosity. In addition, the present measurements were in agreement with the ones of Kuznetsov et al. [215]. As shown in Figure III.12-b, it was also verified that adding urea at a concentration of 0.33 mol L^{-1} did not influence the viscosity of an alkaline solution. Density measurements were performed with a Densito 30 PX densitometer (Mettler Toledo), with a thermoregulation at 293 K. Figure III.12-c shows the variation of the aqueous solution density as a function of KOH concentration in the aqueous solution. The values were in agreement with the ones of from Akerlof et al. [216]. When comparing KOH solutions with and without urea at 0.33 mol L^{-1} ; no difference could be highlighted.

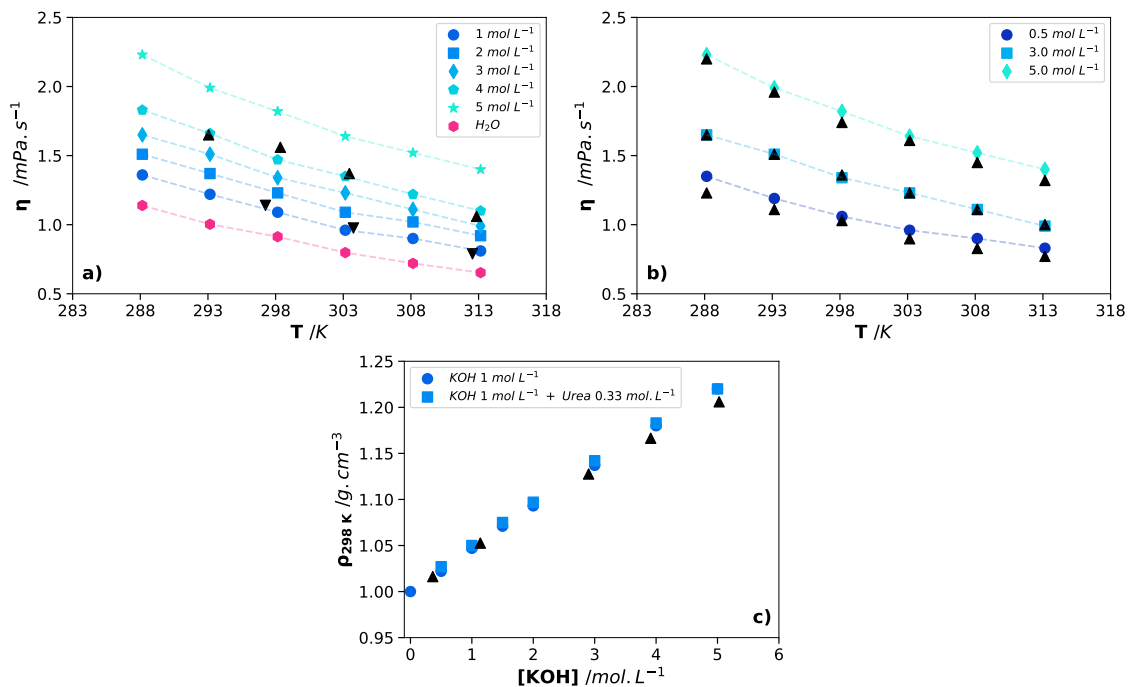


Fig. III.12 – a) Effect of potassium hydroxide concentration on the dynamic viscosity of aqueous solutions. The black triangles up and down present data from the work of Kuznetsov et al. [215] b) Effect of the presence of 0.33 mol L^{-1} urea on the viscosity of alkaline solutions with different concentrations of potassium hydroxide. The triangles correspond to the viscosities of the alkaline solutions when adding urea at 0.33 mol L^{-1} . c) Effects of KOH concentration (dot) and urea presence (square) on the aqueous solution density at 298 K. The values extracted from Akerlof et al. [216] are illustrated with black triangles.

Considering all above assumptions, equations and measurements, the Eqs. III.15-III.16

are obtained.

$$\sum_{\forall \text{ reactions } i} \nu_i r_i = \frac{I}{n\mathcal{F}S_{\text{reaction area for } 0 \leq z \leq \delta+\mu}} = \nabla [\text{CO}(\text{NH}_2)_2]_{\text{for } 0 \leq z \leq \delta+\mu} \times D \quad (\text{III.15})$$

$$= \text{constant} \times D = \text{constant}' \times \frac{k_B T}{6\pi r \eta}$$

$$I = \text{constant}'' \times \frac{T}{\eta} \quad (\text{III.16})$$

The variation of the current measured at the plateau as a function of the ratio T/η exhibits a linearity, expressed by Eq. III.17 ($R^2 = 0.993$), confirming the validity of the assumption made and validating the proposed reaction scheme.

$$I_{\max} = 0.012 \times T \quad (\text{III.17})$$

In order to examine the temperature dependence of the diffusion coefficient D , we assume that it obeys to the Arrhenius' law, Eq. III.18, and the logarithmic analysis of D *vs.* the reverse of T is performed.

$$D_{(T)} = D^0 \times \exp\left(-\frac{E_{a,d}}{RT}\right) \quad (\text{III.18})$$

where D^0 is the diffusion coefficient when the temperature goes to infinity ($\text{m}^2 \text{s}^{-1}$), $E_{a,d}$ the activation energy for diffusion (J mol^{-1}). The results, presented in inset of Figure III.11-b, lead to an activation energy for the urea diffusion $E_{a,d}$ of $(21.2 \pm 0.2) \text{kJ mol}^{-1}$, close to the one obtained by Longworth [217] (18.7kJ mol^{-1}).

With respect to the Eq. III.15, an important question is to determine the reaction that consumes the nickel peroxide; indeed, since the oxidation of urea leads to by-products (see next sections), it is obvious that several reaction intermediates consume nickel(III). One assumes here that only one reaction, r_{HCR} , occurs (*i.e.*, the HCR) and that its rate can be expressed as Eq. III.19.

$$r_{HCR} = k_{\chi(T)} \times \Gamma_{\text{III}}^\beta \times C_{\text{OH}^-}^\gamma \times C_{\text{urea}}^\epsilon \quad (\text{III.19})$$

where $k_{\chi(T)}$ the reaction rate constant ($\text{mol}^{1-\beta-\gamma-\epsilon} \text{m}^{-2(1+\beta)+3(\gamma+\epsilon)} \text{s}^{-1}$), β, γ, ϵ the partial orders of reaction for nickel oxyhydroxide, hydroxide ion and urea respectively (dimensionless). Consequently, the Eq. III.12 can be written as Eq. III.20.

$$I_{\max(T)} = \left(n\mathcal{F}S_{\text{reaction area for } 0 \leq z \leq \delta+\mu} \right) \times 6 \times r_{HCR} \quad (\text{III.20})$$

$$= \left(n\mathcal{F}S_{\text{reaction area for } 0 \leq z \leq \delta+\mu} \right) \times 6 \times k_{\chi(T)} \times \Gamma_{\text{III}}^\beta \times C_{\text{OH}^-}^\gamma \times C_{\text{urea}}^\epsilon$$

Where 6 is the stoichiometric factor of the nickel(III) in the HCR (dimensionless).

Assuming that the $k_{\chi(T)}$ obeys Arrhenius' law, the logarithmic analysis of the variation of the current according to the equation Eq. III.21 leads to the curve indicated in the inset in Figure III.11-a.

$$\ln(I_{\max(T)}) = \ln \left(\mathcal{A}_{HCR} \times n\mathcal{F}S_{\text{reaction area for } 0 \leq z \leq \delta+\mu} \times 6 \times r_{HCR} \right) - \frac{E_{a,HCR}}{RT} \quad (\text{III.21})$$

where \mathcal{A}_{HCR} is the pre-exponential factor, $E_{\text{a,HCR}}$ the activation energy of the HCR (J mol^{-1}). Here, $E_{\text{a,HCR}}$ is estimated to be 49.3 kJ mol^{-1} . The order of magnitude is substantially close to that of the oxidation of methanol on nickel electrode [218]. Note that this $E_{\text{a,HCR}}$ value is relatively low, which means that the {R III.28} between solid NiOOH and urea occurs easily, probably because the system is electrically activated during electro-generation of NiOOH.

III-2.5 Influence of nickel electrode angular velocity on mass transport processes

In this section, the effect on the obtained anodic current of the speed variation of the nickel RDE is studied at two potential scan rates (0.83 and 5 mV s^{-1}) and the obtained curves are illustrated in Figure III.13.

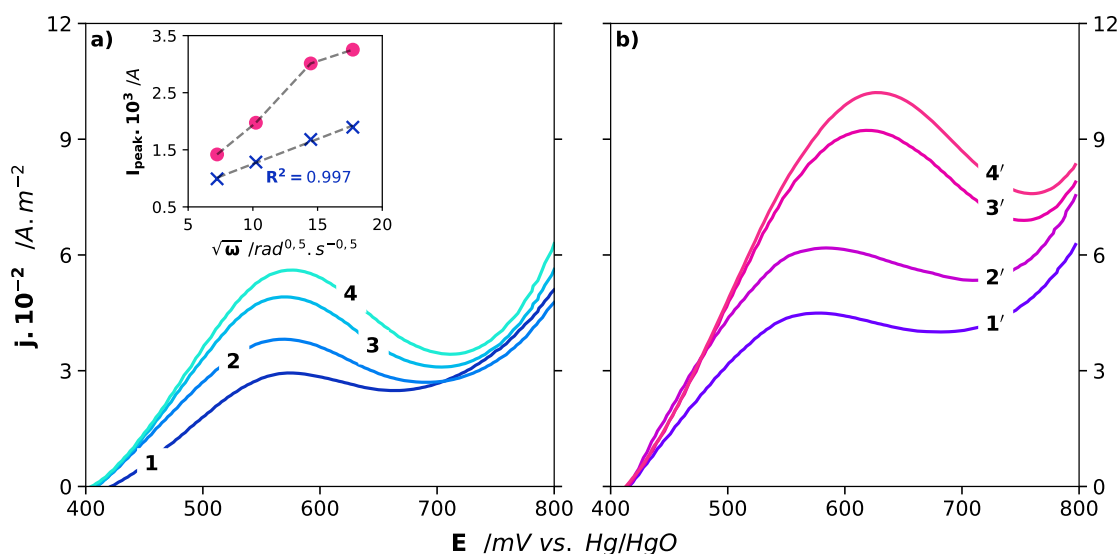


Fig. III.13 – Effect of the solution agitation on the shape of the current potential curves for the urea oxidation on nickel RDE ($S = 3.14 \text{ mm}^2$) and at two potential scan rates: a) 0.83 mV s^{-1} and b) 5 mV s^{-1} . $[\text{CO}(\text{NH}_2)_2]_{t=0} = 0.33 \text{ mol L}^{-1}$; $[\text{KOH}] = 1 \text{ mol L}^{-1}$; $T = 298 \text{ K}$; Rotational speed of the RDE was 500 RPM (1-1'), 1000 RPM (2-2'), 2000 RPM (3-3') and 3000 RPM (4-4'). Inset shows the Levich plot at each scan rate 0.83 mV s^{-1} (cross) and 5 mV s^{-1} (dots).

Both potential scan rates are small enough to consider that at each applied potential, the system operates at steady state for NiOOH. The results shown in Figure III.13 highlight that in general, the current increases with the angular velocity of the RDE, ω , and the potential scan rate, ν . Furthermore, as ω and ν increase, the shape of the curves is deformed from a plateau to a peak.

Considering the curves obtained at the lowest agitation (500 RPM) for the two potential scan rates (0.83 and 5 mV s^{-1}), both curves **1** and **1'** exhibit a pseudo plateau which, as before, is considered to indicate a limitation of mass transfer due to the diffusion of urea from the bulk to the HCR zone. Indeed, recall that the anodic ER requires hydroxide anions. However, since the hydroxide concentration is in excess of the metallic nickel atoms, the current limitation is not due to the OH^- transfer to the anode. Besides, since both potential scan rates used are low, the time required for HCR to occur is sufficient, thus implying, for each applied potential, an immediate and continuous electro-generation of NiOOH. Therefore, as the current increases, urea is consumed in the reaction zone ($\delta \leq z \leq \delta + \mu$) and its concentration cancels, the plateau indicates a mass transfer limitation.

As the angular velocity increases ($\mathbf{1} \rightarrow \mathbf{2}$ and $\mathbf{1}' \rightarrow \mathbf{2}'$), the current increases, which (*i*) reflects an increase of the urea diffusion flux arriving in the reaction zone ($\delta \leq z \leq \delta + \mu$) and (*ii*) confirms the previous assumption made (*i.e.*, there is no internal diffusion limitation ($\delta \leq z \leq \delta + \mu$) (independent of the stirring) and thus only external diffusion limitation ($z \leq \delta$) is considered for the urea). However, simultaneously with increasing current, the shape of the curves (520 to 650 mV) shifts from the plateau to the peak (a similar variation is observed with temperature, in Figure III.11-a). The phenomenon is amplified for the highest ω studied ($\mathbf{2} \rightarrow \mathbf{4}$ and $\mathbf{2}' \rightarrow \mathbf{4}'$). The same explanation as before is proposed, and due to this passivation phenomenon, the magnitude of the peak current could be smaller than the limiting current; therefore, although a linear variation is observed between the current and the square root of the rate of rotation, the slopes of the straight lines are underestimated and the results are not analyzed according to the Levich' law.

III-3 Study of the indirect electro-oxidation of urea under potentiostatic conditions: population distribution establishment

This first part of the study highlights the mediation of nickel(III)/nickel(II) system to the urea oxidation and will serve as solid basis for further kinetic and mechanistic studies. The study emphasizes that there is no direct oxidation of urea. Although the hydroxide ion concentration enhances the reversibility of the nickel(III)/nickel(II) system, a trade-off is necessary to achieve a more environmentally sustainable process. In a second set of experiences, electrolysis, for which complete mass balances in liquid phase are systematically established, are performed, using undivided and divided EC cells. In these experiments, particular attention is paid to make varying the concentrations of urea and KOH in a wide range and to be in excess of KOH over urea. The expected objective is to use all the significant data acquired, in order to select the optimal operating conditions, allowing (*i*) to reach a high degradation rate of urea and (*ii*) to reduce the electro-generated adducts concentration more toxic than urea.

In this part, the objectives are twofold: (*i*) to identify and quantify the intermediates generated during the oxidation of urea in order to propose more accurate reaction pathways than the one given by the mineralisation reaction {R III.28} (*ii*) to determine the optimal operating parameters in the perspective of designing a pilot capable of treating several liters of urea per day. Electrolyses are performed in potentiostatic mode since selective conditions are required. The applied potential (550 mV) is determined from voltammograms obtained in steady state (*i.e.*, at a potential scan rate of 0.83 mV s^{-1}), in the case where the current reaches a limit value. As shown in Chapter II, two cell configurations are used, either divided (anodic and cathodic compartments) or undivided.

III-3.1 Identification of the electro-generated adducts and mass balance on carbon and nitrogen elements

In order to identify the intermediate species generated during the UEO, an electrolysis is performed using mild operating conditions *i.e.*, room temperature, low alkalinity (1 mol L^{-1} of KOH) and an undivided cell. The results are summarised in Figure III.14 in the form of

temporal (Fig. a), and even coulometric (Figs. b and c) variation of the concentrations of the different species detected and analyzed.

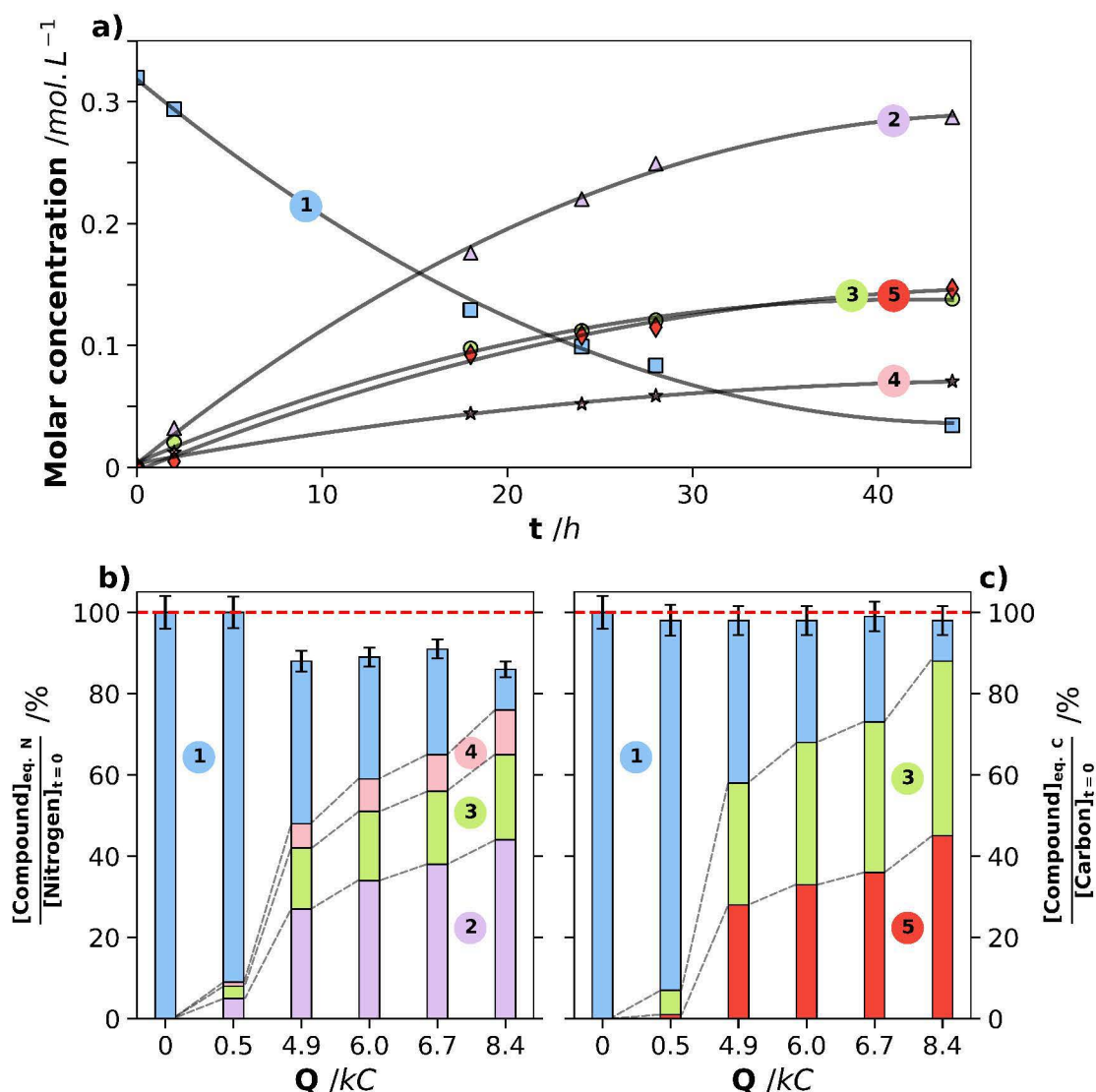


Fig. III.14 – Results of a typical potentiostatic electrolysis on nickel electrode. $S = 4 \text{ cm}^2$; $[\text{KOH}] = 1.5 \text{ mol L}^{-1}$; $[\text{CO}(\text{NH}_2)_2]_{t=0} = 0.33 \text{ mol L}^{-1}$; $E_{\text{applied}} = 550 \text{ mV}$; $T = 298 \text{ K}$; $V = 50 \text{ mL}$. The graph a) shows the molar urea concentration profiles over the electrolysis time, as well as those for the obtained by-products (the line curves are plotted with the aim of interpolating the concentration behavior, and thus do not correspond to modeling). The error bars in part a) are smaller than the size of labels and evaluated at 4%. The graph b) presents the nitrogen mass balance while the right part c) focuses on the carbon mass balance. The red dotted lines (in b) and c)) show a mass balance of 100 %. The error bars represent the total error of the percentages. Labels : ①-□ $\text{CO}(\text{NH}_2)_2$, ②-△ NH_4^+ , ③-○ OCN^- , ④-☆ NO_2^- and ⑤-◇ CO_3^{2-} .

Figure III.14-a presents the time variation of the urea concentration (curve 1) as well as the identified intermediates (curves 2 – 5) generated during electrolysis. As a first approximation, the variation of urea concentration as a function of time is modeled by an apparent first-order kinetic model as Eq. III.22.

$$[\text{CO}(\text{NH}_2)_2]_{(t)} = [\text{CO}(\text{NH}_2)_2]_{(t=0)} \times \exp^{-k_{\text{app}}t} \quad (\text{III.22})$$

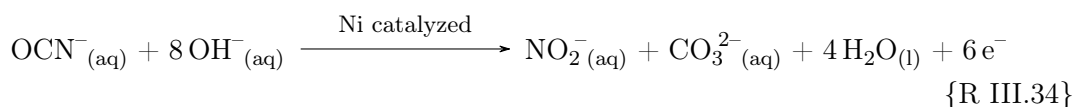
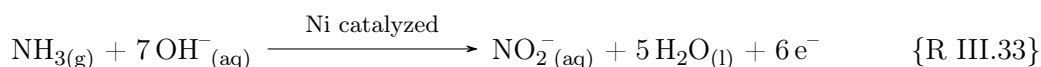
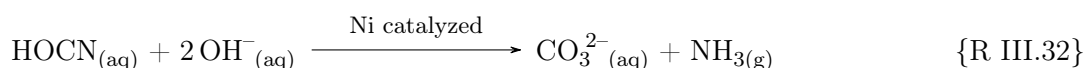
Figure III.14-a also indicates the intermediates species identified into the liquid electrolyte,

namely cyanate (OCN^-), nitrite (NO_2^-), carbonate (CO_3^{2-}) and NH_4^+ (in the ammonia form because the electrolyte is alkaline and pKa is equal to 9.25). Indeed, the ammonium form is obtained during the injection in the ion chromatography which leads to acidify the sample. Moreover, it should be noted that the formation of cyanate and carbonate occurs under equimolar conditions.

Figure III.14-b and c present the variation, as a function of the amount of charge supplied, of the mass balances of total nitrogen (b) and total carbon (c) determined into the liquid electrolyte, and normalized by their respective initial quantities.

Figure III.14-c) highlights that, given the error bars, the carbon mass balance is quantitative at any instant of the electrolysis, meaning that all the disappearing urea is converted to CO_3^{2-} or OCN^- . With respect to the nitrogen mass balance, Figure III.14-b) evidences that (i) the main nitrogen by-products of urea oxidation in alkaline medium are in mineral form, NH_4^+ and NO_2^- , and in organic form, OCN^- , and (ii) these by-products accumulate over time. Moreover, ammonium remains the main species at more than 44mol.% at the end of the electrolysis. While the mass balance of total carbon is almost quantitative, the mass balance of total nitrogen presents a deviation of up to 12% after 20 h of electrolysis, and is therefore significant compared to the error bars. This can be explained in two ways. First, the uncertainty on the nitrogen is higher than on carbon, due to a larger number of nitrogen intermediates. Secondly, the gas phase has not been analyzed, and certainly contains nitrogen compounds such as N_2 or N_2O that may be stripped during the electrolysis.

In summary, under the chosen conditions, most of the urea oxidation products remain in the liquid phase and the gas produced (N_2 or N_2O), does not exceed 12% of the urea. This result is in agreement with the ones obtained by Li et al. [143], and Medvedev al. [147]. At this point, several pathways indicated by {R III.30 - R III.34}, can be proposed in order to better understand the observed formation of by-products at the Ni anode.



where 1e^- represents one reduction of NiOOH to $\text{Ni}(\text{OH})_2$. It has been verified that during the same duration of the experiments, without external energy input, no conversion of urea or formation of by-products is observed, which excludes the assumption of a ‘natural’ hydrolysis of urea.

III-3.2 Influence of the presence (or not) of the ionic separator (undivided cell vs divided cell)

The use of a membrane as separator introduces an ohmic drop, and thus induces an increase in energy consumption, in addition to its relatively high cost and the possible

risks of its poisoning by organic compounds [219, 220]. The H-shaped EC cell, described in **Chapter II**, is used with or without separator; in fact, due to its geometric shape, it enables an easy separation of the cathodic electro-generated hydrogen, avoiding its oxidation in the anodic compartment [21]. The following section is devoted to the study of the impact of the separator on the mechanism path, the nature and concentration of electro-generated adducts. As mentioned above, the volume chosen for the anolyte (for electrolysis with a membrane) is the same as the volume of the electrolyte in the case of no membrane. Figure III.15 presents the mass balances in the liquid phase, for electrolysis carried out with (circles) and without (triangles) membrane. Figs III.15 a to f indicate the variation, against the amount of charge supplied, of the concentrations of urea, cyanate, ammonium, nitrite, total N and total C, respectively, normalized by the initial urea concentration. The repeatability of the experiments is checked by performing each electrolysis twice.

As shown in Figure III.15-a, the presence of an ionic separator has no impact on the conversion rate of urea during electrolysis. This result is important because it shows that urea is not reducible and that there is no hydrogen produced at the cathode that oxidizes at the anode. Figs. III.15 b and c, indicate similar results for cyanate and ammonium respectively. Indeed, an almost perfect overlap of the experimental points can be observed for both conditions, which means that the formation of cyanate and ammonium ions is not affected by the presence of the membrane. Similar conclusions to the previous ones can be made: none of these species reduces at the cathode. Conversely, a different behavior is observed for nitrites, plotted in Figs. III.15-d, whose concentration, at equivalent amount of charge supplied, is decreased by more than two times in the absence of membrane, which means that nitrites are reduced at the Pt cathode [221]. The products related to the nitrite reduction have not been detected in the liquid electrolyte, so the formation of gaseous products, degassed during electrolysis, would be privileged. It should be noted that a quantitative analysis of the gas phase will be considered in a future study. Despite uncertainties, the balance on the carbon element, Figure III.15-f, appears to be quantitative. The deviations are larger in the case of the nitrogen balance, Figure III.15-e. However, one cannot know whether significant amounts of N_2 are produced or not. These results show that in the absence of a membrane separator, electrolysis leads to lower amounts of nitrite, without impacting the concentration of other compounds which means that the product of this reduction should be formed in low concentration and degassed during electrolysis. As a consequence, the use of an undivided cell is interesting as it avoids the issues related to technological complexity, increased ohmic drop, as well as fouling of the membrane surface. However, it should be kept in mind that, for an equivalent amount of charge supplied, such undivided configuration reduces the amount of nitrite but also the amount of hydrogen formed at the cathode. With regard to the prospect of a larger scale process, the application of a potential may allow a better control of by-products formation, compared to galvanostatic electrolysis. Indeed, at higher potentials, oxidation of nitrite to nitrate has been observed [143].

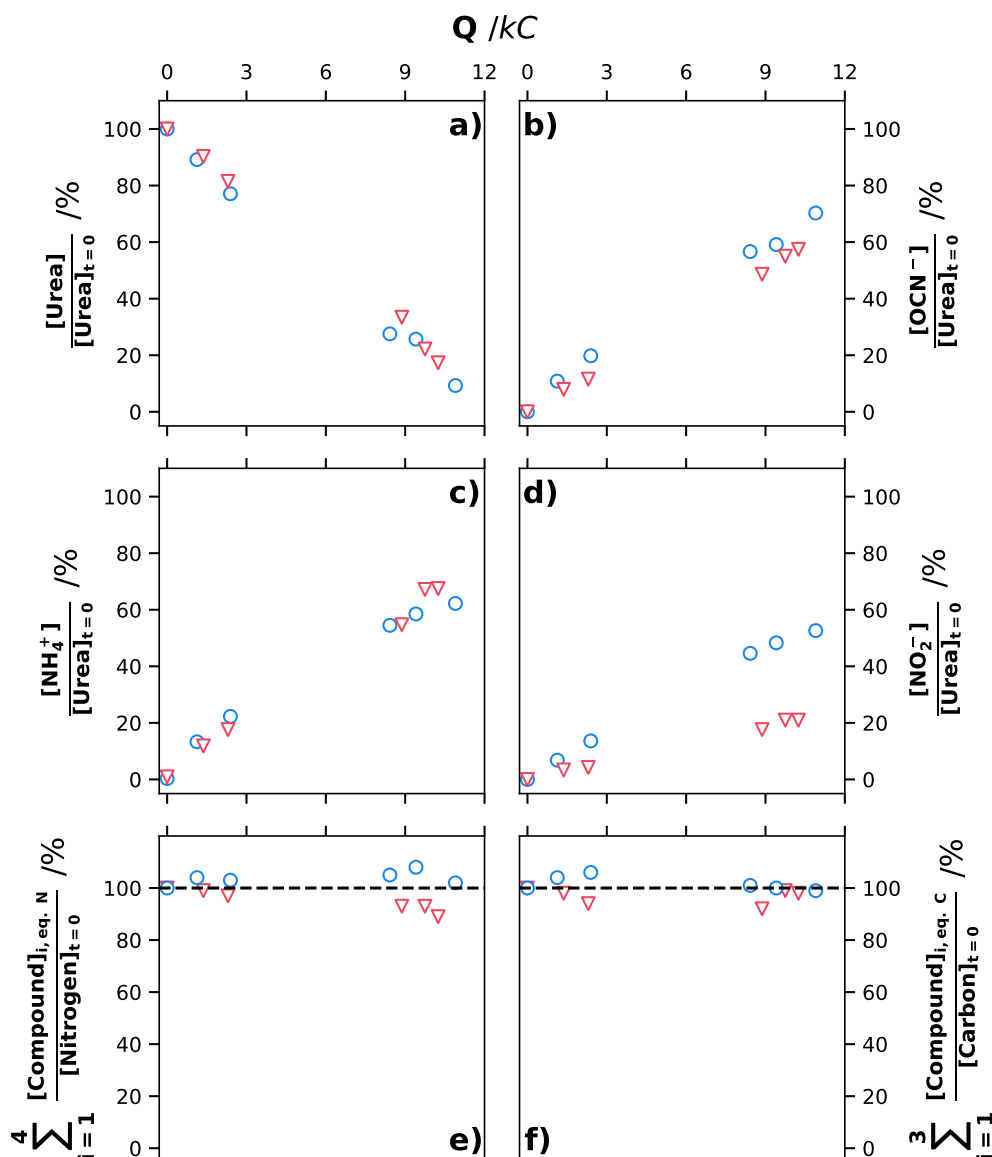


Fig. III.15 – Results of an indirect electro-oxidation of the urea carried out in a H-shaped EC cell (cell c) in Fig. 1). $E_{applied} = 550$ mV; $T = 298$ K; $[CO(NH_2)_2]_{t=0} = 0.33$ mol L⁻¹; $[KOH] = 2$ mol L⁻¹; $S = 15.7$ cm²; $V = 70$ mL. The results are presented as the variation of the normalized concentration of the various products against the amount of supplied charge. Urea, cyanate, ammonium and nitrite are represented, respectively, in part a), b), c) and d). The nitrogen mass balance, e), and carbon balance, f), are normalized in initial concentration. Uncertainties are lower than 4.6%. Circles correspond to the experiments carried out with a membrane. Triangles correspond to the experiments carried out without a membrane.

III-3.3 Influence of the alkalinity

Potassium hydroxide is a strong base and remains a corrosive and toxic reagent whose use should be limited (or even avoided) especially in a wastewater treatment perspective. However, the preliminary study of voltammograms have shown that KOH contributes to increase the rate of the overall process (hydroxide ions are needed for the ER {R I.19}) and the HCR {R III.27}. Consequently, a compromise has to be found in order to operate with the minimum KOH required for avoiding additional environmental problems and of course for minimizing the cost of the electrolysis. Its influence on the urea oxidation products is studied in this sub-section, varying the concentration in a wide range (1 to 5 mol L⁻¹). Figure III.16-a shows that urea conversion, independent of the KOH concentration, can

reach values of 90%. For an equivalent amount of charge supplied, even though the overall process increases with the KOH concentration, the urea conversion is unchanged. A similar variation is observed with the other by-products (ammonium and cyanate, respectively, Figs. b and c) where their compositions are not affected by the KOH concentration (in the range of 1 to 5 mol L⁻¹). The final concentration of nitrite ($\sim 20 \text{ mol.}\%$) is identical to that in the previous sub-section (without membrane) for the same amount of charge supplied. However, some differences appear for urea conversion above 80 %. Note that the amount of ammonium obtained corresponds to the same amount of urea oxidized, meaning that one nitrogen of the urea leads to one nitrogen of ammonium. The other nitrogen of the urea is transformed to cyanate, nitrite and probably N₂ gas. Comparatively to the previously used H-shaped undivided cell (*i.e.*, Figure III.15), the cell used here (Metrohm type undivided cell) present a more efficient mixing efficiency at the anode and to a lesser extent, at the cathode (because the hydrogen variation), thus implying an increase of the mass transfer of (*i*) an electro-active species going to the electrode or (*ii*) any species going to the active area ($\delta \leq z \leq \delta + \mu$) to be adsorbed. Therefore, the rate of the corresponding process is higher in the Metrohm type cell compared to the H-shaped cell. Comparing the final concentrations of cyanate and ammonium, obtained from the electrolysis performed in cell-c), with the final concentrations, obtained from the electrolysis carried out in cell-b), one can observe a decrease of 20mol.% and a 40mol.% increase in concentration at equivalent amount of charge supplied of cyanate and ammonium respectively. This behavior appears to be consistent with stirring-promoted pathways suggested in {R III.30 - R III.34}. Figure III.16-f confirms that the carbon mass balance is close to 100% regardless of KOH concentration. As shown in Figure III.16-e, the mass balance of nitrogen presents a deviation that tends to increase during electrolysis, with a maximum of 20% after 45 h of electrolysis. Such a deviation would suggest that nitrogen gas is produced. In summary, the KOH concentration has no impact on by-product production and composition; increasing its concentration has the advantage of reducing the electrolysis time, but using concentrated alkaline solution remains difficult to recycle. A compromise must be found for larger scale operation.

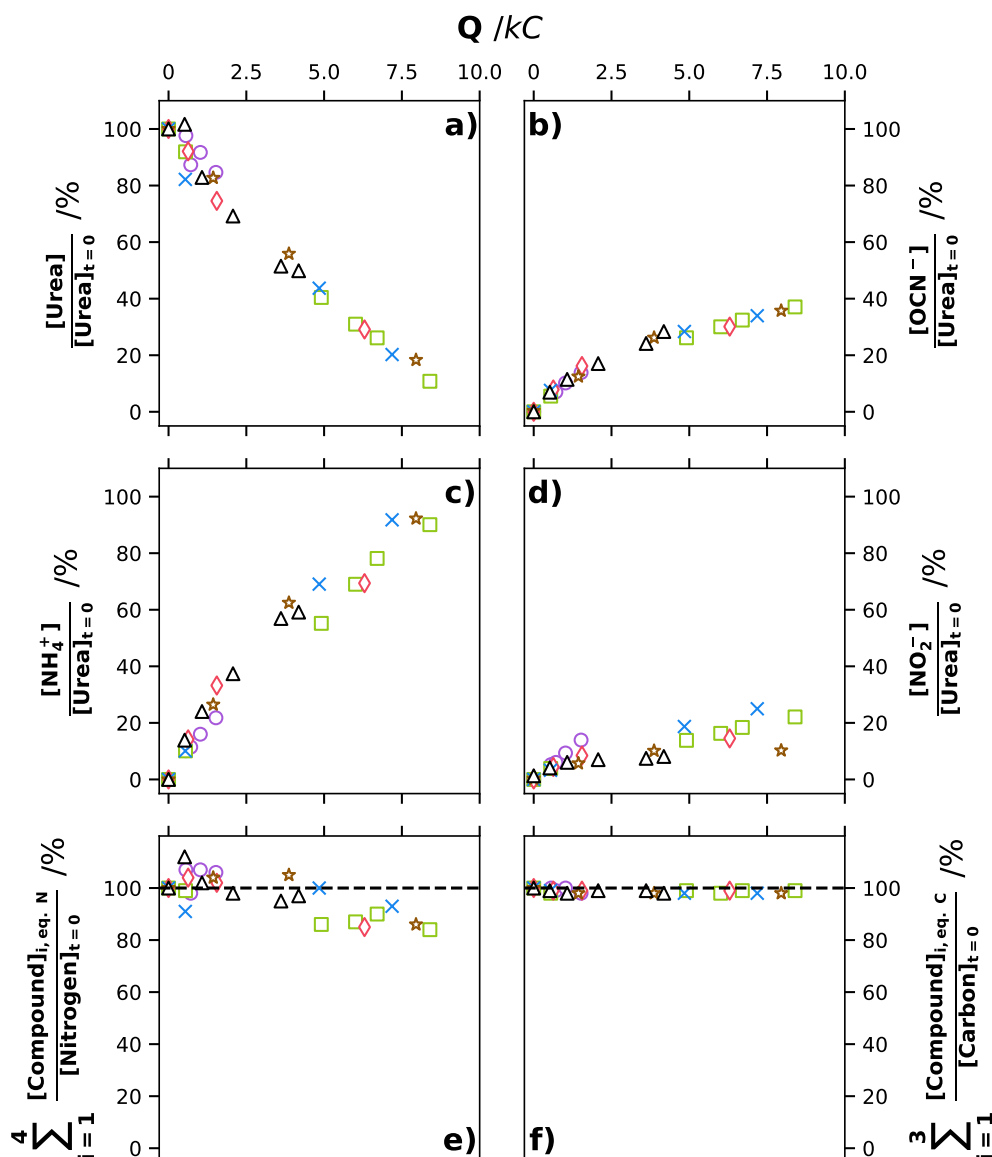


Fig. III.16 – Results of an indirect electro-oxidation of urea in a stirred undivided cell (Metrohm type cell) using various KOH concentration. $E_{applied} = 550$ mV; $T = 298$ K; $[CO(NH_2)_2]_{t=0} = 0.33$ mol L⁻¹; $S = 4$ cm²; $V = 50$ mL; stirred by magnetic bar ($\omega = 500$ RPM, length of the bar: 2 cm; diameter of the bottom area of the cell: 4 cm). The results are presented as the variation of the normalized concentration of the different by-products as a function of the amount of supplied charge. Urea, cyanate, ammonium, and nitrite are shown in parts (a), (b), (c), and (d), respectively. The nitrogen mass balance, e), and carbon mass balance, f), are normalized with respect to the initial concentration. The KOH concentrations used are \circ 1, \square 1.5, \diamond 2.5, \times 3, \star 4, and \triangle 5 mol L⁻¹. The uncertainties are smaller than 5.1%.

III-3.4 Influence of the temperature

Temperature is a parameter affecting the rate of chemical reactions of the HCR and those of {R III.30 - R III.34} as well as the diffusion coefficient of urea. So theoretically, it positively impacts the overall rate of urea oxidation, even if, in the perspective of the process development at pilot-scale, it would induce higher operating cost. The influence of the temperature on urea oxidation is carried out at various temperatures (ranging 293 to 313 K), and the results are presented in the Figure III.17, giving the composition of the different adducts as a function of the amount of charge supplied. The electrolysis times result in nearly complete urea conversions ($\sim 90\%$) for all the operating temperatures. Note that

because temperature causes an increase in anodic current (at constant potential) (Figure III.17-g), the electrolyses durations decrease as the temperature increases. The profiles of normalized concentrations of urea, cyanate, ammonium and nitrite as a function of amount of charge supplied (Figs. III.17-a, b, c and d, respectively) appear similar regardless of the temperature ranging from 293 to 313 K (this indirectly validates the relatively low value of the activation energy, determined previously). At the same amount of charge supplied, the concentrations of urea and by-products are similar to those obtained in the previous sub-section, meaning that neither KOH concentration nor temperature significantly affects the reaction pattern of urea oxidation. Nitrite formation is not impacted by temperature. The total mass balances exhibit the same behavior as in the previous sub-sections: the carbon balance (Figure III.17-f), is close to 100% and, conversely, the balance of nitrogen compounds (Figure III.17-e) shows losses, which increase as a function of the amount of charge supplied (*i.e.*, duration of electrolysis) and should correspond to the gas produced (up to about 20%). Figure III.17-g evidences the resulting current profiles as a function of time. The decrease in current is not related to any poisoning but to the direct decrease in urea concentration in the bulk (urea conversions reach 90%). In the same way as when KOH concentration is increased, the increase of temperature leads to:

- an increase in the current magnitude, due to the increase in both the urea diffusion coefficient and the kinetic constant of HCR;
- a more pronounced decrease in current due to the more rapid decrease in urea concentration.

In brief, the increase of temperature allows to go faster and reduce the electrolysis time against an additional energy input for heating. In view of these results, the use of a heated reactor is not required in a scale-up perspective.

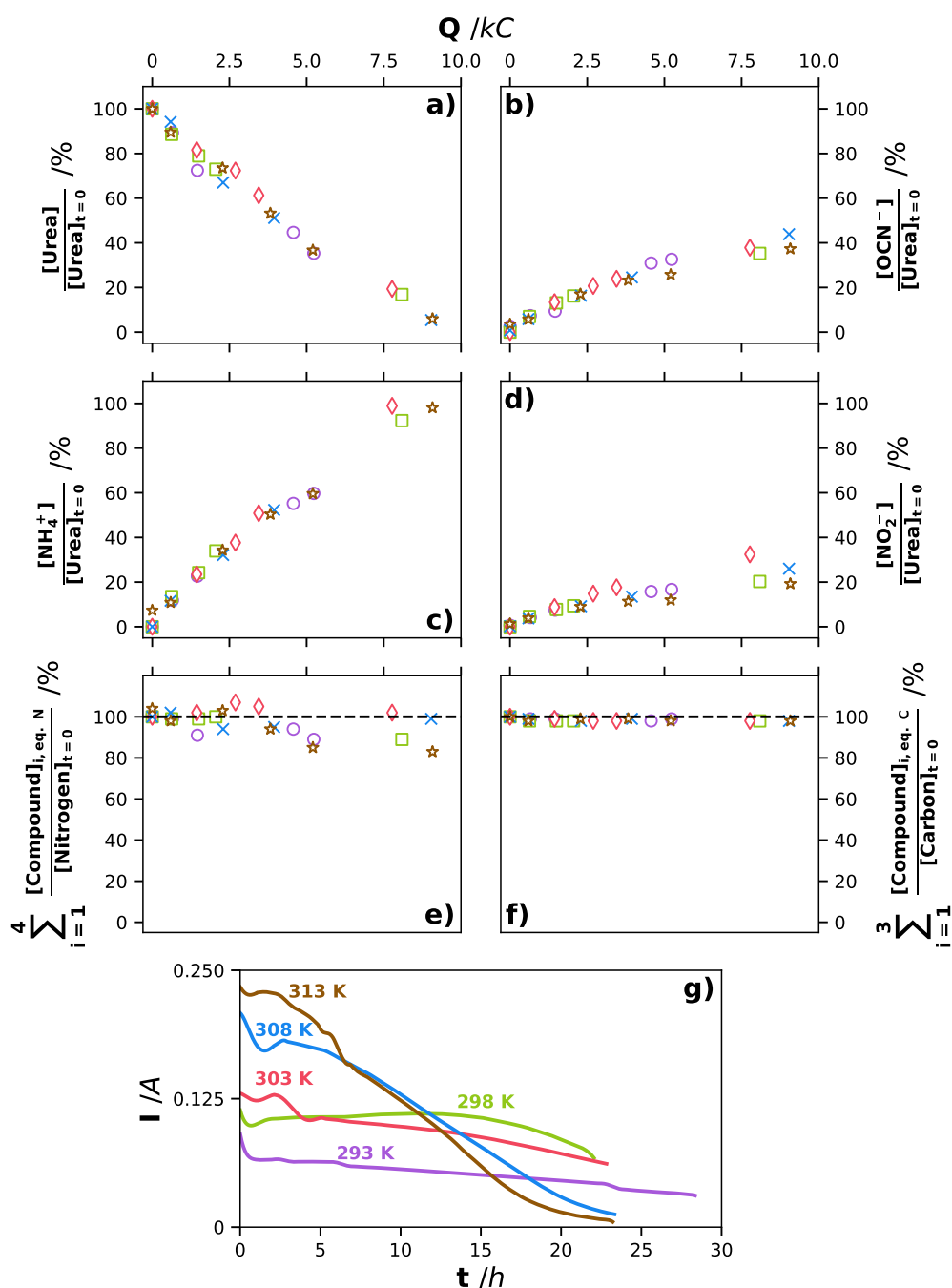


Fig. III.17 – Results of an indirect electro-oxidation of urea in a stirred undivided cell (Metrohm type cell) using various temperature. $E_{applied} = 550$ mV; $[CO(NH_2)_2]_{t=0} = 0.33$ mol L⁻¹; $[KOH] = 2$ mol L⁻¹; $S = 4$ cm²; $V = 50$ mL. The results are presented as the variation of the normalized concentration of the different by-products as a function of the amount of charge supplied. Urea, cyanate, ammonium, and nitrite are shown in parts (a), (b), (c), and (d), respectively. The nitrogen mass balance, e), and carbon balance, f), are normalized with respect to initial concentration. The temperatures are \circ 293, \square 298, \diamond 303, \times 308 and \star 313 K. The uncertainties are smaller than 5.9%. The current profiles over the electrolysis time are presented in part g).

III-4 Conclusion of Chapter 3

In this Chapter, the UEO in alkaline media was intensively investigated at lab-scale.

Firstly, the results provided evidence for the mediation of the nickel(III)/nickel(II) system in urea oxidation via the decoupling of nickel(II) electro-oxidation step (upper to 5 mV s^{-1}) from the indirect heterogeneous urea oxidation (lower to 5 mV s^{-1}), creating a consistent context for further kinetic and mechanistic study. By introducing the TON, the study demonstrated that no direct urea oxidation occurred. The hydroxide ion concentration strongly influenced the reversibility of the nickel(III)/nickel(II) system. Towards more environmentally sustainable process, decreasing this concentration, at least to 1 mol L^{-1} seems to be a relevant strategy. From the analysis of the viscosities, the urea diffusion coefficient was determined as well as the corresponding activation energy from the voltammograms.

Secondly, lab-scale-scale electrolyses were carried out with urea conversions close to 90%, contrary to most of the published works. By implementing various analytical methods, mass balances in the liquid phase could be established; while they were found complete for the carbon element, they deviated by up to 20% for the nitrogen element, showing that some gaseous compounds should be produced. Another original result was the identification of the cyanate, ammonium, nitrite, and carbonate ions as the major by-products of UEO. In the perspective of larger scale implementing UEO, the amount of these by-products had to be reduced in order to orientate the mineralisation of urea towards non-polluting compounds. Experiments performed in a mono-compartment cell configuration showed that nitrites could be reduced at the cathode, thereby reducing the amount of environmentally harmful by-products by 50%, but at the expense the production of hydrogen. Furthermore, by varying from 293 to 313 K, the temperature of the reactional medium had no influence on the formation of by-products. From an environmental process perspective, it would be interesting to perform a mass balance on the nickel electrode in order to exclude any pollution due to nickel release.

From this Chapter, some guidelines could be proposed in order to design and operate an electrolyser able to treat urea by this EC method. They would consist in implementing an undivided cell configuration, containing an electrolyte with 1 mol L^{-1} KOH and at room temperature. The results in **Chapter V** will enable us to study the change of scale under such conditions.

From kinetics and mechanisms to reactor modeling of the reactions involving urea and nickel(III)

Outline of the current chapter

IV-1 Introduction	100
IV-2 Methodology of the kinetic study	101
IV-2.1 Kinetic study on nickel synthesized powders	101
IV-2.2 Kinetics investigations of the reaction between urea and chemically synthesized nickel(III) sites in alkaline medium . . .	105
IV-2.3 Kinetic investigations of the reaction between urea and the electrochemically generated nickel(III) sites in alkaline medium	108
IV-3 Results on the kinetic of the urea catalytic indirect oxidation	108
IV-3.1 Case 1: with chemically synthesized nickel(III) sites	108
IV-3.2 Case 2: with the electrochemically synthesized nickel(III) sites on bare nickel electrode	113
IV-4 Establishment of a complete mechanism for the whole urea electro-oxidation	116
IV-5 Macro- and micro-modeling of the UEO	119
IV-5.1 Establishment of the predictive model	119
IV-6 Conclusion of Chapter 4	127

This chapter presents the results obtained from the article “G. Hopsort*, L. Latapie, K. Groenen Serrano, K. Loubière, T. Tzedakis* (2023). Progress toward a better understanding of the urea oxidation by electromediation of nickel(III)/nickel(II) system in alkaline media. *American Institute of Chemical Engineers J.*, e18113. [10.1002/aic.18113](https://doi.org/10.1002/aic.18113)".

Consequently, to maintain consistency, the introduction have been rewritten and the material and methods section removed.

IV-1 Introduction

To the best of our knowledge, only two studies have been devoted to these investigations (see **Chapter II**, section **I-2.3.b**). By neglecting the catalytic regeneration of the couple NiOOH/Ni(OH)₂ and using Tafel plots, Vedharathinam et al. [142] were the first to propose the following simplified kinetic law as in Eq. **IV.1** without determining the kinetic constant k .

$$\text{rate}_{\text{urea}} = k \times [\text{CO}(\text{NH}_2)_2]^{0.3} \times [\text{OH}^-]^2 \quad (\text{IV.1})$$

Later, partial orders of 1.22 and 0.26 for hydroxide ions and urea respectively on a β -NiOOH covered electrode were obtained using cyclic voltammetry and Tafel plots by Singh et al. [141]. The authors have claimed that: (i) the reaction order of urea concentration is independent of the applied potential and (ii) increasing the applied potential causes the reaction order of the hydroxide ions to decrease. However, in these studies, experiments were carried out in transient state conditions (*i.e.*, high potential scan rate), in which nickel(III) was not constantly regenerated at the electrode surface, as pointed out in the previous **Chapter III**. As obtained in the mixed ER/HCR regime and at low urea conversion rates, the related values of partial reaction orders allowed neither the understanding of the impact that the secondary reactions (occurring at higher urea conversion rates) may have on the EC system, nor obtaining access to relevant intrinsic kinetic information.

To fill this gap, this chapter aims at investigating the kinetics of NiOOH catalytic urea oxidation in an alkaline medium. For this purpose, and since neither explicit rate law nor kinetic models are described in the literature, a novel approach will be suggested, combining studies of the urea action according to (i) specifically synthesized NiOOH powder and to (ii) electrochemically generated NiOOH sites, carried out under steady state conditions.

By implementing catalytic urea oxidation in a suspension of NiOOH solid particles, one can expect to bring new insights on the reaction kinetics by comparing chemophysical phenomena taking place in the presence of (i) non-regenerated NiOOH sites (adsorption, HCR, desorption) on solid particles or (ii) electro-generated NiOOH sites (HCR/ER coupling). Results on oxidation kinetics with the synthesized nickel particles will first be studied. The experiments performed in a lab-scale electrolysis cell at low scan rates enabled to determine the key parameters of the kinetic law for the UEO reaction. Furthermore, by combining the newly-established kinetic rate law with the electrolysis results obtained at high urea conversion rates, a detailed mechanism of urea oxidation in alkaline medium on nickel(III) active sites was proposed, allowing the formation of the liquid phase by-products identified by Tatarchuk et al. [146] and also in the previous **Chapter III**.

Finally, one can regret a lack of Electrochemical Engineering approach of the UEO processes (cell design, geometry and optimization at pilot and industrial scale) [89, 222] in the state of the art. The present study also proposes an original modelling approach enabling the coupled phenomena (electro-oxidation, adsorption, kinetic and mass transport) that occurs during the UEO process to be described. This approach is based on the previously determined kinetic law and can predict the conversion rate of urea during electrolysis at high conversion rates and on a large scale.

This Chapter will be structured as follows:

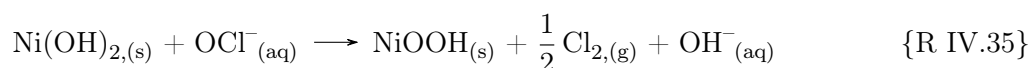
- (i) the kinetic parameters deduced from both chemically and electrochemically synthesized nickel(III) particles;
- (ii) the establishment of a complete mechanism for the whole UEO;
- (iii) the construction of a model and the validation by comparison with experimental data.

IV-2 For a better understanding of the mechanism of action of urea on active nickel(III) sites: a parallel study of the contribution of nickel(III)/nickel(II) electromediation

IV-2.1 Kinetic study on nickel synthesized powders

IV-2.1.a Synthesis protocol

The NiOOH powder was synthesized following the protocols developed by Pan et al. [223] and Thimmasandra et al. [224]. It consisted of oxidizing a Ni(OH)₂ powder at room temperature in presence of sodium hypochlorite NaOCl and sodium hydroxide NaOH, as {R IV.35}.



Specifically, NiOOH particles were prepared by mixing 5 g of a commercially available nickel(II) powder with a solution containing 400 mL of sodium hypochlorite and 2 g of sodium hydroxide. The reaction was achieved after 4 h of magnetic stirring and the mixture obtained was filtered using a Büchner sintered glass filter, and then washed with 6 × 60 mL of deionized water. The NiOOH powder was finally dried in oven at 80 °C during three days. Using two different concentrations of hypochlorite (1.76 × 10⁻¹ mol L⁻¹ and 7.68 × 10⁻¹ mol L⁻¹) powders called Sample 1 and Sample 2 respectively were synthesized to vary the nickel(III) purity.

IV-2.1.b Powder characterization techniques

Various techniques were used to characterize the initial and the synthesized powders.

Firstly, the purity of the nickel(III) particles was quantified by potentiometric back titration using Mohr's salt. An excess of ferrous salt was introduced into a suspension of

NiOOH/Ni(OH)₂ particles. After reaction, the excess of ferrous salt was titrated by an acidic solution of potassium dichromate in accordance with {R IV.36 - R IV.37}.

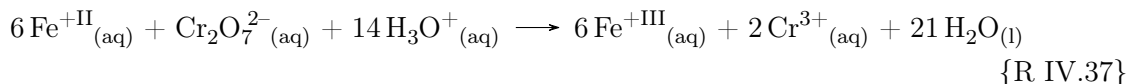
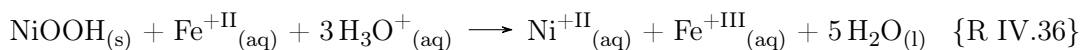


Figure IV.1 describes the experimental set-up used to evaluate the purity of nickel(III) in the synthesized powder. A precise amount of powder (137 mg) was mixed in a beaker filled with a solution composed of 30 mL of deionized water and 2 mL of hydrochloric acid. 882 mg of Mohr's salt was added, corresponding to a large excess of ferrous ions. A stirring period of 5 min was applied to obtain a total oxidation reaction between ferrous ions and nickel(III) particles. The last step consisted in determining the remaining ferrous ions (*i.e.*, the ones that did not react) by a potentiometric titration with K₂Cr₂O₇ dichromate(VI) potassium.

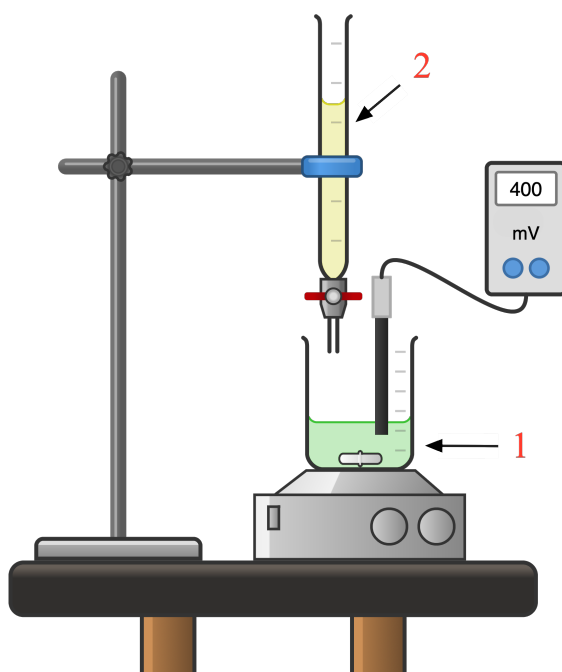


Fig. IV.1 – Schematic representation of the experimental set-up used for determining the purity of the synthesized nickel(III) powder. Label 1 represents the nickel(III) particles dissolved in an acidic oxidized Fe^{+III} solution at $7.2 \times 10^{-2} \text{ mol L}^{-1}$ and label 2 represents the K₂Cr₂O₇ solution at $3.75 \times 10^{-2} \text{ mol L}^{-1}$.

The equivalent volume was deduced from the rise in potential measured by a combined Pt ring electrode Metrohm. An example of a potential *vs.* poured volume is shown in Figure IV.2. The purity was determined as the ratio of the mass of nickel(III) deduced from the titration to the initial mass of the Ni(OH)₂ powder used in the trial. At last, the amount of nickel(III) was equal to the amount of ferrous ions that reacted according to Eq IV.2.

$$n_{\text{nickel(III)}} = n_{\text{Fe}^{+II}}^{\text{in excess}} - n_{\text{Fe}^{+II}}^{\text{titration}} \quad (\text{IV.2})$$

The crystalline structure of the nickel synthesized powders was studied by X-Ray powder Diffraction (XRD) analysis using a diffractometer (MiniFlex600 - D/Tex Ultra2, Rigaku,

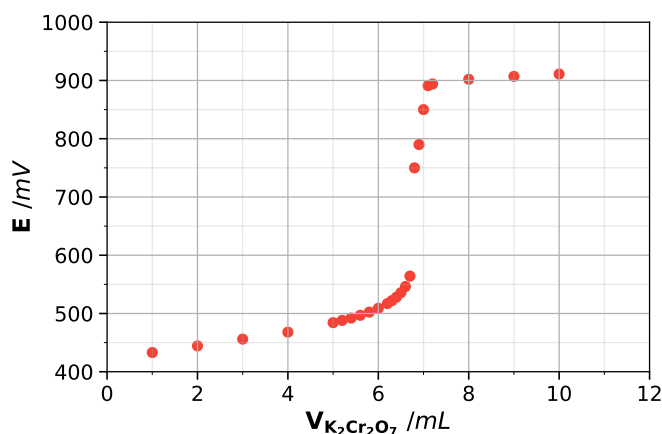


Fig. IV.2 – Potentiometric titration curve involving 32 mL of a solution of nickel(III) particles dissolved in acidic oxidized Fe^{+III} at $7.20 \times 10^{-2} \text{ mol L}^{-1}$, and a solution $K_2Cr_2O_7$ at $3.75 \times 10^{-2} \text{ mol L}^{-1}$.

Japan) with Cu- $K\alpha$ radiation (40 kV, 15 mA). Data, illustrated in Figure IV.3, were collected in the 2θ range of $5-92^\circ$. The step width was 0.02° with a scan speed of $10^\circ \text{ min}^{-1}$. From the literature on nickel(III) XRD characterizations [224–228], the initial powder was well identified as nickel(II) hydroxide $\beta\text{-Ni(OH)}_2$ with a brucite-type structure. After synthesis, samples 1 and 2 were founded to be nickel(III) as $\beta\text{-NiOOH}$ according to diffraction peaks for (001) and (002) crystal faces at 19 and 37° [229]. It is noted that the peaks associated with $Ni(OH)_2$ have disappeared. The differences in peak intensities between spectra 2 and 3 could be explained by some differences in crystallinity (a slight amorphous phase could be present in sample 2) which could broaden the diffraction peaks.

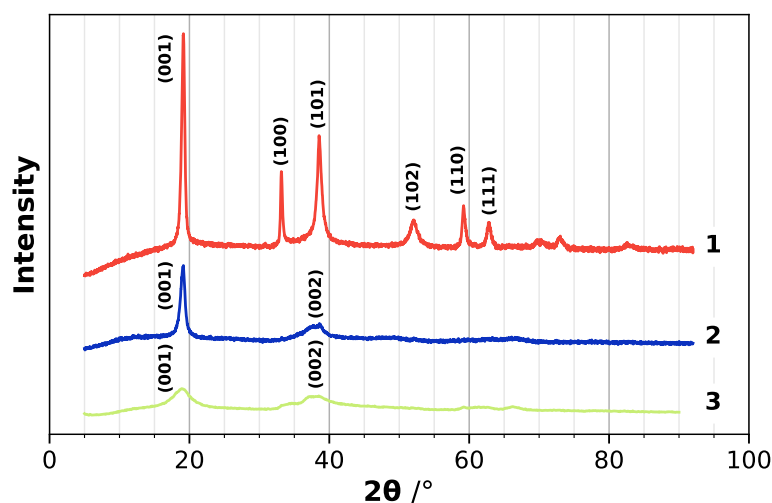


Fig. IV.3 – XRD patterns of (1) commercial $Ni(OH)_2$ powder, (2) and (3) powders obtained by $Ni(OH)_2$ oxidation using respectively 0.176 and 0.768 mol L^{-1} hypochlorite solutions.

Scanning Electron Microscope (SEM) images were obtained using a microscope (JSM 7100F, JEOL, Benelux) operated at 10 kV. As shown in Figure IV.4, the morphology of the various particles did not significantly change after the reaction with hypochlorite and the resulting particles could be assumed as spherical in shape with a wide size distribution from 1 to $30 \mu\text{m}$. These particles, or at least the shell around the particle, are supposed to be composed by $NiOOH$ sites.

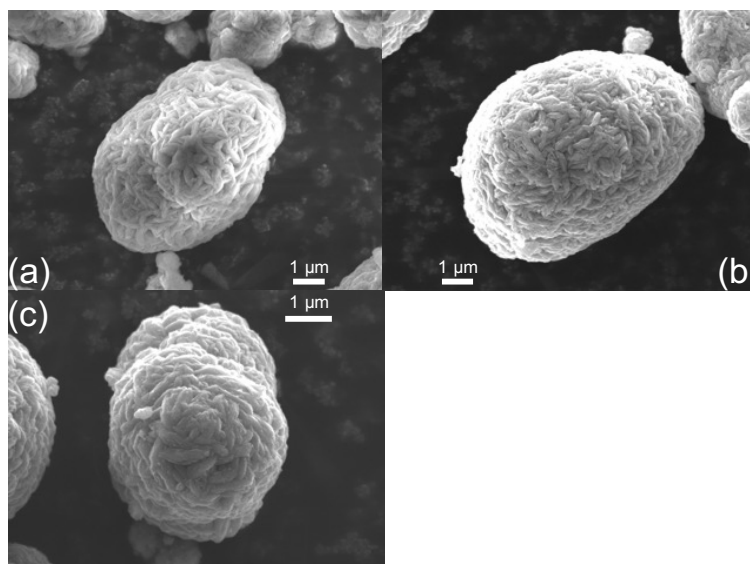


Fig. IV.4 – SEM images of the samples (a) $\text{Ni}(\text{OH})_2$ commercial powder (b) nickel(III) powder – sample 1 (c) nickel(III) powder – sample 2.

A laser diffraction particle size analyzer (Mastersizer MS3000, Malvern Instruments, United-Kingdom) was used to determine the particle size distributions in terms of number and volume. The characteristic diameters of the number and volume distributions of the initial and synthesized powders are reported in Table IV.1. Relative densities of the nickel particles were measured via a helium pycnometer (AccuPyc 1330, Micromeritics, United States). They underwent minor modifications both before and after the synthesis (see Table IV.1). Brunauer, Emmett and Teller (BET) measurements (BELSORP-mini II, BEL, Japan) were made to quantify the porosity and specific area of the particles. As the synthesis reaction of nickel(III) particles consisted in exchanging an electron and a proton, the properties of the particles (porosity, pore diameter, particle size) were slightly modified before and after synthesis. Table IV.1 summarises all the physical properties of the initial nickel(II) powder and of the synthesized nickel(III) powders.

	Particle size analysis (μm)					Purity (%) of nickel(III) content	Density (g cm^{-3})
	<i>Volume distribution</i>						
	d_{10}	d_{50}	d_{90}	d_{32}	d_{43}		
Initial nickel(II) powder	3.9	9.0	16.9	5.4	9.8	0	3.7 ± 0.1
Nickel(III) powder Sample 1	5.5	12.3	24.0	9.9	13.7	79 ± 2	3.9 ± 0.1
Nickel(III) powder Sample 2	4.5	10.0	20.5	7.9	11.4	29 ± 2	3.8 ± 0.1
	<i>Number distribution</i>					Specific surface area ($\text{m}^2 \text{g}^{-1}$)	Mean pore diameter (nm)
	d_{10}	d_{50}	d_{90}	d_{32}	d_{43}		
	Initial nickel(II) powder	0.4	0.5	0.8	5.5		
Nickel(III) powder Sample 1	1.3	3.4	8.1	9.9	13.7		
Nickel(III) powder Sample 2	0.7	1.3	5.3	7.9	11.4	8.51 ± 0.12	7.7 ± 0.1

Table IV.1 – Physical properties of the initial nickel(II) powder and of the nickel(III) powders.

IV-2.2 Kinetics investigations of the reaction between urea and chemically synthesized nickel(III) sites in alkaline medium

IV-2.2.a Experimental set-up and reaction monitoring

The experimental set-up, illustrated in Figure IV.5 and used to monitor the catalytic oxidation of urea by nickel(III) particles in alkaline medium, consisted of a closed double-walled thermoregulated reactor operating under nitrogen atmosphere (nitrogen was previously humidified to avoid any decrease of the reaction volume).

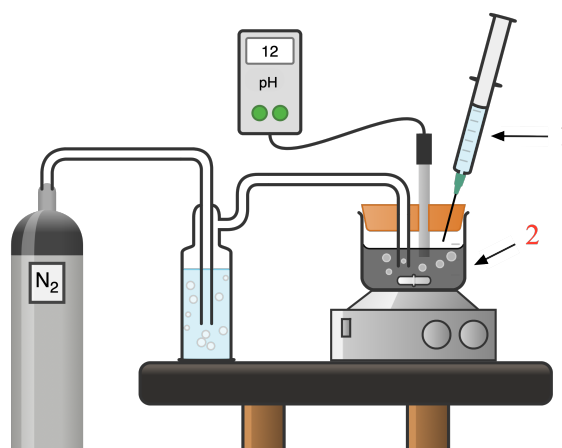


Fig. IV.5 – Schematic representation of the experimental set-up used for studying the kinetics of the catalytic oxidation between urea and nickel(III) particles. Label 1 represents urea in a KOH solution and label 2 represents NiOOH particles in KOH solution in a thermoregulated cell under N_2 atmosphere.

The reactor initially contained a suspension of 5 g of synthesized powder into 45 mL volume of KOH solution at different concentrations. Ultrapure water $18.2 \text{ M}\Omega \text{ cm}$ was

systematically used to prepare suspensions. A strong stirring created by a suitable magnetic bar ($\frac{\phi_{\text{reactor}}}{\phi_{\text{magnetic bar}}} = \frac{6.5}{4.8}$, 800 RPM) ensured that all of the particles were thoroughly suspended. Before introducing urea, the suspension containing NiOOH/Ni(OH)₂ particles was stirred during 5 min in order to finely disperse the nickel powder into the whole KOH volume. The aqueous deaerated alkaline solution of urea was then injected with a syringe through a septum. Each experiment was performed twice to ensure repeatability. The consumption of hydroxide ions was monitored via the pH to study the reaction kinetics. To succeed, this method required a precise pH meter (3 digits), a calibration at the appropriated pH range (pH 13-14), and a glass electrode resistant to the involved suspension. To fill these conditions, a Metrohm Unitrode electrode was used enabling to record the pH every 0.5 s with an accuracy of ± 0.001 pH units. Typical examples of the temporal variation of pH recorded in this study are shown in Figure IV.6.

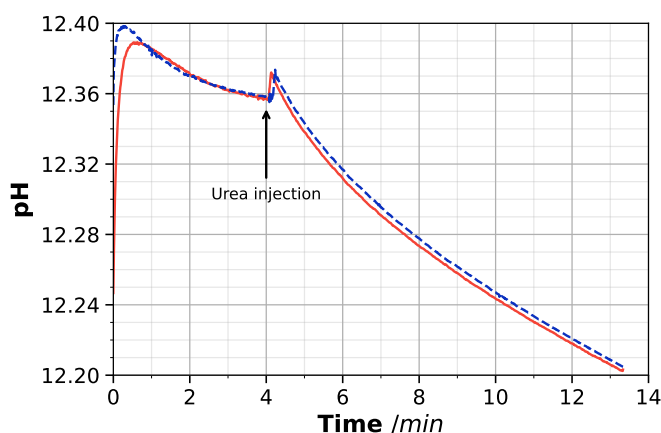


Fig. IV.6 – Typical temporal variations of the pH when an alkaline urea solution was brought into contact with chemically synthesized nickel(III) sites. The repeatability of the results is represented here with two trials (solid and dashed lines).

One could observe that, at the beginning of the recording, a transitional stage occurred corresponding to the time required to reach the perfectly mixed state of the liquid-solid suspension, before injecting the urea alkaline solution (5 mL). The two curves plotted on this figure also highlighted the satisfactory repeatability of the experiments when two different solutions of urea in hydroxide solutions were injected in two identical suspensions of nickel(III) particles. To understand how the reagent concentrations could affect the oxidation kinetic, and subsequently to identify the relevant kinetic parameters, an experimental work plan was established. It allowed varying the hydroxide concentrations from 5×10^{-3} to $5 \times 10^{-2} \text{ mol L}^{-1}$ and the urea concentrations from 10^{-2} to $3 \times 10^{-1} \text{ mol L}^{-1}$ (note that the latter value corresponded to the order of magnitude of the urea concentration in human urine). In addition, the nickel(III) concentration was modified by working with both powders of nickel(III) of different purities. As a preliminary step, it was verified that (i) the chemical reaction occurring when an alkaline urea solution was put into contact with chemically synthesized nickel(III) particles led to identical by-products in the liquid phase when compared to the ones taking place on nickel bare electrode, and (ii) the TOC concentration decreased during the reaction course. For this purpose, the analytical procedure involved IC and NPOC, as described in **Chapter II**.

IV-2.2.b Post-processing of the temporal pH-curves

The instantaneous rate of the reaction {R III.27}, expressed in $\text{mol}(\text{m}^3 \text{g}_{\text{cat}} \text{s})^{-1}$ and noted r_χ , was defined as the derivative of the extent of reaction, ξ , with respect of time, as shown in Eq. IV.3.

$$\begin{aligned} r_\chi &= -\frac{1}{m_{\text{cat}} \times V} \frac{d\xi}{dt} = -\frac{1}{m_{\text{cat}} \times V} \frac{dn_{\text{CO}(\text{NH}_2)_2}}{dt} \\ &= -\frac{1}{m_{\text{cat}} \times V \times \nu_{\text{nickel(III)}}} \frac{dn_{\text{nickel(III)}}}{dt} \\ &= -\frac{1}{m_{\text{cat}} \times \nu_{\text{OH}^-}} \frac{d[\text{OH}^-]}{dt} \end{aligned} \quad (\text{IV.3})$$

where m_{cat} is the nickel(III) mass (expressed in grams of catalyst, g_{cat}), ν_i the stoichiometric coefficient of the reactant i in {R III.27}, V the reaction mixture volume (assuming the volume constant *vs.* time, m^3) and $n_{\text{nickel(III)}}$ the amount of nickel(III) sites into the solid particles of $\text{NiOOH}/\text{Ni}(\text{OH})_2$ that were accessible to the reagents (urea and OH^-). The kinetic law of the chemical reaction was assumed to obey to Eq. IV.4.

$$r_\chi = k_\chi \times [\text{CO}(\text{NH}_2)_2]^{\alpha_\chi} \times [\text{OH}^-]^{\beta_\chi} \times (\rho_{\text{cat}})^{\gamma_\chi} \quad (\text{IV.4})$$

where α_χ , β_χ , γ_χ are the partial orders of the reaction, respectively related to urea, hydroxide, and chemically synthesized nickel(III) sites, k_χ the reaction rate constant ($\text{mol}^{1-(\alpha_\chi+\beta_\chi)} \text{m}^{-3[1-(\alpha_\chi+\beta_\chi)]} \text{g}_{\text{cat}}^{-1[1-\gamma_\chi]} \text{s}^{-1}$) and ρ_{cat} the mass concentration of nickel(III) per unit of volume ($\text{g}_{\text{cat}} \text{m}^{-3}$).

Despite the similarity in terms of by-products, the fundamental mechanisms underlying the urea degradation (in particular the adsorption/desorption ones) were different, depending whether the nickel(III) sites used was electrochemically generated or chemically synthesized. For this reason, distinct notations were used for the kinetic law: r_χ for chemically synthesized sites (defined in Eq. IV.4) and $r_{E\chi}$ for electro-generated sites. The conversion rate of the HCR reaction, noted X , could be calculated from the pH measurements, according to Eq. IV.5.

$$X_{(t)} = 1 - \frac{10^{\text{pH}_{(t)}-14}}{10^{\text{pH}_{t=0}-14}} \quad (\text{IV.5})$$

The experimental curves, $\text{pH}_{(t)}$, were systematically smoothed using a polynomial of order 6 as the raw data were slightly noisy, mainly due to disturbances caused by the stirring and specifically by the flow of the solid particles across the pH electrode. In this work, the initial reaction rates, r_χ^0 , were determined for conversions never exceeding 5% of the initial hydroxide concentration, and calculated from the slope of the $\text{pH}_{(t)}$ curve measured some seconds after the urea injection. The time period considered to calculate these slopes (typically between 5 s and 50 s) slightly impacted the obtained valued, as shown in Appendix E.

IV-2.3 Kinetic investigations of the reaction between urea and the electrochemically generated nickel(III) sites in alkaline medium

IV-2.3.a Expression of reaction rate

The reaction rate of the HCR on electro-generated nickel(III) sites, standardized by the electrode surface, was expressed in $\text{mol m}_{\text{elec}}^{-2} \text{m}_{\text{bulk}}^{-3} \text{s}^{-1}$ and defined as the flux density of the superficial chemical reaction by Eq. IV.6.

$$r_{E\chi} = k_{E\chi} \times [\text{CO}(\text{NH}_2)_2]_{(t)}^{\alpha_{E\chi}} \times [\text{OH}^-]_{(t)}^{\beta_{E\chi}} \times (S_{\text{elec}})^{\gamma_{E\chi}} \quad (\text{IV.6})$$

where $k_{E\chi}$ as the reaction rate constant ($\text{mol}^{1-[1-(\alpha_{E\chi}+\beta_{E\chi})]} \text{m}_{\text{bulk}}^{-3[1-(\alpha_{E\chi}+\beta_{E\chi})]} \text{m}_{\text{elec}}^{-2[1-\gamma_{E\chi}]} \text{s}^{-1}$), S_{elec} the surface of the bare nickel electrode (m^2) and $\alpha_{E\chi}$, $\beta_{E\chi}$, $\gamma_{E\chi}$ the partial orders of urea, hydroxide, and electrochemically generated nickel(III), respectively.

IV-3 Results on the kinetic of the urea catalytic indirect oxidation

IV-3.1 Case 1: with chemically synthesized nickel(III) sites

IV-3.1.a Determination of the initial kinetic rate law

The initial rate method is a well-known approach [230, 231], enabling to determine the partial orders of each reactant by varying its concentration while keeping constant the other reactant concentrations and the operating conditions (temperature, stirring). To determine the partial order of urea, noted α_χ , several temporal pH-measurements are performed and the related initial rates, r_χ^0 , determined. By varying the initial concentration of urea between 0.02 and 0.25 mol L^{-1} , and by keeping $[\text{OH}^-] = 0.005 \text{ mol L}^{-1}$ and the nickel particle mass equal to 30 $\text{kg}_{\text{cat}} \text{ m}^{-3}$ (nickel(III) powder - sample 2), the initial kinetic rate law (Eq. IV.4) can be written as the Eq. IV.7.

$$r_\chi^0 = k_{\text{app}} \times [\text{CO}(\text{NH}_2)_2]^{\alpha_\chi} \quad (\text{IV.7})$$

where k_{app} is the related apparent constant ($\text{mol}^{1-[1-\alpha_\chi]} \text{m}^{-3[1-\alpha_\chi]} \text{g}_{\text{cat}}^{-1} \text{s}^{-1}$).

The variation of the logarithmic initial reaction rate versus the logarithmic urea concentration, plotted in Figure IV.7-a, can be assumed linear despite a rather strong dispersion. From the slope of the related straight line, the partial order of urea is found equal to $\alpha_\chi = 0.2 \pm 0.1$. This low value suggests that the kinetic rate slightly depends on the urea concentration, which could be explained by several reasons:

- the strong affinity of the nickel peroxides particles for the urea. Let's consider that the adsorption of urea on nickel(III) sites obeys to a Langmuir isotherm as shown in Eq. IV.8.

$$\Gamma = \frac{\Gamma_{\text{max}} \times K \times [\text{CO}(\text{NH}_2)_2]}{1 + K \times [\text{CO}(\text{NH}_2)_2]} \quad (\text{IV.8})$$

where Γ the nickel surface concentration (mol m^{-2}), Γ_{max} the maximum nickel surface concentration available on nickel oxide particles (mol m^{-2}) and K is the equilibrium

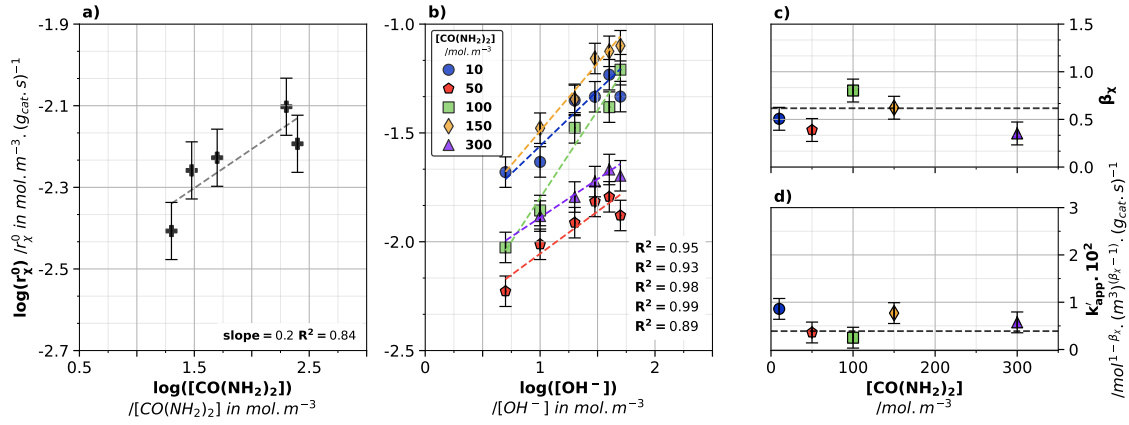


Fig. IV.7 – Kinetic experiments with chemically synthesized nickel(III) sites: measurements of the initial rate versus the concentration of a) urea and b) potassium hydroxide. Graph c) provides the values of β_χ as a function of the KOH concentration for different urea concentrations. k'_{app} remains constant whatever the urea concentration, as shown in the graph d). Graph a) was achieved with a 5 mmol L^{-1} KOH solution. All these results were obtained with nickel(III) synthesized powder – Sample 2.

constant of the adsorption step. In this case, the urea superficial concentration on the nickel(III) sites can be simplified ($K \times [\text{CO}(\text{NH}_2)_2] \gg 1$) as Eq. IV.9.

$$\Gamma = \Gamma_{\max} \quad (\text{IV.9})$$

This means that adsorption is rapid and limited by accessible nickel(III) sites. Regardless of the volume concentration of urea, its superficial concentration remains constant and equal to Γ_{\max} , and thus the nickel(III) surface is saturated with urea.

- the mass transfer limitations of the reagents into the internal nickel oxides layers of core-shell particles.

The same method was implemented for determining the hydroxide partial order, β_χ , by varying the related concentration between 0.005 and 0.05 mol L^{-1} . Here, the simplified initial kinetic rate law can be deduced from Eq. IV.4 and can be written as Eq. IV.10.

$$r_\chi^0 = k'_{app} \times [\text{OH}^-]^{\beta_\chi} \quad (\text{IV.10})$$

where k'_{app} is the related apparent constant (as $k'_{app} = k_\chi \times [\text{CO}(\text{NH}_2)_2]^{0.2} \times (\rho_{cat})^{\gamma_\chi}$, in $\text{mol}^{[1-\beta_\chi]} \text{ m}^{-3[1-\beta_\chi]} \text{ g}_{cat}^{-1} \text{ s}^{-1}$). Figure IV.7-b presents the variation of the logarithmic initial reaction rate *vs.* the logarithm of the hydroxide concentration, for five different urea concentrations ranging from 0.01 to 0.3 mol L^{-1} . These variations are assumed linear and their slopes, determined for various urea concentrations, are reported in Figure IV.7-c. This leads to $\beta_\chi = 0.6 \pm 0.2$. As urea has been found to slightly impact the reaction rate, a small variation of the apparent constants, k'_{app} , as a function of the urea concentration is observed in Figure IV.7-d, likely due to some measurement errors. From this, an average value of the apparent constant is found equal to $0.38 \times 10^{-2} \text{ mol}^{0.4} \text{ m}^{-1.2} \text{ g}_{cat}^{-1} \text{ s}^{-1}$.

By modifying the nickel(III) purity of the synthesized powders (Samples 1 and 2, see Table IV.1) and keeping constant the initial concentrations of urea at 0.3 mol L^{-1} and of

hydroxide at 0.005 mol L^{-1} , the partial order of nickel(III), γ_χ , can be deduced as Eq. IV.11.

$$r_\chi^0 = k''_{app} \times (\rho_{cat})^{\gamma_\chi} \quad (\text{IV.11})$$

where k''_{app} is the related apparent constant ($\text{mol} (\text{m}^3_{\text{bulk}})^{\gamma_\chi-1} \text{g}_{\text{cat}}^{-(1+\gamma_\chi)} \text{s}^{-1}$). Considering that the mass concentration of nickel(III), ρ_{cat} , is the product of the mass of powder introduced and the nickel(III) content in the powder, the slope of the Eq. IV.12 allows to determine the reaction order of nickel(III).

$$\ln(r_\chi^0) = \ln(k''_{app}) + \gamma_\chi \times \ln(\text{mass of powder} \times \text{purity}) \quad (\text{IV.12})$$

At last, γ_χ is found almost equal to 1.9 ± 0.2 which can be interpreted as the number of nickel(III) sites (NiOOH in fact) involved in the urea oxidation reaction. Once the partial orders are determined, the kinetic constant, k_χ , is calculated using the values of (i) initial concentrations of the reagents and of (ii) initial rates measured for 35 trials according to Eq. IV.4. As illustrated in Figure IV.8, k_χ is ranging from $k_{\chi,low} = 0.24 \times 10^{-12}$ to $k_{\chi,high} = 7.7 \times 10^{-12} \text{ mol}^{0.2} \text{ m}^{5.1} \text{ g}_{\text{cat}}^{-2.9} \text{ s}^{-1}$, the average value being equal to is $k_{\chi,mean} = 3.8 \times 10^{-12} \text{ mol}^{0.2} \text{ m}^{5.1} \text{ g}_{\text{cat}}^{-2.9} \text{ s}^{-1}$.

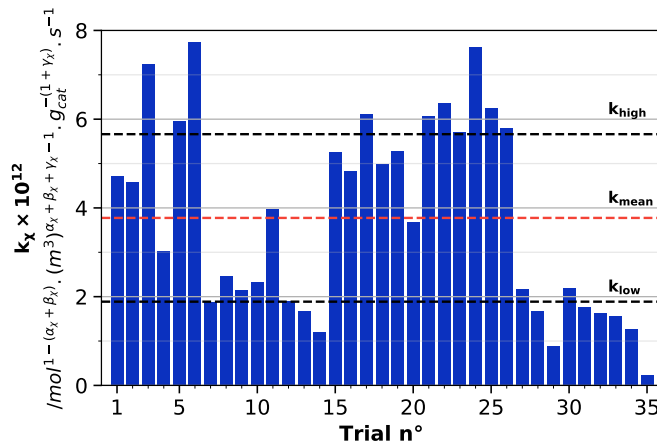


Fig. IV.8 – Distribution histogram of the determined kinetic constant k_χ for the 35 experiments carried out. The values were ranged between 2.4×10^{-13} and $7.7 \times 10^{-12} \text{ mol}^{0.2} \text{ m}^{5.1} \text{ g}_{\text{cat}}^{-2.9} \text{ s}^{-1}$ with a mean value at $3.8 \times 10^{-12} \text{ mol}^{0.2} \text{ m}^{5.1} \text{ g}_{\text{cat}}^{-2.9} \text{ s}^{-1}$.

Therefore, the overall empirical kinetic law of urea oxidation in presence of chemically generated nickel(III) sites can be expressed by Eq. IV.13.

$$r_\chi = (3.8 \pm 2.0) \times 10^{-12} \times [\text{CO}(\text{NH}_2)_2]^{0.2 \pm 0.1} \times [\text{OH}^-]^{0.6 \pm 0.2} \times \rho_{\text{cat}}^{1.9 \pm 0.2} \quad (\text{IV.13})$$

It should be kept in mind that (i) as the urea molecules penetrate into the NiOOH/Ni(OH)₂ particles, they are oxidized and the NiOOH is reduced to Ni(OH)₂ and (ii) the urea oxidation products generated have then to diffuse deeper into the particle to encounter another nickel(III) active site and to continue their mineralisation. As mentioned above, the occurrence of mass transfer limitations could also contribute to slow down the reaction rate. In the case of such synthesized nickel particles, the regeneration of nickel(III) sites cannot occur after being consumed by urea, which will inevitably modify the rate law here obtained.

IV-3.1.b Validation of the initial kinetic rate law by the integral method

In this section, it is assumed that there is no limitation by the mass transport (urea or/and OH^-), inside or outside of the $\text{NiOOH}/\text{Ni}(\text{OH})_2$ particles. Following this assumption, the validity of the kinetic rate law determined previously (Eq. IV.13) must be confirmed. To this end, it is necessary to numerically integrate the equation as a function of time and to confront the theoretical temporal variations of the reactant concentrations with the experimental data. Using the integral method for kinetic investigations offers the advantage [232] to validate the reaction orders and the rate constant obtained using the initial rate method (*i.e.*, at short times and very low OH^- conversions below 5%) for longer periods where high conversions are achieved and where secondary reactions can also occur. The method for doing so entails a comparison between the experimental and predicted temporal variations in OH^- concentration in order to validate the law derived from initial kinetics. Table IV.2 presents the chemical amounts of reactants, initially and at any time, where X represents the hydroxide conversion rate.

	moles of $\text{CO}(\text{NH}_2)_2$	moles of OH^-	moles of NiOOH	moles of accessible NiOOH
$t=0$	$a = [\text{CO}(\text{NH}_2)_2]^0 \times V$	$b = [\text{OH}^-]^0 \times V$	$c = \frac{m_{\text{cat}} \times \text{purity}}{M_{\text{NiOOH}}}$	$c' = c \times \epsilon$
t	$a - \frac{bX}{6}$	$b(1 - X)$	$c - bX$	$c' - bX$

Table IV.2 – Extent of urea oxidation reaction by chemically synthesized nickel(III) sites where V represents the liquid reaction volume ($4.5 \times 10^{-5} \text{ m}^3$), m_{cat} the mass of powder (5 g), M_{NiOOH} the NiOOH molar mass (91.7 g mol^{-1}) and X the conversion in hydroxide ions. The corresponding overall reaction is written as $\text{CO}(\text{NH}_2)_2 + 6 \text{OH}^- + 6 \text{NiOOH} \rightarrow \text{products}$.

Without considering the real accessibility of the nickel(III) sites in the synthesized core-shell particles, the theoretical profiles tend towards the experimental values but significant deviations of magnitude are obtained (deviation $> 50\%$) and even more for the highest reactant concentration (results not shown). In order to describe the physics of the system (*i.e.*, spherical layers of NiOOH around a core of $\text{Ni}(\text{OH})_2$), a surface accessibility factor of nickel(III), noted ϵ , is voluntarily introduced. Such choice is motivated by the fact that (*i*) the spatial distribution of nickel(III) on solid particles is probably not uniform, and (*ii*) the oxidation reaction of urea on nickel particles is a surface reaction, and the by-products and reaction intermediates formed inside the particle are consuming the OH^- ions. This latter consumption, not considered in the kinetic model here studied, will lead to a diffusional limitation of hydroxide ions within the particles. The parameter, ϵ , offers the advantage to fill this bias. Note that the relating value, not measured, will be the single fitting parameter of the model. By coupling Eq. IV.3 expressed as a function of hydroxide ions and Eq. IV.13, it comes Eq. IV.14.

$$\frac{dX}{dt} = \frac{6m_{\text{cat}}k_{\text{X}}b^{0.6}}{[\text{OH}^-]^0} \times \left(\frac{6a - bX}{6V}\right)^{0.2} \times \left(\frac{(1 - X)}{V}\right)^{0.6} \times \left(\frac{(c' - bX) \times M_{\text{NiOOH}}}{V}\right)^{1.9} \quad (\text{IV.14})$$

The previous equation is numerically solved (using `scipy.integrate.odeint` Python package solving a system of ordinary differential equations), and the theoretical temporal conversion of hydroxide with time is obtained, as reported in Figure IV.9 The surface accessibility factor of nickel(III), ϵ , used to plot these figures is equal to 2.6%, suggesting then that a

small amount of nickel(III) is available for the chemical reaction. Indeed, after a first cycle of adsorption onto the powder, the urea molecules having a strong affinity to nickel(III) could induce a “screen effect”, thus reducing the number of nickel(III) sites into the internal layers of the particles. Figure IV.9 also reports a sensitivity study with respect to the chemical kinetic constant, k_{χ} : a maximum deviation of 20% is observed for the reaction times longer than 600 s. The validity of the kinetic rate law is then checked by considering several initial concentrations of urea and hydroxide ions. Whatever the concentrations, the numerical profiles of the conversion of OH^- do not deviate (maximum deviation of 6%) from the experimental data for $X < 20\%$ ($\epsilon = 2.6\%$). As expected, higher conversions are observed when the initial hydroxide ions concentration is decreased. Figure IV.9 shows that the temporal profiles obtained using the kinetic rate law constant $k_{\chi,low}$, $k_{\chi,mean}$ or $k_{\chi,high}$ determined from the previous section are in very good agreement (maximum deviations of 10%) with the experimental ones for a period longer than 200 s. It can be noted that for unfavorable conditions, illustrated in Figure IV.9-c (*i.e.*, the lowest ratio between initial concentration of hydroxide ions and urea, almost equal to 1.7×10^{-2}), the deviation between the experimental and predictive profiles is higher than 20% after 600 s. This slowing down of the urea oxidation could be explained in several ways: (*i*) an internal diffusional limitation of the reactants (urea and hydroxide) and by-products in the particles could limit the reaction process after consuming all the nickel(III) active sites on the catalyst surface and (*ii*) a competitive adsorption between the by-products and the reactants could also occur.

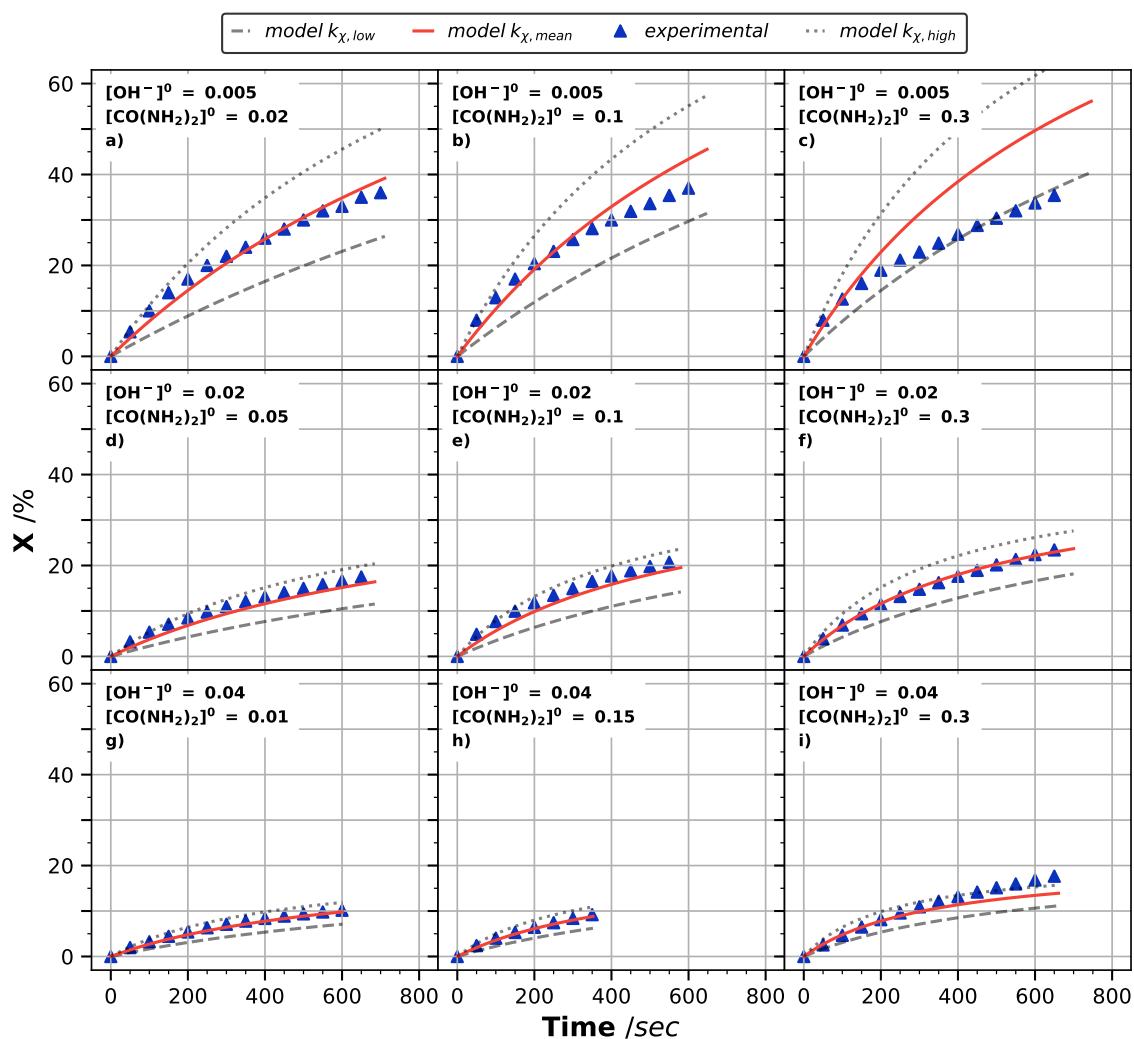


Fig. IV.9 – Comparison of the experimental temporal variations of the hydroxide ion conversion to the ones obtained by numerical solving of the Eq. IV.14 for different initial concentrations of urea and hydroxide (molar concentration are expressed in mol L^{-1}). The surface accessibility factor of nickel(III), ϵ , is equal to 2.6% whatever the graphs.

IV-3.2 Case 2: with the electrochemically synthesized nickel(III) sites on bare nickel electrode

In the present section, the NiOOH sites are electrochemically regenerated on a bare nickel anode and react with urea. As shown in the previous Chapter, the coupling of the HCR (Urea/NiOOH) with the ER (NiOOH/Ni(OH)₂) allows to continuously regenerate the active nickel(III) sites if the nickel oxides anode is polarized to the appropriated potential. It becomes then possible to study only the HCR and thus to avoid the adsorption/desorption processes as well as the mass transport of urea and oxidation products from one nickel(III) molecule to the other. For that, the current potential curves have been plotted by applying a potential scan rate lower than 1 mV s^{-1} . This technique has been here applied for different operating parameters, with the aim of establishing the kinetic law of the UEO in presence of electro-generated NiOOH sites at the anode. The $I=f(E)$ curves obtained at steady state conditions are showed in Figure IV.10-a-b-c. From them, the partial orders of urea, hydroxide ions and nickel(III) sites has been determined, as shown in Figure IV.10 respectively.

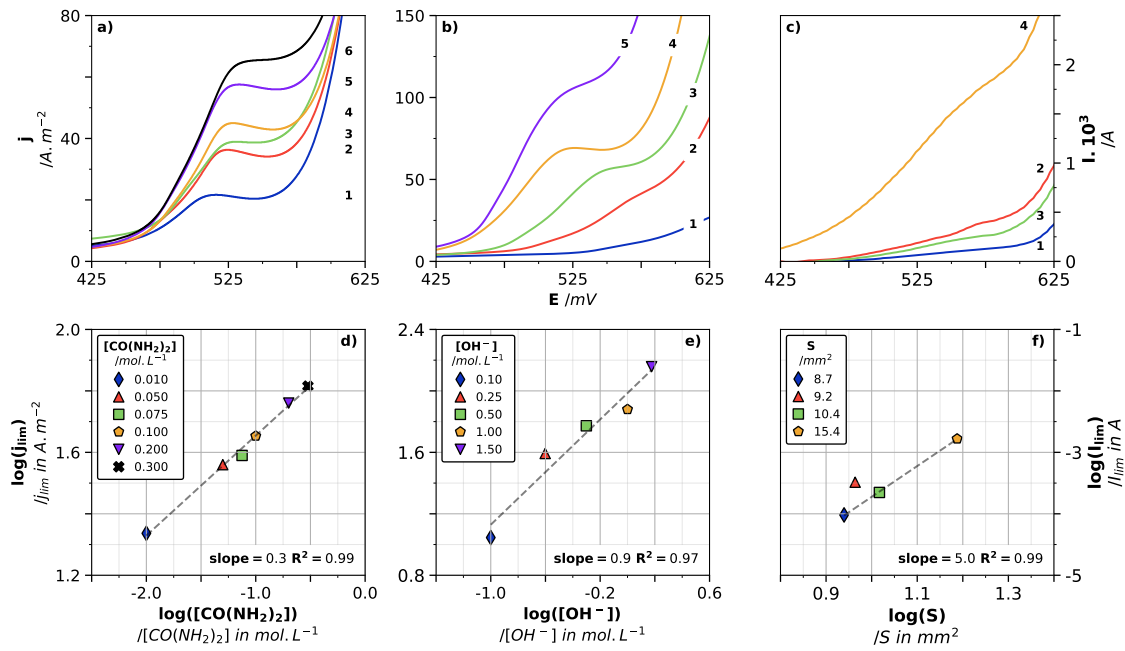


Fig. IV.10 – Kinetic experiments with electrochemically synthesized nickel(III) sites on bare nickel electrode. *Top*: Graphs a), b) and c) present $j/I=f(E)$ curves obtained at the steady state (0.12 mV s^{-1}) using a Ni WE immersed in 100 mL of alkaline solutions of urea, thermoregulated at 298 K.

Graph a) effect of urea concentration on the shape of the $I=f(E)$ curves obtained on nickel RDE in alkaline solution of KOH (1 mol L^{-1}) at 1000 RPM with urea concentrations at 0.01 mol L^{-1} (1), 0.05 mol L^{-1} (2), 0.075 mol L^{-1} (3), 0.1 mol L^{-1} (4), 0.2 mol L^{-1} (5) and 0.3 mol L^{-1} (6).

Graph b) effect of KOH concentration on the shape of the $I=f(E)$ curves obtained on nickel RDE in urea solution of 0.3 mol L^{-1} stirred at 1000 RPM with hydroxide concentrations at 0.1 mol L^{-1} (1), 0.25 mol L^{-1} (2), 0.5 mol L^{-1} (3), 1 mol L^{-1} (4) and 1.5 mol L^{-1} (5).

Graph c) effect of the geometric surface area (rectangular area) of the nickel electrode on the shape of the $I=f(E)$ curves obtained with an urea concentration of 0.3 mol L^{-1} and a KOH concentration of 1 mol L^{-1} , using geometrical electrode surfaces equal to 8.7 (1), 9.2 (2), 10.4 (3) and 15.4 mm^2 (4).

Bottom: The partial orders of urea ($\alpha_{E\chi}$), hydroxide ions ($\beta_{E\chi}$) and nickel(III) ($\gamma_{E\chi}$) were determined from the curves respectively plotted in Figures d), e) and f), deduced from the logarithm plot of the limiting current density magnitude (at the diffusion limitation area) as a function of the logarithmic reactant concentration.

The potentiostatic polarization of the nickel electrode at the plateau of the $I=f(E)$ curves allows the anode to be covered by Ni(OH)_2 which oxidizes into NiOOH . The urea is oxidized by chemical reaction with NiOOH which is reduced into the Ni(OH)_2 , immediately oxidized on the nickel electrode into NiOOH , thus releasing its electron. The newly regenerated NiOOH goes on a new cycle with the urea oxidation intermediate, thus meaning that the urea and its intermediates formed could be oxidized by the same nickel system, without any mass transfer limitation. The oxidation process continues until obtaining the final products (N_2 , CO_2 , etc.). Under steady state conditions, the mass balance on nickel(III) is expressed as the Eq. IV.15.

$$\frac{d\Gamma_{\text{III}}}{dt} = \frac{I_{\text{plateau}}}{n\mathcal{F}S_{\text{electrode}}} - \nu_{\text{nickel(III)}} \times \Gamma_{E\chi} \times V \quad (\text{IV.15})$$

where Γ_{III} is the nickel surface concentration (mol m^{-2}), I_{plateau} as the limiting current, observed at the plateau signal (A), n_e the number of exchanged electron (1, dimensionless),

\mathcal{F} the Faraday constant (C mol^{-1}), $\nu_{\text{nickel(III)}}$ the stoichiometric coefficient of nickel(III) and $r_{E\chi}$ the reaction rate of the HCR on electro-generated nickel(III) sites ($\text{mol m}_{\text{elec}}^{-2} \text{m}_{\text{bulk}}^{-3} \text{s}^{-1}$). It is obvious that after a certain time, the redox system $\text{NiOOH}/\text{Ni}(\text{OH})_2$ will reach a steady state until the concentration of urea is sufficient to supply the system. In this case, the accumulation of the nickel(III) at the nickel surface can be assumed equal to zero. The current intensity of the plateau is thus proportional to the reaction rate as Eq. IV.16.

$$I_{\text{plateau}}^{\infty} = n\mathcal{F} \times V \times \nu_{\text{nickel(III)}} \times k_{E\chi} \times [\text{CO}(\text{NH}_2)_2]^{\alpha_{E\chi}} \times [\text{OH}^-]^{\beta_{E\chi}} \times (S_{\text{electrode}})^{\gamma_{E\chi}+1} \quad (\text{IV.16})$$

where $I_{\text{plateau}}^{\infty}$ is the limiting current in steady state conditions (A). As for the initial rate method, by applying the logarithm to Eq. IV.16 and by varying the molar concentration of one reactant, the partial orders can be deduced, according to Eqs. IV.17 - IV.19

$$\log(j_{\text{plateau}}^{\infty}) = \log\left(n\mathcal{F} \times k_{E\chi} \times [\text{OH}^-]^{\beta_{E\chi}} \times (S_{\text{electrode}})^{\gamma_{E\chi}}\right) + \alpha_{E\chi} \times \log([\text{CO}(\text{NH}_2)_2]) \quad (\text{IV.17})$$

$$\log(j_{\text{plateau}}^{\infty}) = \log(n\mathcal{F} \times k_{E\chi} \times [\text{CO}(\text{NH}_2)_2]^{\alpha_{E\chi}} \times (S_{\text{electrode}})^{\gamma_{E\chi}}) + \beta_{E\chi} \times \log([\text{OH}^-]) \quad (\text{IV.18})$$

$$\log(I_{\text{plateau}}^{\infty}) = \log\left(n\mathcal{F} S_{\text{electrode}} \times k_{E\chi} \times [\text{CO}(\text{NH}_2)_2]^{\alpha_{E\chi}} \times [\text{OH}^-]^{\beta_{E\chi}}\right) + \gamma_{E\chi} \times \log(S_{\text{electrode}}) \quad (\text{IV.19})$$

where $j_{\text{plateau}}^{\infty}$ is the limiting current density corresponding to the plateau of the signal in steady state (A m^{-2}).

The related plots are reported in Figure IV.10-d-e-f. A value of $\alpha_{E\chi} = 0.3 \pm 0.1$ is obtained for the partial order of urea, which is in agreement with the value obtained with chemically synthesized nickel(III) sites. The partial order of hydroxide ions is found equal to $\beta_{E\chi} = 0.9 \pm 0.1$. This value is slightly higher than the previously one ($\beta_{\chi} = 0.6$), which can be attributed to the fact that additionally to the urea oxidation, the electro-generation of nickel(III) requires one hydroxide ion and thus implies a stronger dependence of the chemical rate by hydroxide ions. At last, the partial order of nickel(III) is found equal to $\gamma_{E\chi} = 5.0 \pm 0.5$. This high value would suggest that, during the potentiostatic polarization, a nickel active site is regenerated 5 times on the electrode surface per adsorbed urea. Since the number of urea adsorption sites onto nickel(III) is continuously electro-regenerated, the adsorbed urea molecule can be completely oxidized without any desorption of intermediates, contrary to the case with chemically synthesized particles, containing sacrificial NiOOH . Once the partial orders known, the kinetic constant, noted $k_{E\chi}$, is deduced using the same method than in the previous section. On the basis of eleven experiments carried out and illustrated in Figure IV.11, $k_{E\chi}$ is found to vary in the range from 2.32×10^{24} to $4.24 \times 10^{24} \text{ mol}^{-0.2} \cdot \text{m}_{\text{elec}}^{-12} \cdot \text{m}_{\text{bulk}}^{0.6} \cdot \text{s}^{-1}$. The average value is equal to $2.86 \times 10^{24} \text{ mol}^{-0.2} \text{m}_{\text{elec}}^{-12} \text{m}_{\text{bulk}}^{0.6} \text{s}^{-1}$ and used for the following calculations.

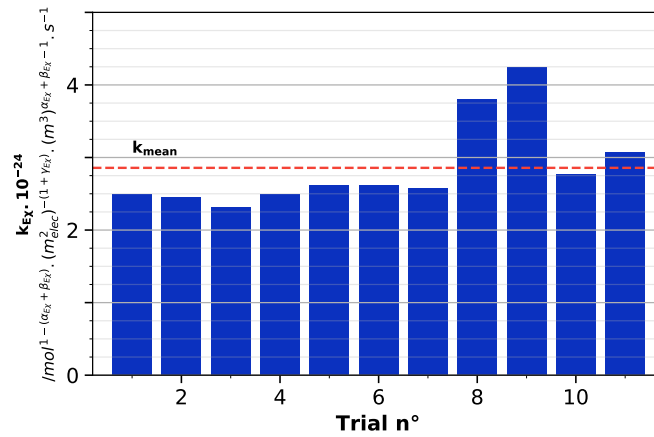


Fig. IV.11 – Distribution histogram of the determined kinetic constant k_{EX} for the 11 experiments carried out. The values were ranged between 2.32×10^{24} and 4.24×10^{24} with a mean value at $2.86 \times 10^{24} \text{ mol}^{-0.3} \text{ m}_{\text{elec}}^{-12} \text{ m}_{\text{bulk}}^{0.6} \text{ s}^{-1}$.

Finally, the proposed kinetic law for the urea oxidation by the electrochemically generated nickel(III) sites can be written as the Eq. IV.20.

$$r_{EX} = (2.86 \pm 1.38) \times 10^{24} \times [\text{CO}(\text{NH}_2)_2]^{0.3} \times [\text{OH}^-]^{0.9} \times (\text{S}_{\text{electrode}})^5 \quad (\text{IV.20})$$

IV-4 Establishment of a complete mechanism for the whole urea electro-oxidation

Based on the current state-of-art, Figure 1.8-a-b propose an overall mechanism for urea degradation involving electrochemically generated nickel(III) sites. The reaction scheme is composed of different pathways leading to the formation of by-products previously identified in the liquid phase in Chapter III. The urea degradation mechanism from electro-generated nickel(III) site can be classified into the nucleophilic oxidation reaction class [233, 234] (as for the methanol oxidation on nickel(III) [235]), involving two pathways: successive (i) electro-generated $\text{Ni}(\text{OH})_2$ catalyst dehydrogenation reaction followed by (ii) a spontaneous nucleophilic dehydrogenation reaction. Firstly, the urea is adsorbed on a nickel(III) site [236], formed by the catalyst dehydrogenation reaction of nickel(III) oxidation. By analogy to the urease action on urea [81, 237], a second active nickel(III) site is required to pursue the oxidation (step 2). Following the first nucleophilic attack onto a hydroxide group, two reactional pathways (step 3 and/or step 20) can be considered, favoring the formation of either ammonia (step 5), nitrite (steps 4, 8-19), and carbonate ions (steps 4-7), or cyanate ions (steps 20-22). The formation of ammonia and carbonate ions belongs to the same reactional pathway, thus suggesting an equimolar formation of these by-products over time. The nitrification route on nickel sites shown in Figure IV.12-b leads to the formation of nitrite. This route has been already studied by Density Functional Theory (DFT) [148], voltammetry and electrolyses [238]. This latter route does not rule out the production of nitrogen during oxidation, even if several works [147] have reported the overoxidation of nitrogen into undesired NO_x compounds at the expense of a nitrogen production. It should be noted that (i) the formation of cyanate (steps 21-22) and nitrite (steps 4, 18, 19) ions occurs in equimolar way, and (ii) most of the reactions constituting the proposed mechanism

require hydroxide ions, and consequently directly decrease the local pH at the electrode surface. This reaction scheme, reflects the complexity of a fully detailed kinetic approach that will require a very large number of experiments so as to be able to determine each elementary kinetic constant (from k_1 to k_{22} , forward and backward).

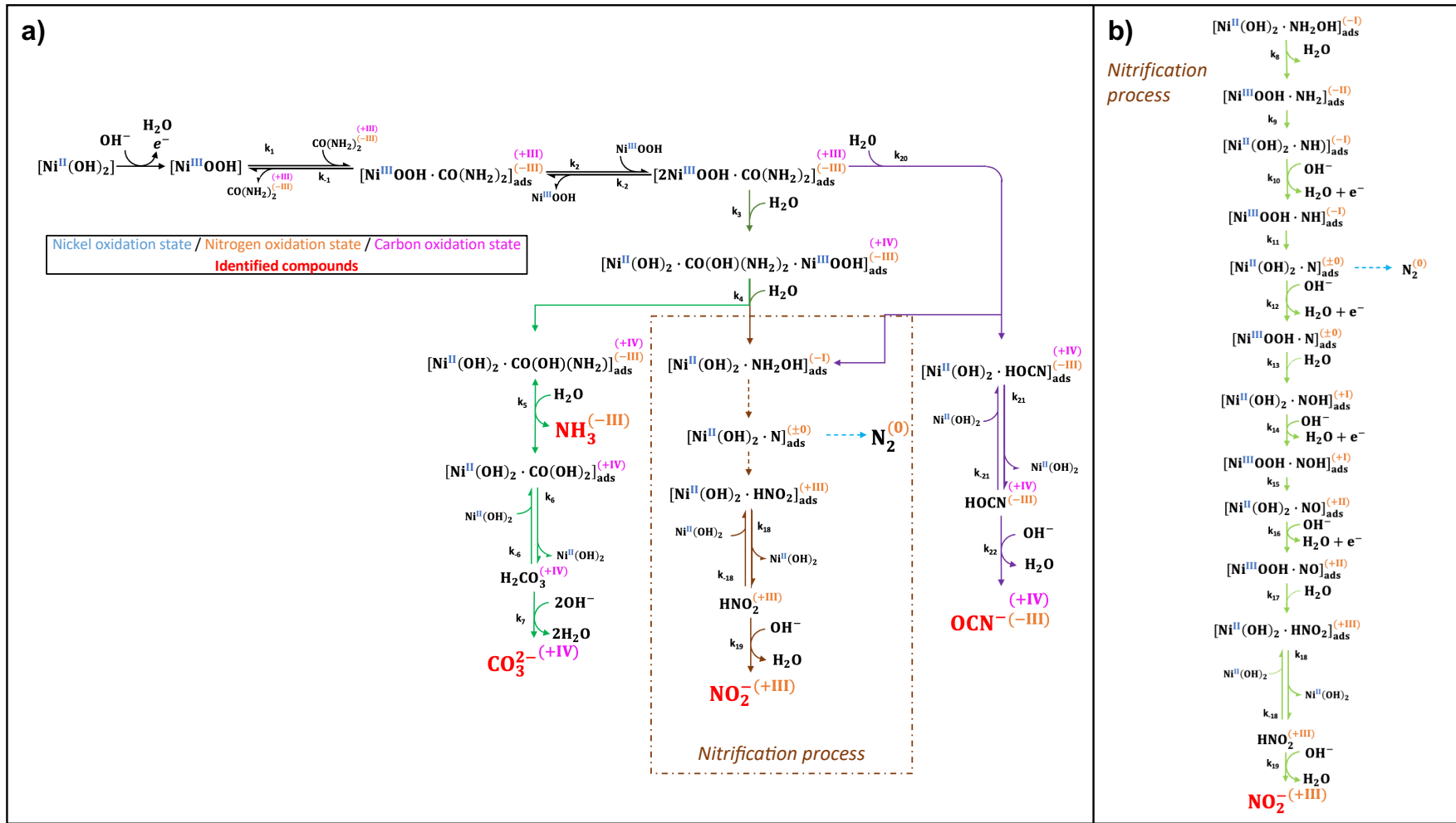


Fig. IV.12 – Proposed overall mechanism for UEO in alkaline media on a bare nickel anode covered after polarization by the system NiOOH/Ni(OH)₂. On the left side, a) the mechanism shows the main and side chemical pathways leading to N₂ and CO₂ (under CO₃²⁻ form) as well as the by-products previously identified in the liquid phase and b) detailed nitrification route.

IV-5 Global microscopic and macroscopic modeling of the coupling of electromediation and heterogeneous chemical reaction between urea and nickel(III)

IV-5.1 Establishment of the predictive model

Various potentiostatic electrolyses with high conversions of urea have been performed in the previous **Chapter III**, for which the variations of the concentrations of urea and by-products with electrolyses times have been determined and can be thus used to validate the model. The latter is based on the kinetic data obtained in the previous sections and involves all the physical processes occurring at the anode and in the bulk. Besides, the model is expected to be applicable at larger scale. Let's consider that a one-dimensional description, depending on the distance to the electrode, is sufficient (for parallelepipedal EC cells and planar anodes) to solve the mass transport phenomena coupled to the HCR in a porous catalytic layer. A schematic representation of the half-cell is given in Figure IV.13

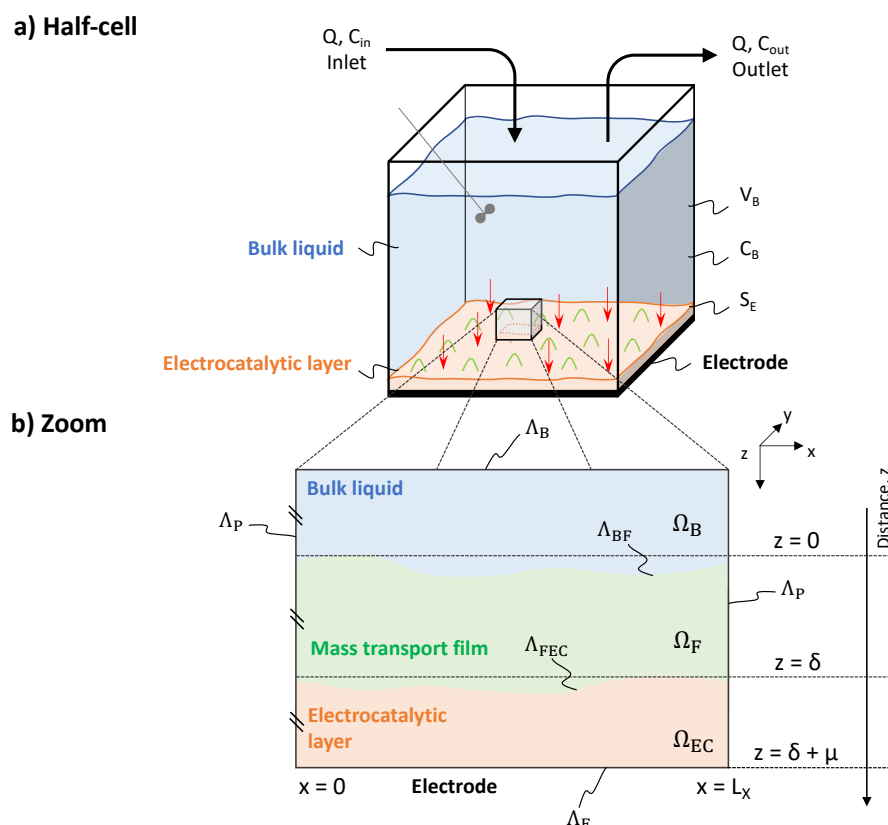
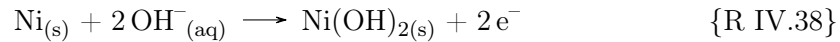


Fig. IV.13 – a) Schematic representation of the EC half-cell. The large scale includes a perfectly stirred liquid phase and an electroactive layer of nickel oxide mixtures on the metal electrode surface. b) View of the various sensitive areas including possible limiting physical phenomena. The enlargement scheme contains three subdomains characterized by the occurrence of different phenomena: (1) a perfectly mixed zone, Ω_B , that is connected to the bulk liquid, (2) a mass transport film Ω_F , and (3) the matrix of the electrocatalytic nickel oxide layer Ω_{EC} at the electrode surface. Each boundary of the system is labeled by Λ . Λ_{BF} represents the boundary between the bulk Ω_B and mass transport film Ω_{EC} areas. Λ_{FEC} represents the boundary between the film Ω_F and electrocatalytic film Ω_{EC} areas. Λ_E and Λ_B represent the massive electrode and wall boundaries of the system, respectively (illustration adapted from Picioreanu et al. [239]).

The aim is here to model the behavior of the EC system during potentiostatic electrolyses

on a massive nickel electrode (supposed in equipotential conditions) of a stirred aqueous solution of urea in alkaline medium. During the electrode polarization, the following reactions will take place on the nickel compounds; starting by the {R III.25} and followed by the {R I.19}. At the applied electrolyses potential (*i.e.*, the one measured at the diffusion plateau of I=f(E) curves, 0.55 V as illustrated in Figure IV.10), the reaction described in {R IV.38} occurs until the electrode is completely covered by Ni(OH)₂ layer. Then the catalytic cycle urea/NiOOH/Ni(OH)₂ occurs.



IV-5.1.a Model assumptions

With the objective of building a robust model, it is necessary to formulate a clear framework and the appropriated assumptions:

- Nickel(II) oxidation reaction occurs in a layer of a constant thickness μ which porosity ω , tortuosity τ and surface in contact with the solution remain unchanged throughout the electrolysis. Such assumption is supported by the fact that no significant release of nickel oxides has been measured by Inductively Coupled Plasma - Optical Emission Spectroscopy (ICP-OES) measurements performed at the end of each electrolysis (detection limit equals to 100 ppb). Porosity is evaluated considering that the nickel sites in the reactive layer are disposed as face-centered cubic unit cell with an atomic packing factor estimated at 0.74. Moreover, the tortuosity, τ , is estimated at $\pi/2$ as the ratio between the half-circumference of a sphere ($\pi \times r$) and the diameter of the sphere ($2 \times r$) (corresponding to the shortest path). The diffusion coefficient in the reactive layer ($\delta < z < \delta + \mu$) is then calculated as an effective diffusion coefficient $D_{i,w}^{\text{eff}}$ according to the Eq. IV.21.

$$D_{i,w}^{\text{eff}} = D_{i,w} \times \frac{\omega}{\tau} \quad (\text{IV.21})$$

where $D_{i,w}$ is the diffusion binary coefficient of the specie i in the water ($\text{m}^2 \text{s}^{-1}$), ω the porosity of the layer of thickness μ (dimensionless) and τ the tortuosity (dimensionless). The values of the urea diffusion coefficient were previously calculated for different KOH concentrations, from the Stokes-Einstein equation as presented in the previous Chapter.

- The nickel oxides Ni(OH)₂ and NiOOH are here considered as electronic conductors [209, 210], making the electronic transfer invariant in the whole μ layer. On the other hand, most of the electrolyses are performed under potentiostatic conditions. Since the applied potential is sufficiently anodic to allow (energetically speaking) the immediate conversion of any Ni(OH)₂ released from the HCR to NiOOH, one can assume that after a few minutes of electrolysis, the surface concentrations of Ni(OH)₂ and NiOOH become constant and that the term related to the accumulation of these species is null. The urea concentration profiles are supposed to be independent of the length and width of the reactive layer and the radial diffusion to be negligible. Once formed,

NiOOH will react with urea and hydroxide ions according to Eq. IV.22.

$$\begin{aligned} r_{\text{EX}}(\delta \leq z \leq \delta + \mu, t) &= k_{\text{EX}} \times [\text{OH}^-]^{\beta_{\text{EX}}} \times (S_{\text{elec}})^{\gamma_{\text{EX}}} \times [\text{CO}(\text{NH}_2)_2]_{(\delta \leq z \leq \delta + \mu, t)}^{\alpha_{\text{EX}}} \\ &= k_{\text{app}} \times [\text{CO}(\text{NH}_2)_2]_{(\delta \leq z \leq \delta + \mu, t)}^{\alpha_{\text{EX}}} \end{aligned} \quad (\text{IV.22})$$

where k_{app} is the apparent constant ($\text{mol}^{1-\alpha_{\text{EX}}} \text{m}_{\text{elec}}^{-2} \text{m}^{-3[1-\alpha_{\text{EX}]} \text{s}^{-1}$). Firstly, it should be noted that the proposed kinetic equation does not take into account the consumption of nickel peroxide and hydroxide ions during the chemical reactions leading to the products and by-products. Secondly, it is assumed that this kinetic law is intrinsic and does not take into account experimental bias via diffusive phenomena.

- The concentration of urea and hydroxide ions in the layer μ is considered as a spatially continuous function; the nickel sites are assumed to be small enough not to impact the spatial concentration profile.

IV-5.1.b Governing equations: urea mass balances

From these assumptions, the predictive model gives the urea concentration profile in all areas indicated in Figure IV.13. Into the bulk, the anolyte is assumed to be perfectly stirred, and the urea concentration is therefore considered uniform in the bulk volume, Ω_{B} . The macroscopic balance of urea can be written as Eq. IV.23.

$$\begin{aligned} \text{Accumulation} + \text{Diffusion} + (\text{Feed} + \text{Output})_{\text{in continuous reactor}} &= 0 \\ \Omega_{\text{B}} \quad z \leq 0 \quad V^{\text{bulk}} \times \frac{\partial [\text{CO}(\text{NH}_2)_2]}{\partial t} + \left[D_{\text{urea,w}} \times S_{\text{electrode}} \times \frac{\partial [\text{CO}(\text{NH}_2)_2]}{\partial z} \right]_{z=0} & \quad (\text{IV.23}) \\ + Q_v \times ([\text{CO}(\text{NH}_2)_2]_{\text{Feed}} - [\text{CO}(\text{NH}_2)_2]_{\text{Output}}) &= 0 \end{aligned}$$

where Q_v is the volumetric flow rate ($\text{m}^3 \text{s}^{-1}$). In the present work, the results are obtained in a batch electrolyser ($Q_v = 0$). Unlike in Ω_{B} , the urea concentration in the mass transport film Ω_{F} , is subject to spatial variation caused by the urea diffusion phenomenon due to the chemical reaction in Ω_{EC} . The microscopic mass balance can be written as the Eq. IV.24.

$$\begin{aligned} \Omega_{\text{F}} \quad \text{Accumulation} + \text{Diffusion} &= 0 \\ 0 \leq z \leq \delta \quad (S_{\text{electrode}} \times \delta) \times \left[\frac{\partial [\text{CO}(\text{NH}_2)_2]}{\partial t} - \left[D_{\text{urea,w}} \times \frac{\partial^2 [\text{CO}(\text{NH}_2)_2]}{\partial z^2} \right] \right] &= 0 \quad (\text{IV.24}) \end{aligned}$$

In the Ω_{EC} area, the coupling of the HCR to the urea diffusion into the porous solid are the main occurring phenomena. The microscopic mass balance can be written according to the Eq. IV.25.

$$\begin{aligned} \text{Accumulation} + \text{Chemical reaction} + \text{Diffusion effective} &= 0 \\ \Omega_{\text{EC}} \quad \delta \leq z \leq \delta + \mu \quad V_{\text{EC layer}} \times \left[\frac{\partial [\text{CO}(\text{NH}_2)_2]}{\partial t} + S_{\text{electrode}} \times r_{\text{EX}} \right. & \quad (\text{IV.25}) \\ \left. - D_{\text{urea,w}}^{\text{eff}} \times \frac{\partial^2 [\text{CO}(\text{NH}_2)_2]}{\partial z^2} \right] &= 0 \end{aligned}$$

where $V_{\text{EC layer}}$ is the volume of the EC layer (m^3) equal to $S_{\text{electrode}} \times \mu \times \frac{\omega}{\tau}$ (ω the porosity of the layer of thickness μ and τ the tortuosity).

Eq. IV.25 represents a classical situation of a boundary value problem and its resolution (shooting method) is well documented in other works [240, 241]. The resolution state of the model is a pseudo-steady state where the resolution is established by a succession of steady states, in the mass transport area as well as the electroactive layer, and a transient state in the bulk. The model resolution method is presented in Appendix F.

IV-5.1.c Boundary and initial conditions

The following initial and boundary conditions are applied:

- At initial time, the urea concentration is assumed to be uniform throughout the whole system and equal to the initial concentration in the volume according to Eq. IV.26.

$$\forall \Omega \quad C(z, 0) = C_{\text{ini}} \quad (IV.26)$$

$$t = 0$$

- It is considered that the urea does not directly react at the electrode neither with $\text{Ni}(\text{OH})_2$ nor Ni ; therefore, the mass flux arriving at the surface of the metal electrode Λ_E and at both frontiers Λ_P of the system, are assumed to zero according to Eq. IV.27.

$$\forall \Lambda_E, \Lambda_P \quad \left. \frac{\partial [\text{CO}(\text{NH}_2)_2]}{\partial z} \right|_{z=\Lambda_E, \Lambda_P} = 0 \quad (IV.27)$$

$$\forall t$$

- The continuity of the concentrations in each Ω domain, especially in the Ω_{EC} area, is ensured by the equality of the concentrations at each Λ boundary of the system following the Eqs. IV.28.

$$\forall t \quad \begin{aligned} C_{\Omega_B, \Lambda_{BF}}(0, t) &= C_{\Omega_F, \Lambda_{BF}}(0, t) \\ C_{\Omega_F, \Lambda_{FEC}}(\delta, t) &= C_{\Omega_{EC}, \Lambda_{FEC}}(\delta, t) \end{aligned} \quad (IV.28)$$

- Since the mass transport properties are significantly different in the domains Ω_F and Ω_{EC} in terms of diffusion constant but also of thickness and concentration continuity, the equality of urea flux can be described as Eq. IV.29.

$$\forall t \quad D_{\text{urea},w} \times \left. \frac{\partial [\text{CO}(\text{NH}_2)_2]}{\partial z} \right|_{z=\delta} = D_{\text{urea},w}^{\text{eff}} \times \left. \frac{\partial [\text{CO}(\text{NH}_2)_2]}{\partial z} \right|_{z=\delta} \quad (IV.29)$$

These changes can be expressed according to a Biot dimensionless number as shown in Eq. IV.30.

$$\text{Biot} = \frac{k_{m, \Omega_F}}{k_{m, \Omega_{EC}}} = \frac{D_{\text{urea},w}}{\delta} \times \frac{\mu}{D_{\text{urea},w}^{\text{eff}}} \quad (IV.30)$$

where k_m is the mass transport coefficient (m s^{-1}).

Finally, the boundary condition can be expressed as:

$$\text{Biot} \times \frac{\partial [\text{CO}(\text{NH}_2)_2]}{\partial z} \Big|_{z=\Lambda_{\text{FEC}}}^{\Omega_{\text{F}}} = \frac{\partial [\text{CO}(\text{NH}_2)_2]}{\partial z} \Big|_{z=\Lambda_{\text{FEC}}}^{\Omega_{\text{EC}}} \quad (\text{IV.31})$$

IV-5.1.d Comparison between predictions and experimental data

IV-5.1.d.i Thicknesses of the diffusion film and the electrocatalytic layer

Two physical dimensions of the system need to be determined prior to the application of the model: the thickness of the diffusion layer, δ , and the thickness of the electrocatalytic layer, μ . Concerning the diffusion layer, the anodic oxidation limit current, observed on the urea diffusion plateau, is proportional to the concentration of the electroactive species. Here, nickel(III) is the electroactive specie, but its concentration will vary proportionally to that of urea according the catalytic cycle already mentioned in the previous section. Then, the following Eq. IV.32 can be applied.

$$\delta = \frac{n \times \mathcal{F} \times D_{\text{urea,w}} \times [\text{CO}(\text{NH}_2)_2]_{z \leq 0}}{j_{\text{plateau}}^{\infty}} \quad (\text{IV.32})$$

where $j_{\text{plateau}}^{\infty}$ is the limit current density current measured at the diffusion plateau in steady state (A m^{-2}) at a potential varying in the range of 0.51 and 0.55 V (see Figure IV.10), n the number of exchanged electrons (dimensionless, 1 in case of nickel(III)/nickel(II)). Considering the values obtained in Figure IV.10-a for the lowest urea concentration (where the concentration of urea at the electrode is close to 0, the molar flux arriving at the electrode becomes constant), a value of $\delta = (3.4 \pm 0.2) \times 10^{-5}$ m is determined. The thickness of the electrocatalytic layer have been estimated in the previous Chapter and found equal to $\mu = (4.9 \pm 0.4) \times 10^{-8}$ m.

IV-5.1.d.ii Urea electrolysis on nickel electrode : case results and comparison

In order to evaluate the veracity of the model, the urea concentrations experimentally measured in the bulk for various electrolyses for which high conversions are achieved, will be considered and compared to the ones predicted by the model.

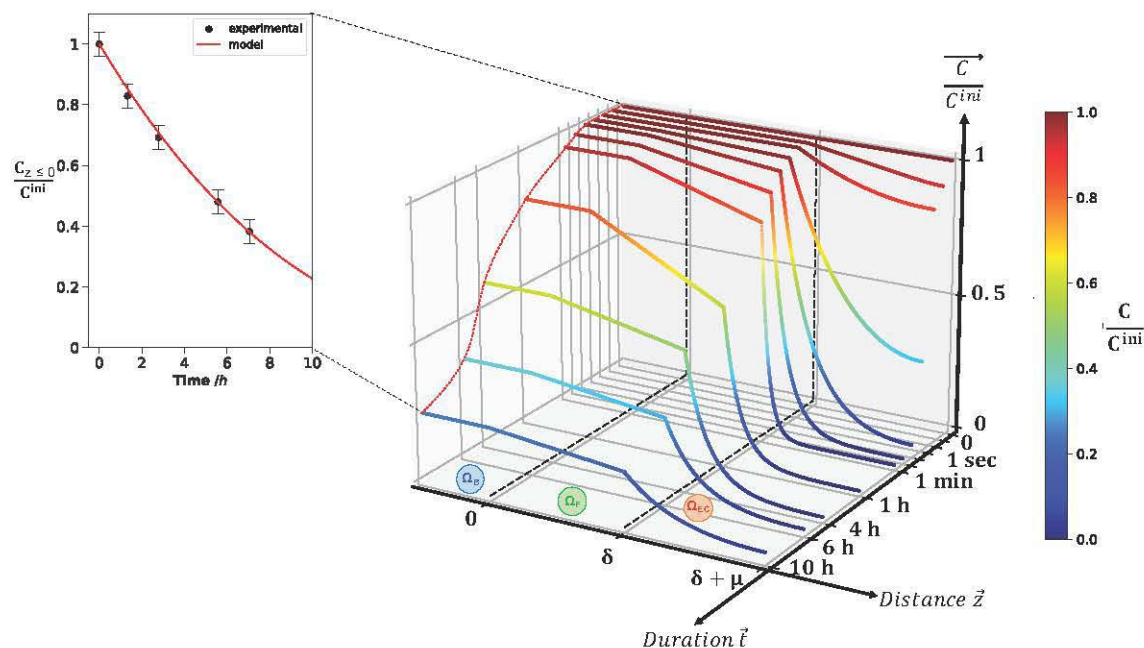


Fig. IV.14 – Spatio-temporal profiles of the urea concentration during a potentiostatic electrolysis at 0.55 V of a 0.33 mol L^{-1} urea solution in alkaline media (5 mol L^{-1} KOH), on nickel massive electrode. *Inset*: dimensionless urea concentrations in the bulk Ω_B measured experimentally (black filled circles) and predicted by the model (red line).

Figure IV.14 illustrates the spatio-temporal profiles of the urea concentration predicted by the model. The three spatial zones are quite distinct and well represented, allowing a good understanding of the involved processes (Ω_B , Ω_F : transport phenomena / Ω_{EC} : transport phenomena and heterogeneous reaction). A non-linear time scale is represented for a better readability of the phenomena occurring. In the reaction area Ω_{EC} , the flux at the metal electrode (at $z = \delta + \mu$) equals to 0. The concentration in this Ω_{EC} zone starts to decrease according and tends towards a steady state until the chemical regime competes with the diffusion flux from the diffusion film Ω_F . A linear concentration profile in the Ω_F zone is thus obtained. In the bulk area Ω_B , the assumption of a perfectly stirred batch reactor is equivalent to an identical concentration at all points (at $z \leq 0$). The breaking slope observed at $z = \delta$ is representative of the urea transfer to the electrode. They indicate the discontinuities in the urea concentration between the two media: liquid Ω_F and the catalytic Ω_{EC} layer of $\text{NiOOH}/\text{Ni}(\text{OH})_2$. Both layers exhibit different mass transport properties in terms of diffusion constant, but also thickness and concentration continuity according to the Biot number in Eq. IV.30. In the experimental conditions related to Figure IV.14, and at a KOH concentration of 5 mol L^{-1} , this ratio between the mass transfer constants in the diffusion film and in the electrocatalytic layer, respectively, is estimated to be 112, thus reflecting a diffusional limitation in the porous zone compared to the diffusion film. The inset in Figure IV.14 illustrates the simulated temporal variation of the urea concentration in the bulk (continuous line), and a good agreement is observed with the experimental points obtained in the previous Chapter.

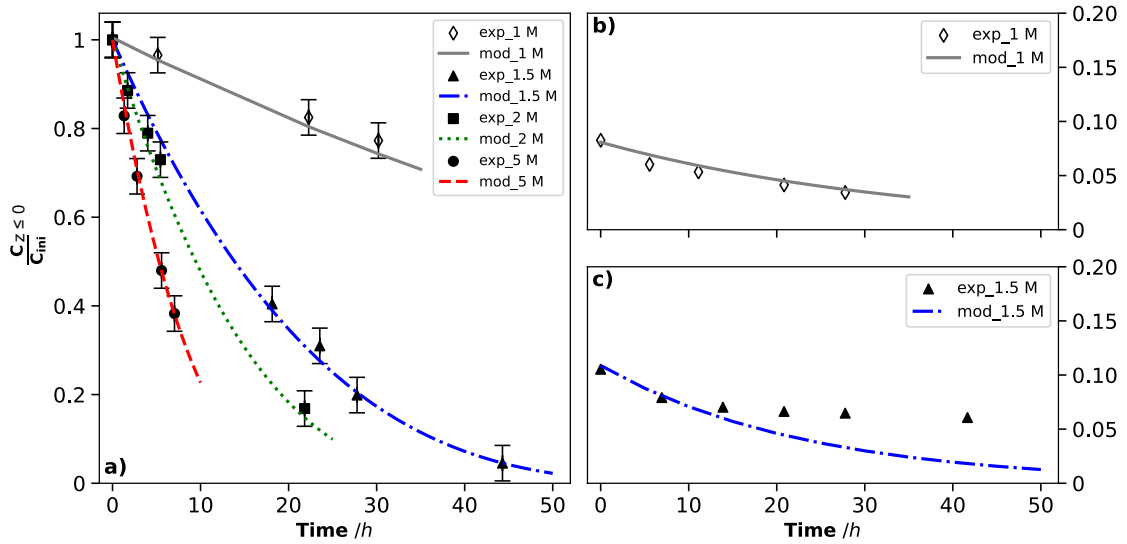


Fig. IV.15 – *Left*: a) Temporal variations of the normalized urea concentration in the bulk during potentiostatic electrolysis on nickel massive electrode in alkaline media. Experimental results are plotted for different KOH concentrations: 1 mol L^{-1} (\diamond), 1.5 mol L^{-1} (\blacktriangle), 2 mol L^{-1} (\blacksquare) and 5 mol L^{-1} (\bullet). Filled symbols are obtained with an S/V ratio of 8 m^{-1} . The unfilled symbols are obtained with an S/V ratio equal to 20 m^{-1} . The lines represent the temporal profiles of the urea concentration predicted by the model at each KOH concentration.

Right: (b-c) Experimental and predicted profiles of the current intensity during electrolysis with a distance between electrodes of b) 15 cm using a H-type cell without separator and c) 3 cm using an undivided Metrohm type-cell.

Figure IV.15-a compares the predicted (continuous line) and experimental (dots) normalized urea concentrations in the bulk, obtained during electrolyses at different KOH concentrations, using two S/V ratios, where significant conversion rates of urea were reached. Data obtained at S/V ratio of 8 are extracted from the previous Chapter also. In addition to examine the validity of the model on an enhanced value of S/V ratio, an alkaline electrolysis was carried out using an anode surface of 26 cm^2 into 130 mL of electrolyte. A good agreement is observed between the experiments and the model since the maximum deviation of urea concentration is observed at 6%. An additional validation of the model is performed by comparing the temporal variation of the current predicted by the model according to Eq. IV.33 with the experimental one.

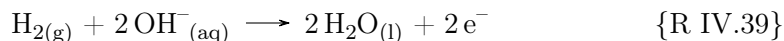
electro – generated $\text{Ni}(\text{III})$ flux = $6 \times$ Urea chemically reacted flux

$$\begin{aligned}
 I &= nFSV\nu_{\text{Ni}(\text{III})} \int_{z=\delta}^{z=\delta+\mu} r_{E\chi}(z) \times dz \\
 &= \left[nFV\nu_{\text{Ni}(\text{III})} k_{E\chi} \times [\text{OH}^-]^{\beta_{E\chi}} \times (\text{S}_{\text{electrode}})^{\gamma_{E\chi}+1} \right] \\
 &\quad \times \int_{z=\delta}^{z=\delta+\mu} [\text{CO}(\text{NH}_2)_2]^{\alpha_{E\chi}} \times dz
 \end{aligned} \tag{IV.33}$$

As shown in Figure IV.15-b, the model predicts the current with a maximum deviation of 4%, thus implying that the main assumption considering a constant temporal superficial concentration of nickel(III) would be verified. Results of electrolysis indicated in Figure IV.15-c were obtained using an undivided Metrohm type cell, containing a strongly stirred (1000 RPM) solution. In these conditions, the electro-generated hydrogen at the cathode

(diameter < 1 mm) dispersed in the bulk, and consequently in the immediate environment of the anode. Strong dispersion of gaseous H_2 increase the gas/liquid interface and facilitates its dissolution (the stationary concentration of hydrogen can achieve its solubility). Under the applied anodic potential (0.55 V), the dissolved hydrogen can be oxidized, and in these conditions the observed current is composed by:

- the urea oxidation current (temporally decreasing);
- the hydrogen oxidation current [21, 242, 243] induced by the {R IV.39}, first increasing until the steady state is reached, *i.e.*, a constant gaseous H_2 flux arrived at the anode area.



These facts explain the observed difference of the current between the model and the experimental data, which varies from 1 to 80%. Note that, this difference will decrease as a function of time. Indeed, as the urea concentration is depleted, the corresponding fraction of anodic current is decreased, thus implying the overall current to decreases. In these conditions the hydrogen electro-generated flux at the cathode decreases. As the hydrogen is not maintained in the reactor, its contribution to the anode current will also decrease until to be cancelled (simultaneously to urea). The difference in current intensity between the theoretical and experimental data corresponds to the current 'lost' due to the absence of a physical separator.

IV-6 Conclusion of Chapter 4

This Chapter allowed to highlight and characterize the kinetics of urea indirect electro-oxidation on active nickel(III) sites in alkaline medium.

NiOOH particles, synthesized from commercial Ni(OH)₂ powder using NaOCl, were characterized by SEM, BET, XRD and particle size analysis. They exhibited spherical shape and their content in nickel(III) reached 80%. Compared to Ni(OH)₂ solids, the crystallinity of the synthesized NiOOH particles appears to be much lower than that of the starting powder, reflecting a core-shell geometry. The particles after synthesis, were composed of an amorphous NiOOH shell and a Ni(OH)₂ core.

Firstly, the kinetic study was performed using chemically synthesized nickel(III) particles. By using the method of initial rate of OH⁻ disappearance, the partial reaction order of urea was evaluated at 0.3, highlighting a limitation of the urea adsorption on the active sites of nickel. Subsequently, the partial orders of 0.6 and 1.9, respectively attributed to hydroxide ions and nickel active sites, were determined using the same type of experimental measurements. The dependence of the kinetic rate on hydroxide ions appeared to be low, whereas it was higher on nickel ($\gamma_{\chi} \approx 2$). Although more experiments would be required to precisely identify the reaction mechanism, an order of 2 against the nickel(III) suggesting that urea would bind to two nickel sites either (i) via both amine groups or (ii) via one of the amine groups and the ketone group. Besides, this low dependence of the kinetic rate to dissolved species concentrations would suggest possible mass transport limitations in the solid spherical particles; indeed, after a consumption of nickel(III), the transformed urea or even the by-products must desorb, and find another nickel(III) available to absorb, to pursue the oxidative process. Moreover, the performed BET analysis showed particles having low specific surface area (8.51 m² g⁻¹), which would tend to incriminate limitation by the mass transport into the particles. This initial kinetic law did not consider the effect of the urea oxidized intermediates on OH⁻ or nickel(III) consumption, as their initial concentration was close to zero. Since the limitation of the overall process, at least initially, appears to be due to the adsorption, these intermediates do not accumulate; they rapidly convert to observed products, and therefore do not affect the kinetic rate. This fact was validated by the integration as a function of time, of the initial kinetic law *i.e.*, for higher conversion rates. The obtained theoretical variation of the OH⁻ concentration was successfully compared with the experimental one (maximum deviation of 6%).

Secondly, the kinetics of indirect electro-oxidation of urea was studied by polarizing a massive nickel electrode which enabled the formation of a catalytic layer NiOOH/Ni(OH)₂, and thus ensured the urea oxidation thanks to the EC continuous regeneration of the nickel(III) active sites. Under these assumptions, the kinetic rate law showed a partial order of urea close to the previous value (*i.e.*, 0.3). However, the order of the nickel surface was found to be high ($\gamma_{E\chi} \approx 5$), signifying that the adsorption of urea onto nickel(III) sites was followed by complete oxidation of this urea by five nickel(III) generated electrochemically, almost instantaneously due to potentiostatic polarization of the anode at the required potential.

Coupled with the previously performed mass balances carried out our electrolyses (which demonstrated the presence of various by-products in the liquid phase), the present kinetic study made possible to build up a relatively complete multi-pathway (22 sequential steps, four different ways and 5 urea oxidation products) mechanism able to describe the process of indirect electro-oxidation of urea.

Finally, this kinetic study was implemented into a more general predictive model combining *(i)* mass transport phenomena, in a liquid film and in a solid porous catalytic layer with *(ii)* the indirect electrocatalytic chemical reaction occurring in the previous layer, and finally *(iii)* assisted by the quasi-instantaneous regeneration of the reaction driving factor *i.e.*, the nickel(III) catalytic sites. The resolution of the established model on the basis of the shooting method allowed to predict spatio-temporal urea concentration profiles for various operating conditions. These predicted results were compared to the experimental ones for different hydroxide concentrations and S/V ratio. A satisfactory agreement was observed with low ($< 5\%$) deviations, thus opening interesting perspectives for further larger-scale operations in the urea mineralisation.

Toward the process scaling-up: real effluent treatment and pilot-scale experiments

Outline of the current chapter

V-1 EC treatment of real matrix at lab-scale	130
V-1.1 Complete mass-balances and proof of concept	130
V-1.2 Linear voltammetry experiments as a tool to better understand the matrix effect during the electro-oxidation of human urine	145
V-2 From the lab-scale scale to the pilot-scale	157
V-2.1 Complete mass balances during the course of the urea electrolysis at pilot-scale	157
V-2.2 Effect of some key operating parameters on the urea synthetic solution electrolyses at pilot-scale	159
V-2.3 Human urine electrolysis at pilot-scale	164
V-2.4 Evaluation of energy consumption at pilot-scale	166
V-3 Conclusion of Chapter 5	168

This chapter presents two major advances towards the process implementation at industrial scale: (i) the applicability when using real matrix and (ii) the scaling up from lab-scale-scale to pilot-scale.

With this in view, this chapter has been divided into two main sections:

1. The first section deals with the study of the EC treatment of real human urine solutions by combining two different approaches: (i) establishment of gas and liquid mass balances during the electrolysis's course and (ii) linear voltammetry investigations.
2. The second section will focus on the results obtained from the UEO carried out in the pilot-scale reactor described in **Chapter II**. In presence of urea synthetic solutions, complete mass balances will be first presented and the influence of operating parameters (electrode surface, flow rate, applied potential) then investigated. Lastly, the proof of concept will be established during the electrolysis of a real urine solution.

The section **V-1.1** of this chapter presents the results obtained from the article "G. Hopsort*, L. Latapie, K. Groenen Serrano, K. Loubière, T. Tzedakis* (2023). New insights into urea electro-oxidation: complete mass-balances and proof of concept with real-matrix effluent. *Journal of The Electrochemical Society*. [10.1149/1945-7111/acf87e](https://doi.org/10.1149/1945-7111/acf87e)".

The rest of this Chapter presents the results obtained from the article "G. Hopsort, E. Piguet, L. Latapie, K. Groenen Serrano, K. Loubière, T. Tzedakis*. (2023). Towards an industrial perspective for urea-to-hydrogen valorization by electro-oxidation on nickel (III): real effluents and pilot-scale proof of concept. submitted in: *Electrochimica Acta*".

V-1 EC treatment of real matrix at lab-scale

This section will be composed of two sub-sections. First, complete mass balances will be established in both liquid and gaseous phases during the course of lab-scale electrolysis with urea synthetic solution, and then with human urine. From them, energy assessments will be then proposed.

In a second time, LSV experiments will be discussed as a tool to better understand the matrix effect during the electro-oxidation of human urine.

V-1.1 Complete mass-balances and proof of concept

As discussed in **Chapter I**, the issue related to the by-products formed during the UEO process has been addressed only very recently where five research papers have reported the occurrence of several by-products in the liquid phase (OCN^- , NO_x ($x = 2$ and/or 3), NH_3 and CO_2) [140, 143, 146, 244, 245]. In addition, in the case of electrolysis with large urea conversion rates, complete mass balances are scarcely made, even if complex mechanisms have been suggested [140, 143, 146, 246]. To fill these gaps, in the previous **Chapters III** and **IV**, we have established for the first time (i) complete mass balances in the liquid phase during the course of potentiostatic electrolyses with high urea conversion rates ($>80\%$), and (ii) kinetics laws and reaction mechanisms based on a chain of reactional adsorption of urea on nickel(III) active sites. However, no mass balance in the gas phase has been made, thus

pointing out the need of additional investigation for the part of the mechanism leading to the gaseous products.

Some works have reported electrolyses on real human urine electrolysis by using BiO_x - TiO_2 [247] or IrO_2 [71] anodes. However, to the best of our knowledge, none exists with nickel electrode and real human urine previously alkalinized. Such lack makes difficult to validate the efficiency of the UEO processes with real effluents in a view of a future industrial implementation.

To fill this gap, the present section aims at elucidating the performances of a lab-scale EC reactor operating with real human urine and at rigorously comparing them to the ones in presence of urea synthetic solutions. For this purpose, the analytical methods need to be optimized so as to perform complete analysis of all electro-generated by-products in both aqueous and gaseous phases. This preliminary study will thus pave the way for operating the process at larger scale.

V-1.1.a Experimental information

Human urine samples were obtained from two healthy male volunteers (aged between 25 and 30 years old). The entire sample of urine was stored at 4 °C between experiments. All assays were duplicated using the same batch of urine to ensure repeatability.

Note that a special care was taken to ensure that no nitrogenous or carbonaceous compounds present in the anolyte migrated to the catholyte via the IONAC anionic separator used (the composition of the catholyte was analyzed at the end of the electrolyses).

Electrolyses of urea synthetic solution and human urine were carried out in the H-type cell with a membrane. The creatinine electrolysis presented later was performed in a single-compartment cell.

Electrolytes were analyzed by IC-CD/MS, TOC, and GC according to the methods presented in **Chapter II**. Figure V.1 presents the different cationic (part a) and anionic (part b) chromatograms over time of a potentiostatic electrolysis (0.55 V *vs.* Hg/HgO) of a human urine solution. This reveals the accumulation of by-products such as:

- Formic Acid (FA) (CH_2O_2) and OA ($\text{C}_2\text{H}_2\text{O}_2$) (not observed in the case of urea synthetic solution electrolyses);
- OCN^- , NH_4^+ , NO_2^- and CO_3^{2-} (already observed in the case of urea synthetic solution electrolyses).

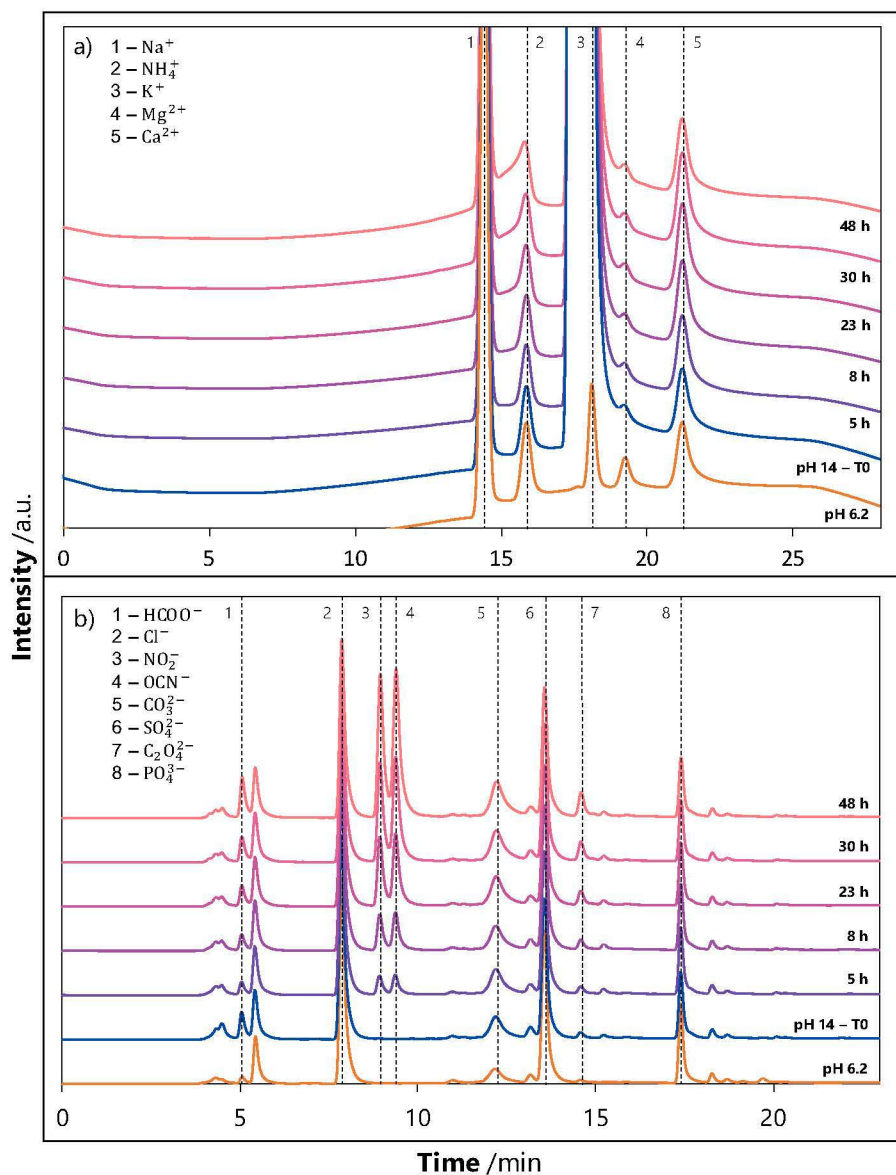


Fig. V.1 – Typical a) cationic and b) anionic chromatograms obtained during IC analysis during potentiostatic electrolysis (0.55 V vs. Hg/HgO) of urine solution in alkaline medium at pH = 14.

As FA and OA were formed in the case of human urine electrolysis (as discussed in the next section), it was necessary to establish calibration curves for these compounds. The latter obtained by IC for formic and oxalic acids are shown in the Figure V.2. They enabled to quantify their quantity present in urine during electrolysis. The linear relationships between the molar concentrations and the peak area signals obtained in IC are presented in Eqs. V.1-V.2.

$$\text{Peak area}_{\text{FA}} = 16.06 \times [\text{FA}]_{\text{molL}^{-1}} \text{ with } T_{\text{r}} = 4.5 \text{ min \& } R^2 = 0.999 \quad (\text{V.1})$$

$$\text{Peak area}_{\text{OA}} = 28.69 \times [\text{OA}]_{\text{molL}^{-1}} \text{ with } T_{\text{r}} = 25.2 \text{ min \& } R^2 = 0.999 \quad (\text{V.2})$$

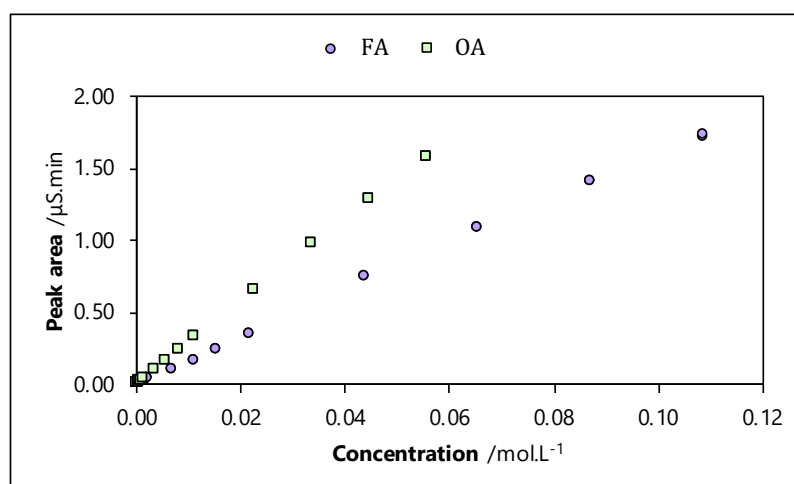


Fig. V.2 – Calibration curves of formic and oxalic acids obtained by IC analysis.

The Faraday efficiency of the compound *i*, represented as FE_i (%), was defined by Eq. V.3.

$$FE_i = \frac{n_i \times n_e \times \mathcal{F}}{Q_{\text{total}}} \times 100 \quad (\text{V.3})$$

where n_i is the amount of the compound *i* (mol) and n_e represents the number of electrons exchanged (dimensionless) which was equal to:

- 1 for OCN^- and NH_4^+ (the formation of these species indirectly implies nickel(II)→nickel(III) oxidation system, as described in **Chapter IV**);
- 6 for N_2 ;
- 6 for NO_2^- .

V-1.1.b Results and discussion

The following results will concern:

- (i) electrolysis of urea synthetic solution;
- (ii) electrolysis of human urine (including effect of alkalization and chronoamperometry);
- (iii) electrolysis of creatinine;
- (iv) energy cost assessments.

Note that, the results presented here in the case of urea synthetic solutions are complementary to the ones reported in **Chapter III** and **IV**, in particular because they include mass balance in the gaseous phase (N_2 , H_2). They also serve as benchmark a case when comparing the performances with urine.

V-1.1.b.i Electrolysis of urea synthetic solutions

The first set of experiments concerns the performance of chrono-amperometry electrolysis of a urea solution at 0.55 V *vs.* Hg/HgO performed in undivided Metrohm-type cell.

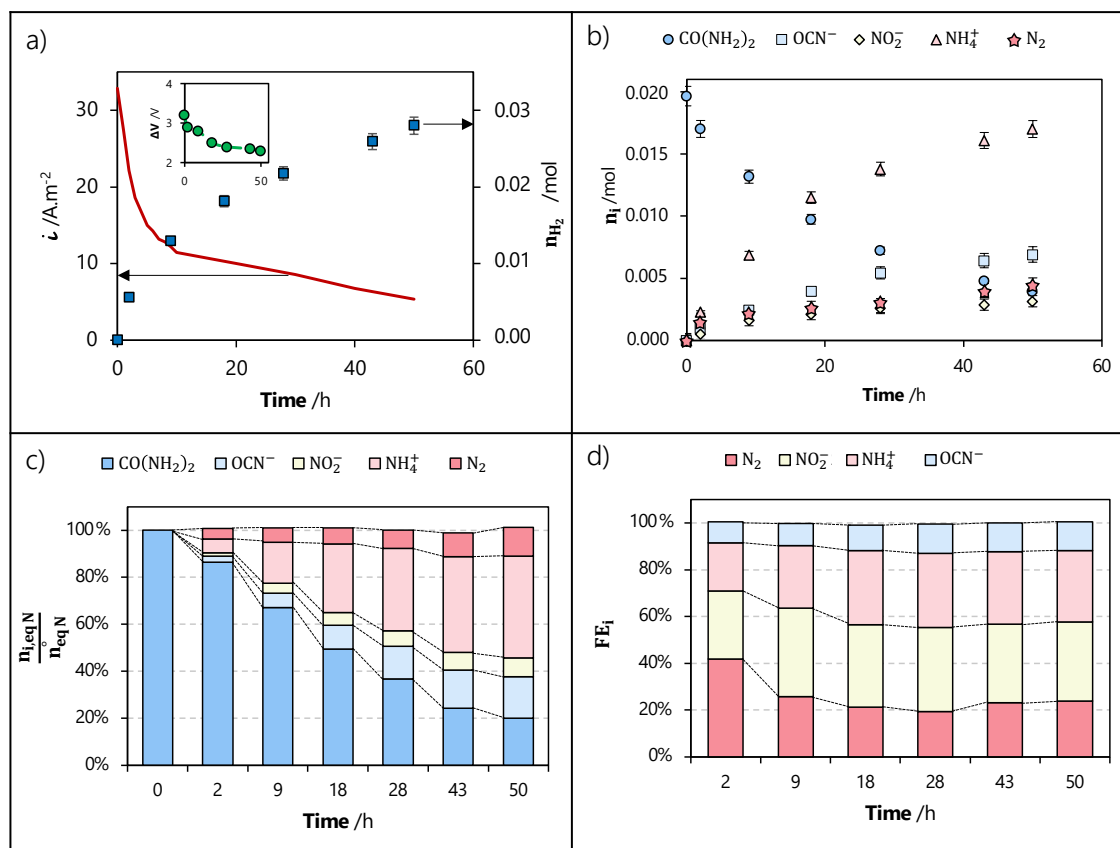


Fig. V.3 – Typical results obtained from chronoamperometric electrolysis of a urea synthetic solution (0.33 mol L⁻¹) in alkaline medium (1 mol L⁻¹ KOH): a) current density and the amount of formed H₂ (inset: cell voltage), b) temporal profiles of molar quantity of identified N-species, c) N-mass balance, and d) N-FE balance.

Figure V.3-a illustrates the temporal variation of the UEO current density, with the cell voltage shown in the inset. The observed decrease in cell voltage (from 3.1 V to 2.2 V) is attributed to both a decrease in cathodic overvoltage and an ohmic drop. Figure V.3-b reports the temporal profiles of the number of moles for each identified N-specie (the raw data are provided in Appendix H). The urea degradation achieves a conversion rate of 80% over 50 h, predominantly forming NH₃ (at 43%, observed as NH₄⁺ in IC analysis). A simultaneous variation was observed with the current density (Figure V.3-a), thus confirming the absence of poisoning phenomena during the electrolysis. Figure V.3-c presents, for the first time, a complete mass balance of the N-species formed in both liquid and gas phases. Interestingly and unequivocally, OCN⁻, NO₂⁻, NH₃ and N₂ are the main (> 98%) N-compounds produced during the electrolysis since the sum of their molar quantities remains equal to the N-amount initially present in the EC cell (2 × initial moles of urea), and this whatever the electrolysis time. As mentioned in **Chapter III** and illustrated in V.4, the mass balance of the C-species (namely CO(NH₂)₂, OCN⁻ and CO₃²⁻) is also validated (more than 98%).

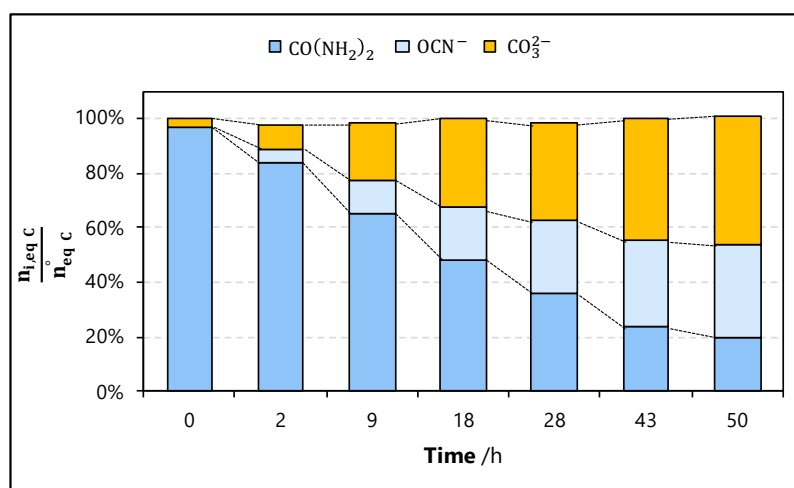


Fig. V.4 – Typical results obtained from chrono-amperometry electrolysis of a urea synthetic (0.33 mol L^{-1}) solution in alkaline medium (1 mol L^{-1} KOH): carbon mass balance.

Figure V.3-d reports the FE for all the identified N-compounds. The total FE_i reaches 100% (with a maximal deviation of 2%), showing that the charge balance is validated for 50 h. The following conclusions can be drawn:

- (i) After 9 h of electrolysis (corresponding to the disappearance of 35% of the urea initially present), the distribution of the concentrations of the various compounds does not evolve anymore (*i.e.*, their FE_i tends to become constant). Such trend could be explained as follows. Urea is oxidized according to a pathway that produces intermediate products as well as nitrites. These intermediates accumulate over time and, once enough concentrated in the medium, would oxidize into nitrites. Then, the ratio of the number of electrons released for nitrite formation to the total electrons remains constant, as far as the urea is consumed. Once the main pathways for urea oxidation and by-product formation are established - by setting up the indirect massive nickel electrode process (nickel(0)→nickel(II)→nickel(III)) - a constant pattern emerges. The ratio of the molar fluxes formed by each reaction pathway, and thus the related FE_i remains constant, regardless of the residual urea concentration.
- (ii) Between the four detected products (Figure V.3-d), only N₂ and NO₂⁻ exhibit a higher oxidation state of nitrogen (0 and +III respectively) compared to urea (-III). Together they represent more than 60% of the total charge. The N-oxidation state for the two other compounds (NH₄⁺ and OCN⁻, both at (-III)) does not change, which is in agreement with the previously presented mechanism (in **Chapter IV**). The formation of these compounds (NH₄⁺ and OCN⁻) results from a catalytic reaction of nickel(III) with urea, which requires the prior formation of nickel(III) from the oxidation of nickel(II) with an exchange of an electron. By applying $n_e = 1$, according to the nickel(II)→nickel(III) oxidation reaction, the FE balance is validated, thus indirectly confirming the previous mechanism [246].
- (iii) Unfortunately, the formation of OCN⁻ and NO₂⁻ occurs to the detriment of N₂, thus making the process less interesting from a sustainable point of view. To overcome this issue, several attempts are very recently made to orient the mechanism towards N₂, for example by electrode material functionalisation [245, 248].

The production of H_2 estimated from Eq. V.4 is reported in Figure V.3-a, leading to a value of $1.78 \text{ mol}_{H_2} \cdot \text{mol}_{\text{urea}}^{-1}$ after 50 h of electrolysis. This means that, overall, the oxidation of 1 mole of urea releases 3.5 electrons, instead of the 6 electrons expected for the generation of 1 mole of N_2 . Finally, in this section, the by-products of the synthetic UEO were identified and quantified, demonstrating that less than 30% of the urea was converted into N_2 .

V-1.1.b.ii Electrolysis of human urine

The industrial development of EC processes inevitably involves the trial phase with real matrices. In this section, the UEO will be studied, with human urine previously alkalinized, during chrono-amperometry electrolysis.

Effect of alkalinization

Urine was alkalinized by adding KOH pellets (until reaching $\text{pH} = 14$), and the effect of this alkalinization on the concentration of the major compounds contained in urine was examined. The results are shown in Table V.2.

Two phenomena can be noticed:

- (i) The alkalinization of urine solutions results in the precipitation of a whitish solid which has been characterized. Table V.1 presents ICP-OES analysis (experimental details provided in Appendix G). Figure V.5 provides optical microscopy images. Some of the mineral salts identified are whewellite ($\text{Ca}(\text{C}_2\text{O}_4) \cdot \text{H}_2\text{O}$) and struvite ($\text{NH}_4\text{MgPO}_4 \cdot 6\text{H}_2\text{O}$) [249]. The ICP-OES analysis of the precipitate has confirmed such trends by revealing that the elements Ca (7.3wt.%), Mg (16.0wt.%) and P (3.8wt.%) are present in majority.

Elementary analyte	Weight fraction (%)
Ca	7.3
Mg	16.0
K	5.3
Na	1.0
P	3.8
S	0.1

Table V.1 – Elementary composition of the precipitate formed when urine is alkalinized (ICP-OES analysis).

- (ii) The degradation of organic matter (*i.e.*, 7% decrease in TOC) caused by the alkalinization of the biological solution leads to an increase in the concentrations of NH_3 (+42%), oxalic acid (+23%) and the appearance of FA. Note that the formation of low-molecular-weight organic acids (LMWOA), such as FA and OA, has been already observed [250] during the alkalinization of water from a brown water lake.

	Analyte											
	$(\text{mol L}^{-1} \pm 0.1) \times 10^3$											
	CO(NH ₂) ₂	NO ₂ ⁻	NO ₃ ⁻	SO ₄ ²⁻	PO ₄ ³⁻	Cl ⁻	NH ₄ ⁺	Na ⁺	Mg ²⁺	Ca ²⁺	FA	OA
Before alkalization	248.8	/	1.4	12.0	18.0	85.8	17.8	104.3	4.0	3.0	/	0.7
After alkalization	233.6	/	1.3	11.4	15.1	82.9	25.3	104.3	/	2.8	1.6	0.9
Deviation (%)	↓7	/	↓7	↓5	↓16	↓3	↑42	=	↓	↓6	↑	↑28
	$(\text{g L}^{-1} \pm 0.1)$											
	TOC	CO(NH ₂) ₂ (eq. C)	FA (eq. C)	OA (eq. C)								
Before alkalization	7.1	3.0	/	0.017								
After alkalization	6.6	2.8	0.019	0.020								
Deviation (%)	↓7	↓7	↑	↑17								

Table V.2 – Effect of the alkalization (pH = 6.2 and pH = 14 before and after alkalization respectively) on the main compounds in urine. The deviation values were calculated as the ratio of the difference between the concentrations before and after alkalization by the concentration before alkalization, namely as $\frac{C_{i,\text{before alkalization}} - C_{i,\text{after alkalization}}}{C_{i,\text{before alkalization}}} \times 100$.

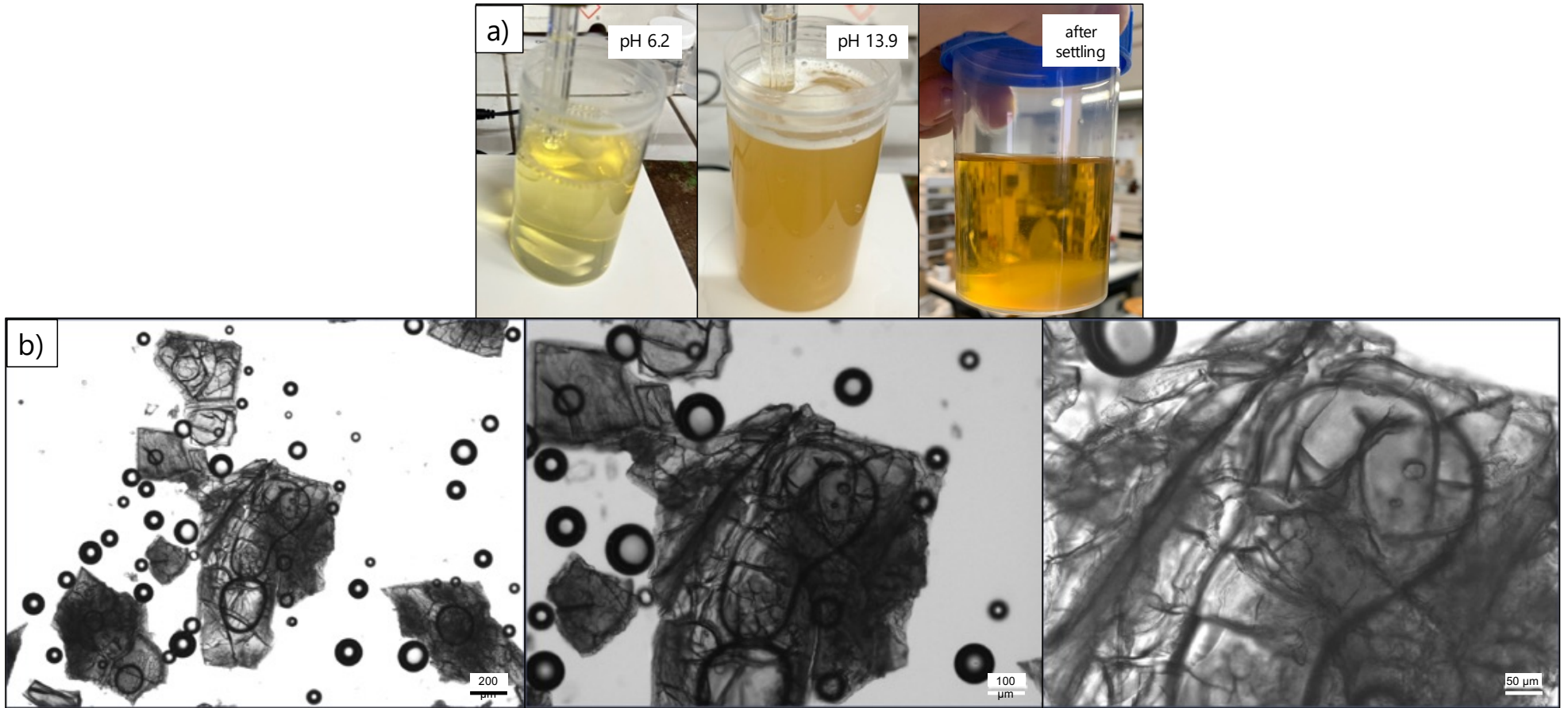


Fig. V.5 – a) Observation of a precipitate in a human urine sample (pH 6.2) formed after adding KOH pellets to reach pH 14 and b) optical microscope images of the crystals obtained.

Chronoamperometry results

Figure V.6 presents the results related to electrolysis at constant potential (0.55 V *vs.* Hg/HgO) carried out with freshly excreted urine solution after alkalization in undivided Metrohm-type cell (described in Chapter II, section II-1.1, Figure II.2). Note that the corresponding urea concentration in the urine was measured at 0.23 mol L^{-1} (equivalent to 42% of TOC measured), a value lower than the generally admitted urea concentration into the urine (*i.e.*, 0.33 mol L^{-1}).

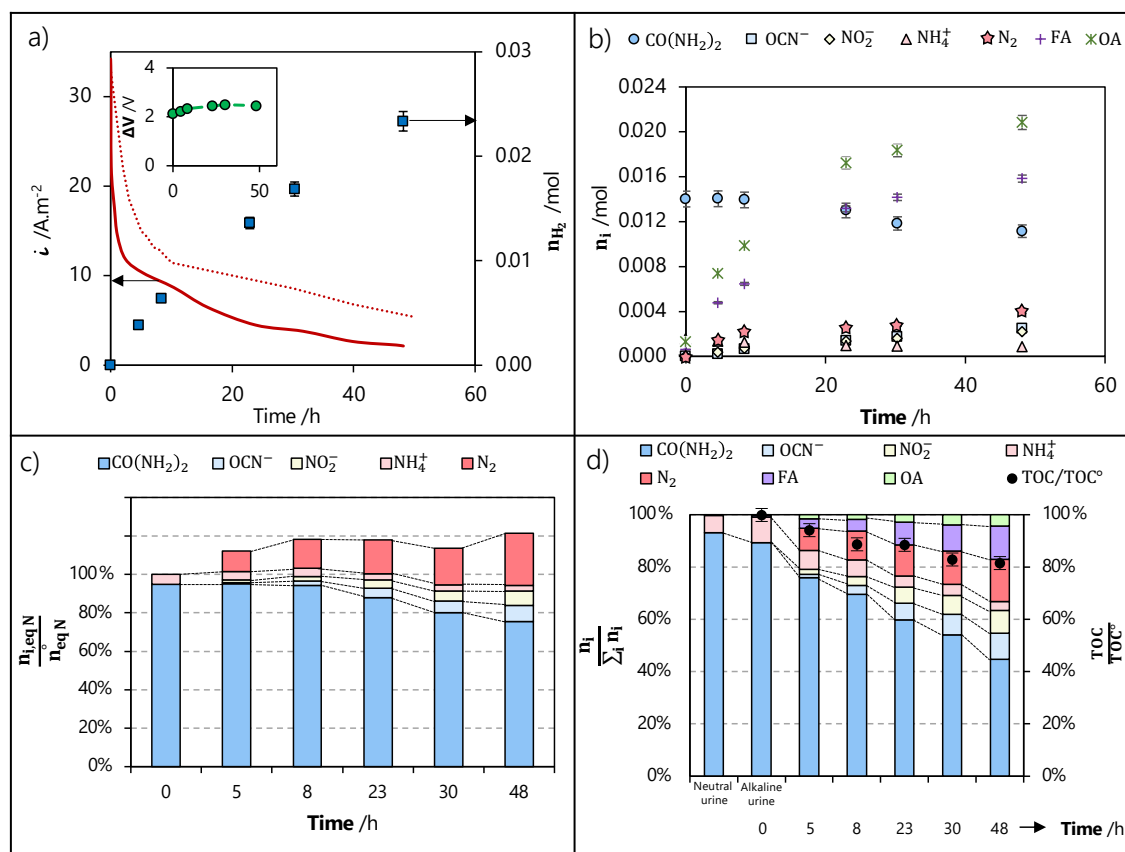


Fig. V.6 – Typical results obtained from chronoamperometric electrolysis of a human urine solution in alkaline medium (1 mol L^{-1} KOH): a) time profiles of the current density (dashed line corresponds to urea synthetic solution, reported in Figure V.3) and the formed H_2 amount (inset: cell voltage), b) temporal profiles of molar quantity of identified species, c) urea mass-balance and d) amount proportions of identified substances in the urine.

Figure V.6-a presents the temporal variations of the current density during electrolysis of both (i) urea synthetic (dashed line extracted from Figure V.3 and (ii) human urine (solid line) solutions. The initial current density value, after immediate polarization, is higher for urine electrolysis (34 A m^{-2} with urea concentration of 0.23 mol L^{-1}) than for urea synthetic solution (31 A m^{-2} with urea concentration of 0.33 mol L^{-1}), thus suggesting an EC activity at the applied potential other than the one observed between urea and nickel(III)→nickel(II) redox system. This additional activity could be direct or indirect, and would involve other organic molecules present into urine, as already depicted for creatinine [251] or ascorbic/uric acids and glucose [252]. Immediately after the start of urine electrolysis, the current density decreases more rapidly over time than it does during urea synthetic electrolysis. However, the same type of temporal variation was observed for both types of electrolysis. Figure V.6-b presents the temporal variation of the molar quantity of the urea in the case of the

urine electrolysis under the applied potential. The molar quantity reduces from 0.014 mol to 0.010 mol after 50 h of electrolysis, resulting a low conversion. Table V.3 compares the temporal trends, after 50 h of electrolysis, in terms of (i) urea conversion rate X (for urea synthetic electrolysis in Figure V.3-b) and for urine electrolysis in Figure V.6-b) and (ii) current density i .

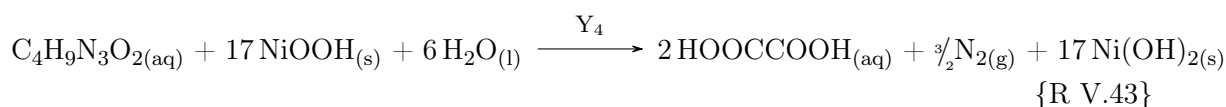
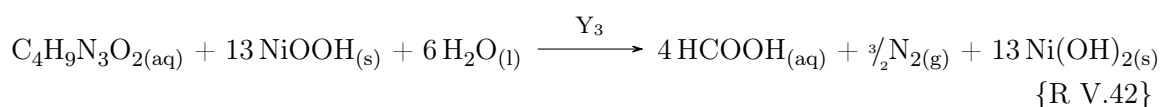
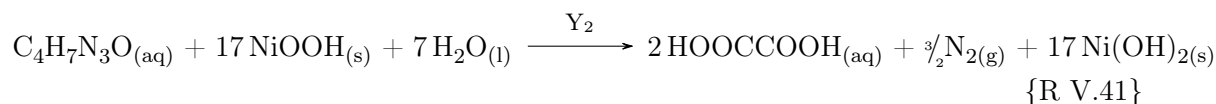
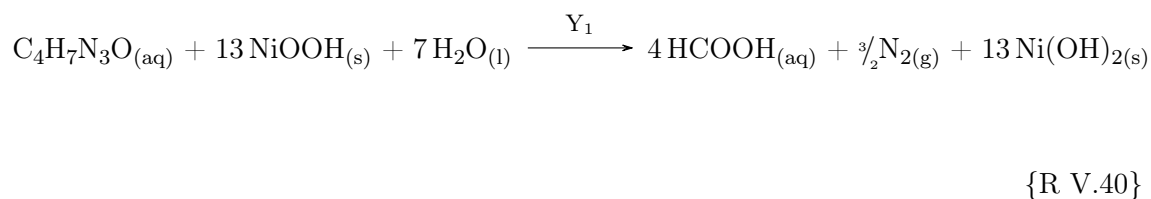
Electrolyzed solution	Urea conversion rates (%)	Final current density ($A\ m^{-2}$)
Synthetic urea	80	$0.19 \times$ initial current density
Urine	20	$0.07 \times$ initial current density

Table V.3 – Comparison of conversion rates and current densities during chronoamperometric electrolysis after 50 h at 0.55 V *vs.* Hg/HgO of (i) urea synthetic and (ii) urine solutions.

From these results, several comments can be made:

- (i) in the case of urine, the current decreases and the urea consumption remains low ($X \leq 20\%$);
- (ii) it cannot be ruled out that the degradation of urea might be induced by other oxidant molecules (such as hypochlorite [253] possibly formed by oxidation of Cl^- naturally present in human urine) produced by electro-oxidation;
- (iii) the measured current results from the oxidation of both urea and other organic molecules;
- (iv) the species contained in urine seems to limit the UEO without inhibiting it. Indeed, even if the measured currents remain significant, higher values could be expected taking into account the urea residual concentrations. This would suggest a competition between urea and other organic molecules present into the urine against the nickel sites.

Figure V.6-b also presents the temporal variation of the molar amount of the products detected during the urine electrolysis. The by-products (OCN^- , NO_2^- , NH_3 , N_2) observed during the UEO are still present (for more details, Appendix H provides raw data (molar amount) of all the reactants and by-products present in the process against time and charge). However, their quantities remain lower compared to the ones detected in the case of urea, which is in agreement with the low urea conversion rates. Besides, supplementary products are detected and in relatively significant quantities: typically, FA and OA achieve 0.016 and 0.02 mol after 50 h respectively. These quantities are higher than the initial molar quantity observed into the urine, thus suggesting an electro-generation of these acids by oxidation with another organic molecule. In particular, organic molecules (such as creatinine $C_4H_7N_3O$, creatine $C_4H_9N_3O_2$, etc.) electro-oxidation could generate FA ($HCOOH$) and OA ($HOCCOOH$) with possible reactions described by {R V.40-R V.43}.



where Y_i could be a catalyst or complexing agent present in the matrix.

In order to gain a more precise understanding of the formation of these by-products, a further representation has been provided in Figure V.6-c, where the mass balance of five N by-products (including urea) is presented over the electrolysis time. On the y-axis, it has been chosen to plot the ratio of the molar amount of compound i by the total molar amount of nitrogenous compounds initially detected. Note that larger nitrogenous molecules (creatinine, creatine, glycine, etc.) cannot be included, as they have not been titrated. The N by-products monitored can be released by both UEO and electro-oxidation of the larger molecules, thus explaining why the total molar ratio are greater than 100%. This result indirectly demonstrates the electro-oxidation of molecules such as creatinine and creatine, and/or the competition existing between UEO and the electro-oxidation of these molecules. Some previous works have already pointed out this production, such as the formation of cyanate from the oxidation of glycine [254] or the N_2 generated by the oxidation of creatinine [251, 255].

Figure V.6-d shows the molar distribution of the identified species present in the matrix. The term $\sum_i n_i$ represents the sum of the moles of the seven identified and quantified compounds in the mixture (provided values in Appendix H). First, one can observed that FA appears through simple alkalization which could be due to chemical reactions involving (i) urea or another organic compound and dissolved oxygen, or (ii) even another oxidant molecules present into urine [256, 257]. The rise of temperature during the alkalization step could catalyze this reaction [258]. All these findings clearly demonstrates that the matrix has a significant effect to orientate the products of the UEO, typically to obtain FA and OA instead of carbonate (as identified in the case of urea synthetic electrolysis). Simultaneously to the electrolysis, 60 mL of alkalized urine have been stored at room temperature and the concentration of the various species monitored. For comparison's purposes, no degradation of organic matter is observed after alkalization and without applying potential in alkaline and neutral urine solutions (the amounts of initial and final urea/FA/OA have been measured and remain constant). As also observed in Figure V.6-d, nitrite accounts for 4 mol.% of the total substance amount at the end of electrolysis, while it represents 7 mol.% in the case of urea synthetic solution (Appendix H). The same trends are

observed for ammonia with 38mol.% being produced in the case of urea synthetic electrolysis compared to 1.5mol.% for urine electrolysis (already present in the initial sample); and cyanate where 4.3mol.% with urine *vs.* 15mol.% with urea were obtained at the end. The presence of organic molecules other than urea can cause significant modifications of these proportions. Indeed, these compounds can exhibit an electrocatalytic behavior against nickel (FA [259], dopamine [260], glucose [261], etc.), and thus possibly presenting oxidative behavior against the urea electro-generated adducts.

As a reminder, about 3,100 compounds have been identified in urine, according to Bouatra et al. [58]. Figure V.7 (raw data provided in Appendix H) show the distribution of the identified carbonaceous species compared with the measured TOC. The identified carbonaceous molecules (urea, cyanate, FA, OA) represent only 43% of the total TOC before alkalization of urine. This confirms that urine contains significant quantities (57%) of other carbon-containing molecules (such as creatinine, urobilin, etc.), not quantified in this study.

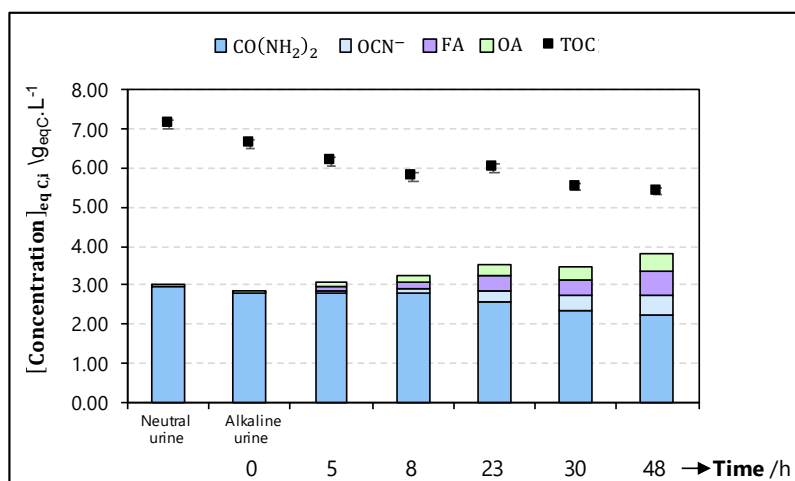


Fig. V.7 – Histogram of concentrations of identified carbon species and TOC measured during electrolysis of a urine solution.

The reactions delineated in {R V.40-R V.43} involve the usage of nickel(III) sites between 13 and 17 times, corresponding to the exchange of 13 to 17 electrons. This results in the release of approximately 3.3 to 4.3 electrons per mole of carbon, depending on the nature of the products. For comparison, the hydrogen production occurring during the electrolysis of urea synthetic involves 3.5 electrons for oxidizing one mole of carbon urea. This data provides further evidence for the matrix effect: the presence of other organic molecules in urine, such as creatinine and creatine, alters the urea degradation pathway established with synthetic solution. The electro-oxidation of organic molecules, which involves such a high number of electron exchanges, can be explained by the continuous electro-regeneration of the active nickel(III) adsorption sites. In addition, the adsorption on nickel sites of higher size organic molecules (such as creatinine [251]), limits the urea adsorption on these nickel sites and consequently completely modifies the reaction pathway.

V-1.1.b.iii Electrolysis of creatinine

The objective of this new set of experiments is to elucidate the EC behavior of creatinine. For that, chrono-amperometry electrolysis of a creatinine solution was performed for 40 h

in the undivided EC lab-cell (described in **Chapter II**, section II-1.1, Figure II.1-a), in which a massive nickel electrode (18 cm^2 , single face) was used and a potential of 0.55 V *vs.* Hg/HgO. The concentration of creatinine was chosen to be close to the maximal physiological concentration (*i.e.*, the maximal concentration encountered in human urine), namely 0.013 mol L^{-1} . The results (based on the monitoring of the liquid phase only) are shown in Figure V.8.

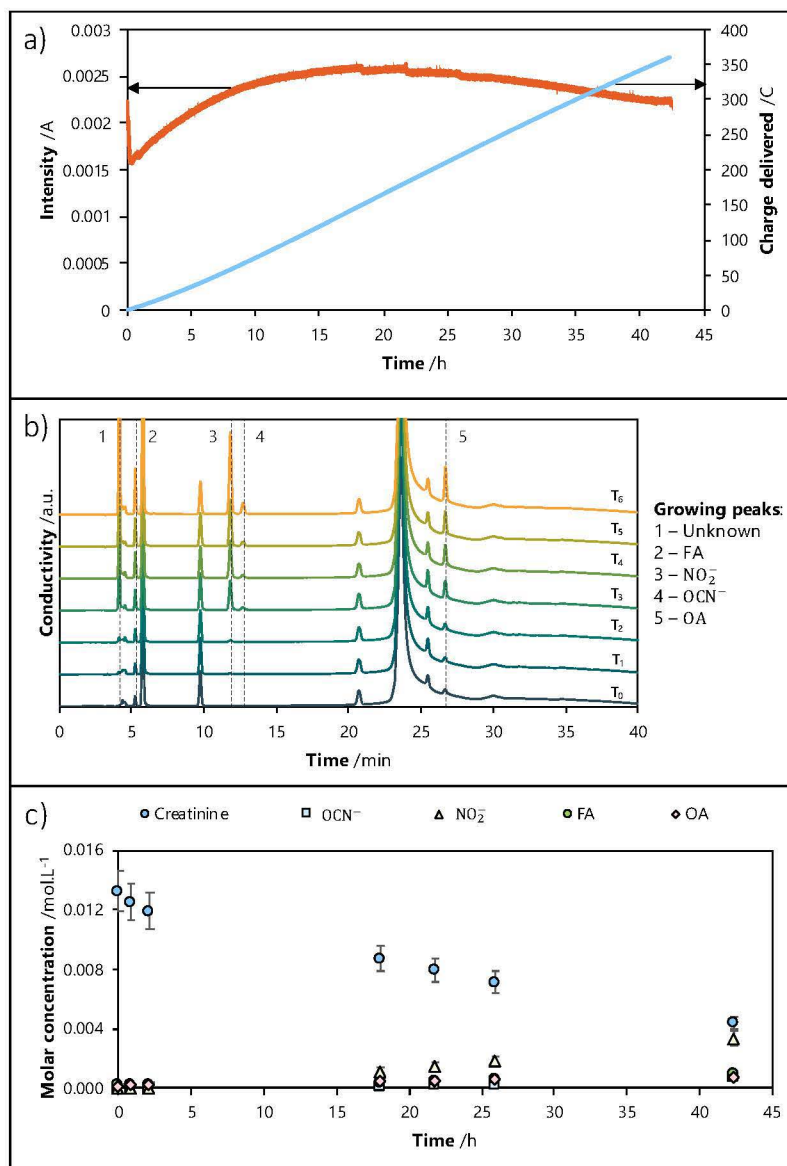


Fig. V.8 – Results of chrono-amperometry of a creatinine solution (0.013 mol L^{-1}) on nickel electrode (18 cm^2) in alkaline solution ($\text{KOH } 1\text{ mol L}^{-1}$): temporal profiles of a) current intensity and charge delivered, b) the anion chromatograms, and c) concentration of creatinine and identified products.

Figure V.8-a shows the temporal profile of the current during the electrolysis. Its shape is atypical as describing first a rapid decrease, then an increase until reaching a plateau (83 A m^{-2}) and finally a slight decrease. At the end of the electrolysis, almost 350 C were supplied to the system. The observed current corresponds to the oxidation of nickel(II) to nickel(III). The creatinine oxidizes, probably by some indirect pathways since the $I=f(E)$ of creatinine does not show any additional peak other than nickel(II) oxidation (it will be discussed later, in section V-1.2.b.i). Regarding the intensity profile, it seems that before oxidation, the creatinine needs to be adsorbed on nickel electrode. The duration required

to achieve the equilibrium state between adsorption and oxidation could then explain the shape of the current curve.

In order to determine if creatinine was oxidized, the reaction medium was sampled over time, and analyzed by IC. Figure V.8-b shows the results only on the anion side (no change being observed on the cation side). It can be observed that the amount of 5 compounds increases: (i) FA, (ii) nitrite, (iii) cyanate, (iv) OA and (v) an unidentified molecule. The creatinine signal measured by MS reveals a degradation of 67% at the end of electrolysis.

The temporal variations of both reagent and product concentrations in the bulk are provided in Figure V.8-c which confirms the degradation of creatinine under these pH conditions and on nickel electrodes.

All these findings support the idea that:

- (i) during the electrolysis of urine solution (as presented in the previous section), a competition for accessing to active nickel(III) sites takes place between urea (the main compound in urine) and creatinine (the second abundant compound in urine). To go further, more investigations on the relative degradation rate for each molecule need to be done;
- (ii) the formation of oxalic and formic acids, observed during the electrolysis of urine (and not with urea), could be induced by the creatinine electro-oxidation

V-1.1.b.iv Energy cost assessments

Since the electrolysis was performed in a divided cell, the sole cathodic reaction involved was the reduction of water to H₂. As a consequence, the amount of H₂ formed, n_{H₂} (mol), corresponded to the one supplied by Eq. V.4.

$$n_{\text{H}_2} = \frac{Q_{\text{total}}}{\mathcal{F} \times 2} \quad (\text{V.4})$$

where Q_{total} represents the total charge supplied to the EC cell.

Q_{total} was calculated by integrating the current I(t) obtained at the applied potential of 0.55 V vs. Hg/HgO with time during chrono-amperometry measurements.

The energy consumption of the EC cell, denoted as E_{consumed} (Wh), was defined by Eq. V.5.

$$E_{\text{consumed}}(t) = \int_0^t I(t) \times \Delta U_{\text{electrolyser}}(t) \times dt \quad (\text{V.5})$$

where ΔU_{electrolyser} is the cell voltage (V).

The energy related to the produced H₂, denoted as E_{eq. H₂ produced} and expressed in Wh, could be calculated using Eq. V.6.

$$E_{\text{eq. H}_2 \text{ produced}} = V_{\text{H}_2, \text{ produced}} \times \rho_{\text{H}_2} \times \lambda_{\text{H}_2} \quad (\text{V.6})$$

where V_{H₂, produced} was the total amount of H₂ formed during electrolysis (L), λ_{H₂} the H₂ gravimetric energy density (kWh kg_{H₂}⁻¹) and ρ_{H₂} the volumetric density of hydrogen in STP conditions which was evaluated at 8.4 × 10⁻⁵ kg L⁻¹ [262]. At 25 °C and under atmospheric pressure, λ_{H₂} is reported equal to 33.33 kWh kg_{H₂}⁻¹ [263] and represents an estimate of the energy that would be produced for a complete H₂ combustion.

In order to estimate the overall energy consumption of the process, the actual consumption, ΔE (Wh), was then expressed according to Eq. V.7.

$$\Delta E = E_{\text{consumed}} - E_{\text{eq. H}_2 \text{ produced}} \quad (\text{V.7})$$

The energy consumption of electrolysis is here compared with (i) urea synthetic and (ii) urine.

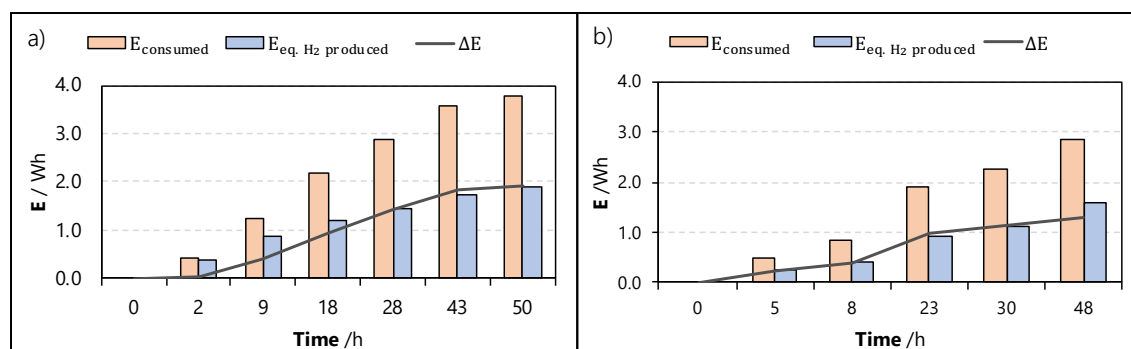


Fig. V.9 – Energy data corresponding to the EC-cell consumption, the equivalent energy resulting from H_2 production, and the deviation between the consumption and the added-value energy during the UEO in the case of a) urea synthetic and b) urine electrolyses.

For urea synthetic electrolysis, Figure V.9-a shows that after 50 h of electrolysis, the UEO process consumes 34 kWh of electricity to produce 1 kg of H_2 . This value is in the same order of magnitude as the one reported by Boggs et al. [20] in 2009 ($38 \text{ kWh kg}_{\text{H}_2}^{-1}$) who carried out chronoamperometric measurements under severe conditions of alkalinity (at 1.4 V *vs.* Hg/HgO and 5 mol L^{-1} KOH).

In the case of urine electrolysis (Figure V.9-b), as time progresses, the energy consumed by the system increases until reaching 2.9 Wh. Similar to the energy consumption, the energy equivalent of H_2 increases in the same manner up to 1.6 Wh, resulting in an energy differential (ΔE) of 1.3 Wh. Given the total amount of H_2 formed during electrolysis (*i.e.*, 2.34×10^{-2} mol, Figure V.6-a, *vs.* 2.80×10^{-2} mol, Figure V.3-a in the case of urea synthetic solution), the energy consumption for urine treatment is $28 \text{ kWh kg}_{\text{H}_2}^{-1}$, and thus reduced by 18% when compared to the electrolysis of urea ($34 \text{ kWh kg}_{\text{H}_2}^{-1}$). However, this consumption remains almost 30% lower than the one required to obtain the same amount of H_2 from water electrolysis [264], assuming identical levels of purity and electrolyte alkalinity.

This energy comparison needs to be taken further, in order to improve the comparability by investigating under more similar industrial conditions (in terms of current density in particular).

V-1.2 Linear voltammetry experiments as a tool to better understand the matrix effect during the electro-oxidation of human urine

As discussed in the previous section, the EC response of human urine is significantly different from that obtained with urea, which is not surprising with respect the complexity

of the real matrix. In the present section, linear voltammetry experiments will be carried out so as to provide more information of the processes occurring during electro-oxidation of human urine. This exploratory study will be structured into 3 parts which objectives are:

- (i) to highlight the phenomenon of urea hydrolysis in urine; for that, the $I=f(E)$ curves will be plotted after different sampling periods and under various storage conditions;
- (ii) to evaluate the influence of the matrix effect on the EC response; for that, the $I=f(E)$ curves will be plotted at various concentrations of the main compounds contained in urine (as presented in **Chapter I**, section I-1.3, Figure I.5) using the spiking's method;
- (iii) to determine the partial kinetic order of urea for the chemical reaction between NiOOH and urea in the case of a real matrix and comparing it with the case of urea synthetic solutions (**Chapter IV**); for that, the $I=f(E)$ curves will be plotted at low potential scan rates.

V-1.2.a Electrochemical behavior of urine stabilized by alkalization

Figure V.10 shows typical linear voltammetric curves obtained with an urine solution, freshly excreted and alkalinized at $\text{pH} = 14$ (equivalent to a KOH concentration of 1 mol L^{-1}). It was obtained on nickel RDE, at 10 mV s^{-1} and 1000 RPM (see section II-1.1 in **Chapter II** for EC set-up).

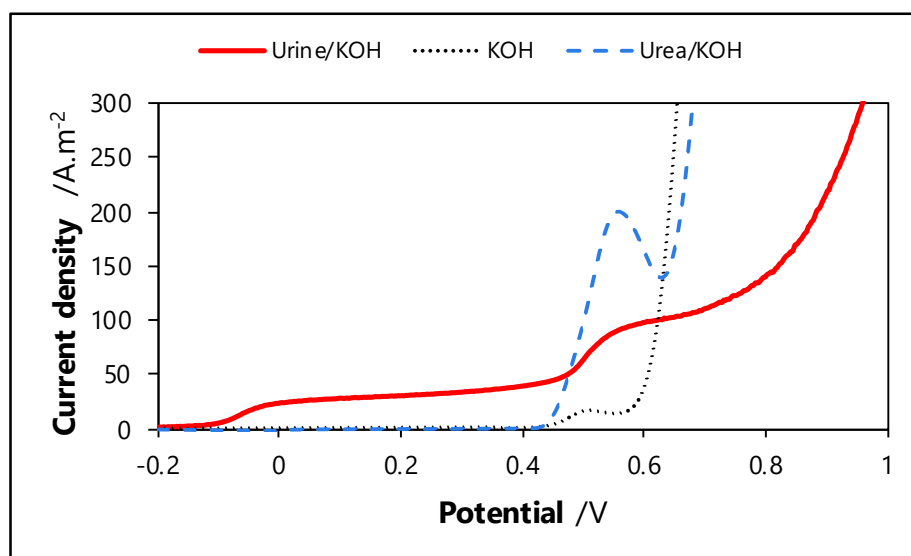


Fig. V.10 – Linear voltammetry of a freshly excreted human urine immediately alkalinized ($\text{KOH } 1 \text{ mol L}^{-1}$, unknown urea concentration, solid line), KOH solution (1 mol L^{-1} , dotted line) and urea solution 0.33 mol L^{-1} alkalinized with KOH (1 mol L^{-1} , dashed line), all obtained at $\nu_{scan} = 10 \text{ mV s}^{-1}$.

Two plateau can be observed:

- (i) a first anodic signal occurs at $-0.1 \text{ V vs. Hg/HgO}$, exhibiting a plateau ($\sim 25 \text{ A m}^{-2}$) in the potential range between -0.05 and 0.45 V . This wave is not observed in the case of urea synthetic solutions, while, it is observed for the different human urine samples. However, considering the fact that oxidation begins at low (*i.e.*, -0.1 V) potentials, this would orient towards easily oxidative compounds, such as thiol type molecules known to be present in urine (see Appendix A). To go ahead, additional investigation is required to fully validate this assumption.

(ii) a second oxidation signal is observed at 0.55 V *vs.* Hg/HgO, and presents a plateau ($\sim 100 \text{ A m}^{-2}$) as already observed with urea synthetic solutions, and is attributed to the oxidation peak of nickel(II) to nickel(III). Note that the potential of this wave appears to be independent of the “urine” matrix.

To investigate the stability of urine samples and thus the urea hydrolysis (as discussed in **Chapter I**, section I-1.3, Table I.2), the curves $I=f(E)$ have been plotted over several days by implementing two situations for the same batch of urine:

Case (i): a part of the urine sample is alkalinized on the first day of the study, and the $I=f(E)$ curves are plotted with the same sample after several days’ storage;

Case (ii): the other part of this urine sample is stored at room temperature, and each day an aliquot is undertaken, alkalinized and analyzed.

Figure V.11 shows the $I=f(E)$ curves plotted with urine solutions alkalinized at different ages, expecting to study the urea hydrolysis kinetics in urine. As shown in Figure V.11-a, the first oxidation signal ($-0.1 \text{ V vs. Hg/HgO}$) remains unaffected over time, while the anodic signal attributed to the nickel(II) oxidation decreases over time.

Figure V.11-b reports the temporal variation of the ratio of the net current to the initial net current (Eq. V.8).

$$I_{\text{net}} = I_{(E = 0.6 \text{ V})} - I_{(E = 0.4 \text{ V})} \quad (\text{V.8})$$

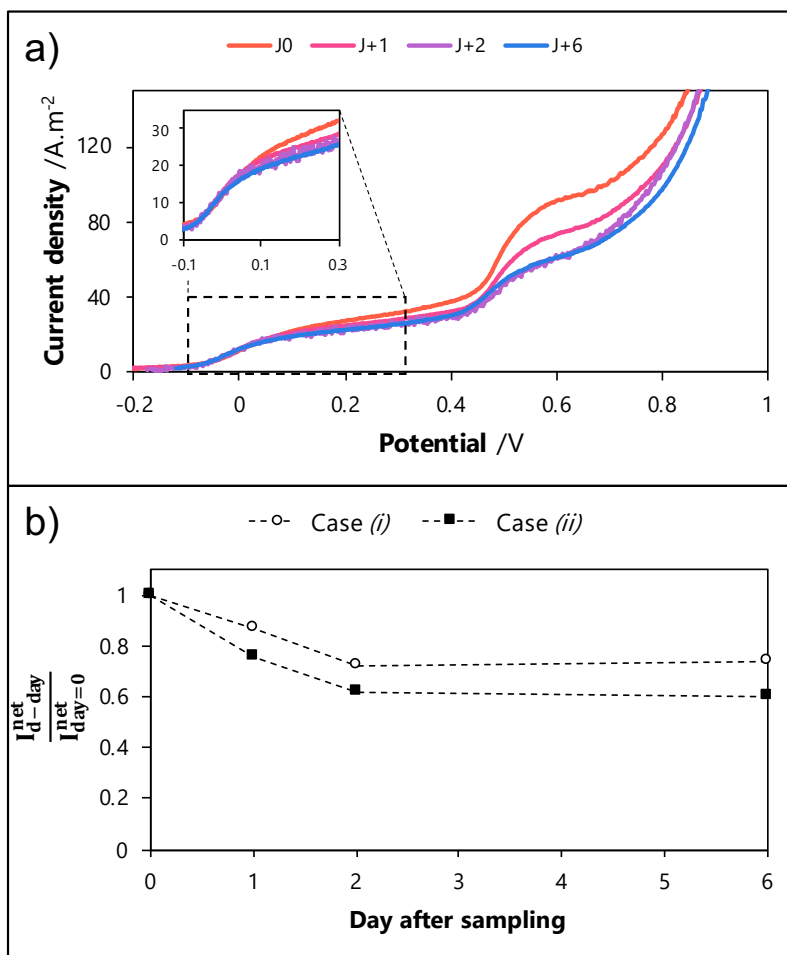
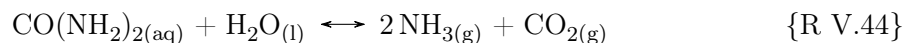


Fig. V.11 – Investigations of the stability of urine samples: a) linear voltammograms of a urine solution at different times after excretion (alkalinized day-after-day, KOH 1 mol L⁻¹, case (ii)) and b) temporal variation of the ratio of the net current to the net initial current (observed at 0.55 V vs. Hg/HgO) obtained from urine solutions alkalinized initially (case (i)) or day-after-day (case (ii)).

These results enable to conclude that:

- (i) the nickel(II) oxidation current decreases with time in both cases. The urea is hydrolyzed, according to reaction {R V.44}, and its concentration decreases (as presented in **Chapter II**, section I-1.3). As this nickel(II) oxidation is catalyzed by the presence of urea, the current magnitude logically falls down.



- (ii) an equilibrium state seems to be reached. The observed normalised current ($\sim 75\%$ for case (i) and $\sim 60\%$ for case (ii)) remains unchanged after 2 days of urine storage.
- (iii) the hydrolysis kinetics of urea seems to be affected by alkalinity conditions. Indeed, the decrease in current is more rapid and more important when urine is stored at neutral pH ($\sim -40\%$) than at pH = 14 ($\sim -25\%$). Indeed, when the solution is stored at pH 14, the equilibrium of the {R V.44} is shifted to the indirect way of Eq. R V.44, limiting its degradation. It can be seen that the plateau value when urine is stored at pH 14 is higher (-25%) than in the neutral case (-40%).

These findings point out that the alkalinity of the solution enables to slightly slow down the urea hydrolysis.

V-1.2.b Voltammetric response of different matrices spiked by each one of the most concentrated compounds in urine

The previous section (V-1.1) have shown how the presence of molecules other than urea in urine could have a strong impact on the UEO process. To deeply understand this matrix effect, various linear voltammetry experiments will be carried out by spiking three different matrices: KOH, urea/KOH and urine/KOH. As a first approach, a focus has been made on the most concentrated compounds present in urine and on the ones formed especially during the urine electrolysis (*i.e.*, FA and OA). As a result, the solution spiking will involve:

- Either organic molecules: creatinine ($C_4H_7N_3O$), hippuric acid ($C_9H_9NO_3$), creatine ($C_4H_9N_3O_2$), histidine ($C_6H_9N_3O_2$), OA ($C_2H_2O_4$) and FA (CH_2O_2);
- Or ion compounds: phosphate (PO_4^{3-}), sulfate (SO_4^{2-}), chloride (Cl^-) and ammonia (NH_3).

Appendix I shows all the curves $I=f(E)$ measured, namely for each matrix, each the nature of the doped compound and each concentration after doping.

All these $I=f(E)$ curves exhibit an EC behavior. However, to validate a certain electroactivity, electrolyses with significant conversion is required. Between the examined compounds:

- hippuric acid, sulfate and phosphate do not seem to significantly affect the nickel(III)/nickel(II) signal. Indeed, the current remains constant whatever the added concentrations.
- creatine, creatinine and histidine seem to react with the NiOOH; indeed the corresponding signal increases as a function of the added concentration. However, this effect appears to be enhanced in the case of urea/KOH matrix. For urine, except the creatinine, the two other compounds do not influence the nickel(II) signal. Doping the urine/KOH matrix by histidine impacts the current magnitude which decreases as function of the added concentration.

Figure V.12 summarises these results by reporting the ratio of the net current magnitude of the nickel(II) oxidation at each spike to the net intensity before spiking.

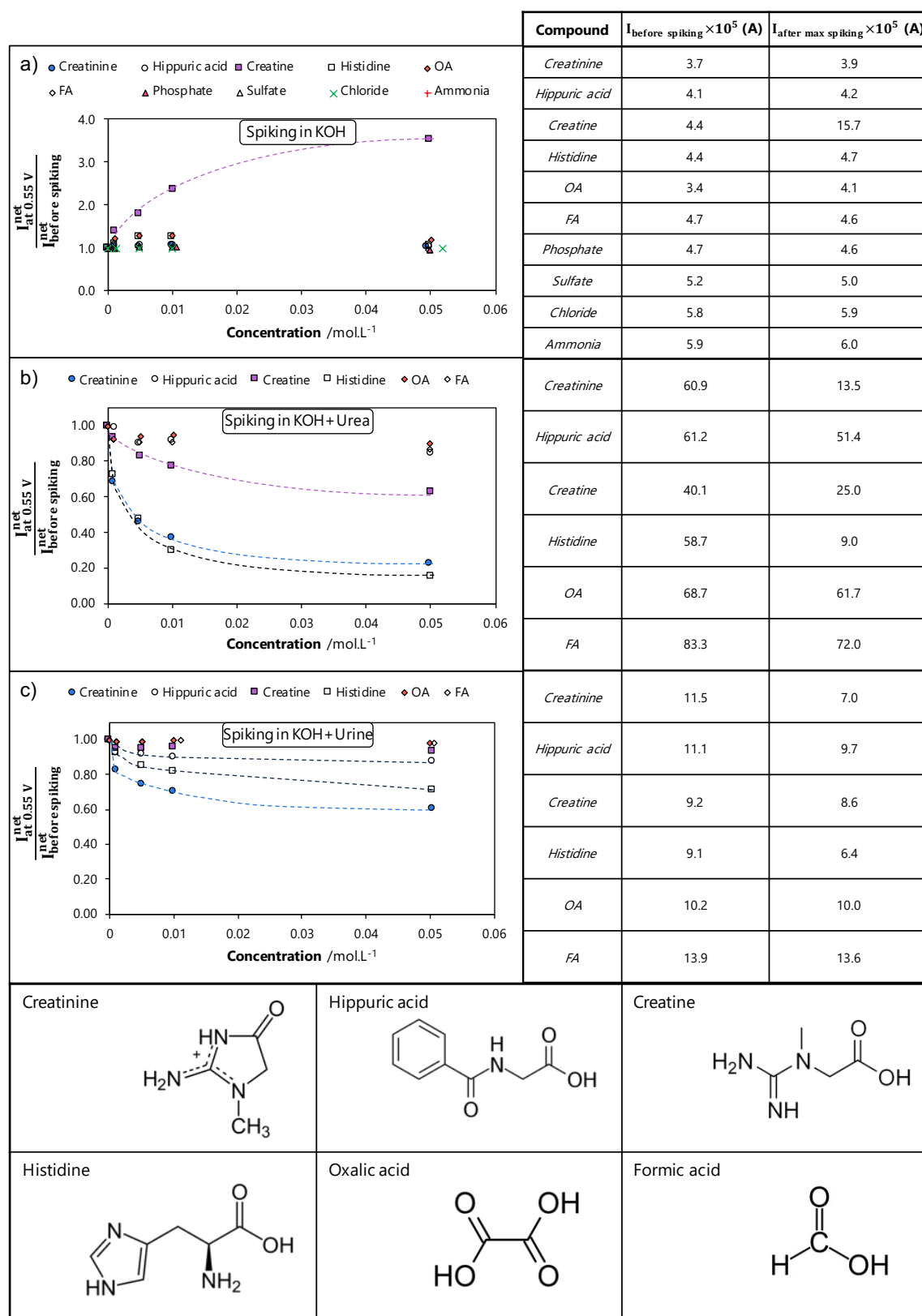


Fig. V.12 – Summary of the curves $I=f(E)$ obtained by linear voltammetry plot when spiking various major compounds in urine in the cases of matrix: a) KOH, b) urea/KOH and c) urine/KOH.

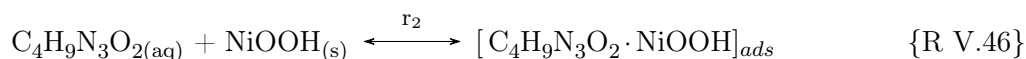
Different conclusions can be drawn depending on the matrices studied and the concentrations (chosen to be close to physiological concentrations present in urine), as discussed in the following sub-sections.

V-1.2.b.i KOH matrix

In this case, the oxidation of nickel(II) to nickel(III) takes place without catalysis and continuous regeneration of nickel(II) by the chemical reaction with urea. If the ratio increases, nickel(II) oxidation is exacerbated following two possible ways:

1. by chemical reaction between NiOOH and the added species;
2. by direct oxidation of the species added at the same potential than the oxidation of nickel(II).

From the graph V.12-a, the main effect is observed with the creatine ($C_4H_9N_3O_2$) since the signal is multiplied by 4 when 0.05 mol L^{-1} creatine is added. Indeed, the magnitude of the current oxidation of nickel(II) over the creatine concentration increases, but not linearly, thus excluding the direct oxidation of creatine. For creatine concentration higher than 0.05 mol L^{-1} , the current stabilizes, meaning that the kinetic rates, r_1 is rapid and the forward direction of r_2 is major. The limitation comes from r_3 , as shown in {R V.45-R V.47}



The effect of the concentrations of the other compounds appears minor, except probably for histidine ($\sim + 0.03 \text{ V}$) and creatinine ($\sim + 0.02 \text{ V}$) which seem to poison the electrode, as the nickel(II) oxidation potential increases over the concentration.

The curves obtained with various concentrations of histidine (Appendix I, Figure. I.1) are represented in Figure V.13-a in a potential scale going to the anodic direction until 2 V vs. Hg/HgO. The goal is to get a better understanding of the observed shift of the potential of both signals (*i.e.*, nickel(II) and OH^- oxidation reactions) to the anodic direction as a function of the increased concentration of histidine. The inset shows the nickel(II) oxidation signal.

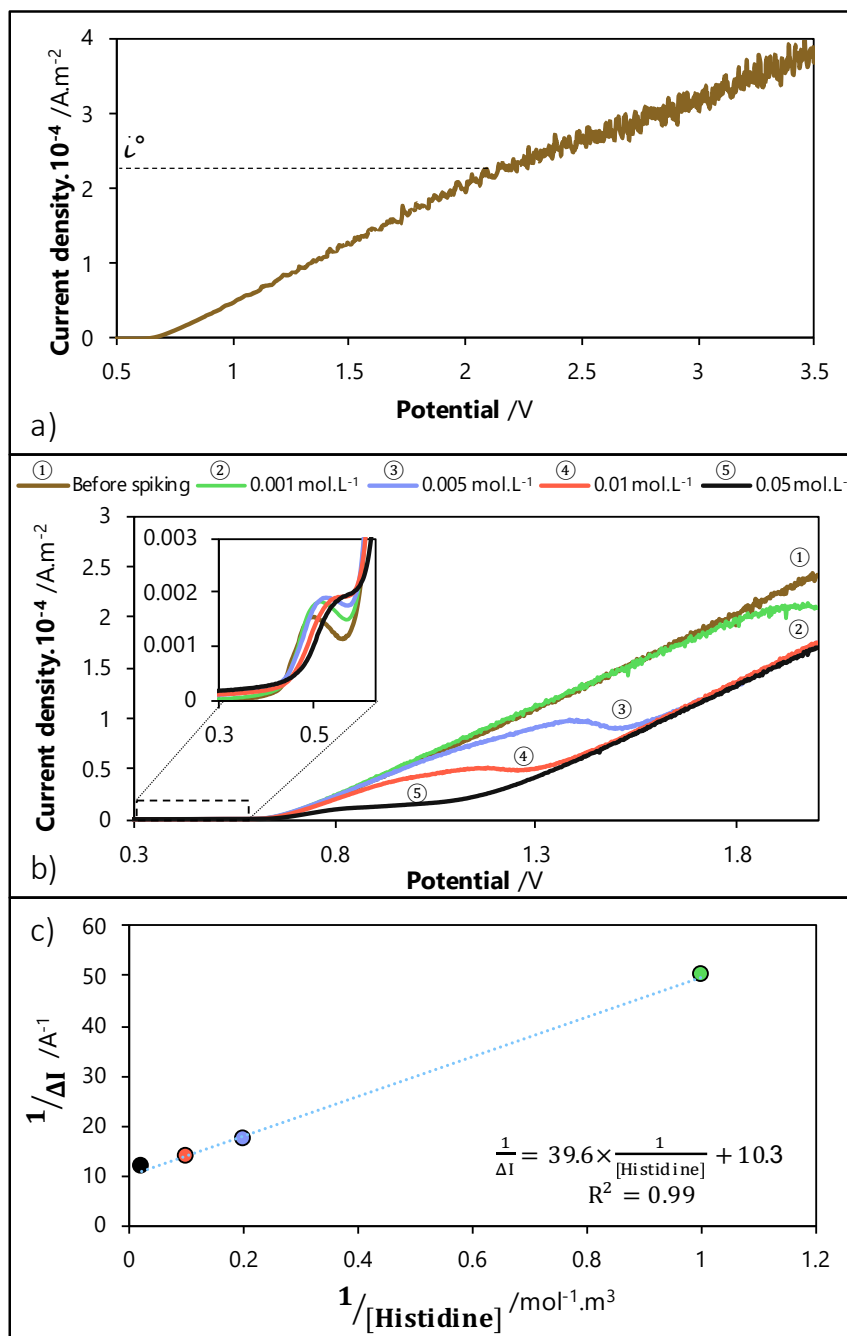
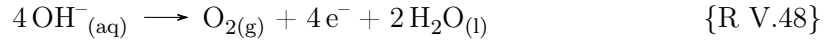


Fig. V.13 – a) Linear voltammogram obtained on nickel RDE ($3.14 \times 10^{-6} \text{ m}^2$) at 10 mV s^{-1} of KOH (1 mol L^{-1}) solution, b) linear voltammograms obtained on nickel RDE ($3.14 \times 10^{-6} \text{ m}^2$) at 10 mV s^{-1} when doping a KOH solution (1 mol L^{-1}) with histidine between 0.001 and 0.05 mol L^{-1} and c) determination of the affinity adsorption of histidine on nickel sites.

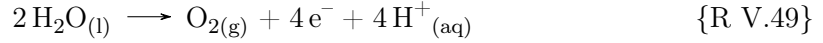
Nickel(II) oxidation is affected by histidine concentration as the potential of the beginning of the nickel(II) oxidation increases with the concentration of the added histidine. This confirms an adsorption of histidine on nickel(II) and the consequent blocking of the nickel sites. As a result, the access of OH^- to nickel(II) is forbidden and requires more energy. Besides the amount of charge of the nickel(II) oxidation signal decreases with histidine concentration (-30% between the signal before doping and doping at 0.05 mol L^{-1}).

For potentials higher than $0.6/0.7 \text{ V}$, the oxidation of the solvent occurs following the

reaction {R V.48}.



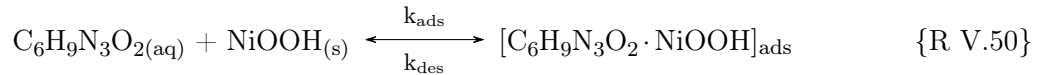
Curve ① (Figure V.13-a) is the signal, exponentially shaped, obtained without any doping of the KOH solution. For very high over-voltage ($E_{\text{anode}} \geq 2 \text{V}$), the curve tends to become horizontal (*i.e.*, to exhibit a diffusion limited plateau). This means that for potentials higher than 2 V, the interfacial concentration of OH^- reaches zero and the new additional reaction occurring is the water oxidation as in the reaction {R V.49}. This also induces the acidification of the electrode.



In Figure V.13-b, one can note that the corresponding part of the water oxidation does not appear in curve ① and ②; but it is clearly observable for curves ③ to ⑤.

Curves ② to ⑤ have been obtained in presence of histidine by increasing its concentration from 1 to 50 mmol L^{-1} . They show that both the observed plateau current magnitude and the potential of the OH^- oxidation signal decrease.

The next part expects to determine if the histidine ($\text{C}_6\text{H}_9\text{N}_3\text{O}_2$) adsorption could be modeled by the Langmuir model, assuming the following reaction {R V.50}.



As detailed in Appendix J, the following relationship can be established as Eq. V.9:

$$\frac{1}{\Delta I} = \frac{1}{I^\circ} + \frac{1}{K \times I^\circ \times [\text{Histidine}]} \quad (\text{V.9})$$

where ΔI is the difference in the oxidation currents of hydroxide ions in the presence of histidine and in its absence (A), I° is the limiting current in absence of histidine (A) and K is the equilibrium constant of the adsorption of {R V.50} between histidine and nickel sites ($K = k_{\text{ads}}/k_{\text{des}}$, dimensionless).

Figure V.13-b shows the variation of the inverse of the current difference as a function of the inverse of the histidine concentration. A good agreement is found (correlation coefficient 0.99), validating the Langmuir-modeled adsorption of histidine onto nickel sites. The y-intercept of the straight line (equal to $1/I^\circ$, Eq. V.9), enables to determine the mass transfer coefficient of the hydroxide ions (in the case of 1 mol L^{-1} and a anode surface area of 3.14 mm^2), as highlighted in Eq. V.10. It is found equal to $8.4 \times 10^{-5} \text{ m s}^{-1}$.

$$k_{\text{OH}^-} = \frac{1}{y_{\text{intercept}} \times n_e \times \mathcal{F} \times [\text{OH}^-] \times S \times \frac{1}{1-t_{\text{OH}^-}}} \quad (\text{V.10})$$

Assuming a diffusion coefficient of $5.3 \times 10^{-9} \text{ m}^2 \text{ s}^{-1}$ for hydroxide ions [265] and a transport number t_{OH^-} equal to 0.75, a diffusion layer of 65 μm is obtained, which is in agreement with usual values.

Having determined the k_{OH^-} coefficient, the histidine adsorption equilibrium constant, K , can be deduced and found equal to 0.22, meaning a low affinity of histidine against nickel.

V-1.2.b.ii Urea/KOH matrix

In the case of this matrix, remember that urea catalyzes the oxidation of nickel(II) to nickel(III) by chemical reaction. A matrix effect is undeniably observed. Compared with the previous section (KOH matrix, V-1.2.b.i), the presence of organic molecules reduces the nickel(II) oxidation signal. Competition is created with other molecules for the nickel(III) sites available to urea. From the Figure V.12-b, it appears that increasing the concentration of creatinine, creatine, histidine and hippuric acid, makes decreasing the current of the nickel(II) oxidation signal. The decrease is strongly pronounced in the case of histidine and creatinine, but when considering the one at physiological concentrations.

- (i) creatine decreases the signal by 40% (maximum physiological concentration of $2 \times 10^{-2} \text{ mol L}^{-1}$);
- (ii) creatinine decreases the signal by 80% (maximum physiological concentration $3 \times 10^{-3} \text{ mol L}^{-1}$);
- (iii) histidine decreases the signal by 85% (maximum physiological concentration $2 \times 10^{-3} \text{ mol L}^{-1}$).

This common behavior could translate a competitive adsorption on nickel(III) sites with the urea. Decreasing the amount of urea adsorbed leads to a decrease in the rate of the urea/nickel(III) reaction, and consequently the nickel(III) amount density Γ_{III} (mol m^{-2}) implying the current. This can be highlighted by comparing the current observed after the maximum concentration spiking (all at 50 mmol L^{-1}) in Eq. V.11 (reported in the table of Figure V.12).

$$I_{\text{FA}} \geq I_{\text{OA}} \geq I_{\text{Hippuric acid}} \geq I_{\text{Creatine}} \geq I_{\text{Creatinine}} \sim I_{\text{Histidine}} \quad (\text{V.11})$$

From this, one can deduce the order of the adsorption affinity of these adducts against the nickel(III) can be deduced as follows:

$$\text{Creatinine} \sim \text{Histidine} \geq \text{Creatine} \geq \text{Hippuric acid} \geq \text{OA} \geq \text{FA} \quad (\text{V.12})$$

V-1.2.b.iii Urine/KOH matrix

In order to come as close as possible to the actual conditions under which UEO occurs in urine, the compounds have also been spiked in this urine/KOH matrix.

The effect of the various compounds added into an alkalized solution of urine, on the current of the nickel(II) oxidation signal is presented in Figure V.12-c. Compared to the effect previously observed (sections V-1.2.b.i and V-1.2.b.ii), the effect seems here minor ($\leq 30\%$ of decrease of the current for creatinine, compared to 80% in the case of urea/KOH matrix). As previously observed, only three compounds (creatinine, histidine and hippuric acid) exhibit a negative effect on the current.

Note that the histidine (Appendix I, Figure I.3) seems to affect also the signal of the solvent oxidation. As previously, all the observed effects could be explained by an adsorption of the corresponding species onto the NiOOH sites and the subsequent poisoning of the electrode against, at the least urea oxidation. Quantitative analysis of these results needs more investigation.

This study provided clear evidence of the effect of the matrix on nickel(II) oxidation in alkaline media, and above all of the competition in the chemical reaction between urea/OH⁻/nickel(III) and the other compounds present in urine.

V-1.2.c Matrix effect illustrated by means of kinetic study

In this last sub-section, the UEO kinetics will be carried out with urine matrix expecting to determine the partial order of urea (for the chemical reaction urea/OH⁻/NiOOH). By comparing with the value obtained with urea/KOH matrix (see Chapter IV, section IV-3.2), one can expect to evidence eventual effect of the urine matrix.

The urea partial order was determined by plotting $I^{\text{net}}=f(E)$ curves at very low scan rates (0.83 mV s^{-1}) with various concentrations of the (added) urea into urine. The net current was calculated as Eq. V.13.

$$I^{\text{net}} = I_{E=0.57\text{ V}} - I_{E=0.40\text{ V}} \quad (\text{V.13})$$

As indicated in the Chapter IV (*i.e.*, section IV-3.2 in Figure IV.10), operating in this way avoids limitation of the rate of the chemical reaction by the oxidation of nickel(II) to nickel(III).

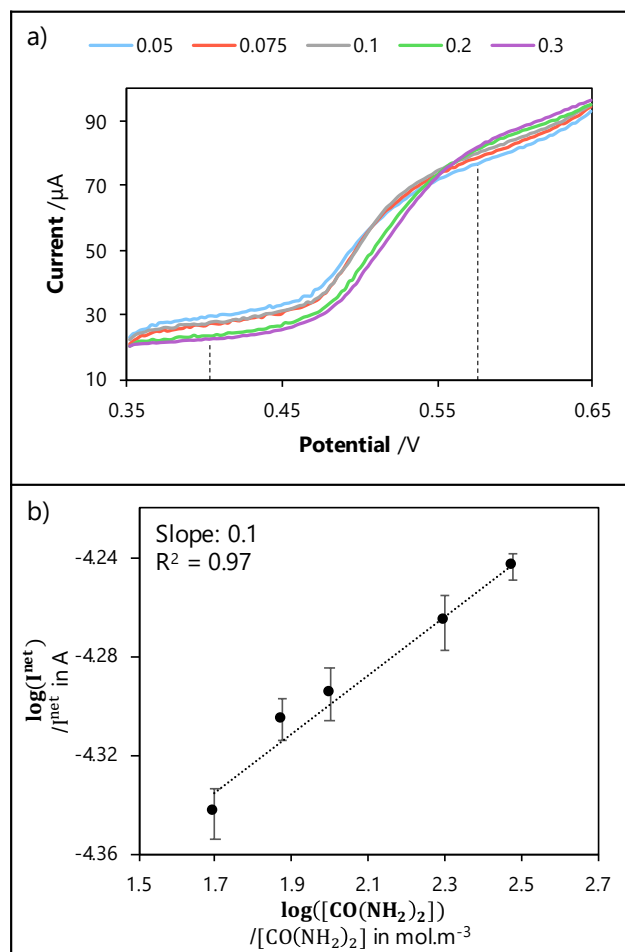


Fig. V.14 – a) $I=f(E)$ curves plotted at low potential scan rate (0.83 mV s^{-1}) and b) logarithmic variation of the nickel(II) oxidation net current against the urea (added) concentration at low potential scan rates.

A straight line is obtained when plotting the logarithmic variation of the nickel(II) oxidation current against the urea (added) concentration.

As demonstrated earlier (section, **Chapter IV**, section **IV-3.2**), the slope of this straight line is directly related to the value of the urea partial order. As a reminder, a value of 0.3 was obtained in a urea/KOH matrix. In the case of the urine matrix, the partial order of urea is found equal to 0.1. This low value can be explained by the low dependence of the nickel(II) oxidation current by the urea concentration ; indeed as discussed in the section **V-1.2.b.ii**, there is competition between the adsorption and also the indirect oxidation of both creatinine and urea.

V-2 From the lab-scale scale to the pilot-scale

This section is devoted to the transfer of the UEO process from lab-scale cells (**Chapters III-IV**) to the pilot-scale reactor. For reminder, the latter of 1 L in volume has a cylindrical vertical geometry in which a nickel anode in the form of a wound grid and a central tubular cathode made of 316 L stainless steel were inserted. It operates under multi-pass mode: the reaction medium continuously circulates according to a closed recycling loop between the reactor and the storage tank. The details of the reactor are given in **Chapter II** (section II-1.2) and in Appendix C.

The present section will be composed of 4 parts aiming at:

- (i) implementing and discussing complete mass balances (in both liquid and gaseous phases) during the whole course of the UEO process in presence of urea synthetic solutions,
- (ii) studying the influence of operating parameters on the UEO performances in presence of urea synthetic solutions;
- (iii) establishing the proof of concept for pilot-scale electrolysis in presence of human urine solution;
- (iv) proposing a brief comparison of the energy performances of the UEO process.

V-2.1 Complete mass balances during the course of the urea electrolysis at pilot-scale

This section focuses on the performance of a potentiostatic electrolysis of an urea solution (0.55 V *vs.* Hg/HgO, where a plateau is observed during nickel(II) oxidation coupled to the UEO).

The electrolysis was carried out using the undivided configuration described in section II-1.2. Periodically aliquots ($\sim 1.5 \text{ cm}^3$) were undertaken and analyzed following the analytical methods described in **Chapter II**. All obtained results are indicated in Figure V.15.

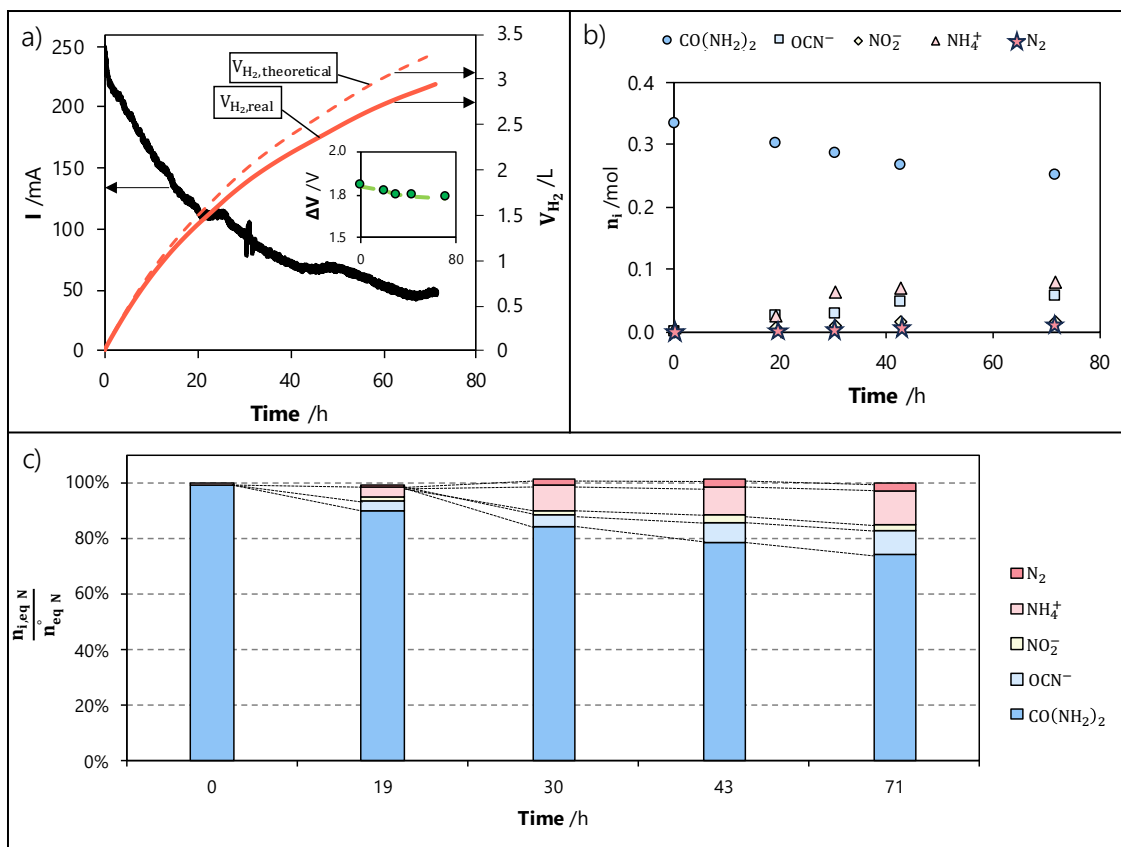


Fig. V.15 – Results obtained during potentiostatic electrolysis at pilot-scale (described in section II-1.2) of a urea synthetic solution (0.33 mol L^{-1}) in alkaline medium ($1 \text{ mol L}^{-1} \text{ KOH}$) (anode surface of 734 cm^2 equivalent of 2 cylinder variations, $30 \text{ kg h}^{-1} \sim 29 \text{ L h}^{-1} \sim \text{Re} = 155 \sim$ reactor residence time τ_{reactor} of 116 s, undivided configuration, 1 L): a) current density and the amount of formed H₂ (solid line: measured by GC, dashed line: theoretical amount)(inset: cell voltage), b) temporal profiles of molar quantity of identified N-species, and c) N-mass balance.

Figure V.15-a indicates both the recorded current (black curve) and the H₂ produced volume (red curve, in STP conditions) over time. The current seems to decrease exponentially although that the curve exhibits some distortions. The initial value (0.25 A , equal to 3.41 A m^{-2}) is relatively low and decrease 5 times in 70 h, possibly due to poisoning of the nickel.

Figure V.15-b introduces the time-dependent amount for the main analyzed compounds (urea, OCN⁻, NO₂⁻, NH₄⁺ and N₂). The rate of urea degradation reaches 28% after 70 h.

Assuming that only urea is oxidized at the anode (which is wrong considering that H₂ can also oxidize), one can conclude that at the end of electrolysis, the magnitude of the current should be equal to 75% of the initially observed current. That is not the case because the magnitude of the current decrease 5 times, suggesting a certain deactivation of the nickel electrode.

Besides, because the absence of separator, a fraction of the dissolved H₂ can move to the anode and undergo subsequent oxidation, thus contributing to increase the current magnitude. This can be demonstrated by comparing:

- (i) the actual quantity produced $V_{\text{H}_2, \text{real}}$, determined by GC;
- (ii) the quantity, $V_{\text{H}_2, \text{theoretical}}$, estimated from the charge considering that no H₂ oxidation

is present according to Eq. V.14.

$$V_{\text{H}_2, \text{ theoretical}} = \frac{\text{Charge } Q}{n_e \times \mathcal{F}} \times 22.4 \quad (\text{V.14})$$

where n_e is the number of electrons exchanged (dimensionless, 2 in the case of $2 \text{ H}_2\text{O} + 2 \text{ e}^- \rightarrow \text{H}_2 + 2 \text{ OH}^-$)

At the end of electrolysis, a 10% difference is observed between the volume of hydrogen measured by GC ($V_{\text{H}_2, \text{ real}}$) and the volume theoretically formed without oxidation ($V_{\text{H}_2, \text{ theoretical}}$). This last result confirms the occurrence of either hydrogen oxidation at the anode or by-products reduction at the cathode at the expense of H_2 (such as NO_2^- , observed in the **Chapter III**, section III-3.2).

The cell voltage is indicated in the inset of Figure V.15-a. The slight decrease in cell voltage (from 1.8 V down to 1.73 V, already observed at lab-scale) is ascribed to the decrease of both cathodic over-voltage and ohmic drop.

Figure V.15-b outlines the time-dependent profiles of mole number for identified N-species. The degradation of urea reaches 25%, primarily resulting in NH_3 (accounting for 13 mol.% at the end of the electrolysis, appearing as NH_4^+ in IC analysis) Cyanate is also significantly ($\sim 10 \text{ mol.}\%$) present. Note that the N_2 gas and NO_2^- are present as traces ($\leq 5 \text{ mol.}\%$).

Figure V.15-c introduces, for the first time, a complete mass balance of the N-species generated in both liquid and gas phases. Regardless of the electrolysis duration, the predominant ($> 97\%$) N-compounds created during electrolysis at pilot-scale are OCN^- , NO_2^- , NH_3 , and N_2 . This further confirms the lab-scale results presented in the previous section V-1.1.

As previously explained in the same section V-1.1, the mass balance of the C-species (specifically $\text{CO}(\text{NH}_2)_2$, OCN^- , and CO_3^{2-}) is also corroborated (exceeding 97% and not shown here).

In conclusion, this section identified and measured the by-products of the synthetic UEO at pilot-scale for the first time. All these results confirm those obtained previously at lab-scale, since the trends remain identical.

V-2.2 Effect of some key operating parameters on the urea synthetic solution electrolyses at pilot-scale

In this section, the impact on the UEO performances of three operating parameters will be investigated by carrying out urea potentiostatic electrolyses, namely:

- (i) the anode surface area;
- (ii) the circulating flow rate of the urea solution into the undivided reactor;
- (iii) the applied potential.

V-2.2.a Influence of the surface of the nickel grid anode

Figure V.16 shows the results of two potentiostatic electrolyses with two different anode surfaces: (i) 734 cm² (2 cylinder variations of nickel grid in the reactor, S/V = 78 m⁻¹) and (ii) 1,101 cm² (3 cylinder variations, S/V = 117 m⁻¹).

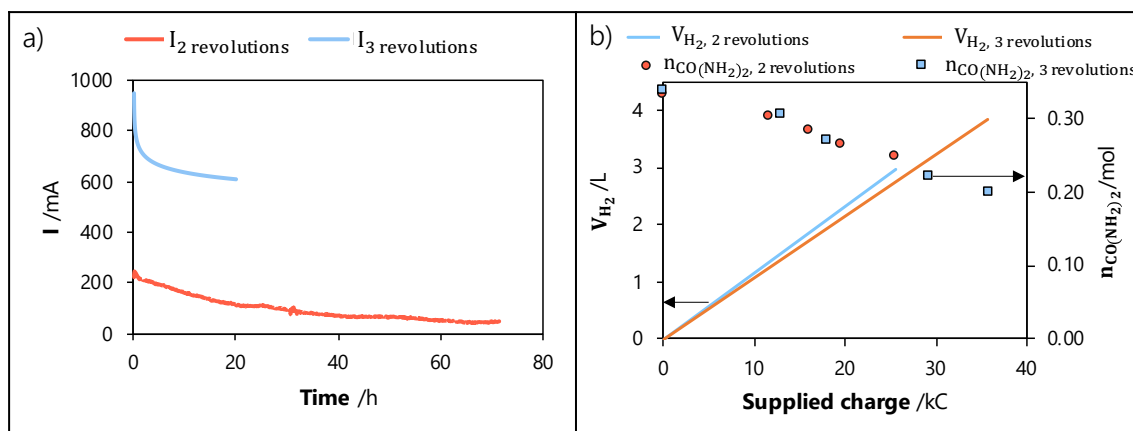


Fig. V.16 – Results of the potentiostatic electrolyses of a urea synthetic solution (0.33 mol L⁻¹) in alkaline medium (1 mol L⁻¹ KOH) carried out at pilot-scale (30 kg L⁻¹, undivided electrolyser, 1 L) for two different anodic surface area: a) the time profile of the current and b) the volume of the produced H₂ and the molar amount of unconverted urea during electrolysis.

Some conclusions can be drawn:

- (i) in Figure V.16-a, when the surface is multiplied by 1.5, the initial current goes from 0.23 A (734 cm²) to 0.96 A (1.101 cm²) and is therefore multiplied by approximately 4. It could be explained by (i) an experimental bias (electrode surface), (ii) a stoichiometric ratio in favor of nickel(III) and (iii) the chemical kinetic rate law. This would be consistent with the partial order of nickel(III) determined in **Chapter IV** (value of 5, section IV-3.2). Indeed, the chemical rate is not a linear function of the nickel site surface concentration, but proportional to Γ_{III}^5 .
- (ii) Figure V.16-b confirms that the variation of the volume of H₂ formed during electrolysis as a function of charge is not affected by the electrolysis surface. The time over which hydrogen is formed is shortened with a larger electrode surface area (3 L_{H₂} in 71 h *vs.* 4 L_{H₂} in 20 h).
- (iii) in Figure V.16-b, the variation of the degraded urea number with the delivered charge does not exhibit any influence with the anode surface. However, the rate of urea degradation is accentuated with larger electrode surface area (−0.08 mol_{urea} in 71 h *vs.* −0.14 mol_{urea} in 20 h).
- (iv) The nature of the by-products is found to remain identical whatever the anode surface, as well as their proportions according to the charge delivered (data not presented here).

V-2.2.b Influence of the flow rate

Figure V.17 shows the temporal variation of the current magnitude measured during potentiostatic electrolyses carried out with two different flow rates: (i) 30 kg h⁻¹ (*i.e.*, 29 L h⁻¹) and (ii) 60 kg h⁻¹ (*i.e.*, 58 L h⁻¹).

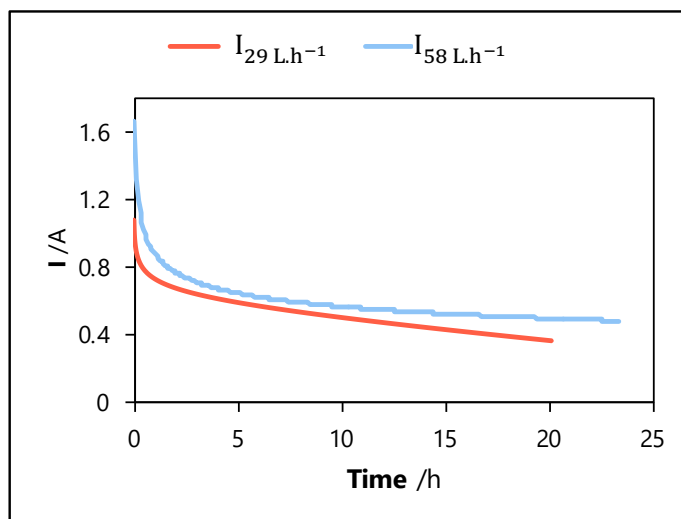


Fig. V.17 – Results of the potentiostatic electrolyses of a urea synthetic solution (0.33 mol L^{-1}) in alkaline medium (1 mol L^{-1} KOH) carried out at pilot-scale (3 revolutions or 1101 cm^2 , undivided electrolyser, 1 L) for two different flow rates: temporal profiles of the current.

When the flow rate is multiplied by 2, the current is increased by 20%. The decaying profile is practically identical in both situations and does not seem to be affected by the flow rate.

In view of values of the Reynolds number presented in **Chapter II** (*e.g.*, ≤ 300), the flow regime in the reactor is laminar, thus meaning that a possible limitation by mass transfer could exist, even when operating under multi-pass mode. For technical limitations (pump), it was unfortunately not possible to implement higher flow rates.

Concerning the formation of UEO by-products or urea degradation, no change was observed between both flow rates, consequently analytical results were not presented.

V-2.2.c Influence of the applied potential

Figure V.18 shows the results of potentiostatic electrolyses performed at three different applied potentials: (i) 0.45 V, (ii) 0.55 V and (iii) 0.65 V (*vs.* Hg/HgO). One can refer to $I=f(E)$ curve reported in section III-2.1, page 73, to get an idea of the potential ranges.

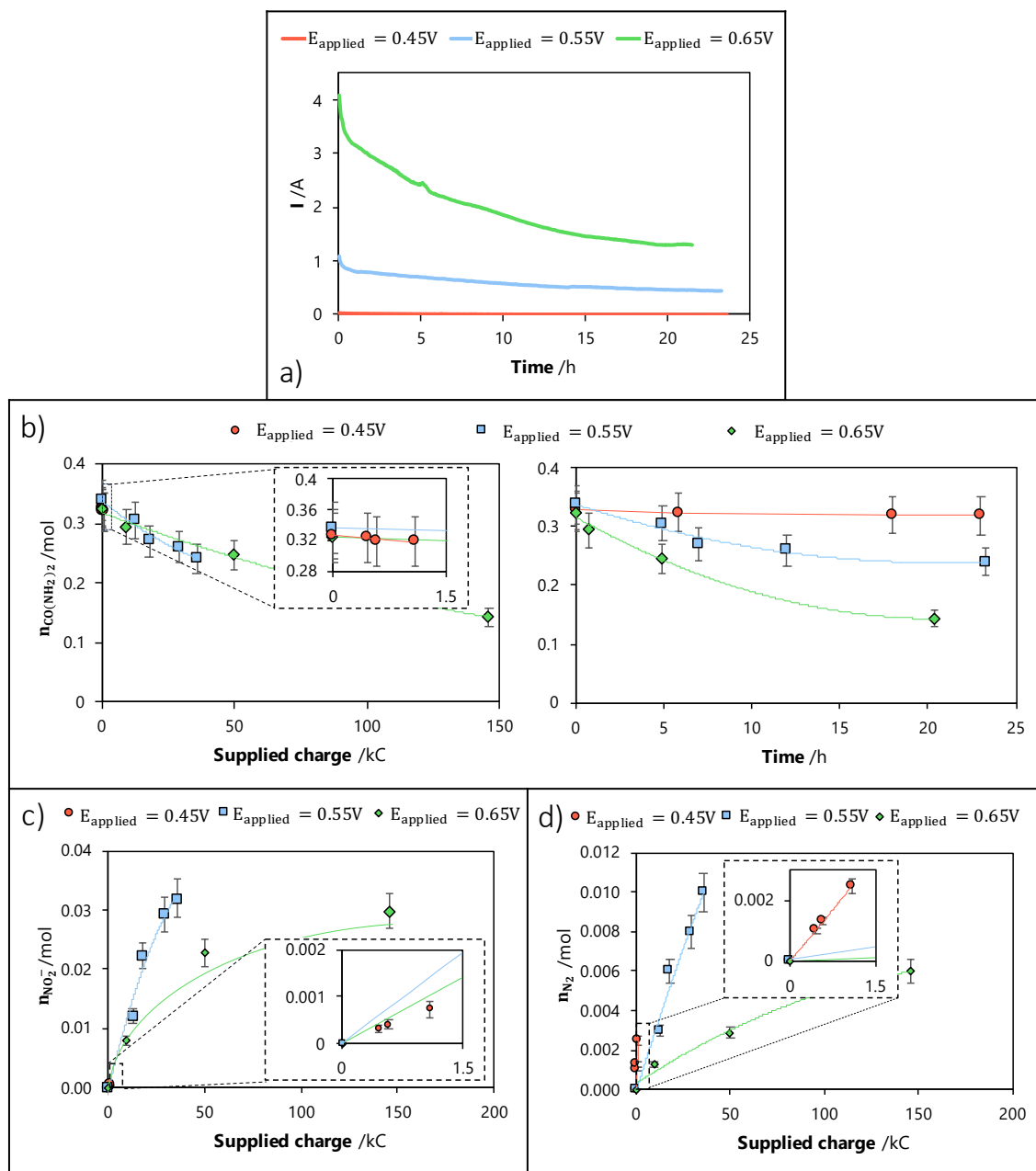


Fig. V.18 – Results of the potentiostatic electrolyses of a urea synthetic solution (0.33 mol L^{-1}) in alkaline medium ($1 \text{ mol L}^{-1} \text{ KOH}$) carried out at pilot-scale ($1,101 \text{ cm}^2$, 60 kg h^{-1} , undivided electrolyser, 1 L) for three different applied potentials: the time profiles a) the current, b) urea molar amount, c) NO_2^- molar amount and d) N_2 amount during electrolysis.

Various conclusions can be drawn from these results:

- (i) In general, the initial current magnitude increases as the applied potential increases (0.04 A at 0.45 V , 1.09 A at 0.55 V and 4.10 A at 0.65 V) as illustrated in V.18-a. At 0.55 V , the nickel(II) oxidation plateau is reached. At 0.65 V , the solvent oxidation zone is started, while at 0.45 V , the intensity is well below $\frac{I_{\text{plateau}}}{2}$. The decrease in intensity is not identical in each case, and intensity is more unstable at high potentials.
- (ii) The urea degradation profiles are shown in Figure V.18-b as a function of delivered charge and electrolysis time. The graph on the left shows that the urea degradation is not affected by the applied potential against the supplied charge. The residual molar amount of urea decreases as the supplied charge increases. Increasing the

applied potential causes, at identical electrolysis duration, an increase of the current magnitude, thus implying also an increase of the urea conversion as indicated in the Table V.4.

Applied potential E (V)	Electrolysis duration (h)	Urea conversion (%, Figure V.18-b, right)	Current decrease $\frac{I_{\text{initial}} - I_{\text{end}}}{I_{\text{initial}}}$ (%, Figure V.18-a)
0.45	24	3	87
0.55	23	29	59
0.65	22	56	68

Table V.4 – Influence of the potential applied during electrolysis on urea conversion and current.

However, comparing the current decrease to the urea conversion evidences strong discrepancies, since the current appears to decrease more rapidly (a similar behavior to the one observed in section V-2.1)

(iii) The influence of applied potential on the molar amount of nitrite is also investigated. In NO_2^- and N_2 , the N-oxidation state is +III and 0, respectively. In previous **Chapter IV** (section IV-4), a mechanism of the UEO was proposed in which both NO_2^- and N_2 were produced by two different ways. This is confirmed here with the variation of the applied potential. Indeed, from the Figure V.18-c, one can compare the molar amount of nitrite produced. Increasing the applied potential seems to favor the NO_2^- -formation (Figure V.18-d). As presented in the Table V.5, the applied potential significantly influences the molar ratio of electro-generated N_2 and NO_2^- .

Applied potential E (V)	Electrolysis duration (h)	NO_2^- molar amount (mmol, Figure V.18-c)	N_2 molar amount (mmol, Figure V.18-d)	$\frac{n_{\text{NO}_2^-}}{n_{\text{N}_2}}$
0.45		0.73	2.50	0.30
0.55	23	32.00	10.00	3.2
0.65		30.00	6.00	5.0
Delivered charge (kC)				
0.45		0.71	2.20	0.3
0.55	1	1.30	0.30	4.3
0.65		0.60	0.07	8.6

Table V.5 – Influence of the potential applied during electrolysis on NO_2^- and N_2 formations.

These results are similar to those obtained at lab-scale by Tatarchuk et al. [146] for both NO_2^- and N_2 . Note that nitrate formation was also observed in their work at potentials higher than 0.77 V *vs.* Hg/HgO. This range of potential values has not been investigated in this Chapter, but will be the subject of further investigation.

Finally, to maximize the reactor's performance from an industrial point of view (decrease operation time), we need to increase the anode surface area and increase the flow rate. Consequently in order to maximize the current, the urea conversion and the N_2 molar

amount at the expense of the NO_2^- , the applied potential appears as the key parameter to orientate N-compound formation mechanism.

V-2.3 Human urine electrolysis at pilot-scale

This section compares the results obtained from pilot-scale electrolysis of real urine solutions with those obtained at lab-scale scale (section V-1.1.b.ii).

Figure V.19 illustrates results obtained during chrono-amperometry electrolysis at 0.55 V *vs.* Hg/HgO on freshly excreted urine that has been alkalized.

Note that the corresponding urea concentration in the urine was determined to be 0.22 mol L^{-1} (which is equal to 30% of the initial measured TOC), a value that is lower than the commonly accepted urea concentration in urine (*i.e.*, 0.33 mol L^{-1}).

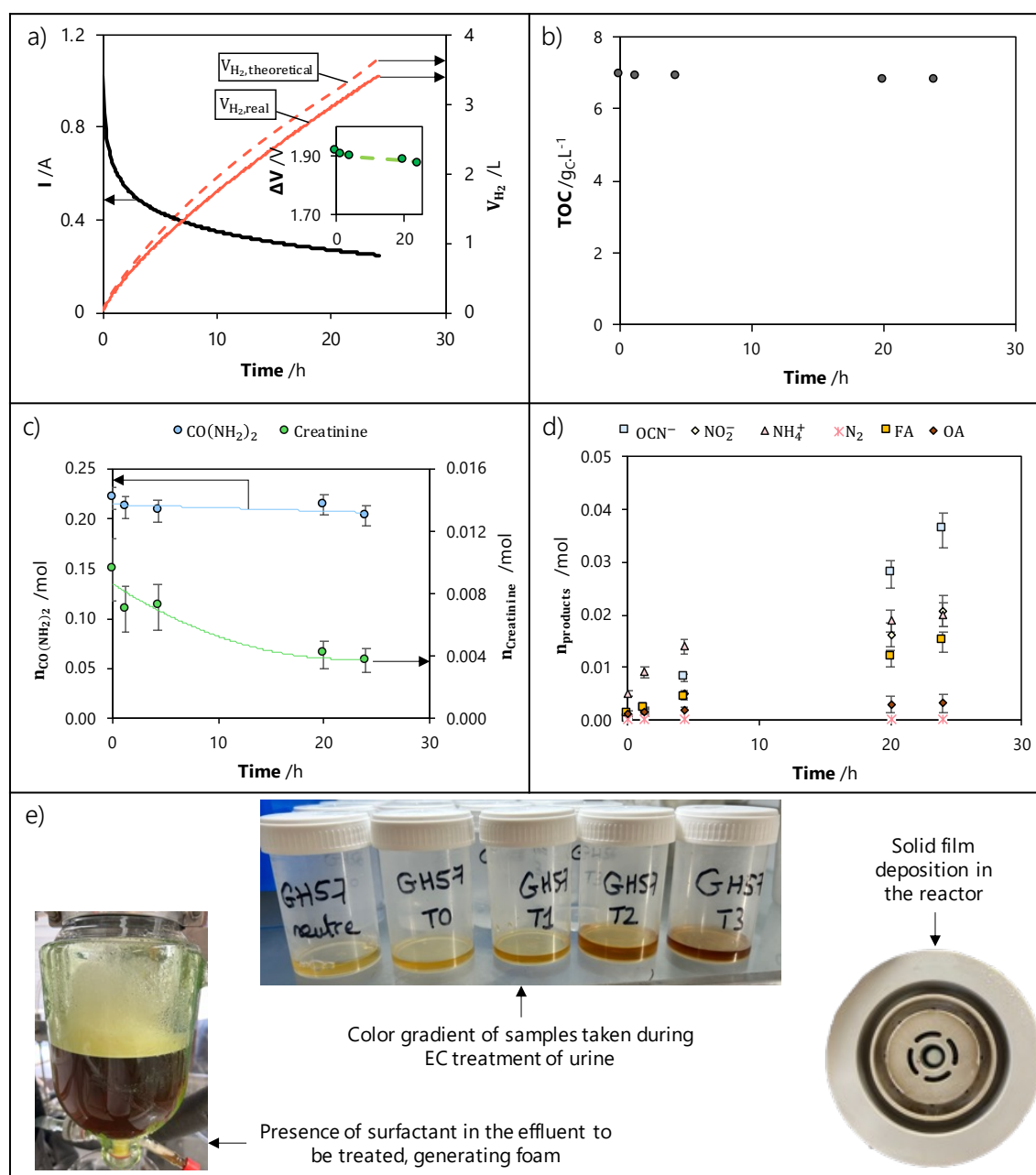


Fig. V.19 – Results of the potentiostatic (0.55 V *vs.* Hg/HgO) electrolyses of a human urine solution (urea concentration of 0.22 mol L^{-1}) in alkaline medium (1 mol L^{-1} KOH) carried out at pilot-scale ($1,101 \text{ cm}^2$, 60 kg h^{-1} , undivided electrolyser, 1 L): temporal profiles of a) the current density and the formed H_2 amount (inset: cell voltage), b) TOC amount, c) urea and creatinine molar amount, d) molar amount of *identified* generated products and some illustrations are given in e) related to the foam formed, the coloring of the samples and the deposit formed, all observed at the end of electrolysis.

Figure V.19-a presents the time-based variation in current during the electrolysis of a human urine solution. The initial current value is relatively high (1.1 A) but drops drastically immediately after polarization (-0.9 A in 1 h). This highlights a stabilization time for the system (typically the electrode surface state), before stabilizing at around 0.3 A. After that, the current variation exhibits an exponential decreases. Concerning the H_2 variation, the same conclusion than for urea synthetic solution (section V-2.1) can be drawn. Dissolved H_2 molecules diffuse towards the anode and oxidize into water, thus causing a decrease of the faradic efficiency and a possible reduction of molecules at the cathode.

Figure V.19-b reports the temporal variation of the TOC. A slight decrease ($\sim 3\%$) was observed after 24 h of electrolysis, although more than 30 kC was supplied to the system. This means that oxidation of organic molecules occurs but there is no mineralisation (*i.e.*, the oxidation does not generate $\text{CO}_2/\text{CO}_3^{2-}$). This fact is also confirmed by the color of the electrolysed urine (Figure V.19-e) which becomes dark brown as the electrolysis duration increases.

Figure V.19-c shows the temporal variation of the molar amount of urea and creatinine both initially present into the urine in significant quantities. Both compounds are oxidized. However, the molar amount of creatinine decreases faster than urea. Final conversion reaches 5 and 85% for urea and creatinine respectively. The initial concentration of creatinine ($9.5 \times 10^{-3} \text{ mol L}^{-1}$) is lower than the one of urea (0.22 mol L^{-1}). Although this lower concentration, creatinine oxidizes first and even appears to block/limit the urea oxidation. This behavior was also suggested at lab-scale and thus clearly appears to be a serious drawback for the UEO process. Indeed, if creatinine oxidation led to CO_2 , then it is reasonable to imagine that, after creatinine oxidation, the urea oxidation would pursue. In fact, the creatinine oxidation products seem to present a poisoning behavior against the nickel(II) oxidation, that could explain why the current magnitude decreases, despite the fact that the urea conversion is practically equal to 0.

In conclusion, (*i*) the substances present in urine, at the least the creatinine, hinders UEO as already observed in lab-scale experiments, (*ii*) the stabilized current was very low compared to the one expected when considering the residual concentrations of urea. This again validates competition between urea and at the least creatinine for nickel sites.

Figure V.19-d depicts the temporal profiles of the *identified* compound concentrations during potentiostatic electrolysis of human urine solution. OCN^- , NH_3 , NO_2^- , FA and OA are the main electrolysis products. The concentrations of NO_2^- , OCN^- , NH_4^+ , FA and OA increase over time, suggesting oxidation of organic compounds. It has been demonstrated on a lab-scale scale that creatinine oxidizes into various by-products (*e.g.*, OCN^- , NO_2^- , FA and OA, section V-1.1.b.iii).

Despite the degradation of organic compounds caused by alkalization (-20% of TOC at the time of alkalization and before electrolysis), the presence of surfactants in the treated urine is observed, as a significant cloud of foam is seen in the storage tank (Figure V.19-e). Similarly, a brownish deposit can be seen on the reactor walls.

It should be noted that after each electrolysis of the section V-2, an ICP-OES analysis was carried out. The presence of nickel, possibly due to dissolution of the anode, is always reported below $100 \mu\text{g L}^{-1}$.

V-2.4 Evaluation of energy consumption at pilot-scale

As already performed at lab-scale (section V-1.1.b.iv), an estimation of the energy has been carried out on the same principle. The results are indicated in Table V.6.

- (*i*) the consumed energy during the electrolysis is estimated using the cell voltage (E_{consumed}), and ranges from 16 to $28 \text{ kWh kg}_{\text{H}_2}^{-1}$;

- (ii) the equivalent energy that could be obtained, by combustion of the H_2 formed ($E_{\text{eq. } H_2 \text{ produced}}$);
- (iii) the difference between these two energies is used to estimate the energy after hydrogen recovery (ΔE).

	Urea (0.33 mol L ⁻¹)							Urine ([CO(NH ₂) ₂]=0.21 mol L ⁻¹)	Commercial electrolyser Water splitting [266]
	Surface (cm ²)		Flow rate (kg h ⁻¹)		E (V)				
	734	1101	30	60	0.45	0.55	0.65		
E_{consumed} (kWh kg _{H₂} ⁻¹)	82.9	79.1	79.1	74.3	70.9	74.3	74.5	80.1	53.0
$E_{\text{eq. } H_2 \text{ produced}}$ (kWh kg _{H₂} ⁻¹)	39.4								
ΔE (kWh kg _{H₂} ⁻¹)	43.5	39.7	39.7	34.9	31.5	34.9	35.1	40.7	13.6

Table V.6 – Process energy performance as a function of operating parameters.

These values are of the same order of magnitude than those obtained on a lab-scale scale (34 kWh kg_{H₂}⁻¹ when treated with a 0.33 mol L⁻¹ urea synthetic solution in the section V-1.1.b.iv). From this table, the following observations can be made:

- (i) the energy density (per kg of H₂) consumed in the EC process decreases as the surface area and flow rate increase. This suggests a more efficient conversion process with a larger surface area and higher flow rate.
- (ii) as the potential increases from 0.45 V to 0.65 V, the energy consumed increases, but the oxidation rate also increase.
- (iii) the ΔE for urine show a relatively higher value compared to urea synthetic solution.
- (iv) the energetic experimental values obtained in the case of this thesis are significantly higher than those obtained in the case of a commercial water splitting electrolyser. This paves the way for multiple optimizations to reduce the energy consumption in the current process such as designed.

V-3 Conclusion of Chapter 5

First, potentiostatic electrolyses were carried out, at lab-scale, in alkaline media and on a Ni massive electrode, in presence of urea synthetic and human urine solutions. Thanks to the IC-CD/MS combined with GC, the concentrations of reactants and by-products were monitored during the electrolysis, and complete mass balances of the N-compounds ($\text{CO}(\text{NH}_2)_2$, OCN^- , NO_2^- , NH_3 , N_2) were performed for the first time.

In the case of urea synthetic solution, it was observed that:

- the urea degradation rate reached 80% over a period of 50 h;
- the sum of the concentrations of all the identified N-by-products represented 98% of the initial N-urea involved;
- NH_3 was the predominant N-compound generated during the UEO and its content reached 43*mol.*% of the initial urea at the end of the electrolysis;
- a competition existed between the formation of OCN^- and NO_2^- and N_2 which was evaluated to represent 23*mol.*% of initial urea at the end of electrolysis;
- at the end of electrolysis, the quantification of the H_2 produced, led to a FE (for the cathodic process of H_2) of 90%. Other compounds (NO_2^-) thus reduced at the cathode or H_2 oxidizes at the anode because of the absence of separator. However, this loss of 10% could be assumed insignificant compared to the cost and investment of the separator.
- the FE for N-compounds achieved $100\% \pm 4\%$, thus confirming the interest of potentiostatic electrolyses;
- these quantitative mass and charge balances, and the electro-generated products, confirmed the previously proposed reaction mechanism in **Chapter IV**.

In the case of human urine, before electrolysis, the alkalization step (until pH reached 14) caused the precipitation of organic matter and mineral salts (phosphorus, sulfur, calcium) in the form of whewellite or struvite. Besides, the formation of NH_3 was evidenced. The $I=f(E)$ curves showed that alkalization marginally affected the urea degradation by hydrolysis (less than 20%). The potentiostatic electrolysis carried out, at the same condition as the one for the urea synthetic solution, enabled to conclude that:

- the urine contained various organic molecules which would compete with urea electro-oxidation for the electroactive nickel sites;
- FA and OA were formed during the electrolysis at 10*mol.*% and 5*mol.*% *vs.* of the initial urea (into the urine) respectively. Electrolysis of creatinine synthetic solution led to produce these FA and OA;
- the urea degradation rate reached 20% which was much lower the one obtained in the case of the electro-oxidation of the urea synthetic solution (80%). This was the direct consequence of the electro-oxidation of other organics present into the urine;

- the energy consumption for H₂ production was estimated to 28 kWh kg_{H₂}⁻¹, a value decreased by approximately 18% compared to urea synthetic solution electrolysis. This result remained difficult to explain. The adsorption of creatinine at the anode could reduce the H₂ oxidation rate, thus enabling to lower the consumed energy. Besides, lowering the urea oxidation rate would reduce the quantity of NO₂⁻ produced and consequently losses of H₂ by the NO₂⁻ reduction at the cathode.

These results clearly pointed out the need to study, for the organics (present into the human matrix), (*i*) the effect of the nickel(III) sites availability against the urea adsorption, as well as (*ii*) their eventual poisoning effects on the nickel electro-oxidation.

For this reason, a voltammetric study was performed at the steady state, expecting to better understand the individual effect of each organic adduct present (at significant concentration $\geq 0.02 \text{ mol L}^{-1}$) in human urine. The main results were summarised below:

- the spiking of urine solutions with organic compounds (primarily found in urine in significant levels), clearly demonstrated (via I=f(E) curves) that the urea adsorption on the nickel(III) sites and its subsequent electro-oxidation were affected by a competitive adsorption of molecules like creatinine, histidine, and creatine. When spiking at higher concentrations, these adsorptions caused the lowering of the magnitude of the nickel(II) oxidation signal's. However, the effect of these molecules (and especially the histidine, and creatine) at their physiological concentrations, remained minor. For creatinine, the maximum decrease of the magnitude of the nickel(II) oxidation signal in the urine matrix was about 20%;
- the oxidation rate of the urea in urine, by the nickel(III) followed a very low (0.1) reaction order against urea, roughly three times lower than the one determined in the case of the KOH matrix. This was in agreement with the competitive adsorption for nickel(III) sites between the urea and at the least the creatinine.

In a second part, the scale-up of the UEO process, was investigated using a pilot designed and built at the lab-scale. The pilot was used to study the effect of the key operating parameters (anode surface area, feed rate and applied potential) by performing complete mass balances on both liquid and gas phases during potentiostatic electrolyses with urea synthetic and human urine solutions.

Electrolyses in potentiostatic mode (0.55 V *vs.* Hg/HgO), of urea synthetic solution (marking for the first time such an assessment) showed that:

- Interestingly, the current decreased five times during the 70 h duration of the electrolysis, and the urea degradation rate did not exceed 30%. This result, not observed at the lab-scale electrolyses, could be due to a certain poisoning of the nickel grid used;
- the predominant N-compounds created during the urea degradation, irrespective of electrolysis duration, were OCN⁻ (9mol.% of urea) and NH₃, (12mol.% of urea). Trace amounts of N₂ gas and NO₂⁻ were also detected. The mass balance of the C-species was also confirmed at more than 98%;

- the surface area of the anode had an impact on the electrolysis process. Obviously, a larger ($\times 2$ or $\times 3$) surface area amplified the initial current and increased the rate of H_2 formation as well as the urea degradation. Despite this, the nature and proportions of the compounds produced remained constant, meaning that increasing the surface did not affect the reaction pathway;
- there was no observable change in UEO by-products or urea degradation rate when increasing the flow rate by a factor of two (keeping laminar flow in the reactor), even the magnitude of the current increased by 20%, which would suggest an urea mass transfer limitation;
- the applied potential mainly affected the nitrite and nitrogen formation rates. Indeed, increasing the anodic potential induced an increase of the nitrite/nitrogen ratio to the detriment of the nitrogen.

Lastly, an electrolysis in potentiostatic mode (0.55 V *vs.* Hg/HgO) was performed with an human urine solution (marking for the first time such an assessment). It revealed that:

- the urea concentration in the fresh urine was found to be 0.22 mol L^{-1} , which was lower than the typically accepted concentration in urine (*i.e.*, 0.33 mol L^{-1});
- the initial current value, relatively high compared to the one obtained with urea, quickly dropped until 80% in 1 h; the subsequent evolution showed an exponential trend, similar to that observed for urea electrolysis;
- a slight decrease in the TOC was observed after 24 h of electrolysis, implying oxidation of organic molecules occurred without mineralisation, as confirmed by the darkening of the electrolysed urine. The temporal variations of the molar amounts of urea and creatinine showed that both compounds oxidized, with a faster kinetics for creatinine. Indeed, even if creatinine had a lower initial concentration than urea, it seemed to block or limit urea oxidation. This could be due to the by-products of creatinine oxidation presenting a poisoning behavior against nickel(II) oxidation;
- the identified compounds during the electrolysis process included OCN^- , NH_3 , NO_2^- , FA and OA. Their concentrations increased over time, indicating the oxidation of organic compounds, as also demonstrated on a lab-scale scale;
- surfactants were formed during the electrolysis of the urine, along with a brownish deposit on the reactor walls, indicating the electro-generation of organic polymeric by products.

All these findings indicate that human urine electrolysis at a pilot-scale induces new challenges that were not identified in synthetic solution, mainly due to interfering substances such as creatinine. Further studies are definitively necessary to optimize the process and overcome these challenges.

General Conclusion and Perspectives

Concluding remarks

As a part of the HyUrea ANR project, this PhD thesis aimed at investigating the potentialities of EC processes for treating urea/urine effluents with simultaneous production of hydrogen and possible photo-assistance. More specifically, the scientific objectives were:

- to gain a better understanding of the physicochemical phenomena occurring during UEO on a massive nickel electrode and in alkaline media;
- to develop a set of analytical techniques enabling to identify and to quantify the UEO by-products, so as to perform complete mass balances in both liquid and gaseous phases during electrolysis with high urea conversion rates;
- to propose a multi-pathway mechanism describing the formation of the previously identified by-products
- to establish an UEO kinetic law with the perspective of engineering and modeling a larger scale EC reactor, potentially with photo-assistance;
- to design, build and optimize a EC reactor prototype enabling urea oxidation while producing H₂ at the cathode, and possibly with photo-assistance.
- to establish the proof-of-concept with real human urine.

Achieving each of the above objectives constitutes a particular challenge when referring the actual state of the art (**Chapter I**). Indeed, even if the UEO was considered as the way to mineralise urea to N₂ and CO₂ and simultaneously producing H₂, no study involving complete mass balances was reported, except very recently, to validate this theoretical full mineralisation.

The contributions of this thesis work can then be structured as follows:

- **Development of a wide range of analytical tools and EC set-ups for a better understanding of the UEO**

Different set-up and analytical methods were implemented to study and monitor the UEO in alkaline media. In particular, the coupling of IC-CD/MS, GC and TOC made possible to evaluate the abatement performances of the process during the various electrolysis, and this in one-shot, short time and without complex sample preparation. The applicability of these techniques was extended to real urine matrix. The different EC reactors used consisted in two reactors typically encountered at lab-scale scale (a Metrohm-type batch cell and a

H-type batch cell) and in a pilot-scale cylindrical reactor (and its environment) that was specially designed for the thesis.

- **Establishment of complete mass balances for N and C, and of FE for electrolysis with high urea conversion rates**

The UEO process in alkaline solutions was deeply investigated at lab-scale with the aim to evaluate the by-products formed and the stability electrode. Potentiostatic electrolyses were successfully achieved (equivalent to 9 kC) with urea conversions nearing 90%, thus surpassing most of the previously reported works. They also highlighted the absence of any poisoning of the anode at lab-scale. For the first time, a complete mass balance was conducted for various N-compounds, including $\text{CO}(\text{NH}_2)_2$, OCN^- , NO_2^- , NH_3 , and N_2 . The total concentration of these identified by-products accounted for nearly 98% of the initial N-urea used. NH_3 emerged as the major N-compound formed during the UEO, at 43 mol.%. A FE of 100% was recorded, validating the charge balance with only a 3.9% maximum deviation, even in presence of high conversion rates. Yet, the emergence of OCN^- and NO_2^- to the expense of N_2 (constituting 23% of the FE at the end of the electrolysis) raises major environmental concerns that should be now solved. The energy consumption of the process was measured to $34 \text{ kWh kg}_{\text{H}_2}^{-1}$ at the end of the electrolysis, which was in agreement with prior studies. The experiments in a mono-compartment cell setup illustrated that nitrites could be minimized at the cathode. This clearly constituted a way to cut down on environmentally detrimental by-products by 50% while avoiding the constraints linked to the use of a separator. Unfortunately, this gain will also affect hydrogen production in the absence of a separator: (i) reduction of by-products decreases the amount of hydrogen formed and (ii) H_2 can move to the anode and oxidize.

In light of these findings, a set of recommendations for designing and operating an electrolyzer capable of treating urea using this EC method was proposed. It consists in the use of an undivided cell configuration, in 1 mol L^{-1} KOH at room temperature.

- **Kinetic study for a better understanding of reaction pathways during UEO**

The EC kinetic study, performed with low ($\leq 5 \text{ mV s}^{-1}$) and high ($\geq 100 \text{ mV s}^{-1}$) potential scan rates, validated (i) the indirect oxidation of the urea by the mediation of the nickel(III)/nickel(II) system, and (ii) the application of the TON concept (thus confirming the absence of direct urea oxidation). This TON quantified the number of EC catalytic cycles regenerating nickel(II) and was evaluated at over 100 (1) at potential scan rates lower (higher) than 5 mV s^{-1} .

As an extension of the previous kinetic study, the idea was to observe the chemical action of urea on nickel(III) without an EC reaction. For that, nickel(III) particles were specifically synthesized, starting from commercial $\text{Ni}(\text{OH})_2$ powder and NaOCl, and then characterized (by SEM, BET, XRD, and particle size analysis). These particles were spherical, made of up to 80% nickel(III) and less crystalline compared to $\text{Ni}(\text{OH})_2$ solids, revealing a structure with an amorphous NiOOH shell surrounding a $\text{Ni}(\text{OH})_2$ core. The kinetic study with these

chemically synthesized nickel(III) particles was carried out through analytical monitoring of hydroxide ion concentration. The partial reaction order of urea was found equal to 0.3. This low value can be explained by the limitation in urea adsorption onto nickel's active sites.

The subsequent partial orders of hydroxide ions and active nickel sites were determined at 0.6 and 1.9, respectively. The kinetic rate thus exhibited moderate dependence on hydroxide ions, but showed a high dependence on nickel(III) ($\gamma_X \sim 2$). The relatively low dependence of the kinetic rate on dissolved species concentrations would indicate some potential mass transport limitations within the solid spherical particles as suggested by the BET analysis that revealed a low specific surface area $\sim 8.51 \text{ m}^2 \text{ g}^{-1}$. The initial kinetic law did not consider the reactions between by-products and OH^- or nickel(III), as these intermediates did not exist at the initial time. Given that, the overall process's limitation would be primarily due to the urea adsorption, these intermediates would not accumulate, but quickly transform into observable products, and, thus, have no impact on the kinetic rate. This was confirmed when integrating the initial kinetic law over time for higher conversion rates. The theoretical variation of the OH^- concentration was successfully compared with the experimental one, yielding a maximum deviation of 6%.

In a second time, the kinetics of indirect UEO was explored by polarizing a solid nickel electrode, thus leading to the formation of a catalytic $\text{NiOOH}/\text{Ni}(\text{OH})_2$ layer, that enabled the urea oxidation through the EC continuous regeneration of nickel(III) active sites. This kinetic rate law showed a partial urea order similar to the value determined with the particles (approximately 0.3). However, the order of the nickel surface was found to be high ($\gamma_{E_X} \sim 5$), indicating that the urea's adsorption onto nickel(III) sites was quickly followed by the complete oxidation of this urea by five electrochemically generated nickel(III), due to potentiostatic polarization of the anode.

By combining this kinetics study with the measurements of the by-products in the liquid phase, a relatively comprehensive multi-pathway mechanism (22 sequential steps, four different paths, and five urea oxidation products) could be proposed to describe the urea's indirect electro-oxidation process.

Lastly, this kinetic study was integrated into a comprehensive predictive model that encompassed the mass transport in liquid and solid catalytic layers, the indirect electrocatalytic reaction in the latter, and the near-instantaneous regeneration of the nickel(III) catalytic sites. The numerical model was solved by the shooting method and able to predict the variations of the urea concentration with the electrolysis time. The comparison of these predictions with experimental results obtained for various hydroxide concentrations and S/V ratios demonstrated a good agreement, with deviations under 5%. This consistency offers promising perspectives for scaling the process.

- **Scaling-up the UEO process from lab- to pilot-scale**

The UEO process was scaled up from lab-scale using a pilot designed especially for the thesis. When electrolysing urea solution at 0.55 V *vs.* Hg/HgO (a first-time assessment), the current dropped 5-times during the 70-hour electrolysis (equivalent to 26 kC), and the urea degradation rate never exceeded 30%. This variation, not seen at lab-scale, could be

explained by different explanations: (i) wrong mass transport conditions (laminar flow) or even (ii) nature of the electrode (nickel grid *vs.* nickel plate, crystallographic phase). The dominant N-compounds produced were OCN^- (9mol.% of urea) and NH_3 (12mol.% of urea), with minor traces of N_2 gas and NO_2^- . The mass balance of C-species was confirmed at almost 98%.

The influence of some key parameters on the process was then studied, namely (i) the anode surface area, (ii) the flow rate and finally (iii) the applied potential.

A larger surface area boosted the initial current, the H_2 formation rate, and the urea degradation. However, the produced compounds' nature and proportions remained unchanged, thus suggesting that the reaction pathway was unaffected when increasing surface area. Doubling the flow rate (from 30 to 60 kg h^{-1} , while keeping laminar flow in the reactor) did not change neither the UEO by-products nor the urea degradation rate, but led to increase the current by 20%, suggesting a urea mass transfer limitation. The applied potential, varying between 0.45 and 0.65 V *vs.* Hg/HgO, had a strong influence on the nitrite and nitrogen formation rates. A higher anodic potential increased the nitrite/nitrogen ratio at the expense of nitrogen (from 0.3 at 0.45 V to more than 8.6 at 0.65 V for the same supplied charge).

- **Highlighting the matrix effect in the EC treatment of human urine solution**

Lastly, the EC treatment of real human urine solutions was carried out to break the glass ceiling of the real matrix.

Before electrolysing human urine, the solution was alkalized to pH=14, leading to the precipitation of organic matter and minerals like phosphorus, sulfur, and calcium in forms like whewellite or struvite. Moreover, NH_3 was formed during this alkalization. This alkalization step had a minor effect on urea, by limiting its hydrolysis degradation rate to 20%. At lab-scale, when conducting potentiostatic electrolysis, several conclusions had been drawn. This work pointed out how the organic molecules present in the urine competed with urea for electroactive nickel(III) sites. FA and OA were formed during the electrolysis, accounting for 10mol.% and 5mol.% compared to initial urea, which could be explained by creatinine oxidation. The maximal urea's degradation rate in urine was 20%, thus significantly lower than the 80% obtained with urea synthetic solutions. This low conversion was likely due to the electro-oxidation of other organics in the urine. The energy consumption for H_2 production was 28 $\text{kWh kg}_{\text{H}_2}^{-1}$, about 18% smaller than that of urea synthetic solution electrolysis, probable consequence of the creatinine adsorption at the anode. The decreased urea oxidation rate also reduced NO_2^- and subsequent H_2 losses.

To better understand the impact of organics in urine on nickel(III) site availability *vs.* urea adsorption and their potential negative effects on nickel(II) oxidation, a voltammetric study was conducted. For that, some organic compounds typically present in large amounts in urine were added to urine solutions. This spiking's method made evident that creatinine, histidine, and creatine competitively adsorbed on nickel(III) sites, thus affecting UEO. Especially for creatinine, the decrease in the nickel(II) oxidation signal was about 20%

when considering the physiological concentration range. The UEO rate in urine, catalyzed by nickel(III), was found to be much slower (urea partial order of 0.1) than in a KOH matrix (urea partial order of 0.3), thus confirming the competitive adsorption of molecules, particularly creatinine, for nickel(III) sites.

At pilot-scale, the first-ever electrolysis of human urine on nickel electrode was conducted in potentiostatic mode (0.55 V *vs.* Hg/HgO). Fresh urine had a urea concentration of 0.22 mol L⁻¹, lower than the typically recognized 0.33 mol L⁻¹. The initial current, although higher than that with urea, rapidly dropped down by 80% in 1 h, then followed an exponential trend similar to urea electrolysis. A minor decline in the TOC was noted after 24 h, suggesting organic molecule oxidation. However, the mineralisation did not occur, as proven by the darkening of the treated urine. Both urea and creatinine oxidized over time, but creatinine degraded faster (conversion rate of 85% *vs.* 5% for urea), inhibiting urea oxidation. The by-products identified during the pilot-scale process were OCN⁻, NH₃, NO₂⁻, FA, and OA. Their rising concentrations over time implied organic compound oxidation, which was in agreement with the lab-scale findings. Some surfactants already present in urine formed a foam in the storage tank and a brown deposit on reactor walls, indicating the formation of organic polymeric by-products. These results showed that human urine electrolysis on a pilot scale is faced with specific challenges, not observed with synthetic solutions, mainly because of interfering compounds like creatinine.

Perspectives

The results obtained in this thesis open promising horizons that would require strong interactions between the fields of Electrochemistry, Materials, Electrochemical and Reactor Engineering. The development of broader collaborations will be key to this undertaking.

Towards a better orientation of by-products The mechanistic orientation of N-by-products towards H₂ remain a priority objective, despite that the treatment of by-products (OCN⁻, NH₃, NO₂⁻) should be considered if N₂ formation becomes impossible. The functionalisation of electrode materials appears as the predominant strategy for orienting the by-product formation mechanism (bi-metallic electrodes or volumetric electrodes) [146]. Initial results have also shown that certain operating conditions (mainly the applied potential) influence the reaction mechanism. A more detailed study of this influence on process energy consumption would enable us to better assess potential gains.

Real human urine The results of **Chapter V** showed that a significant matrix effect was present during the UEO in alkaline media because the EC response was modified by the presence of secondary compounds present in the urine. More detailed study will be required to better understand the related reaction mechanisms, mass transport, adsorption behavior and kinetics, in particular in the perspective of a large-scale industrial implementation. The fact that urea degrades more slowly when creatinine is present is not necessarily problematic, given that the objective is to process organo-nitrogen compounds and produce H₂. However, determining how to achieve high mineralisation in this context requires further investigation:

- (i) the low mineralisation rate of TOC suggests the presence of a wide range of intermediates. Measures of toxicity and biodegradability need to be conducted to verify the sustainability of this process. A more in-depth investigation into the influence of micro-pollutants, like pharmaceutical products often found in urine, is also necessary during urine electro-oxidation;
- (ii) the drop in current needs clarification; indeed, urine electrolysis likely alters the potential range. Regarding material surface functions, transitioning from a plate to a grid revealed noticeable differences. Further research is needed to address this limitation.

The benefit of PEC reactor Solar illumination on the process could enable the coupling of two functions: (i) the photo-degradation of the urine by possible absorption of photons from the organic matter, and (ii) the photo-assistance of the EC process using photo-electrodes or photovoltaic panels, as imagined in the plans for the pilot-scale reactor tubular cell presented in Appendix B. The engineering of such PEC reactors still needs strong efforts, that could however benefit from the current research works developed for applications other than UEO [267].

Toward industrial perspective A first parametric study in the pilot-scale reactor was successfully carried out. This experimental effort should be continued in the future. The development of a EC reactor numerical model, inspired from the design of the one proposed in Chapter V, could be an efficient tool to optimize the pilot-scale reactor, by enabling the prediction of abatement performance and H₂ production under various conditions (feed concentration, flow, temperature, etc.). It would also eliminate the need for a reference electrode within the reactor. Hydrogen is an inexpensive molecule, and water treatment companies are not prepared to spend a lot of money to degrade urine. In this context, an EC process - especially one using electrodes made of Ni, an expensive metal that is destined to remain so - will only become profitable if it works at very high current density.

Fresh urine composition

Table A.1 reports the data from the pioneering work of Putnam et al. [57] that has been formatted to better fit with the thesis purposes. This study carried out in 1971 was the first to identify 68 constituents with a concentration above 10 mg L^{-1} . Nowadays, thanks to the development of advanced analytical techniques, a database with 3,100 molecules can be established for human urine [58].

For reminder, urine contains 98wt% of water (as presented Chapter I, section I-1.3, Figure I.5). The dissolved matter consists, in average, of organic compounds ($\sim 60\text{wt}\%$) and inorganic compounds ($\sim 40\text{wt}\%$). Among the organic compounds, urea represents more than 60wt%, organic ammonium salts more than 20wt%, the rest being creatinine and other compounds.

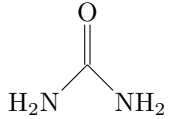
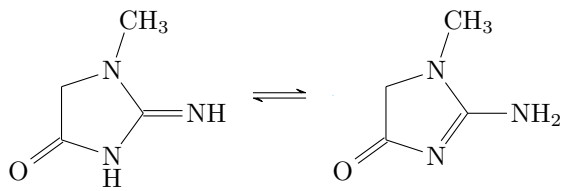
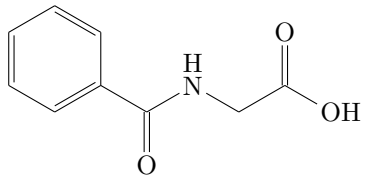
Item	Chemical formula	Structural formula	Molar mass (g mol ⁻¹)	Concentration range (mg L ⁻¹)
Total Solutes				36,700 - 46,700
Urea	CH ₄ N ₂ O		60.1	9,300 - 23,300
Chloride	Cl ⁻		35.5	1,870 - 8,400
Sodium	Na ⁺		23.0	1,170 - 4,390
Potassium	K ⁺		39.1	750 - 2,610
Creatinine (tautomer)	C ₄ H ₇ N ₃ O		113.1	670 - 2,150
Sulfur, inorganic	S		32.1	163 - 1,800
Hippuric Acid	C ₉ H ₉ NO ₃		179.2	50 - 1,670
Phosphorus, total	P		31.0	470-1,070

Table A.1 – Constituents of human urine exceeding 10 mg L⁻¹ (listed in descending order of concentration).

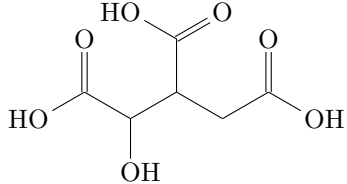
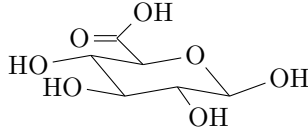
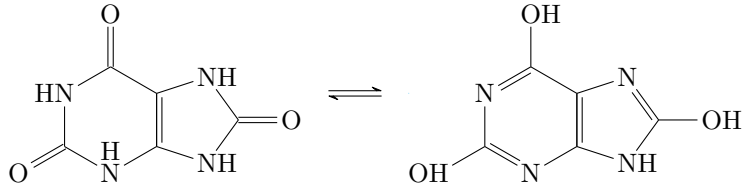
Item	Chemical formula	Condensed formula	Molar mass (g mol ⁻¹)	Concentration range (mg L ⁻¹)
Citric Acid	C ₆ H ₈ O ₇		192.1	90 - 930
Glucuronic Acid	C ₆ H ₁₀ O ₇		194.1	70-880
Ammonia	NH ₃		17	200 - 730
Uric Acid	C ₅ H ₄ N ₄ O ₃		168.1	40 - 670
Uropepsin				70 - 560
Bicarbonate	HCO ₃ ⁻		61.0	20 - 560

Table A.1 (continued).

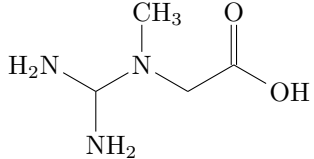
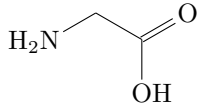
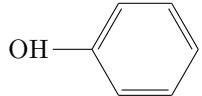
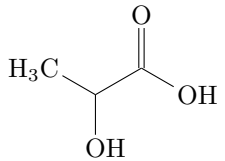
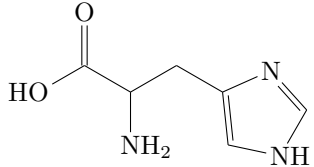
Item	Chemical formula	Condensed formula	Molar mass (g mol ⁻¹)	Concentration range (mg L ⁻¹)
Creatine	C ₄ H ₉ N ₃ O ₂		149.2	0 - 530
Sulfur, organic	S		32.1	77 - 470
Glycine	C ₂ H ₅ NO ₂		75.1	90 - 450
Phenols	C ₆ H ₆ O		94.1	130 - 420
Lactic Acid	C ₃ H ₆ O ₃		90.1	30 - 400
Calcium	Ca ²⁺		40.1	30 - 390
Histidine	C ₆ H ₉ N ₃ O ₂		155.2	40 - 330

Table A.1 (continued).

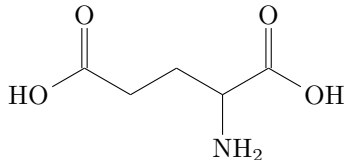
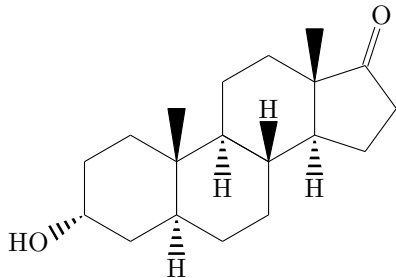
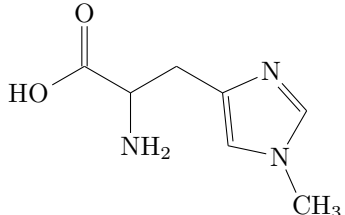
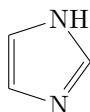
Item	Chemical formula	Condensed formula	Molar mass (g mol ⁻¹)	Concentration range (mg L ⁻¹)
Glutamic Acid	C ₅ H ₉ NO ₄		147.1	7 - 320
Androsterone	C ₁₉ H ₃₀ O ₂		290.5	2 - 280
1-Methylhistidine	C ₇ H ₁₁ N ₃ O ₂		169.2	30 - 260
Magnesium	Mg ²⁺		24.3	20 - 205
Imidazole Derivatives	C ₃ H ₄ N ₂		68.1	90 - 200

Table A.1 (continued).

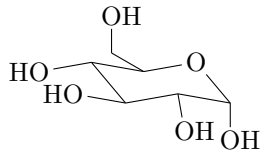
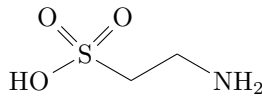
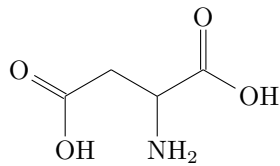
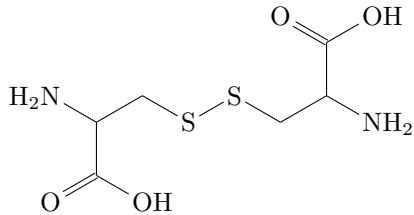
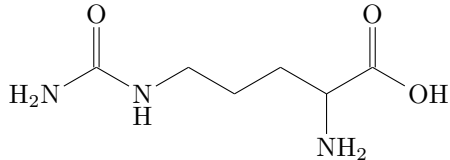
Item	Chemical formula	Condensed formula	Molar (g mol ⁻¹)	mass	Concentration range (mg L ⁻¹)
Glucose	C ₆ H ₁₂ O ₆		390.4		30 - 200
Taurine	C ₂ H ₇ NO ₃ S		125.2		5 - 200
Aspartic Acid	C ₄ H ₇ NO ₄		133.1		7 - 170
Carbonate	CO ₃ ²⁻		60.0		100 - 150
Cystine	C ₆ H ₁₂ N ₂ O ₄ S ₂		240.3		7 - 130
Citrulline	C ₆ H ₁₃ N ₃ O ₃		175.2		0 - 130

Table A.1 (continued).

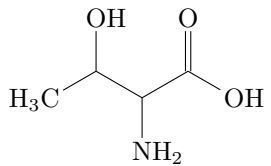
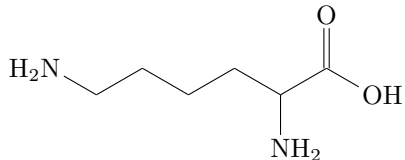
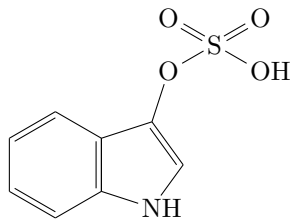
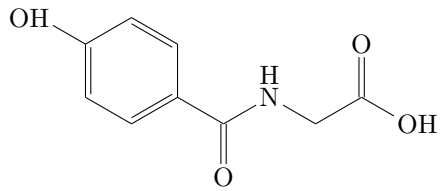
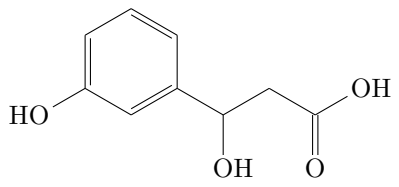
Item	Chemical formula	Condensed formula	Molar (g mol ⁻¹)	mass	Concentration range (mg L ⁻¹)
Threonine	C ₄ H ₉ NO ₃		119.1		10 - 120
Lysine	C ₆ H ₁₄ N ₂ O ₂		146.2		5 - 110
Indoxylsulfuric Acid	C ₈ H ₇ NO ₄ S		231.2		3 - 110
m-Hydroxyhippuric Acid	C ₉ H ₉ NO ₄		195.2		1 - 100
p-Hydroxyphenyl-Hydracrylic Acid	C ₉ H ₁₀ O ₄		182.2		1 - 100

Table A.1 (continued).

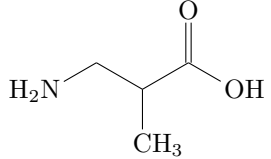
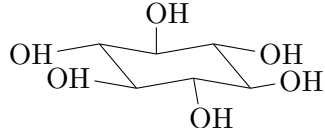
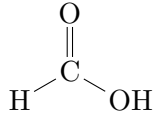
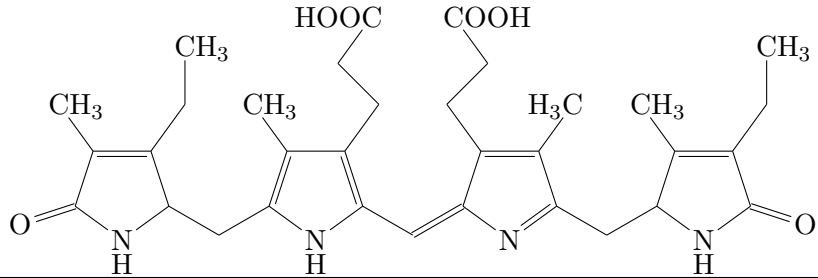
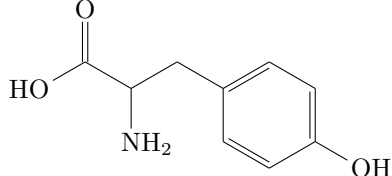
Item	Chemical formula	Condensed formula	Molar (g mol ⁻¹)	mass	Concentration range (mg L ⁻¹)
Aminoisobutyric Acid	C ₄ H ₉ NO ₂		103.1		3 - 120
Inositol	C ₆ H ₁₂ O ₆		180.2		5 - 100
Formic Acid	CH ₂ O ₂		46.0		20 - 90
Urobilin	C ₃₃ H ₄₂ O ₆ N ₄		588.7		7 - 90
Tyrosine	C ₉ H ₁₁ NO ₃		181.2		10 - 70

Table A.1 (continued).

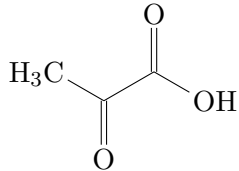
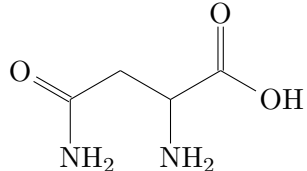
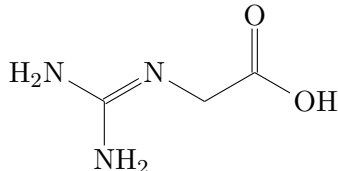
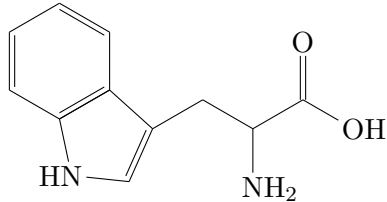
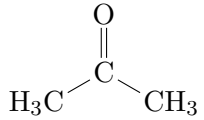
Item	Chemical formula	Condensed formula	Molar (g mol ⁻¹)	mass	Concentration range (mg L ⁻¹)
Pyruvic Acid	C ₃ H ₄ O ₃		88.1		2 - 70
Albumin	C ₁₂₃ H ₁₉₃ N ₃₅ O ₃₇		2,754.1		7 - 70
Asparagine	C ₄ H ₈ N ₂ O ₃		132.1		20 - 70
Glycoxyamine	C ₃ H ₇ N ₃ O ₂		117.1		15 - 70
Tryptophan	C ₁₁ H ₁₂ N ₂ O ₂		286.8		5 - 60
Ketones (as Acetone)	C ₃ H ₆ O		58.1		10 - 50

Table A.1 (continued).

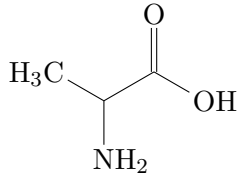
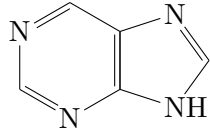
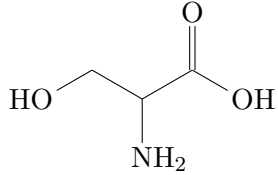
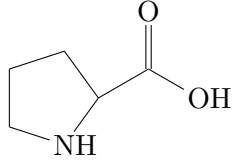
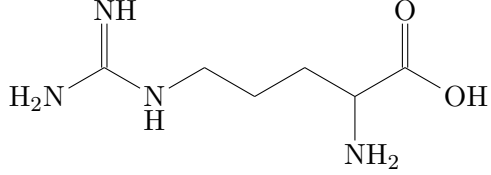
Item	Chemical formula	Condensed formula	Molar (g mol ⁻¹)	mass	Concentration range (mg L ⁻¹)
Alanine	C ₃ H ₇ NO ₂		89.1		15 - 50
Purine Bases	C ₅ H ₄ N ₄		120.1		0 - 50
Serine	C ₃ H ₇ NO ₃		105.1		20 - 50
Proline	C ₅ H ₉ NO ₂		115.1		7 - 40
Arginine	C ₆ H ₁₄ N ₄ O ₂		174.2		7 - 40

Table A.1 (continued).

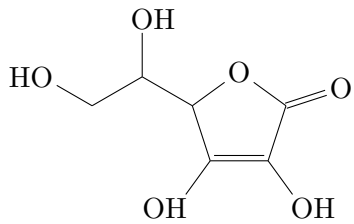
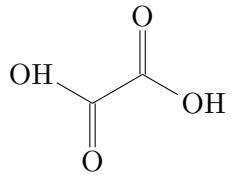
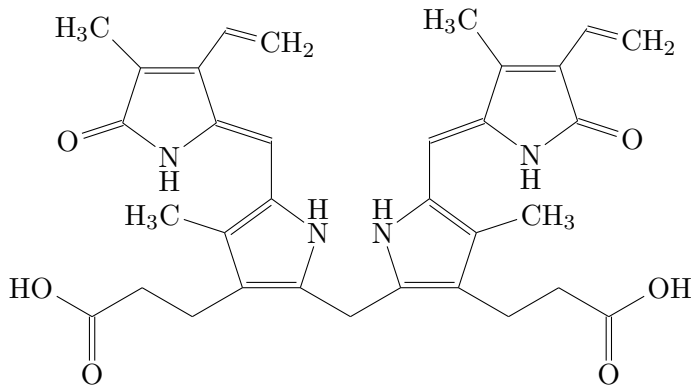
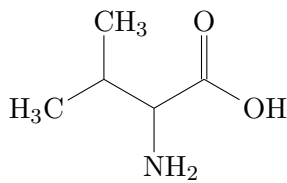
Item	Chemical formula	Condensed formula	Molar (g mol ⁻¹)	mass	Concentration range (mg L ⁻¹)
Ascorbic Acid	C ₆ H ₈ O ₆		176.1		3 - 40
Oxalic Acid	C ₂ H ₂ O ₄		90.0		1 - 30
Bilirubin	C ₃₃ H ₃₆ N ₄ O ₆		584.7		3 - 30
Valine	C ₅ H ₁₁ NO ₂		117.2		7 - 30

Table A.1 (continued).

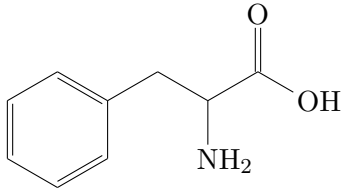
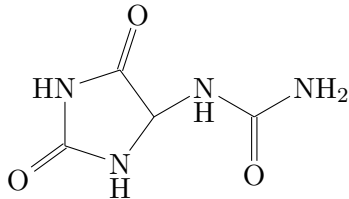
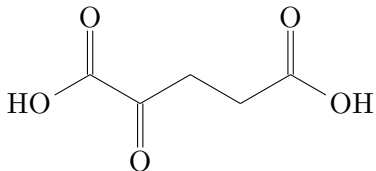
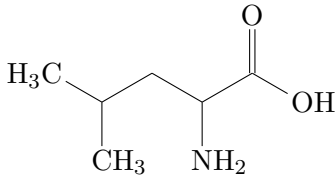
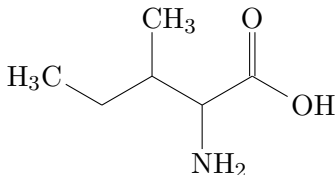
Item	Chemical formula	Condensed formula	Molar (g mol ⁻¹)	mass	Concentration range (mg L ⁻¹)
Phenylalamine	C ₉ H ₁₁ NO ₂		165.2		6 - 30
Allantoin	C ₄ H ₆ N ₄ O ₃		158.1		2 - 25
Oxoglutaric Acid	C ₅ H ₆ O ₅		146.1		13 - 25
Leucine	C ₆ H ₁₃ NO ₂		131.2		8 - 25
Isoleucine	C ₆ H ₁₃ NO ₂		117.1		4 - 22

Table A.1 (continued).

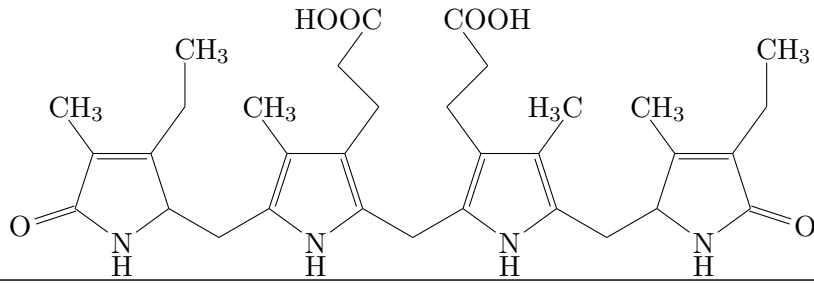
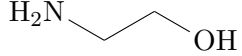
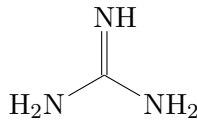
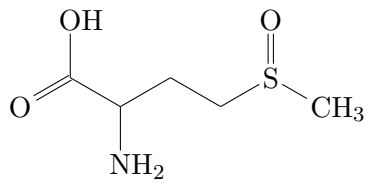
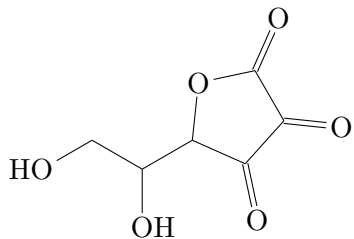
Item	Chemical formula	Condensed formula	Molar (g mol ⁻¹)	mass	Concentration range (mg L ⁻¹)
Urobilinogen	C ₃₃ H ₄₄ N ₄ O ₆		592.7		0 - 17
Ethanolamine	C ₂ H ₇ NO		61.1		3 - 15
Guanidine	CH ₅ N ₃		59.1		7 - 13
Methionine Sulfoxide	C ₅ H ₁₁ NO ₃ S		165.1		0 - 13
Dehydroascorbic Acid	C ₆ H ₆ O ₆		174.1		3 - 13
Other Organics					285

Table A.1 (ended).

Appendix **B**

PEC reactor HyUrea concept

This appendix presents a conceptual idea for a photo-anode-assisted PEC reactor based on the EC reactor developed in this thesis.

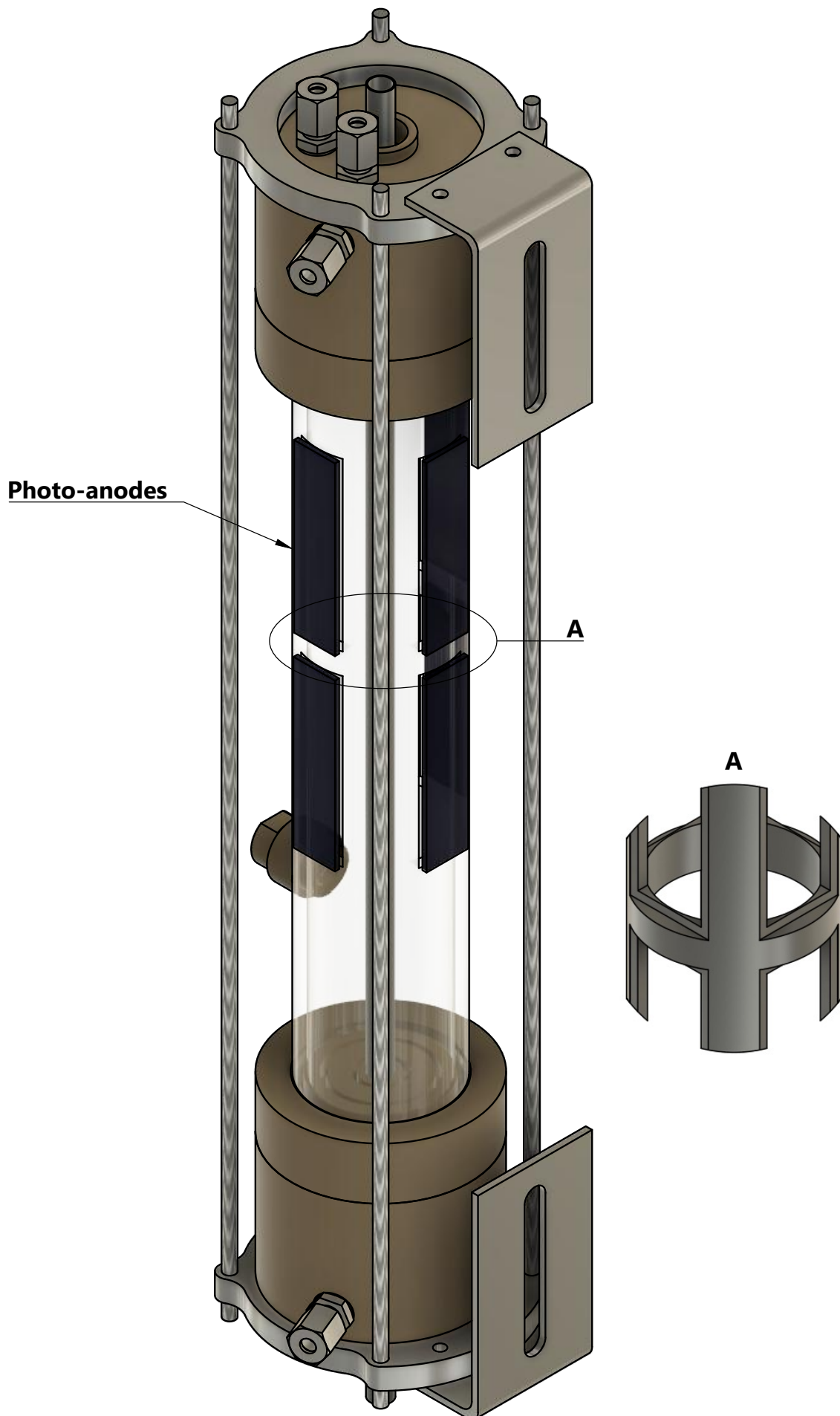


Fig. B.1 – Concept envisaged for the construction of a PEC reactor as part of the HyUrea project.

Pilot-scale plans of the EC cell

In order to guide the reader towards a better understanding of the EC set-up designed at pilot-scale, Figure C.1 provides elementary 3D views. The reactor consists of 5 main parts:

Part n°1 This piece collects fluid(s) from storage tank(s);

Part n°2 This part distributes the solution(s) in the reactor;

Part n°3 The PMMA tube is transparent to visible light, allowing future irradiation of the reactor (via the use of photo-anodes);

Part n°4 This part collects the fluid(s) (liquid and gaseous);

Part n°5 This part features vertical outlets to prevent the accumulation of gases in the reactor.

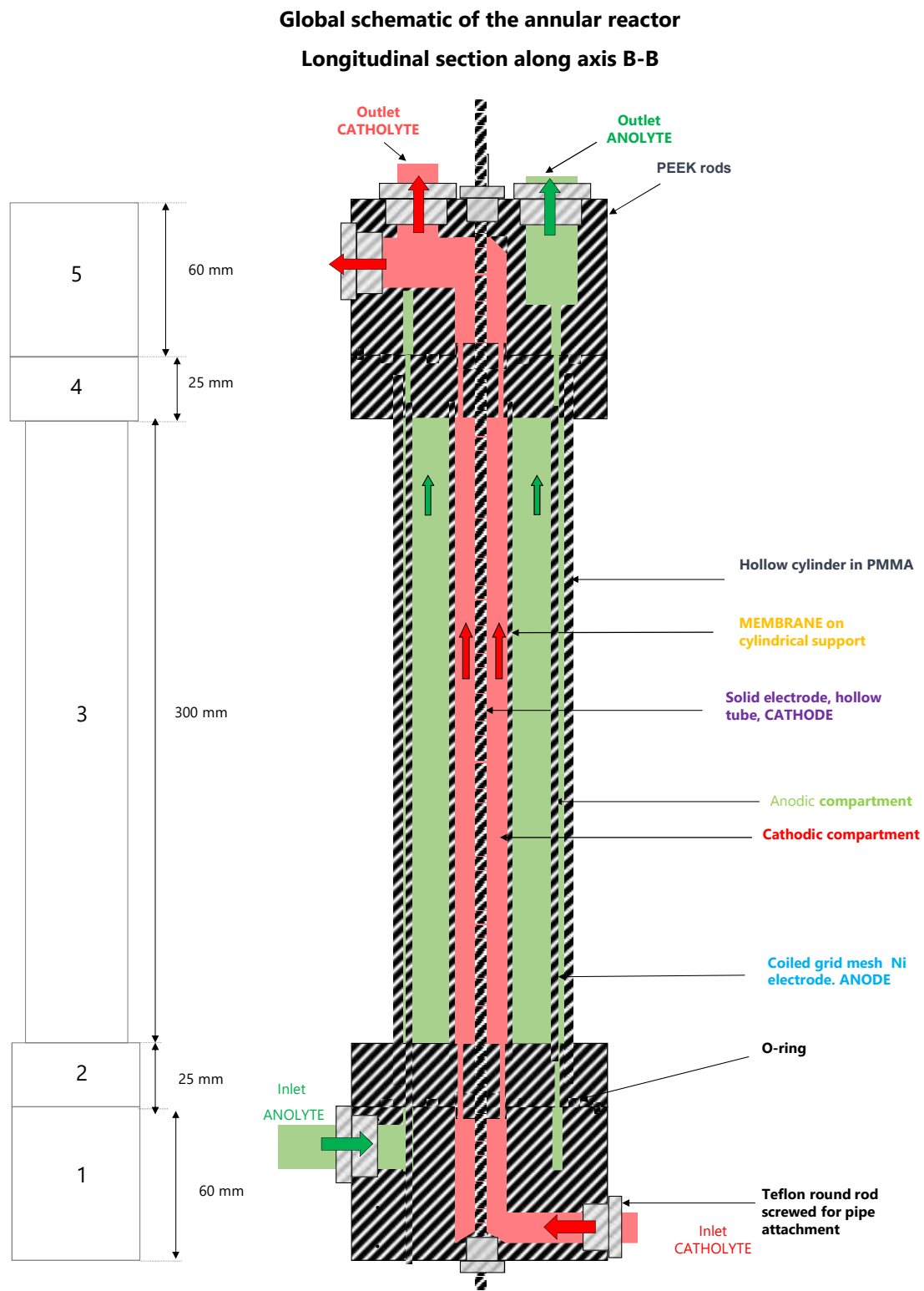


Fig. C.1 – Semi-pilot-scale plans of the electrochemical cell.

Part N°3 of the reactor

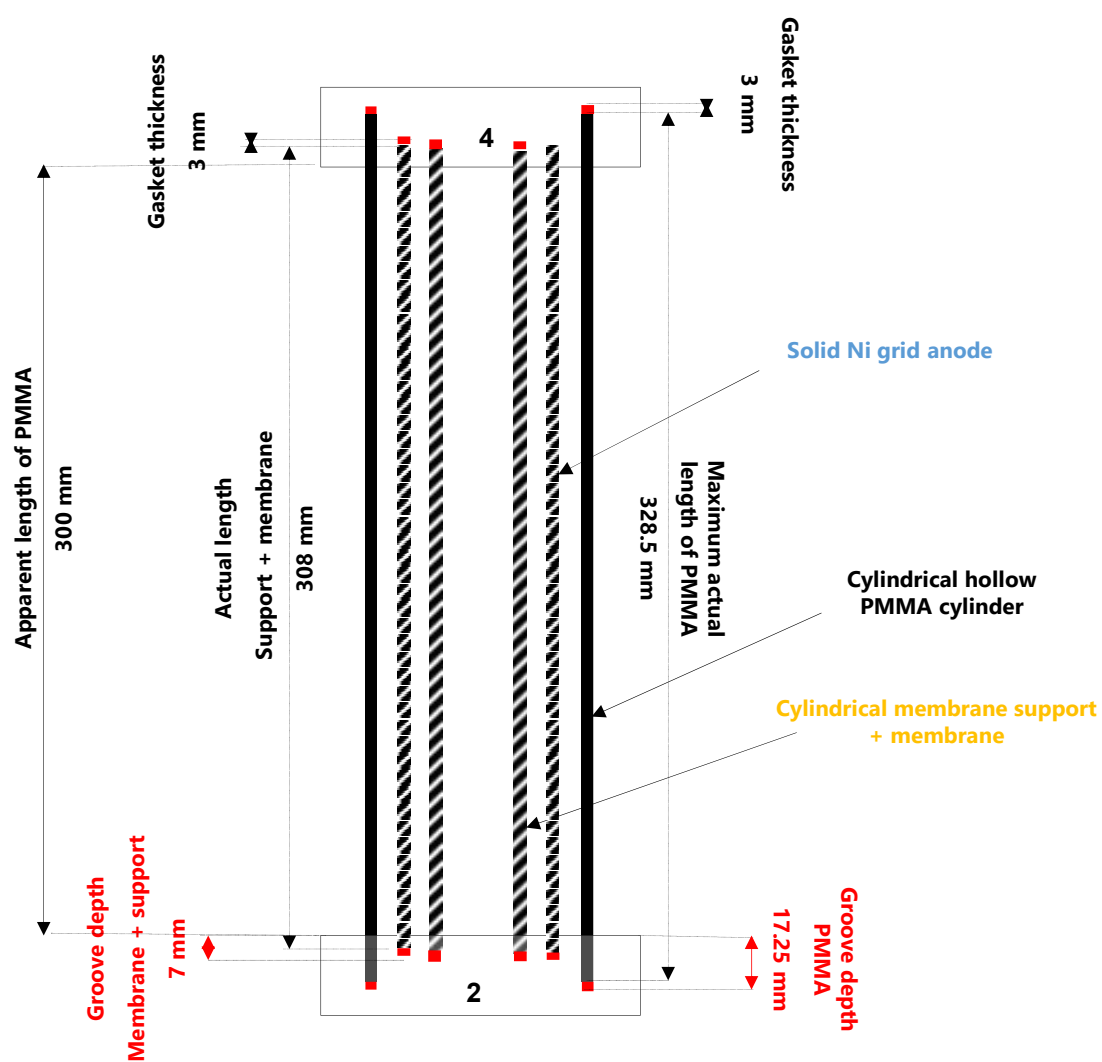


Figure C.1 (continued).

Profiled parts N°1 and N°2 (Bottom of the reactor)

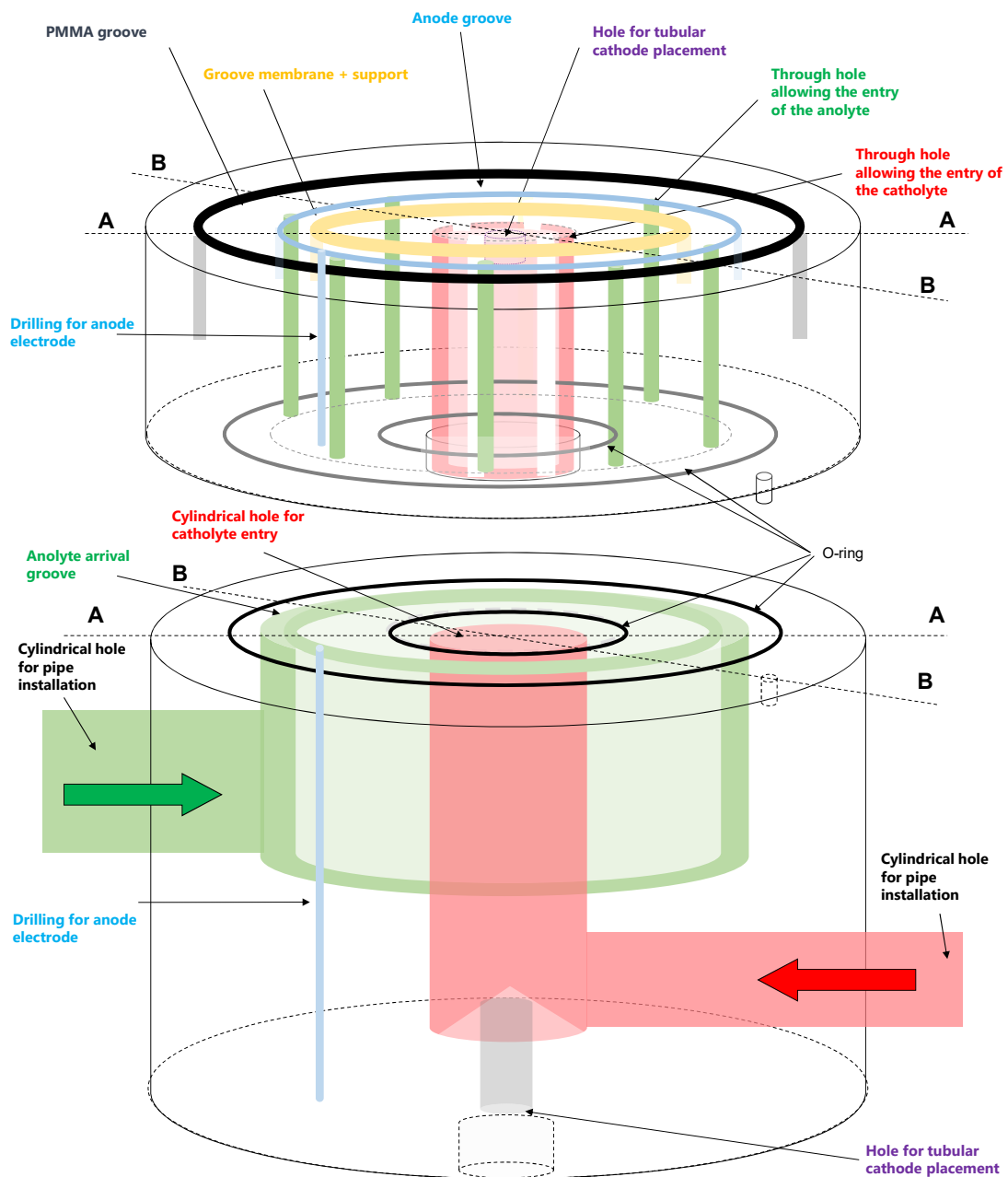


Figure C.1 (continued).

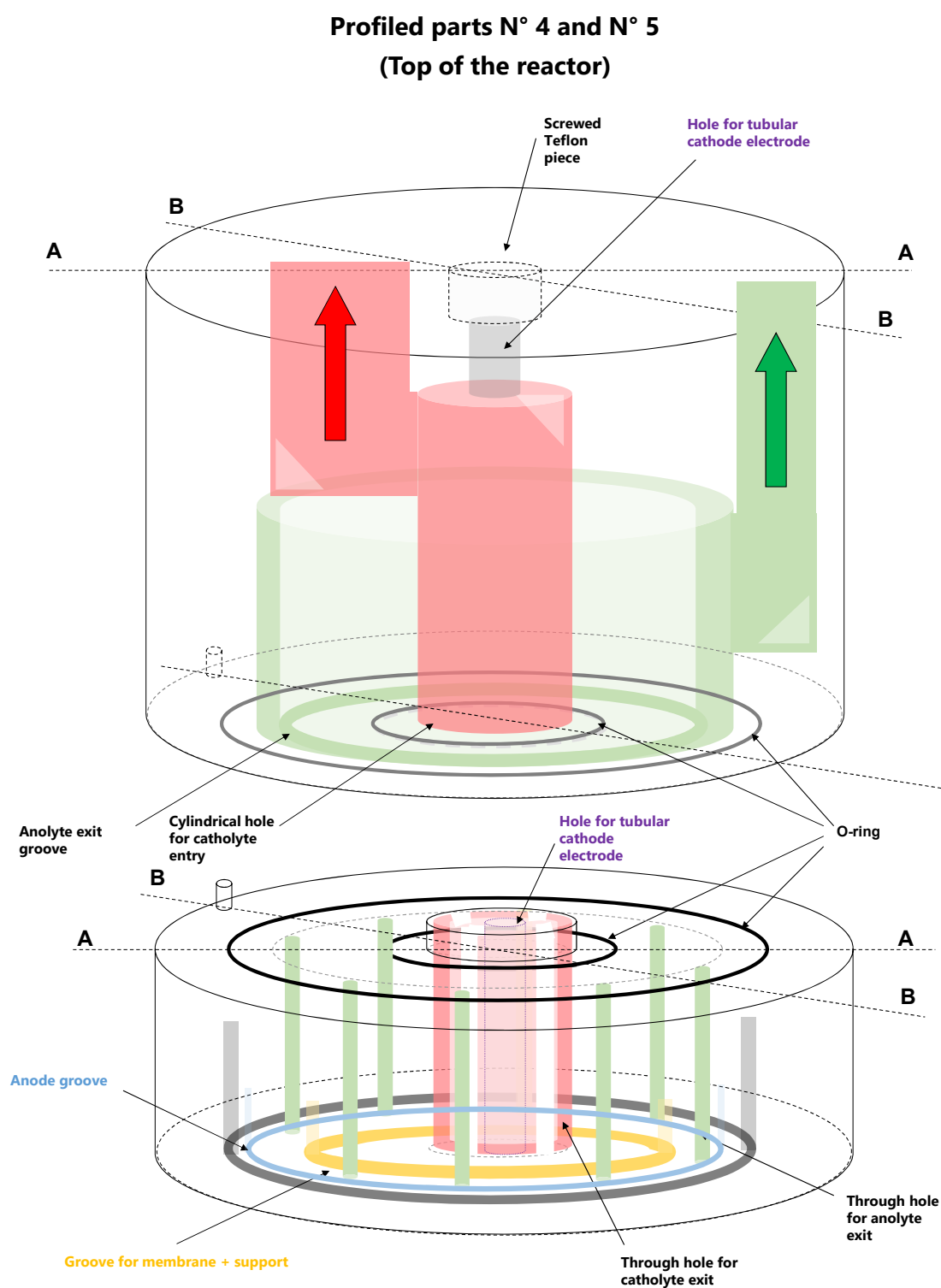


Figure C.1 (continued).

Parts N°1 and N°2 (bottom)
Longitudinal section along axis B - B

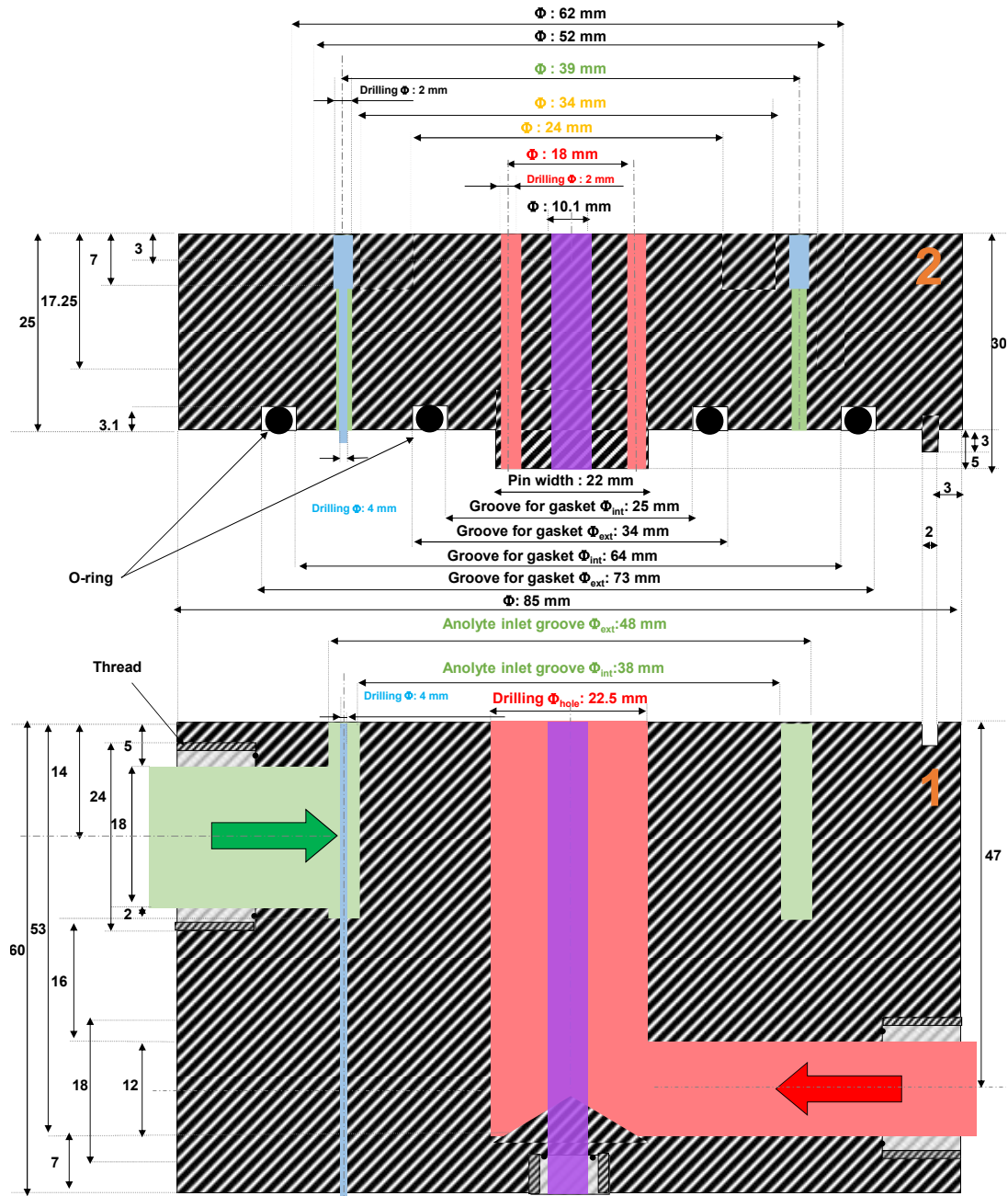


Figure C.1 (continued).

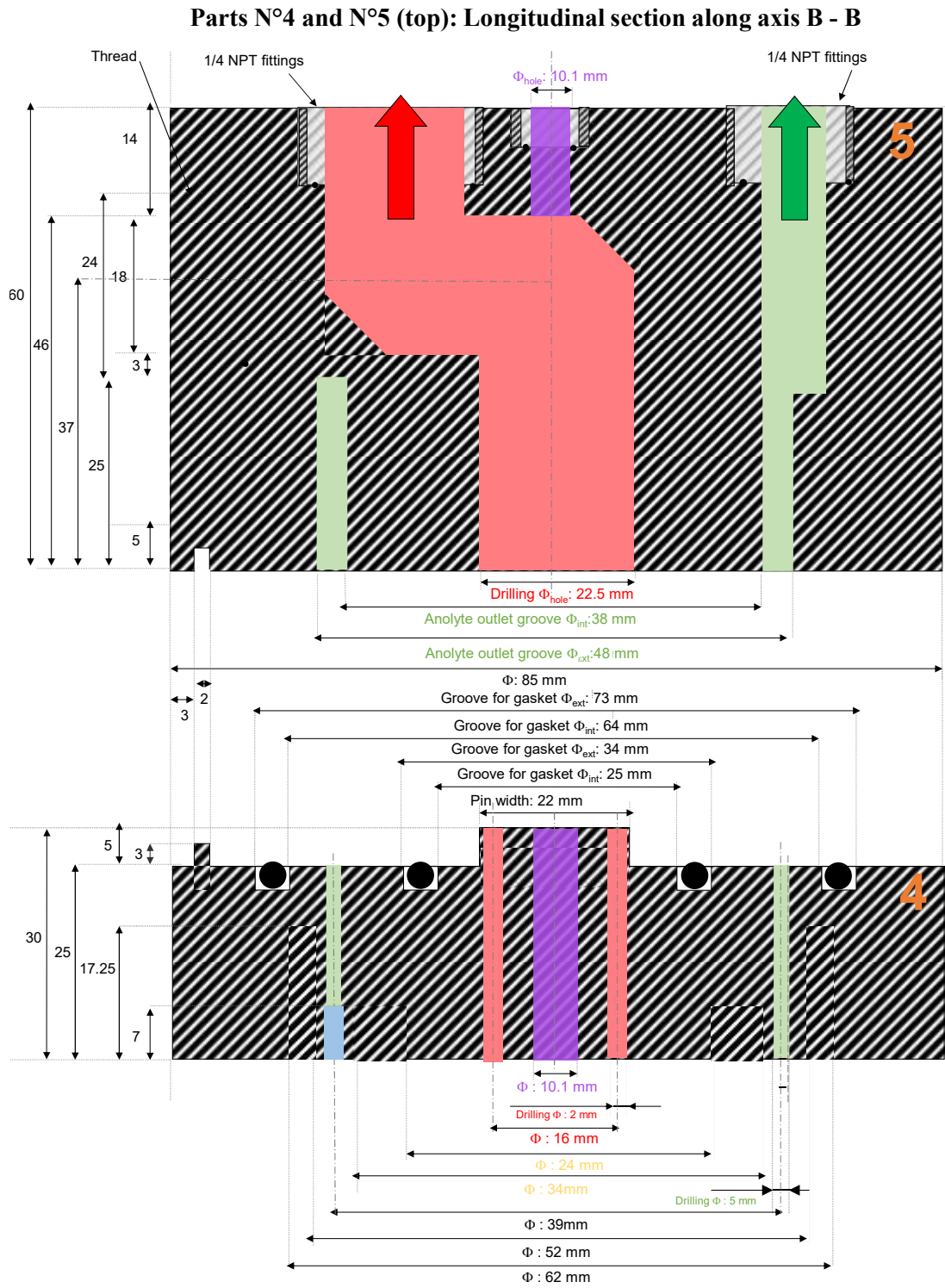


Figure C.1 (continued).

Part N°2 bottom view
 (= Part N°4 top view except for anode drilling and reversed pin position)

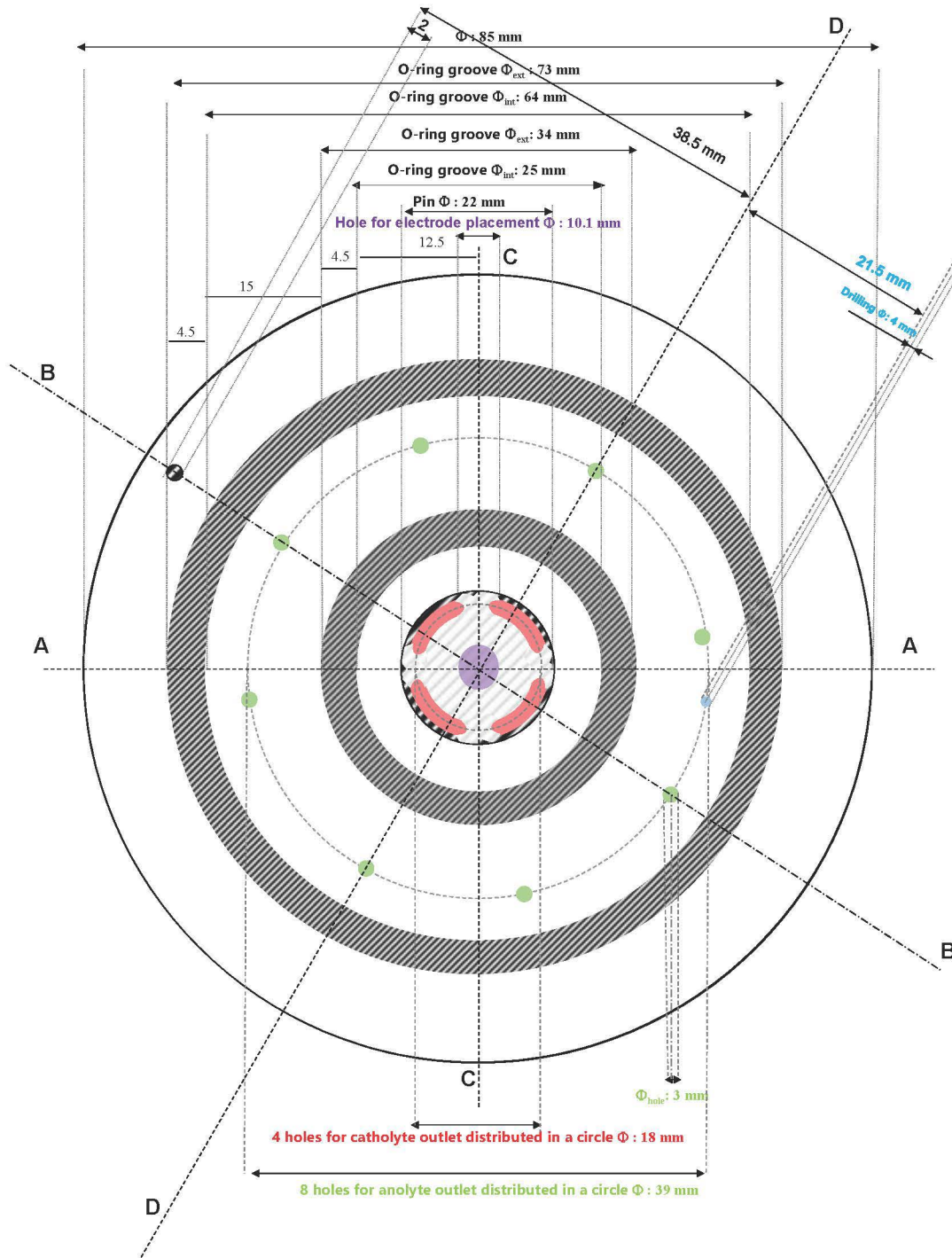


Figure C.1 (continued).

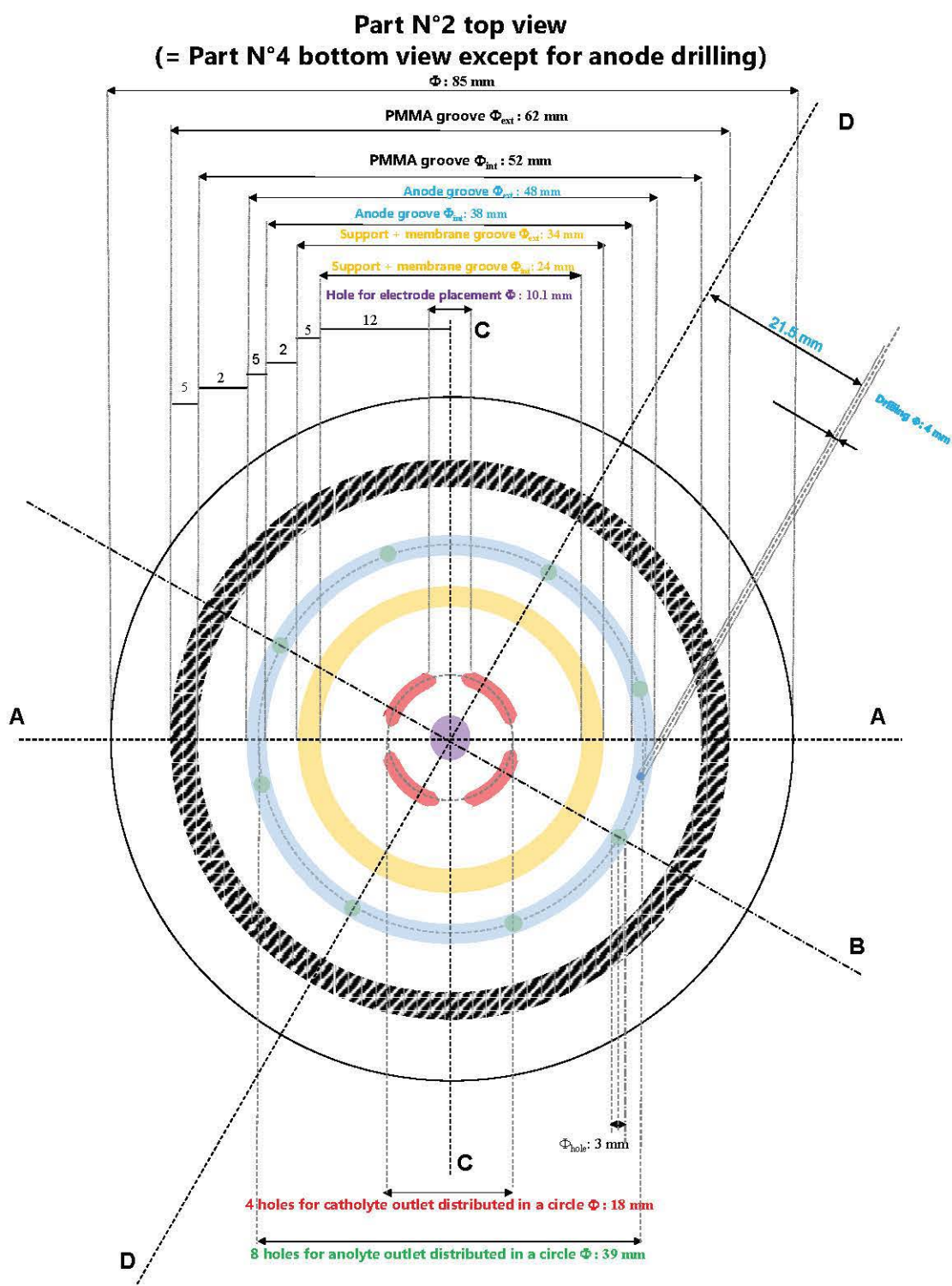


Figure C.1 (continued).

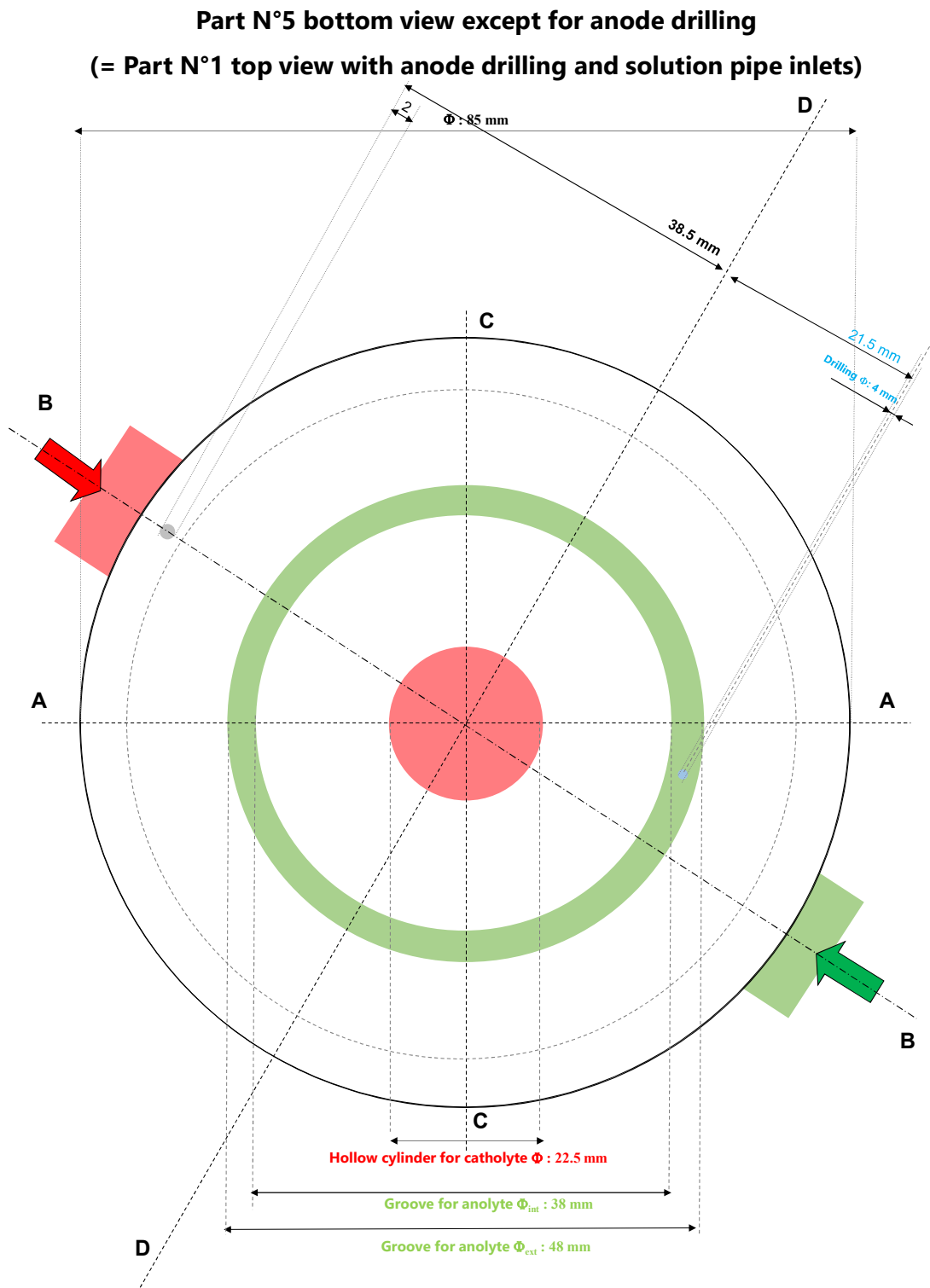


Figure C.1 (continued).

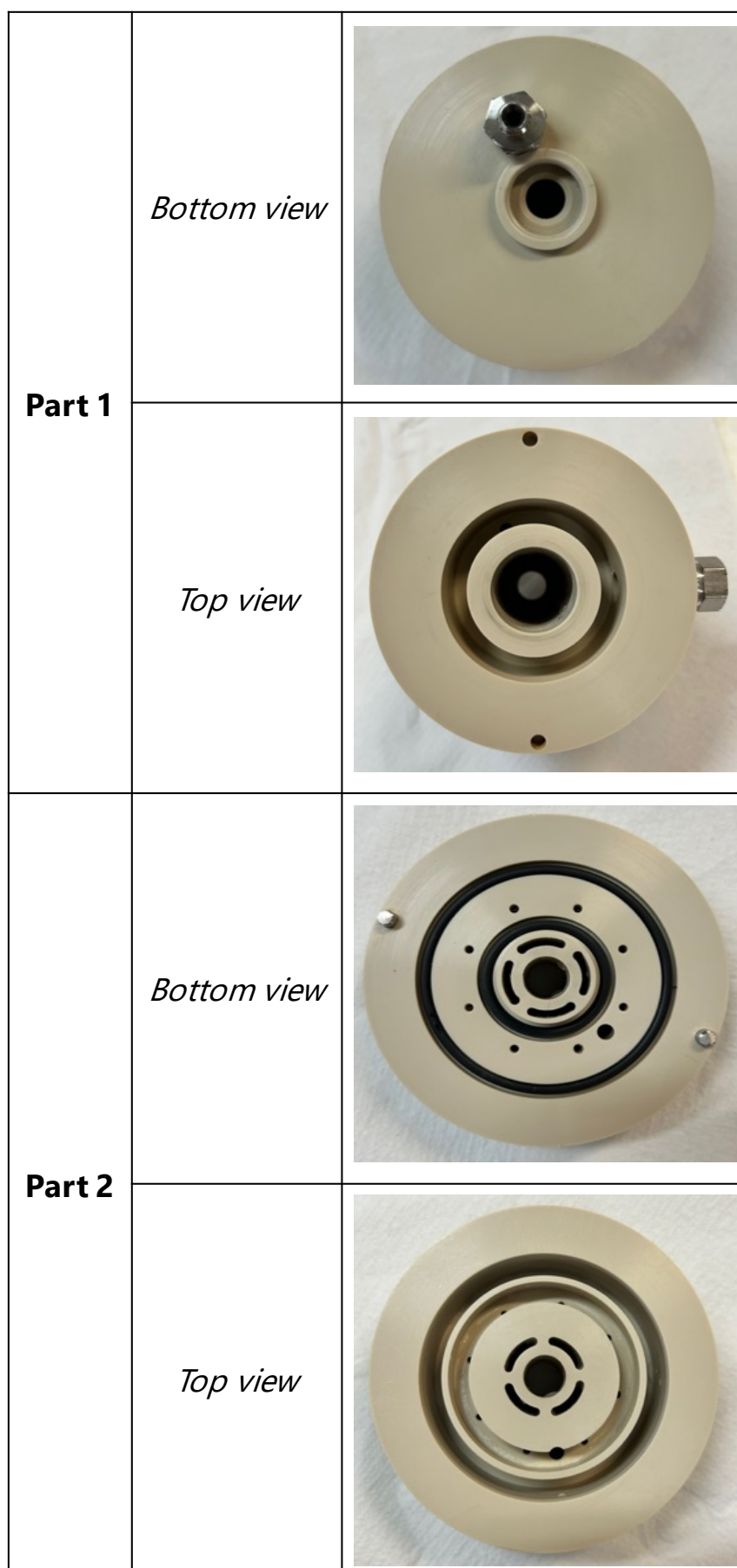


Fig. C.2 – Illustration of Parts n°1 and 2.

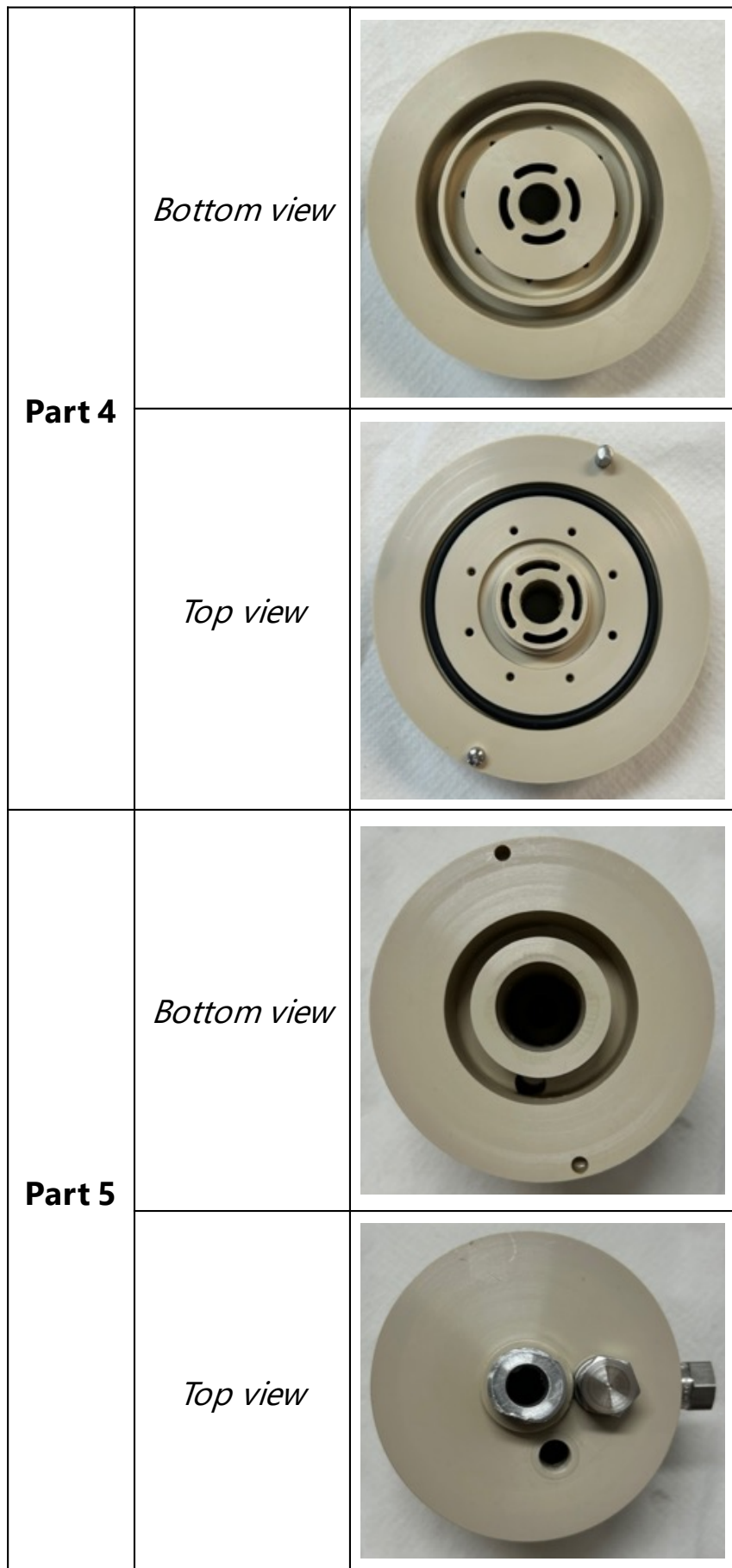


Fig. C.3 – Illustration of Parts n°4 and 5.

Validation of a new IC-MS method for the quantification of analytes in human urine

Outline of the current chapter

D-1 Introduction	206
D-2 Material and methods	207
D-2.1 Chemicals	207
D-2.2 Preparation of standards and urine samples	207
D-2.3 Validation of the method	207
D-3 Results	213
D-3.1 Implementation of the IC-CD/MS method	213
D-3.2 Validation of the IC-CD/MS method	213
D-3.3 Analysis of human urine samples	225
D-4 Discussions	228
D-5 Conclusions	230
D-6 Ethical approval	230

This appendix presents the results obtained from the article “G. Hopsort*, L. Latapie, K. Groenen Serrano, K. Loubière, T. Tzedakis* (2023). Deciphering the human urine matrix: a new approach to simultaneously quantify the main ions and organic compounds by ion chromatography / mass spectrometry (IC-MS). *Analytical and Bioanalytical Chemistry*. 10.1007/s00216-023-04808-2”.

D-1 Introduction

Using the human urine composition as a health indicator is an old method; first known as uroscopy, then as urinalysis, this practice has been in existence for about 6,000 years ago. Early physicians considered urine as a revealing diagnostic tool, allowing them to understand various diseases like infections of the urinary tract, problems with the kidneys and bladder, and liver failure [268–271]. Produced by the kidneys and stored in the bladder between urinations, urine’s composition depends on various factors, such as diet, lifestyle, and individual characteristics (*i.e.*, gender, age, weight, eating habits, etc.). When freshly excreted from the bladder, urine contains more than 95wt% of water. Substances present in urine are split into organic compounds ($\sim 60wt\%$, composed of urea representing more than 60wt%, followed by ammonium salts $\sim 20wt\%$, the rest including creatinine and other compounds) and inorganic compounds ($\sim 40wt\%$, salts such as sodium chlorides, potassium chlorides, sulfates, carbonates, and phosphates). The work of Prof. D.F. Putnam in 1971 pioneered the determination of the human urine composition [57]. They provided, for the first time, a deep analysis demonstrating that human urine is an aqueous solution of urea, creatinine, uric acid, and various other species, such as chloride, sodium, potassium, sulfate, ammonium, and phosphate in smaller quantities. Proteins were also found to be present in urine, but in trace amounts compared to their concentrations in blood plasma. Consequently and after a multitude of research works, Bouatra et al.[58] identified in 2013 more than 3,100 components in human urine. Since then, over 90 compounds were found to be consistently present in urine samples, irrespective of gender or collection time. Later, various analytical methods have emerged to inspect the urine matrix [272, 273], and currently multiple specific techniques are available to quantify traces of many “minor” molecules in urine, such as : HPLC (hormones [274], antidepressants [275], ranitidine [276]), UHPLC-MS/MS (pyrithione metabolites [277], DL-cysteine [278], steroid hormones [279]) or LC-MS/MS (gluten-derived metabolites [280], THC metabolites [281], phytocannabinoids [282]). However, any study has yet been developed allowing efficient quantification of the most concentrated compounds without sample preparation and in a short time. Among the different analytical techniques used to measure separately the majority molecules contained in urine, one can typically cite:

- (i) for urea, electrochemical sensor [283], chemiluminometric [177] and spectrophotometric [181] methods,
- (ii) for creatinine, electrochemical detection [284], HPLC-MS/MS [285], colorimetric method [286],
- (iii) for chlorides, spectrophotometric method [287].

Besides, the simultaneous determination of both uric acid and creatinine has already been reported using HPLC [288, 289] or LC/MS [290]. Sakurai et al. quantified urea, uric

acid and creatinine by LC/MS [190] in real human urine matrices, while Wang et al. focused on the simultaneous potentiometric detection of sodium and potassium [291] in artificial urine solutions. Using paper-based sensors in synthetic urine, Tasoglu et al. successfully detected, in physiological concentrations, the major ions contained in urine, such as sodium, potassium, calcium, chloride and nitrite [292]. All these methods are undeniably accurate but do not allow for one-pot and short-time analysis of the majority of compounds in the urine matrix. To the best of our knowledge, none of them are able to simultaneously determine the concentrations of both ions and organic compounds. For the first time, the present work proposes a simple, rapid and sample-preparation-free method for the simultaneous analysis of the main organic molecules (lactic acid, hippuric acid, citric acid, uric acid, oxalic acid, urea, creatine and creatinine as biomarkers [293–298]) and the most concentrated ions (chloride, sulfate, phosphate, sodium, ammonium, potassium, magnesium and calcium) contained in human urine. This method consists of coupling ion chromatography to mass spectroscopy, which relevancy, accuracy and robustness will be demonstrated through a study involving samples obtained from 10 healthy human volunteers.

D-2 Material and methods

D-2.1 Chemicals

Lactic acid, hippuric acid, citric acid, uric acid, oxalic acid, urea, creatine and creatinine were purchased from Sigma-Aldrich (> 99.5%, St-Louis, USA) with a Normapur[®] grade. Anionic standards were prepared from a mixed solution from CPAChem (Combined seven anions standard II – 7 components, Bogomilovo, Bulgaria), while cationic standards were prepared from a mixed solution from SCP Science (Standard for IC, Baie-D'Urfé, Canada). Water was purified by a Milli-Q water purification system from Elga LabWater (Medica, Lane End, UK). Glassware should be avoided for the preparation and storage of solutions and replaced by synthetic material in order to avoid any ionic salting-out.

D-2.2 Preparation of standards and urine samples

D-2.2.a Preparation of standards

Standard stock solutions of the analytes containing organic molecules at 0.5 g L^{-1} were prepared in Milli-Q water and stored in plastic bottles at 4°C for no more than one week. Then, stock solutions were diluted to standard solutions at different concentrations.

D-2.2.b Preparation of urine samples

Anonymous human urine samples were obtained from 10 healthy volunteers internally (7 male samples #1→#7 and 3 female samples #8→#10 in their 20s to 60s). The samples were stored at 4°C until analysis. Urine samples were (i) filtered through $0.45 \mu\text{m}$ syringe filters, (ii) diluted 250-fold and then (iii) injected to the analytical system.

D-2.3 Validation of the method

An example of the obtained chromatograms for various analyte standard concentrations is provided in Figure D.1. The method was validated for selectivity, sensitivity, linearity,

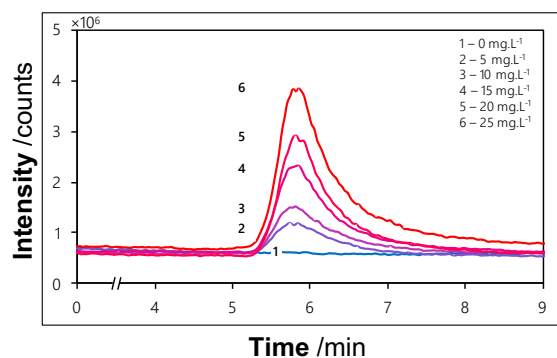


Fig. D.1 – Ion chromatograms extracted from a standard sample containing urea at concentrations ranging from 0 to 25 mg L⁻¹.

accuracy, and precision according to the ICH guidelines [299].

D-2.3.a Selectivity

The method's selectivity to ensure a proper separation of the different ions was examined on standard solutions and blank solvent (Milli-Q water) via conductivity measurements. For the organic molecules, the method's selectivity was examined by analyzing several standard solutions. The signal of the mass spectrum of each pure compound was then compared to the corresponding one obtained in the urine spectrum as illustrated in D.2 and Table D.1.

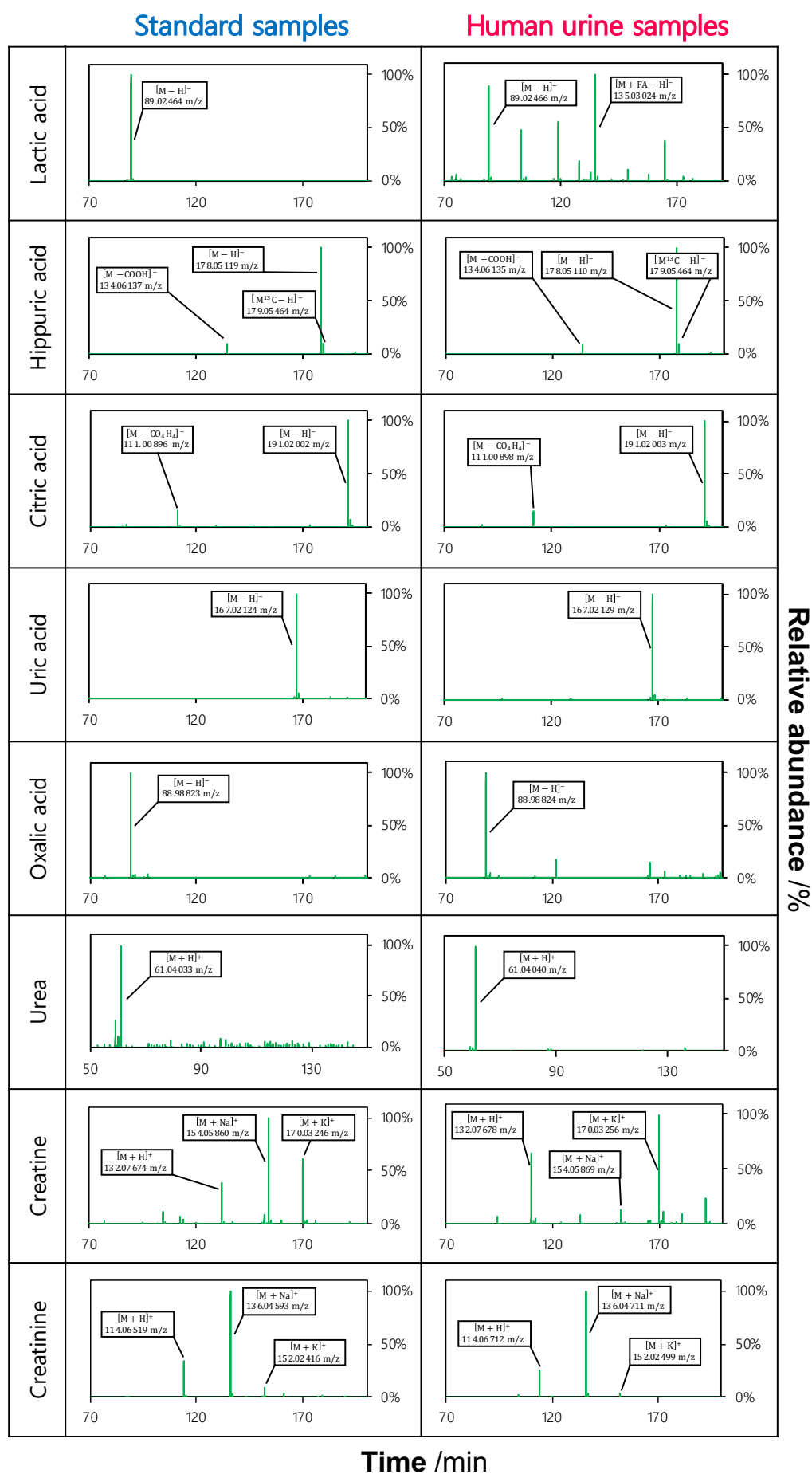


Fig. D.2 – Mass spectra of organic compounds in urine analyzed in standard and real urine samples.

Analyte	$\frac{m}{z}$ [M-H] ⁻ , theoretical	$\frac{m}{z}$ [M-H] ⁻ , standard sample		$\frac{m}{z}$ [M-H] ⁻ , human urine sample	
		Value	RE (%)	Value	RE (%)
Lactic acid	89.02442	89.02464	2.47×10^{-4}	89.02461	2.13×10^{-6}
Hippuric acid	178.05097	178.05119	1.24×10^{-4}	178.05110	7.30×10^{-7}
Citric acid	191.01973	191.02002	1.52×10^{-4}	191.02003	1.57×10^{-6}
Uric acid	167.02106	167.02124	1.08×10^{-4}	167.02129	1.38×10^{-6}
Oxalic acid	88.98803	88.98823	2.25×10^{-4}	88.98824	2.36×10^{-6}

Analyte	$\frac{m}{z}$ [M-H] ⁺ , theoretical	$\frac{m}{z}$ [M-H] ⁺ , standard sample		$\frac{m}{z}$ [M-H] ⁺ , human urine sample	
		Value	RE (%)	Value	RE (%)
Urea	61.03964	61.04033	1.13×10^{-3}	61.04040	1.25×10^{-5}
Creatine	132.07675	132.07674	7.57×10^{-6}	132.07678	2.27×10^{-7}
Creatinine	114.06690	114.06441	2.18×10^{-5}	114.04807	1.65×10^{-4}

Table D.1 – Mass spectroscopic identification of organic compounds in human urine by comparison with standards.

D-2.3.b Sensitivity

The method's sensitivity was determined under the operating conditions used through the LODs and Limits Of Quantification (LOQs) determination at a signal-to-noise ratio of 3 and 10, respectively.

D-2.3.c Linearity

The linearity of the CD or MS signals of each compound against its concentration was examined by plotting the corresponding calibration curves. A set of solutions containing different concentrations of analyte were prepared, covering a wide range of values as reported in Table D.2.

Analyte	Concentration range for calibration rcurves (mg L ⁻¹)	Detection mode	Concentration range for determining recoveries (mg L ⁻¹)
<i>Organic molecules</i>		MS	
Urea	$0 \leq [\text{CH}_4\text{N}_2\text{O}] \leq 25$	+p	$5 \leq [\text{CH}_4\text{N}_2\text{O}] \leq 25$
Uric acid	$0 \leq [\text{C}_5\text{H}_4\text{N}_4\text{O}_3] \leq 20$	-p	$2.5 \leq [\text{C}_5\text{H}_4\text{N}_4\text{O}_3] \leq 20$
Creatine	$0 \leq [\text{C}_4\text{H}_9\text{N}_3\text{O}_2] \leq 10$	+p	$2.5 \leq [\text{C}_4\text{H}_9\text{N}_3\text{O}_2] \leq 10$
Creatinine	$0 \leq [\text{C}_4\text{H}_7\text{N}_3\text{O}] \leq 10$	+p	$2.5 \leq [\text{C}_4\text{H}_7\text{N}_3\text{O}] \leq 10$
Citric acid	$0 \leq [\text{C}_6\text{H}_8\text{O}_7] \leq 7.5$	-p	$2.5 \leq [\text{C}_6\text{H}_8\text{O}_7] \leq 7.5$
Lactic acid	$0 \leq [\text{C}_3\text{H}_6\text{O}_3] \leq 5$	-p	$1 \leq [\text{C}_3\text{H}_6\text{O}_3] \leq 5$
Hippuric acid	$0 \leq [\text{C}_9\text{H}_9\text{NO}_3] \leq 5$	-p	$1 \leq [\text{C}_9\text{H}_9\text{NO}_3] \leq 5$
Oxalic acid	$0 \leq [\text{C}_2\text{H}_2\text{O}_4] \leq 5$	-p	$1 \leq [\text{C}_2\text{H}_2\text{O}_4] \leq 5$
<i>Ionic compounds</i>		CD	
Chloride	$0 \leq [\text{Cl}^-] \leq 20$	⊕	$1 \leq [\text{Cl}^-] \leq 20$
Ammonium	$0 \leq [\text{NH}_4^+] \leq 15$	⊕	$2.5 \leq [\text{NH}_4^+] \leq 15$
Potassium	$0 \leq [\text{K}^+] \leq 10$	⊕	$1.25 \leq [\text{K}^+] \leq 10$
Sodium	$0 \leq [\text{Na}^+] \leq 7.5$	⊕	$1.25 \leq [\text{Na}^+] \leq 7.5$
Sulfate	$0 \leq [\text{SO}_4^{2-}] \leq 5$	⊖	$0.25 \leq [\text{SO}_4^{2-}] \leq 5$
Phosphate	$0 \leq [\text{PO}_4^{3-}] \leq 5$	⊖	$0.25 \leq [\text{PO}_4^{3-}] \leq 5$
Magnesium	$0 \leq [\text{Mg}^{2+}] \leq 2$	⊕	$0.25 \leq [\text{Mg}^{2+}] \leq 2$
Calcium	$0 \leq [\text{Ca}^{2+}] \leq 2$	⊕	$0.25 \leq [\text{Ca}^{2+}] \leq 2$

Table D.2 – Concentration range (ordered by decreasing concentration) used for each analyte to obtain the IC-CD/MS calibration curves and recoveries

D-2.3.d Accuracy

The method's accuracy was assessed by injecting standard solutions at different concentrations. By using calibration curves, the RE between the theoretical and measured concentrations was then determined according to the Eq. D.1.

$$\text{RE} = \left| \frac{\text{Theoretical concentration value} - \text{Experimental concentration value}}{\text{Theoretical concentration value}} \right| \times 100 \quad (\text{D.1})$$

The accuracy was also examined by means of the recovery of some known quantities of organic molecules and ionic compounds added to human urine samples. The latter parameter was already been studied by El Himri et al. [300] and was defined as Eq. D.2.

$$\text{Recovery} = \frac{\text{Measured amount}}{\text{Spiked amount}} \times 100 \quad (\text{D.2})$$

$$\text{Measured amount} = \text{Amount after spiking} - \text{Amount before spiking} \quad (\text{D.3})$$

The dispersion of the measurements is assessed by evaluating the SD as shown in Eq.

D.4.

$$SD = \sqrt{\frac{\sum(x_i - \mu)^2}{N}} \quad (D.4)$$

where x_i represents each value from the population, μ is the population mean and N is the size of the population. The recovery was determined by triplicate analysis of urine samples spiked with standards as shown in Table D.2.

Analyte	Concentration range (mg L ⁻¹)
<i>Organic molecules</i>	
Urea	$5 \leq [\text{CH}_4\text{N}_2\text{O}] \leq 25$
Uric acid	$2.5 \leq [\text{C}_5\text{H}_4\text{N}_4\text{O}_3] \leq 20$
Creatine	$2.5 \leq [\text{C}_4\text{H}_9\text{N}_3\text{O}_2] \leq 10$
Creatinine	$2.5 \leq [\text{C}_4\text{H}_7\text{N}_3\text{O}] \leq 10$
Citric acid	$2.5 \leq [\text{C}_6\text{H}_8\text{O}_7] \leq 7.5$
Lactic acid	$1 \leq [\text{C}_3\text{H}_6\text{O}_3] \leq 5$
Hippuric acid	$1 \leq [\text{C}_9\text{H}_9\text{NO}_3] \leq 5$
Oxalic acid	$1 \leq [\text{C}_2\text{H}_2\text{O}_4] \leq 5$
<i>Ionic compounds</i>	
Chloride	$1 \leq [\text{Cl}^-] \leq 20$
Ammonium	$2.5 \leq [\text{NH}_4^+] \leq 15$
Potassium	$1.25 \leq [\text{K}^+] \leq 10$
Sodium	$1.25 \leq [\text{Na}^+] \leq 7.5$
Sulfate	$0.25 \leq [\text{SO}_4^{2-}] \leq 5$
Phosphate	$0.25 \leq [\text{PO}_4^{3-}] \leq 5$
Magnesium	$0.25 \leq [\text{Mg}^{2+}] \leq 2$
Calcium	$0.25 \leq [\text{Ca}^{2+}] \leq 2$

Table D.3 – Concentration range (ordered by decreasing concentration) used for each analyte to determine the IC-CD/MS method recoveries.

D-2.3.e Precision

The intra-day precision was evaluated through the repeatability defined with RSD, as Eq. D.5, and determined from 5 replicates at a minimum of 3 different concentrations on day 1. The inter-day precision was evaluated by injecting the same solution in triplicate on days 2 and 3.

$$RSD = \left| \frac{SD}{\mu} \right| \times 100 \quad (D.5)$$

D-2.3.f Matrix effect

Calibration standards with equivalent concentration levels were prepared by introducing spiking into blank matrix extracts of the urine sample. Calibration curves were obtained by

plotting the peak areas as a function of the concentrations of their respective calibration standards for each compound. The ME was ascertained by comparing the slopes of the calibration curves formed from the matrix case and the ones formed from solvent-based calibration curves. The method used to quantify ME was derived from the equation proposed by Cho et al. [301] as described in Eq. D.6. A value exceeding 100% (below 100%) means an increase (a decrease) in response signal. This analysis was performed on ten distinct samples.

$$\text{ME} = \frac{\text{slope of matrix calibration curve}}{\text{slope of solvent standard calibration curve}} \times 100 \quad (\text{D.6})$$

D-3 Results

D-3.1 Implementation of the IC-CD/MS method

The operating parameters of the mass spectrometer were optimized (*i.e.*, ESI voltage, gas temperature, etc.), corresponding to IC conditions (*i.e.*, flow rate, eluent composition and concentration) previously described. Under these conditions, all the analytes in this matrix could be efficiently separated and detected within an overall run duration of 35 min. The chromatograms of the mixed standards and urine samples obtained are shown in Figure D.3 and Figure D.3, respectively. The $[\text{M} - \text{H}]^-$ ions of lactic, hippuric, citric, uric and oxalic acids were detected in the negative ion mode as lactate, hippurate, citrate, urate, and oxalate (their identification is also possible in CD but was not applied in this study). The $[\text{M} - \text{H}]^+$ ions of urea, creatine and creatinine were detected in the positive ion mode.

D-3.2 Validation of the IC-CD/MS method

D-3.2.a Linearity, LODs and LOQs

Table D.4 shows, for each analyte, the calibration curve ranges, regression equations, correlation coefficients, LODs and LOQs. Whatever the analyte, a linear relationship is obtained between the peak area and the concentration of standards in water, with correlation coefficients above 0.993. In Figure D.5, the calibration curves shows, for each standard, a good validation of the method by applying the Kohlrausch's law (Eq. D.7) and the Kingdon's principle (Eq. D.8), respectively, for CD and MS detections [302, 303].

$$\sigma = \sum_{\text{compounds } i} \lambda_i \times [\text{Compound } i] \quad (\text{D.7})$$

where: σ is the conductivity of the solution (S m^{-1}), λ_i is the molar conductivity of the compound i ($\text{S m}^2 \text{mol}^{-1}$).

$$\omega = \frac{z \times B}{m} \quad (\text{D.8})$$

where: ω is the angular frequency (rad s^{-1}), B is the magnetic field (T), m/z is the mass-to-charge ratio (kg C^{-1}).

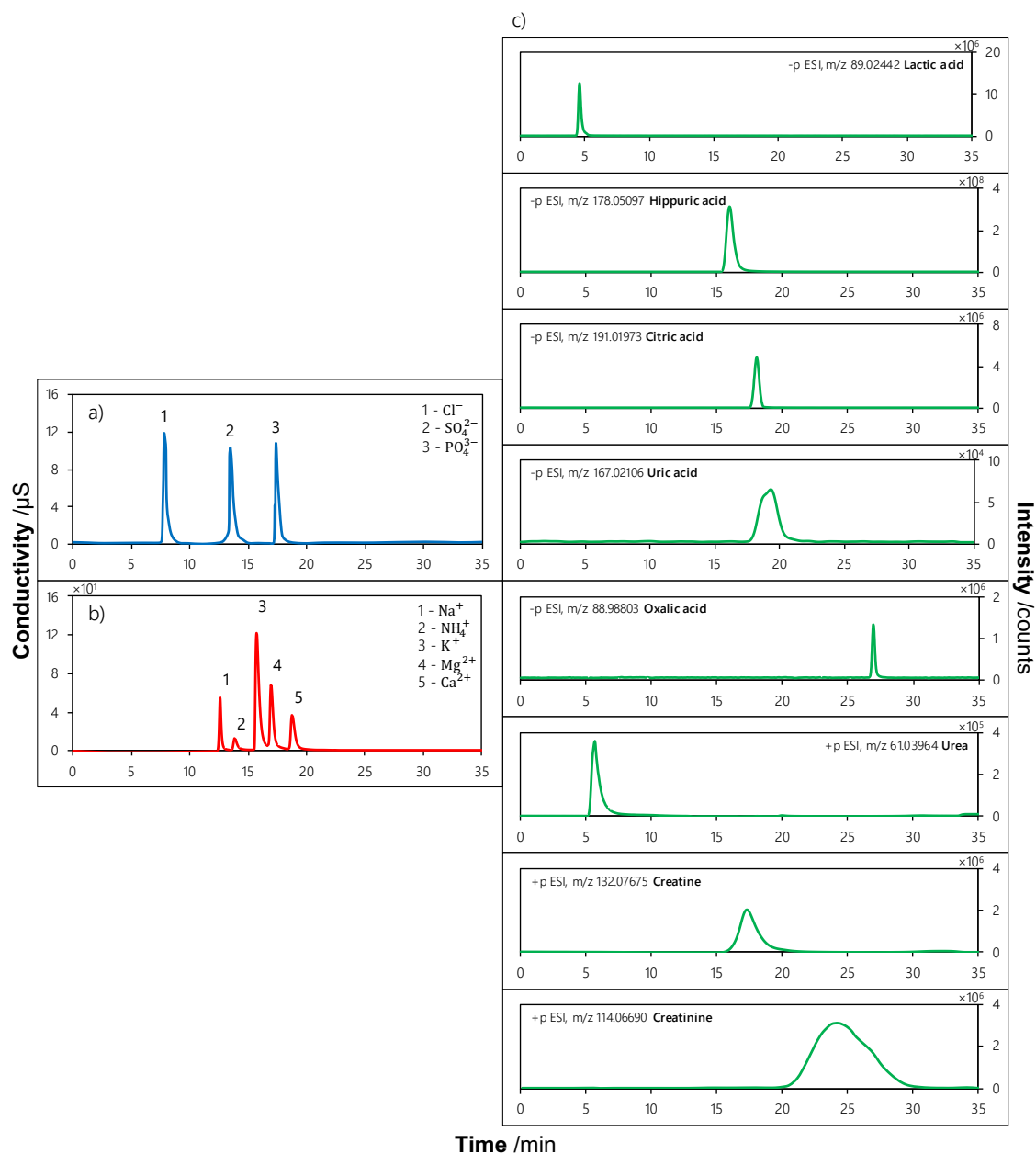


Fig. D.3 – a) Anionic, b) cationic and c) extracted ion chromatograms of a sample containing all the standards in water. Major compounds are identified and labeled.

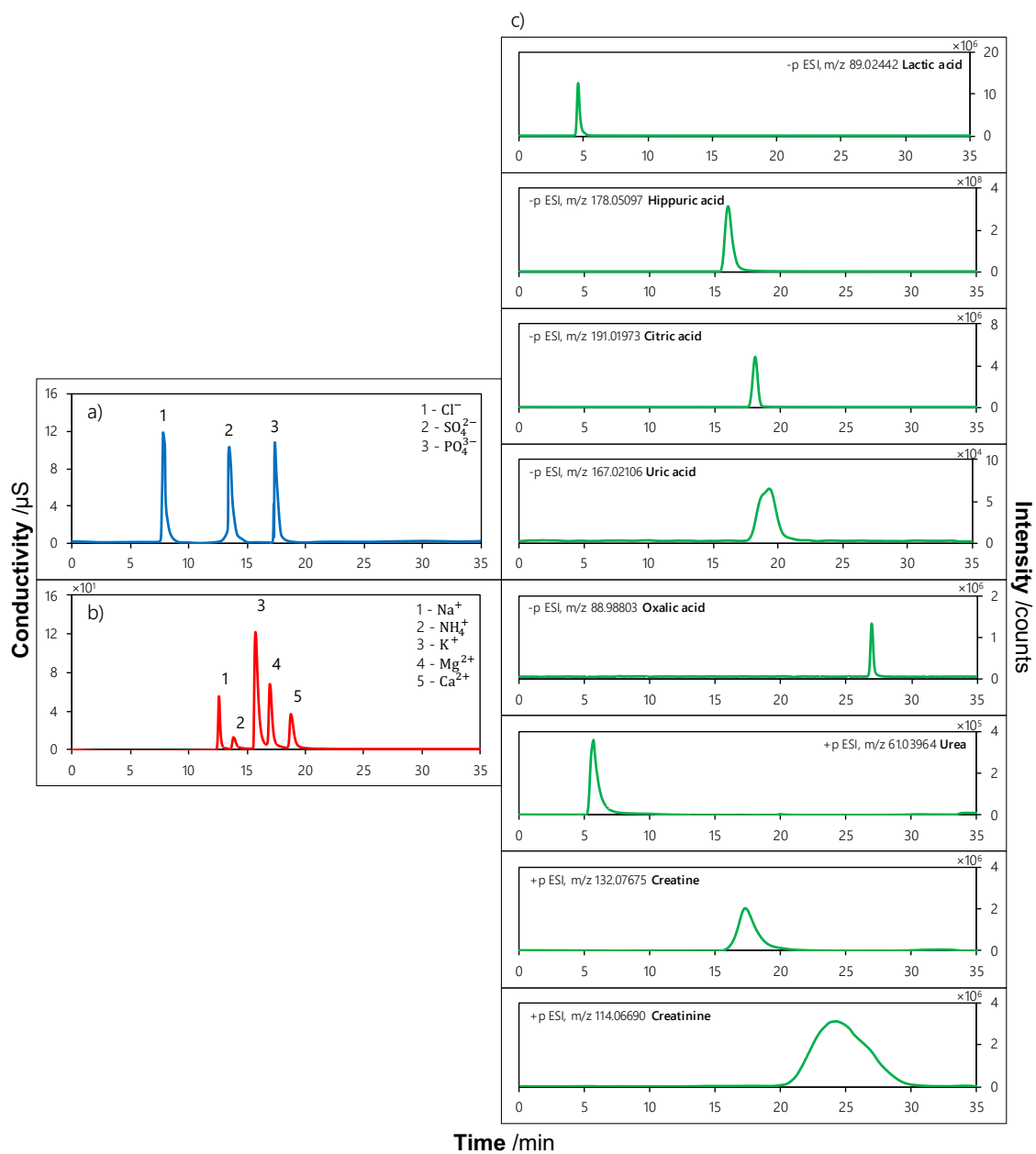


Fig. D.4 – a) Anionic, b) cationic and c) extracted ion chromatograms of a typical human urine sample. Major compounds are identified and labeled.

Analyte	ESI polarity	Retention time (min)	Analyte concentration range (ppm)	Regression equation ([j] in mg L ⁻¹)	Correlation coefficient	LODs (mg L ⁻¹)	LOQs (mg L ⁻¹)
<i>Organic molecules (MS)</i>				(Peak area in counts min)			
Lactic acid	-p	4.6	0-5	Peak area = $3.84 \times 10^6 \times [C_3H_6O_3] + 9.40 \times 10^4$	0.9988	0.19	0.64
Hippuric acid	-p	16.0	0-5	Peak area = $5.08 \times 10^6 \times [C_9H_9NO_3] + 6.01 \times 10^5$	0.9958	0.37	1.22
Citric acid	-p	18.1	0-7.5	Peak area = $5.43 \times 10^4 \times [C_6H_8O_7] + 4.39 \times 10^3$	0.9990	0.30	1.01
Uric acid	-p	19.5	0-20	Peak area = $3.21 \times 10^3 \times [C_5H_4N_4O_3] + 8.42 \times 10^2$	0.9988	0.72	2.41
Oxalic acid	-p	27.0	0-5	Peak area = $3.98 \times 10^5 \times [C_2H_2O_4] + 3.37 \times 10^4$	0.9982	0.24	0.80
Urea	+p	5.9	0-25	Peak area = $1.22 \times 10^6 \times [CH_4N_2O] + 1.51 \times 10^5$	0.9999	0.32	1.07
Creatine	+p	17.3	0-10	Peak area = $3.86 \times 10^5 \times [C_4H_9N_3O_2] + 2.55 \times 10^4$	0.9979	0.59	1.96
Creatinine	+p	23.8	0-10	Peak area = $1.25 \times 10^6 \times [C_4H_7N_3O] + 2.59 \times 10^5$	0.9972	0.63	2.11
<i>Ionic compounds (CD)</i>				(Peak area in μ S min)			
Chloride		7.5	0-20	Peak area = $0.50 \times [Cl^-] + 0.06$	0.9999	0.12	0.41
Sulfate		13.1	0-5	Peak area = $0.40 \times [SO_4^{2-}] + 0.10$	0.9994	0.14	0.47
Phosphate		17.0	0-5	Peak area = $0.17 \times [PO_3^{2-}] + 0.01$	0.9982	0.25	0.84
Sodium	[-]	13.0	0-7.5	Peak area = $8.58 \times [Na^+] + 0.68$	0.9991	0.23	0.77
Ammonium		14.3	0-15	Peak area = $0.72 \times [NH_4^+] + 0.13$	0.9987	0.75	2.59
Potassium		13.1	0-10	Peak area = $0.64 \times [K^+] + 0.06$	0.9994	0.14	0.47
Magnesium		17.8	0-2	Peak area = $2.12 \times [Mg^{2+}] + 0.08$	0.9936	0.16	0.54
Calcium		19.7	0-2	Peak area = $1.09 \times [Ca^{2+}] + 1.05$	0.9950	0.14	0.48

Table D.4 – Retention time, calibration curve ranges, regression equation, correlation coefficients, LODs and LOQs obtained, for each analyte (ordered by increasing retention time) from the curves plotted in Figure D.5.

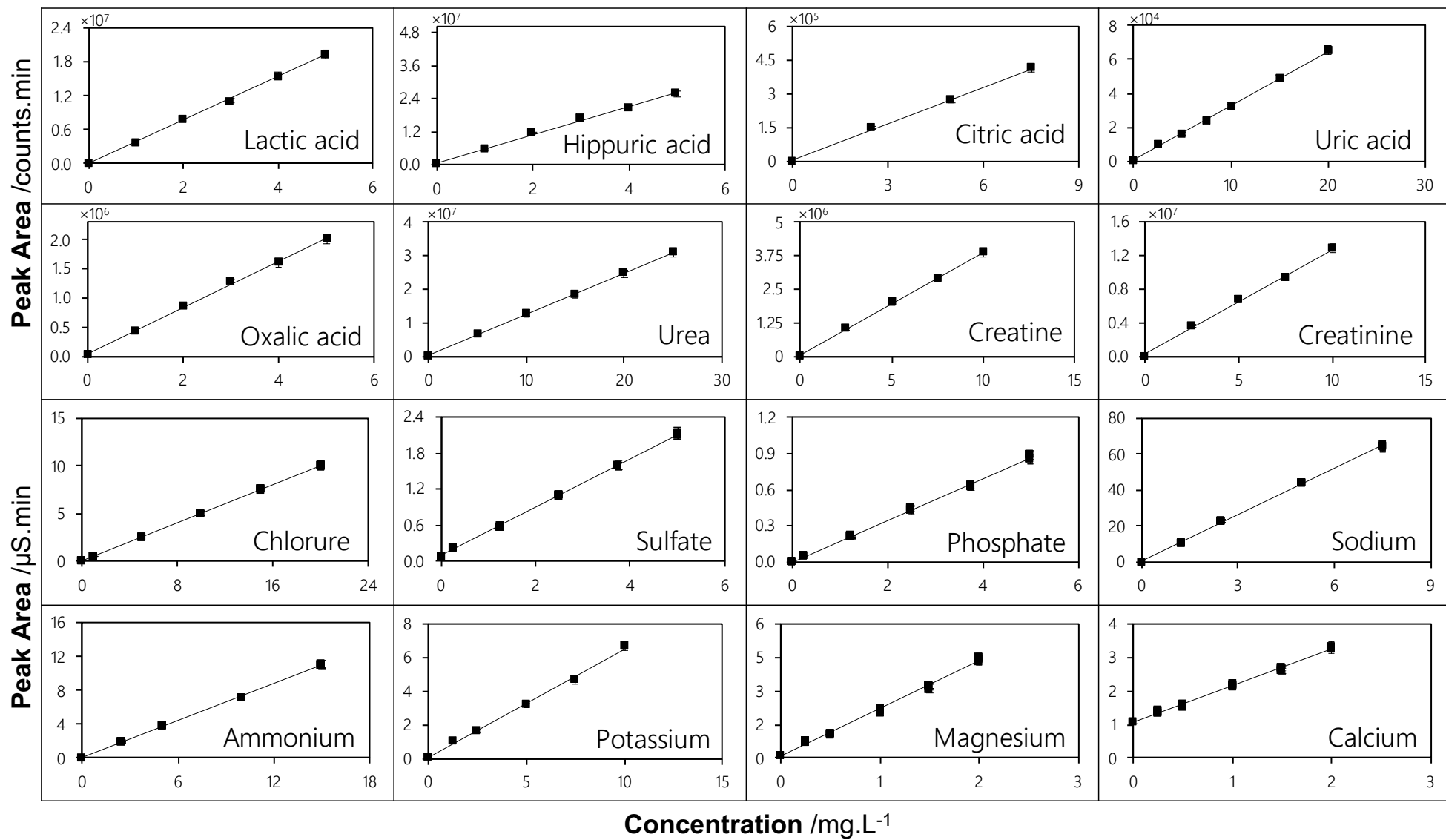


Fig. D.5 – Calibration curves for each standard analyte.

D-3.2.b Precision

As shown in Table D.5, the intra-day precisions for all concentrations of each standard were smaller than 2.5% and the RSD for the inter-day analysis smaller than 4.0% for each analyte, thus demonstrating that the method can be used to obtain accurate results.

Analyte	Concentration range (mg L ⁻¹)	Intra-day (<i>n</i> =5)		Inter-day (<i>n</i> =11)	
		Accuracy RE (%)	Precision RSD (%)	Accuracy RE (%)	Precision RSD (%)
<i>Organic molecules</i>					
Lactic acid	1.00	1.2	1.5	4.3	0.6
	2.00	2.9	0.8	1.8	3.5
	3.00	3.5	3.1	0.2	2.2
	4.00	0.5	1.9	3.4	2.8
	5.00	3.3	2.6	2.5	3.4
Hippuric acid	1.00	3.6	3.2	0.9	1.8
	2.00	0.4	2.1	3.7	2.4
	3.00	1.1	1.4	4.2	0.3
	4.00	2.2	0.9	1.3	3.8
	5.00	1.7	1.2	2.0	2.0
Citric acid	2.50	1.1	1.4	2.6	1.5
	5.00	3.9	0.9	4.2	3.9
	7.50	0.9	2.2	1.1	0.2
Uric acid	2.50	2.5	0.5	3.7	2.8
	5.00	4.1	1.8	5.0	1.9
	7.50	3.9	1.2	2.4	3.1
	10.00	2.8	2.5	0.5	0.7
	15.00	0.6	0.3	3.8	3.7
	20.00	3.2	2.1	1.3	2.4
Oxalic acid	1.00	2.7	2.9	3.1	3.7
	2.00	4.1	1.7	2.6	0.4
	3.00	2.3	3.3	1.9	1.1
	4.00	1.5	3.6	4.4	1.6
	5.00	3.8	0.7	0.1	1.3
Urea	5.00	1.8	0.1	0.9	1.1
	10.00	4.5	1.7	4.1	3.4
	15.00	1.2	2.4	0.2	0.4
	20.00	3.6	1.0	3.3	3.0
	25.00	0.5	0.7	2.0	1.7
Creatine	2.50	1.7	1.6	4.6	2.5
	5.00	2.4	1.3	1.8	1.2
	7.50	3.8	0.4	3.9	4.0
	10.00	0.3	1.9	1.5	0.9
Creatinine	2.50	2.3	0.1	4.9	2.1
	5.00	3.7	2.3	0.0	3.6
	7.50	0.7	1.8	2.3	1.4
	10.00	1.5	2.0	3.1	2.9

Table D.5 – Intra-day and inter-day precision and accuracy.

Analyte	Concentration range (mg L ⁻¹)	Intra-day (n=5)		Inter-day (n=11)	
		Accuracy RE (%)	Precision RSD (%)	Accuracy RE (%)	Precision RSD (%)
<i>Ionic compounds</i>					
Chloride	1.00	1.1	0.6	1.1	0.8
	5.00	0.8	1.0	0.4	0.3
	10.00	0.3	0.4	0.9	1.0
	15.00	1.3	0.9	1.3	0.4
	20.00	0.1	0.2	0.5	0.7
Sulfate	0.25	0.6	0.8	1.0	0.2
	1.25	1.2	0.5	0.2	0.1
	2.50	0.9	0.3	1.2	0.9
	3.75	0.8	1.0	0.7	0.5
	5.00	0.8	0.0	0.1	0.7
Phosphate	0.25	0.2	0.7	1.4	0.1
	1.25	1.7	0.3	1.0	0.9
	2.50	0.6	0.8	0.8	0.6
	3.75	0.3	0.5	0.0	0.2
	5.00	0.4	0.1	0.4	0.8
Sodium	1.25	1.9	1.0	1.1	0.4
	2.50	0.4	0.6	0.6	0.2
	5.00	0.1	0.9	1.3	1.0
	7.50	0.1	0.0	0.9	0.5
Ammonium	2.50	1.4	0.7	0.5	0.5
	5.00	0.8	0.2	1.1	0.6
	10.00	0.4	0.9	1.4	0.7
	15.00	0.6	0.4	0.2	1.0
Potassium	1.25	0.7	0.6	0.6	0.3
	2.50	1.9	0.3	1.2	0.3
	5.00	0.1	0.8	0.9	0.1
	7.50	0.3	0.5	0.1	0.9
	10.00	0.3	0.2	0.4	0.1
Magnesium	0.25	1.4	0.9	0.7	0.4
	0.50	0.7	0.2	1.0	0.7
	1.00	0.1	0.7	1.4	0.5
	1.50	0.7	0.5	0.2	0.1
	2.00	0.1	0.1	1.4	1.7
Calcium	0.25	0.2	1.0	0.6	0.9
	0.50	0.1	0.3	0.3	0.8
	1.00	1.6	0.6	1.2	0.5
	1.50	0.5	0.1	0.1	0.2
	2.00	0.8	0.8	1.3	0.1

Table D.5 (continued).

D-3.2.c Accuracy

Table D.6 shows the recovery of different analytes for various concentrations in spiked human urine samples, ranging from 94.9% to 102.6%. They indicate a good agreement between theoretical and experimental ones.

Analyte	Spiked concentration (mg L ⁻¹)	Recovery rates	
		Mean value (%)	SD (%)
<i>Organic molecules</i>			
Lactic acid	1.00	95.8	3.2
	2.00	98.3	4.1
	3.00	100.5	5.0
	4.00	96.1	3.5
	5.00	101.4	4.8
Hippuric acid	1.00	101.7	5.1
	2.00	95.4	3.9
	3.00	99.9	2.9
	4.00	101.1	4.9
	5.00	97.3	3.7
Citric acid	2.50	95.3	3.4
	5.00	100.7	5.6
	7.50	101.5	4.8
Uric acid	2.50	99.2	4.0
	5.00	102.3	5.2
	7.50	97.8	3.6
	10.00	98.6	4.5
	15.00	100.1	5.7
	20.00	94.9	3.1
Oxalic acid	1.00	99.2	4.7
	2.00	102.1	5.6
	3.00	97.6	4.5
	4.00	100.8	5.3
	5.00	102.5	5.2
Urea	5.00	96.4	2.9
	10.00	102.6	5.1
	15.00	101.8	4.7
	20.00	97.1	3.8
	25.00	100.9	5.8
Creatine	2.50	95.6	3.3
	5.00	98.0	4.3
	7.50	99.7	5.0
	10.00	96.9	3.7
Creatinine	2.50	101.1	4.9
	5.00	95.9	3.0
	7.50	100.4	5.5
	10.00	97.5	3.2

Table D.6 – Recovery of the analytes introduced into a human urine sample ($n = 3$).

Analyte	Spiked concentration (mg L ⁻¹)	Recovery rates	
		Mean value (%)	SD (%)
<i>Ionic compounds</i>			
Chloride	1.00	99.3	0.4
	5.00	100.8	1.2
	10.00	101.5	1.4
	15.00	100.1	0.7
	20.00	99.7	0.9
Sulfate	0.25	101.2	1.1
	1.25	101.8	1.6
	2.50	99.9	0.3
	3.75	100.4	1.3
	5.00	100.6	0.6
Phosphate	0.25	101.1	1.5
	1.25	99.6	0.2
	2.50	101.4	0.8
	3.75	100.0	1.1
	5.00	99.1	0.5
Sodium	1.25	101.7	1.0
	2.50	100.9	1.3
	5.00	100.2	0.1
	7.50	99.5	1.6
Ammonium	2.50	101.3	0.8
	5.00	99.8	1.2
	10.00	100.5	0.3
	15.00	99.4	1.5
Potassium	1.25	100.7	0.9
	2.50	101.0	1.4
	5.00	101.6	0.7
	7.50	99.2	1.0
	10.00	100.3	0.5
Magnesium	0.25	101.9	1.6
	0.50	99.0	0.4
	1.00	101.7	1.1
	1.50	100.4	0.2
	2.00	100.8	1.4
Calcium	0.25	100.1	0.7
	0.50	101.5	1.3
	1.00	99.3	0.6
	1.50	99.8	1.0
	2.00	100.9	0.2

Table D.6 (continued).

D-3.2.d Matrix effect

As explained in section D-2.3.f, the ME are evaluated using ten human urine samples spiked with various analytes, with the objective of evidencing any suppression or enhancement of their signals. A typical example for a human urine sample spiked with commercial urea is presented Figure D.6-a. The y-shift shows the presence of urea initially contained in the human urine sample. As illustrated in Figure D.6-b, the analyte concentration in the urine matrix can be obtained by applying the standard addition method. The same study was performed for all analytes and the results are reported in Table D.7. As described in Eq. D.6, the comparison of the peak areas indicates any significant matrix effect.

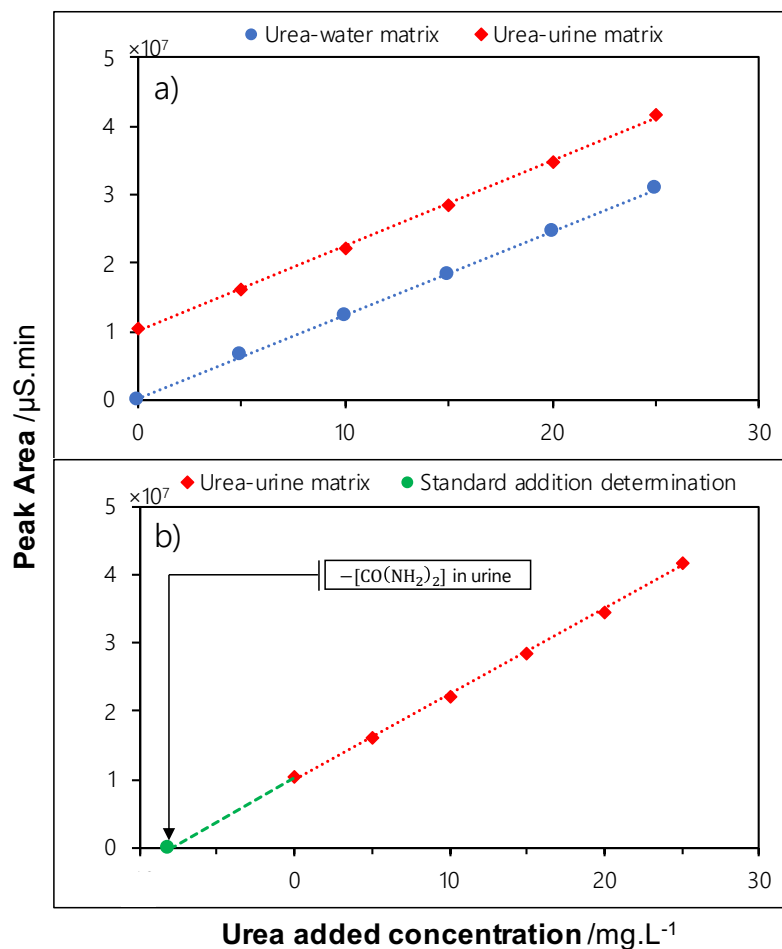


Fig. D.6 – a) Variation of the urea MS signal magnitude with the urea added concentration, into water or into human urine and b) illustrative example of the application of the standard addition method for the determination of the urea concentration in a human urine sample.

Sample	<i>Organic molecules</i>															
	Lactic acid		Hippuric acid		Citric acid		Uric acid		Oxalic acid		Urea		Creatine		Creatinine	
	Mean value (%)	SD (%)	Mean value (%)	SD (%)	Mean value (%)	SD (%)	Mean value (%)	SD (%)	Mean value (%)	SD (%)	Mean value (%)	SD (%)	Mean value (%)	SD (%)	Mean value (%)	SD (%)
#1	97.4	1.7	108.1	8.3	98.7	2.7	97.2	1.5	100.8	4.9	96.7	3.6	94.8	4.8	103.9	7.9
#2	102.6	9.6	104.7	3.1	101.5	7.6	101.8	6.2	101.9	7.5	108.2	10.1	106.3	9.3	99.5	6.5
#3	99.1	5.4	98.7	6.8	97.9	1.9	99.5	4.7	107.8	0.4	91.5	1.9	103.2	8.2	101.6	8.6
#4	104.2	4.1	103.5	2.9	99.6	5.3	96.7	0.6	97.6	8.7	104.3	7.3	97.7	2.7	104.8	9.8
#5	101.3	7.2	106.9	10.5	100.2	8.1	100.3	5.3	103.8	5.9	99.8	5.8	95.6	3.6	96.2	3.2
#6	105.7	3.5	99.5	0.8	102.1	4.2	102.1	2.4	98.3	9.2	100.1	8.4	110.9	7.9	98.3	4.3
#7	106.2	2.6	102.1	6.1	97.4	0.6	98.4	3.9	104.9	8.9	92.5	2.5	109.1	10.1	110.0	11.0
#8	100.1	9.9	107.3	4.5	100.9	6.9	101.0	6.7	102.4	1.3	109.3	9.3	99.2	5.2	92.7	2.7
#9	98.6	10.3	101.7	3.8	101.7	3.5	96.9	4.0	108.3	7.1	97.4	4.4	105.4	6.4	105.1	5.1
#10	103.1	0.6	100.3	5.2	100.4	7.3	100.7	6.5	97.9	2.1	102.6	6.2	90.8	0.8	110.4	6.4

Table D.7 – Matrix effects of the analytes introduced into a human urine sample ($n = 3$).

Sample	<i>Ionic compounds</i>															
	Chloride		Sulfate		Phosphate		Sodium		Ammonium		Potassium		Magnesium		Calcium	
	Mean value (%)	SD (%)	Mean value (%)	SD (%)	Mean value (%)	SD (%)	Mean value (%)	SD (%)	Mean value (%)	SD (%)	Mean value (%)	SD (%)	Mean value (%)	SD (%)	Mean value (%)	SD (%)
#1	95.1	3.1	98.8	6.8	93.4	2.4	98.1	6.1	97.3	4.3	98.6	5.6	97.8	8.3	101.3	3.5
#2	108.6	10.6	96.5	3.5	102.3	7.3	104.0	9.0	100.7	7.7	102.5	7.5	96.1	2.7	93.7	8.2
#3	94.7	4.7	104.1	9.1	100.8	6.8	111.5	8.5	102.8	9.8	100.2	6.2	105.3	5.0	99.0	6.9
#4	106.9	9.9	101.7	8.7	97.2	4.2	93.9	2.9	94.4	3.4	93.1	1.1	100.5	10.1	108.1	2.3
#5	99.3	6.3	95.9	2.9	110.0	11.0	107.6	10.6	103.1	8.1	106.1	9.1	109.2	9.2	104.2	7.1
#6	101.2	8.2	107.4	10.4	96.9	3.9	95.2	3.2	108.9	10.9	95.8	3.8	98.0	3.3	96.3	10.8
#7	109.8	10.8	93.6	1.6	105.7	9.7	109.7	11.7	95.5	2.5	108.4	10.4	94.9	4.0	95.0	4.6
#8	90.6	0.6	102.9	7.9	104.6	8.6	92.1	1.1	99.9	5.9	114.7	8.7	92.8	11.0	110.0	0.9
#9	97.9	2.9	109.5	11.5	99.1	5.1	106.8	9.8	91.1	0.1	99.6	5.6	101.9	1.6	92.6	9.4
#10	104.5	7.5	100.0	5.0	91.8	1.8	90.3	0.3	105.0	6.0	91.4	0.4	97.8	6.1	97.1	5.7

Table D.7 (continued).

D-3.3 Analysis of human urine samples

Ten human urine samples obtained from healthy volunteers have been analyzed using the proposed method, and the quantitative results are reported in Table D.8. The thirteen analytes, present in all samples, are quantified at a concentration within the linear ranges of their calibration curves.

Sample	<i>Organic molecules</i>															
	Lactic acid		Hippuric acid		Citric acid		Uric acid		Oxalic acid		Urea		Creatine		Creatinine	
	Mean value (%)	SD (%)	Mean value (%)	SD (%)	Mean value (%)	SD (%)	Mean value (%)	SD (%)	Mean value (%)	SD (%)	Mean value (%)	SD (%)	Mean value (%)	SD (%)	Mean value (%)	SD (%)
#1	1.62×10^{-2}	0.17	0.78	0.18	0.92	0.60	0,92	0,60	3.16×10^{-2}	2.81	20.37	0.22	0.16	2.80	3.01	0.47
#2	7.17×10^{-3}	0.64	0.42	0.19	0.81	3.38	0,81	3,38	4.12×10^{-2}	0.75	21.34	0.62	1.59	0.35	3.85	0.77
#3	9.67×10^{-3}	2.38	0.09	0.26	0.52	0.21	0,52	0,21	LOD	-	7.79	2.78	0.14	1.94	1.00	3.38
#4	4.25×10^{-3}	2.16	0.19	0.17	0.33	0.83	0,33	0,83	LOD	-	6.20	2.33	<LOD	-	0.72	1.38
#5	1.50×10^{-2}	0.21	0.61	0.57	0.78	1.42	0,78	1,42	5.11×10^{-2}	1.74	9.65	1.50	0.05	3.63	2.24	1.07
#6	LOD	-	0.16	2.24	0.59	0.93	0,59	0,93	3.73×10^{-3}	2.38	11.55	0.13	17.54	0.52	0.91	1.75
#7	3.46×10^{-3}	0.53	0.14	2.23	0.38	1.46	0,38	1,46	3.75×10^{-4}	1.18	5.84	0.99	<LOD	-	0.86	0.76
#8	5.53×10^{-2}	0.02	0.46	0.21	0.77	1.42	0,77	1,42	1.37×10^{-2}	0.06	15.56	0.09	0.65	0.71	1.58	1.81
#9	3.37×10^{-2}	0.38	0.61	0.46	0.72	0.38	0,72	0,38	2.17×10^{-2}	0.10	14.48	1.00	1.73	0.64	2.21	0.26
#10	1.72×10^{-2}	0.54	0.19	0.18	0.93	0.59	0,93	0,59	4.43×10^{-2}	0.20	23.14	1.93	6.88	0.67	1.37	0.11

Table D.8 – Matrix effects of the analytes introduced into a human urine sample ($n = 3$).

Sample	<i>Ionic compounds</i>															
	Chloride		Sulfate		Phosphate		Sodium		Ammonium		Potassium		Magnesium		Calcium	
	Mean value (%)	SD (%)	Mean value (%)	SD (%)	Mean value (%)	SD (%)	Mean value (%)	SD (%)	Mean value (%)	SD (%)	Mean value (%)	SD (%)	Mean value (%)	SD (%)	Mean value (%)	SD (%)
#1	3.37	0.42	1.31	1.01	2.70	0.76	0.32	0.51	0.73	3.86	4.13	1.07	0.08	0.10	0.19	0.61
#2	4.97	0.07	1.42	0.62	4.87	0.11	0.61	0.73	0.51	3.83	4.15	0.73	0.14	1.85	0.08	1.92
#3	3.16	0.11	0.38	2.31	0.44	2.35	0.24	0.14	0.10	2.34	2.98	0.65	0.03	0.25	0.05	1.76
#4	1.51	0.23	0.38	1.17	0.78	1.31	0.09	0.18	0.15	1.51	2.38	1.28	0.04	2.38	LOD	-
#5	5.85	0.06	0.75	1.18	1.29	0.79	0.34	0.75	0.83	0.94	4.23	0.78	0.05	3.61	LOD	-
#6	2.67	0.01	1.07	1.64	0.48	2.14	0.26	0.34	0.16	1.42	2.58	0.64	0.05	1.55	0.10	0.17
#7	2.60	0.14	0.25	1.74	0.25	1.22	0.16	0.42	0.20	0.00	2.80	0.49	0.03	2.86	0.05	1.60
#8	5.49	0.13	1.06	0.41	1.15	0.89	0.67	0.83	0.38	0.63	1.68	0.33	0.16	3.67	0.26	1.24
#9	2.53	0.42	1.16	0.38	2.23	0.46	0.28	0.32	0.64	0.39	2.60	1.07	0.10	1.72	0.09	3.42
#10	3.39	0.10	1.68	0.26	3.84	0.27	0.49	0.67	0.63	1.59	2.58	0.97	0.13	0.07	0.12	1.34

Table D.8 (continued).

D-4 Discussions

To the best of the authors' knowledge, the analytical technique described above (*i.e.*, IC-CD/MS) is applied for the first time for simultaneously determining major compounds in urine. This allows a double analysis and direct dilute-and-shoot approach in 35 min without sample preparation. The validation results demonstrate the reliability of this method for the simultaneous quantification of lactic acid, hippuric acid, citric acid, uric acid, oxalic acid, urea, creatine, creatinine and ions in human urine samples (with a precision within 4.0%, accuracy ranging from 0.1% to 5% and recovery rates varying from 94.9% to 102.6%). Both external calibration and standard-addition approaches enable the quantification of the analyte. Following this procedure, the proposed method provides satisfactory quantitative results (compared to the literature's values presented in D.9), without the need for expensive isotope-labelled compounds [304], thereby supporting its applicability to daily testing of human urine samples. The difference in values can be attributed to different lifestyle practices (such as eating habits, sleep, sex, sports practices, etc.).

According to various studies [190, 303, 304], the identification and characterization of a human urine solution can be performed by evaluating some concentration ratio according to the two following coefficients K_1 and K_2 :

$$K_1 = 20 \times \frac{[\text{Uric acid}]}{[\text{Urea eq nitrogen}]}$$

$$K_2 = \frac{[\text{Uric acid}]}{[\text{Creatinine}]}$$

where concentrations are given g L^{-1} .

These two factors have been evaluated and reported in the Table D.10. Sakurai et al. [190] reported values of K_1 ranging from 0.69 to 2.25, which are consistent with those obtained in this study, ranging from 1.63 to 3.45. As for K_2 , Kwon et al. [290] and Sakurai et al. [190] reported values ranging from 0.28 to 0.66, similar to those obtained in this study (from 0.21 to 0.68). However, the pioneering technique of ion chromatography coupled with mass spectroscopy allows efficient characterization of the more significant analytes contained in human urine.

Analyte	Converted literature values		Ref.
	(g L ⁻¹)		
<i>Organic molecules</i>			
Urea	13.67 ± 2.67		
Uric acid	0.31		
Creatine	0.06		
Creatinine	1.14 ± 0.04		[58]
Citric acid	0.46 ± 0.24		
Lactic acid	0.01		
Hippuric acid	0.46		
Oxalic acid	0.01 – 0.03		
<i>Ionic compounds</i>			
Chloride	5.19 ± 3.18		
Ammonium	0.51 ± 0.16		[58]
Potassium	2.32		
Sodium	0.46		[305]
Sulfate	1.12		[306]
Phosphate	3.01		[307]
Magnesium	0.07 ± 0.02		[58]
Calcium	0.12 ± 0.04		

Table D.9 – Literature values of identified compound concentrations in human urine.

Sample	K ₁		K ₂	
	Value	SD	Value	SD
#1	1.94	0.02	0.31	0.01
#2	1.63	0.05	0.21	0.01
#3	2.85	0.09	0.52	0.02
#4	2.30	0.07	0.46	0.01
#5	3.45	0.01	0.35	0.01
#6	2.20	0.02	0.66	0.02
#7	2.76	0.01	0.44	0.01
#8	2.13	0.03	0.49	0.01
#9	2.12	0.01	0.32	0.03
#10	1.72	0.02	0.68	0.02

Table D.10 – Results in terms of K₁ and K₂ determined for 10 samples expecting the validation of the method ($n = 3$).

D-5 Conclusions

This appendix investigated a new IC-CD/MS method for the simultaneous quantification of the 8 main organic molecules (biomarkers) and 8 ions naturally present in human urine, in two runs and within 35 min. Chromatographic separation was performed using ion-exchange columns coupled to a mass spectroscopy detector. Quantitative concentration values were obtained using the external standard method without requiring the use of expensive isotope-labeled compounds. The results were validated according to ICH guidelines (through selectivity, sensitivity, linearity, accuracy, and precision) and showed that the proposed method provided quantitative values with precision and accuracy higher than 95%. Furthermore, no matrix effects were observed. In the future, the proposed method could be thus used as a basic technique in any analytical field.

D-6 Ethical approval

This is an observational study. No ethical approval was needed for the study. Before gathering any information, we ensured to obtain written approvals from each participant with notice of information and consent form. All procedures performed in studies involving human participants were in accordance with the ethical standards of the institutional and/or national research committee and with the 1964 Helsinki Declaration and its later amendments. This study was conducted with healthy individuals aged 18 and above, who had no previous record of kidney-related ailments. The study excluded those who were currently suffering from a urinary tract infection. Furthermore, female participants were instructed to undertake the test on non-menstrual days.

Repeatability of the measurements of the initial rate, r_{χ}^0 , as a function of time chosen to calculate the initial rate from the curve $pH(t)$

To ensure reliable and accurate measurements, the influence of the sampling time on the initial rate was studied. Table E.1 reports the different measures of the initial rate, noted r_{χ}^0 , obtained for five reactant (urea and OH^-) concentrations and sampling times varying from 5 to 50 seconds. The RSD was calculated from each averaged value of r_{χ}^0 . This criterion allows identifying which sampling time was the best choice for determining r_{χ}^0 . From these findings, a sampling time of 10 seconds was chosen for calculating all the initial reaction rates.

Sampling time (s)		Experiment 1		Experiment 2		Experiment 3		Experiment 4		Experiment 5	
		Trial 1	Trial 2	Trial 1	Trial 2	Trial 1	Trial 2	Trial 1	Trial 2	Trial 1	Trial 2
5	r_{χ}^0 (mol L ⁻¹ s ⁻¹)	1.23×10 ⁻⁵	1.40×10 ⁻⁵	1.57×10 ⁻⁵	1.64×10 ⁻⁵	2.11×10 ⁻⁵	1.67×10 ⁻⁵	2.32×10 ⁻⁵	1.98×10 ⁻⁵	2.01×10 ⁻⁵	2.01×10 ⁻⁵
	Average	1.31×10 ⁻⁵		1.61×10 ⁻⁵		1.89×10 ⁻⁵		2.15×10 ⁻⁵		2.01×10 ⁻⁵	
	Standard deviation (SD, mol L ⁻¹ s ⁻¹)	1.18×10 ⁻⁶		4.97×10 ⁻⁷		3.12×10 ⁻⁶		2.39×10 ⁻⁶		4.11×10 ⁻⁸	
	RSD	9%		3%		17%		11%		0 %	
10	r_{χ}^0 (mol L ⁻¹ s ⁻¹)	1.22×10 ⁻⁵	1.38×10 ⁻⁵	1.55×10 ⁻⁵	1.62×10 ⁻⁵	2.08×10 ⁻⁵	1.66×10 ⁻⁵	2.29×10 ⁻⁵	1.96×10 ⁻⁵	2.01×10 ⁻⁵	2.03×10 ⁻⁵
	Average	1.30×10 ⁻⁵		1.59×10 ⁻⁵		1.87×10 ⁻⁵		2.13×10 ⁻⁵		2.02×10 ⁻⁵	
	SD (mol L ⁻¹ s ⁻¹)	1.15×10 ⁻⁶		5.02×10 ⁻⁷		3.03×10 ⁻⁶		2.32×10 ⁻⁶		1.84×10 ⁻⁷	
	RSD	9%		3%		16%		11%		1 %	
25	r_{χ}^0 (mol L ⁻¹ s ⁻¹)	1.18×10 ⁻⁵	1.33×10 ⁻⁵	1.50×10 ⁻⁵	1.57×10 ⁻⁵	2.01×10 ⁻⁵	1.62×10 ⁻⁵	2.22×10 ⁻⁵	1.92×10 ⁻⁵	2.00×10 ⁻⁵	2.11×10 ⁻⁵
	Average	1.25×10 ⁻⁵		1.54×10 ⁻⁵		1.81×10 ⁻⁵		2.07×10 ⁻⁵		2.05×10 ⁻⁵	
	SD (mol L ⁻¹ s ⁻¹)	1.08×10 ⁻⁶		4.65×10 ⁻⁷		2.76×10 ⁻⁶		2.11×10 ⁻⁶		8.40×10 ⁻⁷	
	RSD	9%		3%		15%		10%		4%	
50	r_{χ}^0 (mol L ⁻¹ s ⁻¹)	1.12×10 ⁻⁵	1.25×10 ⁻⁵	1.43×10 ⁻⁵	1.50×10 ⁻⁵	1.89×10 ⁻⁵	1.56×10 ⁻⁵	2.12×10 ⁻⁵	1.86×10 ⁻⁵	1.97×10 ⁻⁵	2.24×10 ⁻⁵
	Average	1.18×10 ⁻⁵		1.46×10 ⁻⁵		1.73×10 ⁻⁵		1.99×10 ⁻⁵		2.11×10 ⁻⁵	
	SD (mol L ⁻¹ s ⁻¹)	9.67×10 ⁻⁷		4.74×10 ⁻⁷		2.35×10 ⁻⁶		1.82×10 ⁻⁶		1.87×10 ⁻⁶	
	RSD	8%		3%		14%		9%		9%	
	Average global	1.26×10 ⁻⁵		1.55×10 ⁻⁵		1.83×10 ⁻⁵		2.08×10 ⁻⁵		2.05×10 ⁻⁵	
	SD global (mol L ⁻¹ s ⁻¹)	5.70×10 ⁻⁷		6.43×10 ⁻⁷		7.39×10 ⁻⁷		7.14×10 ⁻⁷		4.32×10 ⁻⁷	
	RSD global	5 %		4%		4%		3%		2%	

Table E.1 – Influence of the sampling on the repeatability of the initial reaction rate r_{χ}^0 .

Model resolution

1. Initialization

- define all the partial reactional orders, $\alpha_{E\chi}$, $\beta_{E\chi}$, $\gamma_{E\chi}$, the kinetic constant, $k_{E\chi}$, the tortuosity, τ , and the porosity, ω , of the electrocatalytic layer domain Ω_{EC} , the diffusivity coefficient of urea, $D_{urea,w}$, and the cell volume, V ;
- set the initial concentrations of soluble components in each subdomain: $[\text{OH}^-]_{\forall z,t=0}$ and $[\text{CO}(\text{NH}_2)_2]_{\forall z,t=0}$;
- set the geometrical surface, $S_{elec}^{geometric}$, and the rugosity of the electrode, Sdr . The Sdr parameter can be considered as the ratio between the area of the ‘real’ developed surface and the area of the ‘projected’ surface. In our case, the Sdr is measured by a 3D optical profiler (S-Neox, Sensofar, Spain) and equal to 1.09%.
- calculate the real electrode surface S_{elec} according to Eq. F.1;

$$S_{elec} = S_{elec}^{geometric} \times Sdr \quad (\text{F.1})$$

- calculate the kinetic apparent constant, k_{app} ;
- calculate the effective diffusivity coefficient of urea, $D_{urea,w}^{eff}$, into the Ω_{EC} domain;
- set the time $t = 0$ and the time step size $\tau_n = 1 \text{ s}$;
- set the size and shape of computational sub-domains, Ω_B , Ω_F and Ω_{EC} ;
- initialize all the model fluxes to 0;
- calculate the dimensionless Biot number, Bi defined in Eq. IV.30.

2. Time stepping (pseudo-steady state)

do

Time step n at time τ_n .

- (a) Dynamics of urea concentration in the electrocatalytic layer Ω_{EC} (steady state)

- i. Calculate dimensionless Hatta number

The Hatta number, defined as Eq. F.2, allows to describe the competition, in the Ω_{EC} domain, between the chemical kinetics and the effective diffusion inside the porous solid. Depending on this number, either a chemical or

diffusional regime takes place.

$$\text{Ha} = \sqrt{\frac{k_{\text{app}} \times \mu^2}{D_{\text{urea,w}}^{\text{eff}} \times [\text{CO}(\text{NH}_2)_2]^{0.7}}} \quad (\text{F.2})$$

ii. Solve mass balance

- Solve for urea concentration $[\text{CO}(\text{NH}_2)_2]_{\delta \leq z \leq \delta + \mu, t_n + \tau_n}$, the ODE system according to Eq. F.3.

$$\frac{\partial^2 [\text{CO}(\text{NH}_2)_2]}{\partial x^2} - \text{Ha}^2 \times [\text{CO}(\text{NH}_2)_2]^{0.3} = 0 \quad (\text{F.3})$$

from t_n to $t_n + \tau_n$.

A shooting method for boundary value problems of ODE system was used for stable and accurate integration between t_n and $t_n + \tau_n$. The method consisted in testing different fluxes in $z = \delta$ so as to minimize a target function defined in $z = \delta + \mu$ as a Neumann condition ($\left. \frac{\partial [\text{CO}(\text{NH}_2)_2]}{\partial z} \right|_{z=\Lambda_E} = 0$).

(b) Dynamics of urea concentration in the liquid film layer Ω_F (steady state)

- i. Scaling the diffusion flux by the respective mass transport characteristics to the studied area according to Eq. F.4.

$$\text{Biot} \times \left. \frac{\partial [\text{CO}(\text{NH}_2)_2]}{\partial z} \right|_{z=\Lambda_{\text{FEC}}}^{\Omega_F} = \left. \frac{\partial [\text{CO}(\text{NH}_2)_2]}{\partial z} \right|_{z=\Lambda_{\text{FEC}}}^{\Omega_{\text{EC}}} \quad (\text{F.4})$$

ii. Solve mass balance

- Solve for urea concentration $[\text{CO}(\text{NH}_2)_2]_{0 \leq z \leq \delta, t_n + \tau_n}$ the Eq. F.5.

$$\frac{\partial^2 [\text{CO}(\text{NH}_2)_2]}{\partial x^2} = 0 \quad (\text{F.5})$$

(c) Dynamics of urea concentration in the bulk Ω_B (transient state)

i. Solve mass balance:

- Solve for urea concentration $[\text{CO}(\text{NH}_2)_2]_{z \leq 0, t_n + \tau_n}$ according to the Eq. F.6.

$$V^{\text{bulk}} \times \frac{\partial [\text{CO}(\text{NH}_2)_2]_{z \leq 0}}{\partial t} + D_{\text{urea,w}} \times S_{\text{electrode}} \times \left. \frac{\partial [\text{CO}(\text{NH}_2)_2]}{\partial z} \right|_{z=\Lambda_{\text{BF}}}^{\Omega_F} = 0 \quad (\text{F.6})$$

- Solve for urea concentration $[\text{CO}(\text{NH}_2)_2]_{z=\delta, t_n + \tau_n}$ according to the Eq. F.7.

$$[\text{CO}(\text{NH}_2)_2]_{z=\delta} = [\text{CO}(\text{NH}_2)_2]_{z=0} + \delta \times \left. \frac{\partial [\text{CO}(\text{NH}_2)_2]}{\partial z} \right|_{z=\Lambda_{\text{BF}}}^{\Omega_F} \quad (\text{F.7})$$

ICP-OES experimental details

In **Chapter V**, section **V-1.1.b.ii**, some ICP-OES measurements (HORIBA Ultima 2) with a nitrogen purging were performed to characterize the precipitate formed once human urine was alkalinized.

The sample was nebulized into Ar plasma, specifically Ultra High Purity 4.5 Grade argon with 99.999% purity, via a concentric pneumatic nebulizer paired with a cyclonic spray chamber. The operating guidelines recommended by the manufacturer were strictly adhered to an auxiliary gas flow of 0.2 L per minute (except for alkali compounds, Na and K, where 0.5 L per minute is used), a nebulizer gas flow of 0.6 L per minute, and a radiofrequency power of 1.2 kW. Special care was taken in choosing wavelength to reduce disruption. For S: 181.978 nm, P: 213.618 nm, Mg: 285.213 nm, Ca: 396.847 nm, Na: 589.592 nm and K: 769.896 nm were used. Calibration curves are illustrated in Figure **G.1** and presented in Eqs. **G.1-G.6**.

$$\text{Peak area}_{\text{Ca}} = 3.02 \times 10^6 \times [\text{Ca}] + 6.29 \times 10^5 \text{ with } R^2 = 0.999 \quad (\text{G.1})$$

$$\text{Peak area}_{\text{K}} = 3.67 \times 10^4 \times [\text{K}] - 3.10 \times 10^4 \text{ with } R^2 = 0.997 \quad (\text{G.2})$$

$$\text{Peak area}_{\text{Mg}} = 3.32 \times 10^5 \times [\text{Mg}] + 1.28 \times 10^4 \text{ with } R^2 = 0.999 \quad (\text{G.3})$$

$$\text{Peak area}_{\text{Na}} = 3.80 \times 10^4 \times [\text{Na}] - 1.69 \times 10^4 \text{ with } R^2 = 0.997 \quad (\text{G.4})$$

$$\text{Peak area}_{\text{P}} = 3.71 \times 10^4 \times [\text{P}] - 5.92 \times 10^2 \text{ with } R^2 = 0.999 \quad (\text{G.5})$$

$$\text{Peak area}_{\text{S}} = 2.14 \times 10^4 \times [\text{S}] + 2.07 \times 10^3 \text{ with } R^2 = 0.999 \quad (\text{G.6})$$

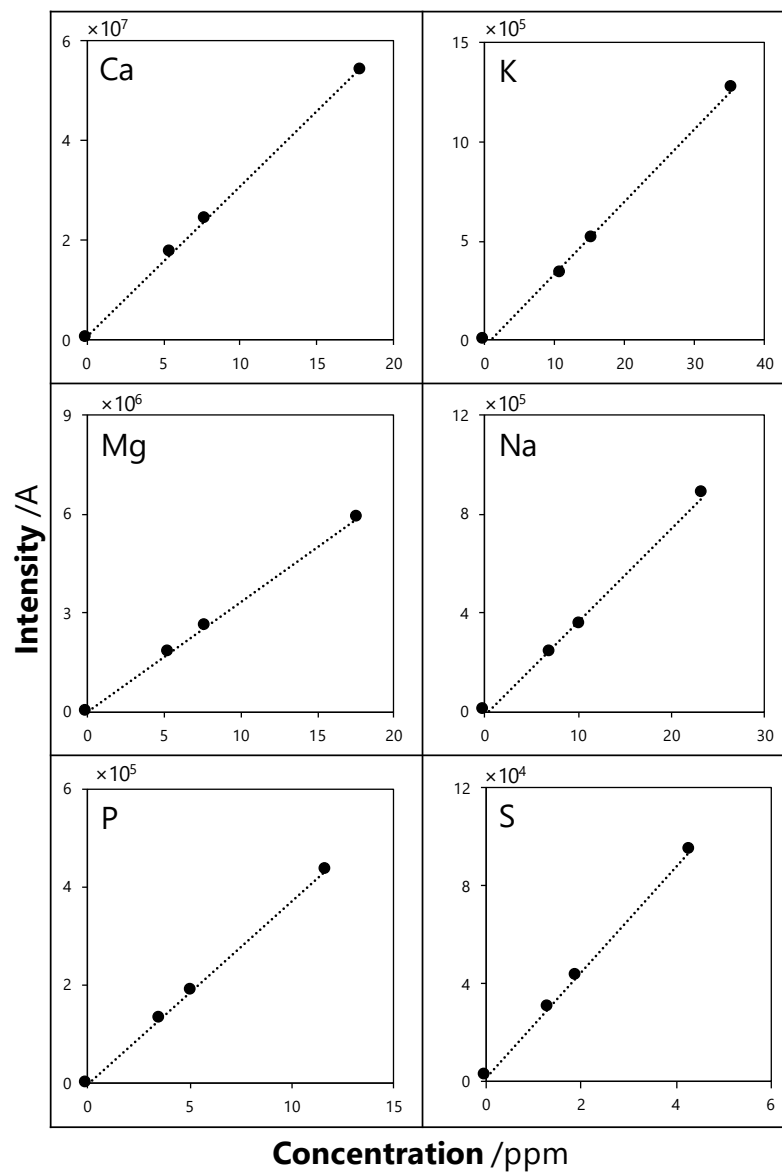


Fig. G.1 – ICP-OES calibration curves.

Raw data of complete mass balance during urea and urine electrolysis

These raw data are presented in the **Chapter V** in the section **V-1.1**. Table **H.1** shows the raw data obtained when determining the quantities of reagents and products during the chronoamperometric electrolysis of a 50 h urea solution. Table **H.2** shows the raw data obtained when determining the quantities of reagents and products during the chronoamperometric electrolysis of a 48 h human urine solution. Table **H.3** shows the raw data obtained when determining the quantities of C- reagents and products during the chronoamperometric electrolysis of a 48 h human urine solution.

Time (h)	Charge (C)	CO(NH ₂) ₂	OCN ⁻	CO ₃ ²⁻	NO ₂ ⁻ (mol)	NH ₄ ⁺	N ₂	Σ
0	0	1.97×10 ⁻²	/	6.00×10 ⁻⁴	/	/	/	2.03×10 ⁻²
2	1080	1.70×10 ⁻²	9.89×10 ⁻⁴	1.80×10 ⁻³	5.44×10 ⁻⁴	2.30×10 ⁻³	1.56×10 ⁻³	2.42×10 ⁻²
9	2500	1.32×10 ⁻²	2.47×10 ⁻³	4.20×10 ⁻³	1.63×10 ⁻³	6.89×10 ⁻³	2.23×10 ⁻³	3.06×10 ⁻²
18	3500	9.75×10 ⁻³	3.95×10 ⁻³	6.60×10 ⁻³	2.12×10 ⁻³	1.15×10 ⁻²	2.59×10 ⁻³	3.65×10 ⁻²
28	4200	7.22×10 ⁻³	5.44×10 ⁻³	7.20×10 ⁻³	2.61×10 ⁻³	1.38×10 ⁻²	2.81×10 ⁻³	3.91×10 ⁻²
43	5000	4.77×10 ⁻³	6.43×10 ⁻³	9.00×10 ⁻³	2.88×10 ⁻³	1.61×10 ⁻²	4.02×10 ⁻³	4.32×10 ⁻²
50	5400	3.96×10 ⁻³	6.92×10 ⁻³	9.60×10 ⁻³	3.16×10 ⁻³	1.70×10 ⁻²	4.46×10 ⁻³	4.51×10 ⁻²

Table H.1 – Molar quantities of reagents and products during electrolysis of urea synthetic solution.

pH	Time (h)	Charge (C)	CO(NH ₂) ₂	OCN ⁻	NO ₂ ⁻	NH ₄ ⁺ (mol)	N ₂	FA	OA	Σ
6.2	0	/	1.49×10 ⁻²	/	/	1.07 × 10 ⁻³	/	/	4.22×10 ⁻⁵	1.60×10 ⁻²
	0	/	1.40 × 10 ⁻²	/	/	1.52 × 10 ⁻³	/	9.56 × 10 ⁻⁵	5.11 × 10 ⁻⁵	1.57 × 10 ⁻²
14	5	740	1.40×10 ⁻²	2.21×10 ⁻⁴	3.59×10 ⁻⁴	1.33×10 ⁻³	1.56×10 ⁻³	7.04×10 ⁻⁴	2.71×10 ⁻⁴	1.85×10 ⁻²
	8	1230	1.39×10 ⁻²	6.48×10 ⁻⁴	7.02×10 ⁻⁴	1.25×10 ⁻³	2.23×10 ⁻³	8.96×10 ⁻⁴	3.42×10 ⁻⁴	2.00×10 ⁻²
	23	2628	1.30×10 ⁻²	1.39×10 ⁻³	1.33×10 ⁻³	9.33×10 ⁻⁴	2.59×10 ⁻³	1.89×10 ⁻³	6.20×10 ⁻⁴	2.18×10 ⁻²
	30	3256	1.18×10 ⁻²	1.75×10 ⁻³	1.58×10 ⁻³	9.00×10 ⁻⁴	2.81×10 ⁻³	2.21×10 ⁻³	8.33×10 ⁻⁴	2.19×10 ⁻²
	48	4508	1.12×10 ⁻²	2.48×10 ⁻³	2.18×10 ⁻³	8.50×10 ⁻⁴	4.02×10 ⁻³	3.20×10 ⁻³	1.06×10 ⁻³	2.49×10 ⁻²

Table H.2 – Molar quantities of reagents and products during electrolysis of human urine.

pH	Time (h)	Charge (C)	TOC	CO(NH ₂) ₂	OCN ⁻ (mol)	FA	OA	Σ
6.2	0	/	7.12	2.99	/	/	0.02	3.00
	0	/	6.61	2.80	/	0.02	0.02	2.84
14	5	740	6.15	2.81	0.04	0.14	0.11	3.10
	8	1230	5.78	2.79	0.13	0.18	0.14	3.23
	23	2628	6.00	2.60	0.28	0.38	0.25	3.50
	30	3256	5.50	2.37	0.35	0.44	0.33	3.49
	48	4508	5.39	2.23	0.50	0.64	0.42	3.79

Table H.3 – Carbonaceous species concentrations during electrolysis of human urine.

Linear voltammetry of main compounds in human urine in various matrices

These raw data are presented in the **Chapter V** in the section **V-1.2.b**. The curves presented in this appendix were obtained in linear voltammetry, during different spiking of the main organic molecules and ions contained in human urine in 3 different matrices: *(i)* KOH (Figure **I.1**), *(ii)* urea/KOH (Figure **I.2**) and *(iii)* alkalized urine (Figure **I.3**).

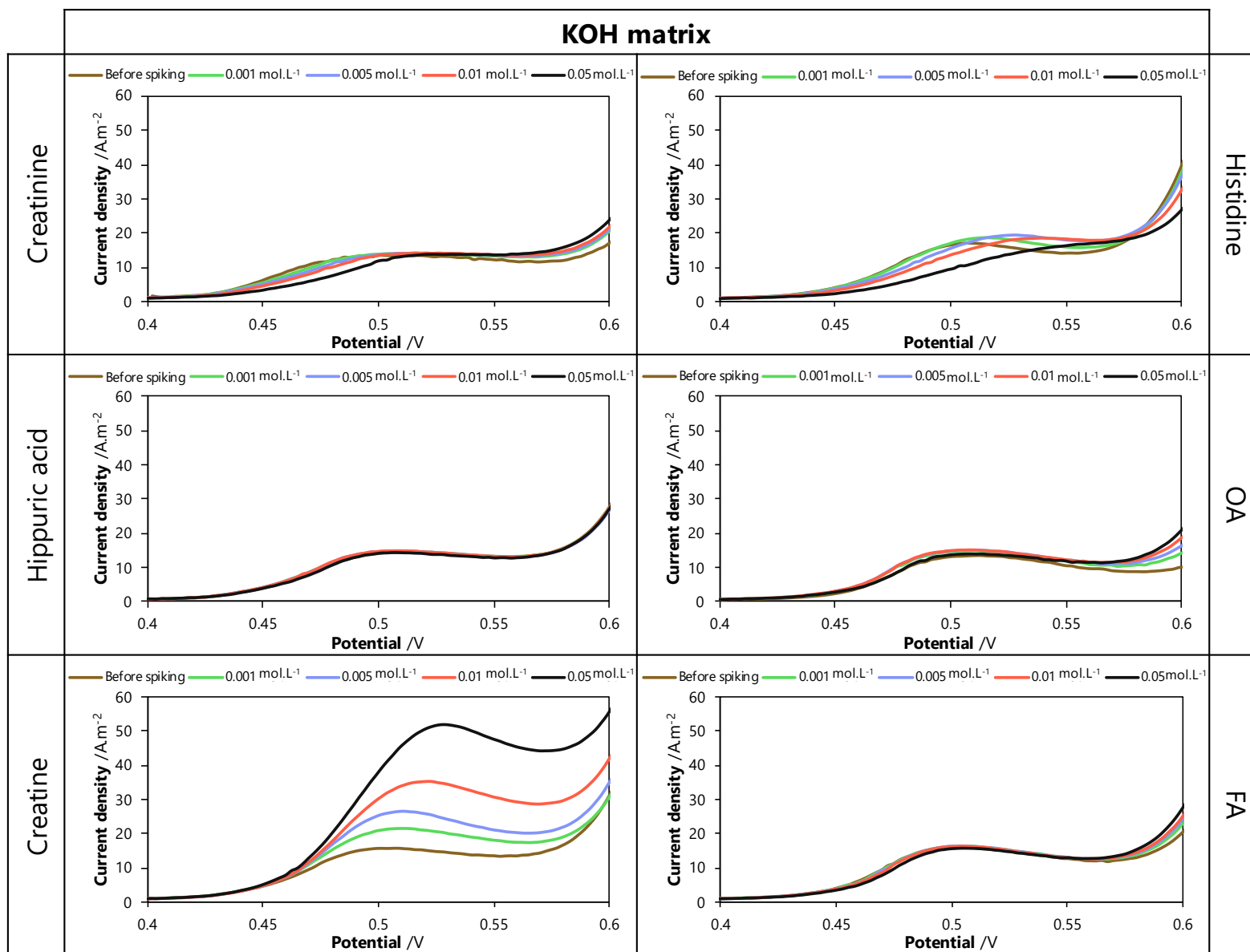


Fig. I.1 – $I=f(E)$ curves obtained by spiking various compounds, mainly present in human urine, into a KOH matrix.

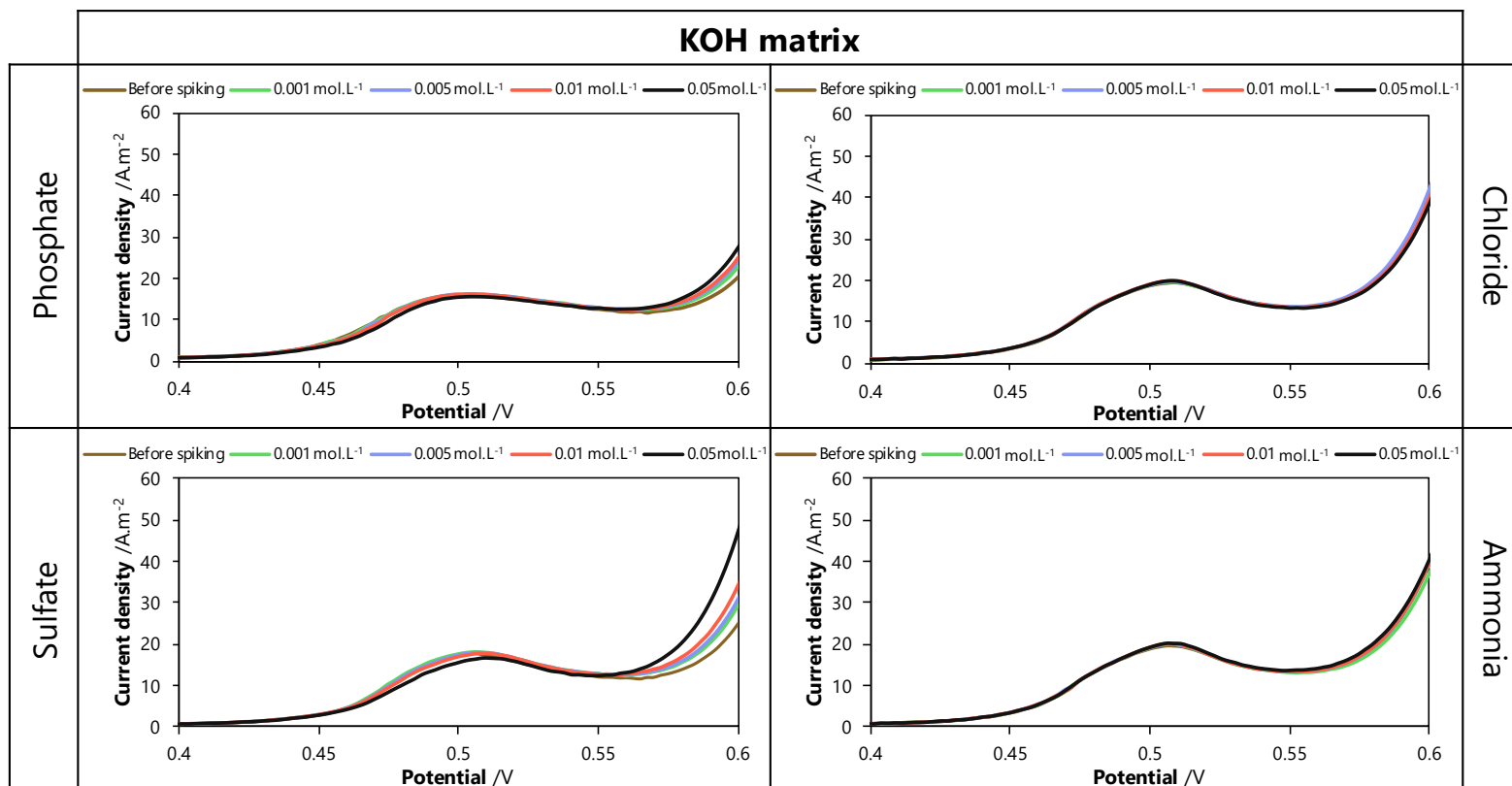


Figure I.1 (continued).

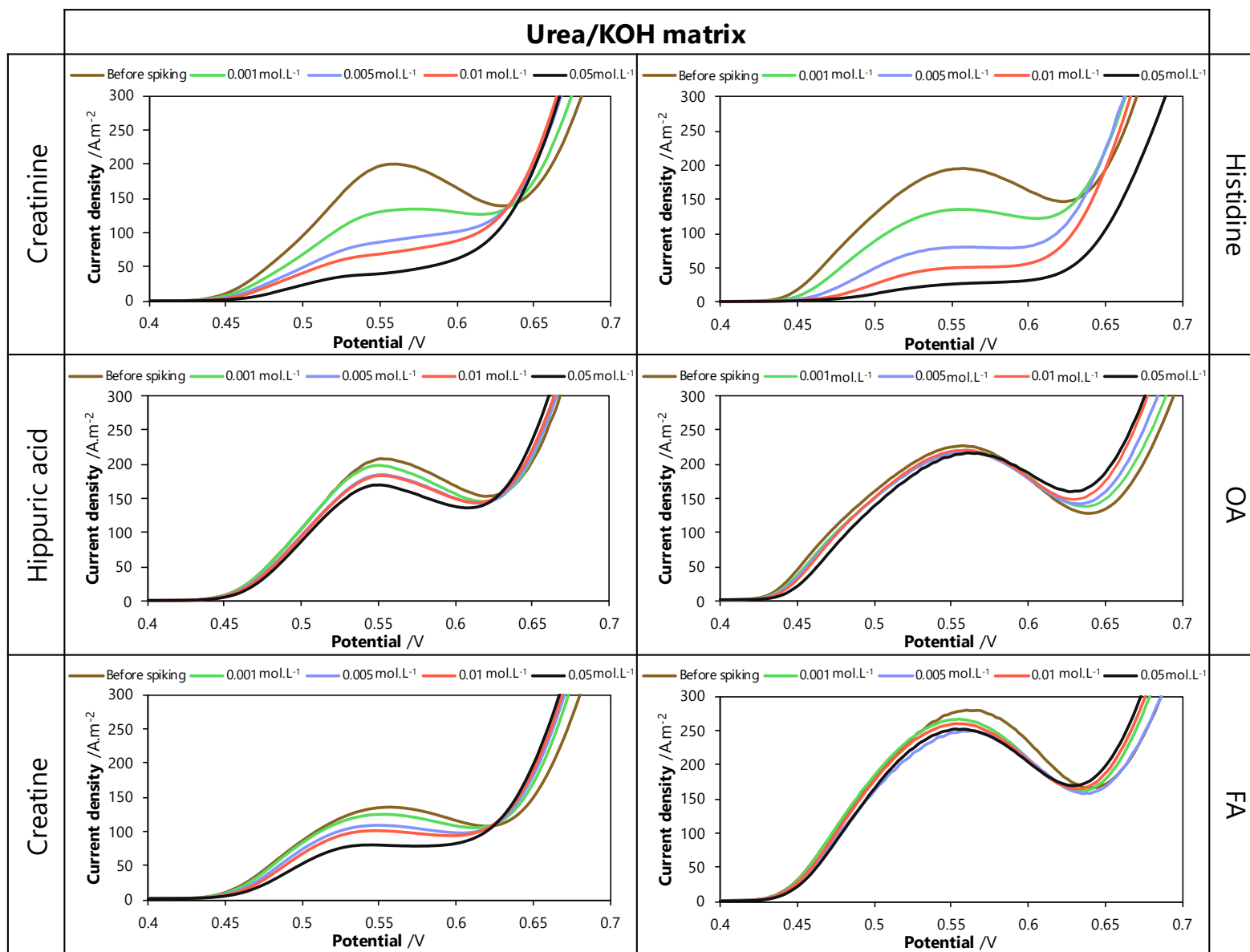


Fig. I.2 – $I=f(E)$ curves obtained by spiking various organic molecules, mainly present in human urine, into a urea/KOH matrix.

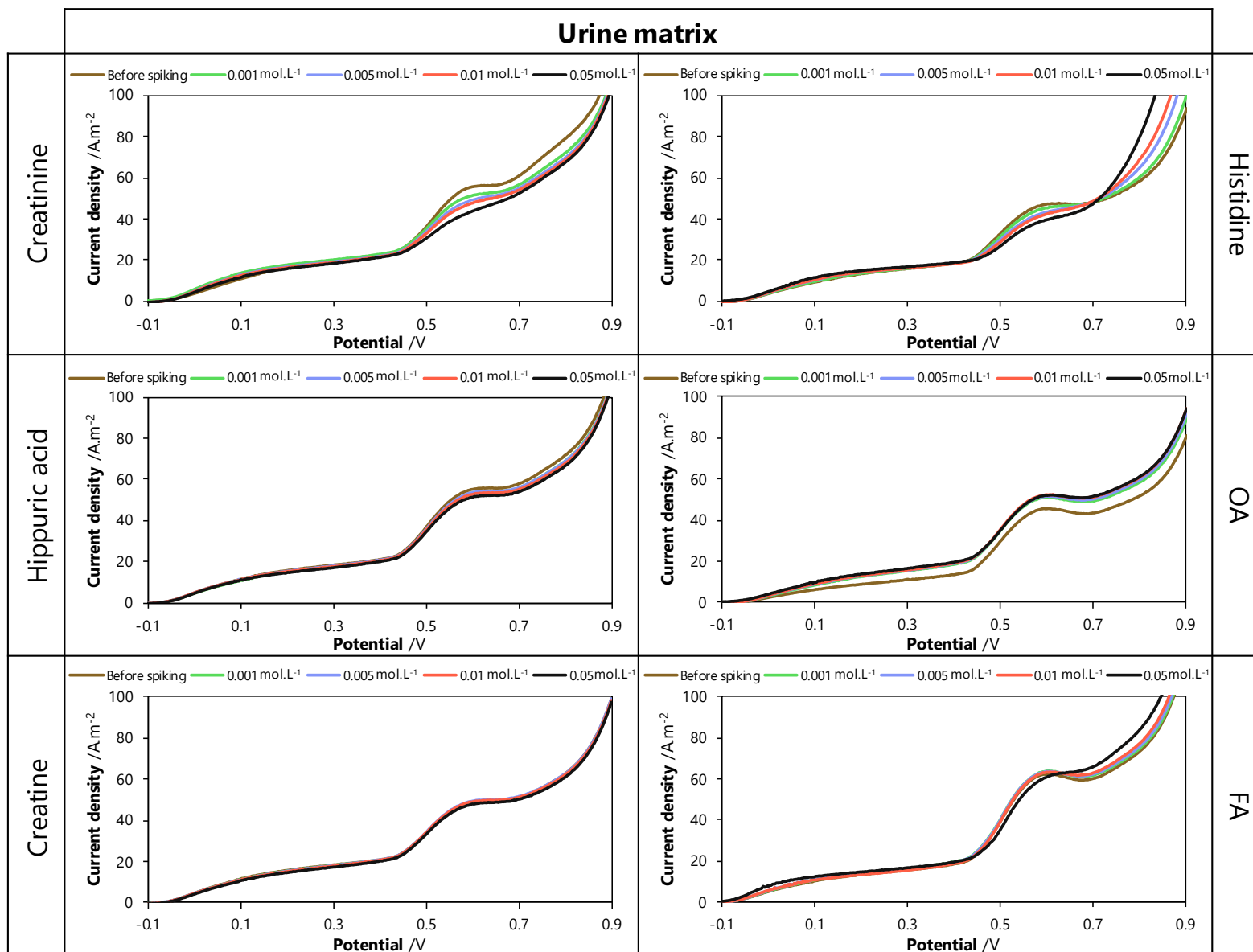


Fig. I.3 – $I=f(E)$ curves obtained by spiking various organic molecules, mainly present in human urine, into a urine/KOH matrix.

Langmuir model for histidine adsorption on nickel(III) sites

The Langmuir model corresponds to adsorbed molecules which form a single mono-layer on the surface. Each site for adsorption is equivalent in terms of adsorption energy. There is no interaction between adjacent molecule.

On the basis of the adsorption reaction, one can established the Eq. J.1.

$$\Theta = \frac{\Gamma_H}{\Gamma_{H,\max}} = \frac{K \times [\text{Histidine}]}{1 + K \times [\text{Histidine}]} \quad (\text{J.1})$$

where Γ_H is the number of nickel sites covered by histidine, $\Gamma_{H,\max}$ is the number of maximum nickel sites available to the histidine adsorption, Θ is the coverage ratio (dimensionless, between 0 and 1), and K is the equilibrium constant of the adsorption reaction between histidine and nickel sites ($K = k_{\text{ads}}/k_{\text{des}}$, dimensionless).

For this signal (0.6 to 2 V), the current, proportional to the OH^- concentration, can be expressed by Eq. J.3. In the absence of histidine (when $\Theta = 0$), a limiting current (I°) can be expressed as Eq. J.2, without adsorption of this molecule, allowing maximum current for hydroxide ion oxidation:

$$\text{without histidine : } I^\circ = n \times \mathcal{F} \times k_{\text{OH}^-} \times [\text{OH}^-] \times S \times \frac{1}{1 - t_{\text{OH}^-}} \quad (\text{J.2})$$

$$\text{with histidine : } I = n \times \mathcal{F} \times k_{\text{OH}^-} \times [\text{OH}^-] \times S \times (1 - \Theta) \times \frac{1}{1 - t_{\text{OH}^-}} \quad (\text{J.3})$$

$$I = I^\circ \times (1 - \Theta) \quad (\text{J.4})$$

where I is the current (A), n is the number of exchanged electrons (1 in the case of $\text{OH}^- \rightarrow 0.25 \text{ O}_2 + 1 \text{ e}^- + 0.5 \text{ H}_2\text{O}$, dimensionless), k_{OH^-} is mass transfer coefficient of hydroxide ion (m s^{-1}), S is the geometrical area of the nickel RDE (m^2), t_{OH^-} is the ion transport number of hydroxide (dimensionless).

The ion transport number of OH^- is estimated via Eq. J.5 and represented the fraction

of the total current carried in an electrolyte by OH^- specie.

$$t_{\text{OH}^-} = \frac{[\text{OH}^-] \times D_{\text{OH}^-}}{[\text{OH}^-] \times D_{\text{OH}^-} + [\text{H}^+] \times D_{\text{H}^+}} \quad (\text{J.5})$$

Assuming diffusion coefficient of $5.3 \times 10^{-9} \text{ m}^2 \text{ s}^{-1}$ for hydroxide ions [265] and $1.83 \times 10^{-9} \text{ m}^2 \text{ s}^{-1}$ for potassium ions [308], the number t_{OH^-} is equal to 0.75.

The difference in the oxidation currents of hydroxide ions (ΔI), in the presence of histidine and in its absence, can then be expressed according to Eq. J.6.

$$\Delta I = I^\circ - I \quad (\text{J.6})$$

$$\Theta = \frac{\Delta I}{I^\circ} = \frac{K \times [\text{Histidine}]}{1 + K \times [\text{Histidine}]} \quad (\text{J.7})$$

Leading to Eq. J.8:

$$\frac{1}{\Delta I} = \frac{1}{I^\circ} + \frac{1}{K \times I^\circ \times [\text{Histidine}]} \quad (\text{J.8})$$

Bibliography

- [1] S. E. Vollset, E. Goren, C.-W. Yuan, J. Cao, A. E. Smith, T. Hsiao, C. Bisignano, G. S. Azhar, E. Castro, J. Chalek, A. J. Dolgert, T. Frank, K. Fukutaki, S. I. Hay, R. Lozano, A. H. Mokdad, V. Nandakumar, M. Pierce, M. Pletcher, T. Robalik, K. M. Steuben, H. Y. Wunrow, B. S. Zlavog, and C. J. L. Murray. In: *The Lancet* (2020). DOI: [10.1016/S0140-6736\(20\)30677-2](https://doi.org/10.1016/S0140-6736(20)30677-2) (cit. on p. 1).
- [2] B. S. Choudri and Y. Charabi. In: *Water Environment Research* (2019). DOI: [10.1002/wer.1157](https://doi.org/10.1002/wer.1157) (cit. on p. 1).
- [3] S. P. de l'assainissement francilien (SIAAP). *L'assainissement des eaux usées en agglomération parisienne : principe et procédés*. Livret pédagogique. Mar. 2013, p. 92 (cit. on p. 1).
- [4] S. Rahimi, O. Modin, and I. Mijakovic. In: *Biotechnology Advances* (2020). DOI: [10.1016/j.biotechadv.2020.107570](https://doi.org/10.1016/j.biotechadv.2020.107570) (cit. on p. 2).
- [5] Y. Law, L. Ye, Y. Pan, and Z. Yuan. In: *Philosophical Transactions of the Royal Society B: Biological Sciences* (2012). DOI: [10.1098/rstb.2011.0317](https://doi.org/10.1098/rstb.2011.0317) (cit. on p. 2).
- [6] W. G. Hines. *A Review of Wastewater Problems and Wastewater-Management Planning in the San Francisco Bay Region, California*. [Menlo Park, Calif.]: U.S. Dept. of the Interior, Geological Survey, 1973. URL: <https://pubs.usgs.gov/of/1973/0112/report.pdf> (cit. on p. 2).
- [7] G. Crini and E. Lichtfouse. In: *Environmental Chemistry Letters* (2019). DOI: [10.1007/s10311-018-0785-9](https://doi.org/10.1007/s10311-018-0785-9) (cit. on p. 2).
- [8] P. Kay, R. Hiscoe, I. Moberley, L. Bajic, and N. McKenna. In: *Environmental Science and Pollution Research* (2018). DOI: [10.1007/s11356-018-2070-7](https://doi.org/10.1007/s11356-018-2070-7) (cit. on p. 2).
- [9] U. Badeti, N. K. Pathak, F. Volpin, U. Dorji, S. Freguia, H. K. Shon, and S. Phuntsho. In: *Process Safety and Environmental Protection* (2021). DOI: [10.1016/j.psep.2021.04.022](https://doi.org/10.1016/j.psep.2021.04.022) (cit. on p. 3).
- [10] K. Mahalik, J. Sahu, A. V. Patwardhan, and B. Meikap. In: *Journal of Hazardous Materials* (2010). DOI: [10.1016/j.jhazmat.2009.10.053](https://doi.org/10.1016/j.jhazmat.2009.10.053) (cit. on pp. 3, 16).
- [11] Y. Qin and J. M. Cabral. In: *Biocatalysis and Biotransformation* (2002). DOI: [10.1080/10242420210154](https://doi.org/10.1080/10242420210154) (cit. on pp. 3, 17).
- [12] A. Muhammad Yusuf., F. Mulana, and S. D. Said. In: *IOP Conference Series: Materials Science and Engineering* (2019). DOI: [10.1088/1757-899X/536/1/012079](https://doi.org/10.1088/1757-899X/536/1/012079) (cit. on pp. 3, 18).
- [13] T. Kameda, S. Ito, and T. Yoshioka. In: *Journal of Dispersion Science and Technology* (2017). DOI: [10.1080/01932691.2016.1219953](https://doi.org/10.1080/01932691.2016.1219953) (cit. on pp. 3, 18).
- [14] B. Koubaissy, J. Toufaily, Z. Yaseen, T. J. Daou, S. Jradi, and T. Hamieh. In: *Adsorption Science & Technology* (2017). DOI: [10.1177/0263617416666084](https://doi.org/10.1177/0263617416666084) (cit. on pp. 3, 18).
- [15] A. M. Bernhard, D. Peitz, M. Elsener, T. Schildhauer, and O. Kröcher. In: *Catalyst. Science Technology* (2013). DOI: [10.1039/C2CY20668D](https://doi.org/10.1039/C2CY20668D) (cit. on pp. 3, 18).

- [16] G. Lourinho and P. S. D. Brito. In: *Waste and Biomass Valorization* (2021). DOI: [10.1007/s12649-020-00951-4](https://doi.org/10.1007/s12649-020-00951-4) (cit. on p. 3).
- [17] S. G. Simoes, J. Catarino, A. Picado, T. F. Lopes, S. Di Bernardino, F. Amorim, F. Gírio, C. Rangel, and T. Ponce de Leão. In: *Journal of Cleaner Production* (2021). DOI: [10.1016/j.jclepro.2021.128124](https://doi.org/10.1016/j.jclepro.2021.128124) (cit. on p. 3).
- [18] A. Kapałka, G. Fóti, and C. Comninellis. “Basic Principles of the Electrochemical Mineralization of Organic Pollutants for Wastewater Treatment”. In: *Electrochemistry for the Environment*. Ed. by C. Comninellis and G. Chen. Springer, 2010, pp. 1–23. ISBN: 978-0-387-36922-8. DOI: [10.1007/978-0-387-68318-8_1](https://doi.org/10.1007/978-0-387-68318-8_1) (cit. on p. 3).
- [19] M. Jafari and G. G. Botte. In: *Journal of Applied Electrochemistry* (2021). DOI: [10.1007/s10800-020-01481-6](https://doi.org/10.1007/s10800-020-01481-6) (cit. on p. 3).
- [20] B. K. Boggs, R. L. King, and G. G. Botte. In: *Chemical Communications* (2009). DOI: [10.1039/b905974a](https://doi.org/10.1039/b905974a) (cit. on pp. 3, 27, 28, 34, 145).
- [21] Z. Zhou, Y. Liu, J. Zhang, H. Pang, and G. Zhu. In: *Electrochemistry Communications* (2020). DOI: [10.1016/j.elecom.2020.106871](https://doi.org/10.1016/j.elecom.2020.106871) (cit. on pp. 3, 92, 126).
- [22] J. Li, S. Wang, J. Chang, and L. Feng. In: *Advanced Powder Materials* (2022). DOI: [10.1016/j.apmate.2022.01.003](https://doi.org/10.1016/j.apmate.2022.01.003) (cit. on p. 3).
- [23] L. Rebiai, D. Muller-Bouvet, R. Benyahia, E. Torralba, M. L. Viveros, V. Rocher, S. Azimi, C. Cachet-Vivier, and S. Bastide. In: *Electrochimica Acta* (2023). DOI: [10.1016/j.electacta.2022.141516](https://doi.org/10.1016/j.electacta.2022.141516) (cit. on p. 4).
- [24] L. Rebiai. “Élaboration et Caractérisation de Matériaux d’électrode Nanostructurés Pour La Conversion Photoélectrochimique de l’urée”. PhD thesis. Paris 12, 2022. URL: <https://www.theses.fr/s226383> (cit. on p. 4).
- [25] E. Guerrini and S. Trasatti. “Electrocatalysis in Water Electrolysis”. In: *Catalysis for Sustainable Energy Production*. Ed. by P. Barbaro and C. Bianchini. Weinheim, Germany: Wiley-VCH Verlag GmbH & Co. KGaA, 2009, pp. 235–269. ISBN: 978-3-527-62541-3. DOI: [10.1002/9783527625413.ch7](https://doi.org/10.1002/9783527625413.ch7) (cit. on p. 8).
- [26] A. J. Hale. *The Manufacture of Chemicals by Electrolysis*. Bertram Blount. A Treatise of Electro-Chemistry. London: Constable & Company Ltd, 1919. 80 pp. URL: http://www.sciencemadness.org/library/books/the_manufacture_of_chemicals_by_electrolysis.pdf (cit. on p. 8).
- [27] R. Kothari, V. Tyagi, and A. Pathak. In: *Renewable and Sustainable Energy Reviews* (2010). DOI: [10.1016/j.rser.2010.05.005](https://doi.org/10.1016/j.rser.2010.05.005) (cit. on p. 8).
- [28] O. Sahu, B. Mazumdar, and P. K. Chaudhari. In: *Environmental Science and Pollution Research* (2014). DOI: [10.1007/s11356-013-2208-6](https://doi.org/10.1007/s11356-013-2208-6) (cit. on p. 8).
- [29] P. Nidheesh, A. Kumar, D. Syam Babu, J. Scaria, and M. Suresh Kumar. In: *Chemosphere* (2020). DOI: [10.1016/j.chemosphere.2020.126437](https://doi.org/10.1016/j.chemosphere.2020.126437) (cit. on p. 8).
- [30] D. Kliaugaitė, K. Yasadi, G.-j. Euverink, M. F. Bijmans, and V. Racys. In: *Separation and Purification Technology* (2013). DOI: [10.1016/j.seppur.2013.01.055](https://doi.org/10.1016/j.seppur.2013.01.055) (cit. on p. 8).
- [31] J. G. Salway. In: *Trends in Biochemical Sciences* (2018). DOI: [10.1016/j.tibs.2018.04.012](https://doi.org/10.1016/j.tibs.2018.04.012) (cit. on p. 9).
- [32] F. Wöhler. In: *Annalen der Physik* (1824). DOI: [10.1002/andp.18240781202](https://doi.org/10.1002/andp.18240781202) (cit. on p. 10).
- [33] T. Berrod and Q. Russel. *Les superpouvoirs de l’urine*. 2014. URL: https://boutique.arte.tv/detail/superpouvoirs_urine (cit. on p. 10).
- [34] A. C. Correa, V. B. Carmona, J. A. Simão, L. H. Capparelli Mattoso, and J. M. Marconcini. In: *Carbohydrate Polymers* (2017). DOI: [10.1016/j.carbpol.2017.03.051](https://doi.org/10.1016/j.carbpol.2017.03.051) (cit. on p. 10).

- [35] J.-W. Kim, K. Carlborn, L. M. Matuana, and P. A. Heiden. In: *Journal of Applied Polymer Science* (2006). DOI: [10.1002/app.23654](https://doi.org/10.1002/app.23654) (cit. on p. 10).
- [36] J.-P. Mazaud. In: *Techniques de l'ingénieur. Procédés chimie - bio - agro | Opérations unitaires. Génie de la réaction chimique* (2001). URL: <https://www.techniques-ingenieur.fr/base-documentaire/procedes-chimie-bio-agro-th2/fabrication-des-grands-produits-industriels-en-chimie-et-petrochimie-42319210/uree-j6660/> (cit. on p. 10).
- [37] M. Johansson. *Urine Separation - Closing the Nutrient Cycle*. Stockholm Water Company, 2000. URL: <https://www.susana.org/en/knowledge-hub/resources-and-publications/library/details/189> (cit. on p. 10).
- [38] L. Rossi, J. Lienert, and T. Larsen. In: *Journal of Environmental Management* (2009). DOI: [10.1016/j.jenvman.2009.01.006](https://doi.org/10.1016/j.jenvman.2009.01.006) (cit. on pp. 10, 13).
- [39] M. Maurer, W. Pronk, and T. Larsen. In: *Water Research* (2006). DOI: [10.1016/j.watres.2006.07.012](https://doi.org/10.1016/j.watres.2006.07.012) (cit. on p. 10).
- [40] T. M. P. Martin, F. Esculier, F. Levavasseur, and S. Houot. In: *Critical Reviews in Environmental Science and Technology* (2022). DOI: [10.1080/10643389.2020.1838214](https://doi.org/10.1080/10643389.2020.1838214) (cit. on p. 10).
- [41] T. H. Boyer and D. Saetta. In: *Accounts of Chemical Research* (2019). DOI: [10.1021/acs.accounts.8b00614](https://doi.org/10.1021/acs.accounts.8b00614) (cit. on p. 11).
- [42] M. Patrick, Y. Tsige, A. Adow, M. Abdirashid, H. Yunis, D. Githiri, E. Hulland, J. Murphy, P. Akers, T. W. Brown, C. Blanton, and T. Handzel. In: *International Journal of Hygiene and Environmental Health* (2021). DOI: [10.1016/j.ijheh.2021.113745](https://doi.org/10.1016/j.ijheh.2021.113745) (cit. on p. 11).
- [43] K. A. Landry and T. H. Boyer. In: *Water Research* (2016). DOI: [10.1016/j.watres.2016.09.024](https://doi.org/10.1016/j.watres.2016.09.024) (cit. on p. 11).
- [44] H. L. Mobley and R. P. Hausinger. In: *Microbiological Reviews* (1989). DOI: [10.1128/mr.53.1.85-108.1989](https://doi.org/10.1128/mr.53.1.85-108.1989) (cit. on p. 11).
- [45] K. M. Udert, T. A. Larsen, and W. Gujer. In: *Water Research* (2003). DOI: [10.1016/S0043-1354\(03\)00071-X](https://doi.org/10.1016/S0043-1354(03)00071-X) (cit. on p. 11).
- [46] K. Udert, T. Larsen, and W. Gujer. In: *Water Science and Technology* (2006). DOI: [10.2166/wst.2006.921](https://doi.org/10.2166/wst.2006.921) (cit. on p. 11).
- [47] K. M. Udert, T. A. Larsen, M. Biebow, and W. Gujer. In: *Water Research* (2003). DOI: [10.1016/S0043-1354\(03\)00065-4](https://doi.org/10.1016/S0043-1354(03)00065-4) (cit. on pp. 11, 15).
- [48] T. A. Larsen, K. M. Udert, and J. Lienert. *Source Separation and Decentralization for Wastewater Management*. IWA Publishing, 2013. ISBN: 978-1-78040-107-2. DOI: [10.2166/9781780401072](https://doi.org/10.2166/9781780401072) (cit. on p. 11).
- [49] T. H. Boyer, K. Taylor, A. Reed, and D. Smith. In: *Environmental Progress & Sustainable Energy* (2014). DOI: [10.1002/ep.11825](https://doi.org/10.1002/ep.11825) (cit. on p. 11).
- [50] K. Udert, T. Larsen, and W. Gujer. In: *Water Supply* (2003). DOI: [10.2166/ws.2003.0010](https://doi.org/10.2166/ws.2003.0010) (cit. on p. 11).
- [51] S. Blume and M. Winker. In: *Water Science and Technology* (2011). DOI: [10.2166/wst.2011.530](https://doi.org/10.2166/wst.2011.530) (cit. on p. 12).
- [52] T. A. Larsen, A. C. Alder, R. I. L. Eggen, M. Maurer, and J. Lienert. In: *Environmental Science & Technology* (2009). DOI: [10.1021/es803001r](https://doi.org/10.1021/es803001r) (cit. on p. 12).
- [53] H. Jönsson and B. Vinnerås. In: *Water Science and Technology* (2007). DOI: [10.2166/wst.2007.558](https://doi.org/10.2166/wst.2007.558) (cit. on p. 12).

- [54] C. Eme, C. Boutin, CREAPURE, and IRSTEA. *Composition des eaux usées domestiques par source d'émission à l'échelle de l'habitation. Etude bibliographique*. Rapport d'étude. 2015. URL: <https://www.documentation.eauetbiodiversite.fr/notice/composition-des-eaux-usees-domestiques-par-source-d-emission-a-l-echelle-de-l-habitation-etude-bibli0> (cit. on pp. 12, 14).
- [55] E. von Münch and M. Winker. *Technology Review of Urine Diversion Components. Overview of Urine Diversion Components Such as Waterless Urinals, Urine Diversion Toilets, Urine Storage and Reuse Systems*. Eschborn: Deutsche Gesellschaft für Internationale Zusammenarbeit (GIZ), 2011. URL: http://www.susana.org/_resources/documents/default/2-875-giz2011-en-technology-review-urine-diversion.pdf (cit. on p. 12).
- [56] J. De Paepe, L. De Pryck, A. R. D. Verliefde, K. Rabaey, and P. Clauwaert. In: *Environmental Science & Technology* (2020). DOI: [10.1021/acs.est.9b06804](https://doi.org/10.1021/acs.est.9b06804) (cit. on p. 13).
- [57] D. F. Putnam. *Composition and Concentrative Properties of Human Urine*. National Aeronautics and Space Administration, 1971, p. 112. URL: <https://ntrs.nasa.gov/citations/19710023044> (cit. on pp. 13, 177, 206).
- [58] S. Bouatra, F. Aziat, R. Mandal, A. C. Guo, M. R. Wilson, C. Knox, T. C. Bjorndahl, R. Krishnamurthy, F. Saleem, P. Liu, Z. T. Dame, J. Poelzer, J. Huynh, F. S. Yallou, N. Psychogios, E. Dong, R. Bogumil, C. Roehring, and D. S. Wishart. In: *PLoS ONE* (2013). Ed. by P. Dzeja. DOI: [10.1371/journal.pone.0073076](https://doi.org/10.1371/journal.pone.0073076) (cit. on pp. 13, 142, 177, 206, 229).
- [59] C. Santoro, M. J. S. Garcia, X. A. Walter, J. You, P. Theodosiou, I. Gajda, O. Obata, J. Winfield, J. Greenman, and I. Ieropoulos. In: *ChemElectroChem* (2020). DOI: [10.1002/celec.201901995](https://doi.org/10.1002/celec.201901995) (cit. on p. 14).
- [60] D. Hellström, E. Johansson, and K. Grennberg. In: *Ecological Engineering* (1999). DOI: [10.1016/S0925-8574\(98\)00074-3](https://doi.org/10.1016/S0925-8574(98)00074-3) (cit. on p. 14).
- [61] H. Ray, D. Saetta, and T. H. Boyer. In: *Environmental Science: Water Research & Technology* (2018). DOI: [10.1039/C7EW00271H](https://doi.org/10.1039/C7EW00271H) (cit. on p. 14).
- [62] I. Kabdaşlı, O. Tünay, Ç. İşlek, E. Erdinç, S. Hüskalar, and M. Tatlı. In: *Water Science and Technology* (2006). DOI: [10.2166/wst.2006.433](https://doi.org/10.2166/wst.2006.433) (cit. on p. 14).
- [63] P. Simha, J. Senecal, A. Nordin, C. Lalander, and B. Vinnerås. In: *Water Research* (2018). DOI: [10.1016/j.watres.2018.06.001](https://doi.org/10.1016/j.watres.2018.06.001) (cit. on p. 14).
- [64] P. H. Arve and S. C. Popat. In: *ACS ES&T Engineering* (2021). DOI: [10.1021/acsestengg.1c00194](https://doi.org/10.1021/acsestengg.1c00194) (cit. on p. 14).
- [65] M. Ikematsu, K. Kaneda, M. Iseki, and M. Yasuda. In: *Science of The Total Environment* (2007). DOI: [10.1016/j.scitotenv.2007.03.028](https://doi.org/10.1016/j.scitotenv.2007.03.028) (cit. on p. 14).
- [66] K. M. Udert, C. Fux, M. Münster, T. A. Larsen, H. Siegrist, and W. Gujer. In: *Water science and technology : a journal of the International Association on Water Pollution Research* (2003). DOI: [10.2166/wst.2003.0031](https://doi.org/10.2166/wst.2003.0031) (cit. on p. 14).
- [67] K. L. Sahrawat. In: *Plant and Soil* (1984). DOI: [10.1007/BF02450373](https://doi.org/10.1007/BF02450373) (cit. on p. 14).
- [68] G. Sachs, D. R. Scott, D. L. Weeks, M. Rektorscheck, and K. Melchers. "Regulation of Urease for Acid Habitation." In: *Helicobacter Pylori: Physiology and Genetics*. Ed. by H. L. Mobley, G. L. Mendz, and S. L. Hazell. Washington (DC): ASM Press, 2001. ISBN: 1-55581-213-9. pmid: [21290728](https://pubmed.ncbi.nlm.nih.gov/21290728/) (cit. on p. 14).
- [69] W. Yang, J. Li, and X. Yang. In: *Frontiers in Sustainability* (2021). DOI: [10.3389/frsus.2021.710739](https://doi.org/10.3389/frsus.2021.710739) (cit. on p. 14).
- [70] Z. Liu, Q. Zhao, K. Wang, D. Lee, W. Qiu, and J. Wang. In: *Journal of Environmental Sciences* (2008). DOI: [10.1016/S1001-0742\(08\)62202-0](https://doi.org/10.1016/S1001-0742(08)62202-0) (cit. on p. 15).

- [71] V. Amstutz, A. Katsaounis, A. Kapalka, C. Comninellis, and K. M. Udert. In: *Journal of Applied Electrochemistry* (2012). DOI: [10.1007/s10800-012-0444-y](https://doi.org/10.1007/s10800-012-0444-y) (cit. on pp. 15, 25, 131).
- [72] D. Wu, Y. Zhang, G. Dong, Z. Du, W. Wu, D. Chadwick, and R. Bol. In: *Environmental Pollution* (2021). DOI: [10.1016/j.envpol.2020.116365](https://doi.org/10.1016/j.envpol.2020.116365) (cit. on p. 16).
- [73] S. N. Behera, M. Sharma, V. P. Aneja, and R. Balasubramanian. In: *Environmental Science and Pollution Research* (2013). DOI: [10.1007/s11356-013-2051-9](https://doi.org/10.1007/s11356-013-2051-9) (cit. on p. 16).
- [74] J. J. Sigurdarson, S. Svane, and H. Karring. In: *Reviews in Environmental Science and Bio/Technology* (2018). DOI: [10.1007/s11157-018-9466-1](https://doi.org/10.1007/s11157-018-9466-1) (cit. on p. 16).
- [75] E. Urbańczyk. In: *Journal of Applied Electrochemistry* (2016). DOI: [10.1007/s10800-016-0993-6](https://doi.org/10.1007/s10800-016-0993-6) (cit. on pp. 16, 18, 24, 26).
- [76] J. N. Sahu, S. Hussain, and B. C. Meikap. In: *Korean Journal of Chemical Engineering* (2011). DOI: [10.1007/s11814-010-0524-9](https://doi.org/10.1007/s11814-010-0524-9) (cit. on p. 16).
- [77] E. Jabri, M. B. Carr, R. P. Hausinger, and P. A. Karplus. In: *Science (New York, N. Y.)* 268.5213 (1995), pp. 998–1004. ISSN: 0036-8075 (cit. on p. 17).
- [78] L. Mazzei, V. Broll, and S. Ciurli. In: *Soil Science Society of America Journal* (2018). DOI: [10.2136/sssaj2017.09.0323](https://doi.org/10.2136/sssaj2017.09.0323) (cit. on p. 17).
- [79] N. E. Dixon, P. W. Riddles, C. Gazzola, R. L. Blakeley, and B. Zerner. In: *Canadian Journal of Biochemistry* (1980). DOI: [10.1139/o80-181](https://doi.org/10.1139/o80-181) (cit. on p. 17).
- [80] S. Benini, W. R. Rypniewski, K. S. Wilson, S. Miletto, S. Ciurli, and S. Mangani. In: *Structure* (1999). DOI: [10.1016/S0969-2126\(99\)80026-4](https://doi.org/10.1016/S0969-2126(99)80026-4) (cit. on p. 17).
- [81] L. Mazzei, F. Musiani, and S. Ciurli. In: *JBIC Journal of Biological Inorganic Chemistry* (2020). DOI: [10.1007/s00775-020-01808-w](https://doi.org/10.1007/s00775-020-01808-w) (cit. on pp. 17, 116).
- [82] F. Musiani, E. Arnofi, R. Casadio, and S. Ciurli. In: *JBIC Journal of Biological Inorganic Chemistry* (2001). DOI: [10.1007/s007750000204](https://doi.org/10.1007/s007750000204) (cit. on p. 17).
- [83] D. Suárez, N. Díaz, and K. M. Merz. In: *Journal of the American Chemical Society* (2003). DOI: [10.1021/ja030145g](https://doi.org/10.1021/ja030145g) (cit. on p. 17).
- [84] T. Chen, Y. Wu, and S. Xiao. “A Method of Producing Chlorine Dioxide Which Employs Alkaline Chlorate in a Mineral Acid Medium and Urea as a Reducing Agent”. U.S. pat. WO2004037746A2 (cit. on p. 18).
- [85] P. Rychen, B. Scheiffelen, and T. Frank. “A process for removing urea from water”. German pat. 3 068 731 B1. Sept. 21, 2016 (cit. on p. 18).
- [86] K. Cho and M. R. Hoffmann. In: *Environmental Science & Technology* (2014). DOI: [10.1021/es5025405](https://doi.org/10.1021/es5025405) (cit. on pp. 19, 25).
- [87] K. Ye, G. Wang, D. Cao, and G. Wang. In: *Topics in Current Chemistry* (2018). DOI: [10.1007/s41061-018-0219-y](https://doi.org/10.1007/s41061-018-0219-y) (cit. on pp. 19, 31, 34).
- [88] R. K. Singh, K. Rajavelu, M. Montag, and A. Schechter. In: *Energy Technology* (2021). DOI: [10.1002/ente.202100017](https://doi.org/10.1002/ente.202100017) (cit. on pp. 19, 28, 31, 34).
- [89] X. Wang, J.-P. Li, Y. Duan, J. Li, H. Wang, X. Yang, and M. Gong. In: *ChemCatChem* (2022). DOI: [10.1002/cctc.202101906](https://doi.org/10.1002/cctc.202101906) (cit. on pp. 20, 22, 23, 27, 34, 101).
- [90] S. B. Tuwiner. *Research, Design, and Development of an Improved Water Reclamation System for Manned Space Vehicles*. NASA, 1966. URL: <https://ntrs.nasa.gov/api/citations/19670013995/downloads/19670013995.pdf> (cit. on p. 21).
- [91] J. Bizot and A. Sausse. “Method for the Purification of a Solution Containing Chloride Ions”. Pat. 7216541 (Dutch Patent). Rhône-Poulenc, S.A. (cit. on pp. 21, 24).
- [92] S. J. Yao, A. J. Appleby, A. Geisel, H. R. Cash, and S. K. Wolfson. In: *Nature* (1969). DOI: [10.1038/224921a0](https://doi.org/10.1038/224921a0) (cit. on p. 21).

- [93] R. W. Keller, S. J. Yao, J. M. Brown, S. K. Wolfson, and M. V. Zeller. In: *Bioelectrochemistry and Bioenergetics* (1980). DOI: [10.1016/0302-4598\(80\)80007-9](https://doi.org/10.1016/0302-4598(80)80007-9) (cit. on p. 21).
- [94] J. F. Patzer, S. J. Yao, S. K. Wolfson, and R. Ruppel-Kerr. In: *Journal of Electroanalytical Chemistry and Interfacial Electrochemistry* (1989). DOI: [10.1016/0022-0728\(89\)87276-6](https://doi.org/10.1016/0022-0728(89)87276-6) (cit. on pp. 21, 22).
- [95] S. J. Yao, J. M. Brown, K. Wolfson, K. V. Thirivikraman, and M. A. Krupper. “Controlled Potential Electrolysis for Urea Removal in Hemodialysis: Improved Efficiency in Urea Clearance”. In: *IEEE Transactions on Biomedical Engineering*. Fourth Annual Conference of the IEEE Engineering in Medicine and Biology Society. Vol. BME-29. Marriott Hotel, Philadelphia, PA, 1982, pp. 590–620. DOI: [10.1109/TBME.1982.324990](https://doi.org/10.1109/TBME.1982.324990) (cit. on p. 22).
- [96] S. Yao, S. Wolfson, M. Krupper, and K. Wu. In: *Bioelectrochemistry and Bioenergetics* (1984). DOI: [10.1016/0302-4598\(84\)85111-9](https://doi.org/10.1016/0302-4598(84)85111-9) (cit. on p. 22).
- [97] J. Patzer, S. Yao, and S. Wolfson. In: *IEEE Transactions on Biomedical Engineering* (1991). DOI: [10.1109/10.99080](https://doi.org/10.1109/10.99080) (cit. on p. 22).
- [98] J. F. Patzer, S. K. Wolfson, and S. J. Yao. In: *Chemical Engineering Science* (1990). DOI: [10.1016/0009-2509\(90\)80170-J](https://doi.org/10.1016/0009-2509(90)80170-J) (cit. on p. 22).
- [99] V. A. Gromyko, T. B. Tsygankova, V. B. Gaidadymov, and B. V. Vasil’ev YuB. In: *Elektrokhimiya* 10 (1974), p. 49 (cit. on p. 22).
- [100] A. Bolzan and T. Iwasita. In: *Electrochimica Acta* (1988). DOI: [10.1016/0013-4686\(88\)80040-9](https://doi.org/10.1016/0013-4686(88)80040-9) (cit. on p. 22).
- [101] G. Horányi, G. Inzelt, and E. Rizmayer. In: *Journal of Electroanalytical Chemistry and Interfacial Electrochemistry* (1979). DOI: [10.1016/S0022-0728\(79\)80288-0](https://doi.org/10.1016/S0022-0728(79)80288-0) (cit. on p. 22).
- [102] P. Rikvold, J. Zhang, Y.-E. Sung, and A. Wieckowski. In: *Electrochimica Acta* (1996). DOI: [10.1016/0013-4686\(96\)00049-7](https://doi.org/10.1016/0013-4686(96)00049-7) (cit. on p. 22).
- [103] M. Gamboa-Aldeco, P. Mrozek, C. Rhee, A. Wieckowski, P. Rikvold, and Q. Wang. In: *Surface Science* (1993). DOI: [10.1016/0039-6028\(93\)90212-3](https://doi.org/10.1016/0039-6028(93)90212-3) (cit. on p. 22).
- [104] P. Rikvold, M. Gamboa-Aldeco, J. Zhang, M. Han, Q. Wang, H. Richards, and A. Wieckowski. In: *Surface Science* (1995). DOI: [10.1016/0039-6028\(95\)00440-8](https://doi.org/10.1016/0039-6028(95)00440-8) (cit. on p. 22).
- [105] A. Łukomska and J. Sobkowski. In: *Journal of Solid State Electrochemistry* (2006). DOI: [10.1007/s10008-006-0101-7](https://doi.org/10.1007/s10008-006-0101-7) (cit. on p. 22).
- [106] F. Altaf, R. Qureshi, S. Ahmed, A. Y. Khan, and A. Naseer. In: *Journal of Electroanalytical Chemistry* (2010). DOI: [10.1016/j.jelechem.2010.02.011](https://doi.org/10.1016/j.jelechem.2010.02.011) (cit. on p. 22).
- [107] J. F. Patzer, S. Yao, and S. Wolfson. In: *Journal of Molecular Catalysis* (1991). DOI: [10.1016/0304-5102\(91\)80163-W](https://doi.org/10.1016/0304-5102(91)80163-W) (cit. on p. 23).
- [108] L. Rutigliano, D. Fino, G. Saracco, V. Specchia, P. Spinelli, and L. Grizzaffi. In: *Journal of Applied Electrochemistry* (2009). DOI: [10.1007/s10800-009-9831-4](https://doi.org/10.1007/s10800-009-9831-4) (cit. on p. 23).
- [109] M. Fels. In: *Medical & Biological Engineering & Computing* (1978). DOI: [10.1007/BF02442928](https://doi.org/10.1007/BF02442928) (cit. on p. 24).
- [110] M. Fels. In: *Medical & Biological Engineering & Computing* (1982). DOI: [10.1007/BF02442789](https://doi.org/10.1007/BF02442789) (cit. on p. 24).

- [111] B. Schuenemann, E. Quellhorst, H. Kaiser, G. Richter, K. Mundt, E. Weidlich, G. Loeffler, M. Zachariae, and O. Schunk. In: *Transactions - American Society for Artificial Internal Organs* 28 (1982), pp. 49–53. ISSN: 0066-0078. pmid: [6761937](#) (cit. on p. 24).
- [112] K. Köster, H. Wendt, J. Gallus, G. Krisam, and H. D. Lehmann. In: *Artificial Organs* (1983). DOI: [10.1111/j.1525-1594.1983.tb04182.x](#) (cit. on p. 24).
- [113] K. Köster, H. Wendt, J. Gallus, G. Krisam, and H.-D. Lehmann. In: *Journal of Chemical Technology and Biotechnology* (2007). DOI: [10.1002/jctb.5030320707](#) (cit. on p. 24).
- [114] J. C. Wright, A. S. Michaels, and A. J. Appleby. In: *AIChE Journal* (1986). DOI: [10.1002/aic.690320906](#) (cit. on p. 25).
- [115] H. Li, Q. Yu, B. Yang, Z. Li, and L. Lei. In: *Journal of Electroanalytical Chemistry* (2015). DOI: [10.1016/j.jelechem.2014.11.018](#) (cit. on pp. 25, 29).
- [116] V. M. Grinval'd, G. M. Leshchinskii, V. V. Rodin, S. I. Strelkov, and A. A. Yakovleva. In: *Biomedical Engineering* (2003). DOI: [10.1023/A:1024727513884](#) (cit. on p. 25).
- [117] W. Simka, J. Piotrowski, and G. Nawrat. In: *Electrochimica Acta* (2007). DOI: [10.1016/j.electacta.2006.12.017](#) (cit. on p. 25).
- [118] W. Simka, J. Piotrowski, A. Robak, and G. Nawrat. In: *Journal of Applied Electrochemistry* (2009). DOI: [10.1007/s10800-008-9771-4](#) (cit. on p. 25).
- [119] H. Zöllig, A. Remmele, C. Fritzsche, E. Morgenroth, and K. M. Udert. In: *Environmental Science & Technology* (2015). DOI: [10.1021/acs.est.5b01675](#) (cit. on p. 26).
- [120] J. A. Clark, Y. Yang, N. C. Ramos, and H. W. Hillhouse. In: *Water Research* (2021). DOI: [10.1016/j.watres.2021.117106](#) (cit. on p. 26).
- [121] A. Schranck and K. Doudrick. In: *Water Research* (2020). DOI: [10.1016/j.watres.2019.115130](#) (cit. on pp. 26, 29).
- [122] S. Cotillas, E. Lacasa, C. Sáez, P. Cañizares, and M. A. Rodrigo. In: *Water Research* (2018). DOI: [10.1016/j.watres.2017.10.072](#) (cit. on p. 26).
- [123] Z. Angeles-Olvera, A. Crespo-Yapur, O. Rodríguez, J. Cholula-Díaz, L. Martínez, and M. Videa. In: *Energies* (2022). DOI: [10.3390/en15051609](#) (cit. on p. 27).
- [124] D. Wang and G. G. Botte. In: *ECS Electrochemistry Letters* (2014). DOI: [10.1149/2.0031409eel](#) (cit. on p. 27).
- [125] D. A. Daramola, D. Singh, and G. G. Botte. In: *The Journal of Physical Chemistry* (2010). DOI: [10.1021/jp105159t](#) (cit. on pp. 27, 84).
- [126] F. Guo, K. Ye, M. Du, X. Huang, K. Cheng, G. Wang, and D. Cao. In: *Electrochimica Acta* (2016). DOI: [10.1016/j.electacta.2016.05.149](#) (cit. on p. 27).
- [127] V. Vedharathinam and G. G. Botte. In: *The Journal of Physical Chemistry C* (2014). DOI: [10.1021/jp5052529](#) (cit. on p. 27).
- [128] V. Vedharathinam and G. G. Botte. In: *Electrochimica Acta* (2013). DOI: [10.1016/j.electacta.2013.06.137](#) (cit. on pp. 27, 28).
- [129] V. Climent, A. Rodes, J. M. Pérez, J. M. Feliu, and A. Aldaz. In: *Langmuir* (2000). DOI: [10.1021/la000639g](#) (cit. on p. 27).
- [130] B. Zhu, Z. Liang, and R. Zou. In: *Small* (2020). DOI: [10.1002/smll.201906133](#) (cit. on pp. 28, 31, 34).
- [131] J. Li, J. Li, M. Gong, C. Peng, H. Wang, and X. Yang. In: *Topics in Catalysis* (2021). DOI: [10.1007/s11244-021-01453-w](#) (cit. on p. 28).
- [132] D. Zhu, H. Zhang, J. Miao, F. Hu, L. Wang, Y. Tang, M. Qiao, and C. Guo. In: *Journal of Materials Chemistry A* (2022). DOI: [10.1039/D1TA09989B](#) (cit. on p. 28).

- [133] Y. Xiao and J. M. Hill. In: *Environmental Science & Technology* (2018). DOI: [10.1021/acs.est.8b03409](https://doi.org/10.1021/acs.est.8b03409) (cit. on p. 28).
- [134] Q. Zhang, T. Li, J. Liang, N. Wang, X. Kong, J. Wang, H. Qian, Y. Zhou, F. Liu, C. Wei, Y. Zhao, and X. Zhang. In: *Journal of Materials Chemistry A* (2018). DOI: [10.1039/C8TA01334A](https://doi.org/10.1039/C8TA01334A) (cit. on p. 28).
- [135] Y. Li and C. Zhao. In: *ACS Catalysis* (2017). DOI: [10.1021/acscatal.6b03497](https://doi.org/10.1021/acscatal.6b03497) (cit. on p. 28).
- [136] N. Chen, Y.-X. Du, G. Zhang, W.-T. Lu, and F.-F. Cao. In: *Nano Energy* (2021). DOI: [10.1016/j.nanoen.2020.105605](https://doi.org/10.1016/j.nanoen.2020.105605) (cit. on p. 28).
- [137] R. F. Gouveia and F. Galembeck. In: *Journal of the American Chemical Society* (2009). DOI: [10.1021/ja900704f](https://doi.org/10.1021/ja900704f) (cit. on p. 28).
- [138] T.-H. Shen, L. Spillane, J. Peng, Y. Shao-Horn, and V. Tileli. In: *Nature Catalysis* (2021). DOI: [10.1038/s41929-021-00723-w](https://doi.org/10.1038/s41929-021-00723-w) (cit. on p. 28).
- [139] R. L. King and G. G. Botte. In: *Journal of Power Sources* (2011). DOI: [10.1016/j.jpowsour.2011.06.079](https://doi.org/10.1016/j.jpowsour.2011.06.079) (cit. on p. 28).
- [140] W. Chen, L. Xu, X. Zhu, Y.-C. Huang, W. Zhou, D. Wang, Y. Zhou, S. Du, Q. Li, C. Xie, L. Tao, C.-L. Dong, J. Liu, Y. Wang, R. Chen, H. Su, C. Chen, Y. Zou, Y. Li, Q. Liu, and S. Wang. In: *Angewandte Chemie International Edition* (2021). DOI: [10.1002/anie.202015773](https://doi.org/10.1002/anie.202015773) (cit. on pp. 29–31, 130).
- [141] R. K. Singh and A. Schechter. In: *Electrochimica Acta* (2018). DOI: [10.1016/j.electacta.2018.05.049](https://doi.org/10.1016/j.electacta.2018.05.049) (cit. on pp. 29, 100).
- [142] V. Vedharathinam and G. G. Botte. In: *Electrochimica Acta* (2012). DOI: [10.1016/j.electacta.2012.07.007](https://doi.org/10.1016/j.electacta.2012.07.007) (cit. on pp. 29, 74, 82, 100).
- [143] J. Li, J. Li, T. Liu, L. Chen, Y. Li, H. Wang, X. Chen, M. Gong, Z.-P. Liu, and X. Yang. In: *Angewandte Chemie International Edition* (2021). DOI: [10.1002/anie.202107886](https://doi.org/10.1002/anie.202107886) (cit. on pp. 29, 30, 33, 91, 92, 130).
- [144] W. Xu, Z. Wu, and S. Tao. In: *Energy Technology* (2016). DOI: [10.1002/ente.201600185](https://doi.org/10.1002/ente.201600185) (cit. on p. 31).
- [145] X. V. Medvedeva, J. J. Medvedev, S. W. Tatarchuk, R. M. Choueiri, and A. Klinkova. In: *Green Chemistry* (2020). DOI: [10.1039/D0GC01754J](https://doi.org/10.1039/D0GC01754J) (cit. on pp. 31, 35).
- [146] S. W. Tatarchuk, J. J. Medvedev, F. Li, Y. Tobolovskaya, and A. Klinkova. In: *Angewandte Chemie International Edition* (2022). DOI: [10.1002/anie.202209839](https://doi.org/10.1002/anie.202209839) (cit. on pp. 32–34, 67, 100, 130, 163, 175).
- [147] J. J. Medvedev, Y. Tobolovskaya, X. V. Medvedeva, S. W. Tatarchuk, F. Li, and A. Klinkova. In: *Green Chemistry* (2022). DOI: [10.1039/D1GC04140A](https://doi.org/10.1039/D1GC04140A) (cit. on pp. 34, 91, 116).
- [148] R. M. Choueiri, S. W. Tatarchuk, A. Klinkova, and L. D. Chen. In: *Electrochemical Science Advances* (2021). DOI: [10.1002/elsa.202100142](https://doi.org/10.1002/elsa.202100142) (cit. on pp. 34, 116).
- [149] H. Shin, K. U. Hansen, and F. Jiao. In: *Nature Sustainability* (2021). DOI: [10.1038/s41893-021-00739-x](https://doi.org/10.1038/s41893-021-00739-x) (cit. on p. 35).
- [150] C. Choi, S. Kwon, T. Cheng, M. Xu, P. Tieu, C. Lee, J. Cai, H. M. Lee, X. Pan, X. Duan, W. A. Goddard, and Y. Huang. In: *Nature Catalysis* (2020). DOI: [10.1038/s41929-020-00504-x](https://doi.org/10.1038/s41929-020-00504-x) (cit. on p. 35).
- [151] Z. Yue, C. Ou, N. Ding, L. Tao, J. Zhao, and J. Chen. In: *ChemCatChem* (2020). DOI: [10.1002/cctc.202001126](https://doi.org/10.1002/cctc.202001126) (cit. on p. 35).
- [152] H. Li, X. Qin, T. Jiang, X.-Y. Ma, K. Jiang, and W.-B. Cai. In: *ChemCatChem* (2019). DOI: [10.1002/cctc.201901748](https://doi.org/10.1002/cctc.201901748) (cit. on p. 35).

- [153] R. Clark, A. Moore, M. MacInnis, and E. Bertin. In: *Journal of Applied Electrochemistry* (2021). DOI: [10.1007/s10800-021-01601-w](https://doi.org/10.1007/s10800-021-01601-w) (cit. on p. 35).
- [154] L. Wang, Y. Zhu, Y. Wen, S. Li, C. Cui, F. Ni, Y. Liu, H. Lin, Y. Li, H. Peng, and B. Zhang. In: *Angewandte Chemie International Edition* (2021). DOI: [10.1002/anie.202100610](https://doi.org/10.1002/anie.202100610) (cit. on p. 35).
- [155] X. Yang, J. Nash, J. Anibal, M. Dunwell, S. Kattel, E. Stavitski, K. Attenkofer, J. G. Chen, Y. Yan, and B. Xu. In: *Journal of the American Chemical Society* (2018). DOI: [10.1021/jacs.8b08379](https://doi.org/10.1021/jacs.8b08379) (cit. on p. 35).
- [156] H. Wang, H. Yu, Z. Wang, Y. Li, Y. Xu, X. Li, H. Xue, and L. Wang. In: *Small* (2019). DOI: [10.1002/smll.201804769](https://doi.org/10.1002/smll.201804769) (cit. on p. 35).
- [157] P. Cañizares, C. Sáez, J. Lobato, and M. A. Rodrigo. In: *Industrial & Engineering Chemistry Research* (2004). DOI: [10.1021/ie034025t](https://doi.org/10.1021/ie034025t) (cit. on p. 36).
- [158] C. L. Forryan and R. G. Compton. In: *Physical Chemistry Chemical Physics* (2003). DOI: [10.1039/b307553m](https://doi.org/10.1039/b307553m) (cit. on p. 36).
- [159] Z. Zeng, Y. Sun, and J. Zhang. In: *Electrochemistry Communications* (2009). DOI: [10.1016/j.elecom.2008.11.055](https://doi.org/10.1016/j.elecom.2008.11.055) (cit. on p. 36).
- [160] S. Sriram, I. M. Nambi, and R. Chetty. In: *Electrochimica Acta* (2018). DOI: [10.1016/j.electacta.2018.07.194](https://doi.org/10.1016/j.electacta.2018.07.194) (cit. on p. 36).
- [161] R. A. Nickell, W. H. Zhu, R. U. Payne, D. R. Cahela, and B. J. Tatarchuk. In: *Journal of Power Sources* (2006). DOI: [10.1016/j.jpowsour.2006.05.028](https://doi.org/10.1016/j.jpowsour.2006.05.028) (cit. on p. 42).
- [162] G. G. Guilbault and J. G. Montalvo. In: *Journal of the American Chemical Society* (1970). DOI: [10.1021/ja00711a052](https://doi.org/10.1021/ja00711a052) (cit. on p. 52).
- [163] G. Guilbault and E. Hrabánková. In: *Analytica Chimica Acta* (1970). DOI: [10.1016/S0003-2670\(01\)80959-4](https://doi.org/10.1016/S0003-2670(01)80959-4) (cit. on p. 52).
- [164] J. L. Renfro and Y. Patel. In: *Journal of Applied Physiology* (1974). DOI: [10.1152/jappl.1974.37.5.756](https://doi.org/10.1152/jappl.1974.37.5.756) (cit. on p. 52).
- [165] M. Mikani, S. Talaei, R. Rahmanian, P. Ahmadi, and A. Mahmoudi. In: *Journal of Electroanalytical Chemistry* (2019). DOI: [10.1016/j.jelechem.2019.04.004](https://doi.org/10.1016/j.jelechem.2019.04.004) (cit. on p. 52).
- [166] C. Pundir, S. Jakhar, and V. Narwal. In: *Biosensors and Bioelectronics* (2019). DOI: [10.1016/j.bios.2018.09.067](https://doi.org/10.1016/j.bios.2018.09.067) (cit. on pp. 52, 54).
- [167] P. Bertocchi, D. Compagnone, and G. Palleschi. In: *Biosensors and Bioelectronics* (1996). DOI: [10.1016/0956-5663\(96\)83708-0](https://doi.org/10.1016/0956-5663(96)83708-0) (cit. on p. 52).
- [168] B. Lakard, G. Herlem, S. Lakard, A. Antoniou, and B. Fahys. In: *Biosensors and Bioelectronics* (2004). DOI: [10.1016/j.bios.2003.12.035](https://doi.org/10.1016/j.bios.2003.12.035) (cit. on p. 52).
- [169] Y. Xu, C. Lu, Y. Hu, L. Nie, and S. Yao. In: *Analytical Letters* (1996). DOI: [10.1080/00032719608001459](https://doi.org/10.1080/00032719608001459) (cit. on p. 52).
- [170] B. Kovács, G. Nagy, R. Dombi, and K. Tóth. In: *Biosensors and Bioelectronics* (2003). DOI: [10.1016/S0956-5663\(02\)00164-1](https://doi.org/10.1016/S0956-5663(02)00164-1) (cit. on p. 52).
- [171] D. E. Gaddes, M. C. Demirel, W. B. Reeves, and S. Tadigadapa. In: *The Analyst* (2015). DOI: [10.1039/C5AN01306B](https://doi.org/10.1039/C5AN01306B) (cit. on p. 52).
- [172] L. C. de Faria, C. Pasquini, and G. d. O. Neto. In: *Analyst* (1991). DOI: [10.1039/AN9911600357](https://doi.org/10.1039/AN9911600357) (cit. on p. 52).
- [173] H. Mana and U. Spohn. In: *Analytica Chimica Acta* (1996). DOI: [10.1016/0003-2670\(96\)00004-9](https://doi.org/10.1016/0003-2670(96)00004-9) (cit. on p. 52).
- [174] Y.-L. Liu, R. Liu, Y. Qin, Q.-F. Qiu, Z. Chen, S.-B. Cheng, and W.-H. Huang. In: *Analytical Chemistry* (2018). DOI: [10.1021/acs.analchem.8b04223](https://doi.org/10.1021/acs.analchem.8b04223) (cit. on p. 52).

- [175] M. Janyasupab, N. Asavakijthananont, N. Chanlek, S. Chio-Srichan, Y. Zhang, W. Surareungchai, and P. Sommani. In: *Journal of The Electrochemical Society* (2023). DOI: [10.1149/1945-7111/acd353](https://doi.org/10.1149/1945-7111/acd353) (cit. on p. 53).
- [176] S. W. Lewis, P. S. Francis, K. F. Lim, and G. E. Jenkins. In: *Analytica Chimica Acta* (2022). DOI: [10.1016/S0003-2670\(02\)00249-0](https://doi.org/10.1016/S0003-2670(02)00249-0) (cit. on p. 53).
- [177] X. Hu, N. Takenaka, M. Kitano, H. Bandow, Y. Maeda, and M. Hattori. In: *The Analyst* (1994). DOI: [10.1039/an9941901829](https://doi.org/10.1039/an9941901829) (cit. on pp. 53, 206).
- [178] W. Qin, Z. Zhang, and Y. Peng. In: *Analytica Chimica Acta* (2000). DOI: [10.1016/S0003-2670\(99\)00805-3](https://doi.org/10.1016/S0003-2670(99)00805-3) (cit. on p. 53).
- [179] I. Gutmann. “Urea”. In: *Methods of Enzymatic Analysis*. Bergmeyer HU. Elsevier, 1974, pp. 1791–1801. ISBN: 978-0-12-091304-6. DOI: [10.1016/B978-0-12-091304-6.X5001-0](https://doi.org/10.1016/B978-0-12-091304-6.X5001-0) (cit. on p. 53).
- [180] K.-I. D. Arnstadt. “Determination of the Urea Content of Milk”. European pat. 0164119A2. ARNSTADT KLAUS INGO. Dec. 11, 1985 (cit. on p. 53).
- [181] N. J. Langenfeld, L. E. Payne, and B. Bugbee. In: *PLOS ONE* (2021). Ed. by G. Signore. DOI: [10.1371/journal.pone.0259760](https://doi.org/10.1371/journal.pone.0259760) (cit. on pp. 53, 54, 206).
- [182] A. Roijers and M. Tas. In: *Clinica Chimica Acta* (1964). DOI: [10.1016/0009-8981\(64\)90094-4](https://doi.org/10.1016/0009-8981(64)90094-4) (cit. on p. 53).
- [183] W. T. Bolleter, C. J. Bushman, and P. W. Tidwell. In: *Analytical Chemistry* (1961). DOI: [10.1021/ac60172a034](https://doi.org/10.1021/ac60172a034) (cit. on p. 53).
- [184] J. R. Huizenga, A. Tangerman, and C. H. Gips. In: *Annals of Clinical Biochemistry: International Journal of Laboratory Medicine* (1994). DOI: [10.1177/000456329403100602](https://doi.org/10.1177/000456329403100602) (cit. on p. 53).
- [185] J. H. Boutwell. In: *Clinical Chemistry* (1957). DOI: [10.1093/clinchem/3.4.205](https://doi.org/10.1093/clinchem/3.4.205) (cit. on p. 54).
- [186] R. Emmet. “Method of Analyzing of Ammonia, Urea, and Tyrosine”. U.S. pat. 3718433A. R Emmet. 1973. URL: <https://patents.google.com/patent/US3718433A/en> (cit. on p. 54).
- [187] M. Urbanowicz, K. Sadowska, A. Paziewska-Nowak, A. Sołdatowska, and D. G. Pijanowska. In: *Membranes* (2021). DOI: [10.3390/membranes11110898](https://doi.org/10.3390/membranes11110898) (cit. on p. 54).
- [188] M. Koebel and M. Elsener. In: *Journal of Chromatography A* (1995). DOI: [10.1016/0021-9673\(94\)00922-V](https://doi.org/10.1016/0021-9673(94)00922-V) (cit. on p. 54).
- [189] H. Grossenbacher, A. M. Cook, and R. Hütter. In: *Journal of Chromatography A* (1985). DOI: [10.1016/0021-9673\(85\)80017-0](https://doi.org/10.1016/0021-9673(85)80017-0) (cit. on p. 54).
- [190] T. Sakurai, T. Irii, and K. Iwadate. In: *Legal Medicine* (2022). DOI: [10.1016/j.legalmed.2021.102011](https://doi.org/10.1016/j.legalmed.2021.102011) (cit. on pp. 54, 207, 228).
- [191] S. Fatt Lee, F. Teh Hui Boon, C. Cheah Hun Teong, and J. Rohrer. *Determination of Urea in Ultrapure Water by IC-MS/MS*. APPLICATION NOTE 72482. Thermo Fisher Scientific, p. 7. URL: https://lcmcs.cz/labrulez-bucket-strapi-h3hsga3/AN_72482_IC_MS_Urea_Ultrapure_Water_AN_72482_EN_3bac26af84/AN-72482-IC-MS-Urea-Ultrapure-Water-AN72482-EN.pdf (cit. on p. 54).
- [192] A. Soni and S. K. Jha. “Saliva Based Noninvasive Optical Urea Biosensor”. In: *2017 IEEE SENSORS*. 2017 IEEE SENSORS. Glasgow: IEEE, 2017, pp. 1–3. ISBN: 978-1-5090-1012-7. DOI: [10.1109/ICSENS.2017.8234302](https://doi.org/10.1109/ICSENS.2017.8234302). URL: <http://ieeexplore.ieee.org/document/8234302/> (cit. on p. 54).
- [193] C. Bruggink and D. Jensen. In: *Analytical Science Advances* (2021). DOI: [10.1002/ansa.202000120](https://doi.org/10.1002/ansa.202000120) (cit. on p. 58).

- [194] A. Bauer, J. Luetjohann, S. Rohn, J. Kuballa, and E. Jantzen. In: *Food Control* (2018). DOI: [10.1016/j.foodcont.2017.11.007](https://doi.org/10.1016/j.foodcont.2017.11.007) (cit. on p. 58).
- [195] J. B. Ngere, K. H. Ebrahimi, R. Williams, E. Pires, J. Walsby-Tickle, and J. S. O. McCullagh. In: *Analytical Chemistry* (2023). DOI: [10.1021/acs.analchem.2c04298](https://doi.org/10.1021/acs.analchem.2c04298) (cit. on p. 58).
- [196] G. Hopsort, L. Latapie, K. Groenen Serrano, K. Loubière, and T. Tzedakis. In: *Analytical and Bioanalytical Chemistry* (2023). DOI: [10.1007/s00216-023-04808-2](https://doi.org/10.1007/s00216-023-04808-2) (cit. on p. 61).
- [197] A. Seghioer, J. Chevalet, A. Barhoun, and F. Lantelme. In: *Journal of Electroanalytical Chemistry* (1998). DOI: [10.1016/S0022-0728\(97\)00498-1](https://doi.org/10.1016/S0022-0728(97)00498-1) (cit. on p. 73).
- [198] W. Visscher and E. Barendrecht. In: *Electrochimica Acta* (1980). DOI: [10.1016/0013-4686\(80\)87072-1](https://doi.org/10.1016/0013-4686(80)87072-1) (cit. on p. 73).
- [199] C. Costentin, S. Drouet, M. Robert, and J.-M. Savéant. In: *Journal of the American Chemical Society* (2012). DOI: [10.1021/ja303560c](https://doi.org/10.1021/ja303560c) (cit. on p. 74).
- [200] P. K. T. Nguyen, J. Kim, Y. S. Yoon, H. H. Yoon, and J. Hur. In: *International Journal of Hydrogen Energy* (2023). DOI: [10.1016/j.ijhydene.2022.10.052](https://doi.org/10.1016/j.ijhydene.2022.10.052) (cit. on p. 74).
- [201] R. Lin, L. Kang, T. Zhao, J. Feng, V. Celorrio, G. Zhang, G. Cibin, A. Kucernak, D. J. L. Brett, F. Corà, I. P. Parkin, and G. He. In: *Energy & Environmental Science* (2022). DOI: [10.1039/D1EE03522C](https://doi.org/10.1039/D1EE03522C) (cit. on p. 76).
- [202] S. Wang, P. Xu, J. Tian, Z. Liu, and L. Feng. In: *Electrochimica Acta* (2021). DOI: [10.1016/j.electacta.2021.137755](https://doi.org/10.1016/j.electacta.2021.137755) (cit. on p. 76).
- [203] J. I. Gowda and S. T. Nandibewoor. In: *Asian Journal of Pharmaceutical Sciences* (2014). DOI: [10.1016/j.ajps.2013.11.007](https://doi.org/10.1016/j.ajps.2013.11.007) (cit. on p. 77).
- [204] N. Aristov and A. Habekost. In: *World Journal of Chemical Education* (2015). DOI: [10.12691/wjce-3-5-2](https://doi.org/10.12691/wjce-3-5-2) (cit. on p. 77).
- [205] R. S. Nicholson and Irving. Shain. In: *Analytical Chemistry* (1964). DOI: [10.1021/ac60210a007](https://doi.org/10.1021/ac60210a007) (cit. on p. 78).
- [206] T. Ohsaka, K. Hirabayashi, and N. Oyama. In: *Bulletin of the Chemical Society of Japan* (1986). DOI: [10.1246/bcsj.59.3423](https://doi.org/10.1246/bcsj.59.3423) (cit. on p. 78).
- [207] M. Pourbaix. *Atlas of Electrochemical Equilibria in Aqueous Solutions*. 2nd ed. National Association of Corrosion, 1974. ISBN: 978-0-915567-98-0 (cit. on p. 81).
- [208] A. J. Tkalych, K. Yu, and E. A. Carter. In: *The Journal of Physical Chemistry* (2015). DOI: [10.1021/acs.jpcc.5b08481](https://doi.org/10.1021/acs.jpcc.5b08481) (cit. on p. 83).
- [209] X. Xiong, D. Ding, D. Chen, G. Waller, Y. Bu, Z. Wang, and M. Liu. In: *Nano Energy* (2015). DOI: [10.1016/j.nanoen.2014.10.029](https://doi.org/10.1016/j.nanoen.2014.10.029) (cit. on pp. 83, 120).
- [210] L. Li, J. Xu, J. Lei, J. Zhang, F. McLarnon, Z. Wei, N. Li, and F. Pan. In: *Journal of Materials Chemistry A* (2015). DOI: [10.1039/C4TA05156D](https://doi.org/10.1039/C4TA05156D) (cit. on pp. 83, 120).
- [211] A. J. Bard, R. Parsons, and J. Jordan. *Standard Potentials in Aqueous Solution*. 1st ed. Routledge, 2017. ISBN: 978-0-203-73876-4. DOI: [10.1201/9780203738764](https://doi.org/10.1201/9780203738764) (cit. on p. 83).
- [212] E. J. Dickinson and A. J. Wain. In: *Journal of Electroanalytical Chemistry* (2020). DOI: [10.1016/j.jelechem.2020.114145](https://doi.org/10.1016/j.jelechem.2020.114145) (cit. on p. 83).
- [213] J. S. Spendelow and A. Wieckowski. In: *Physical Chemistry Chemical Physics* (2007). DOI: [10.1039/b703315j](https://doi.org/10.1039/b703315j) (cit. on p. 84).
- [214] E. Hawlicka and R. Grabowski. In: *Berichte der Bunsengesellschaft für physikalische Chemie* (1994). DOI: [10.1002/bbpc.19940980610](https://doi.org/10.1002/bbpc.19940980610) (cit. on p. 85).

- [215] K. I. Kuznetsov, S. V. Skorodumov, and P. P. Granchenko. In: *High Temperature* (2020). DOI: [10.1134/S0018151X20060127](https://doi.org/10.1134/S0018151X20060127) (cit. on p. 86).
- [216] G. Akerlof and P. Bender. In: *Journal of the American Chemical Society* (1941). DOI: [10.1021/ja01849a054](https://doi.org/10.1021/ja01849a054) (cit. on p. 86).
- [217] L. G. Longsworth. In: *The Journal of Physical Chemistry* (1954). DOI: [10.1021/j150519a017](https://doi.org/10.1021/j150519a017) (cit. on p. 87).
- [218] F. Wu, Z. Zhang, F. Zhang, D. Duan, Y. Li, G. Wei, S. Liu, Q. Yuan, E. Wang, and X. Hao. In: *Catalysts* (2019). DOI: [10.3390/catal9090749](https://doi.org/10.3390/catal9090749) (cit. on p. 88).
- [219] J. Brauns, J. Schönebeck, M. R. Kraglund, D. Aili, J. Hnát, J. Žitka, W. Mues, J. O. Jensen, K. Bouzek, and T. Turek. In: *Journal of The Electrochemical Society* (2021). DOI: [10.1149/1945-7111/abda57](https://doi.org/10.1149/1945-7111/abda57) (cit. on p. 92).
- [220] Z. Liu, S. D. Sajjad, Y. Gao, H. Yang, J. J. Kaczur, and R. I. Masel. In: *International Journal of Hydrogen Energy* (2017). DOI: [10.1016/j.ijhydene.2017.10.050](https://doi.org/10.1016/j.ijhydene.2017.10.050) (cit. on p. 92).
- [221] M. Duca, V. Kavvadia, P. Rodriguez, S. Lai, T. Hoogenboom, and M. Koper. In: *Journal of Electroanalytical Chemistry* (2010). DOI: [10.1016/j.jelechem.2010.01.019](https://doi.org/10.1016/j.jelechem.2010.01.019) (cit. on p. 92).
- [222] W. Sun, M. Zhang, J. Li, and C. Peng. In: *ChemSusChem* (Nov. 8, 2022). DOI: [10.1002/cssc.202201263](https://doi.org/10.1002/cssc.202201263) (cit. on p. 101).
- [223] J. Pan, Y. Sun, P. Wan, Z. Wang, and X. Liu. In: *Electrochemistry Communications* (2005). DOI: [10.1016/j.elecom.2005.05.004](https://doi.org/10.1016/j.elecom.2005.05.004) (cit. on p. 101).
- [224] R. Thimmasandra Narayan. In: *Indian Journal of Materials Science* (2015). DOI: [10.1155/2015/820193](https://doi.org/10.1155/2015/820193) (cit. on pp. 101, 103).
- [225] E. Shangguan, Z. Chang, H. Tang, X. Yuan, and H. Wang. In: *International Journal of Hydrogen Energy* (2010). DOI: [10.1016/j.ijhydene.2010.01.098](https://doi.org/10.1016/j.ijhydene.2010.01.098) (cit. on p. 103).
- [226] M. Kashani Motlagh, A. Youzbashi, F. Hashemzadeh, and L. Sabaghzadeh. In: *Powder Technology* (2013). DOI: [10.1016/j.powtec.2012.12.047](https://doi.org/10.1016/j.powtec.2012.12.047) (cit. on p. 103).
- [227] J. L. Bantignies, S. Deabate, A. Righi, S. Rols, P. Hermet, J. L. Sauvajol, and F. Henn. In: *The Journal of Physical Chemistry C* (2008). DOI: [10.1021/jp075819e](https://doi.org/10.1021/jp075819e) (cit. on p. 103).
- [228] D. S. Hall, D. J. Lockwood, C. Bock, and B. R. MacDougall. In: *Proceedings of the Royal Society A: Mathematical, Physical and Engineering Sciences* (2015). DOI: [10.1098/rspa.2014.0792](https://doi.org/10.1098/rspa.2014.0792) (cit. on p. 103).
- [229] X.-Z. Fu, Y.-J. Zhu, Q.-C. Xu, J. Li, J.-H. Pan, J.-Q. Xu, J.-D. Lin, and D.-W. Liao. In: *Solid State Ionics* (2007). DOI: [10.1016/j.ssi.2007.04.011](https://doi.org/10.1016/j.ssi.2007.04.011) (cit. on p. 103).
- [230] H. L. Pardue. In: *Analytica Chimica Acta* (1989). DOI: [10.1016/S0003-2670\(00\)82005-X](https://doi.org/10.1016/S0003-2670(00)82005-X) (cit. on p. 108).
- [231] J. Casado, M. A. Lopez-Quintela, and F. M. Lorenzo-Barral. In: *Journal of Chemical Education* (1986). DOI: [10.1021/ed063p450](https://doi.org/10.1021/ed063p450) (cit. on p. 108).
- [232] L. C. Thomas, A. Dorizas, and E. Mech. In: *Analytical Letters* (1989). DOI: [10.1080/00032718908051382](https://doi.org/10.1080/00032718908051382) (cit. on p. 111).
- [233] W. Chen, Y. Wang, B. Wu, J. Shi, Y. Li, L. Xu, C. Xie, W. Zhou, Y.-C. Huang, T. Wang, S. Du, M. Song, D. Wang, C. Chen, J. Zheng, J. Liu, C.-L. Dong, Y. Zou, J. Chen, and S. Wang. In: *Advanced Materials* (2022). DOI: [10.1002/adma.202105320](https://doi.org/10.1002/adma.202105320) (cit. on p. 116).
- [234] W. Chen, C. Xie, Y. Wang, Y. Zou, C.-L. Dong, Y.-C. Huang, Z. Xiao, Z. Wei, S. Du, C. Chen, B. Zhou, J. Ma, and S. Wang. In: *Chem* (2020). DOI: [10.1016/j.chempr.2020.07.022](https://doi.org/10.1016/j.chempr.2020.07.022) (cit. on p. 116).

- [235] Y. Qi, Y. Zhang, L. Yang, Y. Zhao, Y. Zhu, H. Jiang, and C. Li. In: *Nature Communications* (2022). DOI: [10.1038/s41467-022-32443-5](https://doi.org/10.1038/s41467-022-32443-5) (cit. on p. 116).
- [236] J. Ge, Z. Liu, M. Guan, J. Kuang, Y. Xiao, Y. Yang, C. H. Tsang, X. Lu, and C. Yang. In: *Journal of Colloid and Interface Science* (2022). DOI: [10.1016/j.jcis.2022.03.152](https://doi.org/10.1016/j.jcis.2022.03.152) (cit. on p. 116).
- [237] L. Mazzei, M. Cianci, S. Benini, and S. Ciurli. In: *Angewandte Chemie International Edition* (2019). DOI: [10.1002/anie.201903565](https://doi.org/10.1002/anie.201903565) (cit. on p. 116).
- [238] Y.-J. Shih, Y.-H. Huang, and C. Huang. In: *Electrochimica Acta* (2018). DOI: [10.1016/j.electacta.2018.01.045](https://doi.org/10.1016/j.electacta.2018.01.045) (cit. on p. 116).
- [239] C. Picioreanu, I. M. Head, K. P. Katuri, M. C. van Loosdrecht, and K. Scott. In: *Water Research* (2007). DOI: [10.1016/j.watres.2007.04.009](https://doi.org/10.1016/j.watres.2007.04.009) (cit. on p. 119).
- [240] J. Lee and D. H. Kim. In: *Chemical Engineering Science* (2005). DOI: [10.1016/j.ces.2005.05.027](https://doi.org/10.1016/j.ces.2005.05.027) (cit. on p. 122).
- [241] S. Natesan and N. Ramanujam. In: *International Journal of Computer Mathematics* (1999). DOI: [10.1080/00207169908804861](https://doi.org/10.1080/00207169908804861) (cit. on p. 122).
- [242] E. S. Davydova, F. D. Speck, M. T. Paul, D. R. Dekel, and S. Cherevko. In: *ACS Catalysis* (2019). DOI: [10.1021/acscatal.9b01582](https://doi.org/10.1021/acscatal.9b01582) (cit. on p. 126).
- [243] P. Trinke, P. Haug, J. Brauns, B. Benschmann, R. Hanke-Rauschenbach, and T. Turek. In: *Journal of The Electrochemical Society* (2018). DOI: [10.1149/2.0541807jes](https://doi.org/10.1149/2.0541807jes) (cit. on p. 126).
- [244] G. Hopsort, D. Pereira Do Carmo, L. Latapie, K. Loubière, K. Groenen Serrano, and T. Tzedakis. In: *Electrochimica Acta* (2023). DOI: [10.1016/j.electacta.2023.141898](https://doi.org/10.1016/j.electacta.2023.141898) (cit. on p. 130).
- [245] P. Wang, X. Bai, H. Jin, X. Gao, K. Davey, Y. Zheng, Y. Jiao, and S.-Z. Qiao. In: *Advanced Functional Materials* (Mar. 16, 2023), p. 2300687. ISSN: 1616-301X, 1616-3028. DOI: [10.1002/adfm.202300687](https://doi.org/10.1002/adfm.202300687). URL: <https://onlinelibrary.wiley.com/doi/10.1002/adfm.202300687> (visited on 05/19/2023) (cit. on pp. 130, 135).
- [246] G. Hopsort, L. Latapie, K. Groenen Serrano, K. Loubière, and T. Tzedakis. In: *AIChE Journal* (2023), e18113. DOI: [10.1002/aic.18113](https://doi.org/10.1002/aic.18113) (cit. on pp. 130, 135).
- [247] J. Kim, W. J. K. Choi, J. Choi, M. R. Hoffmann, and H. Park. In: *Catalysis Today* 199 (Jan. 2013), pp. 2–7. ISSN: 09205861. DOI: [10.1016/j.cattod.2012.02.009](https://doi.org/10.1016/j.cattod.2012.02.009). URL: <https://linkinghub.elsevier.com/retrieve/pii/S0920586112000739> (visited on 07/11/2023) (cit. on p. 131).
- [248] Z. Shen, Y. Qi, W. Ge, H. Jiang, and C. Li. In: *Industrial & Engineering Chemistry Research* (2023). DOI: [10.1021/acs.iecr.3c00802](https://doi.org/10.1021/acs.iecr.3c00802) (cit. on p. 135).
- [249] N. Karki and S. W. Leslie. “Struvite And Triple Phosphate Renal Calculi”. In: *StatPearls*. Treasure Island (FL): StatPearls Publishing, 2023. pmid: [33760542](https://pubmed.ncbi.nlm.nih.gov/33760542/). URL: <http://www.ncbi.nlm.nih.gov/books/NBK568783/> (visited on 05/18/2023) (cit. on p. 136).
- [250] T. Brinkmann, G. Abbt-Braun, and F. H. Frimmel. In: *Acta hydrochimica et hydrobiologica* 31.3 (Nov. 2003), pp. 213–224. ISSN: 0323-4320, 1521-401X. DOI: [10.1002/aheh.200300491](https://doi.org/10.1002/aheh.200300491). URL: <https://onlinelibrary.wiley.com/doi/10.1002/aheh.200300491> (visited on 05/19/2023) (cit. on p. 136).
- [251] K. Carpenter and E. M. Stuve. In: *Journal of Applied Electrochemistry* (2021). DOI: [10.1007/s10800-021-01545-1](https://doi.org/10.1007/s10800-021-01545-1) (cit. on pp. 139, 141, 142).
- [252] K. M. Hassan and M. Abdel Azzem. In: *Journal of Applied Electrochemistry* 45.6 (June 2015), pp. 567–575. ISSN: 0021-891X, 1572-8838. DOI: [10.1007/s10800-015-0805-4](https://doi.org/10.1007/s10800-015-0805-4). URL: <http://link.springer.com/10.1007/s10800-015-0805-4> (visited on 05/23/2023) (cit. on p. 139).

- [253] S. Dbira, N. Bensalah, M. I. Ahmad, and A. Bedoui. In: *Materials* 12.8 (Apr. 16, 2019), p. 1254. ISSN: 1996-1944. DOI: [10.3390/ma12081254](https://doi.org/10.3390/ma12081254). URL: <https://www.mdpi.com/1996-1944/12/8/1254> (visited on 05/23/2023) (cit. on p. 140).
- [254] L.-C. Chen, T. Uchida, H.-C. Chang, and M. Osawa. In: *Electrochemistry Communications* 34 (Sept. 2013), pp. 56–59. ISSN: 13882481. DOI: [10.1016/j.elecom.2013.05.016](https://doi.org/10.1016/j.elecom.2013.05.016). URL: <https://linkinghub.elsevier.com/retrieve/pii/S1388248113001999> (visited on 05/23/2023) (cit. on p. 141).
- [255] A. Schranck, R. Marks, E. Yates, and K. Doudrick. In: *Environmental Science & Technology* 52.15 (Aug. 7, 2018), pp. 8638–8648. ISSN: 0013-936X, 1520-5851. DOI: [10.1021/acs.est.8b01743](https://doi.org/10.1021/acs.est.8b01743). URL: <https://pubs.acs.org/doi/10.1021/acs.est.8b01743> (visited on 06/06/2023) (cit. on p. 141).
- [256] T. Brinkmann, P. Hörsch, D. Sartorius, and F. H. Frimmel. In: *Environmental Science & Technology* 37.18 (Sept. 1, 2003), pp. 4190–4198. ISSN: 0013-936X, 1520-5851. DOI: [10.1021/es0263339](https://doi.org/10.1021/es0263339). URL: <https://pubs.acs.org/doi/10.1021/es0263339> (visited on 06/03/2023) (cit. on p. 141).
- [257] H. W. Schiwarra, H. Siegel, and A. Goebel. In: *European journal of clinical chemistry and clinical biochemistry : journal of the Forum of European Clinical Chemistry Societies* 30.2 (Feb. 1992), pp. 75–79. ISSN: 0939-4974. pmid: [1581412](https://pubmed.ncbi.nlm.nih.gov/1581412/) (cit. on p. 141).
- [258] A. Modvig and A. Riisager. In: *Catalysis Science & Technology* 9.16 (2019), pp. 4384–4392. ISSN: 2044-4753, 2044-4761. DOI: [10.1039/C9CY00271E](https://doi.org/10.1039/C9CY00271E). URL: <http://xlink.rsc.org/?DOI=C9CY00271E> (visited on 06/03/2023) (cit. on p. 141).
- [259] G. H. El-Nowihy and M. S. El-Deab. In: *Renewable Energy* 167 (Apr. 2021), pp. 830–840. ISSN: 09601481. DOI: [10.1016/j.renene.2020.11.156](https://doi.org/10.1016/j.renene.2020.11.156). URL: <https://linkinghub.elsevier.com/retrieve/pii/S0960148120319200> (visited on 05/23/2023) (cit. on p. 142).
- [260] D.-M. Zhou, H.-X. Ju, and H.-Y. Chen. In: *Journal of Electroanalytical Chemistry* 408.1-2 (May 1996), pp. 219–223. ISSN: 15726657. DOI: [10.1016/0022-0728\(95\)04522-8](https://doi.org/10.1016/0022-0728(95)04522-8). URL: <https://linkinghub.elsevier.com/retrieve/pii/S0022072895045228> (visited on 06/03/2023) (cit. on p. 142).
- [261] F. Franceschini and I. Taurino. In: *Physics in Medicine* 14 (Dec. 2022), p. 100054. ISSN: 23524510. DOI: [10.1016/j.phmed.2022.100054](https://doi.org/10.1016/j.phmed.2022.100054). URL: <https://linkinghub.elsevier.com/retrieve/pii/S2352451022000087> (visited on 06/03/2023) (cit. on p. 142).
- [262] K. T. Møller, T. R. Jensen, E. Akiba, and H.-w. Li. In: *Progress in Natural Science: Materials International* (2017). DOI: [10.1016/j.pnsc.2016.12.014](https://doi.org/10.1016/j.pnsc.2016.12.014) (cit. on p. 144).
- [263] E. Tzimas, C. Filiou, S. D. Peteves, and J.-B. Veyret. *Hydrogen Storage: State-of-the-Art and Future Perspective*. EUR 20995 EN. JRC26493, Dec. 16, 2003. URL: <https://publications.jrc.ec.europa.eu/repository/handle/JRC26493> (visited on 05/31/2023) (cit. on p. 144).
- [264] B. C. Tashie-Lewis and S. G. Nnabuife. In: *Chemical Engineering Journal Advances* 8 (Nov. 2021), p. 100172. ISSN: 26668211. DOI: [10.1016/j.cej.2021.100172](https://doi.org/10.1016/j.cej.2021.100172). URL: <https://linkinghub.elsevier.com/retrieve/pii/S2666821121000880> (visited on 05/20/2023) (cit. on p. 145).
- [265] E. Samson, J. Marchand, and K. A. Snyder. In: *Materials and Structures* 36.3 (Apr. 2003), pp. 156–165. ISSN: 1359-5997, 1871-6873. DOI: [10.1007/BF02479554](https://doi.org/10.1007/BF02479554). URL: <http://link.springer.com/10.1007/BF02479554> (visited on 07/15/2023) (cit. on pp. 153, 246).
- [266] A. Hodges, A. L. Hoang, G. Tsekouras, K. Wagner, C.-Y. Lee, G. F. Swiegers, and G. G. Wallace. In: *Nature Communications* 13.1 (Mar. 15, 2022), p. 1304. ISSN: 2041-1723. DOI: [10.1038/s41467-022-28953-x](https://doi.org/10.1038/s41467-022-28953-x). URL: <https://www.nature.com/articles/s41467-022-28953-x> (visited on 07/15/2023) (cit. on p. 167).

- [267] E. Mousset and D. D. Dionysiou. In: *Environmental Chemistry Letters* (2020). DOI: [10.1007/s10311-020-01014-9](https://doi.org/10.1007/s10311-020-01014-9) (cit. on p. 176).
- [268] D. A. Queremel Milani and I. Jialal. “Urinalysis”. In: *StatPearls*. Treasure Island (FL): StatPearls Publishing, 2023. pmid: [32491617](https://pubmed.ncbi.nlm.nih.gov/32491617/) (cit. on p. 206).
- [269] K. Njoku, D. Chiasserini, E. R. Jones, C. E. Barr, H. O’Flynn, A. D. Whetton, and E. J. Crosbie. In: *Frontiers in Oncology* (2020). DOI: [10.3389/fonc.2020.559016](https://doi.org/10.3389/fonc.2020.559016) (cit. on p. 206).
- [270] J. Jing and Y. Gao. In: *Discovery medicine* (2018). ISSN: 1944-7930 1539-6509. pmid: [29579412](https://pubmed.ncbi.nlm.nih.gov/29579412/) (cit. on p. 206).
- [271] B. Sequeira-Antunes and H. A. Ferreira. In: *Biomedicines* (2023). DOI: [10.3390/biomedicines11041051](https://doi.org/10.3390/biomedicines11041051) (cit. on p. 206).
- [272] N. A. Brunzel. *Fundamentals of Urine and Body Fluid Analysis - E-Book*. 5th ed. Philadelphia: Elsevier, 2022. ISBN: 978-0-323-84656-1 (cit. on p. 206).
- [273] B. Das Gupta. *Urine Analysis*. Elsevier. India, 1932. 152 pp. ISBN: 978-1-4831-6769-5. URL: <https://doi.org/10.1016/C2013-0-06676-5> (cit. on p. 206).
- [274] D. Lopes, L. Morés, M. Da Silva, M. Schneider, J. Merib, and E. Carasek. In: *Journal of Chromatography B* (2022). DOI: [10.1016/j.jchromb.2022.123406](https://doi.org/10.1016/j.jchromb.2022.123406) (cit. on p. 206).
- [275] G. G. Mohamed, A. M. Fekry, F. M. A. Attia, N. S. Ibrahim, and S. M. Azab. In: *Journal of Chromatography B* (2020). DOI: [10.1016/j.jchromb.2020.122178](https://doi.org/10.1016/j.jchromb.2020.122178) (cit. on p. 206).
- [276] D. A. Ashiru, R. Patel, and A. W. Basit. In: *Journal of Chromatography B* (2007). DOI: [10.1016/j.jchromb.2007.10.029](https://doi.org/10.1016/j.jchromb.2007.10.029) (cit. on p. 206).
- [277] A. Zoller, K. Wehmeyer, K. Krivos, M. Karb, P. Stoffolano, J. Nash, G. Balan, L. Behymer, M. Seeck, J. Brum, Y. Zou, and J. Price. In: *Journal of Chromatography B* (2021). DOI: [10.1016/j.jchromb.2021.122614](https://doi.org/10.1016/j.jchromb.2021.122614) (cit. on p. 206).
- [278] Q. Ma, C. Qi, X.-L. Li, Q. Shi, C.-Y. Xu, T. Jin, and J. Z. Min. In: *Journal of Pharmaceutical and Biomedical Analysis* (2021). DOI: [10.1016/j.jpba.2021.113939](https://doi.org/10.1016/j.jpba.2021.113939) (cit. on p. 206).
- [279] E. Dmitrieva, A. Temerdashev, A. Azaryan, and E. Gashimova. In: *Journal of Chromatography B* (2020). DOI: [10.1016/j.jchromb.2020.122390](https://doi.org/10.1016/j.jchromb.2020.122390) (cit. on p. 206).
- [280] A. Coglianesi, B. Charlier, F. Mensitieri, A. Filippelli, V. Izzo, and F. Dal Piaz. In: *Journal of Pharmaceutical and Biomedical Analysis* (2023). DOI: [10.1016/j.jpba.2023.115416](https://doi.org/10.1016/j.jpba.2023.115416) (cit. on p. 206).
- [281] B. L. Young and Y. Victoria Zhang. In: *Journal of Chromatography B* (2022). DOI: [10.1016/j.jchromb.2022.123495](https://doi.org/10.1016/j.jchromb.2022.123495) (cit. on p. 206).
- [282] J. D. Reber, E. L. Karschner, J. Z. Seither, J. L. Knittel, and J. P. Walterscheid. In: *Clinical Biochemistry* (2021). DOI: [10.1016/j.clinbiochem.2021.09.005](https://doi.org/10.1016/j.clinbiochem.2021.09.005) (cit. on p. 206).
- [283] J. Liu, W. Lu, L. Zhang, J. Yang, Z.-P. Yao, Y. He, and Y. Li. In: *Biosensors and Bioelectronics* (2021). DOI: [10.1016/j.bios.2021.113534](https://doi.org/10.1016/j.bios.2021.113534) (cit. on p. 206).
- [284] K. Teekayupak, C. Aumnate, A. Lomae, P. Preechakasedkit, C. S. Henry, O. Chailapakul, and N. Ruecha. In: *Talanta* (2023). DOI: [10.1016/j.talanta.2022.124131](https://doi.org/10.1016/j.talanta.2022.124131) (cit. on p. 206).
- [285] L. Caporossi, E. Paci, S. Capanna, B. Papaleo, G. Tranfo, and D. Pignini. In: *URINE* (2023). DOI: [10.1016/j.urine.2023.04.002](https://doi.org/10.1016/j.urine.2023.04.002) (cit. on p. 206).
- [286] G. Musile, Y. Agard, S. Pesavento, E. F. De Palo, R. M. Dorizzi, and F. Bortolotti. In: *Analytica Chimica Acta* (2023). DOI: [10.1016/j.aca.2022.340610](https://doi.org/10.1016/j.aca.2022.340610) (cit. on p. 206).

- [287] D. L. Rocha and F. R. Rocha. In: *Microchemical Journal* (2013). DOI: [10.1016/j.microc.2012.10.020](https://doi.org/10.1016/j.microc.2012.10.020) (cit. on p. 206).
- [288] Y. Zuo, C. Wang, J. Zhou, A. Sachdeva, and V. C. Ruelos. In: *Analytical Sciences* (2008). DOI: [10.2116/analsci.24.1589](https://doi.org/10.2116/analsci.24.1589) (cit. on p. 206).
- [289] S. George, M. Dipu, U. Mehra, P. Singh, A. Verma, and J. Ramgaokar. In: *Journal of Chromatography B* (2006). DOI: [10.1016/j.jchromb.2005.10.051](https://doi.org/10.1016/j.jchromb.2005.10.051) (cit. on p. 206).
- [290] W. Kwon, J. Y. Kim, S. Suh, and M. K. In. In: *Forensic Science International* (2012). DOI: [10.1016/j.forsciint.2012.03.025](https://doi.org/10.1016/j.forsciint.2012.03.025) (cit. on pp. 206, 228).
- [291] F. Wang, Y. Liu, M. Zhang, F. Zhang, and P. He. In: *Analytical Chemistry* (2021). DOI: [10.1021/acs.analchem.1c01203](https://doi.org/10.1021/acs.analchem.1c01203) (cit. on p. 207).
- [292] F. Ghaderinezhad, H. Ceylan Koydemir, D. Tseng, D. Karınca, K. Liang, A. Ozcan, and S. Tasoglu. In: *Scientific Reports* (2020). DOI: [10.1038/s41598-020-70456-6](https://doi.org/10.1038/s41598-020-70456-6) (cit. on p. 207).
- [293] K. Oginawati, A. A. H. Anka, S. H. Susetyo, S. A. Febriana, I. Tanziha, and C. R. S. Prakoeswa. In: *Heliyon* (2021). DOI: [10.1016/j.heliyon.2021.e07775](https://doi.org/10.1016/j.heliyon.2021.e07775) (cit. on p. 207).
- [294] J. Gunst, K. B. Kashani, and G. Hermans. In: *Intensive Care Medicine* (2019). DOI: [10.1007/s00134-019-05810-y](https://doi.org/10.1007/s00134-019-05810-y) (cit. on p. 207).
- [295] X. Wang, M. Wang, J. Ruan, S. Zhao, J. Xiao, and Y. Tian. In: *Journal of Chromatography B* (2019). DOI: [10.1016/j.jchromb.2019.06.022](https://doi.org/10.1016/j.jchromb.2019.06.022) (cit. on p. 207).
- [296] D. Krupp, N. Doberstein, L. Shi, and T. Remer. In: *The Journal of Nutrition* (2012). DOI: [10.3945/jn.112.159319](https://doi.org/10.3945/jn.112.159319) (cit. on p. 207).
- [297] L.-W. Xiang, J. Li, J.-M. Lin, and H.-F. Li. In: *Journal of Pharmaceutical Analysis* (2014). DOI: [10.1016/j.jpha.2013.11.003](https://doi.org/10.1016/j.jpha.2013.11.003) (cit. on p. 207).
- [298] S. Nikolaidis, C. Karpouzi, G. Tsalis, A. Kabasakalis, K. G. Papaioannou, and V. Mougios. In: *Biomarkers* (2016). DOI: [10.3109/1354750X.2016.1138323](https://doi.org/10.3109/1354750X.2016.1138323) (cit. on p. 207).
- [299] ICH. *Validation of Analytical Procedures: Text and Methodology Q2(R2)*. London, UK: EMA, Mar. 31, 2022 (cit. on p. 208).
- [300] M. El Himri, M. Errasfa, A. El Kassimi, A. Naboulsi, A. El Himri, and M. El Haddad. In: *Journal of the Indian Chemical Society* (2022). DOI: [10.1016/j.jics.2022.100684](https://doi.org/10.1016/j.jics.2022.100684) (cit. on p. 211).
- [301] J. Cho, J. Lee, C.-U. Lim, and J. Ahn. In: *Food Additives & Contaminants: Part A* (2016). DOI: [10.1080/19440049.2016.1235800](https://doi.org/10.1080/19440049.2016.1235800) (cit. on p. 213).
- [302] *Practical Aspects of Trapped Ion Mass Spectrometry, Volume IV, Theory and Instrumentation*. Raymond E. March and John F.J Todd. CRC Press, 2017. ISBN: 978-1-138-11344-2 (cit. on p. 213).
- [303] Y. Huang, S.-f. Mou, and K.-n. Liu. In: *Journal of Chromatography A* (1999). DOI: [10.1016/S0021-9673\(98\)00970-4](https://doi.org/10.1016/S0021-9673(98)00970-4) (cit. on pp. 213, 228).
- [304] P. Unak, Ş. Darcan, F. Yurt, Z. Biber, and M. Çoker. In: *Biological Trace Element Research* (1999). DOI: [10.1007/BF02784234](https://doi.org/10.1007/BF02784234) (cit. on p. 228).
- [305] R. Dineen, M. J. Hannon, and C. J. Thompson. “Hyponatremia and Hypernatremia”. In: *Endocrinology: Adult and Pediatric*. Elsevier, 2016, 1953–1964.e4. ISBN: 978-0-323-18907-1. DOI: [10.1016/B978-0-323-18907-1.00112-8](https://doi.org/10.1016/B978-0-323-18907-1.00112-8). URL: <https://linkinghub.elsevier.com/retrieve/pii/B9780323189071001128> (cit. on p. 229).
- [306] M. Y. Said, A. Post, I. Minović, M. Londen, H. Goor, D. Postmus, M. R. Heiner-Fokkema, E. Berg, A. Pasch, G. Navis, and S. J. L. Bakker. In: *Transplant International* (2020). DOI: [10.1111/tri.13600](https://doi.org/10.1111/tri.13600) (cit. on p. 229).

- [307] H. K. Walker, W. D. Hall, and J. W. Hurst, eds. *Clinical Methods: The History, Physical, and Laboratory Examinations*. 3rd. Boston: Butterworths, 1990. pmid: 21250045. URL: <http://www.ncbi.nlm.nih.gov/books/NBK201/> (cit. on p. 229).
- [308] M. He, S. Zhang, Y. Zhang, and S. G. Peng. In: *Optics Express* 23.9 (May 4, 2015), p. 10884. ISSN: 1094-4087. DOI: 10.1364/OE.23.010884. URL: <https://opg.optica.org/abstract.cfm?URI=oe-23-9-10884> (visited on 07/15/2023) (cit. on p. 246).

Scientific production

Publications in peer-reviewed journals

1. **G. Hopsort***, D. Pereira Do Carmo, L. Latapie, K. Loubière, K. Groenen Serrano, T. Tzedakis*. “Progress toward a better understanding of the urea oxidation by electromediation of nickel(III)/nickel(II) system in alkaline media”. In: *Electrochimica Acta* (2023).
[10.1016/j.electa.2023.141898](https://doi.org/10.1016/j.electa.2023.141898).
2. **G. Hopsort***, L. Latapie, K. Groenen Serrano, K. Loubière, T. Tzedakis*. “Indirect urea electro-oxidation by nickel(III) in alkaline medium: From kinetic and mechanism to reactor modeling”. In: *American Institute of Chemical Engineers J.* (2023).
[10.1002/aic.18113](https://doi.org/10.1002/aic.18113)
3. **G. Hopsort***, L. Latapie, K. Groenen Serrano, K. Loubière, T. Tzedakis*. “Deciphering the human urine matrix: a new approach to simultaneously quantify the main ions and organic compounds by ion chromatography / mass spectrometry (IC-MS)”. In: *Analytical and Bioanalytical Chemistry* (2023).
[10.1007/s00216-023-04808-2](https://doi.org/10.1007/s00216-023-04808-2)
4. **G. Hopsort***, L. Latapie, K. Groenen Serrano, K. Loubière, T. Tzedakis*. “New insights into urea electro-oxidation: complete mass-balances and proof of concept with real-matrix effluent”. In: *Journal of The Electrochemical Society* (2023).
[10.1149/1945-7111/acf87e](https://doi.org/10.1149/1945-7111/acf87e)
5. **G. Hopsort***, E. Piguet, L. Latapie, K. Groenen Serrano, K. Loubière, T. Tzedakis*. “Towards an industrial perspective for urea-to-hydrogen valorization by electro-oxidation on nickel (III): real effluents and pilot-scale proof of concept”. submitted in: *Electrochimica Acta* (2023).

Conference contributions

- Oral communication in international events:

1. **G. Hopsort**, L. Latapie, K. Loubière, K. Groenen Serrano, T. Tzedakis
Electro-oxydation photo-assistée de l’urée, simultanée à la production d’hydrogène,
*14^{ème} Congrès international du Groupement de Recherche Universitaire sur les
Techniques de Traitement et d’Épuration des Eaux*, 3rd March 2022, Toulouse,
France.

2. **G. Hopsort**, L. Latapie, K. Loubière, K. Groenen Serrano, T. Tzedakis
Urea indirect oxidation: from kinetics and mechanism to modeling of the physico-chemical phenomena, *13th European Symposium on Electrochemical Engineering*, 26th June 2023, Toulouse, France.
 3. **G. Hopsort**, L. Latapie, K. Loubière, K. Groenen Serrano, T. Tzedakis (accepted)
Progress toward a better understanding of urea electrochemical oxidation on nickel anode, *74th Annual Meeting of the International Society of Electrochemistry*, 5th September 2023, Lyon, France.
 4. **G. Hopsort**, L. Latapie, K. Loubière, K. Groenen Serrano, T. Tzedakis (accepted)
Scaling-up electrochemical valorisation of urea to hydrogen: a comprehensive study of kinetics, mechanisms and pilot-scale reactor design, *2023 AIChE Annual Meeting*, 8th November 2023, Orlando (FL), USA.
- Oral communication in national events:
 1. **G. Hopsort**, L. Latapie, K. Loubière, K. Groenen Serrano, T. Tzedakis
Conception, élaboration et optimisation d'un réacteur photoélectrochimique pour la valorisation d'effluents contenant de l'urée en hydrogène, *Webinar Section Grand Sud-Ouest de la Société Française de Génie des Procédés "L'eau, enjeu du futur"*, 7th January 2022, online.
 2. **G. Hopsort**, L. Latapie, K. Loubière, K. Groenen Serrano, T. Tzedakis
Vers un procédé électrochimique photo-assisté d'oxydation de l'urée et de production simultanée d'hydrogène, *18^{ème} congrès de la Société Française de Génie des Procédés*, 9th November 2022, Toulouse, France.
 - Poster communication:
 1. **G. Hopsort**, L. Latapie, K. Loubière, K. Groenen Serrano, T. Tzedakis
C. Cachet-Vivier, R. Benyahia, L. Rebiai, D. Muller, S. Bastide
Valorisation de l'urée par electro-oxydation photo-assistée, simultanée à la production d'hydrogène, *Journées Nationales sur l'Énergie Solaire, FedEsol*, August 2021, Odeillo, France.
 2. **G. Hopsort**, L. Latapie, K. Loubière, K. Groenen Serrano, T. Tzedakis
Urea oxidation by electromediation of nickel(III) / nickel(II) system in alkaline media with simultaneous H₂ production, *9th European Summer School of Electrochemical Engineering*, October 2022 (online).
 3. **G. Hopsort**, L. Latapie, K. Loubière, K. Groenen Serrano, T. Tzedakis (accepted)
Towards an electrochemical process for the urea valorisation into hydrogen through scale-up methodology: from kinetic and mechanistic studies to pilot-scale reactor development, *244th ECS Meeting*, October 2023.

Other communications during the thesis

1. **G. Hopsort**, L. Latapie, K. Loubière, K. Groenen Serrano, T. Tzedakis
Conception, building and optimization of a photoelectrochemical reactor for H₂ production from urea mineralisation, *PhD students' day of the lab-scale*, 20th October 2021, Toulouse, France.

2. G. Hopsort

Ma thèse en 180 secondes (*i.e.*, 3MT), recorded at this [weblink](#), *Regional Final, France Université, CNRS*, 25th March 2022, Toulouse, France.

3. Internal communications: presentations in the "EC Processes" department and in the "EC Engineering for synthesis, pollution abatement, energy and catalysis" team of the lab-scale

**VALORISATION OF UREA INTO HYDROGEN BY ELECTRO-OXIDATION:
FROM MECHANISM AND KINETIC STUDIES TO PILOT-SCALE REACTOR DESIGN AND
OPTIMISATION**

Abstract

To face energy and environmental challenges, the electro-oxidation of urea offers a promising alternative for wastewater treatment. This operation, implemented at room temperature, allows, in addition to the depolluting action, the generation of hydrogen at the cathode. Using inexpensive electrodes, this method has potential for industrial application, and all the more by photo-assisting the process.

This thesis aims at developing a complete model including the design, implementation and optimisation of an electrochemical process allowing the recovery of urine effluents into hydrogen; optionally being assisted by sunlight. Most of the current studies on this subject focus on the functionalisation of electrode materials, without deeply investigating the electrochemical engineering aspects. It is precisely this gap that the work carried out in this thesis seeks to fill. The understanding of the reaction phenomena taking place during the UEO implies the availability of complementary analytical tools. Thus, a wide range of analytical methods (TOC, IC-CD/MS, GC, SEM, granulometry, BET, XRD) has been developed, adapted and rigorously optimised, enabling to establish complete mass balances on almost all the by-product formed.

Then, an electrochemical kinetic study has been carried out by plotting voltammetric curves under different conditions, in order: (i) to study the impact of the operating parameters ($[j]$, $\theta_{/^\circ\text{C}}$, $\omega_{/\text{RPM}}$) on the rate of each chemico-physical phenomenon (electro-catalytic layer generation, reagent transport, reaction kinetics) and (ii) to access key quantities describing the overall process (activation energy, diffusion and anodic charge transfer coefficients, heterogeneous electron transfer rate constant). The validation of the process on a lab-scale scale has been done by means of complete mass balances performed on electrolyses at a scale of 1 to 2 g of urea and for degradation rates of 50 to 90%, never reached to date, and this at different operating conditions ($[\text{OH}^-]$, $\theta_{/^\circ\text{C}}$, mono/bi-compartmented reactor). One of the noticeable results is that the content of the compounds OCN^- , CO_3^{2-} , NO_2^- ions and NH_3 represents $\sim 80\%$ of the degraded urea.

To better understanding of UEO mechanism, additional kinetic studies have been conducted by implementing an original strategy combining two different methods: either solid particles of NiOOH or electro-generated NiOOH on nickel. The analysis of the two kinetic rate laws obtained, coupled with the study of the nature of the oxidation products identified, has enabled to provide new insights on this complex system and to propose a detailed reactional mechanism of the overall process (adsorption, chemical reaction, desorption).

Then, a model combining the established kinetic law with diffusive transport phenomena has been proposed. Concentration profiles have been solved in the liquid volume, in the diffusion layer and in the porous solid layer of NiOOH at the electrode. Consistent agreement ($>95\%$) has been obtained when comparing the lab-scale electrolysis results with the model predictions, and this for different operating conditions.

Coupling the proposed multi-pathway mechanism with this predictive model paves the way for the design and operation of a pilot-scale reactor, the study of which forms the final part of the thesis. The effect of operating parameters ($[j]^\circ$, flow rate/rate, E) on urea conversion, transport phenomena, electrode stability and energy consumption, has been studied on urea solutions, and also on with real effluents. The findings have allowed the validation of the process at pilot-scale (~ 40 g urea).

At last, this thesis has initiated a multi-disciplinary research dynamic aiming at addressing both depollution and energy challenges by valorizing a waste into an energy vector.

Keywords: Urea, Electrochemical Engineering, Kinetic, Mechanism, Effluent valorization, Hydrogen

**VALORISATION DE L'URÉE EN HYDROGÈNE PAR ÉLECTRO-OXYDATION :
DES ÉTUDES CINÉTIQUE ET MÉCANISTIQUE VERS LA CONCEPTION ET L'OPTIMISATION
D'UN RÉACTEUR À L'ÉCHELLE PILOTE**

Résumé

Répondant aux défis énergétiques et écologiques, l'électro-oxydation de l'urée offre une alternative prometteuse au traitement biologique des eaux usées. Simple à mettre en œuvre et opérant à température ambiante, elle permet, outre l'action dépolluante, de générer du H₂ à la cathode. Utilisant des électrodes peu coûteuses, cette méthode présente un potentiel industriel accentué par la perspective de photo-assister le procédé.

Les travaux réalisés dans le cadre de cette thèse visent à développer un procédé électrochimique (conception, mise en œuvre et optimisation) permettant de valoriser l'urine en hydrogène et capable d'être assisté par la lumière solaire. La majorité des recherches actuelles se concentrent sur les matériaux d'électrode, négligeant la dimension Génie des Procédés, que cette thèse aborde.

La compréhension des phénomènes réactionnels liés à l'oxydation anodique de l'urée, implique de disposer d'outils analytiques et de caractérisation. À cet effet, un ensemble analytique (COT, IC-CD/MS, CPG, MEB, granulométrie, BET, DRX) a été développé, adapté et mis en œuvre, ce qui a permis d'établir des bilans de matière de la quasi-totalité des réactifs/produits impliqués.

L'étude de la cinétique électrochimique du système a été réalisée via les courbes I=f(E) avec un double objectif : (i) étudier l'impact des paramètres opératoires ($[j]$, $\theta_{/^\circ\text{C}}$, $\omega_{/\text{RPM}}$) sur la vitesse de chaque phénomène physico-chimique (génération d'une couche électro-catalytique, transport des réactifs, cinétique de la réaction) et (ii) accéder à des grandeurs clés décrivant le processus global (énergie d'activation, coefficient de diffusion et de transfert électronique, constante de transfert électronique hétérogène). La validation du procédé à l'échelle laboratoire a été effectuée par des bilans de matière complets, sur des électrolyses à l'échelle de 1 à 2 g d'urée et à des taux de dégradation de 50 à 90%, jamais atteints à ce jour, et cela dans une large gamme de conditions opératoires ($[\text{OH}^-]$, $\theta_{/^\circ\text{C}}$, réacteur mono/bi-compartmenté). Le résultat marquant de cette étude est que les ions OCN^- , CO_3^{2-} , NO_2^- et NH_3 représentent $\sim 80\%$ de l'urée dégradée, le N₂ ne dépassant pas $\sim 15\%$.

Des études cinétiques de la dégradation de l'urée ont été par la suite conduites via une méthodologie originale combinant deux approches : l'analyse des lois de vitesse cinétique obtenues (i) sur particules solides de NiOOH et (ii) sur NiOOH électrogénéré. Couplée à l'identification des produits d'oxydation, ces résultats ont permis de mieux comprendre le système et de proposer un mécanisme réactionnel détaillé du processus global (adsorption, réaction chimique, désorption).

Un modèle combinant la loi cinétique établie avec les phénomènes de transport diffusifs et convectifs a été proposé. Les profils de concentration ont été déterminés : dans le liquide, la couche de diffusion et la couche solide poreuse de NiOOH à l'électrode. Les prédictions du modèle s'accordent à plus de 95% aux résultats d'électrolyses à l'échelle laboratoire, et ce pour différentes conditions de fonctionnement.

Du couplage de ce modèle prédictif avec le mécanisme à chemins réactionnels multiples proposé, un réacteur à l'échelle pilote a pu être conçu et élaboré, dont l'étude a fait l'objet de la dernière partie de la thèse. L'effet des paramètres opératoires ($[j]^\circ$, débit/régime d'écoulement,) sur les performances du procédé (conversion en urée, transport de matière, stabilité des électrodes et consommation énergétique) a été étudié avec l'urée commerciale puis avec de l'urine humaine, et a permis la validation du procédé à l'échelle pilote (~ 40 g d'urée).

L'ensemble de ces travaux ont contribué à une dynamique de recherche pluridisciplinaire, visant à valoriser un déchet en vecteur énergétique, qui est essentielle pour répondre aux enjeux contemporains de dépollution et d'énergie.

Mots clés : Urée, Génie Électrochimique, Cinétique, Mécanisme, Valorisation d'effluent, Hydrogène
